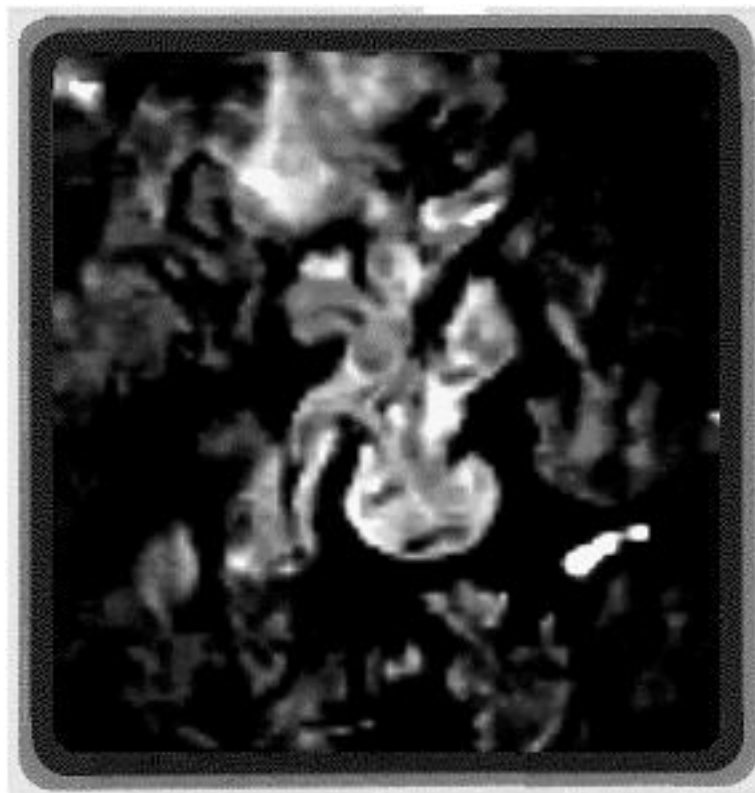Lectures in
Fluid Mechanics

Viscous Flows
and
Turbulence

Lectures in
Fluid Mechanics

Viscous Flows
and
Turbulence

by

Alexander J. Smits

Department of Mechanical Engineering
Princeton University
Princeton, NJ 08544, USA

September 17, 2009

Contents

Preface

These notes are intended for use by students enrolled in Princeton University courses MAE 552, "Viscous Flows and Boundary Layers," and MAE 553, "Turbulent Flow," and they should not be reproduced or distributed without permission of the author.

Alexander J. Smits
Princeton, New Jersey, USA

References for Turbulence Course MAE 537

S.B. Pope, "Turbulent Flows," Cambridge University Press, 2000

P.S. Bernard and J.M. Wallace, "Turbulent Flow: Analysis, Measurement, and Prediction," John Wiley & Sons, 2002

J. Mathieu and J. Scott, "An Introduction to Turbulent Flow," Cambridge University Press, 2000

Hinze, J.O., "Turbulence," McGraw-Hill, New York, 2nd edition, 1975

H. Tennekes and J.L. Lumley, "A First Course in Turbulence," MIT Press, 1972

P. Bradshaw, "An Introduction to Turbulence and Its Measurement," Pergamon Press, 1971

P. A. Libby, "Introduction to Turbulence," Taylor & Francis,1996

J. T. Davies, "Turbulence Phenomena," Academic Press, 1972

M. Lesieur, "Turbulence in Fluids," Kluwer, 3rd edition, 1993

H. Schlichting and K. Gersten, "Boundary-Layer Theory," McGraw-Hill, 8th edition, 2000

D. C. Wilcox, "Turbulence Modeling for CFD," DCW Industries, 1993

B. E. Launder and D. B. Spalding, "Mathematical Models of Turbulence," Academic Press, 1972

U. Frisch, "Turbulence," CUP paperback, 1995

Cebeci, T. and Smith, A. M. O., "Analysis of Turbulent Boundary Layers," Academic Press, 1974

Bradshaw, P., Cebeci, T. and Whitelaw, J. H., "Engineering Calculation Methods for Turbulent Flow," Academic Press, 1981

Cebeci, T. and Bradshaw, P., "Momentum Transfer in Boundary Layers," Hemisphere, 1977

Cebeci, T. and Bradshaw, P., "Physical and Computational Aspects of Convective Heat Transfer," Springer-Verlag, 1984

Smits, A.J. and Dussauge, J.P., "Turbulent Shear Layers in Supersonic Flow," Springer Verlag, AIP Imprint, 1996

Chapter 1

Equations of Motion

Here, we consider the equations of motion briefly. Full derivations can be found in a number of places, notably in Batchelor *Introduction to Fluid Dynamics*, and Currie *Fundamental Mechanics of Fluids*.

We consider only flows of fluids where the continuum hypothesis is valid. That is, the smallest volume of interest (a fluid element) will always contain a sufficient number of molecules for statistical averages to be meaningful. The continuum hypothesis fails when the mean free path is comparable to the smallest significant dimension. This can happen under normal temperatures and pressures when the body dimensions are very small, as for the flow around a very thin wire, such as the sensitive element of a hot wire probe where typical diameters range from 1 to 5 μm, or at very high altitudes, where the densities are very small and the mean free path can be very large. The relevant non-dimensional quantity is the Knudsen number, which is the ratio of the mean free path to a typical flow dimension. When the Knudsen number exceeds unity we expect rarified gas effects to become important. For a hot wire in a supersonic flow, the Knudsen number for the wire filament is about 0.2 at normal temperatures and pressures, and for the region occupied by the shock wave it approaches unity. It is difficult to justify the continuum hypothesis within the shock since for shocks of moderate strength the thickness is equal to a few mean free paths in the downstream gas. Nevertheless, the equations of motion for a continuum gas predict shock structures which agree well with experiment. For the flow over the filament itself, however, slip-flow effects associated with a breakdown in the continuum hypothesis have been observed when the Knudsen number based on the filament diameter is of order 0.1 (Davis, 1972). When Knudsen number effects are negligible, and the flow behavior can be described in term of its macroscopic properties such as its pressure, density, and velocity, the flow of a fluid is described completely by the continuity, momentum and energy equations, together with an equation of state and a suitable set of boundary conditions.

The principles of mass conservation, Newton's Second Law, and the conservation of energy will be used to derive the continuity equation, the momentum equation and the energy equation for fluids in motion. The equations can be written in integral form, appropriate for large control volumes, and in differential form, necessary for understanding the motion of fluid particles.

1.1   Integral Forms

Before we derive the integral equations of motion, we first introduce the concept of flux, which simplifies the derivations considerably.

1.1.1   Flux

When fluid flows across the surface area of a control volume, it carries with it many properties. For example, if the fluid has a certain temperature, it carries this temperature with it across the surface into the control volume. If it has a particular density, it carries this density with it as it crosses the surface. The fluid also carries with it momentum and energy. This "transport" of fluid properties by the flow across a surface is embodied in the concept of *flux*.

> The flux of (something) is the amount of that (something) being transported across a surface per unit time.

Consider <u>volume flux</u>, that is, the volume of all particles going through an area dA in time Δt. For a three-dimensional, time-dependent flow, the velocity and density are functions of three space variables and time. That is, we have a velocity field $\mathbf{V}(x, y, z, t)$ and a density field $\rho(x, y, z, t)$ (figure 1.1a).[1] If we mark a number of fluid particles and visualized their motion over a short time Δt, we could identify the fluid that passes through dA during this time interval (figure 1.1b).

If the area dA is small enough, the distribution of ρ and $\mathbf{V}$ can be approximated by their average values over the area. We can now identify the volume which contains all the particles that will pass through dA in time Δt. This volume $= (V \Delta t \cos \theta) \, dA = (\mathbf{n} \cdot \mathbf{V} \Delta t) \, dA$ where $\mathbf{n}$ is the unit normal which defines the orientation of the surface dA (figure 1.1c). That is,

---

[1]This is called an Eulerian description. See Smits *A First Course in Fluid Mechanics* for further details.
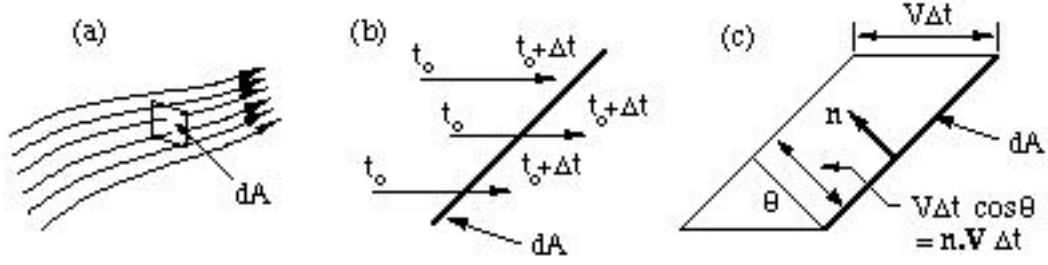
Figure 1.1: (a) Three-dimensional, unsteady flowfield with $\mathbf{V}(x, y, z, t)$ and $\rho(x, y, z, t)$; (b) Edge-on view of element of control surface of area dA; (c) Volume swept through dA in time Δt.

$$\left\{\begin{array}{c} \text{amount of volume per unit time} \\ \text{transported across an area} \\ dA \text{ with a direction } \mathbf{n} \end{array}\right\} = \left\{\begin{array}{c} \text{total} \\ \text{volume} \\ \text{flux} \end{array}\right\} = (\mathbf{n} \cdot \mathbf{V})dA$$

where $\mathbf{n} \cdot \mathbf{V}dA$ is the volume flux (dimensions of $L^3 T^{-1}$), and $\mathbf{n} \cdot \mathbf{V}$ represents the volume flux per unit area (dimensions of LT^{-1}).

Once we have written the volume flux we can easily write down other fluxes, such as

$$\text{mass flux} \qquad \rho(\mathbf{n} \cdot \mathbf{V})\, dA \quad = \quad \mathbf{n} \cdot \rho\mathbf{V}\, dA$$

$$\text{momentum flux} \qquad (\mathbf{n} \cdot \rho\mathbf{V})\mathbf{V}\, dA$$

$$\text{kinetic energy flux} \qquad \tfrac{1}{2}(\mathbf{n} \cdot \rho\mathbf{V})V^2\, dA, \qquad \text{etc.}$$

The dimensions of mass flux are MT^{-1}, momentum flux are MLT^{-2} (= force), and kinetic energy flux are $ML^2 T^{-3}$ (= force × velocity = power).

1.1.2 Continuity equation

The conservation of mass requires that the difference between the mass flow rates in and out of a given control volume is equal to the rate at which mass accumulates inside the volume. Here, we will derive the equation describing mass conservation for an unsteady, three-dimensional flow in its integral form. The differential form will be derived in section 1.3.1.

Consider the fixed control volume *CV* shown in figure 1.2. When the flow is unsteady, the outflux and influx of mass are not equal, so that mass contained inside the control volume may be increasing or decreasing. So:

(a) A fluid element of volume dv has a mass ρdv. Therefore the mass of fluid inside the control volume at any time is $\int \rho dv$. Hence:

$$\text{rate of change of mass in CV} \;=\; \frac{\partial}{\partial t} \int \rho\, dv \qquad (1.1)$$
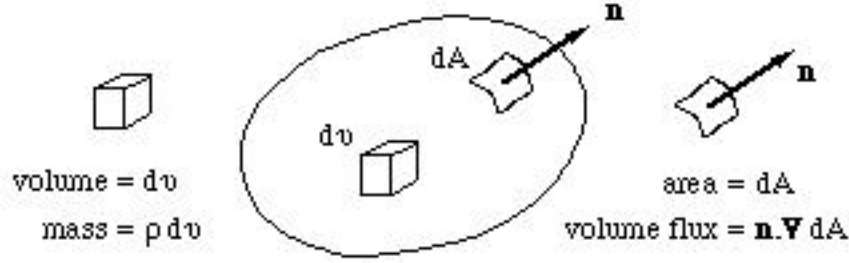
Figure 1.2: Fixed control volume for derivation of the integral form of the continuity equation.

(for a fixed control volume, either the partial or the regular derivative with respect to time can be used, since the volume itself is not changing with time). This rate of change of mass will be negative if the mass inside the control volume is decreasing with time (that is, when the outflux exceeds the influx).

(b) For a small element of surface area dA, the mass outflux through dA per unit time $= \rho \mathbf{V} \cdot \mathbf{n} dA$. Therefore

$$\text{total mass flux out of CV} \; = \; \int \rho \mathbf{V} \cdot \mathbf{n} \, dA. \qquad (1.2)$$

The integrand will be positive when the direction of the flow is in the same direction as the outward-facing unit normal vector $\mathbf{n}$, and negative when the direction of the flow is opposite to that of $\mathbf{n}$.

Hence, from equations 1.1 and 1.2, the conservation of mass requires that

$$\boxed{\frac{\partial}{\partial t} \int \rho \, dv + \int \mathbf{n} \cdot \rho \mathbf{V} \, dA \; = \; 0.} \qquad (1.3)$$

This is the integral form of the continuity equation for a fixed control volume, in a three-dimensional, time-dependent flow. In words:

$$\left\{ \begin{array}{c} \text{rate of increase of mass} \\ \text{inside control volume} \end{array} \right\} + \left\{ \begin{array}{c} \text{net rate of mass flux} \\ \text{out of control volume} \end{array} \right\} = \left\{ 0 \right\}$$

When the mass inside the control volume is fixed,

$$\boxed{\int \mathbf{n} \cdot \rho \mathbf{V} \, dA \; = \; 0} \qquad \text{Fixed mass}$$

(usually, of course, having a fixed mass inside the control volume implies constant density). When the flow is steady the flow properties do not depend on time, and therefore, since the control volume is fixed,

$$\int \mathbf{n} \cdot \rho \mathbf{V} \, dA \; = \; 0. \qquad \text{Steady flow}$$

The same equation is obtained when the mass inside the control volume is fixed, or when the flow is steady. These conditions have somewhat different implications, however, depending on the flow. When the flow is steady, the inlet and outlet mass flow rates, and the mass inside the control volume, do not change with time. When only the mass inside the control volume is constant in time, however, it is possible for the inlet and outlet mass flow rates to be unsteady, as long as they are equal.

For steady or unsteady incompressible flow,

$$\int \mathbf{n} \cdot \mathbf{V} dA \; = \; 0. \qquad \text{Incompressible flow}$$

1.1.3   Momentum equation

We now derive the integral form of the three-dimensional, time-dependent momentum equation. We start with a fixed control volume similar to that used in the derivation of the continuity equation (see figure 1.3). If a resultant force **F** acts on the fluid in the control volume, its momentum will change with time. The momentum of the fluid in the control volume can change in two ways:

1. By a non-zero momentum flux over the surface of the control volume. If the momentum influx is smaller (say) than the momentum outflux, there is a net positive momentum outflux that will tend to decrease the momentum of the fluid in the control volume.

2. By the unsteady variation of momentum contained within the volume, due to unsteady variations in the density or the velocity of the fluid inside the control volume.

This is somewhat similar to the conservation of mass, where a net outflux of mass leads to an unsteady variation of mass contained in the control volume. In other words, the sum of the rate of change of mass in the control
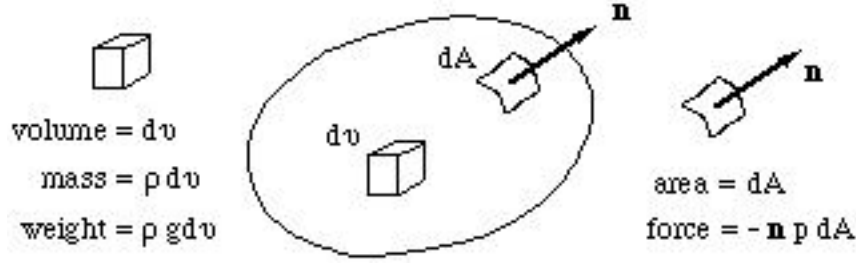
Figure 1.3: Fixed control volume for derivation of the integral form of the momentum equation.

volume and the net outflux of mass from the control volume is zero, since mass must be conserved. That is,

$$
\left\{ \begin{array}{c} \text{rate of change of} \\ \text{mass inside} \\ \text{control volume} \end{array} \right\} + \left\{ \begin{array}{c} \text{net outflux of} \\ \text{mass from} \\ \text{control volume} \end{array} \right\} = \left\{ 0 \right\},
$$

For the momentum, however, the sum of the rate of change of momentum in the control volume and the net outflux of momentum is not necessarily zero: momentum is not conserved if there is a resultant force acting on the fluid. That is,

$$
\left\{ \begin{array}{c} \text{rate of change of} \\ \text{momentum inside} \\ \text{control volume} \end{array} \right\} + \left\{ \begin{array}{c} \text{net outflux of} \\ \text{momentum from} \\ \text{control volume} \end{array} \right\} = \left\{ \begin{array}{c} \text{Resultant forces} \\ \text{acting on fluid} \end{array} \right\}.
$$

We see that the resultant force (equal to the mass of fluid in the control volume times the acceleration of the fluid passing through the control volume) is the sum of an unsteady term and a flux term. Consider each term in the momentum balance, from left to right.

Unsteady term

For the rate of change of momentum inside the control volume, consider an element of volume dv. The mass of this volume is ρdv, and its momentum is $\rho \mathbf{V} dv$. The total momentum contained in the control volume is found by integration, and its rate of change with time is found by differentiating with respect to time. So:

$$
\left\{ \begin{array}{c} \text{rate of change of momentum} \\ \text{inside control volume} \end{array} \right\} = \frac{\partial}{\partial t} \int \rho \mathbf{V} \, dv. \qquad (1.4)
$$

This quantity is positive if the momentum inside the control volume is increasing with time. Note that we have used the partial derivative with respect to time. In fact, we could have used a regular derivative: the control

volume is fixed in shape and location and so the integral (not the integrand) depends only on time.

Flux term

For an element of surface area dA, we have a volume flux $\mathbf{n} \cdot \mathbf{V} dA$ (see section 1.1.1). The flux is positive if the velocity is directed along $\mathbf{n}$, that is, it is positive if the flux is out of the control volume. The mass flux is therefore given by $\mathbf{n} \cdot \rho \mathbf{V} dA$, and the momentum flux is given by $(\mathbf{n} \cdot \rho \mathbf{V}) \mathbf{V} dA$. So:

$$\left\{ \begin{array}{c} \text{net outflux of momentum} \\ \text{from control volume} \end{array} \right\} = \int (\mathbf{n} \cdot \rho \mathbf{V}) \mathbf{V} \, dA. \qquad (1.5)$$

Resultant force

We have surface forces, body forces and forces due to external surfaces.

1. The surface forces include viscous forces acting over the surface of the control volume, and forces due to pressure acting at right angles to the surface. If the vector $\vec{\Sigma}$ is the surface force per unit area due to stress differences acting on the surface of the control volume, then

$$\left\{ \begin{array}{c} \text{net resultant force due to stress} \\ \text{differences acting on the surface} \\ \text{of the control volume} \end{array} \right\} = \int \vec{\Sigma} \, dA \qquad (1.6)$$

2. Body forces include gravitational, magnetic and electrical forces acting over all the fluid contained in the control volume. The only body force considered here is the force due to gravity. An element of volume dv has a mass ρdv, and the vector force due to gravity acting on this mass is $\rho \mathbf{g} dv$. So:

$$\left\{ \begin{array}{c} \text{resultant force due to gravity} \\ \text{acting on the mass contained} \\ \text{in the control volume} \end{array} \right\} = \int \rho \mathbf{g} \, dv = \mathbf{g} \int \rho \, dv = m\mathbf{g},$$
$$(1.7)$$

   where m is the total mass of fluid contained in the control volume.

3. The forces due to external surfaces, $\mathbf{F}_{\text{ext}}$, are the forces applied to the fluid by the walls of a duct, the surfaces of a deflector, or the forces acting in the solid cut by the control volume. An example of the latter is when a control volume is drawn to cut through the solid walls of a duct: we must include the forces transmitted through the walls in the

force balance on the fluid. (Remember: when a fluid exerts a force on a solid surface, an equal but opposite force acts on the fluid.)

By combining the terms given in equations 1.5 to 1.7, and including the viscous forces F_v and the forces due to external surfaces F_{ext}, we obtain the integral form of the momentum equation for a fixed control volume:

$$\mathbf{F_{ext}} + \int \vec{\Sigma} \, dA + \int \rho \mathbf{g} \, dv \;=\; \frac{\partial}{\partial t} \int \rho \mathbf{V} dv + \int (\mathbf{n} \cdot \rho \mathbf{V}) \, \mathbf{V} dA \qquad (1.8)$$

This is a vector equation, so that in Cartesian coordinates it has components in the x-, y- and z-directions.

1.2   Stresses and Strain Rates

The stress term in the momentum equation (equation 1.8) contains normal stresses and shear stresses. To evaluate the components of $\vec{\Sigma}$, consider the elemental control volume shown in figure 1.4. If we take only the stresses that contribute to the x-component of the surface force, we see that there are two kinds:

(a) Normal stresses, acting in the x-direction, normal to the face in the y-z plane (σ_{xx});

(b) Tangential stresses, acting in the x-direction, along faces in the z-x and y-x planes (σ_{yx} and σ_{zx}).

For a large control volume, therefore, the x-component of the surface force is given by

$$\mathbf{i} \cdot \int \vec{\Sigma} \, dA \;=\; \int \left(\sigma_{xx} + \sigma_{yx} + \sigma_{zx} \right) dA.$$

Similar results can be obtained for the surface forces in the y- and z-directions, so that

$$\int \vec{\Sigma} \, dA \;=\; \mathbf{i} \int \left(\sigma_{xx} + \sigma_{yx} + \sigma_{zx} \right) dA$$
$$+ \mathbf{j} \int \left(\sigma_{xy} + \sigma_{yy} + \sigma_{zy} \right) dA$$
$$+ \mathbf{k} \int \left(\sigma_{xz} + \sigma_{yz} + \sigma_{zz} \right) dA.$$
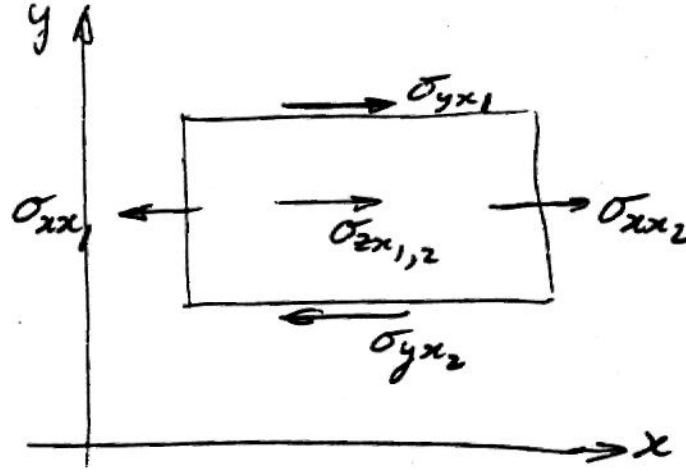
Figure 1.4: Control volume for a steady two-dimensional flow.

Therefore three normal stresses and six tangential stresses contribute to the total surface force. We could write this as

$$\int \Sigma_j \, dA \;=\; \int \sigma_{ij} n_i \, dA,$$

where

$$\sigma_{ij} \;=\; \begin{bmatrix} \sigma_{xx} & \sigma_{yx} & \sigma_{zx} \\ \sigma_{xy} & \sigma_{yy} & \sigma_{zy} \\ \sigma_{xz} & \sigma_{yz} & \sigma_{zz} \end{bmatrix}$$

and n_i is a unit vector defined such that $\sigma_{ij} n_i$ gives the **j**-component of the stress. It is, in fact normal to the surface, pointing out from the control volume.

The parameter σ_{ij} is a tensor known as the stress tensor. The resultant force per unit area, $\vec{\Sigma}$, is a function of space, time and surface orientation. That is,

$$\vec{\Sigma} = \vec{\Sigma}\,(\mathbf{n}, \mathbf{x}, t)\,.$$

Writing $\vec{\Sigma}$ in terms of the stress tensor σ_{ij} makes its dependence on the orientation of the surface clear. The stress tensor itself is independent of the surface orientation, but its scalar product with a unit vector gives the surface force per unit area acting in that direction. That is, the contribution of the surface force in the **j**-direction, Σ_j, is given by the component of the stress tensor acting in that direction, so that

$$\Sigma_j = \sigma_{ij} n_i$$

(see also Batchelor *Introduction to Fluid Dynamics*, p. 10).

The stress tensor σ_{ij}:

(a) The stress tensor σ_{ij} is independent of the surface orientation.

(b) It can be shown that σ_{ij} is symmetric, so that $\sigma_{xy} = \sigma_{yx}$, $\sigma_{xz} = \sigma_{zx}$ and $\sigma_{yz} = \sigma_{zy}$.

(c) By convention σ_{xy} denotes the stress acting in the y-direction, on a face aligned so that x is constant (that is, in the y-z plane.

(d) A fluid is as a medium that will continue to deform under an applied shear stress. Therefore, in a fluid at rest, all shear stresses are zero, by definition, and we are left only with the three normal stresses, σ_{xx}, σ_{yy} and σ_{zz}. What is more,

$$\sigma_{xx} = \sigma_{yy} = \sigma_{zz} = -p,$$

where p is the thermodynamic pressure, and by convention is taken to be positive when it tends to compress (hence the negative sign).

(e) In a fluid in motion, we can define a mean or "bulk" pressure $\bar{p}$, where

$$\bar{p} = -\tfrac{1}{3}\left(\sigma_{xx} + \sigma_{yy} + \sigma_{zz}\right).$$

Now, $\bar{p}$ must equal p when the fluid is at rest, but $\bar{p}$ and p need not be equal when the fluid is in motion (although the differences are usually small, as we shall see).

In order to proceed, we need to find the relationship between the stress tensor and the strain rates, that is, between the stress tensor and the velocity field, so that we can introduce the velocities into the stress term.

1.2.1 Strain rates and deformation

Rate of strain

When a fluid is in motion, every fluid element is, generally speaking, displaced to a new position at every instant. As this displacement takes place, the elements are strained, and the local rate of strain depends on the relative motion between any two points. Consider points A at $\mathbf{x}$ and B at $\mathbf{x} + d\mathbf{x}$. If the velocity at A is $[u, v, w]$, the velocity at B is given by $[u + du, v + dv, w + dw]$, where

$$\begin{aligned}
u + du &= u + \frac{\partial u}{\partial x}dx + \frac{\partial u}{\partial y}dy + \frac{\partial u}{\partial z}dz, \\
v + dv &= v + \frac{\partial v}{\partial x}dx + \frac{\partial v}{\partial y}dy + \frac{\partial v}{\partial z}dz, \\
w + dw &= w + \frac{\partial w}{\partial x}dx + \frac{\partial w}{\partial y}dy + \frac{\partial w}{\partial z}dz.
\end{aligned}$$

Thus the <u>relative</u> motion of B with respect to A is described by the velocity gradient tensor

$$\frac{\partial u_i}{\partial x_j} = \begin{bmatrix} \frac{\partial u}{\partial x} & \frac{\partial u}{\partial y} & \frac{\partial z}{\partial x} \\ \frac{\partial v}{\partial x} & \frac{\partial v}{\partial y} & \frac{\partial v}{\partial z} \\ \frac{\partial w}{\partial x} & \frac{\partial w}{\partial y} & \frac{\partial w}{\partial z} \end{bmatrix}.$$

We can write this as:

$$\frac{\partial u_i}{\partial x_j} = \begin{bmatrix} \frac{\partial u}{\partial x} & \frac{1}{2}\left(\frac{\partial v}{\partial x} + \frac{\partial u}{\partial y}\right) & \frac{1}{2}\left(\frac{\partial w}{\partial x} + \frac{\partial u}{\partial z}\right) \\ \frac{1}{2}\left(\frac{\partial u}{\partial y} + \frac{\partial v}{\partial x}\right) & \frac{\partial v}{\partial y} & \frac{1}{2}\left(\frac{\partial w}{\partial y} + \frac{\partial v}{\partial z}\right) \\ \frac{1}{2}\left(\frac{\partial u}{\partial z} + \frac{\partial w}{\partial x}\right) & \frac{1}{2}\left(\frac{\partial v}{\partial z} + \frac{\partial w}{\partial y}\right) & \frac{\partial w}{\partial z} \end{bmatrix}$$

$$+ \begin{bmatrix} 0 & -\frac{1}{2}\left(\frac{\partial v}{\partial x} - \frac{\partial u}{\partial y}\right) & -\frac{1}{2}\left(\frac{\partial w}{\partial x} - \frac{\partial u}{\partial z}\right) \\ -\frac{1}{2}\left(\frac{\partial u}{\partial y} - \frac{\partial v}{\partial x}\right) & 0 & -\frac{1}{2}\left(\frac{\partial w}{\partial y} - \frac{\partial v}{\partial z}\right) \\ -\frac{1}{2}\left(\frac{\partial u}{\partial z} - \frac{\partial w}{\partial x}\right) & -\frac{1}{2}\left(\frac{\partial v}{\partial z} - \frac{\partial w}{\partial y}\right) & 0 \end{bmatrix}.$$

The first matrix on the right hand side describes the <u>deformation</u> of the fluid element by compression and shearing, and it is called the "rate of strain" tensor, S_{ij}. The second matrix on the right hand side describes the <u>rotation</u> of the fluid element if it were to rotate as a rigid body without deformation, and it is called the "rate of rotation" tensor, R_{ij}. It does not deform the fluid element. Note that the instantaneous angular velocity of the fluid element is given by ω_k where $R_{ij} = \varepsilon_{ijk}\omega_k$.[2] The vector $\vec{\omega}$ is related to the vorticity $\boldsymbol{\Omega}$ by $\vec{\omega} = \frac{1}{2}\nabla \times \mathbf{V} = \frac{1}{2}\boldsymbol{\Omega}$. So:

$$\frac{\partial u_i}{\partial x_j} = S_{ij} + R_{ij}.$$

where

$$S_{ij} = \frac{1}{2}\left(\frac{\partial u_i}{\partial x_j} + \frac{\partial u_j}{\partial x_i}\right) \qquad \text{and} \qquad R_{ij} = \frac{1}{2}\left(\frac{\partial u_i}{\partial x_j} - \frac{\partial u_j}{\partial x_i}\right). \tag{1.9}$$

Stress tensor

It is also convenient to identify the elements of the stress tensor that are connected with fluid motion. When the fluid is at rest, or in rigid body motion, all velocity gradients are zero, and the only stress is due to the

---

[2]ε_{ijk} is the alternating tensor, such that

$$\varepsilon_{ijk} = \pm 1 \qquad \text{for } i \neq j \neq k$$
$$= 0 \qquad \text{for } i = j, j = k, \text{ or } i = k$$

thermodynamic pressure, p. Hence for a fluid in motion, that is, for a fluid where there is relative motion between fluid elements, we can write

$$\sigma_{ij} = -p\,[I] + d_{ij}$$

or

$$\sigma_{ij} = -p\delta_{ij} + d_{ij}$$

where d_{ij} is that part of σ_{ij} which is due to relative motion, and it is called the shear stress tensor, or the deviatoric stress tensor. The matrix $[I]$ is the unit matrix, and δ_{ij} is the Kronecker delta.[3]

Constitutive relationship

To find the relationship between the stress and the strain rate, we need to find only the relationship between d_{ij} and S_{ij}, since they are respectively the stress due to relative motion, and the strain rate due to deformation of fluid elements. The simplest connection is linear, but even a linear relationship between two second order tensors requires 81 coefficients. When combined with the conditions of symmetry and isotropy, the number of coeficients reduces to two, so that,

$$d_{ij} \;=\; 2\mu S_{ij} + \lambda \nabla \cdot \mathbf{V}\,[I]\,,$$

where the coefficient μ is called the "dynamic viscosity" and λ is called the "second coefficient of viscosity." Note that for incompressible flows, where $\nabla \cdot \mathbf{V} = 0$, the second term vanishes. Also,

$$\sigma_{ij} \;=\; -p\,[I] + 2\mu S_{ij} + \lambda \nabla \cdot \mathbf{V}\,[I]\,.$$

The rate-of-strain tensor is the only part of the velocity gradient tensor governed by relative motions among fluid particles. The simplest stress-strain rate relationship is a linear one, and fluids that follow this relationship are called Newtonian. For isotropic Newtonian fluids, the shear stress tensor becomes

$$d_{ij} = \lambda S_{kk}\delta_{ij} + 2\mu S_{ij} \tag{1.10}$$

1.2.2   Normal stresses in a fluid in motion

For a fluid in motion, we defined a bulk pressure $\bar{p}$, where

$$\bar{p} = -\tfrac{1}{3}\left(\sigma_{xx} + \sigma_{yy} + \sigma_{zz}\right).$$

That is,

$$\bar{p} - p \;=\; -\left(\lambda + \tfrac{2}{3}\mu\right)\nabla \cdot \mathbf{V},$$

---

[3]$\delta_{ij} = 1$ for $i = j$, and 0 for $i \neq j$.

where p is the thermodynamic pressure. We see that for a fluid in relative motion, the normal stress is not equal to the pressure p. However, $\bar{p}$ must equal p when:

(a) $\nabla \cdot \mathbf{V} = 0$ (incompressible flow);

(b) $\lambda = -\frac{2}{3}\mu$ ("Stokes Hypothesis"); or

(c) $\left(\lambda + \frac{2}{3}\mu\right)\nabla \cdot \mathbf{V}$ is very small.

For the rest of these notes we will assume that $\lambda = -\frac{2}{3}\mu$ ("Stokes Hypothesis"), so that $\bar{p} = p$. Experience shows this to be a good approximation under a wide variety of conditions. Hence,

$$\sigma_{ij} = -\left(p + \frac{2}{3}\mu\nabla \cdot \mathbf{V}\right)[I] + 2\mu S_{ij}. \tag{1.11}$$

This constitutive relationship holds for all Newtonian fluids, with and without compressibility.

We see that the stress tensor has normal components, such as

$$\sigma_{xx} = -\left(p + \frac{2}{3}\mu\nabla \cdot \mathbf{V}\right) + 2\mu\frac{\partial u}{\partial x}$$

and tangential components such as

$$\sigma_{xy} = \left(\frac{\partial u}{\partial y} + \frac{\partial v}{\partial x}\right) = \sigma_{yx}.$$

Both the normal and the tangential stresses depend on viscosity. The average normal stress $\bar{p} = -\frac{1}{3}\left(\sigma_{xx} + \sigma_{yy} + \sigma_{zz}\right)$ is independent of viscosity, but the individual normal stresses σ_{xx}, σ_{yy} and σ_{zz} are not. This observation holds true for compressible and incompressible flows.

Inviscid flows

In an inviscid or "ideal" fluid, the only stress component is the normal stress, it is equal to the pressure p, and it is isotropic. Hence:

$$\int \vec{\Sigma}\, dA = -\int \mathbf{n}p\, dA$$

(the unit normal $\mathbf{n}$ gives the direction to the force due to pressure differences, and by convention pressure is positive when it acts to compress the fluid — see figure 1.5). So, for an inviscid fluid, the integral form of the momentum
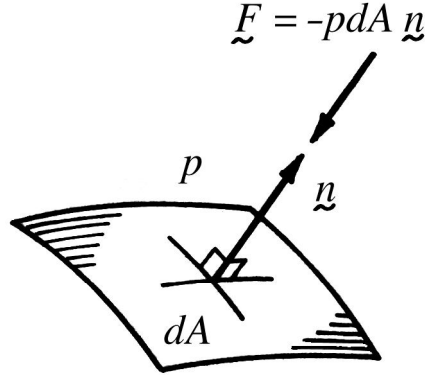
Figure 1.5: The vector force due to pressure acting on an element of surface.

equation is

$$\mathbf{F}_{\text{ext}} - \int \mathbf{n}p\, dA + \int \rho\mathbf{g}dv = \frac{\partial}{\partial t} \int \rho\mathbf{V}dv + \int (\mathbf{n} \cdot \rho\mathbf{V})\,\mathbf{V}dA \qquad (1.12)$$

This is a valid approximation for real fluids when the resultant force components due to viscous stresses are small compared to the forces due to pressure differences (that is, when velocity gradients and relative motions are small).

Viscous flows

To include viscous effects in this momentum balance, we could use (for the j-component)

$$\int \vec{\Sigma}_j\, dA = \int \sigma_{ij}n_i\, dA.$$

However, for many purposes and applications, the variation of σ_{ij} over the surface is not known. In fact, the control volume approach is often taken because we are only interested in gross properties, rather than detailed information on the fluid flow behavior. In that case, we can simply write

$$\mathbf{F}_{\text{ext}} + \mathbf{F}_{\mathbf{v}} - \int \mathbf{n}p\, dA + \int \rho\mathbf{g}dv = \frac{\partial}{\partial t} \int \rho\mathbf{V}dv + \int (\mathbf{n} \cdot \rho\mathbf{V})\,\mathbf{V}dA \qquad (1.13)$$

where $\mathbf{F}_{\mathbf{v}}$ is the resultant force due to viscous effects. It is often possible to choose the control volume so that this viscous force appears only at solid surfaces, and this particular form of the momentum equation can be very useful.

However, we are generally more interested (certainly in these notes) in describing the detailed motion of the fluid inside the control volume. This would allow us to find, for example, the variation of the viscous forces

along the surface of the control volume, not just the overall, integrated viscous force, or (another example) the details of the velocity profile, rather than just the overall momentum outflux.

1.3 Differential Equations of Motion

We can obtain the differential forms of the continuity and momentum equations directly from their integral forms.

1.3.1 Continuity equation

For the continuity equation (equation 10.19):

$$\frac{\partial}{\partial t} \int \rho \, dv + \int \mathbf{n} \cdot \rho \mathbf{V} \, dA = 0.$$

Since the control volume is fixed, the partial derivative can be moved inside the integral, so that

$$\int \frac{\partial \rho}{\partial t} \, dv + \int \mathbf{n} \cdot \rho \mathbf{V} \, dA = 0.$$

The area integral can be converted to a volume integral using the divergence theorem. Hence,

$$\int \left(\frac{\partial \rho}{\partial t} + \nabla \cdot \rho \mathbf{V} \right) dv = 0.$$

Since the control volume is arbitrary, the integrand itself must be zero, so that

$$\frac{\partial \rho}{\partial t} + \nabla \cdot \rho \mathbf{V} = 0.$$

That is,

$$\boxed{\nabla \cdot \rho \mathbf{V} = -\frac{\partial \rho}{\partial t}.} \qquad (1.14)$$

This can be expanded as

$$u \frac{\partial \rho}{\partial x} + \rho \frac{\partial u}{\partial x} + v \frac{\partial \rho}{\partial y} + \rho \frac{\partial v}{\partial y} + w \frac{\partial \rho}{\partial z} + \rho \frac{\partial w}{\partial z} = -\frac{\partial \rho}{\partial t}.$$

Hence:

$$\frac{\partial u}{\partial x} + \frac{\partial v}{\partial y} + \frac{\partial w}{\partial z} = -\frac{1}{\rho} \frac{D\rho}{Dt},$$

or:

$$\nabla \cdot \mathbf{V} = -\frac{1}{\rho}\frac{D\rho}{Dt}. \tag{1.15}$$

Equations 1.14 and 1.15 are two forms of the continuity equation in differential form. Since they are written in vector form, they are independent of the coordinate system.

The total derivative D/Dt represents the rate of change of density following a particle of fluid in an Eulerian system. A fluid particle has a fixed mass m, and therefore a variable volume. In terms of the volume v (= m/ρ):

$$-\frac{1}{\rho}\frac{D\rho}{Dt} = -\frac{v}{m}\frac{D\,(v/m)}{Dt} = \frac{1}{v}\frac{Dv}{Dt}, \tag{1.16}$$

and so the divergence of the velocity is equal to the fractional rate of change of volume of a fluid element of given mass. This is called the rate of dilatation, or simply the dilatation. In tensor notation we have:

$$\frac{\partial \rho}{\partial t} + \frac{\partial \rho u_j}{\partial x_j} = 0. \tag{1.17}$$

By definition, an incompressible fluid is a fluid where $\frac{D\rho}{Dt} = 0$. From equation 1.15, we see that this requires $\nabla \cdot \mathbf{V} = 0$. Constant density is special case of an incompressible fluid, but commonly no distinction is made between an incompressible fluid and one with constant density.

We can also derive the differential form of the continuity equation from first principles, for an Eulerian system in cartesian coordinates. Consider an elemental volume $dx\,dy\,dz$ (figure 1.6). At the point 0, in the middle of the box, at time t,

$$u = u_0, \quad v = v_0, \quad w = w_0, \quad \text{and} \quad \rho = \rho_0.$$

First we find the net mass outflow per unit time. By using a Taylor series expansion, and dropping higher order terms:

On face *abcd*: $u = u_0 - \left(\frac{\partial u}{\partial x}\right)_0 \frac{dx}{2}$,   and $\rho = \rho_0 - \left(\frac{\partial \rho}{\partial x}\right)_0 \frac{dx}{2}$

On face *efgh*: $u = u_0 + \left(\frac{\partial u}{\partial x}\right)_0 \frac{dx}{2}$,   and $\rho = \rho_0 + \left(\frac{\partial \rho}{\partial x}\right)_0 \frac{dx}{2}.$
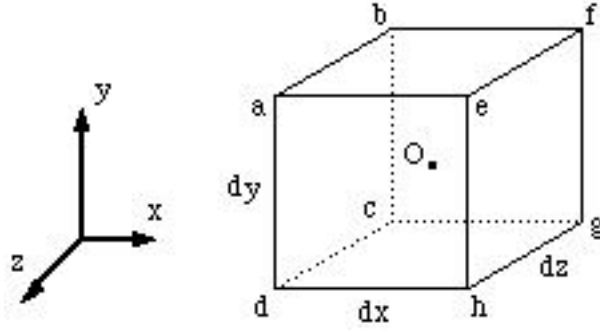
Figure 1.6: Elemental control volume for derivation of the differential form of the continuity equation.

We can find the mass flow through the box by finding the mass flow through each of its six faces and summing the result. We start with faces *abcd* and *efgh*:

$$
\begin{aligned}
\text{Mass influx through } abcd \text{ in time } dt \;&=\; \rho u \, dA \, dt \\[6pt]
&=\; \left(\rho_0 - \left(\frac{\partial \rho}{\partial x}\right)_0 \frac{dx}{2}\right)\left(u_0 - \left(\frac{\partial u}{\partial x}\right)_0 \frac{dx}{2}\right) dy \, dz \, dt
\end{aligned}
$$

$$
\begin{aligned}
\text{Mass outflux through } efgh \text{ in time } dt \;&=\; \rho u \, dA \, dt \\[6pt]
&=\; \left(\rho_0 + \left(\frac{\partial \rho}{\partial x}\right)_0 \frac{dx}{2}\right)\left(u_0 + \left(\frac{\partial u}{\partial x}\right)_0 \frac{dx}{2}\right) dy \, dz \, dt
\end{aligned}
$$

$$
\begin{aligned}
\text{Net outflow through } abcd \text{ and } efgh \;&=\; \left[u_0\left(\frac{\partial \rho}{\partial x}\right)_0 + \rho_0\left(\frac{\partial u}{\partial x}\right)_0\right] dx \, dy \, dz \, dt \\[6pt]
&=\; \left[\frac{\partial(\rho u)}{\partial x}\right]_0 dx \, dy \, dz \, dt.
\end{aligned}
$$

Similar expressions can be derived for the other faces:

$$
\text{Net outflow through } cdhg \text{ and } abfe \;=\; \left(\frac{\partial(\rho v)}{\partial y}\right)_0 dx \, dy \, dz \, dt
$$

$$
\text{Net outflow through } cbfg \text{ and } aehd \;=\; \left(\frac{\partial(\rho w)}{\partial z}\right)_0 dx \, dy \, dz \, dt.
$$

By adding up the contributions over all six faces, we have:

$$
\text{Total net mass outflow in time } dt \;=\; \left[\frac{\partial(\rho u)}{\partial x} + \frac{\partial(\rho v)}{\partial y} + \frac{\partial(\rho w)}{\partial z}\right] dx \, dy \, dz \, dt
$$

(we have dropped the subscript because the result should not depend on the particular point that was considered). This must be equal to the decrease in mass contained in this volume during the same time interval (mass must be conserved). That is,

$$\left[\frac{\partial(\rho u)}{\partial x} + \frac{\partial(\rho v)}{\partial y} + \frac{\partial(\rho w)}{\partial z}\right] dx\, dy\, dz\, dt \; = \; -dx\, dy\, dz\, \frac{\partial \rho}{\partial t}\, dt.$$

Or,

$$\frac{\partial(\rho u)}{\partial x} + \frac{\partial(\rho v)}{\partial y} + \frac{\partial(\rho w)}{\partial z} \; = \; -\frac{\partial \rho}{\partial t},$$

so that

$$\nabla \cdot \rho \mathbf{V} \; = \; -\frac{\partial \rho}{\partial t}.$$

Hence:

$$\frac{\partial u}{\partial x} + \frac{\partial v}{\partial y} + \frac{\partial w}{\partial z} \; = \; -\frac{1}{\rho}\frac{D\rho}{Dt},$$

or:

$$\nabla \cdot \mathbf{V} \; = \; -\frac{1}{\rho}\frac{D\rho}{Dt},$$

as in equations 1.14 and 1.15.

Particular forms

In Cartesian coordinates,

$$\frac{\partial(\rho u)}{\partial x} + \frac{\partial(\rho v)}{\partial y} + \frac{\partial(\rho w)}{\partial z} \; = \; -\frac{\partial \rho}{\partial t}. \tag{1.18}$$

In cylindrical coordinates,

$$\frac{1}{r}\frac{\partial r\rho u_r}{\partial r} + \frac{1}{r}\frac{\partial \rho u_\theta}{\partial \theta} + \frac{\partial \rho u_z}{\partial z} \; = \; -\frac{\partial \rho}{\partial t}. \tag{1.19}$$

1.3.2   Euler equation

We can take a similar approach for the momentum equation. If we start with the integral form for an inviscid fluid (equation 1.12):

$$\mathbf{F}_{\text{ext}} - \int \mathbf{n}\, p\, dA + \int \rho \mathbf{g}\, dv \; = \; \frac{\partial}{\partial t}\int \rho \mathbf{V}\, dv + \int (\mathbf{n} \cdot \rho \mathbf{V})\, \mathbf{V}\, dA.$$

If we look at the interior of the fluid, we can ignore $\mathbf{F}_{\text{ext}}$. Since the control volume is fixed, the partial derivative can be moved inside the integral, so that

$$\int \frac{\partial \rho \mathbf{V}}{\partial t} \, dv + \int (\mathbf{n} \cdot \rho \mathbf{V}) \, \mathbf{V} \, dA \;=\; -\int \mathbf{n} \, p \, dA + \int \rho \mathbf{g} \, dv.$$

Changing the area integrals to volume integrals and collecting terms,

$$\int \left(\frac{\partial \rho \mathbf{V}}{\partial t} + (\nabla \cdot \rho \mathbf{V}) \, \mathbf{V} + (\rho \mathbf{V} \cdot \nabla) \, \mathbf{V} \right) dv \;=\; -\int (\nabla p + \rho \mathbf{g}) \, dv.$$

Simplifying:

$$\int \left(\rho \frac{\partial \mathbf{V}}{\partial t} + \rho \, (\mathbf{V} \cdot \nabla) \, \mathbf{V} + \nabla p - \rho \mathbf{g} \right) dv \;=\; 0.$$

Since the control volume is arbitrary, the integrand itself must be zero, so that

$$\rho \left(\frac{\partial \mathbf{V}}{\partial t} + (\mathbf{V} \cdot \nabla) \, \mathbf{V} \right) + \nabla p - \rho \mathbf{g} \;=\; 0.$$

Therefore:

$$\boxed{\rho \frac{D\mathbf{V}}{Dt} = -\nabla p + \rho \mathbf{g}.} \tag{1.20}$$

This is the differential form of the linear momentum equation for an inviscid fluid, in vector form. This equation is often called the Euler equation, and it holds for compressible and incompressible flows.

We can also derive the differential form of the momentum equation for inviscid flows from first principles.

Consider a fixed, control volume of infinitesimal size (figure 1.7). There is flow through the six faces of the volume, and surface forces and body forces act on the fluid inside the box. The only surface forces taken into account are forces due to pressure differences, and the only body forces considered are forces due to gravity. The volume element $dxdydz$ is similar to the one used to derive the continuity equation except that only one face is shown, and this face has an arbitrary orientation with respect to the gravitational vector $\mathbf{g}$ (that is, $\mathbf{g}$ may have components in or out of the page, as well as being at an angle to the x- and y-axes). The point 0 is at the center of the volume element.

The resultant force in the x-direction, F_x, has two contributions: the force due to pressure differences acting on the two faces of area $dydz$, and the x-component of the force due to the weight of the fluid contained in the
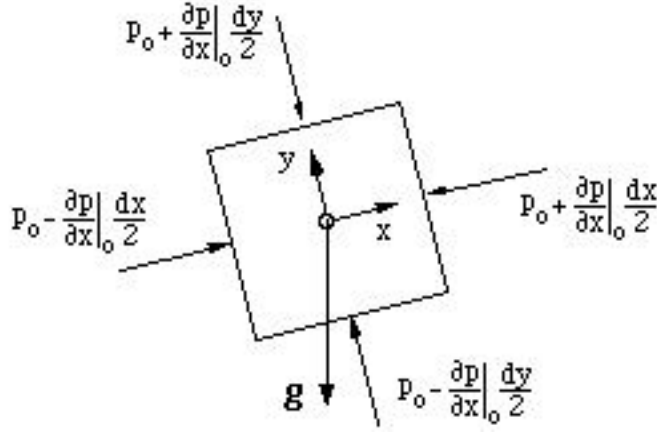
Figure 1.7: Elemental control volume for derivation of the differential form of the momentum equation.

volume *dxdydz*. Using a Taylor series expansion about the center of the volume, and neglecting second-order terms, we have

$$F_x \; = \; \left[p_0 - \frac{\partial p}{\partial x}\bigg|_0 \frac{dx}{2} \right] dy\,dz - \left[p_0 + \frac{\partial p}{\partial x}\bigg|_0 \frac{dx}{2} \right] dy\,dz + \rho_0 \mathbf{g} \cdot \mathbf{i}\,dx\,dy\,dz.$$

That is,

$$F_x \; = \; - \frac{\partial p}{\partial x}\bigg|_0 dx\,dy\,dz + \rho_0 \mathbf{g} \cdot \mathbf{i}\,dx\,dy\,dz$$

Similarly for the *y*- and *z*-directions:

$$F_y \; = \; - \frac{\partial p}{\partial y}\bigg|_0 dx\,dy\,dz + \rho_0 \mathbf{g} \cdot \mathbf{j}\,dx\,dy\,dz$$

$$F_z \; = \; - \frac{\partial p}{\partial z}\bigg|_0 dx\,dy\,dz + \rho_0 \mathbf{g} \cdot \mathbf{k}\,dx\,dy\,dz,$$

so that

$$\begin{aligned}
\mathbf{F} \; &= \; F_x \mathbf{i} + F_y \mathbf{j} + F_z \mathbf{k} \\
&= \; -\left(\mathbf{i}\frac{\partial p}{\partial x} + \mathbf{j}\frac{\partial p}{\partial y} + \mathbf{k}\frac{\partial p}{\partial z} \right) + \rho(\mathbf{g} \cdot \mathbf{i})\,\mathbf{i} + \rho(\mathbf{g} \cdot \mathbf{j})\,\mathbf{j} + \rho(\mathbf{g} \cdot \mathbf{k})\,\mathbf{k} \\
&= \; -\nabla p + \rho \mathbf{g},
\end{aligned}$$

where the subscript has been dropped since the result should be independent of the particular location chosen for the derivation.

By Newton's second law of motion, **F** is equal to the rate of change of momentum following a fluid particle. For a velocity field in an Eulerian system, the acceleration following a fluid particle is given by *D***V**/*Dt*, and

$$\left\{ \begin{array}{c} \text{the rate of change of momentum} \\ \text{following a fluid particle} \end{array} \right\} = \rho \, dx \, dy \, dz \, \frac{D\mathbf{V}}{Dt}$$

Therefore:

$$\rho \frac{D\mathbf{V}}{Dt} = -\nabla p + \rho \mathbf{g},$$

as in equation 1.20.

In words, we can write the Euler equation as

$$\underbrace{\rho \frac{D\mathbf{V}}{Dt}}_{} \qquad = \qquad \underbrace{-\nabla p}_{} \qquad + \qquad \underbrace{\rho \mathbf{g}}_{}$$

inertia force	surface force	body force
(mass x acceleration)	due to pressure differences	due to gravitational attraction

Euler equation in Cartesian coordinates

The Euler equation may also be written as:

$$\frac{D\mathbf{V}}{Dt} = -\frac{1}{\rho}\nabla p + \mathbf{g} = -\frac{1}{\rho}\nabla p - g\nabla h,$$

where we have defined a function h such that $\mathbf{g} = -g\nabla h$ (h may be identified as the elevation of the fluid particle, so that h increases as the particle increases its altitude, and the vector ∇h is a unit vector. Therefore, in Cartesian coordinates, we have:

$$\frac{\partial u}{\partial t} + u\frac{\partial u}{\partial x} + v\frac{\partial u}{\partial y} + w\frac{\partial u}{\partial z} = -\frac{1}{\rho}\frac{\partial p}{\partial x} - g\frac{\partial h}{\partial x}, \tag{1.21}$$

$$\frac{\partial v}{\partial t} + u\frac{\partial v}{\partial x} + v\frac{\partial v}{\partial y} + w\frac{\partial v}{\partial z} = -\frac{1}{\rho}\frac{\partial p}{\partial y} - g\frac{\partial h}{\partial y}, \tag{1.22}$$

$$\frac{\partial w}{\partial t} + u\frac{\partial w}{\partial x} + v\frac{\partial w}{\partial y} + w\frac{\partial w}{\partial z} = -\frac{1}{\rho}\frac{\partial p}{\partial z} - g\frac{\partial h}{\partial z}. \tag{1.23}$$

Euler equation in cylindrical coordinates

In cylindrical coordinates, we have:

$$\frac{\partial u}{\partial t} + u\frac{\partial u}{\partial r} + \frac{v}{r}\frac{\partial u}{\partial \theta} + w\frac{\partial u}{\partial z} - \frac{v^2}{r} = -\frac{1}{\rho}\frac{\partial p}{\partial r} - g\frac{\partial h}{\partial r}, \tag{1.24}$$

$$\frac{\partial v}{\partial t} + u\frac{\partial v}{\partial r} + \frac{v}{r}\frac{\partial v}{\partial \theta} + w\frac{\partial v}{\partial z} + \frac{uv}{r} \;\; = \;\; -\frac{1}{\rho}\frac{1}{r}\frac{\partial p}{\partial \theta} - g\frac{1}{r}\frac{\partial h}{\partial \theta}, \qquad (1.25)$$

$$\frac{\partial w}{\partial t} + u\frac{\partial w}{\partial r} + \frac{v}{r}\frac{\partial w}{\partial \theta} + w\frac{\partial w}{\partial z} \;\; = \;\; -\frac{1}{\rho}\frac{\partial p}{\partial z} - g\frac{\partial h}{\partial z}. \qquad (1.26)$$

1.3.3   Navier-Stokes equations

We will now consider the effects of viscosity. As we saw earlier, the viscous stress for a Newtonian fluid is given by the coefficient of viscosity times the velocity gradient. If the only velocity gradient that acts is the gradient of the x-component of velocity in the y-direction (as in figure 1.8), the principal shear stress is $\tau_{yx} = \mu\,(\partial u/\partial y)$, where the subscript yx denotes a stress that acts in the x-direction and is associated with a velocity gradient in the y-direction. The resultant force acting on the element shown in figure 1.8 due to viscous forces is given by

$$\left(\tau_{yx} + \frac{\partial \tau_{yx}}{\partial y}dy\right)dxdz - \tau_{yx}\,dxdz \;\; = \;\; \frac{\partial \tau_{yx}}{\partial y}\,dxdydz \;\; = \;\; \mu\frac{\partial^2 u}{\partial y^2}\,dxdydz.$$

That is, for this simple case where $(\partial u/\partial y)$ is the only velocity gradient and μ is constant, the resultant force due to viscous friction in the x-direction, per unit volume, is given by:[4]

$$\frac{\partial \tau_{yx}}{\partial y} \;\; = \;\; \mu\frac{\partial^2 u}{\partial y^2}.$$

Note that if the shear stress is uniform throughout the flow, the fluid particles will distort but there will be no resultant force. A resultant force will occur only if the viscous stress varies in the flow, that is, if there are non-zero gradients of the stress τ_{yx}.

In addition to the shear stresses such as τ_{yx}, normal stresses due to extensional strain rates also lead to viscous stresses. A similar analysis to that given above shows that for a flow where $(\partial u/\partial x)$ is the only velocity gradient and μ is constant, the resultant force due to viscous friction in the x-direction, per unit volume, is given by

$$\frac{\partial \tau_{xx}}{\partial x} = \mu\frac{\partial^2 u}{\partial x^2}.$$

In the general case, where velocity gradients act in all directions, the x-component of the viscous force per unit volume in Cartesian coordinates becomes

$$\mu\left(\frac{\partial \tau_{xx}}{\partial x} + \frac{\partial \tau_{yx}}{\partial y} + \frac{\partial \tau_{zx}}{\partial z}\right).$$

---

[4]The dimensions of $\partial \tau_{yx}/\partial y$ are stress/length = force/area $\times$ length = force/volume.
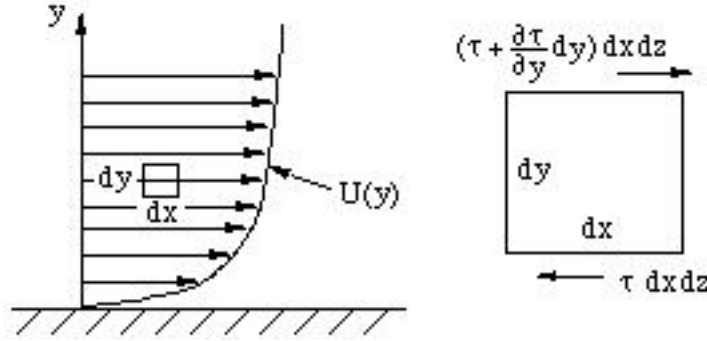
Figure 1.8: Viscous flow showing an element in shear. The velocity $U = U(y)$, only.

By expressing the stresses in terms of the velocity gradients, and using the continuity equation (equation 1.18) to simplify the result, we obtain:

$$\mu\left(\frac{\partial^2 U}{\partial x^2} + \frac{\partial^2 U}{\partial y^2} + \frac{\partial^2 U}{\partial z^2}\right) = \mu\nabla^2 U,$$

where ∇^2 is the Laplacian operator. In vector notation, therefore, the viscous force per unit volume is given by $\mu\nabla^2\mathbf{V}$. In Cartesian coordinates,

$$\nabla^2\mathbf{V} = \frac{\partial^2\mathbf{V}}{\partial x^2} + \frac{\partial^2\mathbf{V}}{\partial y^2} + \frac{\partial^2\mathbf{V}}{\partial z^2}.$$

This viscous force per unit volume can be added to the Euler equation, and we obtain

$$\rho\frac{D\mathbf{V}}{Dt} = -\nabla p + \rho\mathbf{g} + \mu\nabla^2\mathbf{V}. \tag{1.27}$$

This equation is known as the Navier-Stokes equation. It is the momentum equation for the flow of a viscous fluid. In the form written here it only applies to constant property flows (such as incompressible flows) since the viscosity was taken to be constant. The equation carries the names Navier and Stokes because they independently derived it in the early nineteenth century.

More formally, consider the j-component of the total stress term in the integral equation $\int \sigma_{ij}n_i dA$. Using the divergence theorem, we have

$$\int \sigma_{ij}n_i\, dA = \int \frac{\partial\sigma_{ij}}{\partial x_i}\, dv$$

($\int \nabla \cdot \sigma_{ij}\, dA$ in White's notation). Hence:

$$\frac{D\mathbf{V}}{Dt} = \mathbf{g} + -\frac{1}{\rho}\frac{\partial\sigma_{ij}}{\partial x_i}. \tag{1.28}$$
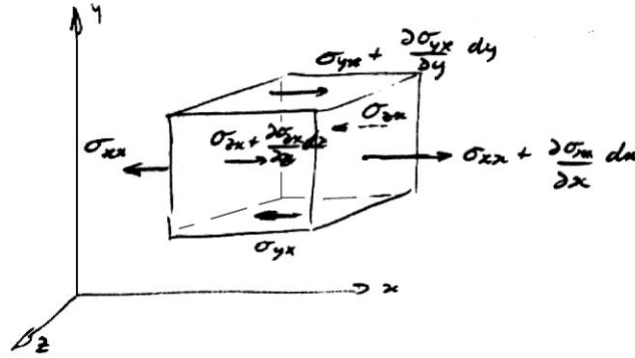
Figure 1.9: Normal and tangential stresses.

This can also be obtained from first principles by considering the stresses (normal and tangential) acting on an element of fluid (figure 1.9). The magnitude of the net force acting in the x-direction

$$= \frac{\partial \sigma_{xx}}{\partial x} dx dy dz + \frac{\partial \sigma_{yx}}{\partial y} dx dy dz + \frac{\partial \sigma_{zx}}{\partial z} dx dy dz$$

$$= \left(\frac{\partial \sigma_{xx}}{\partial x} + \frac{\partial \sigma_{yx}}{\partial y} + \frac{\partial \sigma_{zx}}{\partial z} \right) dx dy dz$$

The net force per unit volume

$$= \mathbf{i} \left(\frac{\partial \sigma_{xx}}{\partial x} + \frac{\partial \sigma_{yx}}{\partial y} + \frac{\partial \sigma_{zx}}{\partial z} \right) + \mathbf{j} \left(\frac{\partial \sigma_{xy}}{\partial x} + \frac{\partial \sigma_{yy}}{\partial y} + \frac{\partial \sigma_{zy}}{\partial z} \right)$$

$$+ \mathbf{k} \left(\frac{\partial \sigma_{xz}}{\partial x} + \frac{\partial \sigma_{yz}}{\partial y} + \frac{\partial \sigma_{zz}}{\partial z} \right).$$

That is, for the j-component,

$$\text{the net force per unit volume} = \frac{\partial \sigma_{ij}}{\partial x_i}.$$

Hence

$$\frac{D\mathbf{V}}{Dt} = \mathbf{g} + \frac{1}{\rho} \frac{\partial \sigma_{ij}}{\partial x_i}.$$

We can write out the components in full. For the x-component,

$$\rho \left(\frac{\partial u}{\partial t} + u \frac{\partial u}{\partial x} + v \frac{\partial u}{\partial y} + w \frac{\partial u}{\partial z} \right) = \rho \mathbf{g} \cdot \mathbf{i} - \frac{\partial p}{\partial x}$$

$$+ \frac{\partial}{\partial x} \left(\mu \left(2 \frac{\partial u}{\partial x} - \frac{2}{3} \nabla \cdot \mathbf{V} \right) \right) + \frac{\partial}{\partial y} \left(\mu \left(\frac{\partial u}{\partial y} + \frac{\partial v}{\partial x} \right) \right) + \frac{\partial}{\partial z} \left(\mu \left(\frac{\partial w}{\partial x} + \frac{\partial u}{\partial z} \right) \right),$$

and similarly for the other two components.

For a constant property fluid, we have, for the *x*-component:

$$\rho\frac{Du}{Dt} = \rho\mathbf{g}\cdot\mathbf{i} - \frac{\partial p}{\partial x} + \mu\left(2\frac{\partial^2 u}{\partial x^2} + \frac{\partial^2 u}{\partial y^2} + \frac{\partial^2 v}{\partial x \partial y} + \frac{\partial^2 w}{\partial x \partial z} + \frac{\partial^2 w}{\partial z^2}\right),$$

and the *y*-component:

$$\rho\frac{Dv}{Dt} = \rho\mathbf{g}\cdot\mathbf{j} - \frac{\partial p}{\partial y} + \mu\left(2\frac{\partial^2 v}{\partial y^2} + \frac{\partial^2 v}{\partial z^2} + \frac{\partial^2 w}{\partial y \partial z} + \frac{\partial^2 u}{\partial x \partial y} + \frac{\partial^2 v}{\partial x^2}\right),$$

and the *z*-component:

$$\rho\frac{Dw}{Dt} = \rho\mathbf{g}\cdot\mathbf{k} - \frac{\partial p}{\partial z} + \mu\left(2\frac{\partial^2 w}{\partial z^2} + \frac{\partial^2 w}{\partial x^2} + \frac{\partial^2 u}{\partial x \partial z} + \frac{\partial^2 v}{\partial y \partial z} + \frac{\partial^2 w}{\partial y^2}\right).$$

Adding them all up, we have

$$\rho\frac{D\mathbf{V}}{Dt} = -\nabla p + \rho\mathbf{g} + \mu\nabla^2\mathbf{V} + \mu\frac{\partial}{\partial x}\left(\frac{\partial u}{\partial x} + \frac{\partial v}{\partial y} + \frac{\partial w}{\partial z}\right)$$

$$+ \mu\frac{\partial}{\partial y}\left(\frac{\partial u}{\partial x} + \frac{\partial v}{\partial y} + \frac{\partial w}{\partial z}\right) + \mu\frac{\partial}{\partial z}\left(\frac{\partial u}{\partial x} + \frac{\partial v}{\partial y} + \frac{\partial w}{\partial z}\right).$$

That is,

$$\boxed{\rho\frac{D\mathbf{V}}{Dt} = -\nabla p + \rho\mathbf{g} + \mu\nabla^2\mathbf{V}.} \tag{1.29}$$

Finally, we can introduce the concept of a potential function. This concept is relatively straightforward in a gravity field because of the related concept of potential energy. We will simply define a function *h* such that

$$\mathbf{g} = -g\nabla\psi.$$

The vector $\nabla\psi$ is a unit vector that points in the direction opposite to the vector **g**. The parameter ψ is called a "potential function," and in this case is identified with the altitude or elevation. Here the word "potential" is clearly connected with the idea of potential energy, which is only a function of elevation. If a body moves from point *a* to point *b*, its potential energy will be unchanged as long as the elevation of the two points is the same. Gravity is called a "conservative" force field since the potential energy of a body depends only on the elevation and not on the particular path used to get from *a* to *b*. The quantity that measures the change in potential energy is the elevation, which is the potential function associated with the conservative force field due to gravity.

The Navier-Stokes equation for a constant property fluid becomes

$$\rho\frac{D\mathbf{V}}{Dt} = -\nabla p - \rho g\nabla\psi + \mu\nabla^2\mathbf{V}. \tag{1.30}$$
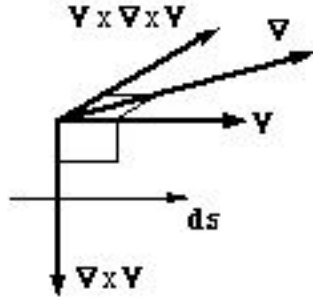
Figure 1.10: Vector notation for the derivation of Bernoulli's equation.

1.4   Bernoulli Equation

The Bernoulli equation states that:

$$p + \tfrac{1}{2}\rho V^2 + \rho g \psi \; = \; \text{constant.} \tag{1.31}$$

This equation holds under the conditions of steady, constant density flow, with no losses along a streamline. It will also apply across streamlines if the flow is irrotational, that is, when $\nabla \times \mathbf{V} = 0$.

We will now derive the Bernoulli equation formally from the momentum equation, first along a streamline, and then for irrotational flow. If the fluid is inviscid, the momentum equation (equation 1.30) states that

$$\rho \left(\frac{\partial \mathbf{V}}{\partial t} + \nabla \left(\tfrac{1}{2} V^2 \right) - \mathbf{V} \times \nabla \times \mathbf{V} \right) = -\nabla p - \rho g \nabla \psi. \tag{1.32}$$

Consider an element $\mathbf{ds}$ along a streamline (figure 1.10). We can find the component of the momentum equation along the streamline by forming the scalar product with the vector $\mathbf{ds}$:

$$\frac{\partial \mathbf{V}}{\partial t} \cdot \mathbf{ds} \; + \; \nabla \left(\tfrac{1}{2} V^2 \right) \cdot \mathbf{ds} \; - \; (\mathbf{V} \times \nabla \times \mathbf{V}) \cdot \mathbf{ds} \; = \; -\left(\frac{\nabla p}{\rho} + g \nabla \psi \right) \cdot \mathbf{ds}.$$

The direction of $\mathbf{V} \times \nabla \times \mathbf{V}$ is perpendicular to $\mathbf{V}$, and, since $\mathbf{ds}$ is in the same direction as $\mathbf{V}$ (see figure 1.10),

$$(\mathbf{V} \times \nabla \times \mathbf{V}) \cdot d\mathbf{ds} = 0.$$

That is,

$$\int_1^2 \frac{\partial \mathbf{V}}{\partial t} \cdot d\mathbf{ds} \; + \; \int_1^2 \nabla \left(\tfrac{1}{2} V^2 \right) \cdot \mathbf{ds} \; + \; \int_1^2 \frac{\nabla p}{\rho} \cdot \mathbf{ds} \; + \; \int_1^2 g \nabla \psi \cdot \mathbf{ds} \; = \; 0.$$

Now, for any scalar ϕ,

$$
\begin{aligned}
\nabla\phi \cdot \mathbf{ds} &= \left(\frac{\partial\phi}{\partial x}\mathbf{i} + \frac{\partial\phi}{\partial y}\mathbf{j} + \frac{\partial\phi}{\partial z}\mathbf{k}\right) \cdot (dx\,\mathbf{i} + dy\,\mathbf{j} + dz\,\mathbf{k}) \\
&= \frac{\partial\phi}{\partial x}dx + \frac{\partial\phi}{\partial y}dy + \frac{\partial\phi}{\partial z}dz,
\end{aligned}
$$

and therefore

$$\nabla\phi \cdot \mathbf{ds} = d\phi.$$

For steady flow, we then obtain:

$$\int_1^2 \left[d\left(\tfrac{1}{2}V^2\right) + \frac{dp}{\rho} + g\,d\psi \right] = 0. \tag{1.33}$$

This equation applies to compressible flows, since no restrictions have so far been placed on the density. Since the integral is independent of the starting and ending point (points 1 and 2 are arbitrary points on a streamline), it follows that

$$d\left(\tfrac{1}{2}V^2\right) + \frac{dp}{\rho} + g\,d\psi = 0. \tag{1.34}$$

This differential form of the Bernoulli equation is also called the one-dimensional Euler equation (the Bernoulli equation as we know it was actually derived by Leonhard Euler). To complete the integration of equation 1.33, we need to know how the density varies as a function of pressure. For frictionless, steady flow of a constant density fluid along a streamline, we obtain the usual form of the Bernoulli equation:

$$\boxed{\frac{V_2^2 - V_1^2}{2} + \frac{p_2 - p_1}{\rho} + g(\psi_2 - \psi_1) = 0.}$$

If we now back up a few steps, we see that the cross-product term $\mathbf{V} \times \nabla \times \mathbf{V}$ was eliminated in this derivation by restricting the flow to be along a streamline. However, if the flow is irrotational, that is, if $\nabla \times \mathbf{V} = 0$, this term is identically zero everywhere and we need not confine ourselves to the flow along a streamline. In fact, for irrotational, inviscid, steady flow of a constant density fluid, the Bernoulli equation applies between any two points in the flow field.

1.5 Constitutive Relationships Revisited

As we saw earlier, the rate-of-strain tensor is the only part of the velocity gradient tensor governed by relative motions among fluid particles. The

simplest stress-strain rate relationship is a linear one, and fluids that follow this relationship are called Newtonian. For isotropic Newtonian fluids, the shear stress tensor becomes (see equation 1.10):

$$d_{ij} = \lambda S_{kk}\delta_{ij} + 2\mu S_{ij}$$

(see, for example, Currie *Fundamental Mechanics of Fluids*), where μ and λ are constants: μ is the *dynamic viscosity*, and λ is usually written in terms of the *bulk viscosity* μ'', where $\mu'' = \lambda + \frac{2}{3}\mu$. The viscosity coefficients relate the shear-stress tensor to the rate-of-strain tensor. They are material properties of a fluid, and may be directly related to the molecular interactions that occur inside the fluid. They may therefore be considered as thermodynamic properties in the macroscopic sense, varying with pressure and temperature. They are proper scalars, independent of direction. Hence:

$$\tau_{ij} = -p\delta_{ij} + \mu'' S_{kk}\delta_{ij} + 2\mu\left(S_{ij} - \tfrac{1}{3}S_{kk}\delta_{ij}\right). \tag{1.35}$$

This is the constitutive equation for stress in a Newtonian fluid. The linear dependence holds over a surprising variety of conditions for compressible and incompressible fluids, and it will be assumed to describe all the flows considered here.

In a fluid at rest only normal stresses are exerted, and the normal stress is independent of the direction of the surface element across which it acts. We see that in a fluid in motion both the normal and the tangential stresses depend on viscosity.

The dynamic viscosity of a gas is the result of momentum exchange among molecules with the same average molecular velocities but with different bulk velocities. Since the interactions will occur within a distance comparable to the mean free path, the dynamic viscosity must depend on the average molecular speed, the number density and the mean free path. The magnitude is very small but the associated stress μS_{ij} can take large values, especially near a solid wall where the velocity gradients are large. Also, as the temperature of the gas increases, the number of collisions will increase and therefore the dynamic viscosity will increase with temperature. It is nearly independent of pressure. The variation with temperature, between $150°K$ to $500°K$, may be approximated by the formula

$$\frac{\mu}{\mu_0} = \left(\frac{T}{T_0}\right)^{0.76}. \tag{1.36}$$

For a wider range of temperatures, between $100°K$ and $1900°K$, Sutherland's formula is more accurate:

$$\frac{\mu}{\mu_0} = \frac{T_0 + 110.3}{T + 110.3}\left(\frac{T}{T_0}\right)^{3/2} \tag{1.37}$$

(NACA Report 1135).

With respect to the bulk viscosity, we can introduce the *mechanical* pressure $\bar{p}$ which is the pressure measured in a moving fluid. That is:

$$p - \bar{p} = \mu'' \frac{\partial u_k}{\partial x_k} = \mu'' \nabla \cdot \mathbf{V}.$$

(see Section 1.2.2). Now $\bar{p} = -\frac{1}{3}\tau_{ii}$, which defines the mechanical pressure in a moving fluid (naturally, for a fluid at rest, $\bar{p} = p$). The mechanical pressure in a moving fluid differs from the thermodynamic pressure by a term proportional to the volumetric dilatation with a coefficient of proportionality called the bulk viscosity. Note that for an incompressible fluid we need not consider the bulk viscosity — it only becomes important for compressible fluid flow.

The pressure $\bar{p}$ is a measure of the *translational* energy of the molecules only, whereas the thermodynamic pressure is a measure of the *total* energy, which includes vibrational and rotational modes as well as the translational modes. Different modes have different relaxation times, so that energy may be transferred between modes, and the bulk viscosity is a measure of this transfer. For a monatomic gas the only mode of molecular energy is translational and the bulk viscosity is always zero. For polyatomic gases the bulk viscosity is never zero, and in fact it may be orders of magnitude larger than the dynamic viscosity (see, for example, Thompson Compressible-Fluid Dynamics). For instance, during the passage of a polyatomic gas through a shock wave, the vibrational modes of energy of the molecules are excited at the expense of the translational modes, so that the bulk viscosity of the gas will be non-zero. However, the stress associated with the bulk viscosity is $\mu'' \nabla \cdot \mathbf{V}$, and in many cases of interest the stress is small enough to be neglected (this is usually called Stokes's Hypothesis). Here, we will assume that $\mu'' \nabla \cdot \mathbf{V}$ is negligible.

The final form of the momentum equation, known as the Navier-Stokes equation, is given by:

$$\rho \frac{\partial u_i}{\partial t} + \rho u_j \frac{\partial u_i}{\partial x_j} = -\frac{\partial p}{\partial x_i} + \frac{\partial}{\partial x_j}\left(\mu\left(\frac{\partial u_i}{\partial x_j} + \frac{\partial u_j}{\partial x_i} - \frac{2}{3}\frac{\partial u_k}{\partial x_k}\delta_{ij}\right)\right). \tag{1.38}$$

1.6 Energy

We now have two equations, the continuity and momentum equations — equations 1.38 and 1.15, with three unknowns: p, u_i and ρ (it is assumed that μ is a known function of the state variables).

For a flow in thermodynamic equilibrium, an extra equation is provided by the equation of state. For the flows considered here it will be assumed

that the pressure, temperature and density are related to each other by the ideal gas law, that is,

$$p = \rho RT \qquad (1.39)$$

where R is the gas constant (= 287.03 m^2s^2K for air). We are interested in systems where velocity, temperature and pressure gradients are present, systems which may not be in perfect equilibrium. When the rates of change are large, the flow does not have time to achieve local equilibrium, and then the equations of state will contain time as a variable. Lagging internal processes such as dissociation, ionization, evaporation, chemical reactions, and the transfer of energy between molecular modes are called relaxation processes. We have already indicated how the transfer of energy among molecular modes can give rise to a non-zero bulk viscosity coefficient. Nevertheless, variables of state can still be used if the rates of change are not too large. If we restrict our attention to the flow of non-hypersonic continuum gases, and we do not consider the flow inside shock waves, the experimental evidence suggests that the assumption of thermodynamic equilibrium appears to be reasonable.

To close this system of equations we need to consider the energy of the system. When the flow can no longer be treated as incompressible, and when heat transfer becomes significant, then the number of variables increases from two for the constant property case (p and $\mathbf{V}$) to include the density ρ, temperature T, viscosity μ, and heat transfer coefficient k (assuming the specific heats C_p and C_v are constant). Generally it is assumed that the equation of state $\rho = \rho(p, T)$ is known, as are the fluid property variations $\mu = \mu(p, T)$ and $k = k(p, T)$. Note that p, $\mathbf{V}$ and T are usually called the primary variables. Thus we need another equation, called the energy equation, which is derived from the first law of thermodynamics applied to a fluid in motion.

It is useful at this stage to distinguish between two general classes of flow: low-speed flows where temperature differences give rise to significant buoyancy effects but the Mach number is small compared to one, and high-speed (gasdynamic) flows where buoyancy effects are negligible but the Mach number is of order one or larger.

1. In the first class of flows, it is usually assumed that the fluid has constant properties (μ and k are constant), and that the temperature effects in the momentum equation are confined to the addition of a buoyancy term as an additional body force. That is, the total body force

$$\begin{aligned} &= (\rho_0 + \Delta\rho)\,\mathbf{g} \\ &= \rho_0\,(1 - \beta\Delta T)\,\mathbf{g} \end{aligned}$$

where β, the coefficient of thermal expansion, is given by

$$\beta = -\frac{1}{\rho}\left(\frac{\partial\rho}{\partial T}\right)_p$$

(=1/T for a perfect gas). Except for this treatment of the body force, the density is assumed to be constant ($\rho = \rho_0$). Of course, in real fluids, ρ, μ, k, and C_p all vary with temperature, especially μ and k, and this approach must be seen as an approximation.

2. In the second class of flows, buoyancy effects are generally negligible, but density variations are now important, and fluid property variations can no longer be neglected.

We will consider some examples from the first class of flows (low speed heat transfer problems with coupled and uncoupled temperature and velocity fields) but concentrate mainly on gasdynamic flows, that is boundary layer flows at supersonic speeds.

1.6.1 Derivation of energy equation

The energy equation is the first law of thermodynamics applied to a fluid flow system. The first law states:

There exists a variable of state E, the internal energy. If a system is transformed from one state of equilibrium to another one by a process in which a certain amount of work dW is done **by** the system, and a certain amount of heat dQ is added **to** the system, then the change in the internal energy is given by

$$dE = dQ - dW.$$

For a process occurring at a finite rate,

$$\frac{dE}{dt} = \frac{dQ}{dt} - \frac{dW}{dt}$$

where the substantial derivatives are used because the mass of the system is fixed, and the time scales for the rate of change are much larger than the time scales necessary to attain thermodynamic equilibrium.

Consider the internal energy balance for a fixed mass of fluid enclosed by a large control volume. The control volume conatins a fixed mass of fluid, so that it is not fixed. The rate of work being done on the fluid in the control

volume is made up of the rate of work done by the body forces $\int \rho \mathbf{g} \cdot \mathbf{V} dv$, plus the rate of work done by the surface forces $\int \vec{\Sigma} \cdot \mathbf{V} dA$. Now,

$$\int \vec{\Sigma} \cdot \mathbf{V} dA \;=\; \int \sigma_{ij} u_j n_i \, dA \;=\; \int \frac{\partial u_j \sigma_{ij}}{\partial x_i} dv$$

$$\;=\; \int \left(u_j \frac{\partial \sigma_{ij}}{\partial x_i} + \sigma_{ij} \frac{\partial u_j}{\partial x_i} \right) dv$$

The first term on the right hand side is associated with small differences in stresses on opposite sides of a fluid element and contributes (together with the rate of work due to body forces) to the gain in kinetic energy of bulk motion of the element. The second term on the right hand side is associated with small differences in velocities on opposite sides of a fluid element and represents the rate of work done in deforming the element without changing its bulk velocity. This work in deforming the element is the only work term which contributes to an increase in the thermodynamic property called the internal energy E.

The other term contributing to the change in E is the heat transfer by conduction (temperature differences are assumed to be small enough to neglect radiative heat transfer). If the rate of heat flow per unit area of control volume surface is $\mathbf{q}$, then the total heat transferred **to** the fluid in the control volume $= - \int \mathbf{n} \cdot \mathbf{q} dA$. With the Fourier heat conduction law, where k = thermal conductivity of fluid (W/mK),

$$\mathbf{q} = -k\nabla T,$$

we get

$$- \int \mathbf{n} \cdot \mathbf{q} \, dA \;=\; + \int \mathbf{n} \cdot -k\nabla T \, dA$$

$$\;=\; + \int \nabla \cdot k\nabla T \, dv.$$

Hence

$$\frac{D(\rho e)}{Dt} = \frac{\sigma_{ij}}{\rho} \frac{\partial u_j}{\partial x_i} + \frac{1}{\rho} \frac{\partial}{\partial x_j} \left(k \frac{\partial T}{\partial x_j} \right)$$

where

$$e \;=\; E/\rho \;=\; \text{internal energy per unit mass}$$
$$\;=\; \text{specific internal energy.}$$

We saw that only a part of the total work term contributes to changing E. The other part contributes to the kinetic energy of the bulk motion. Therefore

we need to consider the total energy, which is the sum of the internal energy E and the kinetic energy of the bulk motion $\frac{1}{2}\rho V^2$. For the control volume with a fixed mass:

$$\frac{D}{Dt} \int \rho \left(e + \tfrac{1}{2}V^2\right) dv = -\int \mathbf{n} \cdot \mathbf{q}\, dA$$

$$+ \int \vec{\Sigma} \cdot \mathbf{V}\, dA + \int \rho \mathbf{g} \cdot \mathbf{V}\, dA.$$

For a fixed control volume, we have

$$\frac{\partial}{\partial t} \int \rho \left(e + \tfrac{1}{2}V^2\right) dv + \int (\mathbf{n} \cdot \rho \mathbf{V}) \left(e + \tfrac{1}{2}V^2\right) dA = \int \mathbf{n} \cdot k\nabla T\, dA$$

$$+ \int \sigma_{ij} n_i u_j\, dA + \int \rho \mathbf{g} \cdot \mathbf{V}\, dA. \tag{1.40}$$

By the usual procedures (Divergence Theorem, Leibniz's Theorem, etc.) we can convert this to a differential equation

$$\frac{\partial}{\partial t}\rho \left(e + \tfrac{1}{2}V^2\right) + \nabla \cdot \rho \mathbf{V} \left(e + \tfrac{1}{2}V^2\right) = \nabla \cdot k\nabla T + \frac{\partial}{\partial x_i}\left(\sigma_{ij} u_j\right) + \rho \mathbf{g} \cdot \mathbf{V}.$$

Using the continuity equation, we can simplify this to

$$\rho \frac{D}{Dt} \left(e + \tfrac{1}{2}V^2\right) = \nabla \cdot k\nabla T + \frac{\partial}{\partial x_i}\left(\sigma_{ij} u_j\right) + \rho \mathbf{g} \cdot \mathbf{V}.$$

By introducing

$$\mathbf{g} = -g\nabla \psi$$
$$\sigma_{ij} = -p\delta_{ij} + d_{ij}$$
$$\text{and} \quad h = e + p/\rho = \text{enthalpy}$$

(where ψ is altitude), we obtain

$$\frac{D}{Dt}\left(h + \tfrac{1}{2}V^2 + g\psi\right) = \frac{1}{\rho}\frac{\partial p}{\partial t} + \frac{\partial}{\partial t}(g\psi) + \frac{1}{\rho}\left[\frac{\partial}{\partial x_i}\left(d_{ij}u_j\right) + \nabla \cdot k\nabla T\right] \tag{1.41}$$

from which we can say that, for a steady flow of an inviscid fluid where heat conduction effects are negligible,

$$h + \tfrac{1}{2}V^2 + g\psi = \text{constant}$$

along along a streamline (streamlines are pathlines in steady flow).

Note that, when the fluid is incompressible as well, the specific internal energy e is constant (as we shall show later), and

$$\frac{p}{\rho} + \tfrac{1}{2}V^2 + g\psi = \text{constant}$$

which is just Bernoulli's equation again.

1.6.2   Enthalpy equation

By using the momentum equation, we can write the energy equation as an enthalpy equation:

$$\rho\frac{Dh}{Dt} \;=\; \frac{Dp}{Dt} + \nabla \cdot k\nabla T + d_{ij}\frac{\partial u_j}{\partial x_i} \qquad (1.42)$$

where

$$d_{ij} \;=\; \mu\left(\frac{\partial u_i}{\partial x_j} + \frac{\partial u_j}{\partial x_i}\right) - \tfrac{2}{3}\mu\delta_{ij}\frac{\partial u_k}{\partial x_k}$$

$$\text{and}\qquad d_{ij}\frac{\partial u_j}{\partial x_i} \;=\; \Phi \quad \text{(the dissipation function)}$$

$$\geq \;\; 0 \quad \text{for } \mu \geq 0.$$

The function Φ represents the part of the viscous work going into deformation, rather than the acceleration of the fluid element.

There is also a positive definite part of the heat conduction term:

$$\nabla \cdot k\nabla T \;=\; T\nabla \cdot \left(\frac{k\nabla T}{T}\right) + \frac{k}{T}\left(\nabla T\right)^2,$$

where the second term on the right hand side is always greater than zero, as long as $k > 0$.

1.6.3   Entropy equation

We have the following two relationships between the thermodynamic properties of pressure, temperature, density, internal energy e and enthalpy h:

$$de \;=\; T\,ds - p\,d\left(\frac{1}{\rho}\right)$$

$$\text{and}\qquad dh \;=\; T\,ds + \frac{1}{\rho}\,dp.$$

These relationships correspond to the first law of thermodynamics when the fluid is at rest (or moving at a constant speed) and in equilibrium, and the process of heat addition is reversible. However, since they are relationships between state variables, and we have neglected non-equilibrium processes whereby the bulk pressure and the thermodynamic pressure could differ, we can simply accept these relationships as definitions of a new quantity

s called entropy, which we could measure even if the fluid is in relative motion.

From the enthalpy equation

$$\rho\frac{Dh}{Dt} - \frac{Dp}{Dt} = \nabla \cdot k\nabla T + \Phi.$$

Using $dh - dp/\rho = Tds$, we get

$$\rho T\frac{Ds}{Dt} = \nabla \cdot k\nabla T + \Phi. \tag{1.43}$$

Note: when $\mathbf{q} = 0$ (adiabatic flow), and there is no dissipation, then the flow is *isentropic* (the rate of change of entropy following a fluid particle is zero). If this is true for all fluid particles, the flow is *homentropic*, that is, *s* is constant everywhere.

If we return to Bernoulli's equation:

$$h + \tfrac{1}{2}V^2 + g\psi = H$$

where H is a constant for a frictionless, non-conducting fluid in steady motion along a streamline (H is sometimes called the stagnation enthalpy). We can see that under these conditions ($\mu = 0$, $k = 0$), the flow is isentropic, and we could say that H is a constant for steady flow along a streamline.

1. For incompressible flow, we see that for isentropic flow, the enthalpy is constant ($dh = Tds + dp/\rho$). Hence the Bernoulli equation for incompressible flow reduces to

$$\frac{p}{\rho} + \tfrac{1}{2}V^2 + g\psi = B$$

where B is a constant for steady, isentropic flow along a streamline.

2. For a compressible, isentropic flow, $dh = (dp/\rho)$, and we get another version of Bernoulli's equation

$$\int \frac{dp}{\rho} + \tfrac{1}{2}V^2 + g\psi = H.$$

For a perfect gas, $p = \rho RT$, and $dh = C_p dT$. When C_p (and C_v) are constant (as is common), $p \propto \rho^\gamma$, and

$$C_p T + \tfrac{1}{2}V^2 + g\psi = H.$$

This equation is often referred to as the one-dimensional energy equation, and it is written in the form

$$C_p T_0 = C_p T + \tfrac{1}{2}V^2$$

when applied to compressible flow. This may be considered as a definition of the "total temperature" T_0, being the temperature measured if the fluid was brought to rest isentropically. We can also write this equation as

$$\frac{T_0}{T} = 1 + \frac{\gamma - 1}{2} Ma^2$$

The energy equation for a compressible fluid may be written as:

$$\rho \frac{\partial}{\partial t} \left(e + \tfrac{1}{2} V^2 \right) + \rho u_j \frac{\partial}{\partial x_j} \left(e + \tfrac{1}{2} V^2 \right) = \frac{\partial \sigma_{ij} u_i}{\partial x_j} - \frac{\partial q_i}{\partial x_i}, \qquad (1.44)$$

where the left-hand-side represents the rate of change of the total energy per unit volume following a fluid particle, and the right hand side is the sum of the rate of work done on the fluid by the surface forces and the rate of heat added to the fluid by conduction. Temperature differences will be assumed to be small enough to neglect radiative heat transfer. For high-speed flows, the work done by the body forces can be neglected since buoyancy effects are rarely important.

The total energy is the sum of the internal energy e and the kinetic energy of the bulk motion $\frac{1}{2} V^2$. The internal energy is a measure of the energy contained in the translational, rotational and vibrational motions of the gas molecules (as well as electron energies), and it is a state variable. It is Galilean invariant (that is, it is independent of translational motion of the observer) whereas the kinetic energy of the bulk motion is not. (Note that any term involving the absolute value of the velocity will depend on the observer, whereas terms which depend on velocity differences will not.)

The rate of work done by the surface forces may be written as:

$$\frac{\partial \sigma_{ij} u_i}{\partial x_j} = u_i \frac{\partial \sigma_{ij}}{\partial x_j} + \sigma_{ij} \frac{\partial u_i}{\partial x_j}. \qquad (1.45)$$

The first part on the right-hand-side arises from small differences in *stresses* on opposite sides of a fluid element, and it contributes to the gain in kinetic energy of the bulk motion of the fluid. The second part is associated with small differences in *velocity* on opposite sides of the fluid element, and it represents the rate of work done in deforming the element without a change in its bulk velocity. The work done in deforming the element is the only work term which contributes to an increase in the internal energy.

By convention, **q** is the conductive heat flux leaving the fluid element (the rate of heat outflow per unit area). Heat conduction contributes to the change in internal energy of the fluid, and makes no contribution to the kinetic energy of the bulk motion. It will be assumed that the heat flux is

given by the Fourier heat-conduction relationship:

$$q_j = -k\frac{\partial T}{\partial x_j}. \tag{1.46}$$

This is a constitutive equation in that it relates a heat flux to a temperature gradient. A single coefficient of proportionality is used, the heat conductivity k, which is a property of the fluid and depends on the temperature and pressure.

For many applications it is more useful to express the energy equation in terms of the enthalpy h, where $h = e + p/\rho$, or the stagnation enthalpy or total enthalpy h_0, where

$$h_0 = h + \tfrac{1}{2}V^2. \tag{1.47}$$

For constant pressure flows, the enthalpy and total enthalpy have conservation properties which make them attractive variables to use. By using the continuity equation, we can write an equation for the total enthalpy:

$$\rho\frac{\partial h_0}{\partial t} + \rho u_j\frac{\partial h_0}{\partial x_j} = \frac{\partial p}{\partial t} - \frac{\partial q_i}{\partial x_i} + \frac{\partial d_{ij}u_i}{\partial x_j}. \tag{1.48}$$

We see that the total enthalpy can change only through the actions of heat transfer, unsteady pressure variations or diffusion of kinetic energy by viscosity. Hence the total enthalpy is constant for the flow of a frictionless, non-conducting fluid with a steady pressure distribution. Even for a turbulent boundary layer in the steady flow of air, it is a matter of observation that the total enthalpy is nearly constant if there is no heat transfer.

For one-dimensional steady flow, equations 1.47 and 1.48 are equivalent, and 1.47 is usually called the one-dimensional energy equation. Under these conditions, equation 1.48 can be integrated between two positions along a streamline, and the total enthalpy will have the same value at these two points if the gradients of velocity and temperature vanish at these locations (see, fro example, Batchelor *Introduction to Fluid Dynamics*). This result is particularly useful when considering shock waves or other discontinuities in the flow. The total enthalpy within the shock can vary along a streamline but its value will be the same at all points that lie outside the shock. In other words, the increase and decrease of h_0 along the streamline due to viscous forces and heat conduction exactly cancel over the particular range covered by the shock. Of course, the entropy always increases.

An equation for the enthalpy may be obtained by using the momentum equation to simplify equation 1.48. Hence,

$$\rho\frac{\partial h}{\partial t} + \rho u_j\frac{\partial h}{\partial x_j} = \frac{\partial p}{\partial t} + u_j\frac{\partial p}{\partial x_j} - \frac{\partial q_i}{\partial x_i} + d_{ij}\frac{\partial u_i}{\partial x_j}. \tag{1.49}$$

The last term on the right-hand-side involves the viscous stresses and it is usually called the dissipation function $\boldsymbol{\Phi}$ (= dissipation rate per unit volume). The dissipation function represents that part of the viscous work going into deformation, rather than acceleration of the fluid particle. If we assume Stokes's Hypothesis,

$$\Phi = d_{ij}\frac{\partial u_j}{\partial x_i} = \tfrac{1}{2}\mu\left(\frac{\partial u_i}{\partial x_j} + \frac{\partial u_j}{\partial x_i}\right)^2, \tag{1.50}$$

and we see that $\boldsymbol{\Phi}$ is always positive.

To write the energy equation in terms of temperature, it is usually assumed that the gas is a perfect gas with constant specific heats. That is, $h = C_pT$ and $h_0 = C_pT_0$, where T_0 is called the *stagnation* or *total temperature*. Then,

$$\rho C_p\frac{DT}{Dt} = \frac{Dp}{Dt} - \frac{\partial q_i}{\partial x_i} + \Phi. \tag{1.51}$$

which shows that the temperature of a fluid particle can change by variations in pressure in the direction of the flow, by heat transfer, and by dissipation of kinetic energy by viscosity and thermal conduction.

The energy equation can also be written in terms of entropy. Entropy is another useful parameter primarily because it may also be taken as constant in many flows. By writing the enthalpy in terms of the entropy,

$$Tds = dh - \frac{1}{\rho}dp$$

we obtain

$$\rho T\frac{Ds}{Dt} = -\frac{\partial q_i}{\partial x_i} + \Phi. \tag{1.52}$$

That is:

$$\frac{Ds}{Dt} = \frac{\Phi}{\rho T} + \frac{1}{\rho T}\frac{\partial}{\partial x_j}\left(k\frac{\partial T}{\partial x_j}\right). \tag{1.53}$$

The heat conduction term can be written as the sum of a flux term (that is, a divergence of a temperature gradient), and term that is quadratic in temperature gradients (positive definite). That is,

$$\frac{Ds}{Dt} - \frac{1}{\rho}\frac{\partial}{\partial x_j}\left(k\frac{\partial \ln T}{\partial x_j}\right) = \frac{\Phi}{\rho T} + \frac{k}{\rho T^2}\left(\frac{\partial T}{\partial x_j}\right)^2. \tag{1.54}$$

The left-hand side is the sum of a rate of change of entropy per unit mass, plus the net outflow of entropy per unit mass. The right-hand side is zero for a reversible process, and positive for an irreversible process, so that it represents the rate of entropy production per unit mass. It depends on the

square of velocity and temperature gradients, and therefore, if the gradients are small, the entropy is changed only by heat conduction.

When there is no heat conduction, the flow is called *adiabatic*. Sometimes, in considering the flow in and out of a control volume, the flow is called adiabatic if there is no heat conduction across the boundaries of the control volume. When there is no heat conduction and the entropy production (called dissipation) is also negligible, then the flow is *isentropic*. A flow is called *homentropic* if this is true for all particles. For an isentropic flow of a simple system (such as a perfect gas), any state variable can be expressed as a unique function of any one other state variable. Isentropic flows are therefore *barotropic*, that is, density is only a function of pressure. Furthermore, $dh = dp/\rho$, and p varies as ρ^γ (for a perfect gas with constant specific heats).

1.7 Summary

The equations of motion for a compressible, viscous, heat conducting fluid are:

$$\frac{\partial \rho}{\partial t} + \frac{\partial \rho u_i}{\partial x_i} = 0, \tag{1.55}$$

$$\rho \frac{\partial u_i}{\partial t} + \rho u_j \frac{\partial u_i}{\partial x_j} = -\frac{\partial p}{\partial x_i} + \frac{\partial d_{ij}}{\partial x_j}, \tag{1.56}$$

$$\rho \frac{\partial h}{\partial t} + \rho u_j \frac{\partial h}{\partial x_j} = \frac{Dp}{Dt} + \frac{\partial}{\partial x_i}\left(k\frac{\partial T}{\partial x_i}\right) + d_{ij}\frac{\partial u_i}{\partial x_j}, \tag{1.57}$$

which are, respectively, the continuity, momentum and energy equations. The deviatoric stress tensor d_{ij} is given by

$$d_{ij} = \mu\left(\frac{\partial u_i}{\partial x_j} + \frac{\partial u_j}{\partial x_i} - \frac{2}{3}\frac{\partial u_k}{\partial x_k}\delta_{ij}\right). \tag{1.58}$$

With the addition of an equation of state and the known variation of viscosity and thermal conductivity with temperature and pressure, this is a complete set of equations describing compressible fluid flow, provided that: the continuum hypothesis holds, the fluid particles are in local thermodynamic equilibrium, body forces can be neglected, the fluid is Newtonian, heat conduction follows Fourier's law and radiative heat transfer can be neglected.

The equations of motion are complete once the boundary conditions are specified. The general formulation of boundary conditions in compressible flow is a specialized topic that will not be addressed here, and we will only consider the specific conditions introduced by the presence of a wall. The

no-slip condition means that the fluid in contact with a solid surface has no relative velocity with respect to the surface. That is, at the wall

$$\mathbf{V} = \mathbf{V}_w. \tag{1.59}$$

When there is heat transfer from the surface, there is an analog to the no-slip condition in that the temperature of the fluid in contact with the solid surface has the same temperature as the surface itself. That is,

$$T = T_{surface}. \tag{1.60}$$

Alternatively, the heat flux must be specified:

$$k\frac{\partial T}{\partial n} = q_w, \tag{1.61}$$

where q_w is the heat flux from the surface to the fluid and n is the direction normal to the surface.

The no-slip condition breaks down at scales comparable to the mean free path of the molecules, and therefore the assumption of continuum flow generally implies that the no-slip condition holds. Under certain conditions, the no-slip condition may break down, even if the fluid still behaves as a continuum. These conditions are usually only found at high Mach numbers, where $U_{slip}/U_\infty \approx MC_f$. A further discussion of the no-slip condition is given by White *Viscous Fluid Flow*, and a fascinating historical note may be found in Goldstein *Modern Developments in Fluid Dynamics*, Page 676.

The Euler equation does not include the viscous stress so that it cannot satisfy the no-slip condition, and slip is allowed. However, relative to the solid surface the velocity of the fluid normal to a solid surface must go to zero so that there is no flow through the surface. That is, at the wall

$$\mathbf{n} \cdot \mathbf{V} = \mathbf{n} \cdot \mathbf{V}_w. \tag{1.62}$$

1.8   Non-Dimensional Equations of Motion

By making the equations of motion non-dimensional, we will be able to identify the important non-dimensional groups that govern the dynamic similarity of fluid flows, and we will also be able to use order-of-magnitude arguments to see when and how different terms in the equations become important.

(a) Choose constant reference properties for the flow:

1. Reference length *L* (might be cylinder diameter, distance from leading edge, chord length, pipe diamter, etc.)

2. Reference velocity V_0 (freestream velocity, velocity difference across a mixing layer, etc. In free convection problems choose v_0/L.)

3. Reference properties p_0, ρ_0, T_0, μ_0, k_0, C_{p0} and $\Delta T = T_w - T_0$. Usually taken to be freestream values, or ambient conditions.)

(b) Define non-dimensional variables:

$$x' = \frac{x}{L}, \quad y' = \frac{y}{L}, \quad z' = \frac{z}{L}$$

$$\mathbf{V}' = \frac{\mathbf{V}'}{V_0}, \quad t' = \frac{tV_0}{L}$$

$$p' = \frac{p - p_0}{\rho V_0^2}, \quad T' = \frac{T - T_0}{T_w - T_0}$$

$$\mu' = \frac{\mu}{\mu_0}, \quad k' = \frac{k}{k_0}, \quad C_p' = \frac{C_p}{C_{p0}}$$

(c) Non-dimensionalize equations.

1.8.1 Continuity

$$\frac{\partial \rho'}{\partial t'} + \nabla' \cdot \rho' \mathbf{V}' = 0$$

(where $\Delta' = L\nabla$). In this non-dimensional form, the coefficients of both terms are unity. If the non-dimensionalizing variables are chosen "correctly" (that is, they are representative of the scales in the problem), the two terms are of the same order.

1.8.2 Energy

$$\rho' C_p' \frac{DT'}{Dt'} = E_c \frac{Dp'}{Dt'} + \frac{1}{RePr} \nabla' \cdot (k' \nabla' T') + \frac{E_c}{Re} \Phi'$$

(where $D/Dt' = (V_0/L)D/Dt$). In this non-dimensional form, three coefficients appear. If the non-dimensionalizing variables are chosen so that they are representative of the scales in the problem, the coefficients indicate the relative magnitude of each term. The coefficients contain three non-dimensional parameters:

$$\text{Reynolds number} \quad Re = \frac{\rho_0 V_0 L}{\mu_0}$$

$$\text{Prandtl number} \quad Pr = \frac{\mu_0 C_{p0}}{k_0}$$

$$\text{Eckert number} \quad Ec \;=\; \frac{V_0^2}{C_{p0}\,(T_w - T_0)}$$

$$\text{Peclet number} \quad Pe \;=\; PrRe \;=\; \frac{\rho_0 V_0 L C_{p0}}{k_0}.$$

In high-speed flows, all three dimensionless groups are important. In low-speed flows, we can usually neglect both the pressure term and the dissipation term, leaving the Peclet number (= $RePr$) as the single non-dimensional parameter. This may be seen from the following simplified analysis:

$$Ec = \frac{V_0^2}{C_{p0}\Delta T} = \frac{V_0^2}{C_{p0} T_0} \frac{T_0}{\Delta T}.$$

Now, for a perfect gas,

$$R = C_p - C_v = C_p\left(1 - \frac{1}{\gamma}\right) = \frac{\gamma - 1}{\gamma}C_p.$$

Therefore,

$$Ec = \frac{V_0^2}{\gamma R T_0} \frac{\gamma R}{C_{p0}} \frac{T_0}{\Delta T} = \frac{V_0^2}{a_0^2}(\gamma - 1)\frac{T_0}{\Delta T} = (\gamma - 1)\,Ma^2\frac{T_0}{\Delta T}.$$

Thus the work of compression and that due to friction are important when the freestream velocity is comparable to the speed of sound, and when the temperature difference between the wall and the fluid is comparable to the freestream temperature.

With $Ec \to 0$, we have

$$\rho' C_p' \frac{DT'}{Dt'} \;=\; \frac{1}{Pe}\nabla' \cdot (k'\nabla'T').$$

But for large Peclet number, we then get $T' = $ constant along a streamline. This implies that for subsonic heat transfer problems (where the variation of T' must be known to determine buoyancy effects), and where the Peclet number is large, the scales used to define the Peclet number must be redefined so that it is of order unity. This, in turn, implies that we need a new scaling analysis similar to the problem of non-dimensionalizing $p - p_0$ with $\frac{1}{2}\rho V_0^2$ at high Re and $\mu_0 V_0 / L_0$ at low Reynolds numbers.

Note that for low-speed flows, in order to neglect the dissipation term and the pressure term, we require $Ec \ll 1$. That is, we need

$$(\gamma - 1)\,Ma^2\frac{T_0}{\Delta T} \ll 1.$$

(a) If temperature differences are due to compressibility effects, then

$$\frac{\Delta T}{T_0} = f(Ma)$$

(= non-dimensional adiabatic temperature rise), and we require $\frac{Ma^2}{f(Ma)} \rightarrow 0$. We can calculate $f(Ma)$ (= adiabatic temperature rise) and show that $\frac{Ma^2}{f(Ma)}$ is small for low Mach number flows.

(b) If temperature differences are due to heat transfer from the wall, then $\frac{\Delta T}{T_0}$ can be $\ll 1$. In some cases, it may still be possible to have $Ec \ll 1$. For air, for example, at $Ma = 0.1$ ($\approx 33\,m/s$), we have $Ec < 0.1$ for $\frac{\Delta T}{T_0} < \frac{1}{25}$, that is, about $12°$ at NTP. For very small temperature differences, viscous effects can no longer be neglected. On the other hand, the temperature field becomes less interesting (from an engineering viewpoint) and so for many practical cases we can assume that $Ec \ll 1$ (see also Panton pp.254–258).

Now, what is the cut-off point between a "low-speed" flow and a "high-speed" flow? Some sense of this distinction is obtained by considering when changes in density due to compressibility become significant in an isentropic flow. Then we have:

$$\Delta p = \left. \frac{\partial p}{\partial \rho} \right|_s \Delta \rho.$$

That is,

$$\frac{\Delta \rho}{\rho} = \frac{\Delta p}{\rho} \left(\left. \frac{\partial p}{\partial \rho} \right|_s \right)^{-1} = \frac{\Delta p}{\rho a^2}.$$

Using Bernoulli's equation (since the flow is sentropic), we see that $\Delta p = O\left(\frac{1}{2}\rho V_0^2\right)$. Hence,

$$\frac{\Delta \rho}{\rho} = \frac{u^2}{2a^2} = \frac{1}{2}Ma^2,$$

and we see that the flow may be considered incompressible when $Ma \ll 1$. Now for air at sea level, $a = 330\,m/s$. If we take $\Delta \rho / \rho = 0.05$ to be the upper limit for "incompressible" flow approximations to be valid, we get $u = 100\,m/s$ ($Ma \approx 0.3$) for the upper limit of a "low-speed" flow. Note that for water, $a \approx 8,000\,m/s$, and compressibility effects are almost always negligible.

1.8.3 Momentum equation

We begin with

$$\rho \frac{D\mathbf{V}}{Dt} = -\nabla p + \rho \mathbf{g} + \frac{\partial \sigma'_{ij}}{\partial x_i}.$$

(see equation 1.28). It's best to consider low-speed (constant property, except for the additional body force due to buoyancy) separately from high-speed flows (body forces negligible). Starting with the latter, we obtain

$$\rho' \frac{D\mathbf{V}'}{Dt'} = -\nabla'p' + \frac{1}{Re}\frac{\partial \sigma'_{ij}}{\partial x_i}{}'$$

(only the Reynolds number appears, although the Prandtl and Eckert numbers are also important, appearing through the energy equation).

Low-speed heat transfer problems

Here it is usually assumed that the fluid has constant transport properties, so that the viscosity and coefficient of thermal conductivity are constant), and that the momentum equation is modified to take account of the "additional" body force due to buoyancy. That is,

$$\text{Total body force} = (\rho_0 + \Delta\rho)\,\mathbf{g} \approx \rho_0\,(1 - \beta\Delta T)\,\mathbf{g}$$

where β is the coefficient of thermal expansion at constant pressure ($1/T$ for a perfect gas). Otherwise, the density is assumed constant.
The momentum equation then becomes

$$\rho \frac{D\mathbf{V}}{Dt} = -\nabla p + \rho_0\,(1 - \beta\Delta T)\,\mathbf{g} + \mu\nabla^2\mathbf{V}$$

where $\Delta T = T - T_0$, the difference between the temperature at some point in the flow, and the temperature at some constant reference point (the wall, the freestream, etc.). Non-dimensionalizing, we get

$$\frac{D\mathbf{V}'}{Dt'} = -\nabla'p' - \mathbf{g}' - \frac{Gr}{Re^2}\beta'T'\mathbf{g}' + \frac{1}{Re}\nabla'^2\mathbf{V}',$$

or

$$\frac{D\mathbf{V}'}{Dt'} = -\nabla'P' - \frac{Gr}{Re^2}\beta'T'\mathbf{g}' + \frac{1}{Re}\nabla'^2\mathbf{V}',$$

where

$$P' = p' + \frac{gh}{V_0^2}, \qquad \mathbf{g}' = \frac{\mathbf{g}}{g}.$$

The Reynolds number has reappeared in a very important way: we see now that it indicates the relative magnitude of the viscous forces in producing an acceleration. In addition, a new parameter called the Grashof number,

$$Gr = \frac{g\beta_0\rho_0^2L^3\,(T_w - T_0)}{\mu_0^2},$$

indicates the strength of the buoyancy or free convectionterms in the flow. If there is a freestream (called "forced" convection, or "mixed" convection, depending on the strength of the buoyancy effects), the Grashof number is effectively a Froude number. That is, for forced convection,

$$\frac{Gr}{Re^2} = \beta\Delta T\frac{gL}{V_0^2} = \frac{\beta\Delta T}{Fr^2},$$

and when the Froude number Fr is large ($V_0^2 \gg gL$), buoyancy is not important.

High-speed compressible flow

Here the momentum equation reads

$$\rho\frac{D\mathbf{V}}{Dt} = -\nabla p + \frac{\partial\sigma'_{ij}}{\partial x_i}$$

where all gravitational acceleration effects have been neglected (all Froude numbers are large). When we non-dimensionalize,

$$\rho'\frac{D\mathbf{V}'}{Dt'} = -\nabla'p' + \frac{1}{Re}\frac{\partial\sigma'_{ij}{}'}{\partial x_i}$$

which has only the Reynolds number as the important non-dimensional parameter. Since temperature variations are always important in high-speed gas flows, the Prandtl and Eckert numbers also influence such flows through the energy equation. Note that the Mach number does not make an explicit appearance anywhere, except that it is contained within the Eckert number.

1.9 Vorticity Transport Equation

Equations 1.55 to 1.57 represent a complete set of equations describing compressible fluid flow. However, the concept of vorticity can be very useful for gaining further insight, especially in turbulent flows where rotational fluid is often distributed in space in rather compact forms such as vortex tubes and sheets.

For a compressible fluid, the vorticity transport equation is written in terms of the specific vorticity $\mathbf{\Omega}/\rho$. By taking the curl of the momentum equation, we obtain:

$$\begin{aligned}
\frac{\partial\left(\Omega_k/\rho\right)}{\partial t} + u_j\frac{\partial\left(\Omega_k/\rho\right)}{\partial x_j} &= \frac{\Omega_j}{\rho}\frac{\partial u_k}{\partial x_j} + \frac{1}{\rho^3}\nabla\rho\times\nabla p \\
&+ \frac{1}{\rho}\varepsilon_{ijk}\frac{\partial^2}{\partial x_i\partial x_j}\left(\mu\left(\frac{\partial u_i}{\partial x_j} + \frac{\partial u_j}{\partial x_i}\right)\right).
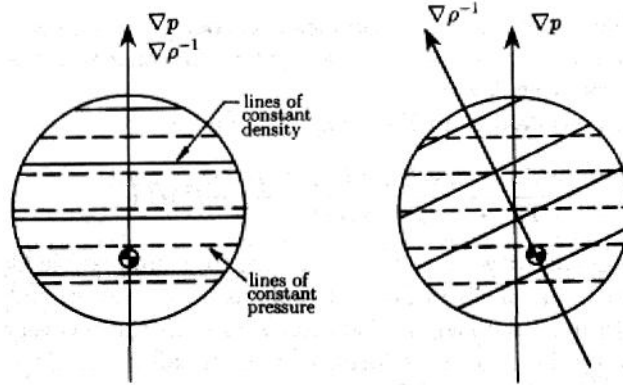\end{aligned} \tag{1.63}$$

Figure 1.11: Generation of vorticity through baroclinic torques.

The first term on the right-hand side of equation 1.63 is sometimes called the *stretching and tilting* term: part of this term describes the exchange of vorticity between components because of the rotation of vortex lines due to presence of velocity gradients; another part gives the rate of change of vorticity due to stretching of vortex lines. The third term on the right-hand-side represents the rate of change of vorticity due to molecular diffusion. The second term is the baroclinic term and it is of particular interest here because it can be an important source term for vorticity in compressible flows. We see from the baroclinic term that in a compressible flow the pressure still appears in the vorticity transport equation. If the density is only a function of pressure, pressure and density gradients are always parallel, and this term does not contribute to the vorticity transport. Under these conditions, the pressure force acting on a fluid element will pass through the center of gravity of the fluid element and no moment results (see figure 1.11). The flow is then called *barotropic* (for example, isentropic flow of a perfect gas). If the pressure gradients are not parallel to the density gradients, there is a contribution to the rate of change of vorticity: the pressure force does not pass through the center of gravity, a moment about the center of gravity exists and the rotation vector will change with time. The flow is called *non-barotropic*.

When the flow is inviscid, barotropic and two-dimensional, the right-hand side is zero, and the specific vorticity remains constant following a fluid particle: for example, if the flow was initially irrotational, it remains irrotational. So vorticity can change by stretching and tilting, barotropic torques and viscous diffusion.

Consider a constant property fluid:

$$\rho \frac{D\mathbf{V}}{Dt} = -\nabla p - \rho g \nabla h + \mu \nabla^2 \mathbf{V}.$$

Taking the curl of both sides, we obtain

$$\frac{D\vec{\Omega}}{Dt} = \left(\vec{\Omega} \cdot \nabla\right)\mathbf{V} + \nu\nabla^2\vec{\Omega}.$$

Note that the pressure and gravitational terms have been eliminated. Now:

$$\frac{D\vec{\Omega}}{Dt} = \text{rate of change of vorticity following a fluid element}$$

$$\nu\nabla^2\vec{\Omega} = \text{rate of change of vorticity due to molecular diffusion of vorticity}$$

$$\left(\vec{\Omega} \cdot \nabla\right)\mathbf{V} = \text{part of this term describes the exchange of vorticity among different components because of the tilting of vortex lines due to the presence of velocity gradient; another part gives the rate of change of vorticity due to stretching of vortex lines.}$$

Now, $\left(\vec{\Omega} \cdot \nabla\right)\mathbf{V} = 0$ in two-dimensional flow, where we get

$$\frac{D\vec{\Omega}}{Dt} = \nu\nabla^2\vec{\Omega}.$$

Remember, the energy equation for a constant property fluid (low-speed flow) is given by a very similar equation

$$\frac{DT}{Dt} = \alpha\nabla^2 T.$$

In fact, both equations are diffusion equations, and

$$\nu = \frac{\mu}{\rho} = \text{viscous diffusivity}$$

$$\alpha = \frac{k}{\rho C_p} = \text{thermal diffusivity.}$$

In addition, if C represents the proportion of marked molecules in a fluid mixture (the concentration of one component of the mixture), then the concentration obeys obeys a simple conservation law, where the concentration of a given fluid particle can only change by molecular transport across its surface. That is,

$$\frac{DC}{Dt} = \wp\nabla^2 C$$
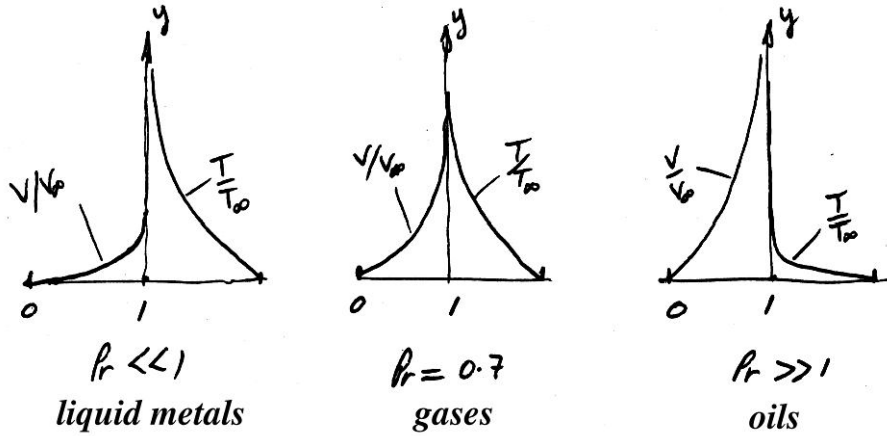
where $\wp$ is the mass diffusivity.

Figure 1.12: Velocity and temperature profiles for (a) liquid metals ($Pr \ll 1$), (b) gases ($Pr \approx 0.7$), (c) oils ($Pr \gg 1$).

The ratios of these diffusivities give a measure of the relative diffusivity of vorticity, heat and mass:

$$
\frac{\nu}{\alpha} = \frac{\mu C_p}{k} = Pr = \frac{\text{viscous diffusion rate}}{\text{thermal diffusion rate}}
$$

$$
\frac{\nu}{\wp} = \frac{\mu}{\rho\wp} = Sc = \frac{\text{viscous diffusion rate}}{\text{mass diffusion rate}}
$$

$$
\frac{\wp}{\alpha} = \frac{\rho C_p \wp}{k} = Le = \frac{\text{mass diffusion rate}}{\text{thermal diffusion rate}}
$$

Note that $Pr = Sc\,Le$ and some typical values are

$$
Pr_{Hg} = 0.024, \quad Pr_{air} = 0.72, \quad Pr_{H_2O} = 7.0, \quad Pr_{SAE30} = 3,500.
$$

Thus, if we were to compare the temperature and velocity profiles in the suddenly accelerated (hot) flat plate case, we see that only for gases (where $Pr \approx 1$) do the thermal and velocity profiles almost coincide (see figure 1.12).

A useful result for inviscid compressible flows may be obtained directly from the momentum equation:

$$
\frac{\partial \mathbf{V}}{\partial t} + (\mathbf{V} \cdot \nabla)\,\mathbf{V} = -\frac{1}{\rho}\nabla p. \tag{1.64}
$$

That is:

$$
\frac{\partial \mathbf{V}}{\partial t} + \nabla \frac{1}{2} V^2 - \mathbf{V} \times \mathbf{\Omega} = -\frac{1}{\rho}\nabla p. \tag{1.65}
$$

When the pressure is eliminated in terms of the entropy and enthalpy, we obtain Crocco's equation for inviscid flows with no body forces:

$$\mathbf{V} \times \boldsymbol{\Omega} + T\nabla s = \nabla\left(h + \frac{1}{2}V^2\right) + \frac{\partial \mathbf{V}}{\partial t}. \tag{1.66}$$

If the flow is steady and adiabatic,

$$\mathbf{V} \times \boldsymbol{\Omega} + T\nabla s = \nabla h_0 \tag{1.67}$$

and the total enthalpy will be constant along each streamline. Hence ∇h_0 is a vector which is perpendicular to the streamlines. Since $\mathbf{V} \times \boldsymbol{\Omega}$ is also perpendicular to the streamlines, the remaining vector $T\nabla s$ is also. Equation 1.67 can then be written in scalar form:

$$V\Omega + T\frac{ds}{dn} = \frac{dh_0}{dn}. \tag{1.68}$$

where n is the coordinate perpendicular to the streamlines. Crocco's equation shows that when the total enthalpy is constant everywhere, the vorticity in a homentropic flow must be zero. More interestingly, as a flow passes through a curved shock, the total enthalpy remains constant but the entropy will increase by an amount which depends on the local strength of the shock. Therefore an initially irrotational flow will acquire vorticity proportional to the entropy gradient generated by the curved shock. This is another example of the production of vorticity by baroclinic torques: the term $T\nabla s$ in equation 1.67 corresponds to the baroclinic term in the vorticity transport equation.

There are a number of other useful properties of vorticity and circulation in inviscid compressible flow. For example, the circulation Γ is defined as:

$$\Gamma = \oint \mathbf{V} \cdot d\ell \tag{1.69}$$

where counter-clockwise contour integration is taken to be positive. That is, the circulation contained within a closed contour in a body of fluid is defined as the integral around the contour of the velocity vector which is locally tangential to the contour itself. In the absence of shocks and other discontinuities, we can use Stokes's Theorem, so that:

$$\Gamma = \iint \boldsymbol{\Omega} \cdot \mathbf{n}\, dS. \tag{1.70}$$

So the circulation can also be expressed as an area integral of the vorticity component normal to the surface enclosed by the contour, as it is in incompressible flow.

From the definition of vorticity, we have as a vector identity

$$\nabla \cdot \mathbf{\Omega} = \nabla \cdot \nabla \times \mathbf{V} = \mathbf{0}. \tag{1.71}$$

That is, there are no sources or sinks of vorticity inside the fluid, and vorticity can only be generated at the boundaries of the fluid. Therefore vortex tubes must close on themselves or terminate on the boundaries, which may be either a solid surface, or in a compressible flow, a shock wave (since it can be a source of vorticity). Furthermore, in the absence of sources or sinks of vorticity:

$$\iiint \nabla \cdot \mathbf{\Omega} \, dv = \iint \mathbf{n} \cdot \mathbf{\Omega} \, dS. \tag{1.72}$$

A vortex tube is a tube defined by vortex lines (lines which are tangent to the local vorticity vector). There is no flux of vorticity normal to the surface of the vortex tube, and equation 1.72 shows that the flux of vorticity along the vortex tube is constant, that is, the circulation around a vortex tube in an inviscid flow is constant. This result, known as Helmholtz's Theorem, will hold for compressible and incompressible flows since it is based on the vector identity given in equation 1.71. Since the circulation remains constant along the length of the vortex tube, the vorticity will increase if the area decreases. What about the rate of change of the circulation as the vortex tube moves? Consider the circulation about a fluid circuit, that is, a circuit which is defined by fluid particles of fixed identity. We need to find $D\Gamma/Dt$, where the symbol D/Dt is understood to be the rate of change following a fluid circuit. For an inviscid fluid, the momentum equation can be used to show that:

$$\frac{D\Gamma}{Dt} = - \oint \frac{\delta p}{\rho}, \tag{1.73}$$

where δp is the pressure difference between adjacent fluid particles on the closed contour (see Batchelor *Introduction to Fluid Dynamics*). If the fluid is also barotropic (so that the pressure is only a function of density), the right-hand side of equation 1.73 is zero, and the circulation around any closed material curve is invariant. This is Kelvin's Theorem, and it will apply to compressible and incompressible flows as long as the flow is barotropic. Using the definition of circulation, we can also write

$$\frac{D}{Dt} \left(\iint \mathbf{\Omega} \cdot \mathbf{n} \, dS \right) = 0.$$

Thus the flux of vorticity across an open material surface is invariant.

For an inviscid, barotropic flow we can therefore make the following observations: If at some instant the flow is without vorticity (such that the circulation around any contour is zero), Kelvin's Theorem states that the circulation must remain without vorticity at any future time. In particular,

a fluid initially at rest has no vorticity, and must remain without vorticity; vortex tubes are in some sense permanent — a vortex tube specified at an initial instant by the vortex-lines that intersect a given closed curve in the fluid has a continuing identity. We may say that in a barotropic, inviscid fluid a vortex-tube moves with the fluid and its strength remains constant. Since the fluid making up the vortex tube retains its identity as the vortex tube moves and deforms, we must conserve mass. In an incompressible flow, therefore, stretching a vortex tube will inevitably increase its vorticity because the cross-sectional area will always decrease. In a compressible flow, we need to know how the density varies before we can say what is happening to the vorticity: it was clear from the vorticity transport equation that we need to consider the specific vorticity.

1.10   Summary:Equations of motion

1.10.1   Continuity equation

Integral forms of the continuity equation for a fixed control volume:

$$\frac{\partial}{\partial t} \int \rho \, dv + \int \mathbf{n} \cdot \rho \mathbf{V} \, dA \;=\; 0$$

$$\int \mathbf{n} \cdot \rho \mathbf{V} \, dA \;=\; 0 \qquad \text{Fixed mass}$$

$$\int \mathbf{n} \cdot \rho \mathbf{V} \, dA \;=\; 0 \qquad \text{Steady flow}$$

$$\int \mathbf{n} \cdot \mathbf{V} dA \;=\; 0 \qquad \text{Incompressible flow}$$

Differential forms of the continuity equation:

$$\frac{\partial \rho}{\partial t} + \nabla \cdot \rho \mathbf{V} \;=\; 0$$

$$\nabla \cdot \mathbf{V} \;=\; -\frac{1}{\rho} \frac{D\rho}{Dt}$$

In tensor notation:

$$\frac{\partial \rho}{\partial t} + \frac{\partial \rho u_i}{\partial x_i} = 0$$

1.10.2   Linear momentum equation

Integral form of the momentum equation for a fixed control volume, where gravity is the only body force:

$$\mathbf{F}_{\text{ext}} + \int \vec{\Sigma} \, dA + \int \rho \mathbf{g} dv \;=\; \frac{\partial}{\partial t} \int \rho \mathbf{V} dv + \int (\mathbf{n} \cdot \rho \mathbf{V}) \, \mathbf{V} dA$$

For an inviscid fluid:

$$\int \vec{\Sigma} \, dA = \int p \, dA$$

Differential form of the momentum equation (the Navier-Stokes equation):

$$\rho \frac{Du_i}{Dt} = \rho \frac{\partial u_i}{\partial t} + \rho u_j \frac{\partial u_i}{\partial x_j} = \rho g_i + \frac{\partial \sigma_{ij}}{\partial x_j}$$

or

$$\frac{\partial (\rho u_i)}{\partial t} + \frac{\partial (\rho u_i u_j)}{\partial x_j} = \rho g_i + \frac{\partial \sigma_{ij}}{\partial x_j}$$

where

$$\sigma_{ij} = -p\delta_{ij} + d_{ij}$$

and d_{ij} depends on the motion of the fluid only and it is called the shear stress tensor, or the deviatoric stress tensor (= σ'_{ij} in my notes, or τ_{ij} in Currie). For isotropic, Newtonian fluids,

$$d_{ij} = \lambda S_{kk} \delta_{ij} + 2\mu S_{ij}$$

where λ is called the "second viscosity coefficient" (μ'' in Batchelor),

$$\frac{\partial u_i}{\partial x_j} = S_{ij} + R_{ij}$$

$S_{ij} = e_{ij}$ and $R_{ij} = \xi_{ij}$ in my notes, and

$$S_{ij} = \tfrac{1}{2} \left(\frac{\partial u_i}{\partial x_j} + \frac{\partial u_j}{\partial x_i} \right) \;\; \text{and} \;\; R_{ij} = \tfrac{1}{2} \left(\frac{\partial u_i}{\partial x_j} - \frac{\partial u_j}{\partial x_i} \right).$$

With the definition of the bulk viscosity μ'' (K in Currie, and κ in Batchelor):

$$\mu'' = \lambda + \tfrac{2}{3}\mu$$

we have

$$d_{ij} = \mu'' S_{kk} \delta_{ij} + 2\mu \left(S_{ij} - \tfrac{1}{3} S_{kk} \delta_{ij} \right)$$

and

$$\sigma_{ij} = -p\delta_{ij} + \mu'' S_{kk}\delta_{ij} + 2\mu\left(S_{ij} - \tfrac{1}{3}S_{kk}\delta_{ij}\right).$$

Differential form of the momentum equation where only the dynamic viscosity is retained:

$$\rho\frac{\partial u_i}{\partial t} + \rho u_j\frac{\partial u_i}{\partial x_j} = -\frac{\partial p}{\partial x_i} + \frac{\partial}{\partial x_j}\left(\mu\left(\frac{\partial u_i}{\partial x_j} + \frac{\partial u_j}{\partial x_i} - \tfrac{2}{3}\frac{\partial u_k}{\partial x_k}\delta_{ij}\right)\right)$$

For a constant-property fluid:

$$\rho\frac{D\mathbf{V}}{Dt} = -\nabla p + \rho\mathbf{g} + \mu\nabla^2\mathbf{V}$$

or, with ψ = altitude:

$$\rho\frac{D\mathbf{V}}{Dt} = -\nabla p - \rho g\nabla\psi + \mu\nabla^2\mathbf{V}.$$

For an inviscid fluid we obtain Euler's equation:

$$\rho\frac{D\mathbf{V}}{Dt} = -\nabla p + \rho\mathbf{g}$$

1.10.3   Energy equation

Integral form of the energy equation for a fixed control volume:

$$\frac{\partial}{\partial t}\int \rho\left(e + \tfrac{1}{2}V^2\right)dv + \int (\mathbf{n}\cdot\rho\mathbf{V})\left(e + \tfrac{1}{2}\rho V^2\right)dA = \int \mathbf{n}\cdot k\nabla T\,dA$$

$$+ \int \sigma_{ij}n_i u_j\,dA + \int \rho\mathbf{g}\cdot\mathbf{V}\,dA.$$

Differential form ($h = e + p/\rho$):

$$\frac{D}{Dt}\left(h + \tfrac{1}{2}V^2 + g\psi\right) = \frac{1}{\rho}\frac{\partial p}{\partial t} + \frac{\partial}{\partial t}(g\psi) + \frac{1}{\rho}\left[\frac{\partial}{\partial x_i}\left(d_{ij}u_j\right) + \nabla\cdot k\nabla T\right]$$

Therefore, for a steady flow of an inviscid fluid where heat conduction effects are negligible, along along a streamline (streamlines are pathlines in steady flow):

$$h + \tfrac{1}{2}V^2 + g\psi = \text{constant}$$

When the fluid is incompressible as well, the specific internal energy e is constant, and

$$\frac{p}{\rho} + \tfrac{1}{2}V^2 + g\psi = \text{constant}$$

which is Bernoulli's equation.

Enthalpy equation

By using the momentum equation, we can write the energy equation as an enthalpy equation:

$$\rho \frac{Dh}{Dt} \;=\; \frac{Dp}{Dt} + \nabla \cdot k\nabla T + d_{ij}\frac{\partial u_j}{\partial x_i}$$

where

$$d_{ij}\frac{\partial u_j}{\partial x_i} = \Phi \quad \text{(the dissipation function)}$$

Entropy equation

From the enthalpy equation

$$\rho\frac{Dh}{Dt} - \frac{Dp}{Dt} \;=\; \nabla \cdot k\nabla T + \Phi.$$

Using $dh - dp/\rho = Tds$, we get

$$\rho T\frac{Ds}{Dt} \;=\; \nabla \cdot k\nabla T + \Phi$$

Note: when $\mathbf{q} = 0$ (adiabatic flow), and there is no dissipation, then the flow is *isentropic* (the rate of change of entropy following a fluid particle is zero). If this is true for all fluid particles, the flow is *homentropic*, that is, s is constant everywhere.

1.10.4   Summary

The equations of motion for a compressible, viscous, heat conducting fluid are:

$$\frac{\partial \rho}{\partial t} + \frac{\partial \rho u_i}{\partial x_i} \;=\; 0, \tag{1.74}$$

$$\rho\frac{\partial u_i}{\partial t} + \rho u_j\frac{\partial u_i}{\partial x_j} \;=\; -\frac{\partial p}{\partial x_i} + \frac{\partial d_{ij}}{\partial x_j}, \tag{1.75}$$

$$\rho\frac{\partial h}{\partial t} + \rho u_j\frac{\partial h}{\partial x_j} \;=\; \frac{Dp}{Dt} + \frac{\partial}{\partial x_i}\left(k\frac{\partial T}{\partial x_i}\right) + d_{ij}\frac{\partial u_i}{\partial x_j}, \tag{1.76}$$

which are, respectively, the continuity, momentum and energy equations. The deviatoric stress tensor d_{ij} is given by

$$d_{ij} = \mu\left(\frac{\partial u_i}{\partial x_j} + \frac{\partial u_j}{\partial x_i} - \tfrac{2}{3}\frac{\partial u_k}{\partial x_k}\delta_{ij}\right). \tag{1.77}$$

With the addition of an equation of state and the known variation of viscosity and thermal conductivity with temperature and pressure, this is a complete set of equations describing compressible fluid flow, provided that: the continuum hypothesis holds, the fluid particles are in local thermodynamic equilibrium, body forces can be neglected, the fluid is Newtonian, heat conduction follows Fourier's law and radiative heat transfer can be neglected.

Chapter 2

Exact Solutions

We begin with incompressible flow, or, more generally, with constant-property flows. The Navier-Stokes equation for a constant property fluid is given by equation 1.30, that is,

$$\rho \frac{D\mathbf{V}}{Dt} = -\nabla p - \rho g \nabla h + \mu \nabla^2 \mathbf{V}. \tag{2.1}$$

Each term in the equation is of the form force per unit volume. The first term on the right hand side is the acceleration due to pressure gradients, and the last term is the acceleration due to viscous stress gradients. Resultant forces exist only when there are gradients of stresses: when stresses are uniform in space, no resultant forces will act. The momentum equation for a constant property fluid can also be written as

$$\frac{D\mathbf{V}}{Dt} = -\nabla \left(\frac{p}{\rho} + gh \right) + \nu \nabla^2 \mathbf{V}. \tag{2.2}$$

where $(p/\rho + gh)$ is sometimes called the "hydrostatic pressure."

The main source of difficulty in solving the momentum equation is not the viscous term but the acceleration term. The acceleration term is nonlinear, in that it involves products of velocity (note that $u\partial u/\partial x$ can be written as $\frac{1}{2}\partial u^2/\partial x$). The Euler and Navier-Stokes equations are nonlinear, partial differential equations, and no general solutions exist. Solutions exist only under particular conditions, such as incompressible, irrotational flow, or "fully-developed" flows where the acceleration term is zero. Numerical solutions are possible, and it is now routinely possible to solve the Euler equation for an entire airplane at transonic Mach numbers, as long as it is not maneuvering too quickly. When viscous effects are included, however, numerical solutions require a great deal more computer speed and memory, and full Navier-Stokes solutions are only possible at Reynolds numbers not much greater than the value where transition to turbulence occurs.

2.1   Parallel Flows

Here we deal with flows which are two-dimensional, and where the velocity is uni-directional. That is, the flow is between parallel plates, and there is no component of the velocity normal to the plates. The flow can also be axisymmetric, as for the flow in a circular pipe, or flowing out radially from a source at the center of two parallel disks (figure 2.1).

The main feature of these flows is that they are "fully-developed," which means that flow properties do not change in the direction of the flow. If the flow is steady as well, then the acceleration is zero ($D\mathbf{V}/Dt = 0$), and the velocity field is determined by a balance between pressure gradients and viscous stress gradients, that is,

$$\nabla p = \mu \nabla^2 \mathbf{V} \tag{2.3}$$

where the body force has been included in the pressure term.

In Cartesian coordinates, if the flow is in the x-direction,

$$v = w = 0$$

and

$$\frac{\partial \mathbf{V}}{\partial x} = \frac{\partial \mathbf{V}}{\partial z} = 0,$$
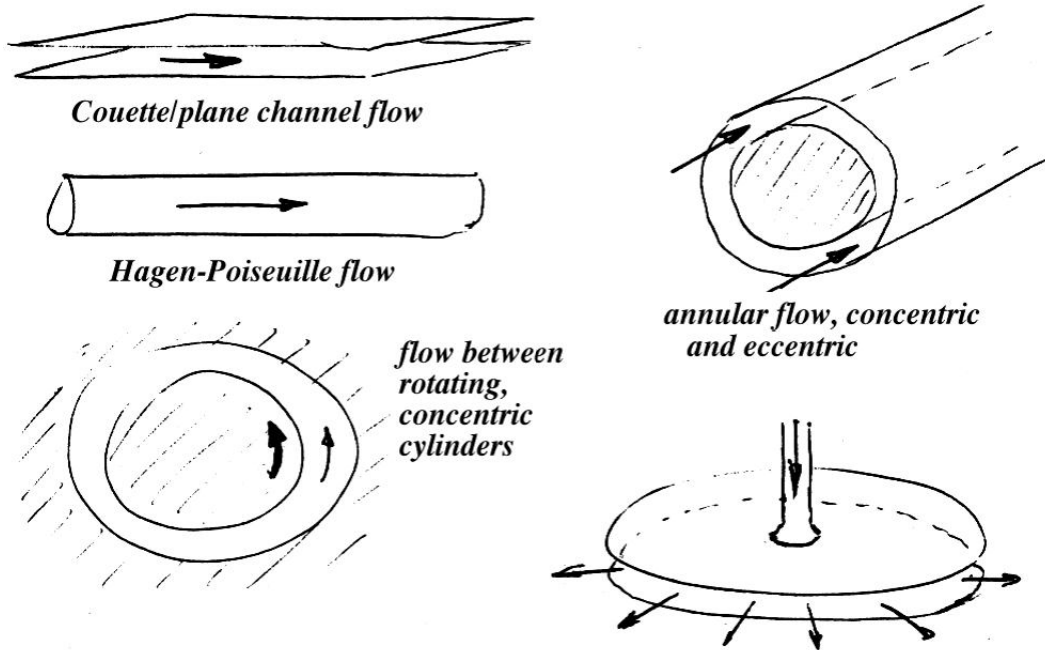

Couette/plane channel flow

Hagen-Poiseuille flow

flow between rotating, concentric cylinders

annular flow, concentric and eccentric

Figure 2.1: Parallel flow examples.

and therefore

$$\frac{dp}{dx} = \mu \frac{d^2\mathbf{V}}{dy^2}. \tag{2.4}$$

2.1.1 Plane Couette flow

In plane Couette flow, two plates are a fixed distance h apart, and the top plate moves at a speed U_0 with respect to the bottom plate (see figure 2.2). Due to the no-slip condition, a flow is generated so that

$$\begin{aligned} \text{at} \quad y &= 0, & u &= 0, \\ \text{and} \quad y &= h, & u &= U_0. \end{aligned}$$

With these boundary conditions, with a constant pressure gradient, equation 2.4 gives

$$\frac{u}{U_0} = \frac{y}{h} + B\frac{y}{h}\left(1 - \frac{y}{h}\right) \tag{2.5}$$

where B is the pressure gradient parameter,

$$B = -\frac{h^2}{2\mu U_0}\frac{dp}{dx}.$$

When $dp/dx = 0$, the velocity gradient is linear (see figure 2.2), and the shear stress is constant:

$$\tau = \mu \frac{du}{dy} = \frac{\mu}{h}U_0.$$

When $B < -1$, there is backflow in the lower part of the flow.

2.1.2 Poiseuille flow

For a smooth pipe of length L and diameter D, dimensional analysis can be used to show that

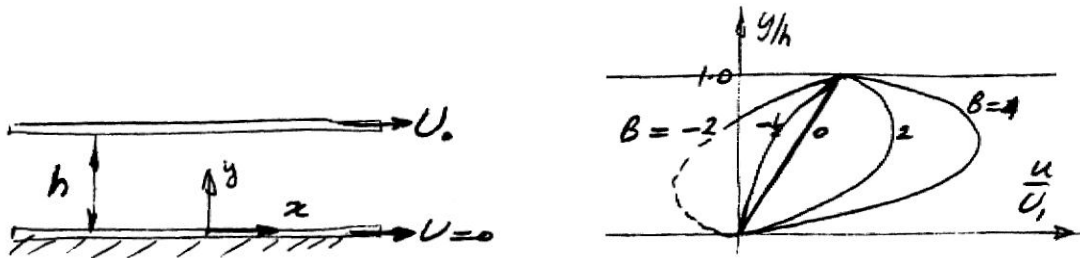$$\frac{\Delta p}{\frac{1}{2}\rho \bar{V}^2} = \phi_1\left(\frac{\rho \bar{V} D}{\mu}, \frac{L}{D}\right)$$

Figure 2.2: Couette flow geometry and velocity profiles.

where the pressure drop over the length L is Δp, and $\bar{V}$ average velocity integrated across the cross-section (= volume flow rate/area). Since pipes are typically long compared to their diameter, an asymptotic, fully-developed state exists where the flow properties do not change with further increase in length. This happens after a distance of 20–40 diameters from the entrance, and the flow properties become free of entrance effects. The mean velocity profile is then independent of the distance along the pipe. In that case, the parameter L/D is no longer important, and the resistance relationship for fully-developed pipe flow becomes:

$$f = \frac{\left(\frac{\Delta p}{L}\right)D}{\frac{1}{2}\rho\bar{V}^2} = \phi\left(\frac{\rho\bar{V}D}{\mu}\right),$$

where f is the friction factor, defined by

$$f = \frac{\left(\frac{\Delta p}{L}\right)D}{\frac{1}{2}\rho\bar{V}^2}.$$

For fully-developed flow in a smooth pipe, therefore, the friction factor is only a function of the Reynolds number based on average velocity and pipe diameter.

It is possible to find exact solutions of the Navier-Stokes equations for fully-developed pipe flow, as long as the flow is laminar and not turbulent (this is called Poiseuille flow). In practice, this requires that the pipe flow Reynolds number is less than about 2,300. It is also possible to find a solution for fully-developed, laminar channel flow (this is called plane Poiseuille flow). Here, we will derive the solutions for these two cases, starting with channel flow. The results are very similar, and they differ only in the constants that appear in the equations.

2.1.3   Fully-developed duct flow

Consider laminar, two-dimensional, steady, constant density duct flow, far from the entrance, so that the flow is fully-developed. The duct is rectangular in cross-section, of width w and height D, and it is horizontal, so we do not have to include the forces due to gravity. For a duct, laminar flow requires that the Reynolds number $\bar{U}D/\nu$ is less than about 2,000, where $\bar{U}$ is the average velocity.

First, we use an integral analysis applied to a large control volume of length dx (figure 2.3). The pressure varies in the streamwise direction, but it does not vary across the flow since the streamlines are parallel. The pressure over the inflow area is $p - \frac{1}{2}dp$, and over the outflow area it is $p + \frac{1}{2}dp$. If the flow is fully-developed, the influx and outflux of momentum have the
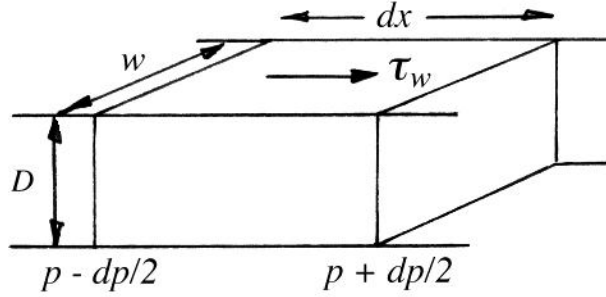
Figure 2.3: Integral control volume for fully-developed flow in a rectangular duct.

same magnitude and so they cancel. Since there is no change in the flow momentum, the flow must be in equilibrium under the applied forces: the force acting on the fluid due to the pressure drop is balanced by the force due to the viscous stress acting on the interior surface of the duct. The pressures act on the cross-sectional area wD. The flow is fully-developed and therefore the velocity gradient is independent of x, and the viscous stress τ_w will not vary in the streamwise direction. If we assume that τ_w is constant over the perimeter of the duct, it acts on the area $2\,(w + D)\,dx$. Hence,

$$\left(p - \tfrac{1}{2}dp\right)wD - \left(p + \tfrac{1}{2}dp\right)wD \;=\; 2\tau_w\,(w + D)\,dx$$

and so

$$\frac{dp}{dx} \;=\; -\,2\tau_w\frac{(w + D)}{wD}.$$

The duct was taken to be two-dimensional, which implies that $w \gg D$. Hence,

$$\frac{dp}{dx} = -\frac{2}{D}\,\tau_w. \tag{2.6}$$

The pressure gradient is negative because the pressure drops due to viscous friction.

Second, we use a differential analysis applied to a small control volume of size $dxdydz$ (figure 2.4), located at a distance y from the centerline. (We could use equation 2.4 directly, but we choose to start from first principles.) The flow is two-dimensional, and there is no variation of the velocity in the spanwise direction. Since the flow is also fully-developed, there is no variation of velocity in the streamwise direction. The only velocity variation that exists is in the cross-stream direction, that is, in the y-direction. Therefore, the only shearing stresses acting on the elemental volume will act on its top and bottom faces which have an area $dxdz$. Let τ be the shear stress in the middle of the control volume. Using a Taylor series expansion, and retaining only the first-order terms, the net viscous force F_v acting in the
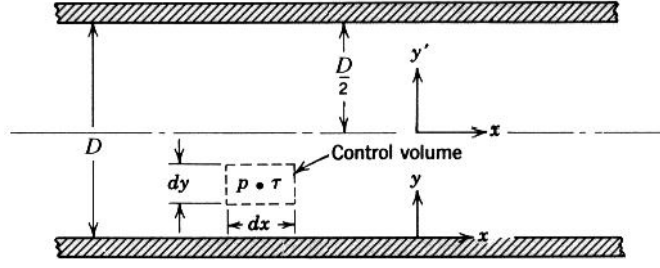
Figure 2.4: Differential control volume for fully-developed flow in a rectangular duct.

x-direction is given by

$$F_v = \left(\tau + \frac{\partial \tau}{\partial y}\frac{dy}{2}\right)dxdz - \left(\tau - \frac{\partial \tau}{\partial y}\frac{dy}{2}\right)dxdz$$

$$= \frac{\partial \tau}{\partial y}\,dxdydz.$$

we see that the net viscous force only makes a contribution if if the viscous stress varies through the flowfield (that is, if $\partial \tau/\partial y \neq 0$). The viscous stress itself is given by

$$\tau = \mu\frac{dU}{dy},$$

since the velocity only varies in the y-direction. Therefore,

$$F_v = \mu\frac{d^2U}{dy^2}\,dxdydz.$$

We see that the viscous force depends on the second derivative of the velocity field.

   Now we evaluate the force due to pressure differences. If the pressure halfway along the length of the control volume is p, the net force F_p due to pressure acting in the x-direction is given by

$$F_p = \left(p - \frac{\partial p}{\partial x}\frac{dx}{2}\right)dydz - \left(p + \frac{\partial p}{\partial x}\frac{dx}{2}\right)dydz$$

$$= -\frac{\partial p}{\partial x}\,dxdydz.$$

Since the pressure does not vary in the z-direction (the flow is assumed to be two-dimensional so that nothing varies in the z-direction), and it cannot vary in the y-direction (the streamlines are straight and forces due to gravity are neglected),

$$\frac{\partial p}{\partial z} = \frac{\partial p}{\partial y} = 0, \qquad \text{and} \qquad \frac{\partial p}{\partial x} = \frac{dp}{dx},$$

and so

$$F_p = -\frac{dp}{dx}\,dxdydz.$$

Since there is no acceleration, F_v and F_p must sum to zero, so that

$$\boxed{\frac{dp}{dx} = \mu\frac{d^2U}{dy^2}.}$$ (2.7)

This equation can be solved by observing that the pressure term only depends on x, whereas the viscous term only depends on y. The equation can only be satisfied if both terms are equal to a constant, $-K$, say. Hence:

$$\frac{dp}{dx} = -K$$ (2.8)

$$\mu\frac{d^2U}{dy^2} = -K,$$ (2.9)

where K is positive since the pressure decreases with distance down the duct.

We can integrate equation 2.9 twice to obtain the velocity profile. The velocity at the top and bottom surface is zero because of the no-slip condition, and the velocity profile will be symmetric about the centerline where $y = 0$. Therefore the boundary conditions are:

$$U = 0 \quad \text{at} \quad y = \pm\frac{D}{2}$$

$$\frac{dU}{dy} = 0 \quad \text{at} \quad y = 0.$$

Hence:

$$U = \frac{KD^2}{8\mu}\left(1 - \left(\frac{2y}{D}\right)^2\right).$$

That is:

$$U = \frac{D^2}{8\mu}\left(-\frac{dp}{dx}\right)\left(1 - \left(\frac{2y}{D}\right)^2\right).$$ (2.10)

The average velocity $\bar{U}$ is defined by

$$\bar{U} = \frac{1}{A}\int U dA$$

so that $\bar{U}$ is equal to the volume flow rate divided by the cross-sectional area A. For a duct, the average velocity is given by

$$\bar{U} = \frac{1}{wD}\int_{-D/2}^{D/2} Uwdy = \frac{KD^2}{12\mu} = \frac{D^2}{12\mu}\left(-\frac{dp}{dx}\right).$$ (2.11)

From equation 2.10 we obtain,

$$\boxed{\frac{U}{\bar{U}} = \frac{3}{2}\left(1 - \left(\frac{2y}{D}\right)^2\right).}$$ (2.12)

The laminar velocity profile is parabolic, as illustrated in figure 11.7. The friction factor is given by:

$$f = \frac{\frac{\Delta p}{L}D}{\frac{1}{2}\rho\bar{U}^2} = \frac{-\frac{dp}{dx}D}{\frac{1}{2}\rho\bar{U}^2} = -\frac{dp}{dx}\frac{2D}{\rho\bar{U}^2} = \frac{24\mu}{\rho\bar{U}D},$$

where the pressure gradient was eliminated using equation 2.11. That is,

$$\boxed{f = \frac{24}{Re}.}$$ (2.13)

which holds for all two-dimensional rectangular ducts with $Re < 2,000$, where $Re = \rho\bar{U}D/\mu$. It will hold for higher values of Reynolds number if the conditions are such to allow laminar flow to exist.

We can find the stress at the wall ($y = -D/2$) by differentiating equation 2.10. That is,

$$\tau_w = \mu\left.\frac{\partial U}{\partial y}\right|_w = -\frac{D}{2}\frac{dp}{dx},$$

which agrees with the result obtained earlier using a large control volume (equation 2.6).

Finally, examine the Navier-Stokes equation (equation 1.27). For duct flow, the nonlinear acceleration term, $D\mathbf{V}/Dt$, is zero, and equation 2.7 follows directly. This equation holds for all fully-developed flows in the absence of gravity), and therefore it is usually possible to find analytic solutions for the velocity distributions in fully-developed flows, as long as the boundary conditions can be satisfied.

2.1.4   Fully-developed pipe flow

Here we consider fully-developed laminar flow in a smooth, circular, horizontal pipe. For a smooth pipe of length L and diameter D,

$$\frac{\Delta p}{\frac{1}{2}\rho\bar{V}^2} = \phi_1\left(\frac{\rho\bar{V}D}{\mu}, \frac{L}{D}\right)$$

where the pressure drop over the length L is Δp, and $\bar{V}$ is the average velocity over the cross-section of the pipe. Since pipes are typically long compared
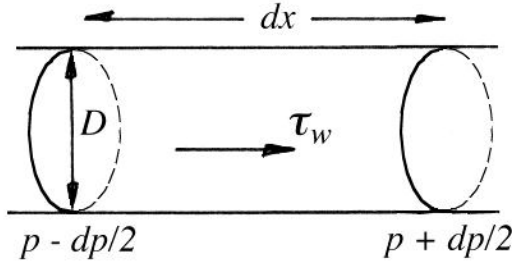
Figure 2.5: Integral control volume for fully-developed flow in a circular pipe.

to their diameter, an asymptotic, fully-developed state exists where the flow properties do not change with further increase in length. This happens after a distance of 20–40 diameters from the entrance, and the flow properties become free of entrance effects. The mean velocity profile is then independent of the distance along the pipe. In that case, the parameter L/D is no longer important, and the resistance relationship for fully-developed smooth pipe flow becomes:

$$f \equiv \frac{\left(\frac{\Delta p}{L}\right)D}{\frac{1}{2}\rho \bar{V}^2} = \phi\left(\frac{\rho \bar{V} D}{\mu}\right) = \phi\left(Re\right),$$

where f is the friction factor. Therefore, the friction factor depends only on the Reynolds number based on average velocity and pipe diameter, Re.

As before, we begin with an integral analysis using a control volume of length dx, as shown in figure 2.5. The pressure over the inflow area is $p - \frac{1}{2}dp$, and over the outflow area it is $p + \frac{1}{2}dp$. Since the flow is fully-developed, the flow is in equilibrium under the applied forces. The pressure drop acts on the cross-sectional area $\pi D^2/4$, and the viscous stress acts on the area $2\pi D dx$. Hence,

$$\left(p - \tfrac{1}{2}dp\right)\frac{\pi D^2}{4} - \left(p + \tfrac{1}{2}dp\right)\frac{\pi D^2}{4} = \tau_w \pi D\, dx$$

so that

$$\frac{dp}{dx} = -\frac{4}{D}\tau_w.$$

Next, we apply a differential analysis by using an annular control volume, located at a distance r from the centerline (figure 2.6). Since the flow is two-dimensional, there is no variation of the velocity in the circumferential direction. Since the flow is fully-developed, there is no variation of velocity in the streamwise direction. The only velocity variation that exists is in the radial, that is, in the r-direction. The only place shearing stresses act are on the inner and outer faces. If the shear stress at the center of the annular control volume is τ, the net viscous force F_v acting in the x-direction is given
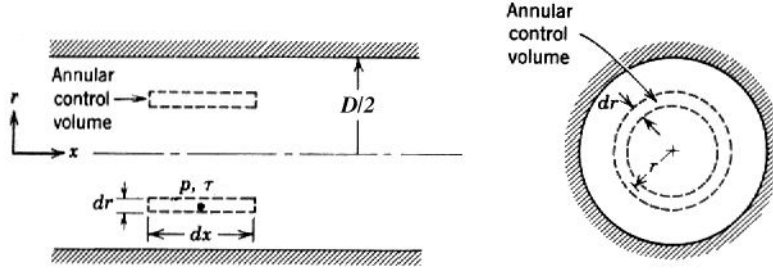
Figure 2.6: Differential control volume for fully-developed flow in a circular pipe.

by

$$F_v = \left(\tau + \frac{\partial \tau}{\partial r}\frac{dr}{2}\right) 2\pi\left(r + \frac{dr}{2}\right) dx - \left(\tau - \frac{\partial \tau}{\partial r}\frac{dr}{2}\right) 2\pi\left(r - \frac{dr}{2}\right) dx$$

$$= \tau\, 2\pi drdx + \frac{\partial \tau}{\partial r}\, 2\pi r drdx,$$

neglecting second-order terms.

The net force due to pressure differences in the x-direction, F_p, is given by

$$F_p = \left(p - \frac{\partial p}{\partial x}\frac{dx}{2}\right) 2\pi r dr - \left(p + \frac{\partial p}{\partial x}\frac{dx}{2}\right) 2\pi r dr$$

$$= -\frac{\partial p}{\partial x}\, 2\pi r drdx,$$

where p is the pressure halfway along the length of the control volume. Since there is no acceleration, F_p and F_v must balance, so that

$$\frac{\partial p}{\partial x} = \frac{\tau}{r} + \frac{\partial \tau}{\partial r} = \frac{1}{r}\frac{\partial (r\tau)}{\partial r}.$$

The pressure term depends only on x and the viscous term can only depend on r. Therefore,

$$\boxed{\frac{dp}{dx} = \frac{1}{r}\frac{d(r\tau)}{dr}.} \tag{2.14}$$

This equation can be satisfied only if the left hand side and the right hand side are equal to a constant, K', say. Hence:

$$\frac{dp}{dx} = -K' \tag{2.15}$$

$$\frac{1}{r}\frac{d(r\tau)}{dr} = -K', \tag{2.16}$$

where K' is positive since the pressure decreases with distance down the duct. Integrating equation 2.16 gives

$$r\tau = -\frac{r^2}{2}K' + c_1$$

or

$$\tau = -\frac{r}{2}K' + \frac{c_1}{r}$$

Since the only velocity gradient is in the r-direction, the viscous stress is given by

$$\tau = \mu\frac{dU}{dr},$$

and

$$\mu\frac{dU}{dr} = -\frac{r}{2}K' + \frac{c_1}{r}$$

and

$$U = -\frac{r^2}{4\mu}K' + \frac{c_1}{\mu}\ln r + c_2$$

Using the boundary conditions:

$$U = 0 \quad \text{at} \quad r = \pm D/2$$
$$\frac{dU}{dr} = 0 \quad \text{at} \quad r = 0,$$

we find

$$U = \frac{K'D^2}{16\mu}\left(1 - \left(\frac{r}{D}\right)^2\right),$$

so that

$$U = \frac{D^2}{16\mu}\left(-\frac{dp}{dx}\right)\left(1 - \left(\frac{2r}{D}\right)^2\right), \tag{2.17}$$

and the velocity profile is parabolic, as found for the duct flow. For a pipe, the average velocity is given by

$$\bar{U} = \frac{D^2}{32\mu}\left(-\frac{dp}{dx}\right), \tag{2.18}$$

so that

$$\boxed{\frac{U}{\bar{U}} = 2\left(1 - \left(\frac{2r}{D}\right)^2\right).} \tag{2.19}$$

The friction factor is then given by:

$$f = \frac{\frac{\Delta p}{L}D}{\frac{1}{2}\rho\bar{U}^2} = \frac{-\frac{dp}{dx}D}{\frac{1}{2}\rho\bar{U}^2} = \frac{64\mu}{\rho\bar{U}D},$$

where equation 2.18 was used to eliminate the pressure gradient. Hence,

$$f = \frac{64}{Re} \tag{2.20}$$

which holds for all circular pipes and tubes with $Re < 2,300$, although it can continue to hold at higher Reynolds numbers under favorable circumstances.

What does $Re < 2,300$ mean? For water at 20°C, $\nu = \mu/\rho \approx 1 \times 10^{-6}\, m^2/s$. If $D = 10\, mm$, then to maintain laminar flow, we need $\bar{U} < 0.23\, m/s$. If $D = 1\, mm$, we need $\bar{U} < 2.3\, m/s$. For air at 20°C, $\nu \approx 15 \times 10^{-6}\, m^2/s$, and if $D = 10\, mm$, $\bar{U} < 3.5\, m/s$. If $D = 1\, mm$, we need $\bar{U} < 35\, m/s$.

2.1.5 Rayleigh flow I

Rayleigh flow is the flow that develops above a suddenly accelerated plane surface. It is an unsteady flow that develops with time (Lord Rayleigh, 1911 Phil. Mag. **21**, 697). Consider a flat plate that is initially at rest in a stationary fluid. At $t = 0$, the plate starts to move with a constant velocity U in the positive x-direction (see figure 2.7). The fluid begins to move, first by the no-slip condition at the surface, and then by the action of viscous stresses within the fluid. For this parallel unsteady flow, the convective acceleration term $\mathbf{V} \cdot \nabla \mathbf{V} = 0$, and the momentum equation reduces to

$$\frac{\partial u}{\partial t} = \nu \frac{\partial^2 u}{\partial y^2}, \tag{2.21}$$

with the boundary conditions

$$
\begin{aligned}
\text{for} \quad & t \leq 0, \quad u = 0 \quad \text{for all } y, \\
\text{for} \quad & t > 0, \quad u = U_0 \quad \text{for } y = 0, \\
\text{and} \quad & u = 0, \quad \text{for } y = \infty.
\end{aligned} \tag{2.22}
$$

This "diffusion" equation is exactly the same as that governing the temperature distribution in a stationary medium of thermal diffusivity ν. The boundary conditions correspond to a suddenly heated wall which is maintained at a constant temperature. This analogy between temperature and velocity, and heat transfer and vorticity, was discussed in more detail in section 1.9.

For now, we obtain the solution (see Carslaw & Jaeger)

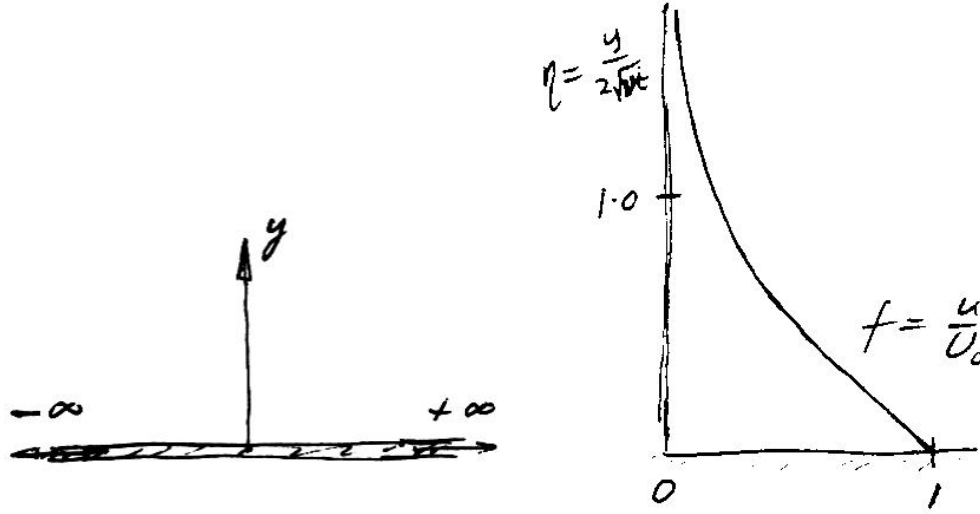$$\frac{u}{U_0} = \mathrm{erfc}\left(\frac{y}{2\sqrt{\nu t}}\right).$$

Figure 2.7: Stokes flow geometry and velocity profile in similarity coordinates.

That is,

$$
\begin{aligned}
f &= \operatorname{erfc} \eta \\
&= \frac{2}{\sqrt{\pi}} \int_{\eta}^{\infty} e^{-\eta^2} \, d\eta \\
&= 1 - \operatorname{erf} \eta
\end{aligned}
$$

so that $\quad f = 1 - \dfrac{2}{\sqrt{\pi}} \displaystyle\int_0^{\infty} e^{-\eta^2} \, d\eta.$

The velocity profiles for varying times are "similar" in that they can be plotted as a unique function of η when u is non-dimensionalized by U_0 (see figure 2.7). The variables f and η are therefore called "similarity" variables.

Similarity is a very useful concept in the analysis of shear layers. In general, the solution of equations 2.21 and 2.22 is

$$
\frac{u}{U_0} = g'(y, \nu, t), \tag{2.23}
$$

where g' is a general function of y, ν and t. There are special cases in which

$$
\frac{u}{U_0} = g(\eta), \tag{2.24}
$$

where η, called a similarity variable, is a specific function of y, ν and t. In such cases, the number of independent variables is reduced from three (y, ν and t) to one (η) so that equations 2.21 becomes an ODE for u. Note that it is a necessary condition that the boundary conditions (equation 2.22) can be expressed in terms of the similarity variables.

Dimensional analysis can help identify the similarity variables. Starting with

$$\frac{u}{U_0} = g'(y, \nu, t),$$

we obtain

$$\frac{u}{U_0} = g\left(\frac{y}{\sqrt{\nu t}}\right).$$

Therefore f and η are similarity variables in that they describe the dynamic similarity of flow fields, as understood in dimensional analysis. In general, similarity variables are used to convert partial differential equations to ordinary differential equations (which are much easier to handle). This is possible because similarity variables reduce the number of parameters describing the flowfield. In the example given here, the dependence of f on y and t is reduced to a dependence on a single variable, η.

To see how this works, we start with the one-dimensional diffusion equation for the Rayleigh flow problem:

$$\frac{\partial u}{\partial t} = \nu \frac{\partial^2 u}{\partial y^2},$$

and convert it to an ordinary differential equation using f and η as similarity variables. Introducing $f = u/U_0$, we get

$$\frac{\partial f}{\partial t} = \nu \frac{\partial^2 f}{\partial y^2}.$$

Then we note that

$$\frac{\partial f}{\partial t} = \frac{\partial f}{\partial \eta}\frac{\partial \eta}{\partial t} = -\frac{\eta}{2t}\frac{\partial f}{\partial \eta}$$

$$\frac{\partial f}{\partial y} = \frac{\partial f}{\partial \eta}\frac{\partial \eta}{\partial y} = +\frac{1}{2\sqrt{\nu t}}\frac{\partial f}{\partial \eta}$$

$$\text{and} \quad \frac{\partial^2 f}{\partial y^2} = \frac{\partial^2 f}{\partial \eta^2}\left(\frac{\partial \eta}{\partial y}\right)^2 = +\frac{1}{4\nu t}\frac{\partial^2 f}{\partial \eta^2}$$

so that

$$\frac{\partial f}{\partial t} - \nu \frac{\partial^2 f}{\partial y^2} = -\frac{\nu}{4\nu t}\frac{\partial^2 f}{\partial \eta^2} - \frac{\eta}{2t}\frac{\partial f}{\partial \eta} = 0.$$

Since the only independent variable is η, we obtain the ordinary differential equation

$$f'' + 2\eta f' = 0.$$

If we take the region of flow affected by the plate motion to be the region where y is such that $u/U_0 < 0.01$, we can see from tables of the
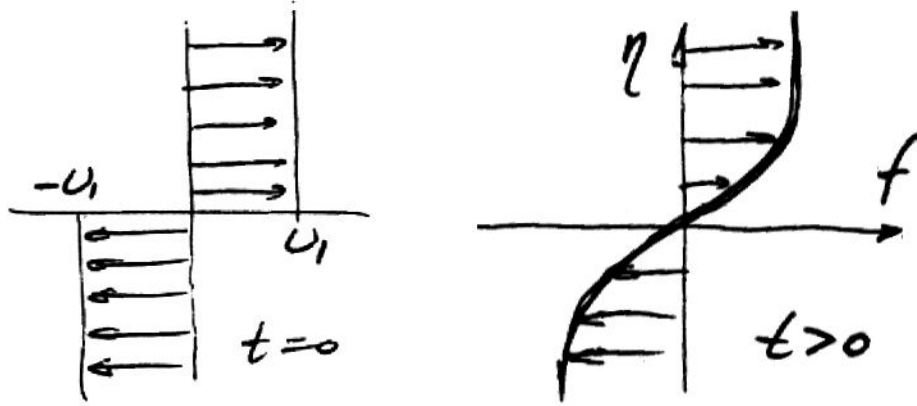
Figure 2.8: Rayleigh flow initial condition and velocity profile in similarity coordinates.

complementary error function that this occurs at $y = 4\sqrt{vt}$. This is the usual definition of a boundary layer thickness δ, and we see that δ depends on $\sqrt{vt}$, where $\sqrt{vt}$ is sometimes called the characteristic length for the diffusion of vorticity, or sometimes simply the Stokes length.

2.1.6 Rayleigh flow II

The second Rayleigh flow is the flow that develops with time starting with a discontinuity in velocity (see figure 2.8). The velocity discontinuity is initially of zero thickness. The momentum equation is the same as for the first Rayleigh flow,

$$\frac{\partial u}{\partial t} = v\frac{\partial^2 u}{\partial y^2},$$

with the boundary conditions

$$
\begin{aligned}
\text{at} \quad t = 0, \quad & u = +U_0 \quad \text{for } y > 0, \\
\text{and} \quad t = 0, \quad & u = -U_0 \quad \text{for } y < 0.
\end{aligned}
$$

We find

$$f = \operatorname{erf}\eta,$$

where $f = u/U_0$, and $\eta = y/\sqrt{2vt}$. The shear layer thickness (to $\pm 0.99U_0$) is equal to $8\sqrt{vt}$ (see figure 2.8).
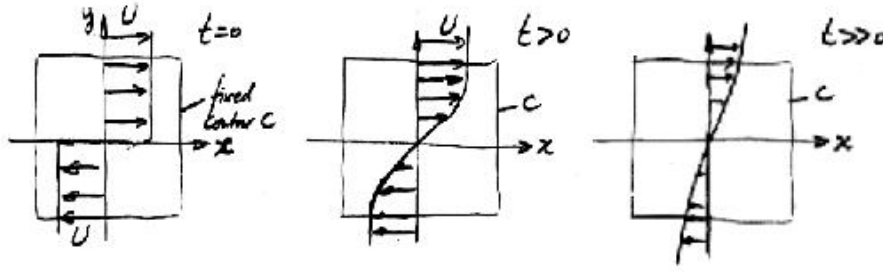
Figure 2.9: Velocity profile evolution as a function of time for the Rayleigh problem (a) $t = 0$, (b) $t > 0$, (c) $t \gg 0$.

2.1.7 Note on vorticity diffusion

The circulation Γ is defined as the line integral of the velocity around a closed contour (see equation 1.69)

$$\Gamma = \oint \mathbf{V} \cdot d\ell$$

where counter-clockwise contour integration is taken to be positive. By Stokes's Theorem

$$\Gamma = \int \mathbf{n} \cdot \nabla \times \mathbf{V} \, dA$$

$$= \int \mathbf{n} \cdot \Omega \, dA,$$

where A is the area enclosed by the contour, and $\Omega = \nabla \times \mathbf{V}$. In cartesian coordinates,

$$\nabla \times \mathbf{V} = \begin{vmatrix} \mathbf{i} & \mathbf{j} & \mathbf{k} \\ \frac{\partial}{\partial x} & \frac{\partial}{\partial y} & \frac{\partial}{\partial z} \\ u & v & w \end{vmatrix}$$

So the circulation can also be expressed as an area integral of the vorticity component normal to the surface enclosed by the contour.

Consider the Rayleigh problem, and evaluate the circulation around the contour C of unit length in the x-direction (see figure 2.9).

$$\text{At } t = 0, \quad \Gamma = -2U \text{ per unit length}$$
$$\text{At } t > 0, \quad \Gamma = -2U \text{ per unit length.}$$

That is, the irculation has remained constant, despite the action of viscosity inside the contour. However,

$$\text{At } t \gg 0, \quad \Gamma < -2U \text{ per unit length}$$

because of viscous diffusion across the contour, out of the control volume.

Of course, if the contour was large enough, the circulation would always remain constant, although the vorticity distribution inside the control volume would be continualy changing.

Another example might be the bucket on a turntable. If at $t < 0$ the fluid was moving with solid body rotation, then the circulation around any contour enclosing all the fluid would be given by $2\pi R^2 \omega$. If at $t = 0$ the bucket was suddenly brought to rest, the no-slip condition at the wall would instantaneously cancel out this circulation. Within the bucket, the vorticity generated at the wall diffuses out with time, until the vorticity everywhere is also zero.

2.2 Fully-Developed Flow With Heat Transfer

Here we consider only low-speed flows where compressibility effects and viscous effects make a negligible contribution to the temperature field. For parallel, steady, fully-developed flows, the momentum equation is independent of the temperature distribution since there are no buoyancy effects (parallel flow) and the fluid properties are taken to be constant. Therefore, the solutions obtained earlier for Couette flow, parallel duct flow, and circular pipe flow apply unchanged.

For these flows, the energy equation reduces to

$$\frac{d^2 T}{dy^2} = 0 \tag{2.25}$$

which shows that (a) the temperature field is independent of the velocity field (the two are "uncoupled"), and (b) the temperature profile is linear.
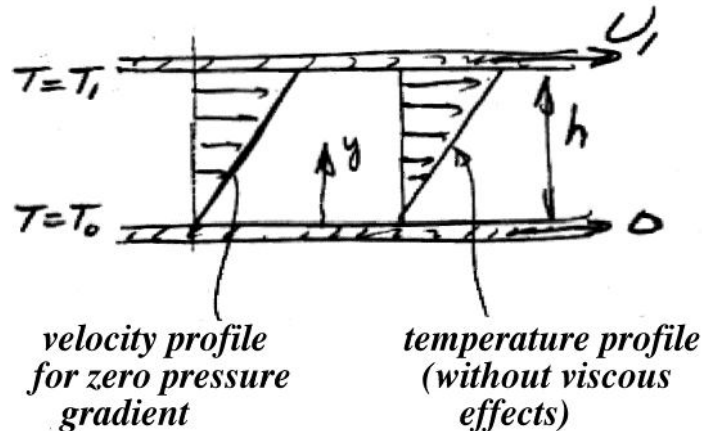

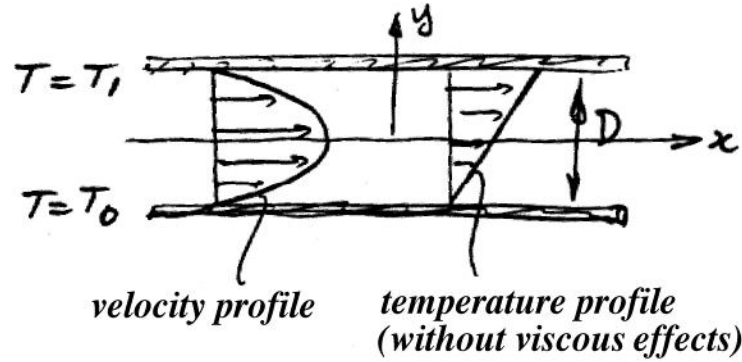Figure 2.10: Incompressible Couette flow with heat transfer.

*velocity profile   temperature profile
                     (without viscous effects)*

Figure 2.11: Incompressible parallel duct flow with heat transfer.

The particular temperature profile depends on the boundary conditions.

2.2.1   Couette flow

Incompressible Couette flow between two parallel plates at different temperature has the boundary conditions:

$$
\begin{aligned}
T &= T_0 \quad \text{at} \quad y = 0 \\
T &= T_1 \quad \text{at} \quad y = D
\end{aligned}
$$

(see figure 2.10). Hence,

$$
\frac{T - T_0}{T_1 - T_0} = \frac{y}{D}
$$

To see how viscous effects can affect the temperature profile, see White *Viscous Flows*, section 3.2.1 (but note especially the last paragraph).

2.2.2   Parallel duct flow

For flow between two fixed plates at different temperatures, the boundary conditions are:

$$
\begin{aligned}
T &= T_0 \quad \text{at} \quad y = -D/2 \\
T &= T_1 \quad \text{at} \quad y = +D/2
\end{aligned}
$$

(see figure 2.11). Hence,

$$
\frac{T - T_0}{T_1 - T_0} = \frac{1}{2}\left(1 + \frac{y}{D}\right)
$$

2.2.3 Circular pipe flow

For flow in a circular pipe, equation 2.25 becomes, in cylindrical coordinates,

$$\frac{d}{dr}\left(r\frac{dT}{dr}\right) = 0.$$

The boundary conditions are:

$$T = T_w \quad \text{at} \quad y = D/2$$
$$\frac{dT}{dr} = 0 \quad \text{at} \quad y = 0$$

(see figure 2.12). Hence,

$$T = T_w$$

So the temperature is constant throughout the fluid. To see the effects of viscous dissipation, see White *Viscous Flows*, section 3.3.5.

2.2.4 Free convection between heated plates

For free convection, there is no imposed velocity field. Consider two parallel plates. For horizontal plates (see figure 2.13),

$$\text{when } T_1 > T_0 \quad \text{the flow is } \underline{\text{stable}}$$
$$\text{when } T_1 < T_0 \quad \text{the flow is } \underline{\text{unstable}} \text{ for large}$$
$$\text{Rayleigh number, } Ra, \text{ where}$$

$$Ra = \frac{\rho^2 C_p g \beta D^3 \Delta T}{\mu}$$

For unstable flows, Bénard cells develop, as seen in figure 5.20.

For vertical plates (see figure 2.14), we get a simple analytical solution. We assume a steady, zero pressure gradient, fully-developed flow. The momentum equation reduces to

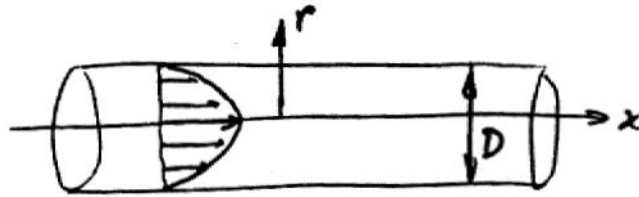$$-\rho \beta g \left(T - \bar{T}\right) = -\mu \frac{d^2 w}{dy^2}$$

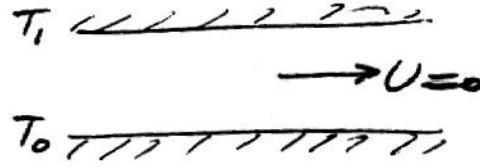Figure 2.12: Incompressible pipe flow with heat transfer.

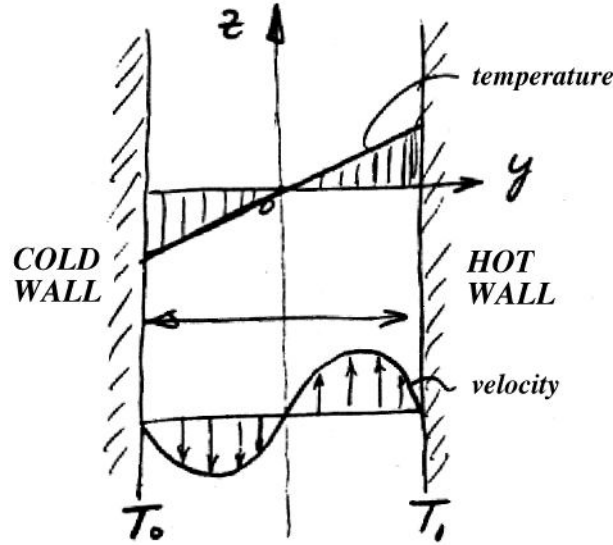Figure 2.13: Free convection between two horizontal plates.

Figure 2.14: Free convection between two vertical plates.

where $\bar{T} = (T_0 + T_1)/2$ is the average temperature and z is positive upwards. The energy equation is again

$$\frac{d^2T}{dy^2} = 0$$

if we neglect viscous effects and compressibility effects. Note that the buoyancy term couples the velocity and temperature fields, and the convective term is then dependent on the driving temperature difference $T_1 - T_0$. However, the temperature field is independent of the velocity.

The boundary conditions are:

$$
\begin{aligned}
w &= 0 & \text{at} \quad y &= \pm D/2 \\
T &= T_0 & \text{at} \quad y &= -D/2 \\
T &= T_1 & \text{at} \quad y &= +D/2
\end{aligned}
$$

Solving for the temperature field:

$$\frac{T - T_0}{T_1 - T_0} = \frac{1}{2}\left(1 + \frac{y}{D}\right).$$

We could also express this as

$$\frac{T - \bar{T}}{T_1 - T_0} = \frac{y}{D}$$

(as in the parallel duct flow). To solve for the velocity field, we begin with

$$-\rho \beta g \left(T_1 - T_0 \right) \frac{y}{D} = \mu \frac{d^2 w}{dy^2}$$

Integrating twice and applying the boundary conditions, we get

$$w = \frac{\rho g D^2 \beta \left(T_1 - \bar{T} \right)}{24 \mu^2} \left(\frac{2y}{D} - \left(\frac{2y}{D} \right)^3 \right).$$

This cubic profile could be written non-dimensionally

$$w^* = \frac{Gr}{24} \left(y^* - y^{*3} \right)$$

where

$$w^* = \frac{\rho w D}{\mu}, \quad y^* = \frac{2y}{D}, \quad Gr = \frac{\rho^2 g D^3 \beta \left(T_1 - \bar{T} \right)}{\mu^2}.$$

To see how viscous effects in the energy equation modify this solution, see White *Viscous Flows*, section 3.2.2.

2.3   Compressible Couette flow

To illustrate the use of the equations of motion, and to introduce some of the concepts encountered in compressible viscous flows, we will consider compressible, laminar Couette flow in some detail. The flow configuration is shown in figure 2.15. Air flows between two parallel plates, where the upper plate moves at a constant velocity U_e relative to the lower plate. By the no-slip condition, the velocity of the air in contact with the upper plate is also U_e relative to the air in contact with the lower plate. The other boundary conditions are as shown. The temperature of the upper and lower plates are T_e and T_w, respectively, and there is a heat flux q_w from the lower plate into the flow and a shear stress τ_w also acts on the lower plate. The flow is two-dimensional so that $\partial/\partial z = 0$; it is fully-developed so that $\partial/\partial x = 0$, and it is steady so that $\partial/\partial t = 0$. We will assume that the gas has constant specific heats.

The continuity equation gives:

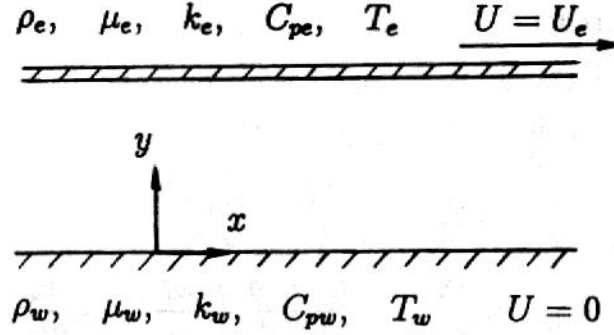$$\frac{\partial \rho v}{\partial y} = 0, \tag{2.26}$$

Figure 2.15: Notation for compressible Couette flow.

where $\mathbf{V} = u\mathbf{i} + v\mathbf{j} + w\mathbf{k}$. Hence, $V = 0$ by symmetry, and the flow is parallel.
The momentum equation gives:

$$\frac{\partial \sigma_{12}}{\partial y} = 0, \qquad \text{that is} \qquad \frac{\partial}{\partial y}\left(\mu \frac{\partial u}{\partial y}\right) = 0. \qquad (2.27)$$

Therefore the shear stresses and pressure are constant throughout the flow field. If the flow were incompressible, the viscosity would be constant and equation 2.27 could be integrated to show that the velocity profile is linear. When the flow is compressible, variations in temperature will produce variations in viscosity, and we need to solve for the temperature distribution before equation 2.27 can be integrated.
The energy equation gives:

$$\frac{\partial}{\partial y}\left(\mu u \frac{\partial u}{\partial y} + k \frac{\partial T}{\partial y}\right) = 0. \qquad (2.28)$$

That is, the diffusion of kinetic energy and heat are in equilibrium. If we write the energy equation in terms of the enthalpy, we find:

$$\Phi - \frac{\partial q_i}{\partial x_i} = 0. \qquad (2.29)$$

That is, the dissipation and the heat flux are in equilibrium. In fact, the two relations give the same result since:

$$\frac{\partial u_i \sigma_{ij}}{\partial x_j} = \Phi + u_i \frac{\partial \sigma_{ij}}{\partial x_j}$$

and the viscous stress is constant. It follows that in this fully-developed flow the temperature distribution depends only on how the kinetic energy is dissipated and how the heat is diffused.

Integrating equation 2.28 from the lower wall outward gives:

$$\mu u \frac{\partial u}{\partial y} + \frac{\mu C_p}{Pr} \frac{\partial T}{\partial y} = -q_w.$$

Here we have introduced the Prandtl number $Pr = \mu C_p / k$. By using the fact that the stress is constant and by assuming that the Prandtl number is constant (this is a good approximation for many gases) we find that:

$$\frac{\partial}{\partial y} \left(C_p T + \tfrac{1}{2} Pr u^2 \right) = -Pr \frac{q_w}{\tau_w} \frac{\partial u}{\partial y}.$$

By further integration:

$$C_p (T - T_w) + \frac{1}{2} Pr u^2 = -Pr \frac{q_w}{\tau_w} u, \tag{2.30}$$

and using the boundary conditions at the upper wall, we obtain:

$$T_w = T_e + \frac{Pr}{C_p} \left(\tfrac{1}{2} U_e^2 + \frac{q_w}{\tau_w} U_e \right). \tag{2.31}$$

Consider the case where the lower wall is adiabatic ($q_w = 0$). Here,

$$T_w = T_r = T_e + \tfrac{1}{2} \frac{Pr U_e^2}{C_p} = T_e \left(1 + Pr \frac{\gamma - 1}{2} M_e^2 \right)$$

where M_e is the Mach number based on the velocity and temperature of the upper wall, and T_r is called the *recovery temperature* or *adiabatic wall temperature.* Since the velocity of the air in contact with the lower wall is zero, T_w is equal to the total temperature at that point. The total temperature at the upper wall is $T_{0e} = T_e + \tfrac{1}{2} U_e^2 / C_p$. We see that if the Prandtl number is not equal to one, the temperature of the stationary wall is not equal to the total temperature at the upper boundary: the kinetic energy is not exactly "recovered" in the form of heat at the lower boundary. The ratio of the recovered energy to the external energy is called the *recovery factor, r,* where

$$r = \frac{T_r - T_e}{T_{0e} - T_e}. \tag{2.32}$$

In the case of laminar Couette flow, the recovery factor is simply equal to the Prandtl number. Note that when the Prandtl number is less than one (for air $Pr = 0.72$ at NTP), the temperature of the stationary wall is lower than the total temperature evaluated at the moving boundary.

Equation 2.31 gives the solution for the heat transfer from the lower wall:

$$q_w = \frac{\tau_w C_p}{Pr U_e} (T_w - T_r) \tag{2.33}$$

which shows that the heat transfer is proportional to the temperature difference $T_w - T_r$, and not $T_w - T_e$ as in low-speed flows. Also, we see that the heat transfer is proportional to the wall shear. That is, for the lower wall,

$$C_h = \frac{1}{2Pr} C_f \tag{2.34}$$

where $\quad C_f = \dfrac{\tau_w}{\frac{1}{2}\rho_e U_e^2}, \quad$ and $\quad C_h = \dfrac{q_w}{\rho_e U_e C_p \left(T_w - T_r\right)}.$

C_f is the skin friction coefficient and C_h is the heat transfer coefficient, or *Stanton number*. Relationships such as Equation 2.34 which connect the heat-transfer and skin-friction coefficients are called Reynolds Analogies, and the ratio $s = 2C_h/C_f$ is called the Reynolds Analogy Factor.

We can find the skin friction coefficient by integrating the momentum equation (equation 2.27). If we assume that the viscosity is proportional to the temperature (the actual variation is given by equations 1.36 and 1.37), we obtain:

$$C_f = \frac{1}{Re}\left(1 + \frac{T_w}{T_e} + \tfrac{2}{3}Pr\left(\gamma - 1\right)M_e^2\right). \tag{2.35}$$

For compressible Couette flow, the skin friction coefficient increases with heating and Mach number (this is not necessarily true for other wall-bounded flows such as boundary layer flows).

In addition, we obtain from equations 2.30 and 2.31:

$$\frac{T}{T_e} = \frac{T_w}{T_e} + \frac{T_r - T_w}{T_e}\left(\frac{u}{U_e}\right) - \frac{\gamma - 1}{2}Pr M_e^2 \left(\frac{u}{U_e}\right)^2. \tag{2.36}$$

This temperature-velocity relationship, derived for compressible Couette flow, is often used in the analysis of laminar and turbulent wall-bounded flows by replacing the Prandtl number in equation 2.36 with the recovery factor appropriate to those flows. In that form, it is often called the Crocco Relation or Crocco's Law. Velocity and temperature profiles for a number of Mach numbers are shown in figure 2.16.

One conclusion we can draw from this example is that in the absence of pressure gradients the kinetic energy of a supersonic flow is of such magnitude that when it is transformed into heat and redistributed in space by molecular diffusion significant temperature variations can occur. This can also be understood from the definition of Mach number: $M = U/\sqrt{\gamma RT}$. Here the numerator (squared) is proportional to the kinetic energy and the denominator (squared) is proportional to the internal energy. When the Mach number is of order unity the two forms of energy are of the same order of magnitude, and changes in the kinetic energy will result in changes in the temperature and its distribution in space.
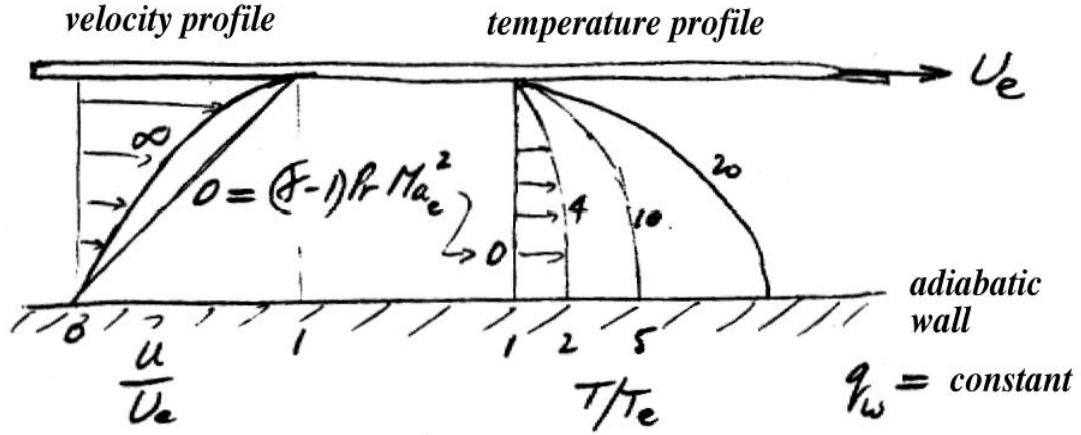
Figure 2.16: Velocity and temperature profiles in compressible Couette flow.

2.4 Similarity Solutions

We saw how it is sometimes possible to change a partial differential equation to an ordinary differential equation by using specially chosen non-dimensional dependent and independent variables. These variables are called similarity variables, and the method is called the method of similarity solutions. We did one example when discussing the Rayleigh problem. Here, we consider some other problems that can be solved using the method of similarity solutions: viscous stagnation point flow, and a suddenly stopped rotating cylinder.

2.4.1 Cylinder rotating at constant speed

Consider a steady laminar flow produced by a long circular cylinder rotating counterclockwise with a constant angular velocity ω in an infinite body of viscous fluid. The equations of motion, in cylindrical coordinates are (with $u = w = 0$), for the radial component

$$\frac{dp}{dr} = \frac{\rho v^2}{r}$$

and for the tangential component

$$\frac{d^2 v}{dr^2} + \frac{1}{r}\frac{dv}{dr} - \frac{v}{r^2} = 0.$$

To solve for v, we note that the tangential momentum equation can be written as

$$\frac{d}{dr}\left(\frac{1}{r}\frac{dvr}{dr}\right) = 0$$

which has the general solution

$$v = ar + \frac{b}{r},$$

that is, a combination of a solid body rotation plus a potential vortex. With the boundary conditions

$$v = r_0\omega \quad \text{and} \quad p = p_0 \quad \text{at} \quad r = r_0$$
$$v = 0 \quad \text{at} \quad r = \infty$$

we obtain

$$v = \frac{r_0^2\omega}{r}.$$

For any closed contour enclosing the spinning cylinder,

$$\Gamma = 2\pi vr = \text{constant} = \Gamma_0$$

so that

$$\boxed{v = \frac{\Gamma_0}{2\pi r}.} \tag{2.37}$$

where Γ is positive for counterclockwise rotation.

We should note that for two-dimensional incompressible flow, we can define a function ψ called the streamfunction, where

$$u = \frac{1}{r}\frac{\partial\psi}{\partial\theta}, \quad \text{and} \quad v = -\frac{\partial\psi}{\partial r}$$

so that the continuity equation is precisely satisfied. For the spinning cylinder problem, $u = 0$, and

$$\psi = \frac{\Gamma}{2\pi}\ln r$$

which is the streamfunction for a line vortex.

Now, for the pressure, we obtain

$$C_p \equiv \frac{p - p_0}{\frac{1}{2}\rho r_0^2\omega^2} = 1 - \left(\frac{r_0}{r}\right)^2$$
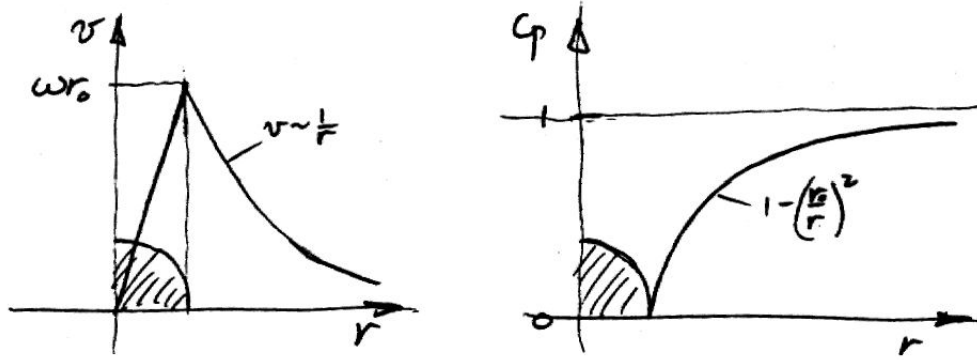
(see figure 2.17).

Figure 2.17: Velocity and pressure distributions for a cylinder rotating at a constant speed in a viscous fluid.

2.4.2 Suddenly stopped rotating cylinder

Consider now the motion that results when the cylinder stops suddenly. The momentum equation becomes

$$\frac{1}{\nu}\frac{\partial v}{\partial t} = \frac{\partial^2 v}{\partial r^2} + \frac{1}{r}\frac{\partial v}{\partial r} - \frac{v}{r^2}$$

with the boundary conditions

$$v = \frac{\Gamma_0}{2\pi r} \quad \text{at} \quad t = 0$$

$$v = 0 \quad \text{at} \quad r = r_0 \ \text{ for } \ t > 0.$$

Consider the case where $r_0 \ll r$ (the far-field solution). Then we could write

$$v = v\left(\Gamma_0, r, \nu, t\right).$$

By dimensional analysis this could be written as

$$\frac{2\pi \nu r}{\Gamma_0} = f(\eta) \quad \text{where} \quad \eta = \frac{r^2}{\nu t}.$$

These similarity variables turn the partial differential equation into an ordinary differential equation:

$$f'' + \tfrac{1}{4}f' = 0$$

with the boundary conditions

$$f = 1 \quad \text{at} \quad \eta = \infty$$
$$f = 0 \quad \text{at} \quad \eta = 0.$$
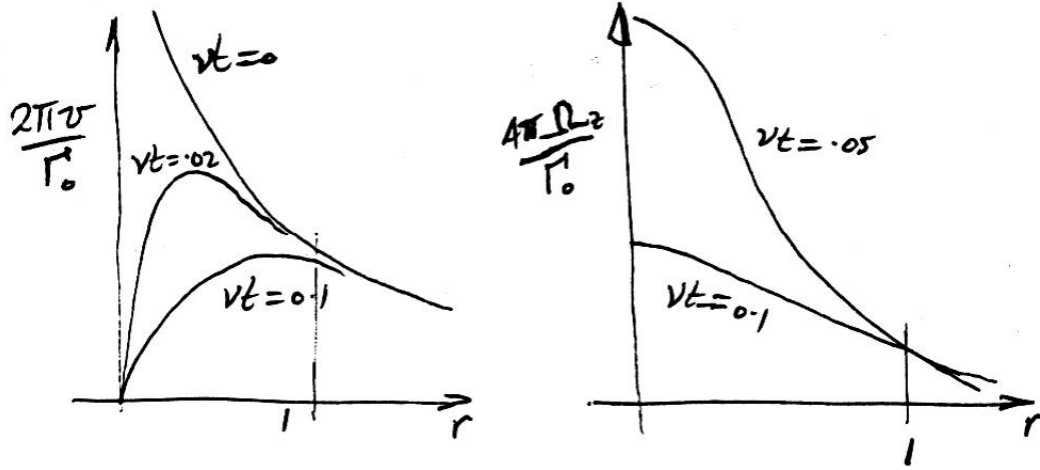
Hence,

$$f = 1 - e^{-\eta/4}.$$

Figure 2.18: Velocity and vorticity distributions for a suddenly stopped cylinder.

Note that

$$\Omega_z \;=\; \frac{1}{r}\frac{\partial rv}{\partial r} - \frac{1}{r}\frac{\partial u}{\partial \theta} \;=\; \frac{1}{r}\frac{drv}{dr} \;=\; \frac{\Gamma_0}{4\pi v t}e^{-\eta/4}.$$

The velocity and vorticity distributions are shown in figure 2.18.

2.4.3   Viscous stagnation point flow

Consider the steady two-dimensional inviscid flow field given by

$$\mathbf{V} = x\mathbf{i} - y\mathbf{j}.$$

For a two-dimensional flow, the shape of the streamlines is given by the solution of:

$$\frac{dy}{dx} \;=\; \frac{v}{u} \;=\; -\frac{y}{x}.$$

The variables can be separated and integrated to give

$$\int \frac{dy}{y} \;=\; -\int \frac{dx}{x}$$

or $\ln y \;=\; -\ln x +$ constant.

This can be written as

$$xy \;=\; C,$$

where C is a constant. The usual notation for a streamline is $\psi =$ constant along a streamline, so that streamlines are given by
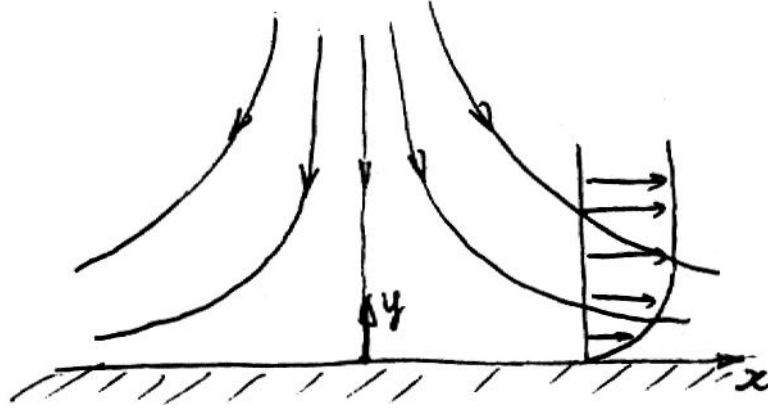
$$\psi = xy$$

Figure 2.19: Viscous stagnation point flow.

$(u = \partial\psi/\partial y, v = -\partial\psi/\partial x)$. That is, the streamlines are parabola in the x-y plane. The flowfield represents a stagnation point flow, as illustrated in figure 2.19 (the stagnation streamline is the one corresponding to $\psi = 0$).

For the viscous flow, we could try a new streamfunction

$$\psi^* = kx\, f(y)$$

which gives

$$u = kx\frac{df}{dy}, \qquad v = -kf.$$

It is not immediately obvious that the modified streamfunction will describe viscous flow near a stagnation point. At first glance, its main justification is that when $\psi^* \propto x$, the viscous terms in the Navier-Stokes equation contains only terms that involve second derivatives with respect to y. However,

(a) ψ^* will satisfy the no-slip condition if

$$f(0) = 0, \quad \text{and} \quad \left.\frac{df}{dy}\right|_{y=0} = f'(0) = 0$$

(so that u and v are zero at the wall for all x).

(b) Far away from the wall, viscous effects should be negligible so that inviscid stagnation point flow is recovered. That is, we require

$$\left.\frac{df}{dy}\right|_{y\to\infty} = 1$$

which means that

$$f(\infty) = y + \text{constant},$$

as required.

So, with the right boundary conditions, ψ^* can represent viscous stagnation point flow.

The Navier-Stokes equation for this two-dimensional flow becomes

$$kf'^2 - kff'' - \nu f''' = -\frac{1}{\rho kx}\frac{\partial p}{\partial x} \tag{2.38}$$

$$\nu f'' + kff' = -\frac{1}{\rho k}\frac{\partial p}{\partial y} \tag{2.39}$$

(the dash represents differentiation with respect to y). The second equation shows that

$$\frac{\partial p}{\partial y} = \text{a function of } y \text{ only,} \tag{2.40}$$

$$\text{and} \quad \frac{\partial^2 p}{\partial x \partial y} = 0. \tag{2.41}$$

Hence

$$\frac{\partial p}{\partial x} = g(x) + C_1. \tag{2.42}$$

$$\text{That is} \quad \frac{1}{\rho kx}\frac{\partial p}{\partial x} = \frac{g(x)}{\rho kx} + \frac{C_1}{\rho kx} \tag{2.43}$$

where C_1 is a constant which must be zero by symmetry. From equation 2.39, we see that the left hand side of equation 2.43 is a function of y only. Since $C_1 = 0$, $g(x)$ must therefore be of the form $C_2 x$. Now what is the value of this constant C_2? At large distances from the origin, the streamlines become nearly parallel, $\partial p/\partial y \to 0$, and $\partial p/\partial x$ must therefore approach the value given by the potential flow (inviscid flow) solution. That is, $C_2 = \rho k^2$. Hence

$$\frac{\partial p}{\partial x} = \rho k^2 x$$

which is independent of y. Note that $\partial p/\partial x$ is given by the inviscid Bernoulli equation, so that $\partial p/\partial x = U(dU/dx)$, where U is the x-component velocity outside the viscous layer. Equation 2.39 becomes

$$\nu f''' + kff'' + k\left(1 - f'^2\right) = 0.$$

To non-dimensionalize this equation, we put

$$\eta = \alpha y, \quad \text{and} \quad f(y) = \beta\phi(\eta)$$

and we find

$$\beta^2 \alpha^2 = 1, \quad \text{and} \quad \beta \alpha^3 = \frac{k}{\nu}. \tag{2.44}$$

That is, $\quad \eta = \sqrt{\frac{k}{\nu}} y, \quad \text{and} \quad \phi(\eta) = \sqrt{\frac{k}{\nu}} f(y). \tag{2.45}$

Finally:

$$\phi''' + \phi \phi'' - \phi'^2 + 1 = 0 \tag{2.46}$$

(the dash represents differentiation with respect to η), with the boundary conditions

$$\phi = 0, \quad \phi' = 0 \quad \text{at} \quad \eta = 0$$
$$\phi' = 1 \quad \text{at} \quad \eta = \infty.$$

Note that when we compare u and v to the inviscid values, we have

$$\frac{u}{U} = f' = \phi', \quad \text{and} \quad \frac{v}{V} = \frac{f(y)}{y} = \frac{\phi}{\eta}.$$

The numerical solution of this nonlinear ordinary differential equation was first given by Hiemenz in 1911. The results are given in table 2.1 and figure 2.20. If we note the distance at which $u/U = 0.99$, we have $\eta = 2.4$. That is,

$$\delta = 2.4 \sqrt{\frac{\nu}{k}}.$$

Thus u/U and δ_{99} are both independent of x.

Finally, we can calculate C_f using

$$\tau_w = \mu \left(\frac{\partial u}{\partial y} + \frac{\partial v}{\partial x} \right)_{y=0}$$

Therefore,

$$C_f = \frac{\tau_w}{\frac{1}{2}\rho U^2} = \frac{\mu k x \sqrt{\frac{k}{\nu}} \phi_0''}{\frac{1}{2}\rho U^2} = 2 \sqrt{\frac{\nu}{Ux}} \phi_0'' = \frac{2\phi_0''}{\sqrt{Re_x}}$$

(note that, as $x \to 0$, $C_f \to \infty$ but $\tau_w \to 0$).

Viscous layer thickness

The viscous layer or "boundary" layer thickness is usually small. For the cylinder example given here, $k = 4U_\infty/D$.

> (a) With $U_\infty = 3\,m/s$, and $D = 30\,cm$, $k = 40\,s^{-1}$. In air, this gives $\delta = 1.4\,mm$. The Reynolds number $Re_D = 60,000$.
>
> (a) With $U_\infty = 0.3\,m/s$, and $D = 30\,cm$, $k = 4\,s^{-1}$, and $\delta = 4.5\,mm$ ($Re_D = 6,000$).

plane				axially symmetrical			
$\eta = \sqrt{\dfrac{a}{\nu}}\, y$	ϕ	$\dfrac{d\phi}{d\eta} = \dfrac{u}{U}$	$\dfrac{d^2\phi}{d\eta^2}$	$\sqrt{2}\cdot\zeta = \sqrt{\dfrac{2a}{\nu}}\, z$	ϕ	$\dfrac{d\phi}{d\zeta} = \dfrac{u}{U}$	$\dfrac{d^2\phi}{d\zeta^2}$
0	0	0	1·2326	0	0	0	1·3120
0·2	0·0233	0·2266	1·0345	0·2	0·0127	0·1755	1·1705
0·4	0·0881	0·4145	0·8463	0·4	0·0487	0·3311	1·0298
0·6	0·1867	0·5663	0·6752	0·6	0·1054	0·4669	0·8910
0·8	0·3124	0·6859	0·5251	0·8	0·1799	0·5833	0·7563
1·0	0·4592	0·7779	0·3980	1·0	0·2695	0·6811	0·6283
1·2	0·6220	0·8467	0·2938	1·2	0·3717	0·7614	0·5097
1·4	0·7967	0·8968	0·2110	1·4	0·4841	0·8258	0·4031
1·6	0·9798	0·9323	0·1474	1·6	0·6046	0·8761	0·3100
1·8	1·1689	0·9568	0·1000	1·8	0·7313	0·9142	0·2315
2·0	1·3620	0·9732	0·0658	2·0	0·8627	0·9422	0·1676
2·2	1·5578	0·9839	0·0420	2·2	0·9974	0·9622	0·1175
2·4	1·7553	0·9905	0·0260	2·4	1·1346	0·9760	0·0798
2·6	1·9538	0·9946	0·0156	2·6	1·2733	0·9853	0·0523
2·8	2·1530	0·9970	0·0090	2·8	1·4131	0·9912	0·0331
3·0	2·3526	0·9984	0·0051	3·0	1·5536	0·9949	0·0202
3·2	2·5523	0·9992	0·0028	3·2	1·6944	0·9972	0·0120
3·4	2·7522	0·9996	0·0014	3·4	1·8356	0·9985	0·0068
3·6	2·9521	0·9998	0·0007	3·6	1·9769	0·9992	0·0037
3·8	3·1521	0·9999	0·0004	3·8	2·1182	0·9996	0·0020
4·0	3·3521	1·0000	0·0002	4·0	2·2596	0·9998	0·0010
4·2	3·5521	1·0000	0·0001	4·2	2.4010	0·9999	0·0006
4·4	3·7521	1·0000	0·0000	4·4	2·5423	0·9999	0·0003
4·6	3·9521	1·0000	0·0000	4·6	2·6837	1·0000	0·0001

Table 2.1: Tabulated flowfield solutions for viscous stagnation point flow (Howarth, 1934).
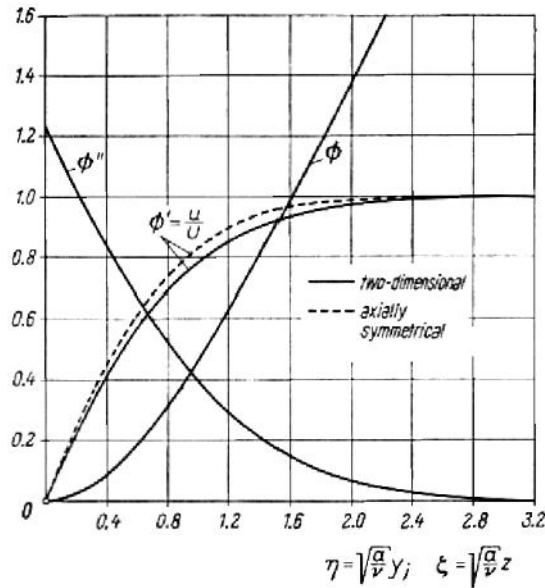

Figure 2.20: Viscous stagnation point flow profiles.

2.5 Creeping Flow and Lubrication Theory

Consider the momentum equation for constant-property, constant-density flows, without heat transfer. In non-dimensional form we had

$$\frac{D\mathbf{V}'}{Dt'} = -\nabla'p' + \frac{1}{Re}\nabla'^2\mathbf{V}',$$

which means that, if we have chosen the reference parameters in a reasonable way, all the derivative terms should be of the same order. This would suggest that at very low Reynolds numbers the inertia term <u>and</u> the pressure gradient term should go to small values compared to the viscous term. However, this is not correct. If the inertia term becomes very small, the dynamic pressure $\frac{1}{2}\rho_0 U_0^2$ goes to very small values, and therefore it is no longer an appropriate scaling parameter for the pressure (the only reason we use the dynamic pressure is because of its prominence in the Bernoulli equation, and in very viscous, low Reynolds number flows, the Bernoulli equation is very wrong). So we should use some kind of viscous scaling, such as

$$p^* = \frac{p - p_0}{\mu_0 V_0/L}.$$

Starting with

$$\frac{D\mathbf{V}}{Dt} = -\nabla p + \mu\nabla^2\mathbf{V},$$

we can re-work the non-dimensionalization, and this time we get

$$\frac{D\mathbf{V}'}{Dt'} = \frac{1}{Re}\left(-\nabla'p^* + \nabla'^2\mathbf{V}'\right),$$

which shows that as the Reynolds number goes to very small values, the inertia terms become negligible but the pressure gradient terms do not. Hence, the momentum equation for very low Reynolds number flows is

$$\boxed{\nabla p = \mu\nabla^2\mathbf{V}} \tag{2.47}$$

This equation looks very much like the one derived for parallel, fully-developed flows, but of course the present case is not restricted to these conditions, only that the Reynolds number is small enough.

2.5.1 Stokes flow

One general solution of this equation is available for flow over a sphere (Stokes flow). The details of the solution are given by White (p.204) and

Batchelor (p.230). In spherical polar coordinates, the radial and tangential velocities are given by

$$u_r \;=\; U_\infty \cos\theta \left(1 + \frac{a^3}{2r^3} - \frac{3a}{2r}\right),$$

$$v_\theta \;=\; U_\infty \sin\theta \left(-1 + \frac{a^3}{4r^3} + \frac{3a}{4r}\right).$$

Note:

(1) The velocities are independent of the viscosity μ.

(2) The streamlines are symmetrical fore and aft (there is no wake). As the Reynolds number increases, the inertia terms will become important, and it is the convective acceleration terms that break the symmetry.

(3) The velocity everywhere is less than U_∞ (unlike potential flow where the velocity at the diameter plane is $1.5 U_\infty$).

(4) The effect of the sphere extends to large distances: at $r = 10a$, $0.85 < |u|/U_\infty < 0.95$ (see figures 2.21 and 2.22).
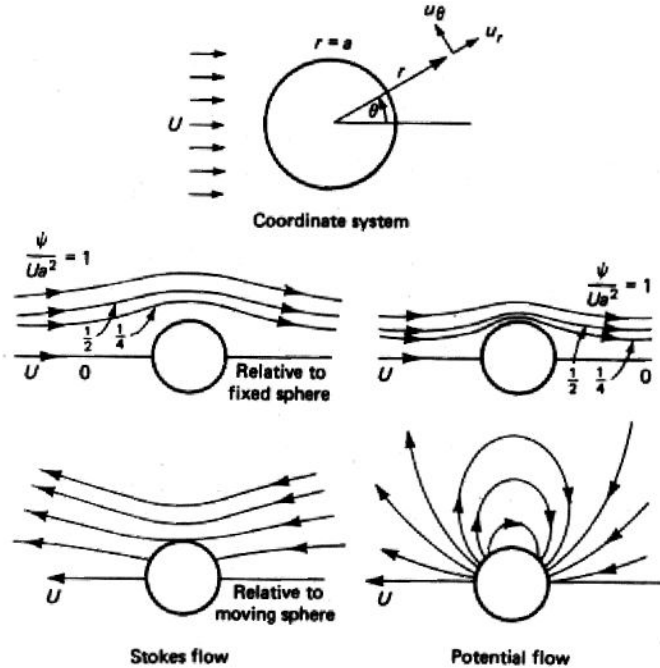

Figure 2.21: Comparison of creeping flow (*left*) and potential flow (*right*) past a sphere. From White *Viscous Flows*.
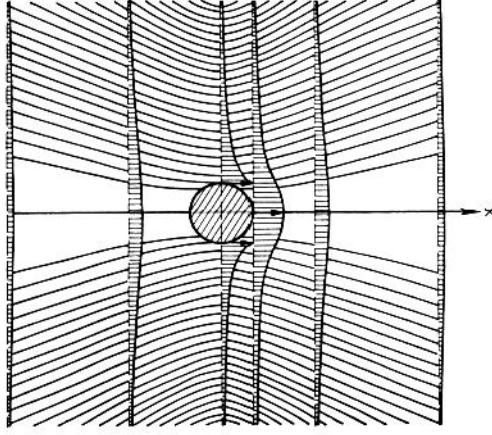
Figure 2.22: Streamlines and velocity distributions in Stokes' solution for a sphere in parallel flow. From Schlichting *Boundary Layers*.

With u_r and u_θ known, the pressure is found by integrating the momentum equation. The result is

$$p = p_\infty - \frac{3\mu a U}{2r^2} \cos \theta$$

where p_∞ is the uniform freestream pressure. Thus the pressure deviation is proportional to μ and antisymmetric, being positive at the front and negative at the rear of the sphere (see figure 2.23). This creates a pressure drag on the sphere. There is also a surface shear stress which creates a drag force. The shear-stress distribution in the fluid is given by

$$\tau = \mu \left(\frac{1}{r} \frac{\partial u_r}{\partial \theta} + \frac{\partial u_\theta}{\partial r} \right) = -\frac{U\mu \sin \theta}{r} \left(1 - \frac{3a}{4r} + \frac{5a^3}{4r^3} \right).$$
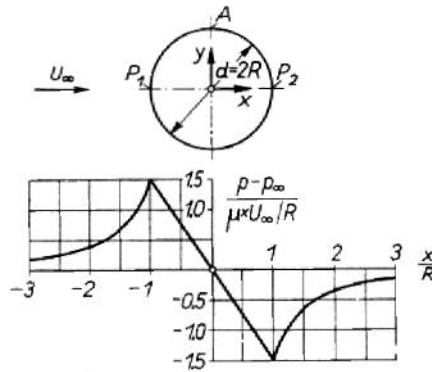

Figure 2.23: Pressure distribution around a sphere in parallel flow. From Schlichting *Boundary Layers*.
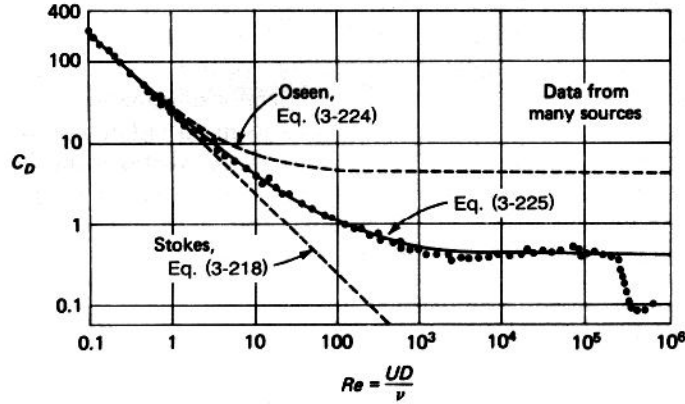
Figure 2.24: Drag on a sphere.

The total drag is found by integrating pressure and shear around the surface:

$$F = -\int_0^\pi \tau_{r=a} \sin \theta \, dA - \int_0^\pi p_{r=a} \cos \theta \, dA$$

$$dA = 2\pi a^2 \sin \theta \, d\theta$$

$$F = 4\pi\mu Ua + 2\pi\mu Ua = 6\pi\mu Ua$$

This is the famous result found by Stokes (1851). For what it is worth, friction in this case contributes two-thirds of the drag and pressure one-third. The formula is strictly valid only for $Re \ll 1$, the "creeping" flow assumption, but figure 2.24 shows that it is accurate up to about $Re = 1$.

2.5.2   Slider bearing

The second example of low Reynolds number flow is the flow in an oil lubricated bearing. This flow is modeled by considering a sliding block moving over a plane guide surface (see figure 2.25). To make the flow steady, we move with the slide block, which is considered to be large in the transverse direction.

We allow the block to be inclined at a small angle α to the guide surface, so that $u(\partial u/\partial x)$, for example, is not zero. However,

$$\frac{\rho u \frac{\partial u}{\partial x}}{\mu \frac{\partial^2 u}{\partial y^2}} \approx \frac{\rho U^2/\ell}{\mu U/h^2} = \frac{\rho U\ell}{\mu}\left(\frac{h}{\ell}\right)^2,$$

and we can neglect the acceleration (inertia) terms when

$$\frac{\rho U\ell}{\mu}\left(\frac{h}{\ell}\right)^2 \ll 1, \quad \text{or} \quad \frac{\rho Uh}{\mu}\left(\frac{h}{\ell}\right) \ll 1.$$
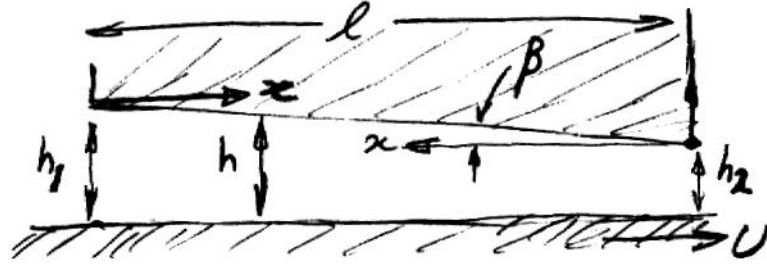
Figure 2.25: Notation for a slider bearing.

Take, for example, $U = 10\,m/s$, $\ell = 100\,mm$, $h = 0.2\,mm$, $v = 40 \times 10^{-6}\,m^2/s$, gives

$$\frac{U\ell}{v} = 25,000, \qquad \frac{\rho U\ell}{\mu}\left(\frac{h}{\ell}\right)^2 = 0.1.$$

Similarly,

$$\frac{\partial^2 u/\partial x^2}{\partial^2 u/\partial y^2} \approx \frac{U/\ell^2}{U/h^2} = \left(\frac{h}{\ell}\right)^2 \ll 1$$

and

$$v \approx 0, \qquad \frac{\partial p}{\partial y} \ll \frac{\partial p}{\partial x}.$$

Finally,

$$\frac{dp}{dx} = \mu \frac{\partial^2 u}{\partial y^2}. \tag{2.48}$$

Note that dp/dx may be a function of x, and so $u = u(x,y)$. This is not an example of fully developed , parallel flow. Therefore we need another equation, since u and p are unknowns. We can use the continuity equation,

$$\int_0^{h(x)} u\,dy = \text{constant} = Q. \tag{2.49}$$

The boundary conditions are

$$\begin{aligned} u = U, \quad y = 0 & \qquad p = 0, \quad x = 0 \\ u = 0, \quad y = h & \qquad p = 0, \quad x = \ell. \end{aligned}$$

Hence, from the momentum equation (equation 2.48, we obtain

$$\frac{u}{U} = \left(1 - \frac{y}{h}\right)\left(1 - \frac{h^2}{2\mu U}\frac{dp}{dx}\frac{y}{h}\right)$$

and from the continuity equation (eqation 2.49,

$$\frac{dp}{dx} = 12\mu\left(\frac{U}{2h^2} - \frac{Q}{h^3}\right)$$

which gives

$$p = 6\mu U \int_0^x \frac{dX}{h^2} - 12\mu Q \int_0^x \frac{dX}{h^3}.$$

With $p = 0$ at $x = \ell$, we get

$$Q = \frac{\frac{1}{2}U \int_0^\ell \frac{du}{h^2}}{\int_0^\ell \frac{du}{h^3}}.$$

Consider a flat slider on a flat guide surface, so that

$$
\begin{aligned}
h &= h_1 - \beta x \\
&= h_1 - \frac{(h_1 - h_2)\,x}{\ell}.
\end{aligned}
$$

This gives

$$Q = \frac{\frac{1}{2}U \int_{h_1}^{h_2} \frac{dh}{h^2}}{\int_{h_1}^{h_2} \frac{dh}{h^3}} = U\frac{h_1 h_2}{h_1 + h_2}$$

and

$$p = 6\mu U \frac{(h_1 - h_2)\,(h - h_2)}{\left(h_1^2 - h_2^2\right)h^2}.$$

(see figure 2.26). Note that

(a) The pressure gradient

$$\frac{dp}{dx} = 12\mu\left(\frac{U}{2h^2} - \frac{Q}{h^3}\right) = 0$$

$$\text{when} \quad h = \frac{2Q}{U} = \frac{2h_1 h_2}{h_1 + h_2}.$$

That is, the pressure has a maximum (or minimum) at $2h_1 h_2/h_1 + h_2$.

(b) For $p > 0$ everywhere, we require $h > h_2$. That is, the block must slope down in the direction of motion.

(c) Back flow occurs in the region of pressure rise near the wall at rest, just as we found in the Couette flow with adverse pressure gradient.

(d) The total pressure load $P = \int_0^\ell p\,dx$ has a maximum value when $h_1/h_2 \approx 2.2$, which gives

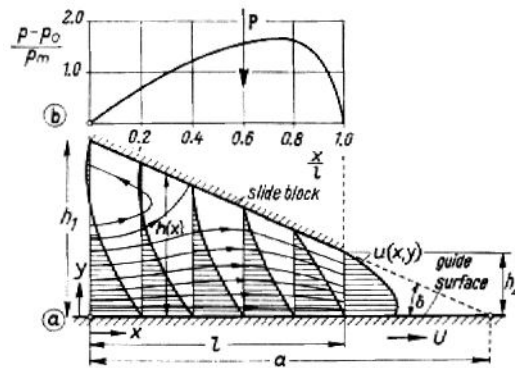$$P = 0.16\frac{\mu U \ell}{h_2}\left(\frac{\ell}{h_2}\right).$$

Figure 2.26: Lubrication in a bearing: a) Flow in a wedge between slide block and plane guide surface; b) Pressure distribution over block, $a/\ell = 1.57$ ($h_1/h_2 = 2.75$). From Schlichting *Boundary Layers*
.

2.6   Additional Exact Solutions

Flow between rotating concentric cylinders (White p.117, Schlichting p.80).

Non-circular duct flows (White p.123).

Eccentric annulus flow (White p.125).

Thermal entrance problem (White p.132).

Starting flow in a circular pipe (White p.141, Schlichting p.84, Batchelor p.193).

Pipe flow with an oscillating pressure gradient (White p.143).

Flow near an oscillating flat plate (White p.148, Schlichting p.85, Batchelor p.191). Note similarity with the case of an unsteady pressure gradient, Lam p.217.

Flow formation in Couette flow (White p.141, Schlichting p.84, Batchelor p.193).

Model of a paint brush (Batchelor p.183).

Chapter 3

Laminar Boundary Layers

Consider again the flow generated by an infinite flat plate set impulsively in motion at $t = 0$ with a constant velocity U. Initially, the fluid velocity is zero everywhere, and the vorticity and circulation are also zero everywhere. At $t = 0$, the no-slip condition sets an infinitely thin layer of fluid into motion. At interior points in the fluid, the velocity and vorticity remain zero, but at the wall, there exists now a discontinuity in tangential velocity, such that the circulation per unit length is $-U$ (constant and finite), and we have therefore a constant strength vortex sheet at the wall. For $t > 0$, the vorticity which was concentrated at the boundary at $t = 0$ diffuses into the fluid by the action of viscosity (figure 3.1). Remember that vorticity in a constant density, constant property fluid obeys a diffusion equation, and therefore the spread of vorticity into the fluid is similar to the spread of temperature away from a suddenly heated plate kept at a constant temperature. The characteristic distance for this diffusion process is $\sqrt{vt}$ for vorticity and $\sqrt{\alpha t}$ for temperature.

In this simple example, the convective acceleration terms were all zero, and we had

$$\frac{D\boldsymbol{\Omega}}{Dt} = \frac{\partial \boldsymbol{\Omega}}{\partial t}, \quad \text{and} \quad \frac{DT}{Dt} = \frac{\partial T}{\partial t}.$$

Let's consider a case where these convective terms are important, such as the case of fluid set in motion by a solid body moving through it. The transport of vorticity away from the body then depends on convection and diffusion, and the convection may limit the parts of the fluid that become vortical. Near the nose of the body, for example, the relative velocity of the fluid toward the body will limit the extent to which the vorticity is spread (figure 3.2). In cases where the convection is strong (U is large), or where the diffusion is weak (v is small), there will be a large region of the fluid, ahead of and to the sides of the body, untouched by the viscous diffusion of vorticity where the fluid is irrotational in the steady state.

When the body is a flat plate of length ℓ, which is put into motion at $t = 0$
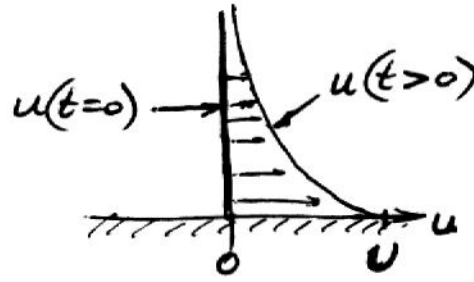
Figure 3.1: Vorticity diffusion for a plate set impulsively into motion.

with a velocity U, and also suddenly heated to a constant temperature, then the vorticity and temperature diffuse out across streamlines to a characteristic distance $\sqrt{vt}$ ($v = \alpha$ when $Pr = 1$). The time t that a material element spends in the vicinity of the flat plate is given by ℓ/U. The ratio of the convection distance ℓ to the diffusion distance $\sqrt{v\ell/U}$ defines a Reynolds number $\sqrt{U\ell/v}$. Thus, if $U\ell/v \gg 1$, the vorticity and heat are convected downstream before they can be diffused very far laterally, and there is a rather narrow region of heated, vortical fluid next to the body. If $U\ell/v \ll 1$, the effect of convection is very small, and both vorticity and temperature rise more or less equally in all directions away from the body, as we saw in the case of Stokes flow over a sphere. (Note that even for $Re \ll 1$, the small convection terms give rise to a wake, as shown by Oseen's correction to Stokes' analysis in figure 2.24.)

(To analyze the flow near the leading edge of the plate, the qualitative statements regarding the convective and diffusive terms will still hold but the quantitative conclusions are different: the analysis must be based on stagnation point flow considerations.)

Thus, in cases where convection <u>and</u> diffusion are important, the effect of increasing Reynolds number is to confine the vorticity diffused from a solid boundary to a layer of relatively small thickness, the magnitude of this vorticity being greater as the layer becomes thinner with increasing Reynolds number. Within this layer (the *boundary layer*), viscous effects are
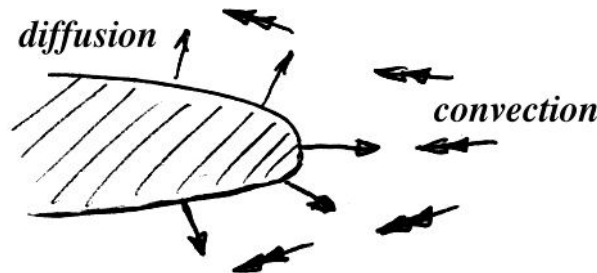

Figure 3.2: The competition between diffusion and convection.

always important, no matter what the Reynolds number, whereas outside this layer the flow may be treated as inviscid (Prandtl's 1904 boundary layer hypothesis). The boundary layer is, in effect, the layer in which the fluid velocity makes a transition from the required value of zero at the boundary to a freestream value which is appropriate to an inviscid fluid.

3.1   Boundary Layer Growth

When a fluid flows over a solid surface, we know that the no-slip condition causes steep velocity gradients to occur in a region near the surface. As the flow proceeds downstream, the thickness of this "boundary" layer grows because lower layers of fluid exert friction on the higher layers, and more and more fluid is decelerated by viscous friction. In a two-dimensional duct, the layers grow on the upper and lower walls, and after some distance they meet, merge, and eventually the flow becomes fully-developed so that further growth stops. A similar process occurs in the entrance region of a pipe.

However, in an external flow, such as the flow over a flat plate placed in the center of a wind tunnel, the boundary layer continues to grow and there is no fully-developed state. The analysis is consequently more difficult because the flow continuous to accelerate and the nonlinear acceleration term in the Navier-Stokes equation is no longer zero. Nevertheless, it is possible to determine approximately the growth rate of the layer and the drag exerted by the flow on the plate by using the integral forms of the continuity and momentum equations.

3.1.1   Control volume analysis

We will begin by analyzing a laminar boundary layer, which is the flow that occurs over a plate when the Reynolds number $Re_x = \rho U_e x / \mu < 100,000$, where x is the distance from the leading edge, and U_e is the velocity of the flow outside the boundary layer. The velocity U_e is taken to be constant so that $\partial p / \partial x = 0$. Also, we will assume that the plate is flat and that the boundary layer is thin, so that the streamlines are nearly parallel and therefore $\partial p / \partial y \approx 0$. The flow is steady and the fluid has a constant density.

Consider a rectangular control volume extending a distance L from the leading edge, with a height equal to the extent of the boundary layer at $x = L$ (figure 3.3). The incoming velocity is uniform, and the outgoing profile is decelerated near the wall because of friction, so that for a distance δ the velocity $U(y) < U_e$. Actually, U approaches the value U_e asymptotically, so that the *boundary layer thickness* δ is defined to be the distance where the U is virtually indistinguishable from U_e. The most common definition of the
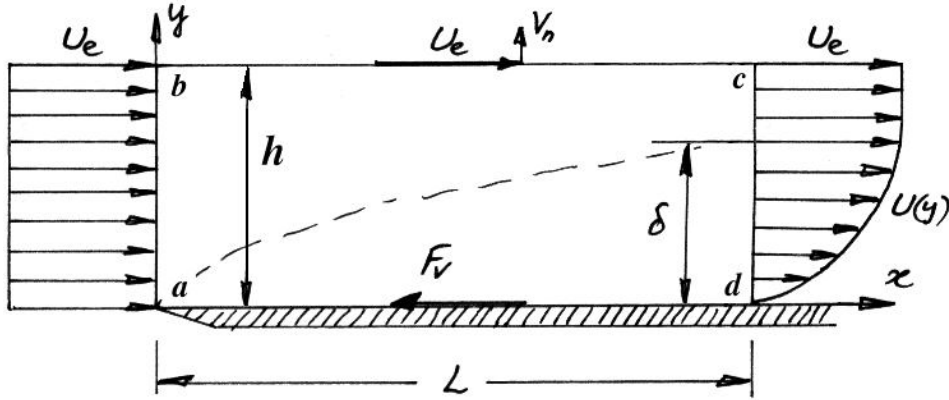
Figure 3.3: Control volume for the analysis of a laminar boundary layer.

boundary layer thickness is

$$U = 0.99U_e \quad \text{at} \quad y = \delta.$$

Note that δ increases with x, so that $\delta = \delta(x)$. For many purposes, the velocity variation outside the boundary layer can be neglected. For example, in applying the continuity and momentum equations, these small velocity variations are routinely ignored because their contributions are negligibly small (see section 3.6).

We begin with the conservation of mass. Since there is a greater mass-flow into the control volume over face ab than out of the control volume over face cd, because $U(y) < U_e$, there must be a mass-flow through face bc. On face bc, the velocity in the x-direction is constant and equal to U_e (remember, $\partial p/\partial x = 0$), but the y-component of the velocity V_n is unknown. For now, we shall simply proceed. Using the continuity equation,

$$\int_0^h (\mathbf{n_1} \cdot U_e\mathbf{i})w dy + \int_0^h (\mathbf{n_2} \cdot U(y)\,\mathbf{i})w dy + \int_0^L (\mathbf{n_3} \cdot (U_e\mathbf{i} + V_n(x)\mathbf{j}))w dx = 0,$$

where w is the width of the plate, and $\mathbf{n_1}$, $\mathbf{n_2}$ and $\mathbf{n_3}$ are the unit normal vectors on faces ab, cd and bc, respectively. That is,

$$-U_e h + \int_0^h U\,dy + \int_0^L V_n\,dx = 0, \tag{3.1}$$

where $U = U(y)$ and $V_n = V_n(x)$.

Next, we use the *x*-component of the momentum equation. It is understood that F_v is the force exerted by the plate on the fluid, so that

$$-F_v \;=\; \mathbf{i}\cdot\int_0^h (\mathbf{n_1}\cdot\rho U_e\mathbf{i})\,U_e\mathbf{i}\,w\,dy + \mathbf{i}\cdot\int_0^h (\mathbf{n_2}\cdot\rho U\mathbf{i})\,U\mathbf{i}\,w\,dy$$

$$+\,\mathbf{i}\cdot\int_0^L (\mathbf{n_3}\cdot\rho\,(U_e\mathbf{i}+V_n\mathbf{j}))\,(U_e\mathbf{i}+V_n\mathbf{j})\,w\,dx.$$

That is,

$$-F_v \;=\; -\int_0^h \rho U_e^2 w\,dy + \int_0^h \rho U^2\,w\,dy + \int_0^L \rho V_n U_e\,w\,dx$$

and so

$$-\frac{F_v}{\rho w} \;=\; -U_e^2 h + \int_0^h U^2\,dy + \int_0^L V_n U_e\,dx.$$

The continuity equation can be used to eliminate the unknown velocity $V_n(x)$. Multiplying equation 3.1 by U_e and subtracting the result from the momentum equation gives

$$-\frac{F_v}{\rho w} \;=\; -U_e^2 h + \int_0^h U^2\,dy + U_e^2 h - \int_0^h UU_e\,dy$$

$$=\; \int_0^h \left(U^2 - UU_e\right)dy.$$

Hence,

$$\frac{F_v}{\rho w U_e^2} \;=\; \frac{1}{U_e^2}\int_0^h \left(UU_e - U^2\right)dy$$

$$=\; \int_0^h \left(\frac{U}{U_e} - \frac{U^2}{U_e^2}\right)dy.$$

Finally,

$$\frac{F_v}{\rho w U_e^2} \;=\; \int_0^h \frac{U}{U_e}\left(1 - \frac{U}{U_e}\right)dy. \tag{3.2}$$

To go further, we need to know (or guess) how the velocity varies with distance from the wall. In other words, we need to know how U varies with y, and δ varies with x.

3.1.2   Similarity solution

It was shown by Prandtl in 1904 that for a boundary layer the full Navier-Stokes equation can be approximated by a simpler equation. The approximations are based on the observation that a boundary layer only grows slowly and the streamlines within the layer are nearly parallel. In particular, the pressure across the layer is nearly constant, (which helps to justify our earlier assumption that the pressure was constant throughout the control volume). These approximations yield an equation called the boundary layer equation, and Paul Richard Heinrich Blasius (1883–1970), one of Prandtl's students, showed that this equation has a "similarity" solution. The boundary layer equation is derived in the next section, but a few preliminary words are useful.

Blasius supposed that the velocity distribution in a laminar boundary layer on a flat plate was a function only of the freestream velocity U_e, the density ρ, the viscosity μ, the distance from the wall y, and the distance along the plate x. Dimensional analysis gives:

$$\frac{U}{U_e} \;=\; f\left(\frac{U_e x}{\nu}, \frac{y}{x}\right).$$

By an ingenious coordinate transformation Blasius showed that, instead of depending on two dimensionless variables, the dimensionless velocity distribution was a function of only one composite dimensionless variable η, so that

$$\frac{U}{U_e} \;=\; f'\left(\frac{y}{x}\sqrt{\frac{U_e x}{\nu}}\right) \;=\; f'\left(\eta\sqrt{2}\right).$$

The variables U/U_e and η $(= y\sqrt{U_e/(2\nu x)})$ are called similarity variables, which means that if the velocity distribution is plotted using these non-dimensional variables (instead of dimensional variables such as U and y), it is defined by a single universal curve, for any Reynolds number and any position along the plate.

These particular similarity variables transform the boundary layer equation (a *PDE*) into an *ODE* which can be solved numerically. The solution is called the Blasius velocity profile, and the results are usually given in the form of a table (see table 3.1). The Blasius velocity profile matches the experimental data, such as those shown in figure 3.4, very well.

The contribution by Blasius was important in that he used similarity arguments (firmly rooted in dimensional analysis) to find an exact solution to an approximate equation describing the flow in a laminar boundary layer (Prandtl's boundary layer equation). Furthermore, the results describe the experimental data very well, thereby justifying the assumptions that were made.

$\eta = y\sqrt{\dfrac{U_\infty}{\nu x}}$	f	$f' = \dfrac{u}{U_\infty}$	f''
0	0	0	0·33206
0·2	0·00664	0·06641	0·33199
0·4	0·02656	0·13277	0·33147
0·6	0·05974	0·19894	0·33008
0·8	0·10611	0·26471	0·32739
1·0	0·16557	0·32979	0·32301
1·2	0·23795	0·39378	0·31659
1·4	0·32298	0·45627	0·30787
1·6	0·42032	0·51676	0·29667
1·8	0·52952	0·57477	0·28293
2·0	0·65003	0·62977	0·26675
2·2	0·78120	0·68132	0·24835
2·4	0·92230	0·72899	0·22809
2·6	1·07252	0·77246	0·20646
2·8	1·23099	0·81152	0·18401
3·0	1·39682	0·84605	0·16136
3·2	1·56911	0·87609	0·13913
3·4	1·74696	0·90177	0·11788
3·6	1·92954	0·92333	0·09809
3·8	2·11605	0·94112	0·08013
4·0	2·30576	0·95552	0·06424
4·2	2·49806	0·96696	0·05052
4·4	2·69238	0·97587	0·03897
4·6	2·88826	0·98269	0·02948
4·8	3·08534	0·98779	0·02187
5·0	3·28329	0·99155	0·01591
5·2	3·48189	0·99425	0·01134
5·4	3·68094	0·99616	0·00793
5·6	3·88031	0·99748	0·00543
5·8	4·07990	0·99838	0·00365
6·0	4·27964	0·99898	0·00240
6·2	4·47948	0·99937	0·00155
6·4	4·67938	0·99961	0·00098
6·6	4·87931	0·99977	0·00061
6·8	5·07928	0·99987	0·00037
7·0	5·27926	0·99992	0·00022
7·2	5·47925	0·99996	0·00013
7·4	5·67924	0·99998	0·00007
7·6	5·87924	0·99999	0·00004
7·8	6·07923	1·00000	0·00002
8·0	6·27923	1·00000	0·00001
8·2	6·47923	1·00000	0·00001
8·4	6·67923	1·00000	0·00000
8·6	6·87923	1·00000	0·00000
8·8	7·07923	1·00000	0·00000

Table 3.1: Dimensionless velocity profile for a laminar boundary layer: tabulated values ($\eta = y\sqrt{U_e/(2\nu x)}$). Adapted from F.M. White, *Fluid Mechanics*, McGraw-Hill, 1986.

The Blasius solution is not an analytical solution, and tabulated values do not reveal the physics very well. It is convenient to have analytical form for the velocity profile, and it turns out that a parabola is a reasonable
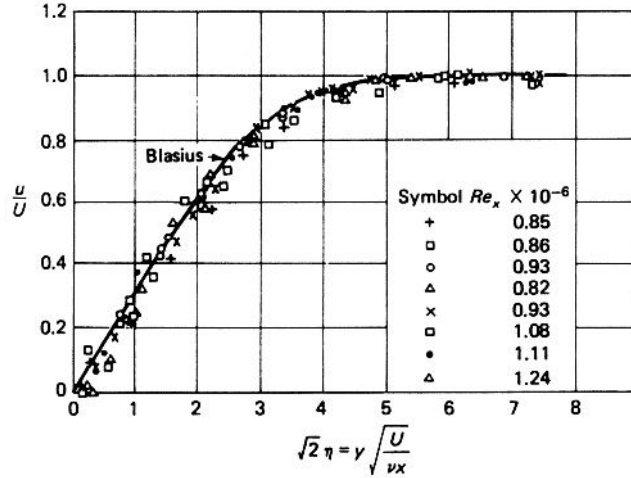
Figure 3.4: Dimensionless velocity profile for a laminar boundary layer: comparison with experiments by Liepmann, *NACA Rept. 890*, 1943. Adapted from F.M. White, *Viscous Flow*, McGraw-Hill, 1991.

approximation (see figure 3.5). That is, we can use the approximation that

$$\frac{U}{U_e} = 2\left(\frac{y}{\delta}\right) - \left(\frac{y}{\delta}\right)^2 \quad \text{for} \quad y \leq \delta \tag{3.3}$$

$$\text{and} \quad \frac{U}{U_e} = 1 \quad \text{for} \quad y > \delta.$$

which satisfies the boundary conditions that $U = 0$ at $y = 0$, and $U = U_e$ at $y = \delta$. Most importantly, it retains the correct similarity scaling, as we shall see. Then, for this particular profile, we have from equation 3.2:

$$\frac{F_v}{\rho w U_e^2 \delta} = \int_0^1 \frac{U}{U_e}\left(1 - \frac{U}{U_e}\right)d\left(\frac{y}{\delta}\right) = \frac{2}{15}. \tag{3.4}$$

To eliminate δ we use the fact that the total force due to friction F_v is the integral of the shear stress at the wall τ_w over the area of the plate:

$$F_v = \int_0^L \tau_w\, w dx.$$

Differentiating and using the Newtonian stress-strain rate relationship gives

$$\frac{1}{w}\frac{dF_v}{dx} = \tau_w = \mu \left.\frac{\partial U}{\partial y}\right|_w. \tag{3.5}$$
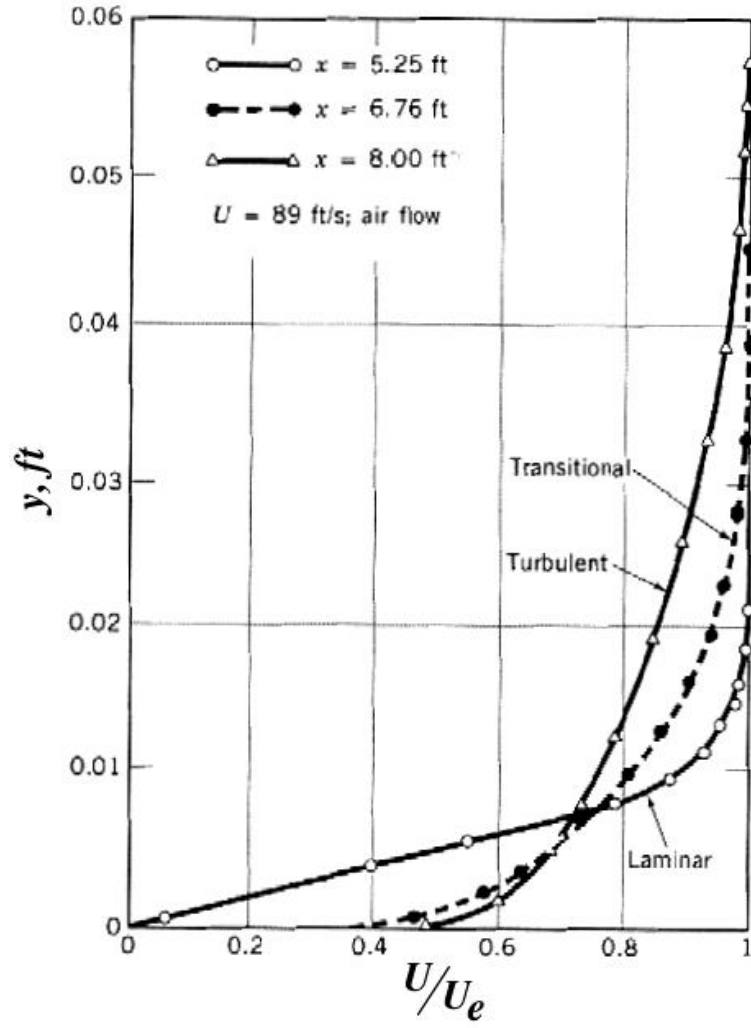
Figure 3.5: Comparison of dimensionless laminar and turbulent flat-plate velocity profiles. Adapted from F.M. White, *Fluid Mechanics*, McGraw-Hill, 1986.

For the parabolic profile approximation,

$$\tau_w = \frac{2\mu U_e}{\delta}.$$ (3.6)

Combining this result with equation 3.4 to eliminate the boundary layer thickness δ, we obtain

$$F_v \frac{dF_v}{dx} = \frac{4}{15}\mu\rho U_e^3 w^2,$$

and by integration,

$$F_v = \sqrt{\tfrac{8}{15}\mu\rho U_e^3 w^2 L}.$$

Non-dimensionalizing F_v gives

$$C_F = \frac{1.46}{\sqrt{Re_L}}$$

for a parabolic velocity profile. The skin friction coefficient C_F and the Reynolds number Re_L are defined by

$$C_F = \frac{F_v}{\frac{1}{2}\rho U_e^2 L w} \qquad \text{and} \qquad Re_L = \frac{\rho U_e L}{\mu}. \tag{3.7}$$

C_F is called the *total* skin friction coefficient since it measures the total viscous drag on the plate.

We can find the variation of boundary layer thickness with streamwise distance by using the result for C_F in equation 3.4 to eliminate F_v. For the parabolic profile approximation:

$$\frac{\delta}{L} = \frac{5.48}{\sqrt{Re_L}}.$$

For any position along the plate, therefore,

$$\frac{\delta}{x} = \frac{5.48}{\sqrt{Re_x}}, \tag{3.8}$$

so that the boundary layer thickness grows as $\sqrt{x}$.

The total skin friction coefficient C_F expresses the magnitude of the viscous <u>force</u> on a plate of width w and length L. We can find the local shear <u>stress</u> variation from equations 3.6 and 3.8. For the parabolic velocity profile:

$$C_f = \frac{0.73}{\sqrt{Re_x}}$$

where the local skin friction coefficient C_f is defined as

$$C_f \equiv \frac{\tau_w}{\frac{1}{2}\rho U_e^2}. \tag{3.9}$$

C_f is called the *local* skin friction coefficient since it measures the local viscous stress on the plate. The stress at the wall decreases with distance downstream because the velocity gradient at the wall decreases as a result of the boundary layer growth.

We can compare these approximate results with the "exact" results obtained by Blasius, who found that

$$\boxed{C_F = \frac{1.328}{\sqrt{Re_L}}, \qquad \frac{\delta}{L} = \frac{5.0}{\sqrt{Re_L}} \qquad \text{and} \quad C_f = \frac{0.664}{\sqrt{Re_x}}.} \tag{3.10}$$

We see that the parabolic velocity profile approximation gave the correct dependence on Reynolds number (that is, it gave the correct scaling), but the skin friction coefficients were about 10% low and the boundary layer thickness was about 10% high.

3.2   Boundary Layer Approximation

Here we derive the boundary layer approximation. Consider constant density, two-dimensional flow. When the boundary layer is thin, compared to some characteristic length of the boundary layer ($\delta/L \ll 1$), then certain approximations to the Navier-Stokes equations are possible. These approximations follow from an order-of-magnitude analysis of the full equations, which begin by making the equations non-dimensional with respect to the characteristic dimensions and velocities of the flow field.

δ = characteristic length scale for variations in the y-direction

L = characteristic length scale for variations in the x-direction (it is the distance over which the velocity U in the x-direction changes appreciably).

U, V = characteristic velocity scales in the x- and y-directions, representative of the velocity differences across the layer, as given by the characteristic freestream velocity components.

Write the non-dimensional variables

$$u' = \frac{u}{U}, \qquad v' = \frac{v}{V}$$
$$x' = \frac{x}{L}, \qquad y' = \frac{y}{\delta}$$
$$p' = \frac{p - p_0}{\rho U^2}, \qquad t' = \frac{tU}{L}$$

The continuity equation becomes

$$\frac{\partial u'}{\partial x'} + \left(\frac{L}{\delta}\right)\left(\frac{V}{U}\right)\left(\frac{\partial v'}{\partial y'}\right) = 0.$$

If we have non-dimensionalized correctly (that is, if we have chosen the characteristic scaling parameters in a way that is representative of the problem), then all non-dimensional derivatives are of the same order, and hence

$$\left(\frac{V}{U}\right) = \mathbf{O}\left(\frac{\delta}{L}\right).$$

The momentum equation in the x-direction becomes

$$\frac{\partial u'}{\partial t'} + u'\frac{\partial u'}{\partial x'} + \left(\frac{V}{U}\right)\left(\frac{L}{\delta}\right)v'\frac{\partial u'}{\partial y'} = -\frac{\partial p'}{\partial x'} + \frac{1}{Re}\left(\frac{\partial^2 u'}{\partial x'^2} + \left(\frac{L}{\delta}\right)^2\frac{\partial^2 u'}{\partial y'^2}\right)$$

where $Re = UL/\nu$. We can see that, from the continuity equation, all terms on the left hand side of the momentum equation are of the same order. On the right hand side, inside the brackets, we see that the first term is much smaller than the second term, when $\delta/L \ll 1$, and it is therefore neglected in further analysis.

The boundary layer is the region where the inertia terms (the left hand side of the momentum equation) and the viscous terms (the second term on the right hand side) are of the same order. If the derivatives have been non-dimensionalized appropriately, we see that

$$\frac{1}{Re} = \mathbf{O}\left(\frac{\delta}{L}\right)^2, \quad \text{that is,} \quad \frac{\delta}{L} = \mathbf{O}\frac{1}{\sqrt{Re}}.$$

As the Reynolds number becomes large, this relationship becomes more exact, since the boundary layer approximations made in this analysis become more exact as the Reynolds number increases. The momentum equation in the x-direction becomes

$$\frac{\partial v'}{\partial t'} + u'\frac{\partial v'}{\partial x'} + \left(\frac{V}{U}\right)\left(\frac{L}{\delta}\right)u'\frac{\partial v'}{\partial y'} = -\left(\frac{U}{V}\right)\left(\frac{L}{\delta}\right)\frac{\partial p'}{\partial y'} + \frac{1}{Re}\left(\frac{\partial^2 v'}{\partial x'^2} + \left(\frac{L}{\delta}\right)^2\frac{\partial^2 v'}{\partial y'^2}\right).$$

With

$$\frac{V}{U}\frac{L}{\delta} = \mathbf{O}\,(1), \quad \frac{\delta}{L} \ll 1, \quad \text{and} \quad \frac{1}{Re} = \mathbf{O}\left(\frac{\delta}{L}\right)^2,$$

we see that the pressure gradient term is very much larger than all the other terms, so that

$$\frac{\partial p}{\partial y} = 0.$$

Thus the pressure is approximately uniform across the boundary layer. The pressure is said to be "impressed" on the boundary layer by the outer, inviscid flow. Near the edge of the layer, the viscous terms must vanish as we approach the inviscid flow, and all velocity gradients in the y-direction must be small, and the x-momentum equation reduces to

$$\frac{\partial U_e}{\partial t} + U_e\frac{\partial U_e}{\partial x} = -\frac{1}{\rho}\frac{\partial p}{\partial x}$$

and for steady flow we get

$$\frac{p}{\rho} + \tfrac{1}{2}U_e^2 = \text{constant}$$

along the streamlines at the outer edge of the boundary layer (the subscript e is used to emphasize the fact that U_e is the velocity at the edge of the layer). Clearly, p can now be regarded as an externally applied boundary condition rather than as an independent variable.

Finally, we have Prandtl's boundary layer equations for two-dimensional, constant density, constant property flow:

$$\frac{\partial u}{\partial t} + u\frac{\partial u}{\partial x} + v\frac{\partial u}{\partial y} = -\frac{1}{\rho}\frac{\partial p}{\partial x} + v\frac{\partial^2 u}{\partial y^2} \tag{3.11}$$

$$0 = -\frac{1}{\rho}\frac{\partial p}{\partial y} \tag{3.12}$$

$$\frac{\partial u}{\partial x} + \frac{\partial v}{\partial y} = 0 \tag{3.13}$$

with the boundary conditions

$$y = 0, \quad u = 0, \quad v = 0$$
$$y = \infty \quad u = U(x, t).$$

3.3 General Observations

<u>First</u>, the boundary layer equation is a second order partial differential equation of parabolic type (unlike the full equation of motion which is elliptic in x and y), and allows straightforward integration with respect to x. Consequently, conditions at any value of x are determined by the upstream history of the boundary layer (when dp/dx is a specified function of x). Note that such an equation cannot describe flows where the boundary layer separates, that is, where there is backflow near the wall and the conditions at x are determined by the upstream <u>and</u> downstream conditions.

<u>Second</u>, from the boundary layer equations, at $y = 0$, where $u = v = 0$,

$$\frac{dp}{dx} = \mu \left.\frac{\partial^2 u}{\partial y^2}\right|_0.$$

That is, the curvature of the velocity profile at the wall is determined by the pressure gradient (figure 3.6).

(a) For $dp/dx = 0$, the curvature of the velocity profile at the wall is zero, and the velocity gradient is constant there. Further from the wall, it must decrease to zero as the edge of the boundary layer is approached.

(b) For $dp/dx < 0$ (accelerating flow: a "favorable" pressure gradient), the curvature of the velocity profile at the wall is negative, and the velocity gradient continually decreases away from the wall.
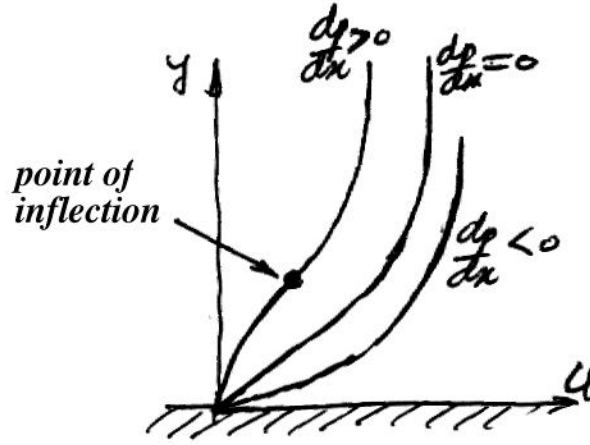
Figure 3.6: Laminar boundary layer profiles in zero, favorable and adverse pressure gradients.

(c) For $dp/dx > 0$ (decelerating flow: an "adverse" pressure gradient), the curvature of the velocity profile at the wall is positive, that is, the velocity gradient increases with distance from the wall. Since the velocity gradient must eventually decrease to zero at the edge of the boundary layer, there must be an "inflection" point in the profile. The pressure force acting on a fluid element due to an adverse pressure gradient acts in a direction opposite to the flow direction, and therefore retards the velcoity of any fluid element. The pressure gradient acts with the same magnitude on all fluid elements within the boundary layer (within the boundary layer approximation), and therefore if the pressure gradient is strong enough those elements next to the wall will be stopped first, and turned around in the direction of the pressure gradient (since they have the least momentum). Therefore, under the action of a persistent adverse pressure gradient (in laminar flows it does not have to be very large), the flow will "separate," that is, a reverse flow region forms (figure 3.7).

Third, the shear stress in a two-dimensional boundary layer is given by

$$\tau = \mu \left(\frac{\partial u}{\partial y} + \frac{\partial v}{\partial x} \right).$$

Non-dimensionally,

$$\frac{\tau}{U\mu/\delta} = \frac{\partial u'}{\partial y'} + \left(\frac{V}{U} \right) \left(\frac{\delta}{L} \right) \frac{\partial v'}{\partial x'}$$

Clearly,

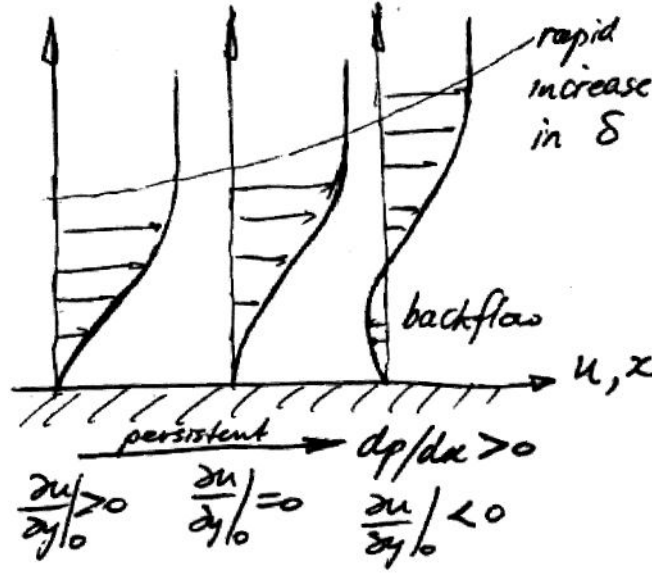$$\tau = \mu \frac{\partial u}{\partial y}$$

Figure 3.7: Laminar boundary layer separating in a persistent adverse pressure gradient.

is a very good approximation.

3.4 Blasius Solution

Here we solve the boundary layer equation for two-dimensional flow over a very thin flat plate, where the freestream velocity U_∞ is (initially) parallel to the plate. The velocity of the potential flow is constant in this case, and therefore $dp/dx = 0$. The boundary layer equation becomes

$$\frac{\partial u}{\partial t} + u\frac{\partial u}{\partial x} + v\frac{\partial u}{\partial y} = \nu\frac{\partial^2 u}{\partial y^2} \tag{3.14}$$

$$\frac{\partial u}{\partial x} + \frac{\partial v}{\partial y} = 0 \tag{3.15}$$

with the boundary conditions

$$y = 0, \quad u = v = 0$$
$$y = \infty \quad u = U_\infty.$$

Because these equations are parabolic, they could be solved by finite-difference techniques, marching downstream in the x-direction. Alternatively, a similarity solution was first derived by Blasius (1908), who recognized that a useful first step is to combine the momentum equation and the continuity

equation using the stream function

$$u = \frac{\partial \psi}{\partial y}, \qquad v = -\frac{\partial \psi}{\partial x},$$

so that the continuity equation is satisfied identically. Thus we get

$$\frac{\partial \psi}{\partial y}\frac{\partial^2 \psi}{\partial x \partial y} - \frac{\partial \psi}{\partial x}\frac{\partial^2 \psi}{\partial y^2} = \nu \frac{\partial^3 \psi}{\partial y^3}.$$

We now introduce the non-dimensional distance from the wall, $\eta = y/\Delta$, where Δ is the characteristic length scale for the viscous layer. With U_∞ as the characteristic velocity scale,

$$\eta = \frac{y}{\Delta} = \frac{y}{\sqrt{\nu t}} = y\sqrt{\frac{U_\infty}{\nu x}}.$$

To non-dimensionalize the stream function, we can use the same variables, so that

$$\psi^* = \frac{\psi}{U_\infty \Delta} = \frac{\psi}{\sqrt{U_\infty \nu x}} = f(\eta)$$

where we note that for the similarity solution to work, $\psi^* = f(\eta)$, that is, ψ^* is a function of η only. Hence $u/U_\infty = F(\eta)$, rather than $u/U_\infty = F(U_\infty x/\nu, y/x)$. That is,

$$\frac{u}{U_\infty} = \frac{df}{d\eta} = f'(\eta)$$

$$\text{and} \qquad \frac{v}{U_\infty}\sqrt{\frac{U_\infty x}{\nu}} = \frac{1}{2}(\eta f' - f).$$

Finally

$$ff'' + 2f''' = 0, \tag{3.16}$$

with boundary conditions

$$\eta = 0, \qquad f = f' = 0$$
$$\eta = \infty \qquad f' = 1.$$

The tabulated solutions for f, f' and f'' are given in table 3.2 and $f' = u/U_\infty$ and v/U_∞ are plotted in figures 3.8 and 3.9, respectively.

Transverse velocity

Note that, as $\eta \to \infty$, $v = 0.8604 U_\infty \sqrt{\frac{\nu}{x U_\infty}}$, which means that at the outer edge of the boundary layer there is flow outward, due to the fact that the increasing boundary layer thickness causes the fluid to be displaced from the wall as it flows along it. That is, the streamlines in the boundary layer diverge.

$\eta = y\sqrt{\dfrac{U_\infty}{\nu x}}$	f	$f' = \dfrac{u}{U_\infty}$	f''
0	0	0	0·33206
0·2	0·00664	0·06641	0·33199
0·4	9·02656	0·13277	0·33147
0·6	0·05974	0·19894	0·33008
0·8	0·10611	0·26471	0·32739
1·0	0·16557	0·32979	0·32301
1·2	0·23795	0·39378	0·31659
1·4	0·32298	0·45627	0·30787
1·6	0·42032	0·51676	0·29667
1·8	0·52952	0·57477	0·28293
2·0	0·65003	0·62977	0·26675
2·2	0·78120	0·68132	0·24835
2·4	0·92230	0·72899	0·22809
2·6	1·07252	0·77246	0·20646
2·8	1·23099	0·81152	0·18401
3·0	1·39682	0·84605	0·16136
3·2	1·56911	0·87609	0·13913
3·4	1·74696	0·90177	0·11788
3·6	1·92954	0·92333	0·09809
3·8	2·11605	0·94112	0·08013
4·0	2·30576	0·95552	0·06424
4·2	2·49806	0·96696	0·05052
4·4	2·69238	0·97587	0·03897
4·6	2·88826	0·98269	0·02948
4·8	3·08534	0·98779	0·02187
5·0	3·28329	0·99155	0·01591
5·2	3·48189	0·99425	0·01134
5·4	3·68094	0·99616	0·00793
5·6	3·88031	0·99748	0·00543
5·8	4·07990	0·99838	0·00365
6·0	4·27964	0·99898	0·00240
6·2	4·47948	0·99937	0·00155
6·4	4·67938	0·99961	0·00098
6·6	4·87931	0·99977	0·00061
6·8	5·07928	0·99987	0·00037
7·0	5·27926	0·99992	0·00022
7·2	5·47925	0·99996	0·00013
7·4	5·67924	0·99998	0·00007
7·6	5·87924	0·99999	0·00004
7·8	6·07923	1·00000	0·00002
8·0	6·27923	1·00000	0·00001
8·2	6·47923	1·00000	0·00001
8·4	6·67923	1·00000	0·00000
8·6	6·87923	1·00000	0·00000
8·8	7·07923	1·00000	0·00000

Table 3.2: The function $f(\eta)$ for a laminar boundary layer along a flat plate at zero incidence, from Howarth (1938).

Skin friction

The drag on one side of a flat plate of length L and width w is given by

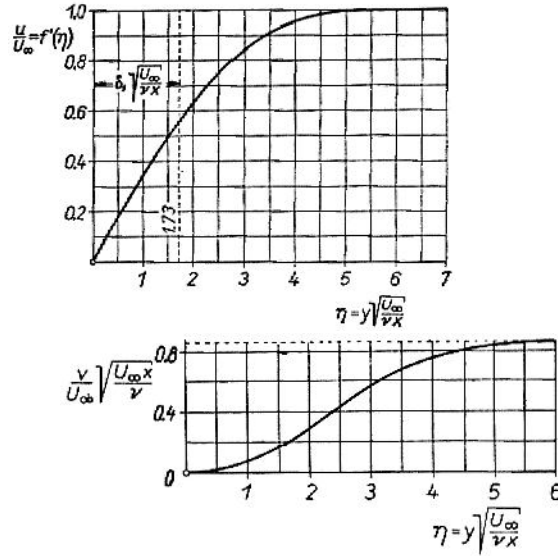$$D \;=\; w \int_0^L \tau_w \, dx. \tag{3.17}$$

Figure 3.8: Velocity distribution in a laminar boundary layer along a flat plate, from Blasius (1908).

Figure 3.9: Transverse velocity distribution in a laminar boundary layer along a flat plate, from Blasius (1908).

The local shear stress at the wall τ_w is given by

$$\tau_w(x) = \mu \left.\frac{\partial u}{\partial y}\right|_{y=0} = \mu U_\infty \sqrt{\frac{U_\infty}{\nu x}} f''(0) = 0.332 \mu U_\infty \sqrt{\frac{U_\infty}{\nu x}}$$

where the value of $f''(0)$ was taken from table 3.2. The dimensionless shear stress becomes

$$\frac{\tau_w}{\rho U_\infty^2} = \frac{1}{2}C_f = 0.332\sqrt{\frac{\nu}{U_\infty x}} = \frac{0.332}{\sqrt{Re_x}}. \qquad (3.18)$$

From equation 3.17 we obtain the drag on one side

$$D = 0.332\mu w U_\infty \sqrt{\frac{U_\infty}{\nu}} \int_0^L \frac{dx}{\sqrt{x}} = 0.664 w U_\infty \sqrt{\mu \rho L U_\infty}$$

so that, for one side, the total skin friction coefficient becomes

$$C_F = \frac{D}{\frac{1}{2}\rho U_\infty^2 A} = \frac{0.664}{\sqrt{Re_L}}. \qquad (3.19)$$

Convective terms

The convective terms near the wall are small and of opposite sign. We can write

$$\frac{u\frac{\partial u}{\partial x}}{v\frac{\partial u}{\partial y}} = -\frac{1}{1 - \left(\frac{f}{\eta f'}\right)}$$

and

$$\frac{f}{\eta f'} = \begin{array}{ll} 0.50 & \text{for } \eta = 1 \\ 0.52 & \text{for } \eta = 2 \\ 0.55 & \text{for } \eta = 3, \end{array}$$

so that

$$u\frac{\partial u}{\partial x} \approx -2v\frac{\partial u}{\partial y} \quad \text{for } y < \frac{\delta}{2}.$$

Boundary layer thickness

The most common definition of the boundary layer thickness is

$$U = 0.99 U_e \quad \text{at} \quad y = \delta.$$

We see that

$$\delta = 4.92 \sqrt{\frac{vx}{U_\infty}},$$

$$\text{that is} \quad \frac{\delta}{x} = \frac{4.92}{\sqrt{Re_x}}. \tag{3.20}$$

Two other thicknesses can be defined, the displacement thickness δ^*, and the momentum thickness θ.

Displacement thickness

We can also define a "displacement thickness" δ^*, which can be thought of as the distance through which the streamlines just outside the boundary layer are displaced laterally by the retardation of fluid in the boundary layer. The decrease in volume flow rate due to the influence of friction is $\int_0^\infty (U_\infty - u)\, dy$, so that δ^* is defined by

$$U_\infty \delta^* = \int_0^\infty (U_\infty - u)\, dy,$$

$$\text{so that} \quad \delta^* = \int_0^\infty \left(1 - \frac{u}{U_\infty}\right) dy. \tag{3.21}$$
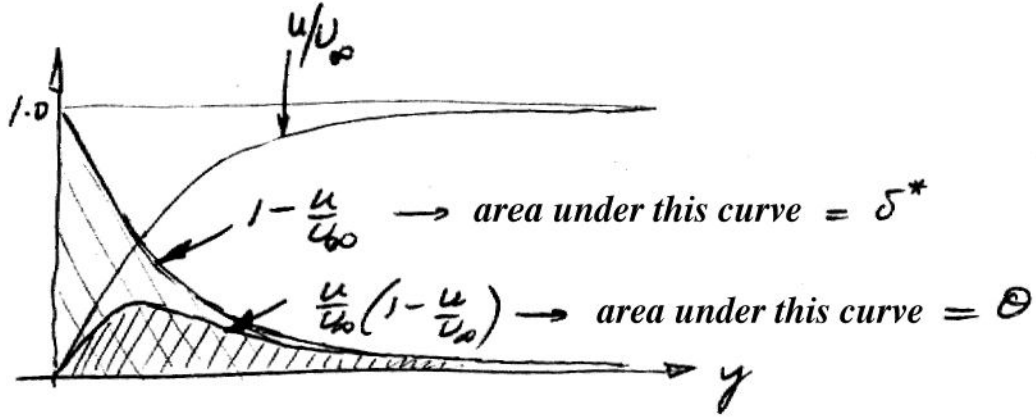
Figure 3.10: The velocity profile and its contribution to the evaluation of the displacement and momentum thicknesses.

For the Blasius boundary layer,

$$\delta^* \;=\; \sqrt{\frac{\nu x}{U_\infty}} \int_0^\infty (1 - f') \, d\eta \;=\; \sqrt{\frac{\nu x}{U_\infty}} \, (\eta_1 - f(\eta_1))$$

where $\eta_1 > 5$ (so that it is outside the boundary layer), and we find

$$\frac{\delta^*}{x} \;=\; \frac{1.721}{\sqrt{Re_x}}. \tag{3.22}$$

Figure 3.10 shows how the integrand contributes to the integral.

Momentum thickness

The loss of momentum in the boundary layer, as compared with potential flow, is given by $\rho \int_0^\infty u\,(U_\infty - u)\,dy$ so that a "momentum thickness" θ may be defined by

$$\rho U_\infty^2 \theta \;=\; \rho \int_0^\infty u\,(U_\infty - u)\,dy,$$

$$\text{so that} \qquad \theta \;=\; \int_0^\infty \frac{u}{U_\infty}\left(1 - \frac{u}{U_\infty}\right) dy. \tag{3.23}$$

For the Blasius boundary layer we find

$$\frac{\theta}{x} \;=\; \frac{0.664}{\sqrt{Re_x}}. \tag{3.24}$$

Figure 3.10 shows how the integrand contributes to the integral.

Shape factor

By definition, $\theta < \delta^*$, and so the ratio δ^*/θ, called the "shape factor" H is always greater than unity. For the Blasius boundary layer, $H = 2.59$.

Experiments

Experiments are in good agreement with the Blasius solution (justifying the assumptions made) as long as the Reynolds number based on x (xU_∞/ν) is less than about 50,000 to 100,000, where the boundary layer is always laminar. laminar flow can persist to higher Reynolds numbers (see, for example, figure 3.4), but at some value the boundary layer will become turbulent, and the preceding analysis no longer holds.

3.5 General Similarity Scaling

In examining the Rayleigh problem, viscous stagnation point flow, and the flat plate (zero pressure gradient) boundary layer equations, we saw how similarity methods combine two independent variables into one, thereby turning a partial differential equation into an ordinary differential equation. Falkner and Skan (1931) investigated the general laminar boundary layer equations to see what specific external flows ($U_e(x)$) would also allow similarity solutions.

They assumed that the non-dimensional wall distance

$$\eta = \frac{y}{\Delta(x)}$$

where $\Delta(x)$ is to be determined. Similarly, the stream function was non-dimensionalized according to

$$\psi^* = \frac{\psi}{U_e(x)\Delta(x)} = f(\eta)$$

where $U_e(x)$ is also to be determined. Hence,

$$\frac{u}{U_e} = \frac{df}{d\eta} = f'$$

$$\text{and} \quad \frac{v}{U_e} = \frac{d\Delta}{dx}\eta f' - \frac{1}{U_e}\frac{dU_e\Delta}{dx}f.$$

Substituting in the boundary layer equation for steady two-dimensional flow

$$u\frac{\partial u}{\partial x} + v\frac{\partial u}{\partial y} = U_e\frac{dU_e}{dx} + \nu\frac{\partial^2 u}{\partial y^2}$$

gives

$$f''' + \alpha f f'' + \beta \left(1 - f'^2\right) = 0$$

where

$$\alpha = \frac{\Delta}{\nu} \frac{d}{dx} (U_e \Delta)$$

$$\text{and} \quad \beta = \frac{\Delta^2}{\nu} \frac{dU_e}{dx}.$$

This equation will only be an ordinary differential equation if α and β are in-dependent of x. The conditions under which this occurs defines the possible external flows which have similarity solutions. Note that

$$2\alpha - \beta = \frac{1}{\nu} \frac{d}{dx} \left(\Delta^2 U_e\right),$$

$$\text{that is} \quad (2\alpha - \beta) x = \frac{1}{\nu} \Delta^2 U_e$$

(the integration constant is arbitrary and was put to zero — it simply defines the origin for x). Hence,

$$\Delta = \sqrt{\frac{(2\alpha - \beta) \nu x}{U_e}}.$$

The factor $2\alpha - \beta$ can take any value, since it is just another scaling factor[1]. the important thing is that α and β are independent of x. To be consistent with the flat plate boundary layer solution, we put $2\alpha - \beta = +1$ (if $\frac{x}{U_e} < 0$, we use -1). Other people (for example, Schlichting, White) use $\alpha = 1$, so that their Δ is $\sqrt{2 - \beta}$ times ours. Hence,

$$\Delta = \sqrt{\frac{\nu x}{U_e}}$$

as in the flat plate boundary layer solution. What about U_e? From the definition of β, we now get

$$\beta = \frac{x}{U_e} \frac{dU_e}{dx}.$$

$$\text{Hence} \quad \frac{U_e}{U_0} = \left(\frac{x}{L}\right)^{\beta} \tag{3.25}$$

where U_0 and L are arbitrary constants ($U_e = U_0$ at $x = L$). Thus similarity solutions of the boundary layer equations are obtained when the velocity

---

[1]If y/Δ is a similarity variable, then $y/(\Delta \times \text{constant})$ is also a similarity variable. To avoid difficulties with η, $2\alpha - \beta \neq 0$.

distribution of the external potential flow is proportional to a power of the distance from the stagnation point.

Hence we get the ordinary differential equation for the non-dimensional stream function

$$f''' + \tfrac{1}{2}(\beta + 1) f f'' + \beta \left(1 - f'^2\right) = 0 \tag{3.26}$$

with boundary conditions

$$\eta = 0, \quad f = f' = 0$$
$$\eta = \infty \quad f' = 1.$$

Note that when different scaling factors were chosen so that $\alpha' = 1$, then $\beta' = \frac{2\beta}{\beta+1}$, and the differential equation becomes

$$f''' + f f'' + \beta' \left(1 - f'^2\right) = 0$$

with the same boundary conditions as before.

Equation 3.26 is a third order, nonlinear ordinary differential equation and we have to worry about non-uniqueness, for example. There exist a wide variety of flow fields that have a potential velocity field modeled by $\frac{U_e}{U_0} = \left(\frac{x}{L}\right)^{\beta}$.

Particular cases

See figure 3.11.

(1) $\beta = 1$ ($\alpha' = 1$, $\beta' = 1$): viscous stagnation point flow, where $U_e = x$.

(2) $\beta = 0$ ($\alpha' = 1$, $\beta' = 0$): U_e = constant, flat plate, zero pressure gradient boundary layer.

(3) $0 \leq \beta \leq \infty$ ($\alpha' = 1$, $0 \leq \beta' \leq 2$): flow past a wedge of angle $\beta'\pi$.

(4) $\beta = -1$ ($\beta' = \infty$): for $U_0 > 0$, flow toward a point sink (Jeffery-Hamel flow in a convergent wedge).

(5) $\beta = -\tfrac{1}{2}$ ($\beta' = -2$): the "fullness" of the profiles decreases, and at $\beta = -0.091$ ($\beta = -0.19884$), $f''(0) = 0$. Called "incipient separation." There are generally two solutions in the range $-0.091 < \beta < 0$, and for $\beta < -0.091$ there exist whole families of solutions.
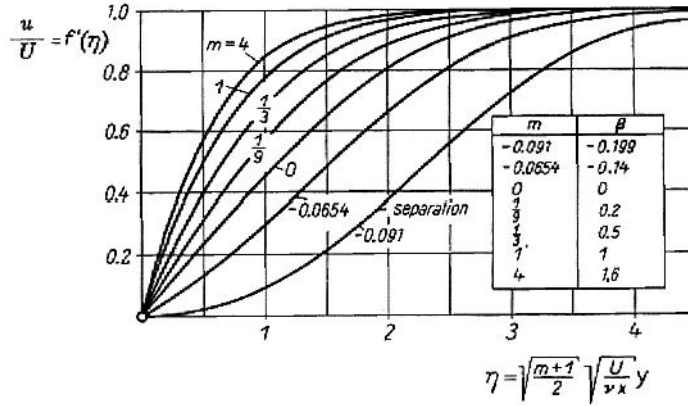
Figure 3.11: Velocity distributions in the laminar boundary layer flow past a wedge (here $m = \beta$). From Schlichting.

3.6   Displacement and Momentum Thickness

As we noted earlier, the velocity U near the edge of the boundary layer approaches the freestream value U_e asymptotically, so that the boundary layer thickness δ is defined to be the distance where the U is "close enough" to U_e. The most common definition of the boundary layer thickness is

$$U = 0.99U_e \quad \text{at} \quad y = \delta.$$

Two other thicknesses were defined, the displacement thickness δ^*, and the momentum thickness θ. Here we consider δ^* and θ in more detail.

3.6.1   Displacement thickness

By definition, the displacement thickness is given by

$$\delta^* \equiv \int_0^\infty \left(1 - \frac{U}{U_e}\right) dy. \tag{3.27}$$

What does this mean, and why is this useful? Equation 3.27 can be rewritten as

$$\rho U_e^2 \delta^* = \int_0^\infty \rho \left(U_e - U\right) dy$$

so that the mass flux passing through the distance δ^* in the absence of a boundary layer is the same as the deficit in mass flux due to the presence of the boundary layer. To make this point further, consider a velocity profile
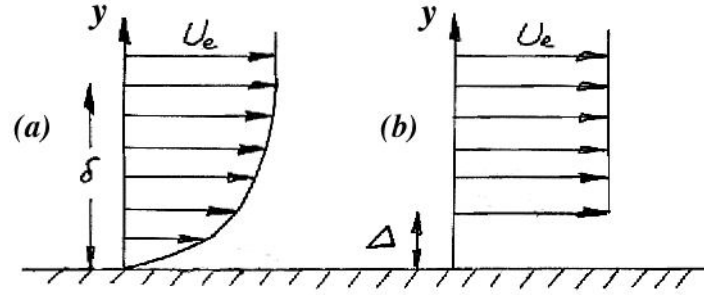
Figure 3.12: Displacement thickness: (a) Velocity profile; (b) Interpretation.
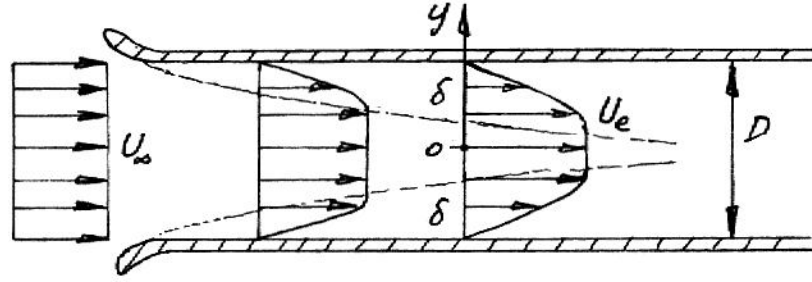
Figure 3.13: Flow in the entrance region of a two-dimensional duct.

where $U = 0$ for $y \leq \Delta$, and $U = U_e$ for $y > \Delta$ (see figure 3.12). For this profile,

$$\delta^* = \int_0^\infty \left(1 - \frac{U}{U_e}\right) dy = \int_0^\Delta dy = \Delta.$$

Therefore, from the point of view of the flow outside the boundary layer, δ^* can be interpreted as the distance that the presence of the boundary layer appears to "displace" the surface outward (hence the name).

To illustrate an application of this concept, consider the entrance region of a two-dimensional duct of width w and height D. The flow is steady and incompressible. Boundary layers will grow on the top and bottom surfaces, as shown in figure 3.13. By continuity, if the flow near the wall is slowed down, the fluid outside the boundary layers (in the "core" region), must speed up. If the incoming velocity has a value U_∞, what is the core velocity U_e at a point where the boundary layer thickness is δ? Take a control volume extending from the entrance plane to the location of interest. The continuity equation gives

$$-U_\infty wD + \int_{-D/2}^{D/2} U\,wdy = 0.$$

$$\text{So,} \qquad U_\infty D \;=\; \int_{-D/2}^{D/2} U_e \, dy - \int_{-D/2}^{D/2} (U_e - U) \, dy$$

$$U_\infty D \;=\; U_e D - 2U_e \int_{(D/2)-\delta}^{D/2} \left(1 - \frac{U}{U_e}\right) dy.$$

That is,

$$U_e \;=\; U_\infty \left(\frac{D}{D - 2\delta^*}\right),$$

where we have made the approximation, that as far as the contribution to the displacement thickness is concerned, $\delta \approx \infty$. This assumption is commonly made. We see that the increase in the freestream velocity is given by the effective decrease in the cross-sectional area due to the growth of the boundary layers, and this decrease in area is measured by the displacement thickness.

3.6.2   Momentum thickness

By definition, the momentum thickness is given by

$$\theta \equiv \int_0^\infty \frac{U}{U_e} \left(1 - \frac{U}{U_e}\right) dy \qquad\qquad (3.28)$$

What does this mean, and why is this useful? Equation 3.28 can be rewritten as

$$\rho U_e \theta = \int_0^\infty \rho U \left(U_e - U\right) dy$$

so that the momentum flux passing through the distance θ in the absence of a boundary layer is the same as the deficit in momentum flux due to the presence of the boundary layer.

To illustrate this concept, we return to the analysis of the laminar, two-dimensional boundary layer. We start by rewriting equation 3.2 as

$$\frac{F_v}{\rho w U_e^2} = \int_0^\delta \frac{U}{U_e} \left(1 - \frac{U}{U_e}\right) dy.$$

If we make the approximation, that as far as the contribution to the momentum thickness is concerned, $\delta \approx \infty$, then

$$\frac{F_v}{\rho w U_e^2} = \theta,$$

so that

$$F_v = \rho U_e^2 \, w\theta.$$

Therefore the momentum flux passing through the cross-sectional area $w\theta$ at $x = L$, say, in the absence of a boundary layer is a measure of the drag on a plate of width w and length L due to the presence of the boundary layer. We can also differentiate this relationship and use equation 3.5 to obtain

$$\frac{d\theta}{dx} = \frac{\tau_w}{\rho U_e^2}.$$

That is,

$$\boxed{\frac{d\theta}{dx} = \frac{C_f}{2},} \tag{3.29}$$

where the local skin friction coefficient C_f was defined in equation 3.9. So the non-dimensional local frictional stress at the wall is equal to the rate of change of the momentum thickness with distance. Equation 3.29 is called the *momentum integral equation* for a boundary layer in a zero pressure gradient. Although we did not show it, this equation applies to laminar and turbulent boundary layers.

3.6.3 Shape factor

Another term that is often encountered in discussions of boundary layer behavior is the *form* or *shape* factor H, where H is defined as the ratio of the displacement thickness to the momentum thickness:

$$H \equiv \frac{\delta^*}{\theta}.$$

Since $\delta^* > \theta$, $H > 1$. For a laminar boundary layer, $H = 2.59$, and for a turbulent boundary layer $1.15 < H < 1.4$, where H decreases with the Reynolds number. Smaller values of H indicate a "fuller" velocity profile (that is, one that is more filled in near the wall). The reduced shape factor for turbulent flow reflects the fact that turbulent boundary layers have fuller velocity profiles.

3.6.4 Momentum integral equation

We begin by integrating the boundary layer equations from the wall to a point h outside the boundary layer. That is,

$$\rho \int_0^h \left(u \frac{\partial u}{\partial x} + v \frac{\partial u}{\partial y} - U_e \frac{dU_e}{dx} \right) dy = -\tau_w$$

since

$$\int_0^h \mu \frac{\partial^2 u}{\partial y^2} dy = \left[\mu \frac{\partial u}{\partial y}\right]_0^2 = -\tau_w.$$

by using the continuity equation,

$$v = -\int_0^y \frac{\partial u}{\partial x} dy,$$

and eventually

$$\mu \frac{d}{dx}\left(U_e^2 \theta\right) + \delta^* U_e \frac{dU_e}{dx} = \frac{\tau_w}{\rho}$$

or

$$\frac{d\theta}{dx} + \theta\,(H+2)\,\frac{1}{U_e}\frac{dU_e}{dx} = \frac{C_f}{2} \tag{3.30}$$

where

$$C_f = \frac{\tau_w}{\frac{1}{2}\rho U_e^2} \quad \text{and} \quad \tau_w = \tau_w = \mu \left.\frac{\partial u}{\partial y}\right|_{y=0}.$$

This is the momentum integral equation for two-dimensional, incompressible boundary layers and it applies to steady laminar <u>and</u> turbulent flows.

For a zero pressure gradient flow,

$$\frac{d\theta}{dx} = \frac{C_f}{2},$$

and we see that, for a single side,

$$C_F = \int_0^L 2\frac{d\theta}{dx} dx = 2\theta_L.$$

That is, the total drag coefficient of a flat plate can be found by measuring the momentum thickness at the trailing edge.

The momentum integral equation has two major uses. First, it is used experimentally to verify that the flow is two-dimensional. If the left hand side equals the right hand side to within a small percentage, then the flow is considered to be two-dimensional. for a zero pressure gradient flow, we usually write the momentum equation as

$$\theta(x) - \theta(x_0) = \frac{1}{2}\int_{x_0}^x C_f(x)\,dx.$$

In a plot of the left hand side versus the right hand side, the data should lie along a 45° slope. Note that the momentum integral equation should not be used to determine C_f from measured values of θ: the value is too sensitive to departures from two-dimensional flow.

Second, it is used in approximate boundary layer calculation methods (such as "profile guessing," Pohlhausen's method, and Thwaites method).

3.7 Other Methods for Solving the Boundary Layer Equations

Similarity solutions are not the only way to solve the boundary layer equations. We also have:

(1) Series Solutions, as in the Blasius Series, the Howarth series, and the Görtler series. These series solutions are used to deal with cases where the equations cannot be cast into similarity form, as in the flow over a cylinder, the flow in a channel with initially parallel walls followed by a convergent or divergent section, and the flow over a flat plate with suction. Details are given in Schlichting chapter 9, and White sections 4.4 and 4.4.1.

(2) Finite Difference Techniques. In explicit techniques, the downstream profile $u(x + \Delta x, y)$ is calculated from $u(x, y)$ by the direct application of a finite difference expression for the streamwise derivative, although these methods require small steps and can easily go unstable. Implicit methods, where the downstream profile is found from a differential equation in the cross-stream direction, are more complicated but they have no stability problems.

(3) Approximate Methods. These are the only methods considered in the sections that follow. They are all based on the momentum integral equation.

3.7.1 Profile guessing methods

For example, with

$$\frac{u}{U_e} = \frac{y}{\delta}$$

which satisfies the boundary conditions of $u = 0$ at $y = 0$, and $u = U_e$ at $y = \delta$, we have

$$\theta = \delta \int_0^1 \eta (1 - \eta) \, d\eta = \tfrac{1}{6}\delta$$

$$\text{and} \quad C_f = \frac{\mu \frac{\partial u}{\partial y}}{\frac{1}{2}\rho U_e^2} = \frac{\mu \frac{U_e}{\delta}}{\frac{1}{2}\rho U_e^2} = \frac{2\nu}{\delta U_e}$$

For zero pressure gradient flow,

$$\frac{d\theta}{dx} = \frac{C_f}{2}$$

$$\text{so that} \quad \frac{d\delta}{dx} = \frac{6\nu}{\delta U_e}.$$

Assumed form for u/u_1	$c_f\sqrt{R_x}$	$C_F\sqrt{R}$	$\frac{\theta}{x}\sqrt{R_x}$	$\frac{\delta^*}{x}\sqrt{R_x}$	$\frac{\delta}{x}\sqrt{R_x}$	H
y/δ	0·577	1·155	0·577	1·732	3·464	3·00
$\frac{3}{2}\frac{y}{\delta} - \frac{1}{2}\left(\frac{y}{\delta}\right)^3$	0·646	1·292	0·646	1·740	4·640	2·70
$2\frac{y}{\delta} - 2\left(\frac{y}{\delta}\right)^3 + \left(\frac{y}{\delta}\right)^4$	0·686	1·372	0·686	1·752	5·840	2·55
$\sin\left(\frac{\pi}{2}\frac{y}{\delta}\right)$	0·654	1·310	0·654	1·741	4·789	2·66
Exact solution	0·664	1·328	0·664	1·721	—	2·59

Table 3.3: Integral parameters for a flat plate laminar boundary layer obtained by approximate methods. From Duncan, Thom & Young.

With $\delta = 0$ at $x = 0$,

$$\int_0^\delta \delta d\delta \ = \ \frac{6\nu}{U_e} \int_0^x dx$$

so that

$$\frac{\delta}{x} \ = \ \frac{\sqrt{12}}{\sqrt{Re_x}} \ = \ \frac{3.464}{\sqrt{Re_x}}$$

$$\text{and} \quad C_f \ = \ \frac{2}{3.464}\frac{1}{\sqrt{Re_x}} \ = \ \frac{0.578}{\sqrt{Re_x}}$$

(see table 3.3).

3.7.2   Pohlhausen method

We <u>assume</u> that the velocity profile can be written as

$$\frac{u}{U_e} = a_0 + a_1\eta + a_2\eta^2 + a_3\eta^3 + a_4\eta^4,$$

where $\eta = y/\delta$. We need five boundary conditions to evaluate the constants $a_0 \to a_4$. We have:

(1) $y = 0$, $u = 0$

(2) $y = \infty$, $u = U_e(x)$

(3) $\nu \left.\frac{\partial^2 u}{\partial y^2}\right|_0 = -U_e\frac{dU_e}{dx}$

(4) $y \to \infty$, $\frac{\partial u}{\partial y} \to 0$

(4) $y \to \infty$, $\frac{\partial^2 u}{\partial y^2} \to 0$

(the last three conditions are actually properties of the solution rather than true boundary conditions). Hence,

$$
\begin{aligned}
a_0 &= 0 \\
a_1 &= 2 + \frac{\Lambda}{6} \\
a_2 &= -\frac{\Lambda}{2} \\
a_3 &= -2 + \frac{\Lambda}{2} \\
a_4 &= 1 - \frac{\Lambda}{6}
\end{aligned}
$$

where Λ is a pressure gradient parameter,

$$
\Lambda = \frac{\delta^2}{\nu} \frac{dU_e}{dx}, \tag{3.31}
$$

representing the ratio of forces due to pressure differences to viscous forces. Finally,

$$
\frac{u}{U_e} = \left(2\eta - 2\eta^3 + \eta^4\right) + \tfrac{1}{6}\Lambda\eta\left(1 - \eta\right)^3 .
$$

Several caveats should be issued. First, the third, fourth and fifth boundary conditions <u>assume</u> something about the expected behavior of the solution. It works when the effects of the pressure gradient (say) on the profile shape are strong. In turbulent boundary layers, the velocity profile shape is affected by the pressure gradient only very near the wall, and the third "boundary condition" would be highly unsuitable. Second, for separating flows, the boundary layer equations themselves break down, and the momentum integral method becomes suspect.

Nevertheless, when the velocity profile shape is known, δ^*, θ can be calculated and the skin friction can be found by eliminating the unknown δ. In addition, since this is an integral method, errors in the velocity profile tend to get washed out, as table 3.3 illustrates for different approximations to the Blasius profile.

$$
\begin{aligned}
\text{Now, when} \quad \Gamma &= 0 && \to \quad \text{flat plate flow} \\
\Gamma &< 0 && \to \quad \text{adverse pressure gradient} \\
\Gamma &> 0 && \to \quad \text{favorable pressure gradient} \\
\Gamma &= -12 \to \quad \left.\frac{\partial u}{\partial y}\right|_w && \to \quad \text{separation}
\end{aligned}
$$
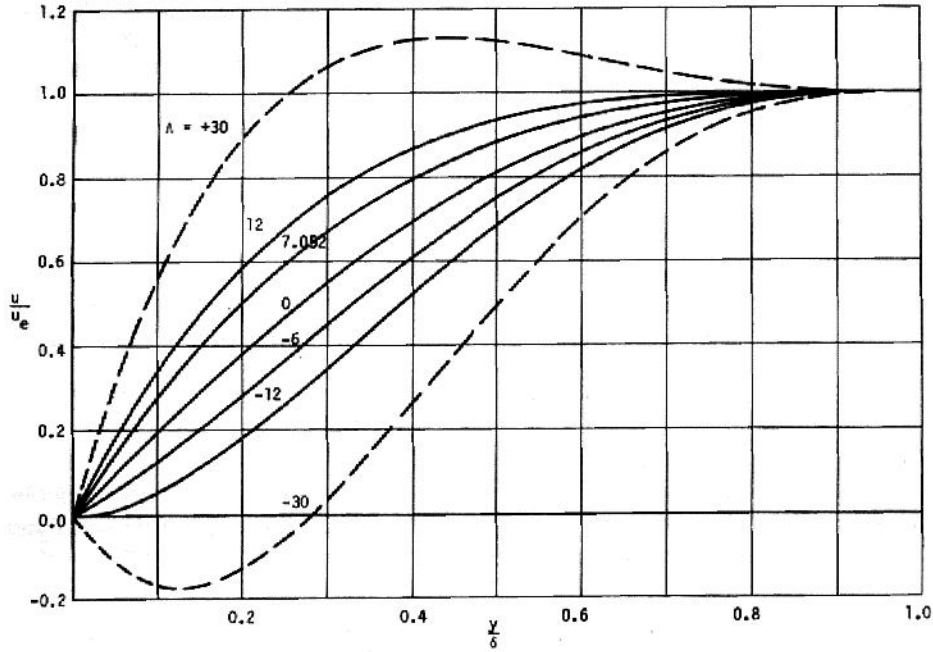
Figure 3.14: Velocity distributions in a laminar boundary layer for different pressure gradients, according to the Pohlhausen solution. From White.

$$\Gamma \; > \; 12 \quad \rightarrow \quad \text{overshoots in profile occur}$$

(see figure 3.14). Despite its limitations, Pohlhausen's method seems to work well for flat plate flow, stagnation point flow, and the accelerating part of flow over a cylinder (although not unexpectedly it breaks down rapidly as the separation point is approached).

3.7.3   Thwaites method

In principle, Thwaites' method is very similar to Pohlhausen's. Pohlhausen used boundary conditions derived from the properties of the solution (in particular, the use of $v \left. \frac{\partial^2 u}{\partial y^2} \right|_0 = -U_e \frac{dU_e}{dx}$) to derive a single profile parameter $\Gamma \; (= \frac{\delta^2}{v} \frac{dU_e}{dx})$ and to develop a "universal" velocity profile description which could then be substituted in the momentum integral relationship to find $\delta(x)$ and C_f. Thwaites bypassed the universal velocity profile idea, and worked directly with the momentum integral equation. He defined a slightly different profile parameter

$$\lambda \; = \; \frac{\theta^2}{v} \frac{dU_e}{dx} \; \left(= \; \frac{\theta^2}{U_e} \left. \frac{\partial^2 u}{\partial y^2} \right|_0 \right).$$
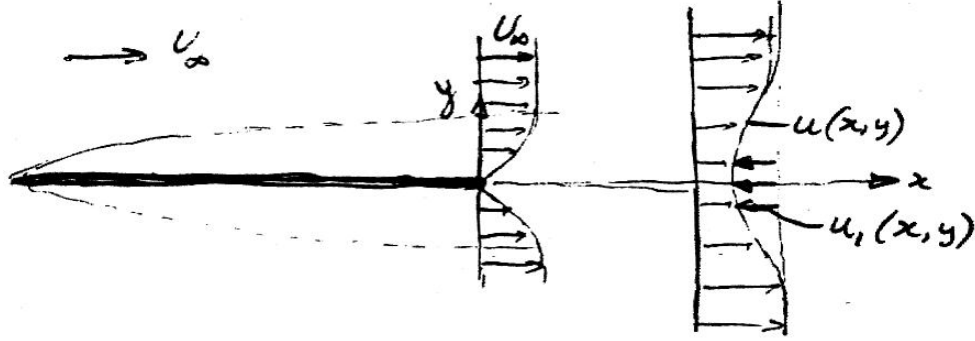
Figure 3.15: Development of a laminar wake downstream of a flat plate at zero incidence.

If we assume that this single parameter describes <u>all</u> boundary layer profiles, it follows that

$$C_f = \frac{2\nu}{U_e\theta}\ell(\lambda) \qquad \left(\text{where} \quad \ell(\lambda) = \left.\frac{\theta}{U_e}\frac{\partial u}{\partial y}\right|_0\right).$$

The momentum integral relationship then reduces to

$$U_e\frac{d\theta^2}{dx} = 2\nu\left(\lambda\left(H+2\right)+\ell\right).$$

Since H must be a unique function of λ, we can write

$$U_e\frac{d\theta^2}{dx} = \nu L(\lambda).$$

It remains to find $\ell(\lambda)$ and $L(\lambda)$. Thwaites used known exact solutions to find these "universal" functions. The method, in general, gives better results than Pohlhausen's in adverse pressure gradients, basically because there are two functions which can be adjusted to favor such flows. See Duncan, Thom & Young, p.273, for a fuller discussion.

3.8   Wake of a Flat Plate

We can also use the boundary layer (or "thin shear layer") approximations in free shear flows where velocity gradients are important in terms of friction, and the convection is strong enough to have slow growth in the direction of the external flow. Examples include the wake of a body at some distance downstream, the flow out of a planar or axisymmetric jet, and the mixing region between two streams of different velocity (a "mixing layer").

Consider the development of a laminar wake downstream of a flat plate at zero incidence (figure 3.15). A similarity solution can be found for $u(x, y)$ if the defect velocity in the wake, u_1 is small compared to U_∞, where

$$u_1(x, y) = U_\infty - u(x, y).$$

Under these conditions, higher order terms drop out, and for a zero pressure gradient the laminar boundary layer equations reduce to

$$-\frac{\partial u_1}{\partial x} + \frac{\partial v}{\partial y} = 0 \tag{3.32}$$

$$-U_\infty \frac{\partial u_1}{\partial x} = \frac{1}{\rho} \frac{\partial \tau}{\partial y} \tag{3.33}$$

where $\tau = -\mu \frac{\partial u_1}{\partial y}$. Note that if we use $\tau = -\mu \frac{\partial u_1}{\partial y} - \rho \overline{u'v'}$ these equations would apply to turbulent flows. The boundary conditions are

$$y = 0, \qquad v = 0, \qquad \frac{\partial u_1}{\partial y} = 0$$

$$y = \infty \qquad u_1 = 0.$$

From the momentum integral equation for the flow over the flat plate we know that, including both sides

$$C_F = \frac{2D}{\frac{1}{2}\rho A U_0^2} = 2\theta_{x=\ell} \tag{3.34}$$

where D is the drag force acting on one side of the plate, and $A = 2w\ell$, where ℓ is the length of the plate. That is,

$$2D = \rho w\ell \int_{-\infty}^{\infty} u \left(U_\infty - u \right) dy.$$

For small defect velocities, this gives

$$2D = \rho w\ell \int_{-\infty}^{\infty} U_\infty u_1 \, dy = \text{constant} = c_0. \tag{3.35}$$

The similarity variables are

$$\eta = \frac{y}{\delta(x)} \quad \text{and} \quad \frac{u_1}{u_c(x)} = f(\eta)$$

where u_c is the centerline velocity defect, so that

$$u = U_\infty - u_c(x) f(\eta).$$

Hence,

$$\frac{\delta^2 U_\infty}{\nu u_c}\frac{du_c}{dx}f - \frac{\delta U_\infty}{\nu}\frac{d\delta}{dx}\eta f' = f'' \tag{3.36}$$

and a similarity solution will be obtained if

$$\frac{\delta^2 U_\infty}{\nu u_c}\frac{du_c}{dx} = \text{constant} = c_1 \tag{3.37}$$

$$\frac{\delta U_\infty}{\nu}\frac{d\delta}{dx} = \text{constant} = c_2. \tag{3.38}$$

One of these constants is arbitrary, so we can put $c_2 = 1$. This gives

$$\delta = \sqrt{\frac{2\nu x}{U_\infty}}. \tag{3.39}$$

and so

$$\eta = \frac{y}{\delta} = y\sqrt{\frac{U_\infty}{2\nu x}}. \tag{3.40}$$

The other constant can be found from the total drag expression given by equation 3.35

$$2D = \rho w \ell \int_{-\infty}^{\infty} U_\infty u_1\, dy = c_0.$$

$$\text{That is,} \quad 2D = -\rho w \ell U_\infty \delta u_c \int_{-\infty}^{\infty} \frac{u_1}{u_c}\, d\frac{y}{\delta} = c_0.$$

That is

$$u_c\delta = -\frac{2D}{\rho w \ell U_\infty \int_{-\infty}^{\infty} f\, d\eta} = \text{constant.} \tag{3.41}$$

Hence

$$u_c = -\frac{A}{\sqrt{x}} \quad \text{where } A = \text{constant.} \tag{3.42}$$

Equations 3.39 and 3.42 show that $c_1 = -1$, and therefore

$$f'' + (\eta f)' = 0. \tag{3.43}$$

The boundary conditions are

$$\eta = 0, \quad f' = 0$$
$$\eta = \infty \quad f = 0.$$

Hence,

$$f(\eta) = B\exp\left(-\eta^2/2\right).$$
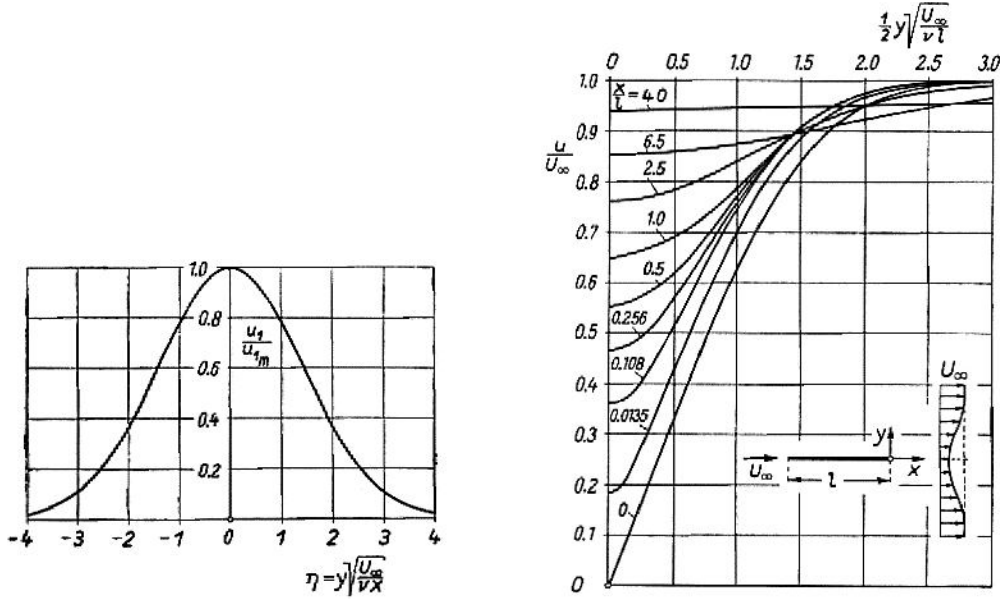
Figure 3.16: Left: Asymptotic velocity distribution in the laminar wake behind a flat plate (similarity coordinates). Right: Approach to asymptotic state in physical variables. From Schlichting.

Equation 3.41, with 3.39 and 3.42 give

$$AB \;=\; -\frac{2D}{\rho w \ell}\,\frac{1}{\sqrt{2\nu U_\infty}}\,\frac{1}{\sqrt{2\pi}}.$$

Hence,

$$u \;=\; U_\infty - \frac{D}{\rho w \ell}\,\frac{1}{\sqrt{\pi \nu U_\infty}}\,\frac{1}{\sqrt{x}}\,\exp\left(-\eta^2/2\right)$$

$$\text{and} \quad 2D \;=\; 1.328 w\,\sqrt{U_\infty^3 \mu \rho \ell}.$$

Finally,

$$\frac{u}{U_\infty} \;=\; 1 - \frac{0.664}{\sqrt{\pi}}\,\sqrt{\frac{x}{\ell}}\,\exp\left(-\eta^2/2\right). \tag{3.44}$$

where the thickness of the plane wake is given by equation 3.39. The velocity distribution in similarity coordinates and the wake development in physical variables is shown in figure 3.16.

3.9   Plane Laminar Jet

Consider a laminar jet emerging from a long, narrow slit and mixing with the surrounding fluid (figure 3.17). Because of friction, the emerging jet

carries with it some of the surrounding fluid which was originally at rest. As a result, the jet spreads out and the centerline velocity decreases. If we neglect pressure gradients, the total momentum in the x-direction remains constant. That is,

$$J = \rho \int_{-\infty}^{\infty} u^2 \, dy = \text{constant}.$$

As usual, we now define the similarity variables

$$\eta = \frac{y}{w}$$

$$\text{and} \quad f = \frac{\psi}{wU_0}.$$

Here we assume

$$w \propto x^q$$

$$\text{and} \quad f \propto x^p.$$

The unknown exponents q and p can be determined from the condition that $J = \text{constant}$, and that the left hand and right hand sides of the x-momentum equation,

$$u\frac{\partial u}{\partial x} + v\frac{\partial u}{\partial y} = v\frac{\partial^2 u}{\partial y^2}$$

are of the same order of magnitude everywhere. This gives $p = -1/3$, $q = 2/3$, and

$$\eta = \frac{1}{3\sqrt{v}}\frac{y}{x^{2/3}}$$

$$f(\eta) = \frac{\psi}{\sqrt{v}x^{1/3}}.$$

$$\text{That is} \quad u = \frac{1}{3x^{1/3}}f'$$

$$v = -\frac{\sqrt{v}}{3}\frac{1}{x^{2/3}}(f - 2\eta f').$$

$$\text{Hence} \quad f'^2 + ff'' + f''' = 0,$$

with the boundary conditions

$$\eta = 0, \quad f = 0, \quad f'' = 0$$
$$\eta = \infty \quad f' = 0.$$

Integrating once gives

$$ff' + f'' = 0.$$
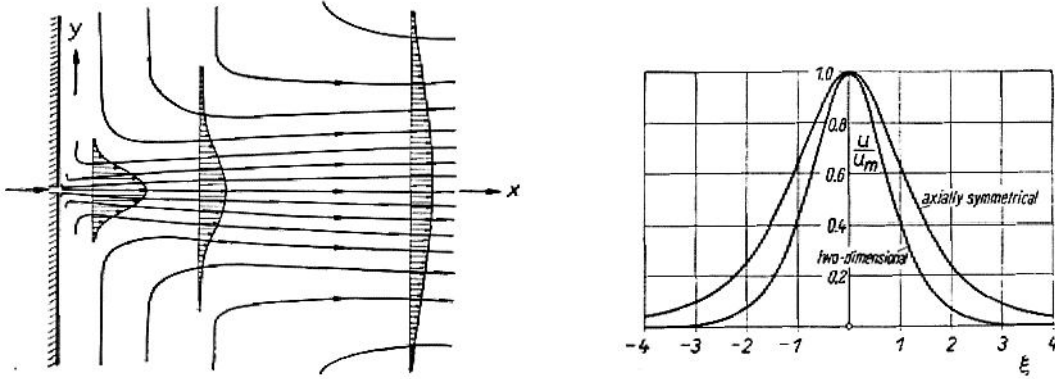
Figure 3.17: Left: Development of a plane jet. Right: Velocity distributions in a two-dimensional and a circular free jet. From Schlichting.

By putting

$$\xi = \alpha\eta, \quad \text{and} \quad f = 2\alpha F(\xi),$$

where α is some constant, and integrating again, we get

$$F' + F^2 = 1.$$

Hence,

$$F = \tanh\xi = \frac{1 - e^{-2\xi}}{1 + e^{-2\xi}}$$

and finally,

$$u = \frac{2}{3}\frac{\alpha^2}{x^{1/3}}\left(1 - \tanh^2\xi\right). \tag{3.45}$$

To find α, we substitute the velocity distribution into the momentum expression $J = $ constant, and so

$$J = \frac{16}{9}\rho\alpha^3\sqrt{\nu},$$

$$\text{that is,} \quad K = \frac{J}{\rho} = \frac{16}{9}\alpha^3\sqrt{\nu}$$

$$\text{so that,} \quad \alpha = 0.8255\frac{K^{1/3}}{\sqrt{\nu}}.$$

The velocity profile in similarity coordinates is shown in figure 3.17, and similar relationships for a variety of laminar jets and wakes are given in table 3.4.
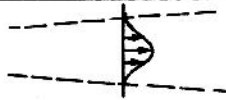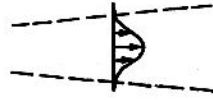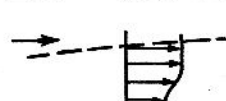
Flow	Sketch	Width, δ	Centerline velocity, $u_c(x)$ or u_1
Two-dimensional jet		$x^{2/3}$	$x^{-1/3}$
Axisymmetric jet		x	x^{-1}
Two-dimensional wake		$x^{1/2}$	$x^{-1/2}$
Axisymmetric wake		$x^{1/2}$	x^{-1}
Two uniform streams		$x^{1/2}$	x^0

Table 3.4: Power laws for width and for centerline velocity of laminar similar free shear layers. From White.

Chapter 4

Compressible Laminar Boundary Layers

For adiabatic, frictionless flow, the energy equation along a streamline gives

$$\rho C_p u \frac{dT}{ds} = u \frac{dp}{ds},$$

that is,

$$C_p (T - T_\infty) = \int_{s_\infty}^{s} \frac{1}{\rho} \frac{dp}{ds} ds = \int_{p_\infty}^{p} \frac{dp}{\rho}.$$

For Bernoulli's equation for compressible flow,

$$\tfrac{1}{2} u^2 + \int \frac{dp}{\rho} = \text{constant}$$

and so,

$$C_p (T - T_\infty) = \tfrac{1}{2} \left(u_\infty^2 - u^2 \right).$$

At a stagnation point, with adiabatic frictionless compression, we obtain

$$\frac{T_0 - T_\infty}{T_\infty} = \frac{(\Delta T)_{ad}}{T_\infty} = \frac{\gamma - 1}{2} M_\infty^2.$$

Thus, at reasonable Mach numbers, the rise in temperature due to adiabatic compression becomes large (for air at $M_\infty = 6$, $\Delta T_{ad} = 2000°$), and since ΔT_{ad} is of the same order of magnitude as the temperature difference across the boundary layer, we can see that the temperature effects will be very important (not that the temperature rise due to friction is of the same order as ΔT_{ad}). For $M_\infty > 6$ dissociation and ionization may become important, and the actual temperature rise may be less than the perfect gas limit.

The variations in temperature cause variations in gas properties, particularly the viscosity μ. It is nearly independent of pressure. A good

approximation to the temperature dependence of μ, between $100°K$ and $1900°K$, is given by Sutherland's formula:

$$\frac{\mu}{\mu_0} = \frac{T_0 + 110.3}{T + 110.3}\left(\frac{T}{T_0}\right)^{3/2}. \tag{4.1}$$

Between $150°K$ to $500°K$, this relationship may be approximated by the formula

$$\frac{\mu}{\mu_0} = \left(\frac{T}{T_0}\right)^m \tag{4.2}$$

Where $m = 0.76$ for air. Similarly, we often use the approximation

$$\frac{k}{k_0} = \left(\frac{T}{T_0}\right)^n. \tag{4.3}$$

Since the Prandtl number $Pr = \mu C_p/k$ is only a weak function of temperature, and C_p is usually taken as a constant for non-hypersonic Mach numbers, $n \approx m$.

4.1   Boundary Layer Approximations

For two-dimensional compressible flow, the equations of motion become

$$\frac{\partial \rho u}{\partial x} + \frac{\partial \rho v}{\partial y} = 0$$

$$\rho\left(u\frac{\partial u}{\partial x} + v\frac{\partial u}{\partial y}\right) = -\frac{\partial p}{\partial x} + \frac{\partial \sigma'_{xx}}{\partial x} + \frac{\partial \sigma'_{xy}}{\partial y}$$

$$\rho\left(u\frac{\partial v}{\partial x} + v\frac{\partial v}{\partial y}\right) = -\frac{\partial p}{\partial y} + \frac{\partial \sigma'_{yx}}{\partial x} + \frac{\partial \sigma'_{yy}}{\partial y}$$

where buoyancy forces have been neglected. For the energy equation,

$$\rho C_p\left(u\frac{\partial T}{\partial x} + v\frac{\partial T}{\partial y}\right) = u\frac{\partial p}{\partial x} + v\frac{\partial p}{\partial y}$$

$$+ \frac{\partial}{\partial x}\left(k\frac{\partial T}{\partial x}\right) + \frac{\partial}{\partial y}\left(k\frac{\partial T}{\partial y}\right)$$

$$+ \sigma'_{xx}\frac{\partial u}{\partial y} + \sigma'_{xy}\frac{\partial u}{\partial y} + \sigma'_{yx}\frac{\partial v}{\partial x} + \sigma'_{yy}\frac{\partial v}{\partial y}.$$

With the boundary layer approximations (see, for example, Cebeci & Smith, p.64), we obtain

$$\frac{\partial \rho u}{\partial x} + \frac{\partial \rho v}{\partial y} = 0 \tag{4.4}$$

$$\rho\left(u\frac{\partial u}{\partial x} + v\frac{\partial u}{\partial y}\right) = -\frac{dp}{dx} + \frac{\partial}{\partial y}\left(\mu\frac{\partial u}{\partial y}\right) \tag{4.5}$$

$$\rho C_p\left(u\frac{\partial T}{\partial x} + v\frac{\partial T}{\partial y}\right) = u\frac{dp}{dx} + \frac{\partial}{\partial y}\left(k\frac{\partial T}{\partial y}\right) + \mu\left(\frac{\partial u}{\partial y}\right)^2, \tag{4.6}$$

and we use the perfect gas relationship

$$p = \rho RT.$$

The energy equation can be written in terms of enthalpy h:

$$\rho\left(u\frac{\partial h}{\partial x} + v\frac{\partial h}{\partial y}\right) = u\frac{dp}{dx} + \frac{\partial}{\partial y}\left(\frac{\mu}{Pr}\frac{\partial h}{\partial y}\right) + \mu\left(\frac{\partial u}{\partial y}\right)^2, \tag{4.7}$$

and total enthalpy H:

$$\rho\left(u\frac{\partial H}{\partial x} + v\frac{\partial H}{\partial y}\right) = \frac{\partial}{\partial y}\left(\frac{\mu}{Pr}\frac{\partial H}{\partial y}\right) + \frac{\partial}{\partial y}\left(\left(1 - \frac{1}{P_r}\right)\mu u\frac{\partial u}{\partial y}\right). \tag{4.8}$$

4.2   Crocco-Busemann Relations

When $Pr = 1$, the total enthalpy equation (equation 4.8) allows the solution $H = $ constant, everywhere. That is, at the wall where $u = 0$, $\frac{\partial h}{\partial y} = 0$ (zero heat transfer). So, when $Pr = 1$, we have an adiabatic wall, and

$$H = h + \tfrac{1}{2}u^2 = \text{constant}.$$

There exists a perfect balance between viscous dissipation and heat conduction ($Pr = 1$) to keep the stagnation enthalpy constant in an adiabatic wall boundary layer. This conclusion applies regardless of pressure gradient and variations in μ, k and C_p individually.

When $Pr = 1$ and $dp/dx = 0$, the energy and momentum equations begin to look very similar. Except for the dissipation term, the enthalpy and velocity could be interchanged. To solve this system of equations, we could try

$$h = h(u),$$

so that

$$\frac{\partial h}{\partial y} = \frac{dh}{du}\frac{\partial u}{\partial y}, \qquad \text{etc.}$$

With $Pr = 1$, we get

$$\frac{dh}{du}\left(\rho u\frac{\partial u}{\partial x} + \rho v\frac{\partial u}{\partial y} - \frac{\partial}{\partial y}\left(\mu\frac{\partial u}{\partial y}\right)\right) = \left(1 + \frac{d^2h}{dy^2}\right)\mu\left(\frac{\partial h}{\partial y}\right)^2.$$

Using the momentum equation for a zero pressure gradient, the left hand side vanishes. Hence, the energy equation reduces to

$$\frac{d^2 h}{dy^2} = -1,$$

so that

$$h = -\tfrac{1}{2}u^2 + C_1 u + C_2.$$

Boundary conditions A

At the wall, $u = 0$, so that $C_2 = h_w$. In the freestream, $u = U_e$ and $h = h_e$, so that $C_1 = (h_e + \tfrac{1}{2}U_e^2 - h_w)U_e$. Hence, for $Pr = 1$, $dp/dx = 0$,

$$H = h + \tfrac{1}{2}u^2 = h_w + (H_e - h_w)\frac{u}{U_e},$$

and for constant C_p,

$$\boxed{\frac{T}{T_e} = \frac{T_w}{T_e} + \frac{T_r - T_w}{T_e}\left(\frac{U}{U_e}\right) - \frac{\gamma - 1}{2}PrM_e^2\left(\frac{U}{U_e}\right)^2.} \tag{4.9}$$

which is identical to the Couette flow result obtained earlier (equation 2.36). This relationship is a useful approximation for gases in laminar <u>and</u> turbulent flows, even when $P \neq 1$, and $dp/dx \neq 0$.

Boundary conditions B

We could alternatively choose, at the wall,

$$u = 0, \qquad \frac{\partial u}{\partial y}\bigg|_w = \frac{\tau_w}{\mu_w}$$

$$\frac{\partial h}{\partial y}\bigg|_w = C_p \frac{\partial T}{\partial y}\bigg|_w = -\frac{C_p}{k_w}q_w,$$

which gives $C_1 = -q_w/\tau_w$, as long as $Pr = 1$ and C_p is constant. Hence,

$$\tfrac{1}{2}u^2 + C_p(T - T_w) = -\frac{q_w}{\tau_w}u.$$

With the freestream boundary conditions $u = U_e$ at $T = T_e$,

$$q_w = \frac{\tau_w C_p}{PrU_e}\left(T_w - T_e - \frac{U_e^2}{2C_p}\right),$$

we see that for adiabatic walls ($q_w = 0$), with $Pr = 1$,

$$T_{aw} = T_r = T_e + \frac{U_e^2}{2C_p}. \tag{4.10}$$

Also, we find

$$C_h = \frac{C_f}{2}. \tag{4.11}$$

When $Pr \neq 1$, a better (empirical) form is

$$C_h = \frac{C_f}{2Pr^{2/3}}.$$

4.3 Howarth-Dorodnitsyn Transformation

To solve the laminar boundary layer equations for compressible flow, a coordinate transformation is often used to reduce the number of equations to a form similar to the incompressible one, which we can can then solve with established techniques.

First, we introduce a stream function that will satisfy the compressible, two-dimensional continuity equation

$$\frac{\partial \rho u}{\partial x} + \frac{\partial \rho v}{\partial y} = 0.$$

That is,

$$\rho u = \rho_\infty \frac{\partial \psi}{\partial y}, \quad \text{and} \quad \rho v = -\rho_\infty \frac{\partial \psi}{\partial x}$$

where ρ_∞ is the upstream, freestream value (assumed to be constant).

Second, we introduce a coordinate transformation, known as the Howarth-Dorodnitsyn Transformation, by introducing a new coordinate $\bar{y}$, where

$$\bar{y} = \int_0^y \frac{\rho}{\rho_\infty} dy. \tag{4.12}$$

Now, in general, if $\psi = \psi(x, y)$,

$$d\psi = \left.\frac{\partial \psi}{\partial x}\right|_y dx + \left.\frac{\partial \psi}{\partial y}\right|_x dy,$$

and so

$$\rho u = \rho_\infty \frac{\partial \psi}{\partial \bar{y}} \frac{\partial \bar{y}}{\partial y} = \rho_\infty \frac{\rho}{\rho_\infty} \frac{\partial \psi}{\partial \bar{y}} = \rho \frac{\partial \psi}{\partial \bar{y}}.$$

$$\text{Hence,} \quad u = \frac{\partial \psi}{\partial \bar{y}},$$

and

$$\rho v \;=\; -\rho_\infty \left(\left.\frac{\partial \psi}{\partial x}\right|_{\bar{y}} + \frac{\partial \psi}{\partial \bar{y}} \left.\frac{\partial \bar{y}}{\partial x}\right|_y \right)$$

so that
$$v \;=\; -\frac{\rho_\infty}{\rho} \left(\frac{\partial \psi}{\partial x} + u \left.\frac{\partial \bar{y}}{\partial x}\right|_y \right).$$

Using Bernoulli's equation in the freestream,

$$\frac{dp}{\rho_e} \;=\; d\!\left(\frac{U_e^2}{2}\right)$$

where ρ_e and U_e are local freestream density and velocity at some position x, so that they are functions of streamwise position x. That is,

$$-\frac{1}{\rho}\frac{dp}{dx} \;=\; \frac{\rho_e}{\rho} U_e \frac{dU_e}{dx}.$$

Hence, the boundary layer equation becomes

$$\frac{\partial \psi}{\partial \bar{y}}\left(\frac{\partial^2 \psi}{\partial y \partial x} + \frac{\partial^2 \psi}{\partial \bar{y}^2}\left.\frac{\partial \bar{y}}{\partial x}\right|_y \right) - \frac{\rho_\infty}{\rho}\left(\frac{\partial \psi}{\partial x} + u \left.\frac{\partial \bar{y}}{\partial x}\right|_y \right)\frac{\partial^2 \psi}{\partial \bar{y}^2}\frac{\rho}{\rho_\infty}$$

$$=\; \frac{\rho_e}{\rho} U_e \frac{dU_e}{dx} + \frac{1}{\rho}\frac{\rho}{\rho_\infty}\frac{\partial}{\partial \bar{y}}\left(\mu \frac{\rho}{\rho_\infty}\frac{\partial^2 \psi}{\partial \bar{y}^2} \right).$$

That is,

$$\frac{\partial \psi}{\partial \bar{y}}\frac{\partial^2 \psi}{\partial x \partial \bar{y}} - \frac{\partial \psi}{\partial x}\frac{\partial^2 \psi}{\partial y^2} \;=\; \frac{\rho_e}{\rho} U_e \frac{dU_e}{dx} + \frac{\partial}{\partial \bar{y}}\left(\mu \frac{\rho}{\rho_\infty^2}\frac{\partial^2 \psi}{\partial \bar{y}^2} \right) \qquad (4.13)$$

The energy equation becomes (term by term):

(a)
$$u\frac{\partial T}{\partial x} + v\frac{\partial T}{\partial y} \;=\; \frac{\partial \psi}{\partial \bar{y}}\left(\frac{\partial T}{\partial x} + \frac{\partial T}{\partial \bar{y}}\left.\frac{\partial \bar{y}}{\partial x}\right|_y \right) - \frac{\rho_\infty}{\rho}\left(\frac{\partial \psi}{\partial x} + \frac{\partial \psi}{\partial \bar{y}}\left.\frac{\partial \bar{y}}{\partial x}\right|_y \right)\frac{\partial T}{\partial \bar{y}}\frac{\rho}{\rho_\infty}$$

$$=\; \frac{\partial \psi}{\partial \bar{y}}\frac{\partial T}{\partial x} - \frac{\partial \psi}{\partial x}\frac{\partial T}{\partial \bar{y}}$$

(b)
$$\frac{\mu}{\rho C_p}\left(\frac{\partial u}{\partial y} \right)^2 \;=\; \frac{\mu}{\rho C_p}\left(\frac{\rho}{\rho_\infty} \right)^2\left(\frac{\partial^2 \psi}{\partial \bar{y}^2} \right)^2 \;=\; \frac{1}{C_p}\frac{\rho \mu}{\rho_\infty^2}\left(\frac{\partial^2 \psi}{\partial \bar{y}^2} \right)^2$$

(c)
$$\frac{1}{\rho C_p}\frac{\partial}{\partial y}\left(k\frac{\partial T}{\partial y} \right) \;=\; \frac{1}{\rho C_p}\frac{\rho}{\rho_\infty}\frac{\partial}{\partial \bar{y}}\left(k\frac{\rho}{\rho_\infty}\frac{\partial T}{\partial y} \right) \;=\; \frac{\partial}{\partial \bar{y}}\left(\frac{k}{C_p}\frac{\rho}{\rho_\infty^2}\frac{\partial T}{\partial \bar{y}} \right)$$

$$=\; \frac{\partial}{\partial \bar{y}}\left(\frac{k}{\mu C_p}\frac{\rho \mu}{\rho_\infty^2}\frac{\partial T}{\partial \bar{y}} \right) \;=\; \frac{\partial}{\partial \bar{y}}\left(\frac{1}{Pr}\frac{\rho \mu}{\rho_\infty^2}\frac{\partial T}{\partial \bar{y}} \right)$$

(d)
$$-\frac{u}{\rho C_p} \;=\; \frac{\rho_e}{\rho C_p} U_e \frac{dU_e}{dx}\frac{\partial \psi}{\partial \bar{y}}.$$

Hence, the energy becomes:

$$\frac{\partial \psi}{\partial \bar{y}} \frac{\partial T}{\partial x} - \frac{\partial \psi}{\partial x} \frac{\partial T}{\partial \bar{y}} = -\frac{\rho_e U_e}{\rho C_p} \frac{d U_e}{dx} \frac{\partial \psi}{\partial \bar{y}}$$

$$+ \frac{\partial}{\partial \bar{y}} \left(\frac{1}{Pr} \frac{\rho \mu}{\rho_\infty^2} \frac{\partial T}{\partial \bar{y}} \right) + \frac{\rho \mu}{C_p \rho_\infty^2} \left(\frac{\partial^2 \psi}{\partial \bar{y}^2} \right)^2. \qquad (4.14)$$

For simplicity, consider the case where $dp/dx = 0$, that is, the flat plate boundary layer case. The boundary conditions are

$$\bar{y} = 0, \quad u = \frac{\partial \psi}{\partial \bar{y}} = 0, \quad v = 0, \quad \rightarrow \quad \psi = 0$$

$$y = \infty, \quad u = U_\infty, \quad T = T_\infty.$$

4.4   Flat Plate Boundary Layer

We look for a similarity solution for the zero pressure gradient case, using the similarity variables

$$\bar{\eta} = \frac{\bar{y}}{\sqrt{\frac{\nu_\infty x}{U_\infty}}}, \qquad f(\bar{\eta}) = \frac{\psi}{\sqrt{\nu_\infty U_\infty x}}, \quad \text{and} \quad T(\bar{\eta}) = T.$$

Now

$$\frac{u}{U_\infty} = \frac{1}{U_\infty} \frac{\partial \psi}{\partial \bar{y}} = \sqrt{\frac{\nu_\infty x}{U_\infty}} \frac{df}{d\bar{\eta}} \frac{\partial \bar{\eta}}{\partial \bar{y}} = f'(\bar{\eta}).$$

Also,

$$\frac{\partial^2 \psi}{\partial x \partial \bar{y}} = -\frac{1}{2} \frac{\bar{\eta}}{x} U_e f''$$

$$\frac{\partial \psi}{\partial x} = \sqrt{\nu_\infty U_\infty x} \left(\frac{1}{2x} f - \frac{1}{2} \frac{\bar{\eta}}{x} f' \right)$$

$$\frac{\partial^2 \psi}{\partial \bar{y}^2} = \sqrt{\frac{U_\infty}{\nu_\infty x}} U_\infty f''$$

$$\frac{\partial T}{\partial x} = -\frac{1}{2} \frac{\bar{\eta}}{x} T'$$

$$\frac{\partial T}{\partial \bar{y}} = \sqrt{\frac{U_\infty}{\nu_\infty x}} T'$$

Hence

$$f f'' + d \frac{d}{d\bar{\eta}} \left(\frac{\rho \mu}{\rho_\infty \mu_\infty} f'' \right) = 0 \qquad (4.15)$$

and

$$\frac{d}{d\bar{\eta}}\left(\frac{1}{Pr}\frac{\rho\mu}{\rho_\infty\mu_\infty}T'\right) + \frac{1}{2}fT' + (\gamma - 1)M_\infty^2 \frac{\rho\mu}{\rho_\infty\mu_\infty}T_\infty f''^2 = 0 \qquad (4.16)$$

Since the pressure is constant everywhere, and it has already been assumed that C_p is constant,

$$\rho \propto t^{-1}, \quad \text{and} \quad \mu = \mu(T),$$

and we see that we have two ordinary differential equations. In particular, when

$$\frac{\mu}{\mu_\infty} = \left(\frac{T}{T_\infty}\right)^m,$$

we have

$$\frac{\rho\mu}{\rho_\infty\mu_\infty} = \left(\frac{T}{T_\infty}\right)^{m-1}.$$

When $m = 1$, we have the "Chapman-Rubesin" approximation

$$\rho\mu = \rho_\infty\mu_\infty,$$

and the momentum equation reduces to

$$ff'' + 2f''' = 0 \qquad (4.17)$$

which is the same as the Blasius equation for incompressible flow, except that the differentiation is with respect to $\bar{\eta}$, instead of η. Thus, we have a universal velocity distribution that is independent of Mach number in the $\bar{y}$ coordinate system. To obtain the velocity profile in the physical coordinate system, we need to obtain the relationship between ρ and y, or alternatively the relationship between the temperature and the velocity. we could solve the energy equation, which with $\rho\mu = \rho_\infty\mu_\infty$ becomes

$$2\frac{d}{d\bar{\eta}}\left(\frac{T'}{Pr}\right) + fT' + 2(\gamma - 1)M_\infty^2 T_\infty f''^2 = 0,$$

or, with $Pr = 1$ we could use the Crocco energy integral

$$\frac{T}{T_\infty} = \frac{T_w}{T_\infty} + \left(1 - \frac{T_w}{T_\infty} + \frac{\gamma - 1}{2}M_\infty^2\right)\frac{u}{U_\infty} - \frac{\gamma - 1}{2}M_\infty^2\left(\frac{u}{U_\infty}\right)^2.$$

4.5 Boundary Layer Properties

4.5.1 Skin friction

To find the skin friction we use

$$
\begin{aligned}
\tau_w \;&=\; \mu_w \left.\frac{\partial u}{\partial y}\right|_w \;=\; \mu_w U_\infty \frac{\partial}{\partial y}\left. f'(\eta)\right|_w \\[2mm]
&=\; \mu_w U_\infty \left(\frac{\partial f'}{\partial \bar\eta}\frac{\partial \bar\eta}{\partial \bar y}\frac{\partial \bar y}{\partial y}\right)\Bigg|_w \;=\; \mu_w U_\infty \left(f''\sqrt{\frac{U_\infty}{\nu_\infty x}}\frac{\rho}{\rho_\infty}\right)\Bigg|_w \\[2mm]
&=\; \frac{(\rho\mu)_w}{\rho_\infty\mu_\infty}\rho_\infty U_\infty^2 \sqrt{\frac{\nu_\infty}{U_\infty x}}f''(0)\,.
\end{aligned}
$$

Therefore

$$
C_f \;=\; \frac{\tau_w}{\tfrac{1}{2}\rho_\infty U_\infty^2} \;=\; \frac{2(\rho\mu)_w}{\rho_\infty\mu_\infty}\sqrt{\frac{\nu_\infty}{U_\infty x}}f''(0)\,.
$$

With the approximation that $\rho\mu = \rho_\infty\mu_\infty$,

$$
C_f \;=\; \frac{2f''}{\sqrt{Re_x}}\,.
$$

As in the Blasius solution, $f'(0) = 0.332$, and

$$
C_f \;=\; \frac{0.664}{\sqrt{Re_x}}, \tag{4.18}
$$

so that the skin friction coefficient is the same as in incompressible flow, at the same Reynolds number.

Since the temperature increases near the wall due to friction, there is also a significant decrease in density. The streamlines diverge and the boundary layer thickens, reducing the velocity gradients at the wall, and τ_w, the stress at the wall. However, at the same time, the viscosity increases because of the rise in temperature. With $m = 1$ in Sutherland's law, these two effects just balance, with the result that the skin friction coefficient remains the same. With $m < 1$, C_f decreases with Mach number (see figure 4.1).

4.5.2 Heat transfer

The heat flux at the wall is given by

$$
q_w = -k_w \left.\frac{\partial T}{\partial y}\right|_w,
$$

and the direction of the heat flux clearly depends on the sign of the temperature gradient at the wall, and

$$\left.\frac{\partial T}{\partial y}\right|_w = \left.\frac{\partial u}{\partial y}\right|_w \left.\frac{\partial T}{\partial u}\right|_w.$$

For attached flows, $\left.\frac{\partial u}{\partial y}\right|_w > 0$, and therefore the sign of $\left.\frac{\partial T}{\partial y}\right|_w$ depends on $\left.\frac{\partial T}{\partial u}\right|_w$. The Crocco relationship

$$\frac{T}{T_\infty} = \frac{T_w}{T_\infty} + \left(1 - \frac{T_w}{T_\infty} + \frac{\gamma - 1}{2}M_\infty^2\right)\frac{u}{U_\infty} - \frac{\gamma - 1}{2}M_\infty^2\left(\frac{u}{U_\infty}\right)^2$$

gives

$$\frac{U_\infty}{T_\infty}\left.\frac{dT}{du}\right|_w = 1 - \frac{T_w}{T_\infty} + \frac{\gamma - 1}{2}M_\infty^2.$$

Consider the following two cases (see figure 4.2):

(a) $\left.\frac{dT}{du}\right|_w < 0$, $q_w > 0$: heat flows from the wall to the fluid (*Hot Wall case*). That is,

$$\frac{T_w - T_\infty}{T_\infty} > \frac{\gamma - 1}{2}M_\infty^2.$$

(b) $\left.\frac{dT}{du}\right|_w > 0$, $q_w > 0$: heat flows from the fluid to the wall (*Cold Wall case*). That is,

$$\frac{T_w - T_\infty}{T_\infty} < \frac{\gamma - 1}{2}M_\infty^2.$$

Remember that for an adiabatic wall, $\left.\frac{dT}{du}\right|_w = 0$, and $Pr = 1$,

$$T_{w,ad} = T_r = T_\infty\left(1 + \frac{\gamma - 1}{2}M_\infty^2\right)$$
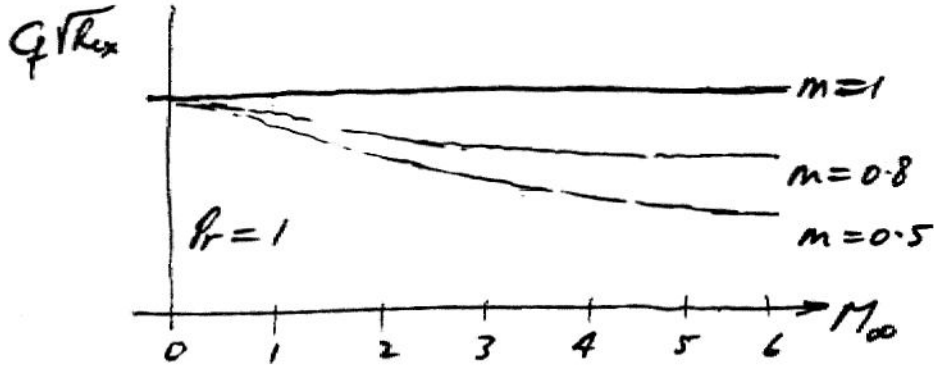
Figure 4.1: Skin friction as a function of Mach number for a laminar boundary layer, for different viscosity-temperature relationships (*m* is the exponent in Sutherland's law).
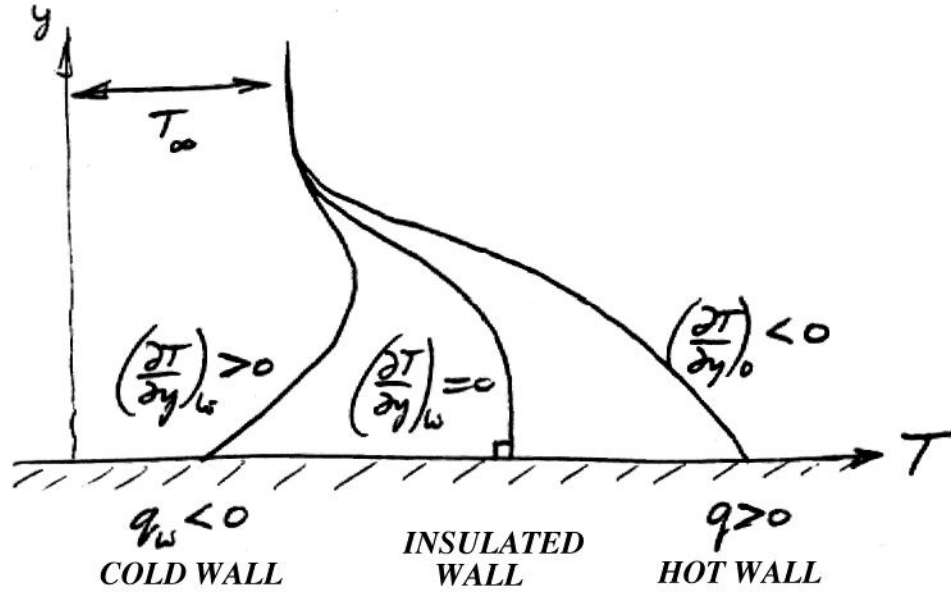
Figure 4.2: Heat transfer for cold wall, hot wall, and adiabatic wall cases.

where $T_r (= T_{w,ad})$ is the "recovery temperature" for $Pr = 1$, and $(T_r - T_\infty)$ is the temperature rise of an adiabatic wall due to frictional heating (that is, due to the presence of a boundary layer).

For the external frictionless flow,

$$T_0 = T_\infty \left(1 + \frac{\gamma - 1}{2} M_\infty^2\right)$$

where T_0 is the total temperature. Hence, for $Pr = 1$, $T_0 = T_r$. However, for $Pr \neq 1$, it can be shown, approximately, that

$$T_{w,ad} = T_r = T_\infty \left(1 + \sqrt{Pr} \, \frac{\gamma - 1}{2} M_\infty^2\right)$$

for laminar boundary layers in air. For air, $\gamma = 1.4$, $Pr = 0.72$, and

$$T_r = T_\infty \left(1 + 0.17 M_\infty^2\right).$$

With $T_\infty = 273°K$ and $M_\infty = 1$, the wall will be heated by about 43°C. With $M_\infty = 2$, this increases to 185°C, and with $M_\infty = 6$, it will be 1670°C (this is probably the limit for the perfect gas assumption).

The equation for the recovery temperature is often written as

$$T_r = T_\infty \left(1 + r\frac{\gamma - 1}{2} M_\infty^2\right)$$

where r is the "recovery factor." The recovery factor is the ratio of the frictional temperature increase of the wall ($T_r - T_\infty$) to that due to adiabatic compression ($= U_\infty^2/2C_p = \frac{\gamma-1}{2}M_\infty^2 T_\infty$).

Let's evaluate q_w from the boundary layer equations. Here, we have

$$
\begin{aligned}
q_w &= -k_w \left.\frac{\partial T}{\partial y}\right|_w = -k_w \left.\left(\frac{\partial T}{\partial \bar\eta}\frac{\partial \bar\eta}{\partial \bar y}\frac{\partial \bar y}{\partial y}\right)\right|_w \\
&= \frac{(\rho\mu)_w}{\rho_\infty\mu_\infty}\frac{C_p}{Pr}\rho_\infty U_\infty \sqrt{\frac{\nu_\infty}{U_\infty x}}T'(0)
\end{aligned}
$$

Now

$$
T' = \frac{\partial T}{\partial \bar\eta} = \frac{\partial T}{\partial u}\frac{\partial u}{\partial \bar\eta} = U_\infty f''(\bar\eta)\frac{T}{u}.
$$

Therefore, when $Pr = 1$,

$$
T'(0) = (T_r - T_w) f''(0)
$$

So for $Pr = 1$ and $\rho\mu = \rho_\infty\mu_\infty$,

$$
q_w = \frac{\rho_\infty U_\infty C_p}{\sqrt{Re_x}}(T_w - T_r) f''(0)
$$

and $f''(0) = 0.332$, so that

$$
C_h = \frac{q_w}{\rho_\infty U_\infty C_p (T_w - T_r)} = \frac{0.332}{\sqrt{\mathfrak{R}_x}} = \frac{C_f}{2} \tag{4.19}
$$

This relationship between C_f and C_h is called "Reynolds Analogy." Accordingly, when

$$
\begin{aligned}
T_w &< T_r & &\text{heat transfer \underline{to wall} (cold wall)} \\
T_w &= T_r & &\text{no heat transfer (insulated wall)} \\
T_w &> T_r & &\text{heat transfer \underline{to fluid} (hot wall)}
\end{aligned}
$$

Note that when $Pr \neq 1$, a more accurate form of the Reynolds Analogy is given by

$$
C_h = \frac{C_f}{2P^{2/3}}. \tag{4.20}
$$

4.5.3   Integral parameters

We would like to retain the same meanings we had for δ^* and θ, that is, δ^* is a measure of the mass deficit and θ is a measure of the momentum deficit.

Displacement thickness

In the presence of the boundary layer, the mass flux at height y is $\rho u \, dy$. In the absence of the boundary layer, it would be $\rho_e U_e dy$. Hence, the mass deficit is given by

$$\int_0^\infty (\rho_e U_e - \rho u) dy,$$

and we define δ^* so that

$$\rho_e U_e \delta^* = \text{mass flux deficit.}$$

Hence,

$$\delta^* = \int_0^\infty \left(1 - \frac{\rho u}{\rho_e U_e}\right) dy. \tag{4.21}$$

For the flat plate boundary layer,

$$\delta^* = \int_0^\infty \left(1 - \frac{\rho u}{\rho_\infty U_e}\right) dy = \int_0^\infty \frac{\rho u}{\rho_e U_e}\left(1 - \frac{\rho u}{\rho_\infty U_e}\right)\frac{\rho_\infty}{\rho} d\bar{y}$$

$$= \int_0^\infty \left(\frac{\rho_\infty}{\rho} - \frac{u}{U_\infty}\right) d\bar{y} = \int_0^\infty \left(\frac{T}{T_\infty} - \frac{u}{U_\infty}\right) d\bar{y}.$$

(for constant pressure). Using the Crocco relation,

$$\delta^* = \int_0^\infty \left(\frac{T_w}{T_\infty} + \left(1 - \frac{T_w}{T_\infty}\right)\frac{u}{U_\infty} + \frac{\gamma - 1}{2}M_\infty^2\frac{u}{U_\infty}\left(1 - \frac{u}{U_\infty}\right) - \frac{u}{U_\infty}\right) dy$$

$$= \int_0^\infty \frac{T_w}{T_\infty}\left(1 - \frac{u}{U_\infty}\right) d\bar{y} + \frac{\gamma - 1}{2}M_\infty^2 \int_0^\infty \frac{u}{U_\infty}\left(1 - \frac{u}{U_\infty}\right) d\bar{y}$$

$$= \frac{T_w}{T_\infty}\overline{\delta^*} + \frac{\gamma - 1}{2}M_\infty^2\bar{\theta}$$

$$= \overline{\delta^*}\left(\frac{T_w}{T_\infty} + \frac{\gamma - 1}{2}M_\infty^2\frac{\bar{\theta}}{\overline{\delta^*}}\right).$$

Hence δ^* depends on the Mach number and the thermal condition of the plate.

Now, from the Blasius solution for incompressible flow, we know that

$$\frac{\bar{\theta}}{\overline{\delta^*}} = \frac{1}{2.59},$$
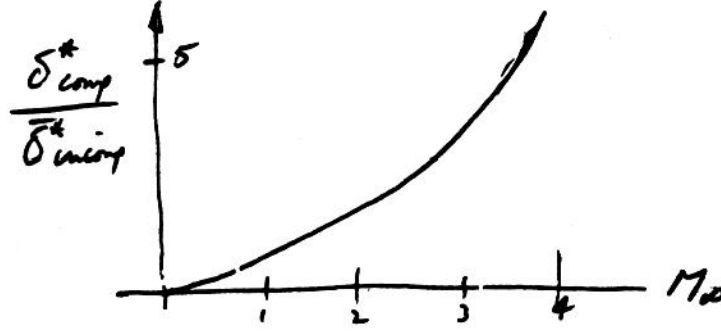
Figure 4.3: Displacement thickness as a function of Mach number for a laminar boundary layer, compared to its incompressible value.

and for insulated walls,

$$\frac{T_w}{T_\infty} = \frac{T_r}{T_\infty} = 1 + \frac{\gamma - 1}{2} M_\infty^2$$

and we get

$$\frac{\delta^*}{\overline{\delta^*}} = 1 + 0.693\,(\gamma - 1)\, M_\infty^2$$

($q = 0$), and we see that δ^* grows rapidly as the Mach number increases (figure 4.3).

Boundary layer thickness

This "stretching" effect caused by compressibility can be deduced easily from the Crocco relation. We know

$$dy = \frac{\rho_\infty}{\rho} d\bar{y} \quad \text{since} \quad \bar{y} = \int_0^y \left(\frac{\rho}{\rho_\infty}\right) dy.$$

Therefore

$$y = \int_0^{\bar{y}} \frac{\rho_\infty}{\rho} d\bar{y} = \int_0^y \left(\frac{T}{T_\infty}\right) d\bar{y}.$$

With $P = 1$ and $dp/dx = 0$, the Crocco relation gives

$$\frac{T}{T_\infty} = \frac{T_w}{T_\infty} + \left(1 - \frac{T_w}{T_\infty} + \frac{\gamma - 1}{2} M_\infty^2\right) f' - \frac{\gamma - 1}{2} M_\infty^2 f'^2$$

$$= 1 + \frac{\gamma - 1}{2} M_\infty^2 \left(1 - f'^2\right) + \frac{T_w - T_r}{T_\infty}\left(1 - f'\right).$$
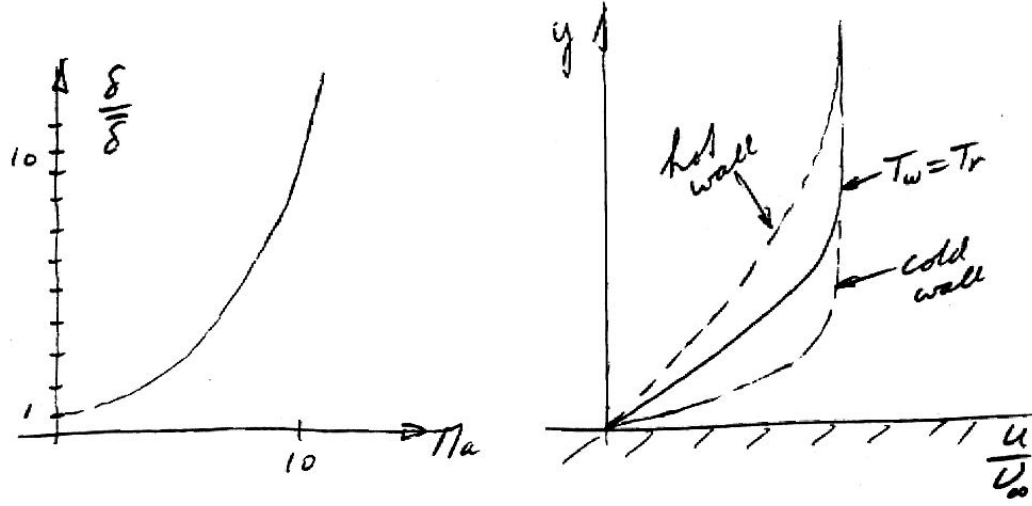
Figure 4.4: Left: Boundary layer thickness as a function of Mach number. Right: Effect of heating on boundary layer thickness.

Therefore,

$$y = \bar{y} + \frac{\gamma - 1}{2} M_\infty^2 \int_0^{\bar{y}} \left(1 - f'^2\right) d\bar{y} + \frac{T_w - T_r}{T_\infty} \int_0^{\bar{y}} (1 - f') d\bar{y}$$

$$\eta = \bar{\eta} + \frac{\gamma - 1}{2} M_\infty^2 \int_0^{\bar{\eta}} \left(1 - f'^2\right) d\bar{\eta} + \frac{T_w - T_r}{T_\infty} \int_0^{\bar{\eta}} (1 - f') d\bar{\eta}$$

This relationship connects η in physical space to $\bar{\eta}$ in transformed space. The second term on the right hand side is always positive, and grows with increasing Mach number. The third term on the right hand side may be positive or negative, depending on the heat transfer.

$$\begin{array}{llll} \text{for} & T_w < T_r & \text{heat transfer \underline{to wall} (cold wall),} & \text{Term } 3 > 0. \\ & T_w = T_r & \text{no heat transfer (insulated wall),} & \text{Term } 3 = 0. \\ & T_w > T_r & \text{heat transfer \underline{to fluid} (hot wall),} & \text{Term } 3 < 0. \end{array}$$

We can see that δ grows rapidly with Mach number (figure 4.4). For the Blasius boundary layer, $f'(\eta) = 0.99$ at $\bar{\eta} = 4.9$, and therefore for an insulated wall where Term 3 is zero,

$$\eta_{physical} = \bar{\eta} + g\left(M_\infty^2\right).$$

At Mach = 5, we have 3.5 times the incompressible value, whereas at $M = 20$ we get 41 times the incompressible value.

If the wall is heated (figure 4.4), the layer would thicken further, and if the wall was cooled, it would thin the layer.

Momentum thickness

In the presence of the boundary layer, the momentum flux at height y is $(\rho u)u \, dy$. If the fluid was not retarded, the momentum flux would be $(\rho u)U_e \, dy$. Hence, the momentum deficit is given by

$$\int_0^\infty \rho u \, (U_e - u) dy,$$

and we define θ so that

$$\rho_e U_e^2 \theta = \text{momentum flux deficit.}$$

Hence,

$$\theta = \int_0^\infty \frac{\rho u}{\rho_e U_e} \left(1 - \frac{u}{U_e} \right) dy. \tag{4.22}$$

For the flat plate boundary layer,

$$\theta \;=\; \int_0^\infty \frac{\rho u}{\rho_e U_e} \left(1 - \frac{u}{U_e} \right) dy \;=\; \int_0^\infty \frac{\rho u}{\rho_e U_e} \left(1 - \frac{u}{U_e} \right) \frac{\rho_\infty}{\rho} d\bar{y}$$

$$=\; \int_0^\infty \frac{u}{U_e} \left(1 - \frac{u}{U_e} \right) d\bar{y} \;=\; \bar{\theta},$$

where the overbar denotes the incompressible value. So the momentum thickness of a flat plate boundary layer in a compressible flow has exactly the same form as the incompressible momentum thickness, and we find

$$\theta = \frac{0.664}{\sqrt{Re_x}}.$$

That is, the momentum thickness is independent of Mach number and thermal conditions at the wall (with $\rho\mu = \rho_\infty \mu_\infty$).

Chapter 5

Stability and Transition

5.1 Introduction

.

So far, we have looked at a variety of problems in laminar viscous flow, including boundary layers, jets and wakes.[1] Often, however, the flows of real fluids differ markedly from the laminar cases considered so far. They exhibit a characteristic feature called *turbulence*. When the Reynolds number increases beyond a certain limit, internal flows (that is, in a pipe) and boundary layers undergo a transition from the laminar to the turbulent regime. In most engineering situations, laminar flows are the exception rather than the rule.

Historically, the incidence of turbulence was first studied in relation to pipe and channel flow. Consider the low Reynolds number flow through a straight pipe of uniform cross section having smooth walls. Each fluid particle moves with a uniform velocity along a straight path. Particles near the wall are slowed down by viscous forces, the flow is well-ordered, and particles travel along neighboring layers (that is, *laminar* flow). At high Reynolds numbers, this orderly flow structure breaks down, and mixing of all the particles occurs. The mixing process in a pipe can be visualized by injection of a thin thread of liquid dye. If the flow remains laminar the dye thread maintains sharply defined boundaries all along the stream. If the flow becomes turbulent the thread diffuses into the stream and the fluid appears uniformly coloured at a short distance downstream. When the fluid becomes turbulent, superimposed on the main motion in the axial direction is a subsidiary motion at right angles to it which affects mixing. At each point the streamline pattern is subjected to continuous fluctuations. The subsequent motion causes an exchange of momentum in the transverse direction and as a consequence, the velocity distribution over the pipe cross section is much

---

[1]Parts of this chapter were adapted from course notes issued by Professor D.S. Dolling at U.T. Austin.
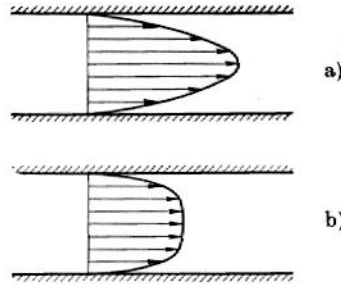
Figure 5.1: Velocity distributions in a pipe. (a) Laminar; (b) Turbulent. From Schlichting.

more uniform in turbulent than in laminar flow (see figure 5.1)

At a given point in the turbulent flow, the pressure and velocity are not constant in time but exhibit irregular high frequency fluctuations.

Osborne Reynolds conducted the first systematic investigation into these two different patterns of flow. He found that the *transition* from laminar to turbulent flow occurs at nearly the same Reynolds number $R = \bar{U}d/\nu$ where $\bar{w}$ is the mean flow velocity ($\bar{U} = Q/A$ where Q is the volume rate of flow and A the cross sectional area. The critical Reynolds number R_{crit} was determined to be about 2,300. Thus if $R < R_{crit}$ one would expect a laminar flow and if $R > R_{crit}$ one would expect a turbulent one. This, of course, would not occur abruptly — there will be a transition region. It turns out however that R_{crit} depends strongly on the conditions in the initial pipe length as well as the inlet itself. Numerical values of $R_{crit} \approx 40,000$ have been reached. The exact upper limit to which R_{crit} can be driven is currently not known. There is however, a lower bound to R_{crit}. It is about 2,300. Below this, the flow remains laminar even in the presence of strong disturbances.

The Moody diagram (figure 5.2) indicates that the friction factor for $Re < 2,300$ follows a single curve: this is the laminar flow regime where the layers of fluid slide over each other, and all the drag is due to viscous stresses set up by the velocity gradient. For $Re > 2,300$, transition to turbulence can take place. When the flow is turbulent, the flow contains eddying motions of all sizes, and a large part of the mechanical energy in the flow goes into the formation of these eddies which eventually dissipate their energy as heat. As a result, at a given Reynolds number, the drag of a turbulent flow is higher than the drag of a laminar flow. In contrast to laminar flow, turbulent flow is affected by surface roughness, so that increasing roughness increases the drag. If the roughness is large enough and the Reynolds number is large enough, the drag becomes independent of Reynolds number, and it depends only on the relative roughness parameter k/D.

Transition to turbulence can occur over a range of Reynolds numbers, depending on many factors, including the level of surface roughness, heat
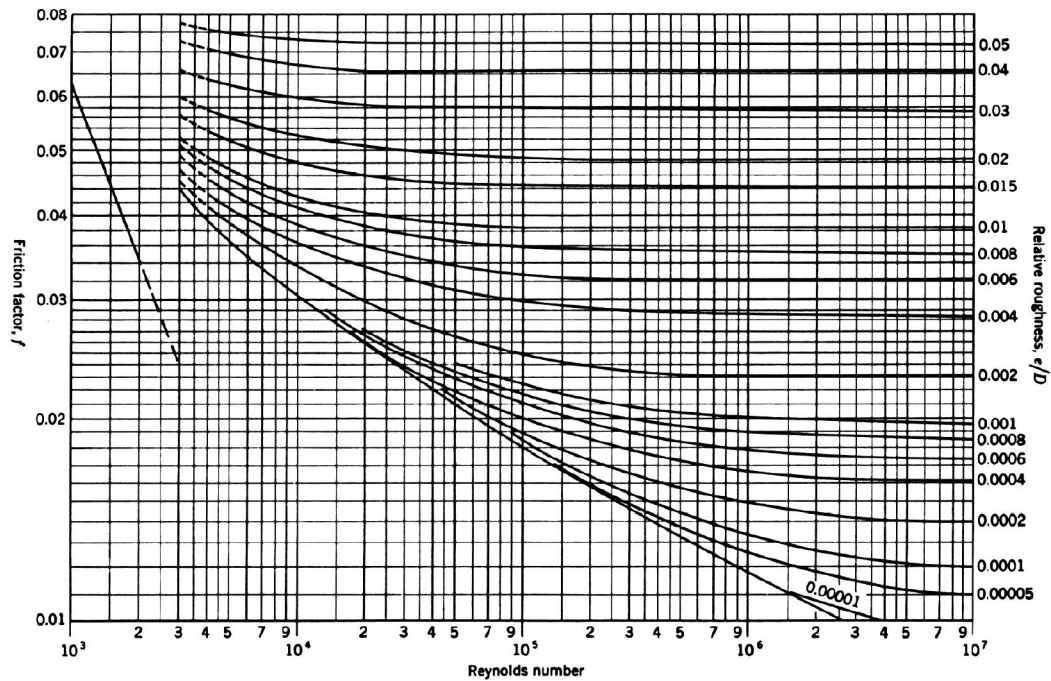
Figure 5.2: Moody diagram for fully-developed flow in circular pipes.

transfer, vibration, noise, and other disturbances. To understand why this is so, and to appreciate the role of the Reynolds number in governing the stability of the flow, it is helpful to think in terms of a spring-damper system such as the suspension system of a car. Driving along a bumpy road, the springs act to reduce the movement experienced by the passengers. If there were no shock absorbers, however, there would be no damping of the motion, and the car would continue to oscillate long after the bump has been left behind. So the shock absorbers, through a viscous damping action, dissipate the energy in the oscillations and reduce their amplitude. If the viscous action is strong enough, the oscillations will die out very quickly, and the passengers can proceed smoothly. If the shock absorbers are not in good shape, the oscillations may not die out. The oscillations can actually grow if the excitation frequency is in the right range, and the system can experience resonance. The car becomes unstable, and it is then virtually uncontrollable.

The stability of a fluid flow is similarly dependent on the relative strengths of the acceleration and the viscous damping. This is expressed by the Reynolds number, which is the ratio of a typical inertia force to a typical viscous force. At low Reynolds numbers, therefore, the viscous force is large compared to the inertia force, and the flow behaves in some ways like a car with a good suspension system. Small disturbances in the velocity field, created perhaps by small roughness elements on the surface, or pres-

sure perturbations from external sources such as vibrations in the surface or strong sound waves, will be damped out and not allowed to grow. This is the case for pipe flow at Reynolds numbers less than the critical value of 2,300. As the Reynolds number increases, however, the viscous damping action becomes comparatively less, and at some point it becomes possible for small perturbations to grow, just as in the case of a car with poor shock absorbers. The flow can become unstable, and it can experience transition to a turbulent state where large variations in the velocity field can be maintained.

The point where the disturbances will grow rather than decay will also depend on the size of the disturbances. If the disturbances are very small, as in the case where the surface is very smooth, or if the wavelength of the disturbance is not near the point of resonance, the transition to turbulence will occur at a higher Reynolds number than the critical value. So the point of transition does not correspond to a single Reynolds number, and it is possible to delay transition to relatively large values by controlling the disturbance environment. At very high Reynolds numbers, however, it is impossible to maintain laminar flow since under these conditions even minute disturbances will be amplified into turbulence.

The flow in a boundary layer can also undergo transition, something which was discovered much later than transition in a pipe. The flowfield around a body immersed in a fluid is strongly dependent on the "state" of
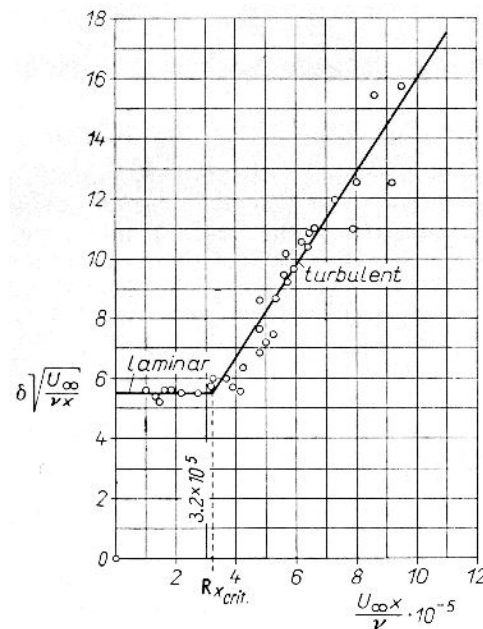
Figure 5.3: Boundary layer thickness plotted agains the Reynolds number based on the current length x along a plate in parallel flow at zero incidence, as measured by Hansen. From Schlichting.

the boundary layer. By "state" we mean laminar, turbulent or transitional. Boundary layer transition is affected by many parameters, the most important being the external pressure gradient, the roughness of the wall surface, and the nature of any disturbances in the external flow.

On a plate with a sharp leading edge and in a normal airstream, transition takes place at distance x downstream, determined by

$$R_{x,crit} = \left(\frac{U_\infty x}{\nu}\right)_{crit} = 3.5 \times 10^5 \quad \text{to} \quad 10^6.$$

Transition is easiest to see through an examination of the velocity profile. When transition occurs, there is an increase in the boundary layer thickness (figure 5.3) and a noticeable change in the shape of the velocity profile (figure 5.4). The shape factor H decreases from about 2.6 (laminar flow) to about 1.4 in the turbulent regime.

Transition also involves a large increase in the surface skin friction (the increase in $(\partial U/\partial y)_{wall}$ can be seen in figure 5.4).

Experiments performed by Emmons, and Schubauer & Klebanoff have shown that in the case of a flat plate the process of transition is intermittent and consists of an irregular sequence of laminar and turbulent regions. This is shown in figure 5.5. At a given point in the boundary layer there occurs a small turbulent area (a turbulent spot), irregular in shape, which then travels downstream in a wedge shaped region, as shown. such turbulent spots appear at irregular intervals in time and at different, randomly distributed points on the plate. Inside of the wedge-like domain the flow is predominantly turbulent, whereas in the adjoining region it alternates continuously
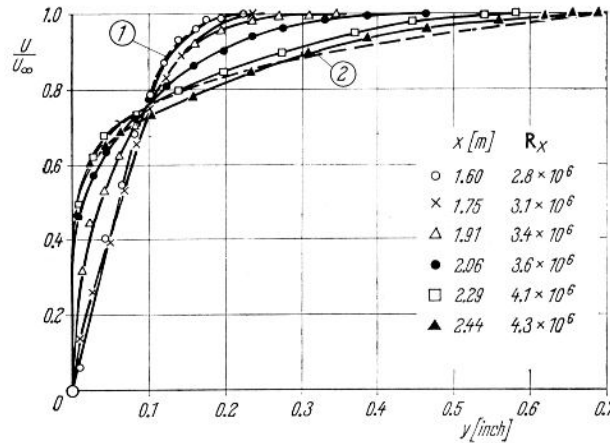
Figure 5.4: Velocity profiles in a boundary layer on a flat plate in the transition region, as measured by Schubauer & Klebanoff. (1) Laminar, Blasius profile; (2) Turbulent 1/7th power law (see section 11.8). From Schlichting.
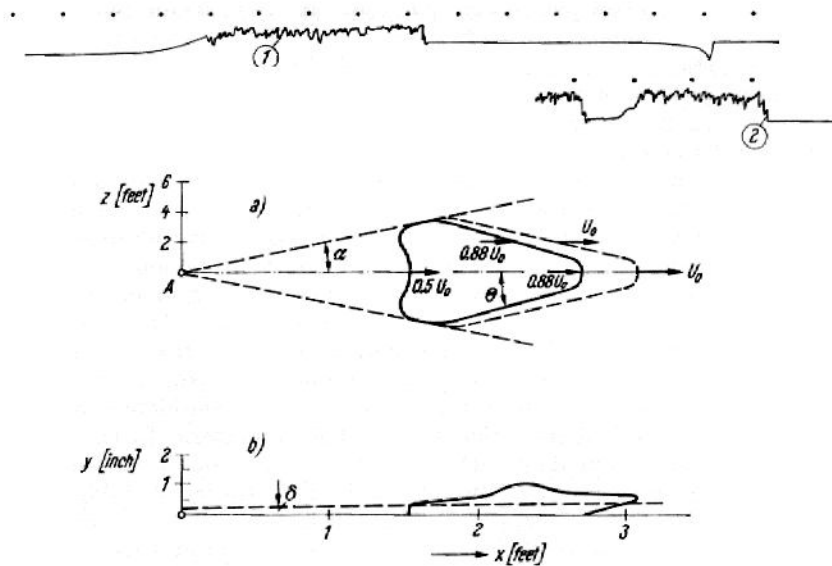
Figure 5.5: Growth of an artificial turbulent spot on a flat plate at zero incidence as measured by Schubauer & Klebanoff: (a) plan view; (b) side view. From Schlichting.

between being laminar and turbulent. An early visualization of a turbulent spot is seen in figure 5.24.

In these brief notes we will be looking at two important topics, namely stability and transition. The first of these two, namely stability, is concerned with the basic question of whether a given physical situation can be disturbed and still return to its original state. The concept of the basic meaning of stability is nicely illustrated by the example given in figure 5.6. As we shall see, figure 5.6d comes closest to the case of boundary layer flow. To examine this phenomenon we will use "small disturbance" theory, which is outlined in the next four pages. We will see that the small disturbance theory will not predict the details of the non-linear process by which the flow changes from laminar to turbulent. It establishes which shapes of velocity profiles are unstable, identifies those frequencies which amplify fastest and indicates how the parameters governing the flow can be changed to delay transition. Transition in the most general way is defined as "the change, over space and time and over a certain Reynolds number range, of a laminar flow into a turbulent one." Although a direct theory linking stability and transition is lacking, several empirical theories leading to a satisfactory prediction of transition exist for two dimensional and axi-symmetric incompressible flows.
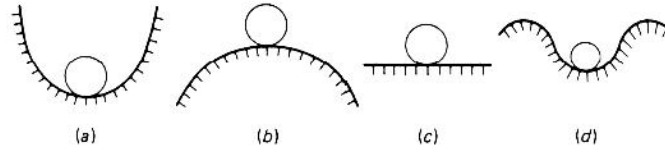
Figure 5.6: Relative stability for a ball at rest: (a) stable; (b) unstable; (c) neutrally stable; (d) stable for small disturbances but unstable for large disturbances. From F. White *Viscous Flows*.

5.2   Stability Analysis

Efforts to clarify and explain theoretically the process of transition started many years ago. Real success has only been achieved in the first 50 years. These theoretical methods are based on the assumption that laminar flows are affected by certain small disturbances. For pipe flow these disturbances may originate in the inlet. For the boundary layer on a body in a stream they may be due to wall roughness or to irregularities in the external (freestream) flow. The theory aims to follow in time the behavior of such disturbances when they are superimposed on the main flow, bearing in mind that their exact form remains to be determined in particular cases.

The important question is whether the disturbances amplify or decay with time. If they decay the main flow is considered stable. If they increase they flow is considered unstable and there exists the possibility of transition to turbulence. In this way a theory of stability is built up with the object being to predict the critical Reynolds number for a given main flow.

The basis of the theory of stability can be traced back to Osborne Reynolds. Much work was done on the mathematical foundations of this stability hypothesis, firstly by Reynolds and later by Rayleigh. It was not until 1930 that Prandtl *et al.* were able to calculate R_{crit} in a satisfactory manner.

5.2.1   Small perturbation analysis

The theory of the stability of laminar flows considers the flow as two parts. Namely, a mean flow (whose stability we wish to investigate) and a disturbance superimposed on it. Let the mean flow, which is steady, be given by its Cartesian velocity components U, V and W, and the pressure by P. The unsteady disturbance quantities will be given by u', v' and w', and p'.

Thus

$$u = U + u', \qquad v = V + v' \quad \text{and} \quad w = W + w', \tag{5.1}$$

and $p = P + p'$. We assume that the quantities related to the disturbance are small compared with the corresponding quantities of the mean flow.

Let us consider a two-dimensional (2-D) incompressible mean flow having a 2-D disturbance. We will further simplify the analysis by assuming that the mean velocity $U = U(y)$ only, whereas the other components V and W are zero everywhere. Such a flow is called "parallel". The boundary layer is a reasonable approximation to a parallel flow since the dependence of U on x is very much smaller than on y. However, for the pressure P, we assume a dependence on both x and y, because the pressure gradient $\partial p / \partial x$ is what maintains the flow. Thus the average mean flow is defined by

$$U = U(y), \qquad V = W = 0, \quad \text{and} \quad P = P(x, y). \tag{5.2}$$

The 2-D disturbance superimposed on the mean flow is a function of both time and space and is given by

$$u'(x, y, t), \qquad v'(x, y, t), \quad \text{and} \quad p'(x, y, t). \tag{5.3}$$

Thus the resultant motion, from equation 5.1 is

$$u = U + u', \qquad v = v', \quad w = 0, \quad \text{and} \quad p = P + p'. \tag{5.4}$$

We assume that the mean flow (equation 5.2) satisfies the Navier-Stokes equations and it is required that the resulting motion (equation 5.4) does also. The fluctuations (equation 5.3) and assumed "small" in the sense that quadratic terms are small compared to linear ones.

If we substitute equation 5.4 into the 2-D, unsteady, incompressible Navier-Stokes equations we get

$$\frac{\partial u'}{\partial t} + U \frac{\partial u'}{\partial x} + v' \frac{dU}{dy} + \frac{1}{\rho} \frac{\partial P}{\partial x} + \frac{1}{\rho} \frac{\partial p'}{\partial x} = \nu \left(\frac{d^2 U}{dy^2} + \nabla^2 u' \right) \tag{5.5}$$

$$\frac{\partial v'}{\partial t} + U \frac{\partial v'}{\partial x} + \frac{1}{\rho} \frac{\partial P}{\partial y} + \frac{1}{\rho} \frac{\partial p'}{\partial y} = \nu \nabla^2 v' \tag{5.6}$$

$$\frac{\partial u'}{\partial x} + \frac{\partial v'}{\partial y} = 0 \tag{5.7}$$

The quadratic terms in the disturbance velocity component have been neglected. If the mean flow satisfies the Navier-Stokes equations (equations 5.5 to 5.7) can be simplified to

$$\frac{\partial u'}{\partial t} + U \frac{\partial u'}{\partial x} + v' \frac{dU}{dy} + \frac{1}{\rho} \frac{\partial p'}{\partial x} = \nu \nabla^2 u' \tag{5.8}$$

$$\frac{\partial v'}{\partial t} + U \frac{\partial v'}{\partial x} + \frac{1}{\rho} \frac{\partial p'}{\partial y} = \nu \nabla^2 v' \tag{5.9}$$

$$\frac{\partial u'}{\partial x} + \frac{\partial v'}{\partial y} = 0 \tag{5.10}$$

Thus we have three equations for u', v' and p'. However, by differentiating equation 5.8 with respect to y and equation 5.9 with respect to x and subtracting the second from the first the pressure can be eliminated leaving two equations for the two unknowns u' and v'.

5.2.2 Orr-Somerfeld equation

The mean laminar flow $U(y)$ in the x-direction is assumed to be influenced by a disturbance (a sinusoidal traveling plane wave, generally known as a Tollmien-Schlichting wave) whose velocities may be expressed in terms of a stream function $\psi(x, y, t)$ such that

$$u' = \frac{\partial \psi}{\partial y}, \quad \text{and} \quad v' = -\frac{\partial \psi}{\partial x}. \tag{5.11}$$

The stream function representing a single oscillation of the disturbance is assumed to be of the form

$$\psi = \phi(y) e^{i(\alpha x - \beta t)} = \phi(y) e^{i\alpha(x - ct)}, \tag{5.12}$$

where $\phi(y)$ is the complex amplitude of the disturbance stream function ($\phi = \phi_r + i\phi_i$), $\alpha = 2\pi/\lambda$, where λ is the disturbance wavelength, and t is time.

The quantity β is complex, so that $\beta = \beta_r + i\beta_i$. The parameter β_r is the angular velocity or $2\pi f$ (f = frequency), and β_i determines the degree of amplification or damping and is called the amplification factor. The disturbances will be damped if $\beta_i < 0$ and the laminar mean flow is stable, where as for $\beta_i > 0$ instability occurs. The ratio β/α is denoted by c where ($c = c_r + ic_i$). The parameter c_r is the velocity of propagation of the wave in the x-direction, and c_i is again the degree of damping or amplification (depending on its sign).

From equations 5.11 and 5.12 we see that

$$u' = \frac{\partial \psi}{\partial y} = \phi'(y) e^{i(\alpha x - \beta t)}, \quad \text{and} \quad v' = -\frac{\partial \psi}{\partial x} = -i\alpha\phi(y) e^{i(\alpha x - \beta t)}. \tag{5.13}$$

Using these results in equations 5.8 and 5.9 and eliminating the pressure term by differentiation and subtraction as mentioned we obtain

$$(U - c)\left(\phi'' - \alpha^2\phi\right) - U''\phi = \frac{i}{\alpha Re}\left(\phi'''' - 2\alpha^2\phi'' + \alpha^4\phi\right) \tag{5.14}$$

This 4th-order ordinary differential equation for $\phi(y)$ is the fundamental differential equation for the disturbance and is commonly known as the Orr-Sommerfeld equation.

In equation 5.14 lengths have been non-dimensionalized by a suitable reference length (that is, it might be the width b of a channel or thickness δ of a boundary layer) and velocities have been divided by the maximum velocity U_m of the main flow. This means that the Reynolds number Re ($= U_m\delta/\nu$, say) is characteristic of the main flow. Terms on the left hand side of equation 5.14 are derived from inertia terms in the equations of motion and those on the right hand side came from the viscous terms. The boundary conditions, say for a boundary layer, require that the perturbation velocities u' and v are zero at the wall and at a large distance from it (that is, in the freestream itself). Therefore the boundary conditions are:

$$\text{At} \quad y = 0, \quad u' \;=\; v' \;=\; 0 \quad \left(\phi \;=\; 0, \quad \phi' \;=\; 0\right) \qquad (5.15)$$

$$\text{At} \quad y = \infty, \quad u' \;=\; v' \;=\; 0 \quad \left(\phi \;=\; 0, \quad \phi' \;=\; 0\right) \qquad (5.16)$$

It is quite reasonable to suggest that disturbances superimposed on a two-dimensional flow pattern do not have to be two-dimensional if a thorough analysis of stability is to be carried out. However, a theorem developed by H.B. Squire (1933), showed that by considering disturbances which were also periodic in the z-direction (that is, including a w'), a given two-dimensional flow became unstable at a higher Reynolds number when the disturbance was taken as three-dimensional than when it was two-dimensional. In this sense, two-dimensional disturbances represent a "worse case" for two-dimensional flows than three-dimensional disturbances do. Thus, the critical Reynolds number (or more accurately, the lowest limit of stability) is obtained by considering two-dimensional disturbance.

Equation 5.14 and its boundary conditions equations 5.15 and 5.16 constitute what is known as a boundary value problem. This implies that for any given velocity profile $U(y)$ there exists a functional relation between the parameters α, R and c ($= c_r + c_i$) which the solution must satisfy. Thus, if the Reynolds number R and the disturbance wavelength λ ($= 2\pi/\alpha$) are considered given, then equations 5.14, 5.15 and 5.16 will give one eigenfunction $\phi(y)$ and one complex eigenvalue c. As we saw earlier, c_r is the propagation velocity of the disturbance whereas the sign of c_i determines whether or not the wave is amplified ($c_i > 0$) or damped ($c_i < 0$). For $c_i < 0$ the flow $[U(y), R]$ is stable for the given value of α, whereas $c_i > 0$ denotes instability. The limiting case, $c_i = 0$, is called *neutral* stability.

The result of such an analysis for a given laminar flow $U(y)$ can be represented graphically in an α-R diagram, since every point of this plane corresponds to a pair values of c_r and c_i. The locus of $c_i = 0$ separates the region of stable and unstable disturbances. This locus is called the curve of neutral stability. An example is shown in figure 5.7 where neutral stability curves for two velocity profiles are shown. For a given velocity profile, the interior of each curve represents a region of instability whereas the exterior
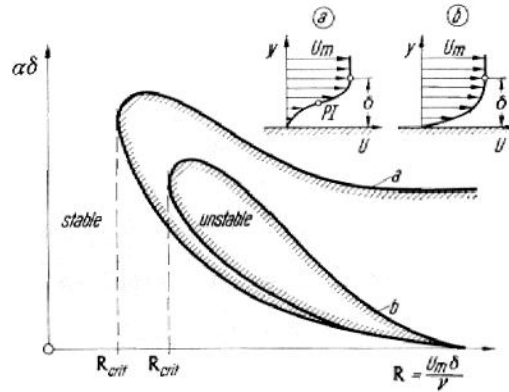
Figure 5.7: Curves of neutral stability for a two-dimensional boundary layer with two-dimensional disturbances: (a) inviscid instability (flow has point of inflection); (b) viscous instability (without point of inflection). From Schlichting.

is a region of stability. The profiles shown in this figure will be discussed in more detail later.

The point on each curve of neutral stability at which the Reynolds number has its smallest value is of great interest since it indicates that value of Reynolds number below which all individual oscillations decay. Above that value, some are amplified. This Reynolds number is the *critical* Reynolds number (R_{crit}) or *limit of stability* for the particular flow being investigated.

It should be pointed out that R_{crit} calculated from stability theory will in general be less than the Reynolds number observed at the point of transition. R_{crit} provides information as to the point on the wall at which amplification of same disturbances begins and continues downstream of it. The transformation of these amplified disturbances into turbulence takes time and the unstable disturbances will have traveled some way downstream. Thus, one would expect that the experimentally observed transition point would be downstream of that point based on the calculated limit of stability. In other words, R_{crit} based on experimental observation would be greater than R_{crit} based on calculation. We often distinguish between these two values by referring to the experimental one as the point of transition" and the theoretical one as the "point of instability". Note that although we use the term "point of transition", we should strictly refer to a "region" of transition. Experimentally it is found that there is no well defined point of transition but that the process whereby a laminar flow becomes a fully developed turbulent flow takes place over a finite distance.

The stability problem, outlined above, poses many difficult mathematical problems. Because of these, success in determining the critical Reynolds number eluded workers for many decades. Early investigators simplified the problem by omitting the viscous terms on the right hand side of the

Orr-Sommerfeld equation. This led to some illuminating results which will be briefly discussed next.

5.2.3 Inviscid stability theory

A limiting but instructive case is that of infinite Reynolds number (or negligible viscosity). Experiments indicate that R_{crit} is large and thus it is natural to simplify the Orr-Sommerfeld equation by dropping the viscous terms (that is, the right hand side of the equation). This gives:

$$(U - c)\left(\phi'' - \alpha^2 \phi\right) - U''\phi = 0 \tag{5.17}$$

Omission of the viscous terms drastically simplifies the problem since the equation has been reduced from 4th to 2nd order, but it also means that we can now only satisfy two boundary conditions, namely

$$y = 0, \quad \phi = 0; \quad y = \infty, \quad \phi = 0.$$

We should also remember that the neglecting viscosity we may lose important properties of the general solution as compared with the simplified form above.

Most of the early work on stability theory used the simplified equation as a starting point. Lord Rayleigh did extensive work published in a series of papers between 1878 and 1915. Obviously, with this approach, no critical Reynolds number is obtainable but questions such as whether a given laminar flow is stable or not (subject to the proviso that viscosity has been neglected) may be answerable. The complete Orr-Sommerfeld equation was not successfully analyzed and critical Reynolds numbers calculated until many years later (Tollmien 1929).

Using the frictionless stability equation Lord Rayleigh derived several theorems concerning the stability of laminar velocity profiles. Their validity when the influence of viscosity was also taken into account was confirmed later.

Rayleigh Theorem 1

The first theorem asserts

> "that velocity profiles having a point of inflexion are unstable."

Rayleigh was only able to prove that this was a necessary condition for instability. Fifty-six years later Tollmien showed that this constituted a sufficient condition for the amplification of disturbances. This "point of

inflexion" criterion is of fundamental importance for stability theory since it provides (except for a viscosity influence correction) a first rough way of classifying laminar flows. We have seen earlier that there is a direct connection between a point of inflexion in the velocity profile and the pressure gradient, so the theorem is important from the practical point of view. Hence the point of inflexion criterion becomes equivalent to a statement about the effect of the pressure gradient in the external flow on the stability of the boundary layer. When applying this theorem to boundary layer flow we can say that a favorable pressure gradient stabilizes the flow, whereas an adverse are promotes instability. Thus the position of the point of minimum pressure on a body in a flow is important in determining the location of transition.

Rayleigh's result produced some confusion in the sense that it was believed for some years that profiles without a point of inflection, such as the Blasius flat plate boundary layer, would be stable for infinitesimal disturbances. In 1921 Prandtl showed that viscosity could be destabilizing for certain wave numbers and certain finite Reynolds numbers. This was verified in 1929 by the computations of Tollmien for the Blasius profile. However, it was not until the 1940's that Schubauer and Skramstad, in a famous low turbulence wind tunnel experiment, verified the theory.

The instability of velocity profiles with points of inflexian is referred to as "frictionless instability" because the laminar mean flow is unstable even without taking into account the effect of viscosity on the oscillating motion. In figure 5.7, this corresponds to curve 'a,' where even at $R = \infty$ there is a certain unstable range of wavelengths.

However, if a profile <u>without</u> a point of inflexion is unstable (curve 'b' of figure 5.7) it is by virtue of the amplification of the disturbances by viscous effects (normally one might expect viscosity to promote damping). This prediction by small disturbance theory was not generally accepted until it was found experimentally. It appears that in this case that the viscous stress fluctuations set up by a traveling wave disturbance can shift the phase of u' with v' so that the product $\rho \overline{u'v'}$ (known as the Reynolds shear stress) is non-zero. The Reynolds stress interacts with the mean velocity gradient to extract kinetic energy from the mean flow and feed it to the disturbance energy. We see in figure 5.7 that at high Reynolds numbers the range of unstable wavelengths is contracted to a point and that unstable oscillations only exist for finite Reynolds numbers.

Rayleigh Theorem 2

The second theorem states that

> "the velocity of propagation of neutral disturbances ($c_i = 0$)
> in a boundary layer is smaller than the maximum velocity
> of the mean flow (that is, $c_r < U_m$)."

This implies that at some point in the flow the wave velocity is equal to the mean velocity, that is, $U - c = 0$. This layer for which $U - c = 0$ corresponds to a singular point of equation 5.17. Here, ϕ'' becomes infinite unless U'' does not vanish simultaneously. The distance $y = y_K$ where $U = c$ is called the *critical layer* of the mean flow.

This mathematical singularity in the frictionless stability equation simply points to the fact that the effect of viscosity cannot be neglected near the critical layer. Inclusion of the effect of viscosity removes this singularity.

The two Rayleigh theorems show that the curvature of the velocity profile affects stability in a fundamental way. The calculation of velocity profiles in laminar boundary layers must be carried out accurately if a proper stability analysis is to be made. Both the profile itself $U(y)$ and its second derivative $U''(y)$ must be known accurately.

5.3   Experimental Evidence

The theory of stability outlined so far assumes that the stability of the boundary layer at a given station on a surface is a function only of its local velocity profile, and the previous history of the layer and its development with distance along the surface play no explicit part. Further, it gives no information on the effect of finite disturbances in promoting transition nor does it tell us anything about the mechanism of transition. In some cases, the calculated limit of stability was found to be close to the measured position of transition but in other cases transition occurred considerably after instability was calculated to begin.

For these reasons, the theory was treated with reserve in some quarters until a classic series of experiments by Schubauer & Skramstad of the National Bureau of Standard in Washington, provided conclusive evidence that within the context of instability to small disturbances the theory was substantially right, at least for the boundary layer on a flat plate in a stream of low turbulence. They demonstrated the existence of the neutral stability curve (see figure 5.8) and obtained substantial agreement with the theoretical predictions of the detailed behavior of the oscillations in the boundary layer. They demonstrated that if the turbulence of the freestream was low

(that is, of intensity $T = \sqrt{\overline{u'^2}}/U < 0.03\%$) sinusoidal oscillations of the kind considered by the theory appeared naturally in the boundary layer well ahead of transition. They also investigated the behavior of artificially induced oscillations over a wide range of frequencies. These were produced by vibrating a metal ribbon held close to the surface and subjected to an oscillating electro-magnetic field. In this way they were able to induce two dimensional disturbances of prescribed frequency, as stipulated by the theory. The existence of natural sinusoidal disturbances could be clearly demonstrated even in the presence of natural oscillations (that is, with no external excitation). See figure 5.9. At the very low turbulence level of the experiment, there are hardly any irregular oscillations left in the boundary layer, but, as the point of transition is approached, there appear almost purely sinusoidal oscillations — their amplitude is initially small and increases rapidly downstream. A short distance ahead of transition, oscillations of very high amplitude appear. At transition, then regular oscillations break down and are suddenly transformed into irregular patterns of high frequency characteristic of turbulent motion.
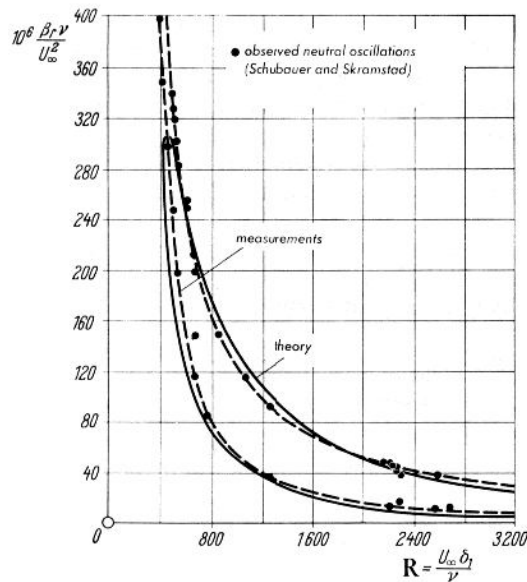
Figure 5.8: Curves of neutral stability for neutral frequencies of disturbance on a flat plate at zero incidence. Measurements by Schubauer & Klebanoff. From Schlichting.

5.4   Effects on Transition

We have seen in the preceding sections that the method of small disturbances can be used to study the phenomenon of transition from laminar to turbulent flow. We might, therefore, expect that this approach should also supply us with information concerning the other parameters which have an important influence on transition, in addition to the single one, the Reynolds number, dealt with so far.

In this set of notes we will briefly review some of the other parameters which are important in determining when transition will occur. These will include effects of pressure gradient, surface suction, surface roughness, and heat transfer.

Only a brief outline is given here. More details are given in, for example, *Boundary Layer Theory* by H. Schlichting.

Influence of pressure gradient

The influence of the pressure gradient on stability manifests itself through the form of the velocity profile given by $U(y)$. We have seen already that the limit of stability of a velocity profile depends strongly on its shape. Those with a point of inflexion possess lower limits of stability than those without one (ie the point of inflexion criterion). We have seen before that the pressure
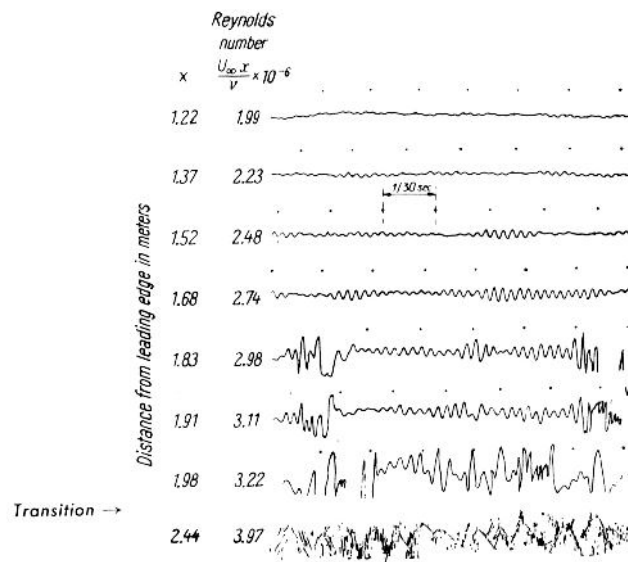
Figure 5.9: Time traces of the u'-component velocity fluctuation caused by natural disturbances in a laminar boundary layer. Measurements by Schubauer & Klebanoff. From Schlichting.

gradient controls the curvature of the velocity profile at the wall. That is,

$$\mu\left(\frac{d^2U}{dy^2}\right)_{wall} = \frac{dp}{dx}.$$

In essence then, the strong dependence of the limit of stability on the shape of the velocity profile amounts to a large influence of the pressure gradient on stability. We can say that accelerated flows ($dp/dx < 0$, favorable pressure gradient) are considerably more stable than decelerated flows ($dp/dx > 0$, adverse pressure gradient). The latter were confirmed experimentally by Schubauer & Skramstad.

To evaluate stability, it is convenient to express the pressure gradient influence by the use of a shape factor for the velocity profile and for simplicity to consider or one parameter family of laminar profiles. An example, which is also an exact solution of the boundary layer equations is the familiar wedge flow, where the freestream velocity is given by $U_m(x) = U_1 x^m$. The exponent m (or β) denotes the "shape factor" of the profiles. The wedge angle, $\beta = 2m/(m + 1)$). This shape factor m is not to be confused with the profile shape factor $H = \delta^*/\theta$. For $m < 0$, the velocity profiles have a point of inflexion, but when in $m > 0$ there is not one. Pretsch carried out the stability calculation for a series of profiles of this family — the results are shown in table 5.1. We can see that the critical Reynolds number is strongly dependent on the pressure gradient. As would be expected, the amplification is much greater with an adverse rather than a favorable pressure gradient.

Pohlhausen's method is a convenient one for calculating laminar velocity profiles and it is instructive to investigate the stability of the associated profile. We have seen that the dimensionless factor $\Lambda = (\delta^2/\nu)(dU_m/dx)$ determines the shape of the velocity profile. It varies between +12 and -12. The latter corresponds to separation. For $\Lambda > 0$ the pressure decreases (dp/dx negative) whereas $\Lambda < 0$ corresponds to an increase in pressure (dp/dx positive). When $\Lambda < 0$ the velocity profiles have a point of inflexion. Schlichting

β	$-0{\cdot}10$	0	$0{\cdot}2$	$0{\cdot}4$	$0{\cdot}6$	$1{\cdot}0$
$m = \dfrac{x}{U}\dfrac{dU}{dx}$	$-0{\cdot}048$	0	$0{\cdot}111$	$0{\cdot}25$	$0{\cdot}43$	$1{\cdot}0$
$\left(\dfrac{U_m \delta_1}{\nu}\right)_{crit}$	126	660	3200	5000	8300	12600
$\left(\dfrac{\beta_i \delta_1}{U_m}\right)_{max} \cdot 10^4$	155	$34{\cdot}5$	$14{\cdot}6$	—	$9{\cdot}1$	$7{\cdot}3$

Table 5.1: Critical Reynolds number (second row) and maximum amplification factor (third row) in terms of the shape factor β of the velocity profile for flows with pressure gradient, as calculated by J. Pretsch. From Schlichting.
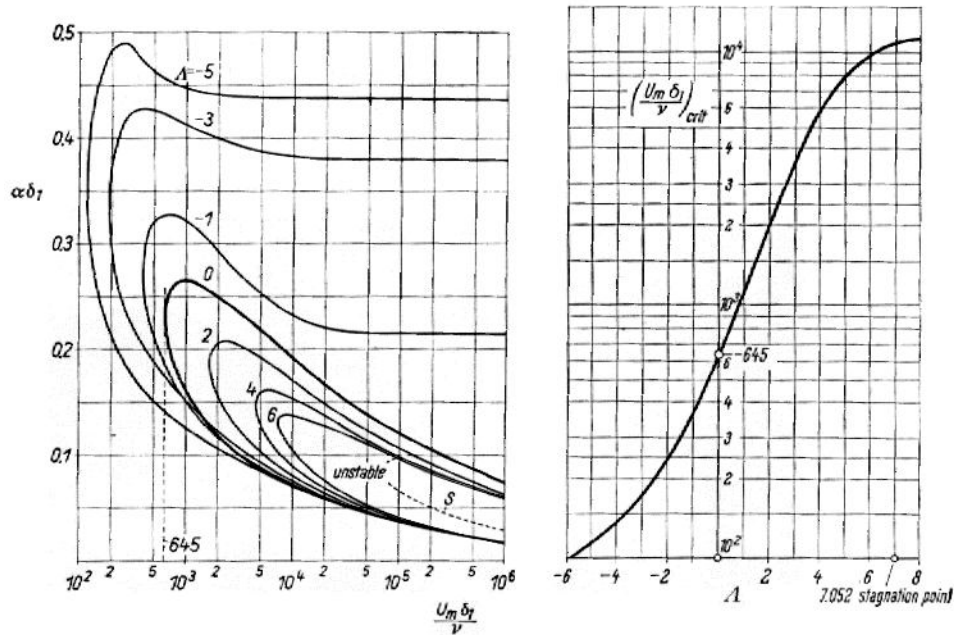
Figure 5.10: Left: curves of neutral stability for laminar boundary layer profiles with pressure decrease ($\Lambda > 0$) and pressure increase ($\Lambda < 0$). Right: critical Reynolds number of boundary layer profiles with pressure gradient as a function of Λ (see equation 3.31 for a definition of Λ). From Schlichting.

& Ulrich carried out stability calculations for this family of profiles. The neutral stability curves are shown in figure 5.10. The right hand figures shows the plot of R_{crit} versus Λ. As might have been anticipated R_{crit} varies strongly with Λ and hence with dp/dx.

We have seen that a pressure increase along a boundary layer strongly favors transition to turbulence. It is interesting to note that conversely, a very strong pressure decrease, such as may be created by a centered expansion in supersonic flow, can cause a turbulent boundary layer to become laminar. Sternberg, making tests on geometry shown in figure 5.11 at a Mach number of 3 observed this. The large favorable pressure gradient at the corner should impresses a strong acceleration on the flow which "extinguishes" the turbulence.

Influence of suction

The effect of suction is to stabilize the boundary layer. Firstly, suction reduces the boundary layer thickness and a thinner boundary layer is less prone to become turbulent. Secondly, suction creates a laminar velocity profile having a higher critical Reynolds number than a velocity profile with no suction.
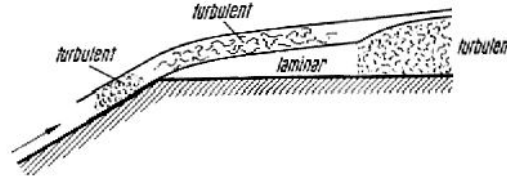
Figure 5.11: Schematic representation of the flow in a laminar boundary layer in supersonic flow around a corner, after Sternberg. From Schlichting.
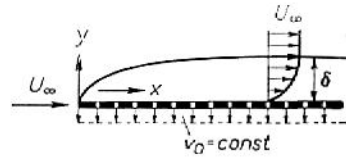
Figure 5.12: Flat plate at zero incidence with homogenous suction. From Schlichting.

For a flat plat at zero incidence and with uniform suction (suction velocity $= -v_0$), as shown in figure 5.12, the velocity profile and hence the boundary layer thickness thickness became independent of the current co-ordinate at a certain distance from the leading edge. From this location onwards we can show that the velocity profile is given by $U(y) = U_\infty(1 - \exp v_0 y / \nu))$ for which the critical Reynolds number is 70,000.[2] Note that for the Basius profile R_{crit} is 520. Thus the critical Reynolds number of this so called "asymptotic" suction profile is more than two orders of magnitude larger than that on a flat plate with neither a pressure gradient or suction. This demonstrates the highly stabilizing effect of suction.

Influence of roughness

The question here is how the process of transition depends on the roughness of the wall over which the boundary layer is flowing. From a practical point of view, the longer the flow over a wing may be kept laminar, the lower will be the overall skin friction drag.

In a general sense, the presence of roughness favors transition. By this, we mean that under otherwise identical conditions, transition occurs at a lower Reynolds number on a rough wall than on a smooth wall. This follow from the theory of stability. Roughness elements produce additional disturbances in the laminar stream which have to be added to those generated by turbulence and already present in the boundary layer.

---

[2]R_{crit} is based on δ^*, that is $R_{crit} = U\delta^*/\nu$. Note that this is the Reynolds number at the point of instability and will be less than the transition Reynolds number found experimentally.

If the disturbances created by roughness are bigger than those due to turbulence, we would expect that a lower degree of amplification would be sufficient to produce transition. Alternatively, if the roughness elements are very small, the disturbances should lie below the "threshold" which is characteristic of those generated by the turbulence of the external freestream — in this case then, we would expect no effect on transition. These propositions show complete agreement with experiment.

When the roughness elements are large, transition occurs at the points where they are actually present. Early workers in the field assumed that the transition point was located at the position of the roughness elements when they were large, or that there was no influence for small elements. However, it turns out that as roughness elements are made progressively higher the point of transition moves steadily upstream until it reaches the position of the roughness elements themselves. This prompts us to ask three basic questions:

1. What is the maximum height of roughness elements below which no influence on transition exists?

2. What is the limiting height of a roughness element which causes transition to occur at the element itself?

3. How do we describe the position of the transition point in the range between items 1 and 2 above.

Experimentally, transition is often provoked by attaching a wire to the wall at right angles to the stream direction. This is called a "trip" wire. Goldstein deduced that the critical height (k_{crit}), that is, the height which does not affect transition is given by

$$\frac{u_{\tau,k} k_{crit}}{\nu} = 7,$$

where $u_{\tau,k} = \sqrt{\tau_{w,k}/\rho}$ is called the "friction" velocity, and $\tau_{w,k}$ is the shear stress at the wall in the laminar boundary layer at the position of the roughness element.

The minimum height for which transition occurs at the element itself was proposed by Tani *et al.* to be $u_{\tau,k} k/\nu_{crit} = 15$ whereas other workers quote a value of 20. The values quoted above are all for single, cylindrical roughness elements (that is, circular wires).

Dryden developed an empirical law for the determination of the position of the transition point, x_{tr}, in terms of the height k of the roughness element and its position x_k. He found that in incompressible flow all the experimental points for the case when transition does not occur at the roughness element itself (that is, $x_{tr} > x_k$) arrange themselves on a single curve in a plot of
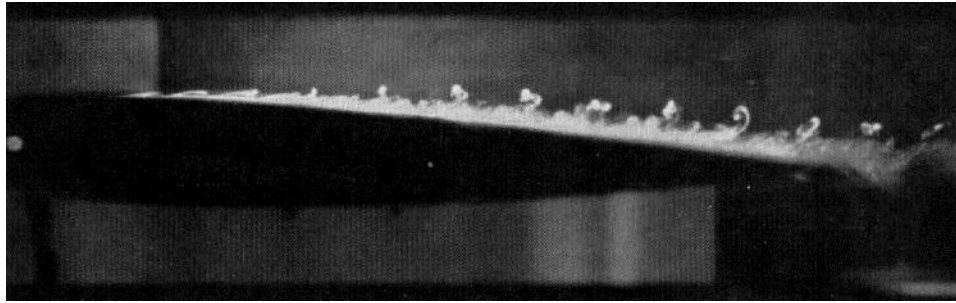
Figure 5.13: Smoke picture of the flow in the boundary layer on an airfoil in the presence of periodic disturbances, after Bergh. From Schlichting.

the Reynolds number $R_{tr} = U\delta^*_{tr}/\nu$ against the ratio k/δ^*_{tr}, where δ^*_{tr} is the displacement thickness at the point of transition, and δ^*_k is the displacement thickness at the position of the roughness element.

Influence of sound and vibration

Sound and vibrations usually produce disturbances over a wide spectrum of frequencies. When there exists good coupling between the boundary layer stability characteristics and the disturbance level, sound and other types of vibration can have a major effect on stability. The coupling between freestream turbulence and transition of the boundary layer on a smooth sphere waas used for a long time to measure the freestream turbulence level: the critical Reynolds number for the drag decrease on the sphere was calibrated in terms of the level of turbulence. As an example of the effects of sound on the boundary layer stability, figure 5.13 illustrates the strong interaction.

Influence of heat transfer

The results given so far are valid only for flows at moderate speeds (that is, incompressible flow). In the case of compressible flows, we must consider the rate of heat transferred from the wall and the wall, in addition to the Mach number. In incompressible flows, heat can be exchanged between the fluid and the wall only if the wall temperature is higher or lower than that of the flowing fluid. In contrast in compressible flows, heat generated within the boundary layer results in an additional important influence. In either case, a thermal boundary layer develops in addition to the velocity boundary layer and this plays a role in the determination of the instability of a small disturbance. We will show in the next few pages that for the subsonic (that is, incompressible or almost so) flow of a gas, heat transfer from the boundary layer to the wall has a stabilizing influence whereas heat

transfer from the wall to the gas has the opposite effect. Both are reversed for flow of a liquid.

The stability of supersonic/hypersonic boundary layers will not be dealt with in these notes. Any interested person should refer to Schlichting *Boundary Layer Theory*.

Using the "point of inflexion" criterion discussed earlier, we can show that in incompressible flow, the transfer of heat from the wall to the fluid ($T_w > T_\infty$) depresses the limit of stability, whereas the transfer of heat from the fluid to the wall ($T_w < T_\infty$) causes it to become larger. We shall see that this is a consequence of the dependence of the fluid viscosity μ on the fluid temperature T.

from the boundary layer equation, the curvature of the main flow velocity profile $U(y)$ at the wall is given by

$$\frac{d}{dy}\left(\mu\frac{dU}{dy}\right)_w = \frac{dP}{dx}.$$

For the flat plate at zero incidence $dP/dx = 0$, and if we differentiate the left hand side (assuming that μ is not a constant but a function of temperature and there of y) we get

$$\mu_w\left(\frac{d^2U}{dy^2}\right)_w + \left(\frac{d\mu}{dy}\right)_w\left(\frac{dU}{dy}\right)_w = 0,$$

and the curvature of the velocity profile at the wall is given by

$$\left(\frac{d^2U}{dy^2}\right)_w = -\frac{1}{\mu_w}\left(\frac{d\mu}{dy}\right)_w\left(\frac{dU}{dy}\right)_w.$$

Now, consider the flow of air for which μ increases with increasing temperature. If the wall is hotter than the gas in the freestream (that is, $T_w > T_\infty$) then we have $(\partial T/\partial y)_w < 0$.

In addition, $(d\mu/dy)_w < 0$ and since $(dU/dy)_w > 0$ it follows that it $T_w > T_\infty$ then $(d^2U/dy^2)_w > 0$. Thus for a heated wall the curvature of the velocity profile at the wall is positive and for a cooled wall it is negative. It follows that for the heated wall there will be a point of inflexion in the boundary layer because the curvature is vanishingly small but negative at $y = \infty$. Thus the velocity profile for a heated wall has a point of inflexion and becomes highly unstable by the criterion given earlier.

This destabilizing effect of heating has been experimentally confirmed (see figure 5.14). It can be seen that the critical Reynolds number decreases as the wall temperature increases, the decrease being steeper for higher turbulence intensities of the freestream. Since the viscosity of a liquid decreases with a temperature increase, the effect outlined above should be reversed. Experiments by Wazzan *et al.* using water have confirmed this.
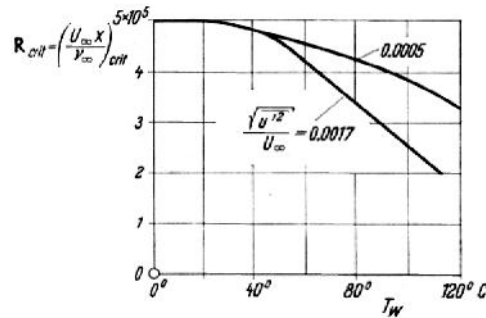
Figure 5.14: The critical Reynolds number of a heated flat plate at zero incidence in an incompressible air stream. Measurements by Liepmann & Fila. From Schlichting.

5.5 The Origin of Turbulence

"In flows which are originally laminar, turbulence arises from instabilities as at large Reynolds number. Laminar pipe flow can become turbulent at a Reynolds number (based on mean velocity and diameter) in the neighborhood of 2,000 unless great care is taken to avoid creating small disturbances that might trigger transition from laminar to turbulent flow. Boundary layers in zero pressure gradient become unstable at a Reynolds number $U_e\delta^*/\nu = 600$ (δ^* is the displacement thickness, U_e is the free-stream velocity, and ν is the kinematic viscosity). Free shear flows, such as the flow in a mixing layer, become unstable at very low Reynolds numbers because of an inviscid instability mechanism that does not operate in boundary-layer and pipe flow. Early stages of transition can easily be seen in the smoke rising from a cigarette." (Tennekes & Lumley).

Two kinds of instability mechanisms can be identified: inviscid instabilities where viscosity is not important in the stability argument, and viscous instabilities where viscosity plays a crucial role in the stability argument. Both kinds are important for the understanding of transition and turbulence.

5.6 Inviscid Stability Examples

The inviscid instability mechanism of thin shear layers can be demonstrated by considering a perturbed vortex sheet (figure 5.15). Initially the pressure and velocity directions are equal on the two sides of the vortex sheet, although the velocity magnitude is not. If a small perturbation occurs on the

initially planar sheet, the streamlines converge on the top and diverge on the bottom, a pressure difference is created, lift is generated, and the initially small perturbation will grow, at least until non-linearities catch up with it. This is called the Kelvin-Helmholtz instability (see figure 5.16).

In a viscous fluid (but not in creeping flow), where the shear layer has a finite thickness, the instability is still governed by the inviscid stability argument and the characteristic roll-up frequency is related to the shear layer thickness and the velocity difference.

Subsequent instabilities can occur which eventually lead to the turbulent state. In the vortex sheet or simple shear layer case, there will always exist imperfections in the flow which can lead to phase differences between roll-ups and eventually to vortex pairing. Three-dimensional disturbances can also become unstable and grow, and the flow quickly takes on all characteristics of fully turbulent flow (see figures 5.17 and 5.18).

Interestingly, at higher Reynolds numbers, where the flow is clearly turbulent, large-scale roll-ups are still evident which look much like the initial Kelvin-Helmholtz roll-ups (see figure 5.19). These are sometimes called "coherent" structures because of their organized form. Superimposed on these large-scales are all other scales, down to very small-scale motions.

Another classic, inviscid instability is Rayleigh-Bénard convection, which is buoyancy driven. A layer of fluid which is heated from below is unstable to small disturbances and convection rolls are formed (see figure 5.20).

5.7   Viscous Stability Examples

Viscous stability problems are more difficult. A good example is given by the instability of a laminar boundary layer as the Reynolds number increases. What we see is that, if very small two-dimensional disturbances are present (this is obviously a rather idealized flow situation), then below a critical Reynolds number the disturbances will dissipate and laminar flow is recovered. Above a critical Reynolds number, the disturbances will grow, first in a two-dimensional manner (called Tollmien-Schlichting (T-S) waves
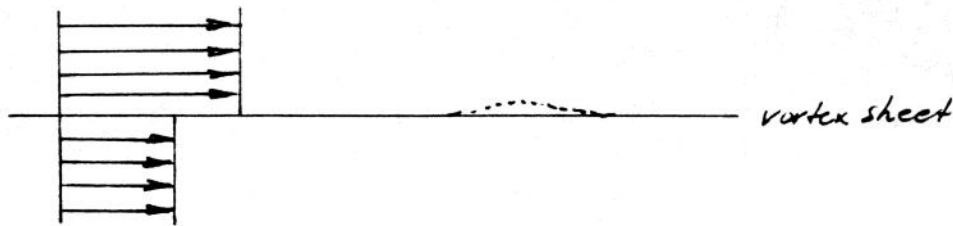
Figure 5.15: Perturbed vortex sheet.
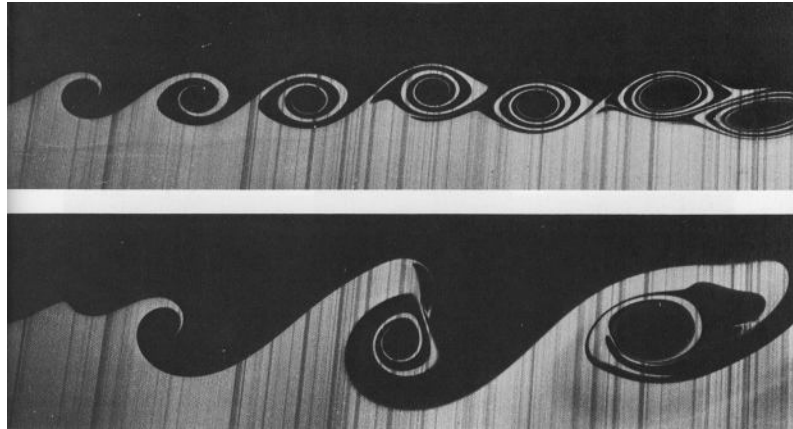
Figure 5.16: Kelvin-Helmholtz instability of a mixing layer.

Figure 5.17: Instability of an axisymmetric jet.

— see figure 5.21), then in a three-dimensional manner as the flow becomes unstable to three-dimensional disturbances, and then finally the flow rapidly becomes turbulent (which in this context means that a wide range of scales are present).

The onset of the two-dimensional instability can be analyzed as a linear problem. The analysis was done by Tollmien in 1929 and presented in its final form by Schlichting in 1933, but the experimental confirmation was not performed until 1947 by Schubauer & Skramstadt — mainly because the experiment is very difficult (see figure 5.8). Note that the most unstable frequency is a function of Reynolds number (it can also be shown that at low Reynolds numbers the most unstable disturbance is two-dimensional so that it is preferentially amplified but at higher Reynolds numbers the three-dimensional instabilities take over and grow very rapidly).

An interesting point about the analysis is that it demonstrated that viscosity can be destabilizing. This is contrary to expectation since we see viscous effects as being dissipative and therefore inherently stabilizing. In agreement with observation, the theory predicts transition in flows that are
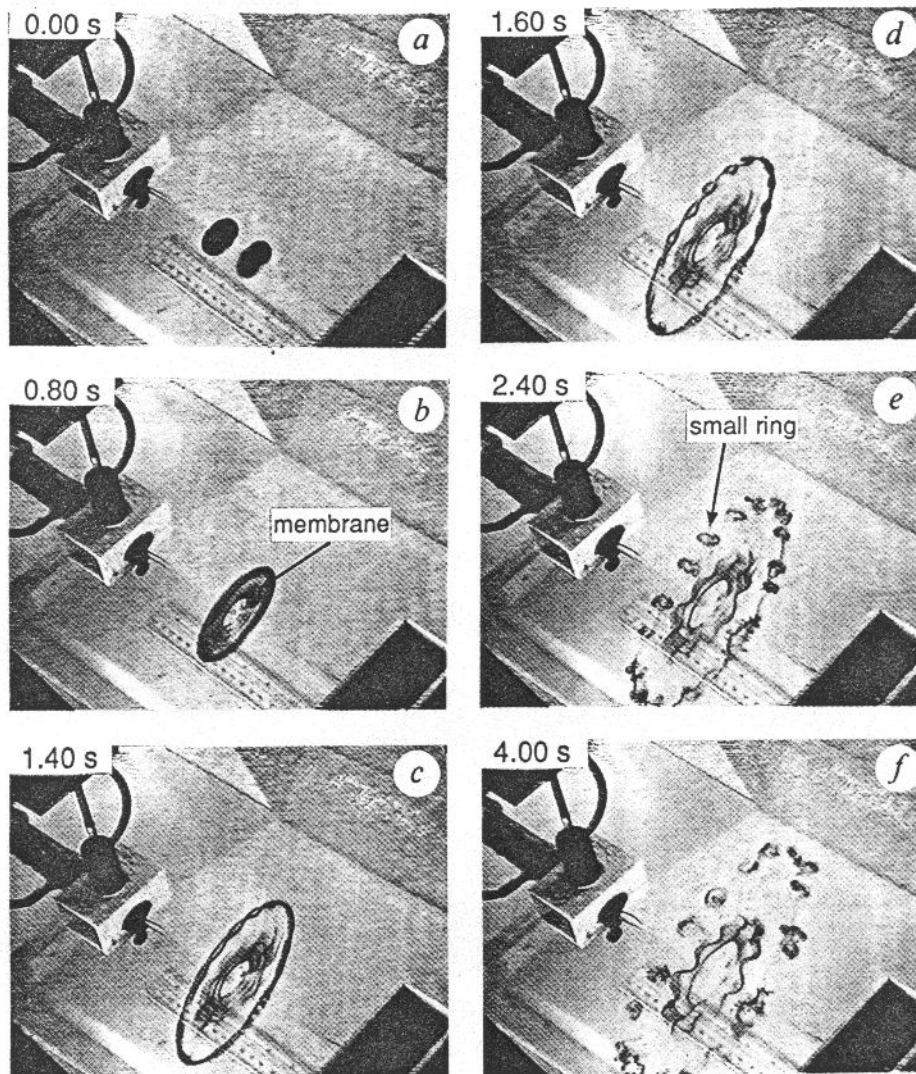
Figure 5.18: Instability and reconnection in the head-on collision of two vortex rings. From Lim & Nickels, 1992.
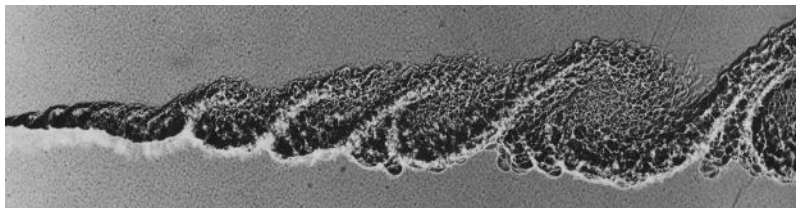
Figure 5.19: Large-scale structure in a turbulent mixing layer.

inviscidly stable (no inflection point in the velocity profile), such as channel flows and boundary layers with favorable pressure gradients. The reason is
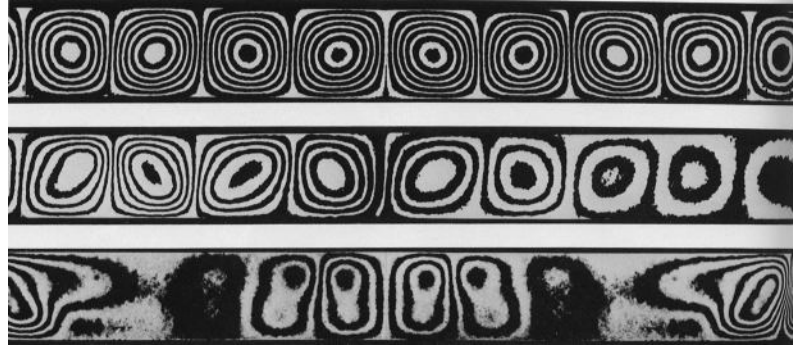
Figure 5.20: Buoyancy-driven convection rolls.
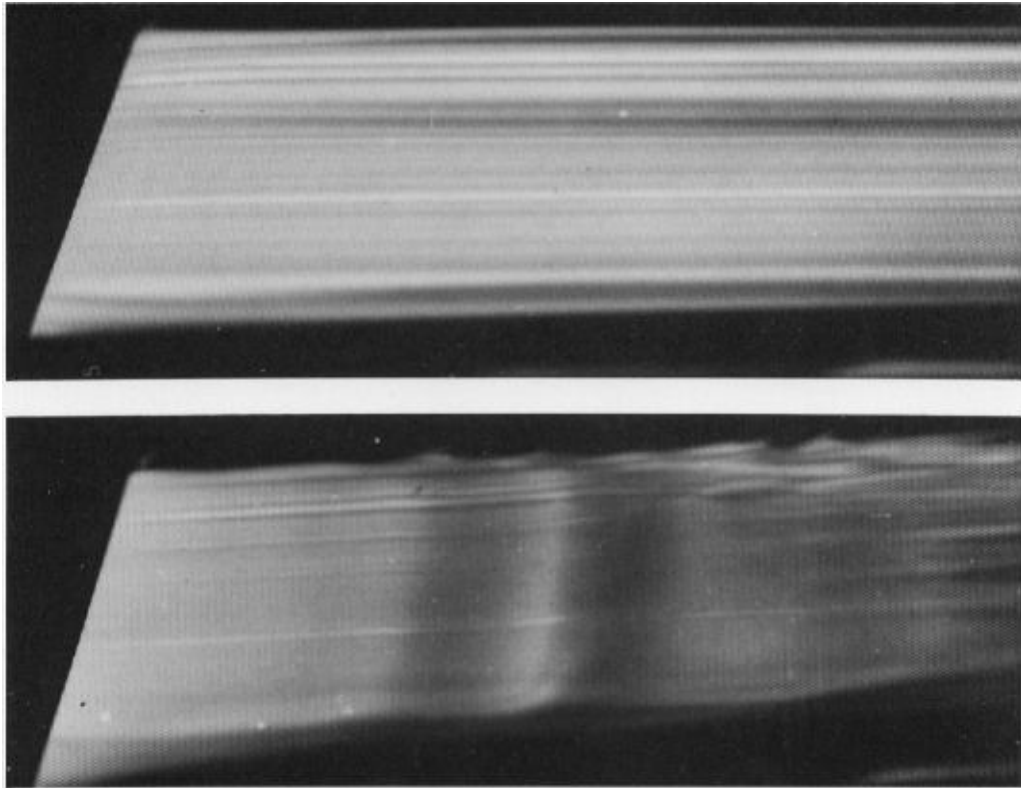
Figure 5.21: Instability of the boundary layer on a flat plate.

that the viscous stress fluctuations set up by a travelling wave disturbance can shift the phase of u' with respect to v' so that the product $\overline{u'v'}$ (the Reynolds shear stress) is non-zero. The Reynolds shear stress interacts with the velocity gradient to extract kinetic energy from the mean flow and feed it to the disturbance energy.

Now there are many roads to turbulence. For example, in Poiseuille flow (laminar pipe and channel flow) and Couette flow (flow between two plates in relative motion), transition does not follow these simple stages to turbu-
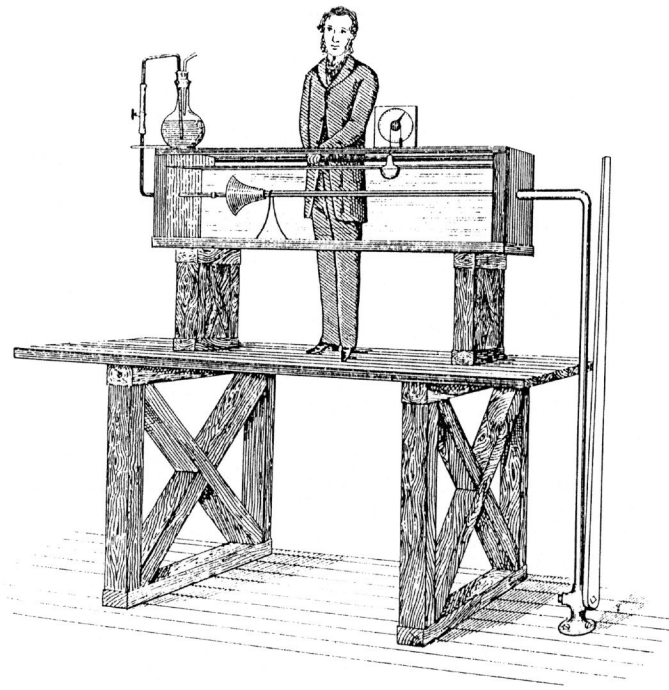
Figure 5.22: Sketch of Reynolds' dye experiment, taken from his 1883 paper.

lence. In fact, Poiseuille pipe flow is not linearly unstable at any Reynolds number (neither is Couette flow), and transition must occur through the effects of large disturbances. From recent work in DNS and experiment we know that pipe flow shows an intermittent transition to turbulence, where "puffs" of "slugs" of turbulent flow occur between periods of laminar flow. The rather simple picture of transition presented by Osborne Reynolds original experiment (see figures 5.22 and 5.23) is not very accurate.

Transition in boundary layers can also occur in different ways. In fact, the most common road to turbulence is through the appearance of "turbulent spots" originating at points of imperfection on the surface. This is sometimes called "bypass" transition in that it by-passes the T-S linear stage. Turbulent spots are sometimes called Emmons spots after the researcher at Harvard who originally described them in detail — although see Schlichting for some very early observations by Prandtl (see figures 5.5 and 5.24). They are very regular in their appearance, grow at well-defined rates, and are separated by regions of laminar flow (see figure 5.25).   The growth process can be described in terms of spanwise vortex tubes which experience a three-dimensional disturbance, that is, they become kinked, thereby generating a self-induced velocity field which lifts up the kink into a region of higher mean velocity, where it is then stretched. These vortex loops distort the adjacent spanwise vortex tubes, and thus the spot grows in a very ordered
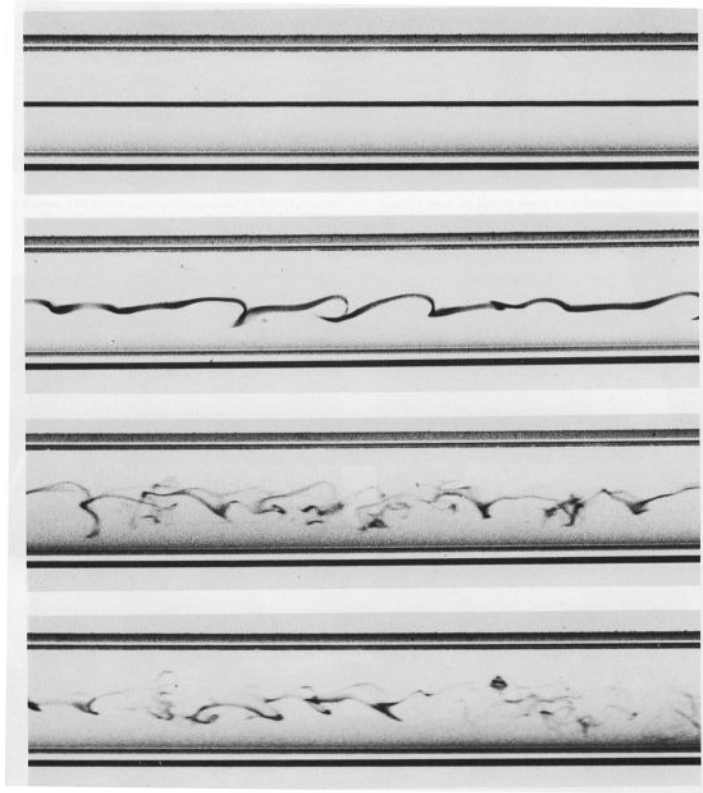
Figure 5.23: Repetition of Reynolds' dye experiment.

fashion (see figure 5.26 from Perry, Lim & Teh, and the analysis by Walker at Lehigh).

When we use ensemble-averaging to investigate the character of the flow inside the spots we see that it closely resembles fully turbulent boundary layer flow (for example — a logarithmic velocity variation is found near the wall). Coles has recently suggested that the turbulent boundary layer (even far downstream of transition) can be thought of as an amalgam of interacting turbulent spots. By inspection we see many regular features in the turbulent spot, which again suggests the presence of "coherent" structures in fully developed turbulent boundary layer flow.

We should also note that transition typically takes some distance. This distance is hard to quantify but there is obviously some distance required before the T-S waves break down, or before the spots amalgamate and produce a flow with no intermittent regions of laminar flow. So we should talk about a transition region rather than a point of transition.

There is also the question about how far downstream the flow is influenced by the details of transition. Clearly, large scale three-dimensional motions are formed as part of the transition process, and it may take some time for these to settle down to their "equilibrium" state. This is particularly
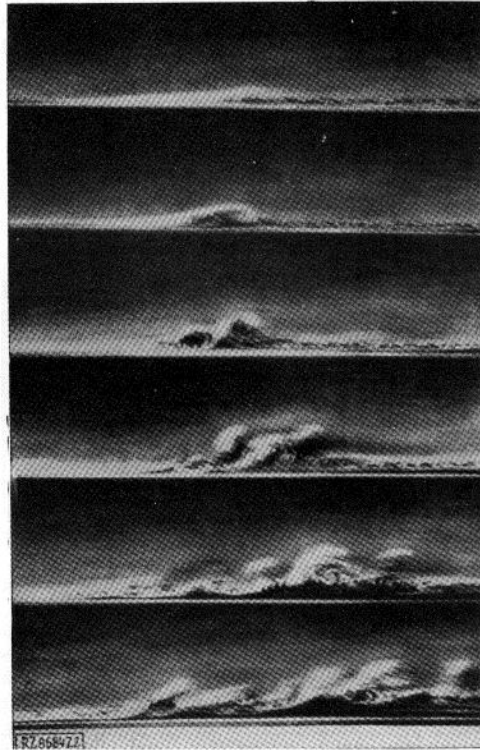
Figure 5.24: Growth of a turbulent spot on a flat plate as visualized by Prandtl. The photographs were taken with the aid of a slow motion camera, which traveled on a trolley along with the flow, in order to follow the same group of vortices. The flow was made visible by sprinkling aluminum dust on the water surface. From Schlichting.

true if the transition was initiated by some "artificial" means (although it could be argued that all disturbances are artificial in some way). For example, in experimental work, transition is often induced by some form of tripping device, typically a circular cylinder place spanwise on the wall. This is done to speed up the transition, and fix it in place so that it does not occur in different places during the course of the experiment. Now if the tripping device is very large, it will produce a large disturbance. Since the disturbance will dissipate slowly (viscous dissipation is always slow) it will affect the flow scaling for a very long distance downstream (see Coles 1962 for a detailed discussion). A similar situation may exist in DNS or LES flows where disturbances are introduced to force transition — a poor choice of disturbance environment may make the results meaningless. Of course, if these kinds of artificially introduced difficulties are avoided, there may exist genuine effects of transition which persist downstream. Or, more to the point perhaps, some part of the flow can be analyzed or modelled using concepts based on stability arguments similar to those used to describe the
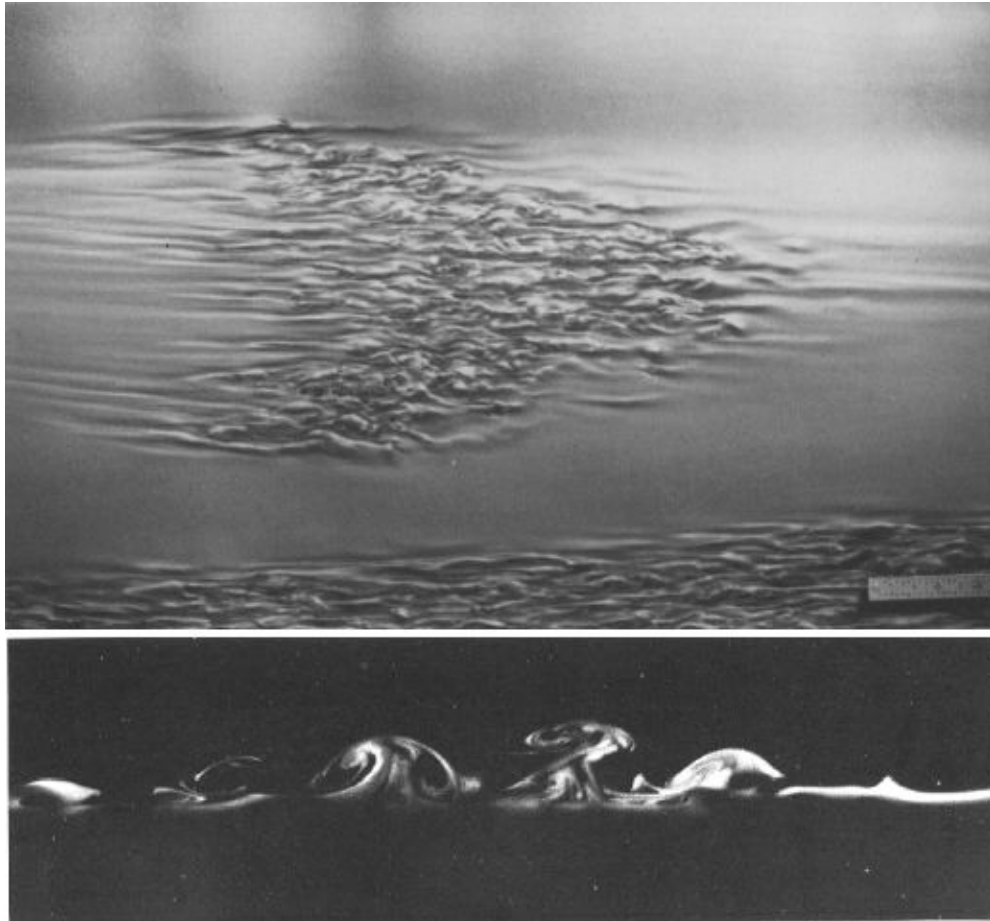
Figure 5.25: Emmons turbulent spot: (top) plan view; (middle) side view; (bottom) cross-section. Visualizations by Cantwell & Coles, and Perry, Lim & Teh.

initially laminar flow (see the large-scale structures in the turbulent mixing layer shown in figure 5.27.

Two more things before we move on. First, we can see the important role of Reynolds number — if the Reynolds number is low enough then there is no turbulence. We will take up this idea more formally later but for now we can think of Reynolds number as the ratio of inertial forces to viscous forces, that is, the ratio of a typical acceleration of a fluid particle to the viscous stress gradients acting on the particle. If a typical length is L and a typical velocity is U, the Reynolds number is $(U^2/L)/(\nu U/L^2) = UL/\nu$. Many different Reynolds numbers can be defined for turbulent flow, depending on the relevant length and velocity scales. In terms of stability arguments, we can think of the analogy with the role of shock absorbers in the suspension of a car. As the car travels over a bumpy road, the shock absorber absorbs the oscillations of the car by viscous dissipation. As the Reynolds number increases, it is as if the shock absorbers become less effective, and the oscillations become
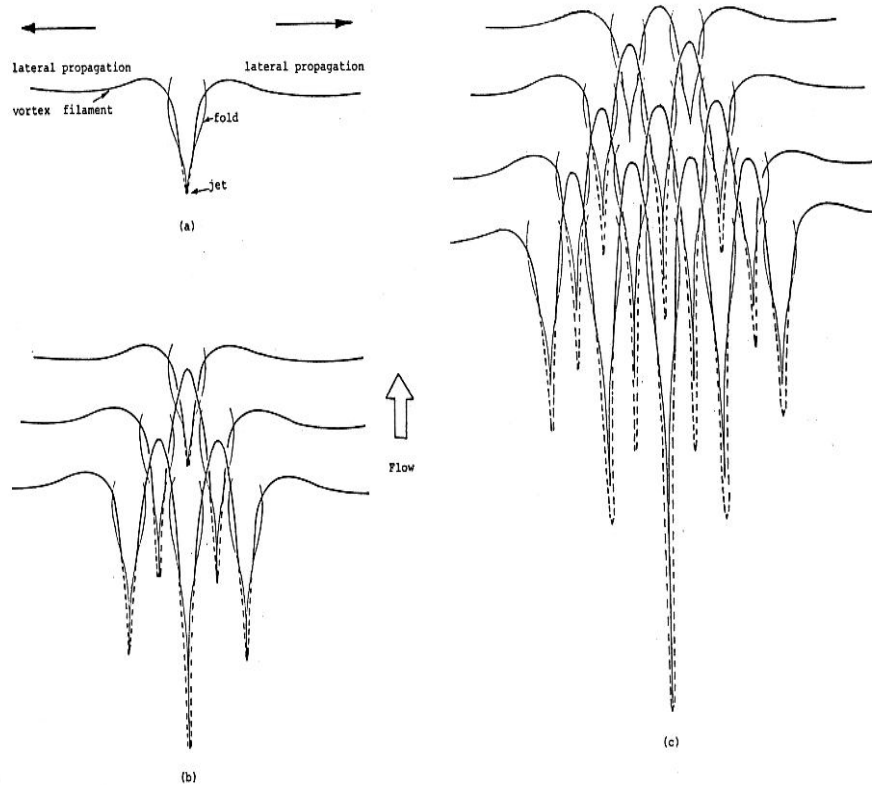
Figure 5.26: Schematic diagram of the sequence of events leading to the formation of a turbulent spot, in terms of vortex filaments. From Perry, Lim & Teh.

larger. At some point in fluid flow, the shock absorbers (viscosity) can actually cause the oscillations to grow and the breakdown follows.

Second, we can see how turbulence arises from a process of successive instability.

> "On the other hand, turbulence cannot maintain itself but depends on its environment to obtain energy. A common source of energy for turbulent velocity fluctuations is shear in the mean flow; other sources, such as buoyancy, enter too. Turbulent flows are generally shear flows. If turbulence arrives in an environment where there is no shear or other maintenance mechanism, it decays: the Reynolds number decreases and the flow tends to become laminar again. The classic example is turbulence produced by a grid in uniform flow in a wind tunnel.
>
> Another way to make a turbulent flow laminar or to prevent a laminar flow from becoming turbulent is to provide for a mechanism that consumes turbulent kinetic energy. This situation prevails in turbulent flows with imposed magnetic fields at low
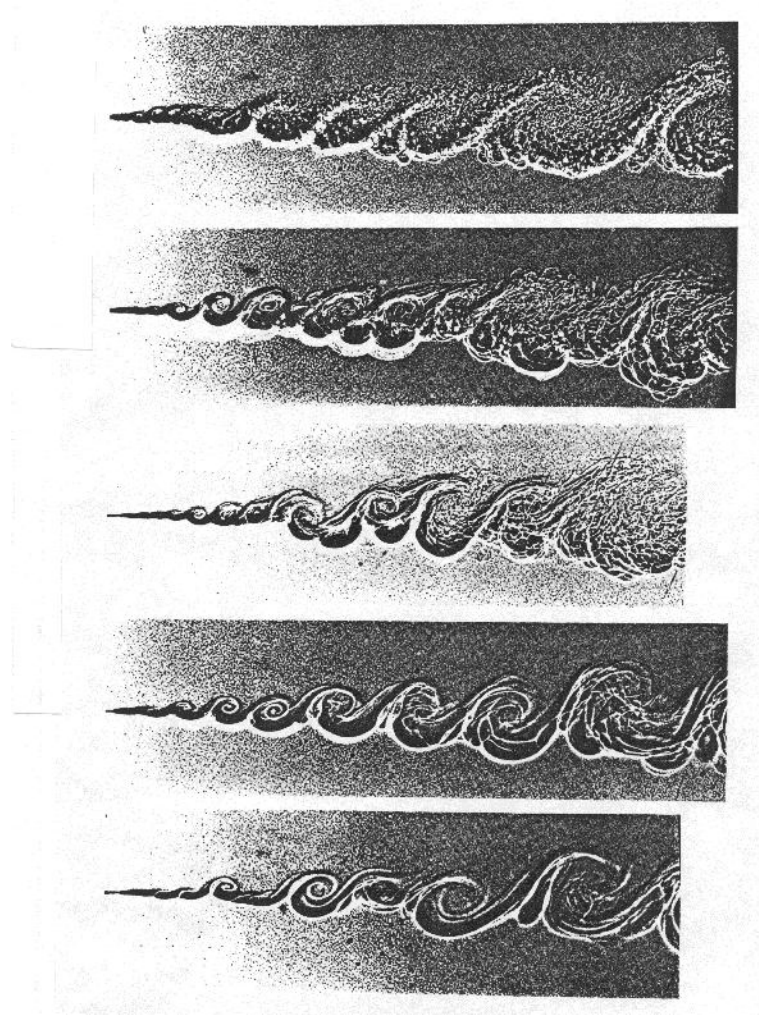
Figure 5.27: Shadowgraphs of mixing layer taken at random times.

magnetic Reynolds numbers and in atmospheric flows with a stable density stratification, to cite two examples." (Tennekes and Lumley).

Chapter 6

Introduction to Turbulent Flow

6.1 The Nature of Turbulent Flow

Turbulent flow is the usual state of fluid motion at high Reynolds numbers. But what does "high Reynolds number" mean? We will deal with this question in some detail but for the moment we can start with the concept that Reynolds number measures the relative importance of inertial forces to viscous forces: if viscous forces are small compared to the inertial forces when we have a high Reynolds number. This implies that at very high Reynolds numbers viscosity is no longer important, and as we shall see, many aspects of turbulent flow can be described without considering viscosity: viscosity is important only in setting the boundary conditions and in dissipating mechanical energy into heat.

Turbulent flow is characterized by:

1. Three-dimensionality. Turbulence is inherently three-dimensional, although some people study two-dimensional turbulence (this may have some application to geophysical flows (see figure 6.1). Note that the "stretching and tilting" term in the vorticity transport equation is absent in two-dimensional flows, and therefore two-dimensional turbulence is considerably simpler than the real-life three-dimensional variety.

2. Time-dependency. That is, turbulence is characterized by unsteady variations in velocity, density, temperature or concentration, and the variation occurs over a wide range of time scales. Turbulence has a broad frequency spectrum.

3. A wide range of length scales. Turbulence has a broad wavenumber spectrum.

4. Effective mixing of all fluid properties. For example, mass, velocity, temperature, momentum energy, etc. are all readily mixed by turbulent

187
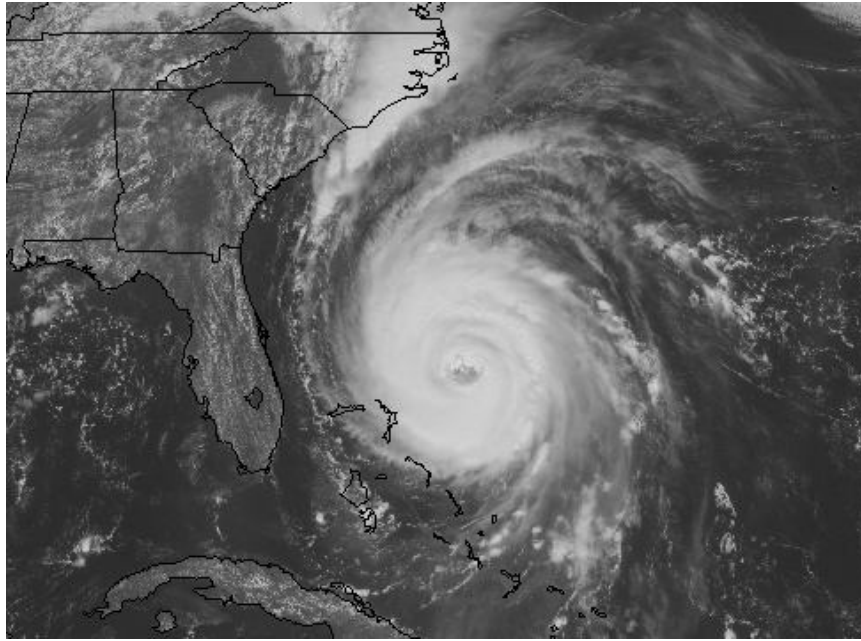
Figure 6.1: Hurricane Fran, September 1996.

motions.

The concept of vorticity is crucial to the understanding of turbulence, and we often talk about turbulence as consisting of an array of vortex tubes and vortex sheets, separated by fluid which is sometimes thought to be irrotational, or sometimes displaying some level of background vorticity. We also often describe turbulence in terms of "eddying" motions with a great range of scales, without being very specific about what that means. We usually think of these eddying motions as having some level of organized vorticity (a mixture of vortex tubes and vortex sheets), although talking in terms of "vortices" can be rather misleading. In fact, there has been perennial disagreement about the definition of a vortex in turbulent flow, and it has recently been the subject of a number of scholarly papers (for example, Kline & Robinson 1990). Nevertheless, the term eddy is widely used, for the reasons that are made clear by figures 6.2, 6.3 and 6.4.

As a further example, consider channel flow at high Reynolds number ($Re \gg 2000$, where $Re = U_{av}h/v$. The pressure drop driving the flow is assumed to be steady (see figure 6.5). At any point in the flow, the magnitude of the velocity in all three directions fluctuates in time. If we insert a probe into the flow so that we can measure the velocity at a given point, we would see the time traces shown in figure 6.6. Note that we can define a

Figure 6.2: Satellite photo of cloud vortices downstream of Guadalupe Island (off Baja California). Courtesy National Oceanic and Atmospheric Administration
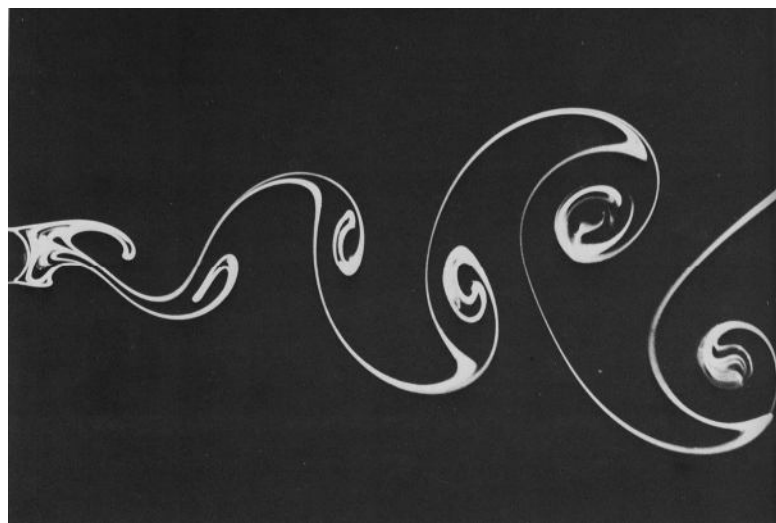
Figure 6.3: Kármán vortex street behind a circular cylinder at a Reynolds number of 140. From Taneda.

Figure 6.4: Kármán vortex street behind a circular cylinder at Reynolds numbers of 200. From Koopmann.

time-averaged velocity:

$$\bar{U}(\vec{x}) = \lim_{T \to \infty} \frac{1}{T} \int_{t_0}^{t_0+T} U(\vec{x}, t)dt$$

and a space-averaged velocity:

$$U_{av} = \frac{1}{A} \int \bar{U}dA = \frac{1}{h} \int_{-h/2}^{+h/2} \bar{U}dy.$$

The concept of a time-averaged velocity also leads to the concept of the flow being composed of a time-averaged field, and a fluctuating field. This is called the Reynolds decomposition where we write: $U = U + w\prime$, $V = V + v\prime$, $W = W + w\prime$, and $p = p + p\prime$.
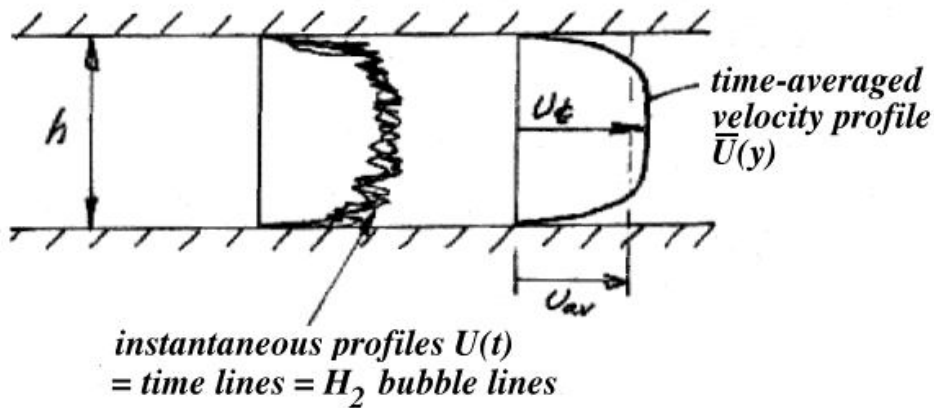
Figure 6.5: Instantaneous and mean velocity profiles in fully-developed channel flow.
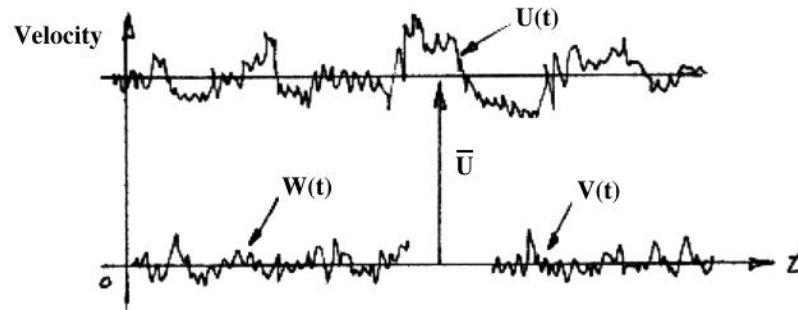
Figure 6.6: Time histories of the three velocity components in turbulent channel flow

However, if we now visualize the flow by putting in some tracers and taking a short-exposure photo, we then have a picture of the instantaneous streamlines. What you see depends on the speed of the observer (see figure 6.7, taken from Schlichting, but originally produced by Prandtl). As the observer moves at different speeds, we see that "eddying" motions become visible in different parts of the flow: slow moving eddies near the wall, and faster ones in the center of the channel. These eddies retain their identity for some distance, and we can see that there is an underlying structure apparent in the turbulent motions. The time traces appeared to show random fluctuations in velocity, yet we can see that these fluctuations are associated with fairly well-defined eddies. It turns out that these eddies are a characteristic feature of turbulent flows, as can be seen from the examples given in figures 6.8 to 6.18.

Figure 6.8: Even Leonardi da Vinci recognized the presence of eddies in turbulent flows.

Figures 6.9 and 6.10: Grid turbulence is the kind of turbulence produced by a flow as it passes through a grid: it is the laboratory approximation of homogeneous, isotropic turbulence. Note how the wakes downstream of the grid interact, merge, and eventually produce a fairly homogeneous flow. The flow visualization technique uses smoke (a passive scalar) to mark the flow. However, the rate at which the vorticity (the turbulence) diffuses compared to the rate the scalar diffuses is given by the Schmidt number, which in the case of smoke is about 2,000. Some distance downstream of its injection point, therefore, the smoke does not mark the vorticity field (see works by Roshko and also by Rockwell).

Figure 6.11: This shadowgraph illustrates the sharp boundary that can occur between turbulent and non-turbulent fluid. Also note the intermittency of the interface: a stationary probe would see periods of turbulent activity
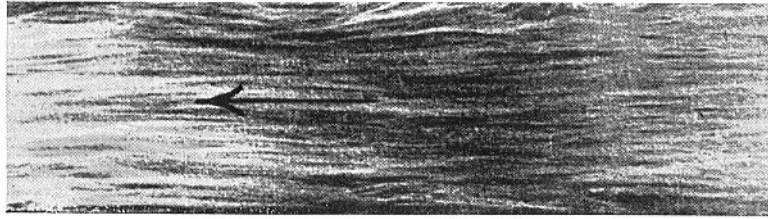
Fig. 18.1 a.   Camera velocity 12·15 cm/sec
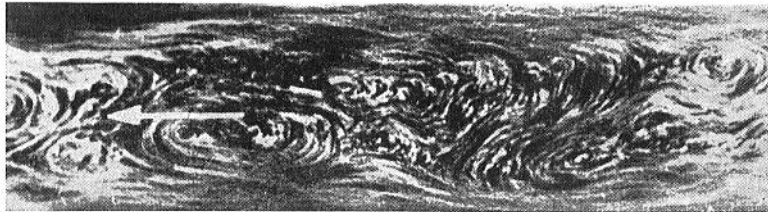
Fig. 18.1 b.   Camera velocity 20 cm/sec

Fig. 18.1 c.   Camera velocity 25 cm/sec
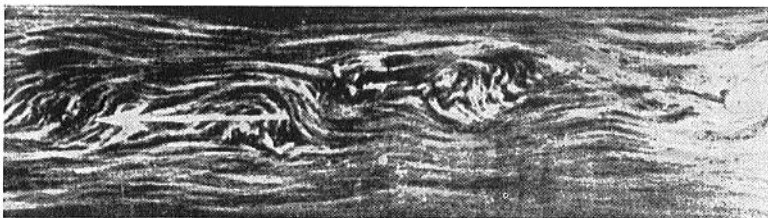
Fig. 18.1 d.   Camera velocity 27·6 cm/sec

Figure 6.7: Turbulent flow in a water channel $6\,cm$ wide, photographed with varying camera speeds. From Schlichting.

(rotational flow), followed by periods of non-turbulent activity (irrotational, potential flow). This picture is often used to demonstrate the wide range of scales present in turbulence. To my eye, only two scales, one based on the wake width and the other about one-fortieth of the wake width, are visible. This is a problem with the visualization technique: shadowgraphs record all the density gradients integrated over the distance from the light source
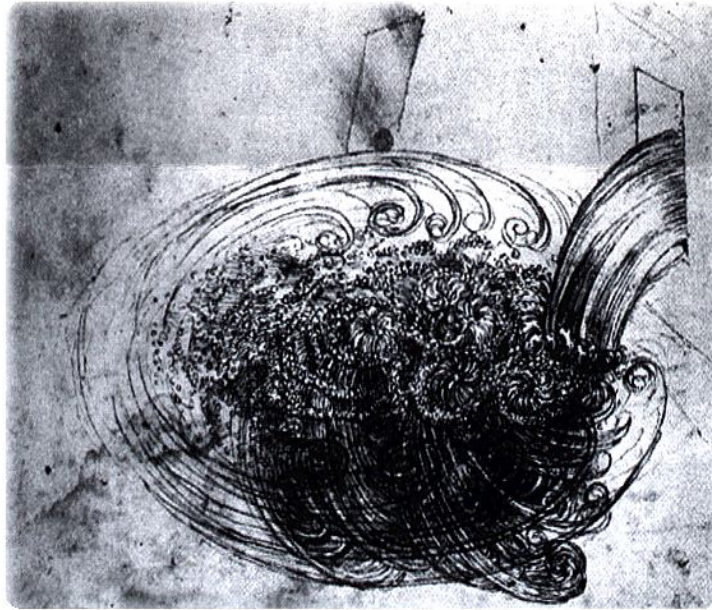
Figure 6.8: Shaft of water issuing from a square hole into a pool, forming bubbles and eddies (Leonardo da Vinci).
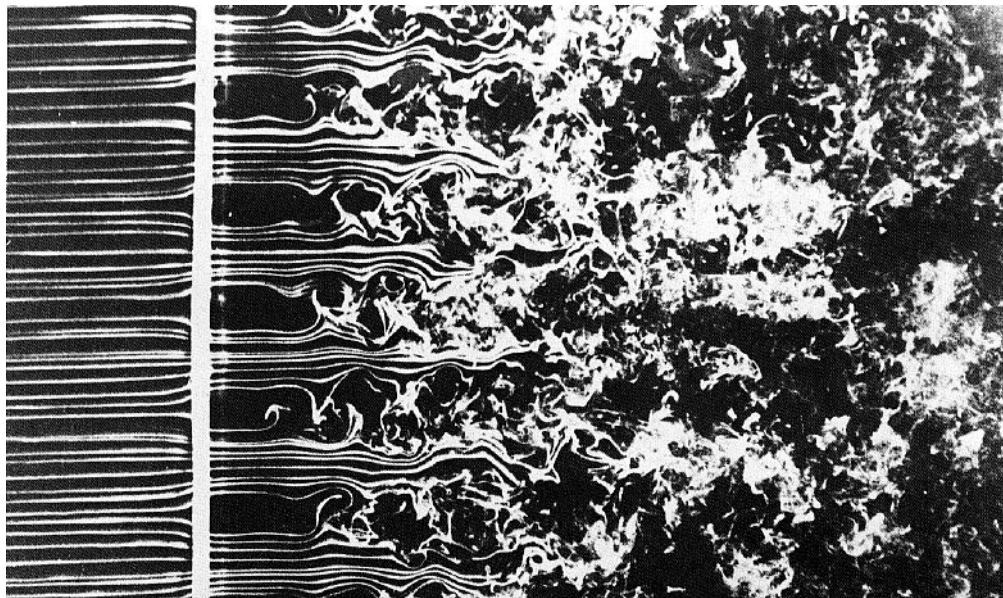
Figure 6.9: Generation of turbulence by a grid. Corke & Nagib.

to the camera (see Liepmann and Roshko for a brief explanantion). Hence the image records the density gradients due to the eddy structures present in the wake but it overlaps them so that the individual eddies are no longer apparent.
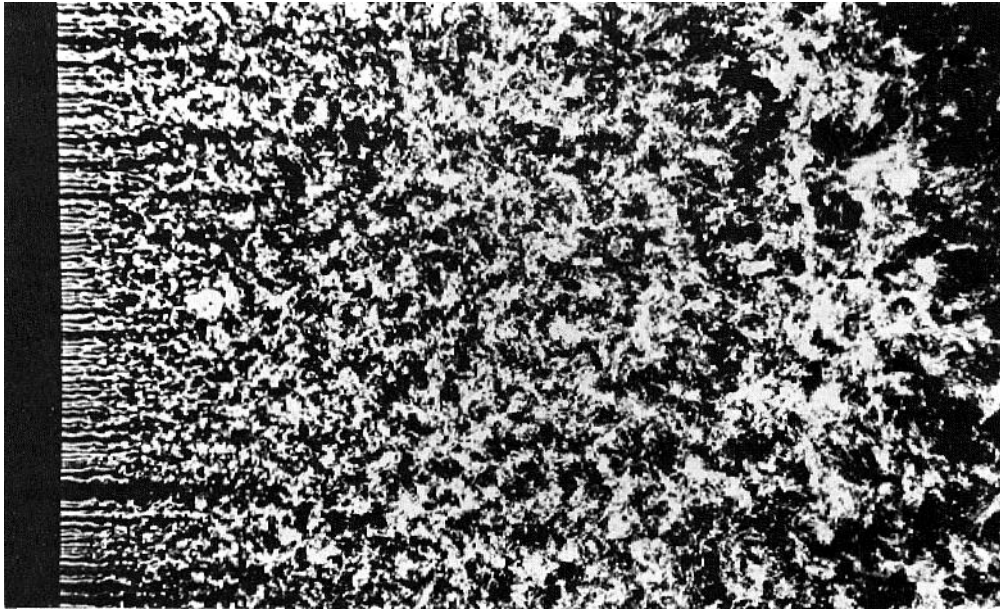
Figure 6.10: Homogeneous turbulence behind a grid. Corke & Nagib.
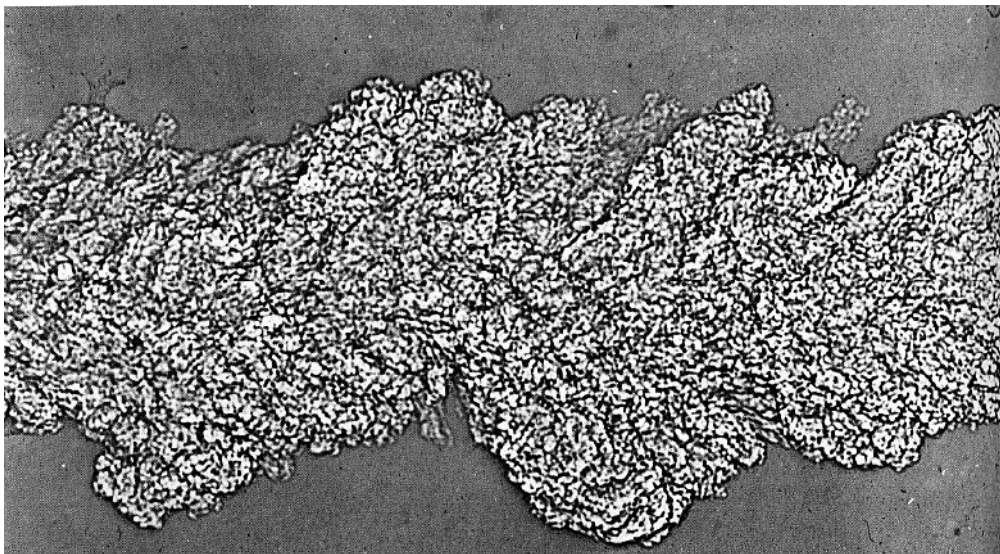
Figure 6.11: Turbulent flow far behind a projectile. Shadowgraph from Ballistic Research Laboratories, Aberdeen Proving Ground.

Figure 6.12: Here, a laser sheet illuminates a fluorescent dye, and therefore we have an image of eddy cross-sections (the same caution about Schmidt number is in effect). The variety of scales, and the evident organization of the turbulence, is clearly seen. Also note that the unmarked fluid occasionally penetrates across the centerline of the jet.
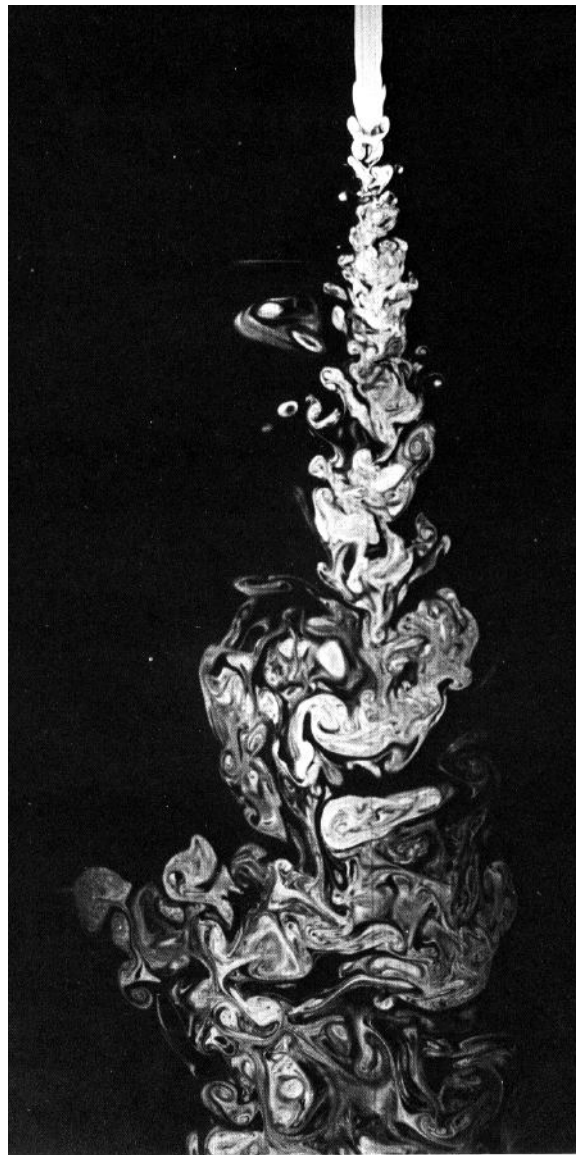
Figure 6.12: Cross-section of a turbulent water jet, at a Reynolds number of about 2300, made visible by laser-induced fluorescence. From Dimotakis, Lye & Papantoniou, 1981.

Figure 6.13: Here is a really high Reynolds number jet (about 10^9). Note the scales of eddies are almost in a geometric progression, where each successive scale is about one-half the previous one.

Figures 6.14 and 6.15: Two views of a turbulent boundary layer at fairly low Reynolds numbers. See how the originally non-turbulent freestream fluid is "entrained" by the boundary layer. Occasionally, we see freestream fluid extending almost to the wall. Presumably this fluid will be eventaully
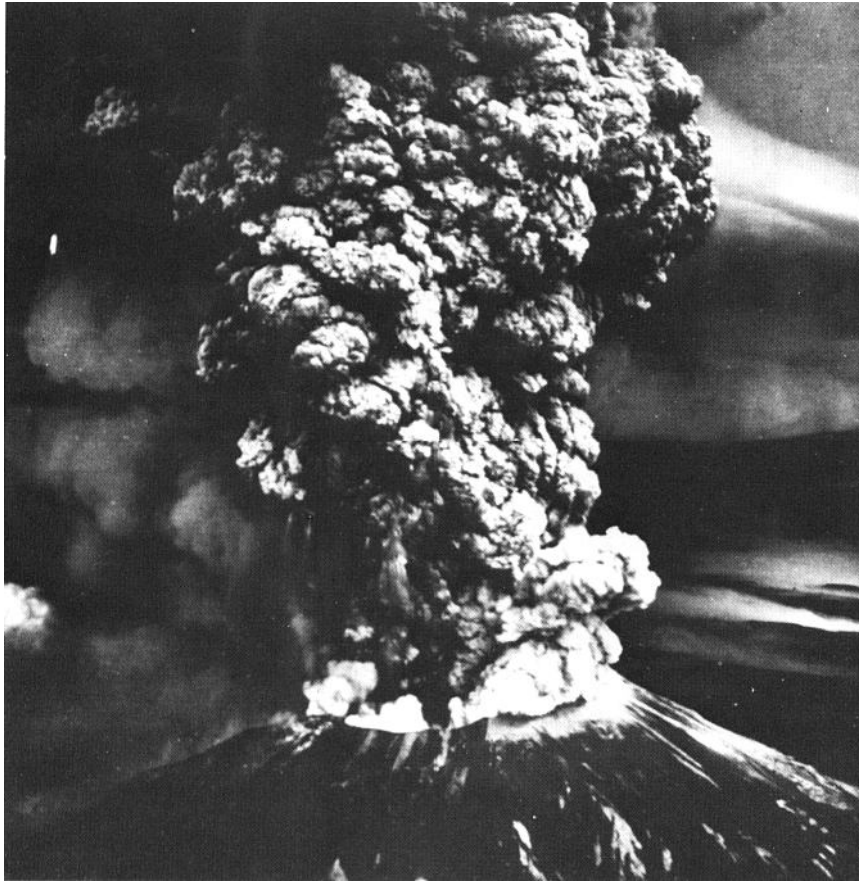
Figure 6.13: Mount St. Helens, 18 May 1980 (US Geological Survey/Popperfoto).

engulfed and become turbulent (rotational) by viscous diffusion of vorticity.

Figure 6.16: Here is a shadowgraph of the turbulent boundary layer on a cylindrical body moving to the left at about Mach 2.3 (taken in a ballistic tunnel by Seiff). The integration effect is not so severe as in figure 7 because of the geometry, and it is now possible to distinguish structures similar to the ones seen at subsonic speeds, as seen in figure 10.

Figure 6.17: By using Rayleigh scattering, the density variations in a streamwise plane are made visible in a turbulent boundary layer at Mach 2.5 (picture by Smith *et al.* at Princeton). The flow is from left to right. This cross section clearly shows the kind of bulges observed at subsonic speeds, as in figures 6.14 and 6.15.

Figure 6.18: Here the Rayleigh scattering technique was used to reveal the density variations in a plane parallel to the wall (the flow is from top to bottom) at a height of about 0.7 times the boundary layer thickness. The
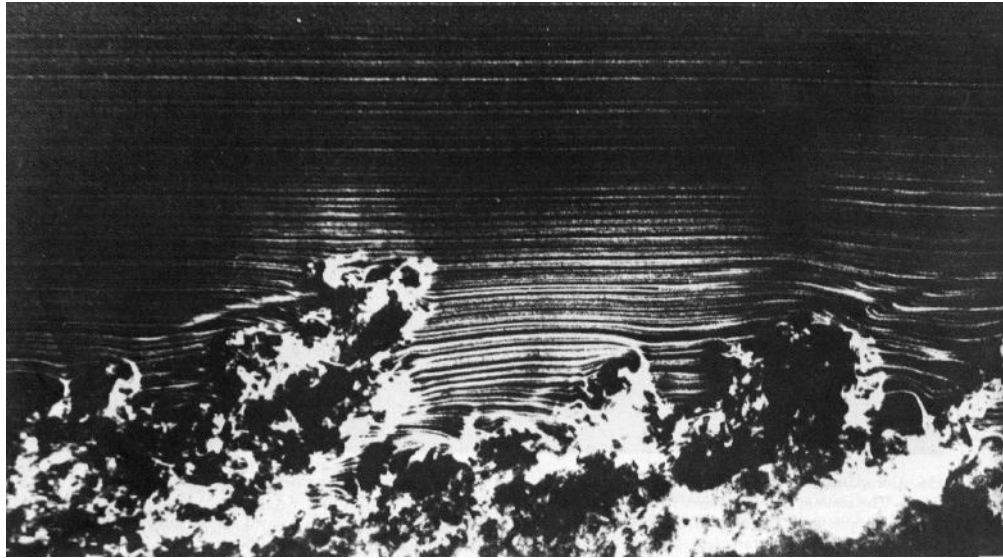
Figure 6.14: Side view of a turbulent boundary layer at $Re_\theta = 3500$. From Corke, Guezennec & Hagib.
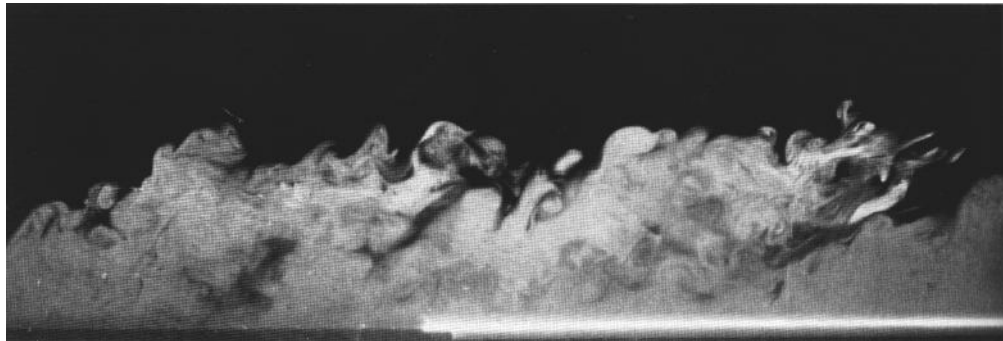
Figure 6.15: Turbulent boundary layer on a wall at $Re_\theta = 4000$. From Falco, 1977.

large islands are about a boundary layer thickness across. Note the three-dimensionality of the density fluctuations.

Figure 6.19: By using Rayleigh scattering, the density variations in a streamwise plane are made visible in a turbulent boundary layer at Mach 8 (picture by Baumgartner *et al.* at Princeton). The flow is from left to right. The same type of structure is observed as at supersonic and subsonic speeds, as in figures 6.17 and 6.15.

6.2   Examples of Turbulent Flow

In the home: water issuing from a faucet, cigarette smoke, stirring a coffee
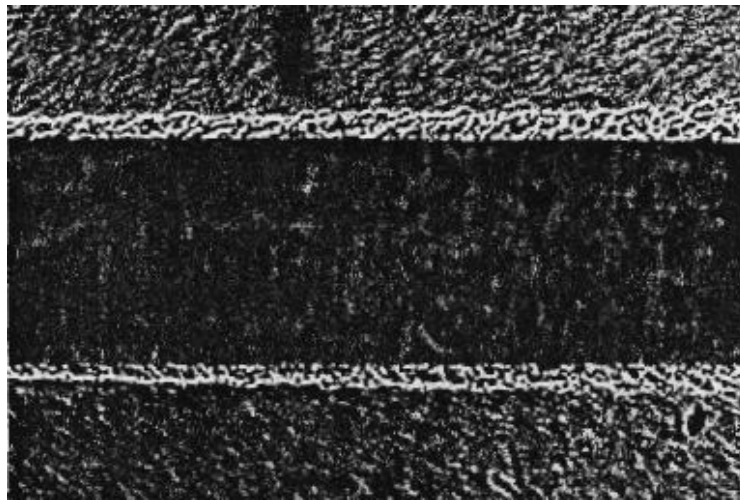
Figure 6.16: Boundary layer on a body of revolution at a Mach number of 2.3. The body is moving to the left. From Seiff.

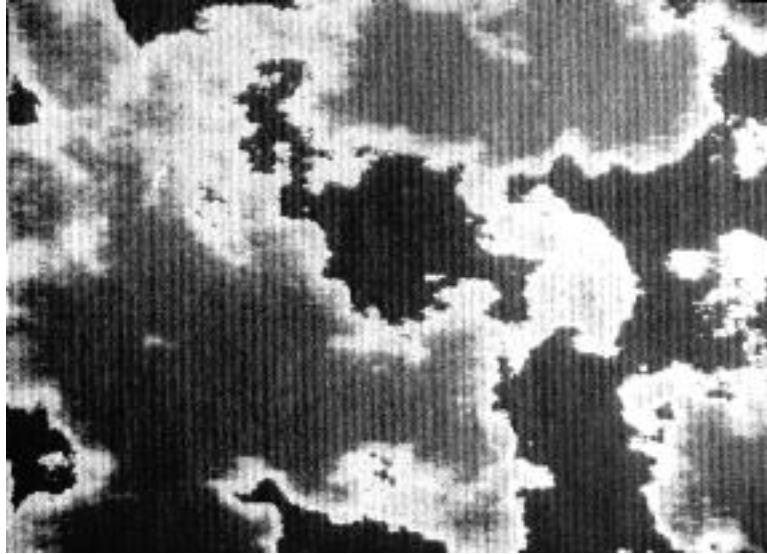Figure 6.17: Side view images of the instantaneous density field in a Mach 3 turbulent boundary layer. Smith & Smits, 1996.

cup, air-conditioning ducts.

Aerodynamical flows: wake of an aircraft, flow over the wings, flow over a ship, aerodynamics of sports balls, separation.

Industrial flows: stirred reactor, pipe flow, flow through valves, constrictions, flows in turbines, combustion furnaces, chimney outlets, pollutant dispersion (not bearings, lubrication applications since these are highly viscous flows where turbulence has no role to play), flow around buildings, internal combustion engines.

Geophysical flows: river flows, channel flows, wake behind a bridge pylon, ocean currents, weather patterns, storms (eg. snow storms), (not settling of small particles which is another highly viscous flow), volcanoes, thermal plumes.

Figure 6.18: Plan view images of the instantaneous density field in a Mach 3 turbulent boundary layer at $y/\delta = 0.7$. Smith & Smits, 1995.
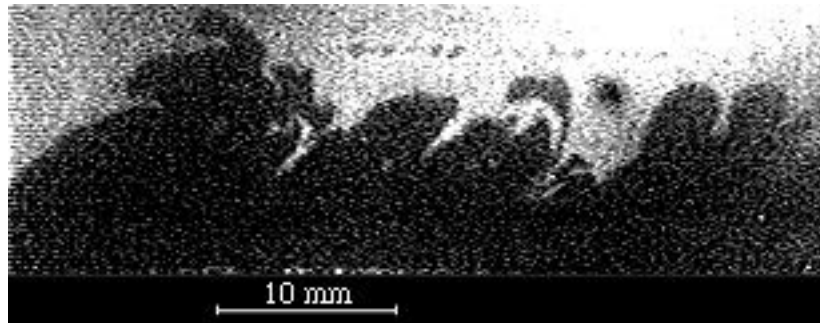
Figure 6.19: Side view images of the instantaneous density field in a Mach 8 turbulent boundary layer. Baumgartner, 1997.

Military flows: flight of bullets, rockets, high-speed (and low-speed) airplanes, helicopter wakes, parachute flows, submarine flows (signatures, noise), propellers.

6.3 The Need to Study Turbulence

Why is turbulence interesting?

If we could predict all the flow states given as examples in section 6.2, or if we had enough insight to develop widely applicable correlation schemes, turbulence would not be an area of research. The truth, of course, is otherwise. It comes down to this: there is no general solution to the Navier-Stokes

equations, which are the governing equations for flow of an incompressible, Newtonian, continuum fluid (for compressible flows, we need an energy equation, and equation of state and some constitutive equations). Particular solutions exist (see Schlichting chapters XX and YY), but in the main they are not useful for the general understanding of turbulent flow. (Sometimes, however, they can be used to give an understanding of particular mechanisms at work in the production, diffusion and dissipation of turbulence).

Historically, studies of turbulence have relied on a very restricted set of "tools":

1. Approximate analysis of average properties of highly idealized turbulent flows (eg. grid turbulence);

2. Analysis of idealized linear stability problems;

3. Measurements of time-averaged properties and ensemble-average properties ($\bar{U}$, $\overline{u'^2}$, $\overline{u'v'}$, $\Phi(\omega)$, $p(u)$, etc.);

4. Flow visualization;

5. Dimensional analysis and scaling arguments.

From this work we have obtained

1. a small set of widely accepted "facts", for example, the logarithmic variation of velocity in a turbulent boundary layer;

2. a small set of widely accepted correlations, for example the friction factor for pipes as a function of Reynolds number;

3. a small set of widely accepted theories eg. Kolmogoroff's inertial range, Batchelor's final decay of grid turbulence;

4. a qualitative notion of energy transfer (the energy cascade);

5. the kinematics and other general features of turbulence and eddies, for example the role of bulges, horshoe-vortices, "typical" eddies, etc.;

6. some useful but rather restricted sets of predictive tools, for example, the k-ε turbulence model;

7. a good appreciation of scaling arguments.

More recently (since late 70's) computers have allowed LES (Large Eddy Simulations) and DNS (Direct Numerical Simulations) of turbulent flows. In DNS, the grid resolution is set small enough to resolve all the scales of motion (at least in principle), whereas in LES only the scales down to the size of the grid are computed, and the smaller scales are modelled in some way.

Both types of computation give time-dependent, three-dimensional flow information, and they have given a great deal of insight into the dynamics of turbulence. However, their overall impact has not been as great as we might have hoped (at least not yet). The difficulty is that turbulence is complex. Extremely complex. If we consider the example of turbulent pipe flow, we have a range of scales which goes from the largest (or order D, the pipe diameter) to the smallest (of order v/u_τ, where u_τ is the friction velocity, which is a velocity scale based on the wall shear stress: it is of the same order as a typical velocity fluctuation). For a pipe flow of water in a 10 cm pipe at 2m/sec we get $Re = \bar{U}Dv = (2 \times 0.1)10^{-6}$. This is not a large Reynolds number for pipe flow. Since

$$C_f = 2 \left(u_\tau/U_{av}\right)^2 \approx 0.003.$$

Hence $u_\tau = 0.04\bar{U}$, and $Du_\tau/v \approx 8,000$. So the largest motions are of order 10^4 times the smallest. In DNS, all these scales must be resolved as a function of time, where at least four variables (U, V, W, p) are carried for each grid point at each time step. In other words, a typical DNS calculation of this relatively simple flow will generate an enormous quantity of information: $\left(4\,(8,000)^3\right) = 2 \times 10^{12}$ pieces of information at each time step. We may be able to do calculations of this magnitude (or at least soon) but it's another thing to understand it. We need to develop simpler models or concepts in turbulence which will give us some understanding and predictive power. Computations will help but in some sense the field of turbulence needs better ideas, not just more data.

So what are the goals of turbulence research? The main goal is:

> To develop approximations to the N-S equations which embody sufficient dynamical information to allow reliable and efficient predictions of turbulent flows.

To get there, we need to develop and test simple models of turbulence which embody the essential physics of turbulence and its scale interactions, and contains the correct scaling information. We need: high quality simulations, high quality experiments, and good ideas.

According to Tony Perry, our methods have evolved from the point where we just had good ideas (figure 6.20a), to where we experiment and theory supported our thought processes (with a little numerics) (figure 6.20b), to where the advent of computers was seen to add a third leg for support figure 6.20c), to the present situation where experiments and theory are both supported by computers to aid our thinking about turbulence. These are the tools. However, there are also different ways to think about turbulence.
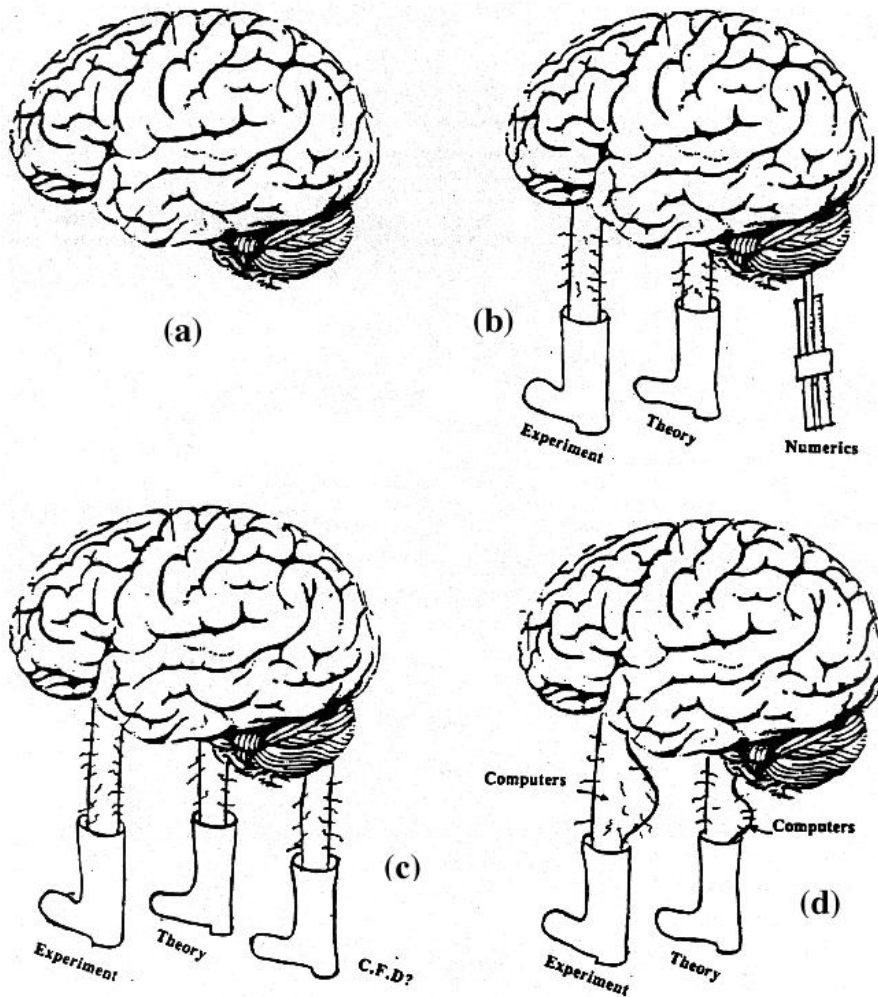
Figure 6.20: The evolving role of computers, experiments and theory. According to Perry.

6.4   Approaches to Turbulence

As noted earlier, turbulence is extremely complex. In order to deal with this complexity, different people take different approaches. The major varieties are the time-averaged approach (also called Reynolds averaged approach), the ensemble-averaged approach, and the instantaneous realization approach. All of these ways of thinking are correct, in the sense that they can all be represented as valid interpretations of the Navier-Stokes equations, but they all give different kinds of information, they have different applications, and they require different kinds of input.
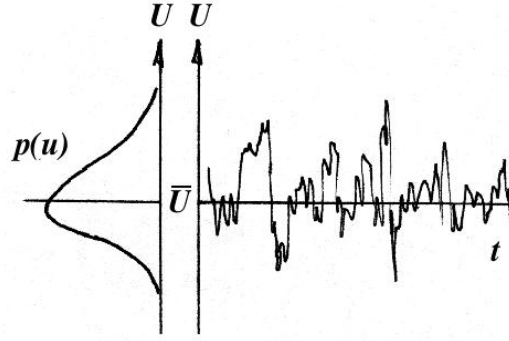
Figure 6.21: Time trace and pdf of the longitudinal velocity fluctuation

6.4.1 Reynolds-averaged approach

This is the most common approach, certainly for engineering purposes. It has the twin distinctions of being the most studied, and being the most limited in terms of understanding. In this approach, turbulence is seen purely as a statistical phenomena. It is assumed that the time-dependent nature of turbulence is far too complicated to incorporate in a physical model (that is, a model which describes the interactions among turbulent scales of motion in a physical way, which could be quantitative or qualitative), or a turbulence model (that is, a model which can be incorporated quantitatively into a set of equations based on the Navier-Stokes (N-S) equations, and that can lead to useful engineering predictions). Hence, the N-S equations are written in terms of mean quantities by using time averages, where a time average is taken over a long enough time to give a stationary mean. Hence,

$$\bar{U}(\mathbf{x}) = \lim_{T \to \infty} \frac{1}{T} \int_{t_0}^{t_0+T} U(\mathbf{x}, t)dt,$$

and

$$U = \bar{U} + u'$$

and

$$\bar{u}' = 0 \quad \text{and} \quad \bar{v}' = 0,$$

etc. (see figure 6.21). But the moments are not zero:

$$\overline{u'^2} = \lim_{T \to \infty} \frac{1}{T} \int_{t_0}^{t_0+T} (U - \bar{U})^2 dt,$$

$$\overline{u'v'} = \lim_{T \to \infty} \frac{1}{T} \int_{t_0}^{t_0+T} (U - \bar{U})(V - \bar{V})dt.$$

When we do this, we obviously lose information. In fact, it can be shown that we need to know all higher order moments of the turbulence (that is,

an infinite number) before we have all the information originally contained in the time-dependent equations. So now we have a subset of equations (typically for the mean velocity and then for the lower-order moments of turbulence) which have more unknown than equations — this is known as the "closure" problem. To close the set of equations some inspired piece of information must be supplied, which may be based on experiment, theory or simulation, or a combination of all three. We will consider this problem in some detail in a later lecture but we should note that this approach (or the closely related pdf method, and the wave-number approach) form the basis of all engineering calculation methods, and it is also the most common approach to measuring turbulence.

NOTE:

> In unsteady but repeatable flows, time-averages are obviously mean-ingless. However, we can form ensemble-averages by accumulating a sufficient number of samples at the same phase in the flow cycle.

6.4.2 Ensemble-averaged approach

This may not be the right name for it, but when I say "ensemble-averaged" approach I don't mean forming the equivalent of Reynolds averages for an unsteady flow. I use the term in a more particular sense to indicate a way of thinking that recognizes that turbulence has an underlying struc-ture, and that it is not just a purely random phenomena as implied by the Reynolds-averaged approach. Here we say that it may be more meaningful to recognize that the eddies which make up turbulence display some similar-ity among themselves, and that we try to determine the average properties of an eddy, and how these properties scale with size, position, etc..

The simplest example is given by the intermittent nature of turbulence in the outer part of a turbulent shear layer. As we can see from the images given in figures 6.11 to 6.18 and figure 6.22, there appear to be periods of turbulent flow (which is rotational) followed by periods of non-turbulent flow (which is irrotational). By forming a detector function (or boxcar function) $I(t)$ which takes the value 0 in non-turbulent flow and 1 in a turbulent flow, then we can form turbulence intensities based on the periods when $I = 1$, rather than over all time (see figure 6.23). That is:

$$\overline{u'^2} = \gamma \overline{u'^2_T} + (1 - \gamma)\overline{u'^2_{NT}}.$$

(Note that $\overline{u'^2_{NT}} \neq 0$ due to irrotational fluctuations in the external potential flow.)

This approach can be used in more sophisticated ways to try to identify eddies of a particular sort, or to identify contributions from two interacting
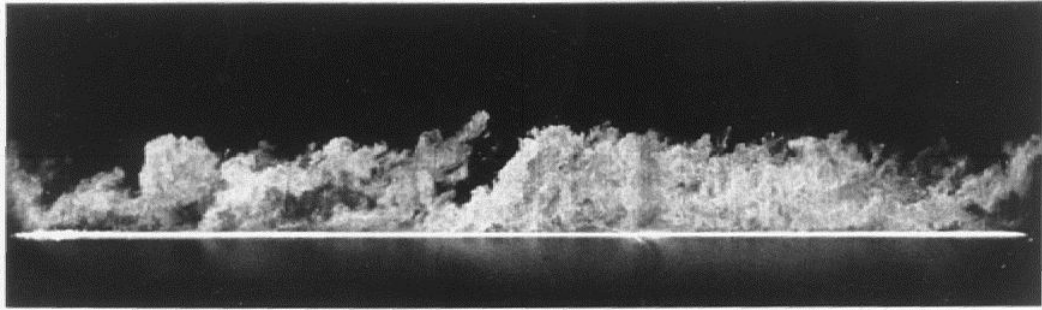
Figure 6.22: Streamwise cross-section of a turbulent boundary layer at Mach 3. From Smith & Smits, 1988.
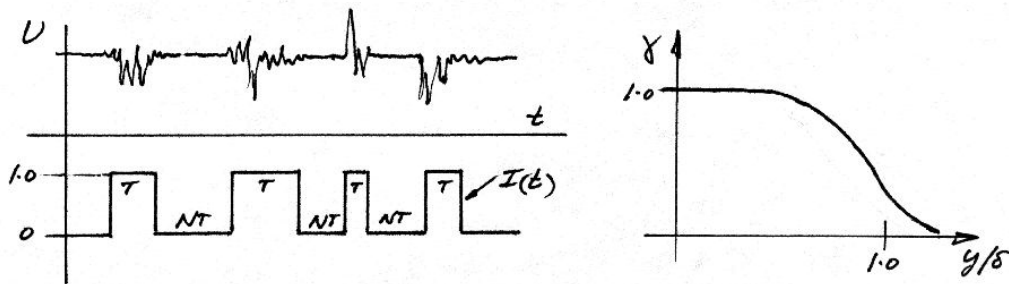

Figure 6.23: The intermittency function and the distribution of the intermittency factor γ.

turbulent flows. A similar approach can be used if the flow has a well-defined periodicity because it is then possible to use phase-averaging to identify the details of the large-scale structure (see Cantwell and Coles, Perry and Lim, and Perry and Tan). Of course there are many problems in defining $I(t)$ and in interpreting the results, but this approach is an attempt to take some of the turbulent structure into account. It has been widely used in turbulence research, for the interpretation of experimental and numerical results (see, for example, the VITA approach of Blackwelder & Kaplan used by Spina, Donovan & Smits 1991). Some examples of ensemble-averaged interpretations of outer-layer structures in turbulent boundary layers are given in figures 6.24 and 6.25.

6.4.3 Instantaneous realization approach

Another awkward name, but here I mean the method where we try to understand turbulence by looking at individual events. Of course, we try to generalize our observations by picking out features which occur often enough to be important (and here we have a link to the ensemble-averaged approach), but of necessity we are looking at a relatively small number of
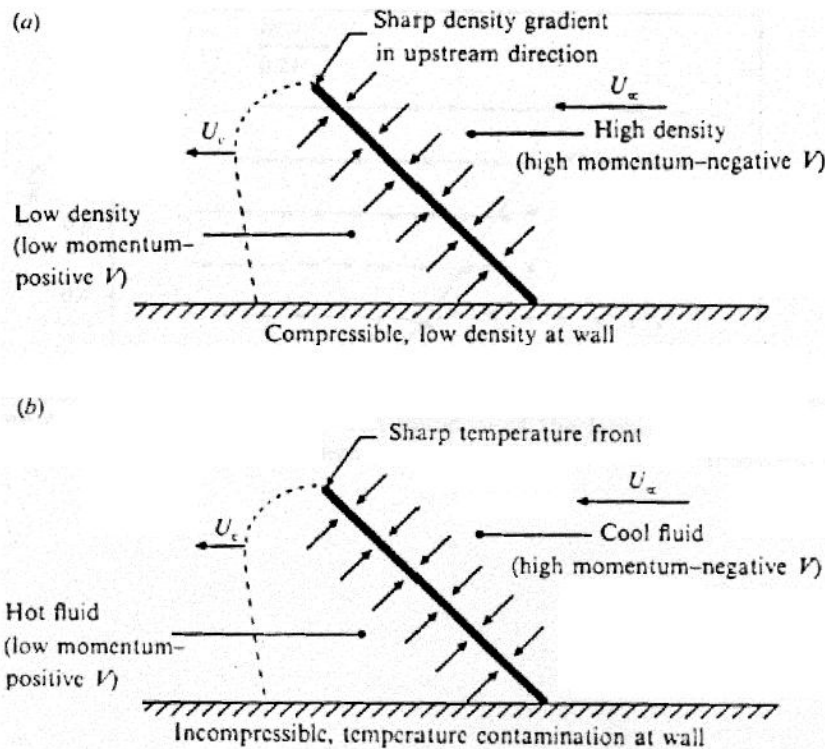
Figure 6.24: Qualititative comparison between the ensemble-averaged structures of: (a) Smith & Smits (1988) in a supersonic boundary layer (visual detection); (b) Chen & Blackwelder (1978) in a subsonic boundary layer over a heated wall (temperature probe detection).

events. We can do this in experiments by using techniques which give information about the whole of the flow field, such as some forms of flow visualization (see figure 6.26 which shows pairs of Rayleigh scattering images of a Mach 2.9 turbulent boundary layer separated by intervals of 60 μs), or time-resolved PIV (Particle-Image Velocimetry), but it is particularly easy to do in numerical simulations where all the properties of turbulence over some relatively short time period can be inspected and analyzed in great depth (see, for example, Robinson's work).

6.4.4   Connections among the approaches

The boundaries between these three main approaches are not clear cut, and most workers in turbulence move freely among them to gain the maximum of useful information. For example:

 (1) the observation that turbulent flows can be intermittent has found its
     way in developing Reynolds'averaged turbulence models (see, for
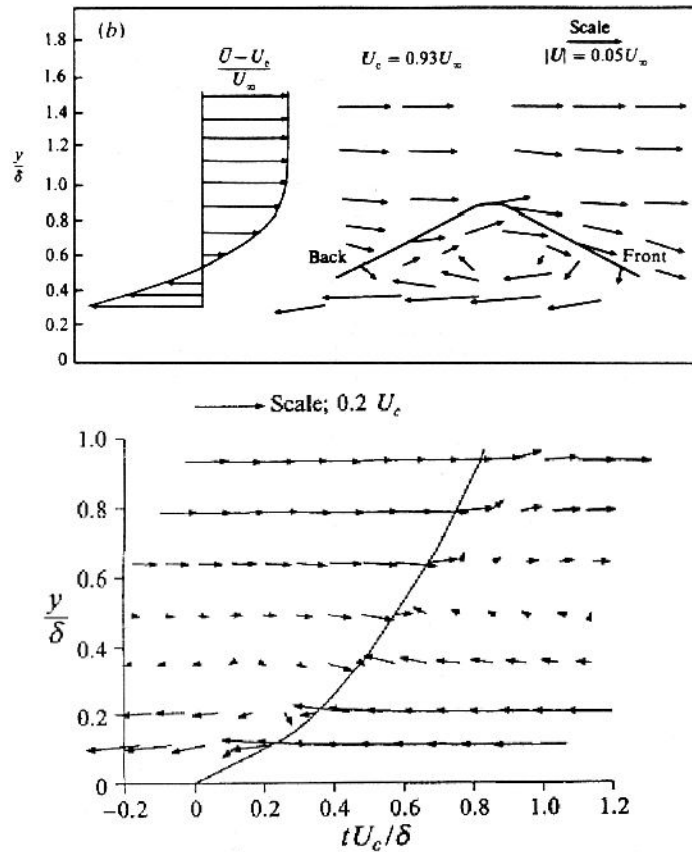
Figure 6.25: (a) Schematic of a large-scale turbulent "bulge" in incompressible flow. From Blackwelder & Kovasznay, 1972; (b) Ensemble-averaged flowfield in a Mach 3 turbulent boundary layer. From Spina, Donovan & Smits, 1992.

example, Cebeci and Smith 1974);

(2) ensemble-averaged results are often studied in terms of their contributions to the Reynolds-averaged turbulent moments (sometimes called Reynolds stresses);

(3) Individual realizations are probably only useful if they reveal something about the average behavior of eddies (ensemble-average approach) or the Reynolds stresses (Reynolds-average approach).

We should also make clear (or try to) what we mean by "structure" in turbulence. Turbulence (in one view: see Bradshaw, p.22) is the sum of a large number of events or processes (the velocity at any point is a product of the whole field, and as a function of time will reflect all influences) that are not quite independent - like a slow hand clap superimposed on a general audience response. So turbulence usually displays departures from
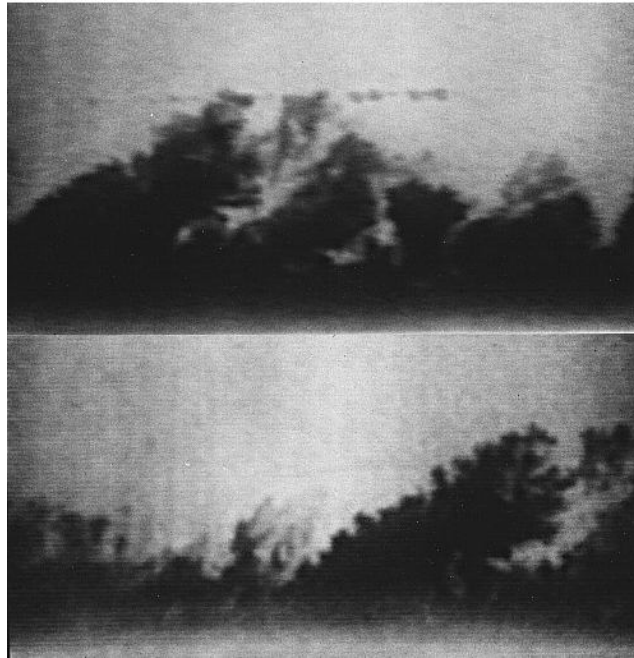
Figure 6.26: Pair of double-pulsed Rayleigh scattering images of a Mach 2.9 turbulent boundary layer, separated in time by intervals of $60\,\mu s$. Flow is from left to right.

Gaussian behavior - these departures may be called structure, and might be embodied in terms of the moments of the pdf's of u', v' and w'.

The term structure is also used in connection with the description of individual eddying motions that are observed to be part of turbulence. These are sometimes called "coherent structures" if they represent some sort of entity which can be followed in time. Here we can talk about the "outer-layer bulges" for example, which can be seen in the flow visualizations of turbulent boundary layers. These bulges evolve somewhat as they move but we can identify some typical properties such as their angle of inclination (which is always leaning downstream), their average size, and frequency of occurrence.

Structure is a widely used word, and people move between its different interpretations, often without being precise.

6.5   Model Flows

The study of turbulence is usually restricted to rather simple model flows, such as grid turbulence (with and without a mean shear), pipe and channel flows, boundary layers, jets, wakes, swirling flows, etc. From these flows we try to extract "universal" information which we can then apply to

more complex flows such as that found in engineering applications. Eventually, we need to know the effects on turbulence of shear, wall constraint, pressure gradient, curvature, divergence, compression, rotation, buoyancy (stratification), chemical reactions (with and without heat release), three-dimensionality, magneto-hydrodynamic effects, separately and in combination.

We need to determine basic mechanisms, and find their sensitivity to changes in boundary conditions or initial conditions. It is of little use to construct an edifice of understanding based on one highly particular flow (for example, the flat plate, zero pressure gradient boundary layer) and then find that the edifice must be rebuilt everytime a boundary condition is changed (for instance when the wall is curved, or the flow is accelerating).

Chapter 7

Reynolds-Averaged Equations

Let us begin with the straight statistical approach where we use the decomposition (in Cartesian coordinates, where $\mathbf{V} = U\mathbf{i} + V\mathbf{j} + W\mathbf{k}$):

$$U(\mathbf{x}, t) = \bar{U}(\mathbf{x}) + u'(\mathbf{x}, t)$$

(V, W and the pressure p are decomposed similarly). As before we have

$$\bar{a} = \lim_{T \to \infty} \int_{t_0}^{t_0+T} a \, dt,$$

where t_0 is an arbitrary start sampling time, and the rules for averaging are:

$$\overline{a'} = 0$$

$$\overline{a + b} = \bar{a} + \bar{b}$$

$$\overline{\bar{a}} = \bar{a}$$

$$\overline{\bar{a} \cdot b} = \bar{a} \cdot \bar{b}$$

$$\overline{\frac{\partial a}{\partial s}} = \frac{\partial \bar{a}}{\partial s}.$$

Start with the continuity and Navier-Stokes equations (for incompressible flow and no body forces):

$$\nabla \cdot \mathbf{V} = 0 \tag{7.1}$$

$$\frac{D\mathbf{V}}{Dt} = \frac{\partial \mathbf{V}}{\partial t} + \mathbf{V} \cdot \nabla \mathbf{V} = -\frac{1}{\rho} \nabla p + \nu \nabla^2 \mathbf{V} \tag{7.2}$$

or

$$\frac{\partial u_i}{\partial t} + u_i \frac{\partial u_i}{\partial x_j} = -\frac{1}{\rho} \frac{\partial p}{\partial x_i} + \nu \frac{\partial^2 u_i}{\partial x_j^2}. \tag{7.3}$$

In the momentum equation, the first term on the left hand side is the rate of change of momentum due to unsteady flow at a point, and the second term

on the left hand side is the rate of change of momentum due to convection of fluid particles to regions where the velocity is different. The first term on the right hand side is the force per unit volume due to pressure differences, and the second term on the right hand side is the force per unit volume due to differences in viscous shear stresses that drag fluid elements about.

7.1 Continuity Equation

With the Reynolds decomposition, the continuity equation becomes:

$$\frac{\partial \bar{U}}{\partial x} + \frac{\partial \bar{V}}{\partial y} + \frac{\partial \bar{W}}{\partial z} + \frac{\partial u'}{\partial x} + \frac{\partial v'}{\partial y} + \frac{\partial w'}{\partial z} = 0. \tag{7.4}$$

Taking the time average we obtain:

$$\frac{\partial \bar{U}}{\partial x} + \frac{\partial \bar{V}}{\partial y} + \frac{\partial \bar{W}}{\partial z} = 0. \tag{7.5}$$

That is,

$$\nabla \cdot \bar{\mathbf{V}} = 0.$$

By subtracting equation 7.5 from 7.4 we obtain:

$$\frac{\partial u'}{\partial x} + \frac{\partial v'}{\partial y} + \frac{\partial w'}{\partial z} = 0. \tag{7.6}$$

That is,

$$\nabla \cdot \mathbf{v}' = 0.$$

Note that the mean and fluctuating velocities individually satisfy the continuity equation.

7.2 Momentum Equation

Consider the *x*-component of the momentum equation. Using the Reynolds decomposition, we obtain:

$$\frac{\partial \bar{U}}{\partial t} + \frac{\partial u'}{\partial t} + \bar{U}\frac{\partial \bar{U}}{\partial x} + u'\frac{\partial u'}{\partial x} + u'\frac{\partial \bar{U}}{\partial x} + \bar{U}\frac{\partial u'}{\partial x}$$

$$+ \bar{V}\frac{\partial \bar{U}}{\partial y} + v'\frac{\partial u'}{\partial y} + v'\frac{\partial \bar{U}}{\partial y} + \bar{V}\frac{\partial u'}{\partial y}$$

$$+ \bar{W}\frac{\partial \bar{U}}{\partial z} + w'\frac{\partial u'}{\partial z} + w'\frac{\partial \bar{U}}{\partial z} + \bar{W}\frac{\partial u'}{\partial z}$$

$$= -\frac{1}{\rho}\frac{\partial \bar{p}}{\partial x} - \frac{1}{\rho}\frac{\partial p'}{\partial x} + \nu\nabla^2\bar{U} + \nu\nabla^2 u'. \tag{7.7}$$

Now we take the time average and consider each term in turn.

(a) $\partial \bar{U}/\partial t = 0$ since by definition $\bar{u}$ is a time average. Hence to apply Reynolds averaging the flow must be stationary. We can apply a more restricted form of averaging of the time constant associated with the unsteadiness is much larger than any time constant associated with the turbulence but we must be very careful: if u_i is a function of t_0, the definition of a time average is meaningless and ensemble averages must be used.

(b) $\qquad \overline{\dfrac{\partial u'}{\partial t}} = 0, \quad$ since $\quad \overline{u'} = 0$

(c) $\qquad \overline{u'\dfrac{\partial u'}{\partial x}} = \dfrac{1}{2}\dfrac{\overline{\partial u'^2}}{\partial x} = \dfrac{\partial\left(\frac{1}{2}\overline{u'^2}\right)}{\partial x}$

(d) $\qquad \overline{u'\dfrac{\partial \bar{U}}{\partial x}} = \overline{v'\dfrac{\partial \bar{U}}{\partial y}} = \overline{w'\dfrac{\partial \bar{U}}{\partial z}} = 0$

(e) $\qquad \dfrac{\overline{\bar{U}\partial u'}}{\partial x} = \dfrac{\overline{\bar{V}\partial u'}}{\partial y} = \dfrac{\overline{\bar{W}\partial u'}}{\partial z} = 0$

(f) $\qquad \overline{v'\dfrac{\partial u'}{\partial y}} = \dfrac{\overline{\partial u'v'}}{\partial y} - \overline{u'\dfrac{\partial v'}{\partial y}}$

(g) $\qquad \overline{w'\dfrac{\partial u'}{\partial z}} = \dfrac{\overline{\partial u'w'}}{\partial z} - \overline{u'\dfrac{\partial w'}{\partial z}}$

(h) $\qquad \dfrac{\overline{\partial p'}}{\partial x} = 0$

(i) $\qquad \overline{\nu\nabla^2 u'} = 0.$

Also note from the continuity equation 7.5 that

$$u'\frac{\partial u'}{\partial x} + u'\frac{\partial v'}{\partial y} + u'\frac{\partial w'}{\partial z} = 0.$$

That is, $\qquad \dfrac{\partial\left(\frac{1}{2}\overline{u'^2}\right)}{\partial x} + \overline{u'\dfrac{\partial v'}{\partial y}} + \overline{u'\dfrac{\partial w'}{\partial z}} = 0.$

Hence the x-component Reynolds-averaged equation becomes:

$$U\frac{\partial U}{\partial x} + V\frac{\partial U}{\partial y} + W\frac{\partial U}{\partial z} =$$

$$-\frac{1}{\rho}\frac{\partial p}{\partial x} - \left(\frac{\partial \overline{u'^2}}{\partial x} + \frac{\partial \overline{u'v'}}{\partial y} + \frac{\partial \overline{u'w'}}{\partial z}\right) + \nu\nabla^2 U \qquad (7.8)$$

where we have dropped the overbars on the mean velocities and pressure. Note that if the flow was not turbulent, we recover the x-momentum equation for steady (laminar) flow.

Similarly, we have for the y- and z-components:

$$U\frac{\partial V}{\partial x} + V\frac{\partial V}{\partial y} + W\frac{\partial V}{\partial z} \; =$$

$$-\frac{1}{\rho}\frac{\partial p}{\partial y} - \left(\frac{\partial \overline{u'v'}}{\partial x} + \frac{\partial \overline{v'^2}}{\partial y} + \frac{\partial \overline{v'w'}}{\partial z}\right) + \nu\nabla^2 V \qquad (7.9)$$

$$U\frac{\partial W}{\partial x} + V\frac{\partial W}{\partial y} + W\frac{\partial W}{\partial z} \; =$$

$$-\frac{1}{\rho}\frac{\partial p}{\partial z} - \left(\frac{\partial \overline{u'w'}}{\partial x} + \frac{\partial \overline{v'w'}}{\partial y} + \frac{\partial \overline{w'^2}}{\partial z}\right) + \nu\nabla^2 W. \qquad (7.10)$$

We see that the process of Reynolds averaging has given us an equation for the mean flow. However, in so doing, terms involving time-averages of velocity fluctuations have appeared, and we have no information on these new terms. Therefore the system of time-averaged equations describing p and $\mathbf{V}$ is not closed. This is the fundamental difficulty of the Reynolds-averaged approach: second-order mean products of fluctuating quantities appear in the equation for the mean flow. This is sometimes called the closure problem.

These second-order products are of two kinds:

(i) Mean squares, or the variances, such as $\overline{u_i^2}$ (no summation). The root mean square, $\sqrt{\overline{u_i^2}}$, is known as the intensity of the turbulence component i, while the intensity of the turbulence is given by:

$$\sqrt{\overline{q^2}} = \left(\overline{u^2} + \overline{v^2} + \overline{w^2}\right)^{\frac{1}{2}} \qquad (\,\sqrt{\overline{q^2}} = 2k \text{ in some books}).$$

This is related to the kinetic energy of the turbulence (per unit volume) $\frac{1}{2}\rho\overline{q^2}$.

(ii) Cross-products, which can also be interpreted as the single-point correlations (or co-variances) between two velocity fluctuations u_i and u_j. The correlation coefficient is defined as:

$$R_{1,2} \; = \; \frac{\overline{u_1 u_2}}{\sqrt{\overline{u_1^2}}\,\sqrt{\overline{u_2^2}}} \; \leq \; 1.$$

Note that if u_i and u_j are independent then the correlation $u_i u_j = 0$.
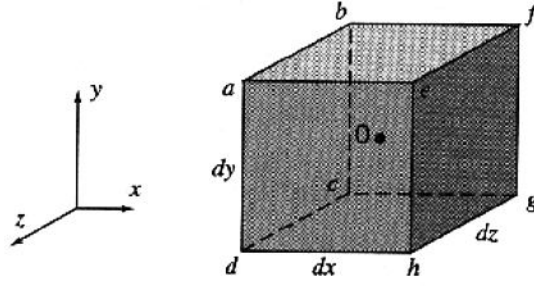
Figure 7.1: Elemental control volume.

7.3 The Reynolds Stresses

When we write the last two terms in equation 7.8 as:

$$\frac{1}{\rho}\left[\mu\nabla^2 U - \rho\left(\frac{\partial\overline{u'^2}}{\partial x} + \frac{\partial\overline{u'v'}}{\partial y} + \frac{\partial\overline{u'w'}}{\partial z}\right)\right]$$

we see that the viscous terms represent a force per unit volume, because it involves the gradients of stresses (for example $\frac{\partial}{\partial y}\left(\mu\frac{\partial U}{\partial y}\right)$). Similarly, we always call $\rho\overline{u^2}$, $\rho\overline{uv}$, $\rho\overline{uw}$, etc., the Reynolds stresses since their gradients have the dimensions of a force per unit volume. They are, of course, only apparent stresses since they arose from the non-linear convective terms in the Navier-Stokes equations.

To see this interpretation more clearly consider the mean x-momentum flux through one of the faces $dydz$ of an elemental control volume

$$= \overline{(\rho U dydz)\,U} = \overline{\rho(U+u)^2}\,dydz = \rho\left(\bar{U}^2 + \overline{u^2}\right)dydz,$$

as shown in figure 7.1.

The additional mean momentum flux due to the turbulent motion can be interpreted as an extra stress ($= \rho\overline{u^2}$). This is an extra normal stress in that it acts normal to the face across which the transport occurs.

Now consider the mean x-momentum flux across one of the faces $dxdz$:

$$= \overline{(\rho V dydz)\,U} = \rho\left(\bar{U}\bar{V} + \overline{uv}\right)dydz,$$

Here $\rho\overline{uv}$ represents an extra mean shear stress on the face $dxdz$. A similar term will arise when we consider the mean y-momentum passing through the face $dydz$, so that the Reynolds stress sensor is symmetric.

So we can find the total x-momentum flux. What is important are the gradients of these fluxes, since these are equal to the resultant forces in the

x-direction:

$$\rho\left(\frac{\partial \bar{U}^2}{\partial x} + \frac{\partial \bar{U}\bar{V}}{\partial y} + \frac{\partial \bar{U}\bar{W}}{\partial z} + \frac{\partial \overline{u^2}}{\partial x} + \frac{\partial \overline{uv}}{\partial y} + \frac{\partial \overline{uw}}{\partial z}\right) dx dy dz.$$

Note that the turbulent fluctuations also lead to extra fluxes of quantities other than momentum. For example, if there are temperature fluctuations θ', then there is an extra rate of enthalpy transfer $\rho C_p \overline{\theta' u}$ in the *x*-direction, etc., in addition to the enthalpy transfer by molecular conduction.

Now *rms* velocity fluctuations of about ±10% will produce Reynolds stresses of about $\rho(0.1U)^2/4$. In a pipe, if we are not too close to the wall, the mean velocity gradients are of order U/D, giving viscous stresses of order $\mu U/D$. The ratio is $0.0025\mu U/D$, or 250 if $\mu U/D = 100,000$. So Reynolds stresses (and other turbulent transport rates) are much larger than viscous stresses (and other molecular transport rates), outside the near-wall region.

Note, in addition, that whether a stress is a "normal" or a "shear" stress depends solely on the axes chosen, and, as in solids, we can always find a set of principal axes with respect to which only normal stresses remain. Since q^2 is the trace of the Reynolds stress tensor it is invariant with rotation of axes.

If we add up the three components of the mean momentum equation we get

$$\bar{U}_j \frac{\partial \bar{U}_i}{\partial x_j} = \frac{1}{\rho}\frac{\partial}{\partial x_j}\left(-p\delta_{ij} + 2\mu \bar{S}_{ij} - \rho\overline{u_i u_j}\right) \tag{7.11}$$

where

$$\bar{S}_{ij} = \frac{1}{2}\left(\frac{\partial \bar{U}_i}{\partial x_j} + \frac{\partial \bar{U}_j}{\partial x_i}\right).$$

We also use

$$\tau_{ij} = -\rho\overline{u_i u_j} = \tau_{ji}.$$

Two examples of turbulent stress distributions are given in figures 7.2 and 7.3. Figure 7.2 gives the results of a study of a two-stream mixing layer by Mehta & Westphal (1984). Note that the mean velocity profiles collapse on a curve that looks like an error function. The maximum streamwise turbulence intensity occurs near the centerline and it is about 18% of the velocity difference across the layer, and the shear stress $-\rho\overline{uv}$ is about one-third of the streamwise normal stress ρu^2. It is particularly interesting that the correlation coefficient R_{uv} is positive (that is, negative v is correlated with positive u, and vice versa), and quite high (about 0.5 over most of the layer). Figure 7.3 shows the results obtained by Alving *et al.* (1990) in a zero pressure gradient boundary layer. All the stress levels are lower than the corresponding values in the mixing layer (this is the influence of the wall
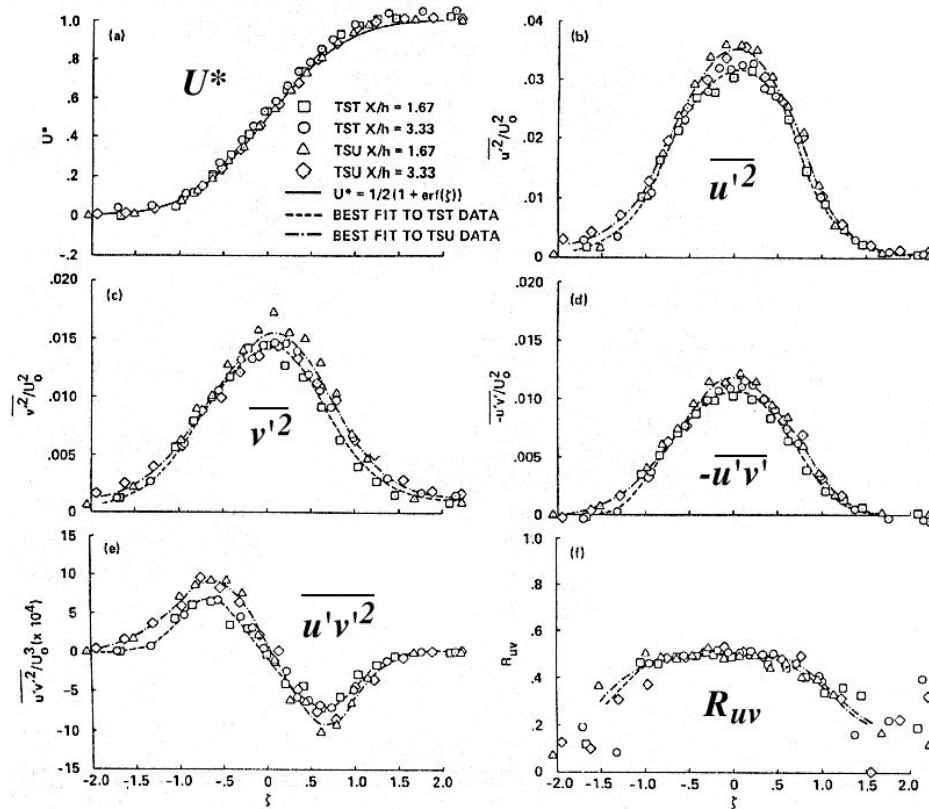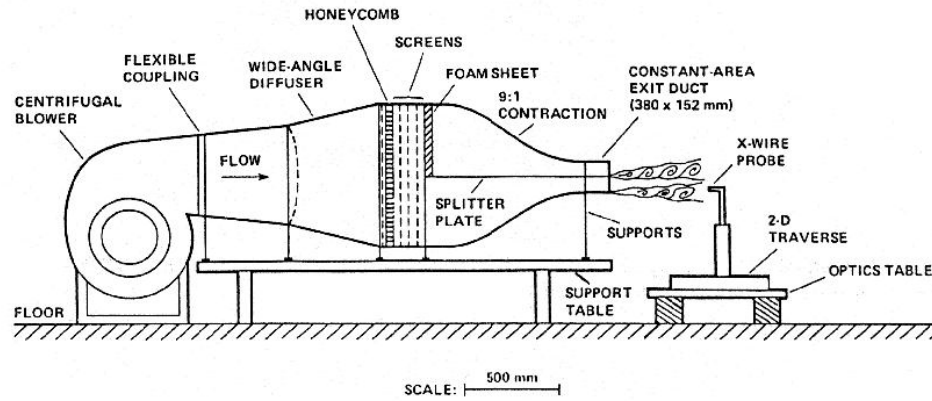
Figure 7.2: Free shear layer stress distributions. Here, $u_0 = U_1 - U_2$ = velocity difference between the two streams, and $U^* = (U - U_2)/(U_1 - U_2)$. From Mehta & Westphal, 1984.

constraint), and the levels of v^2 and w^2 are considerably lower than the level of u^2. The maximum streamwise turbulence intensity occurs near the wall and it is about 10% of the velocity in the freestream. The shear stress $-\rho\overline{uv}$ is about one-fourth of the streamwise normal stress ρu^2. Again, the correlation
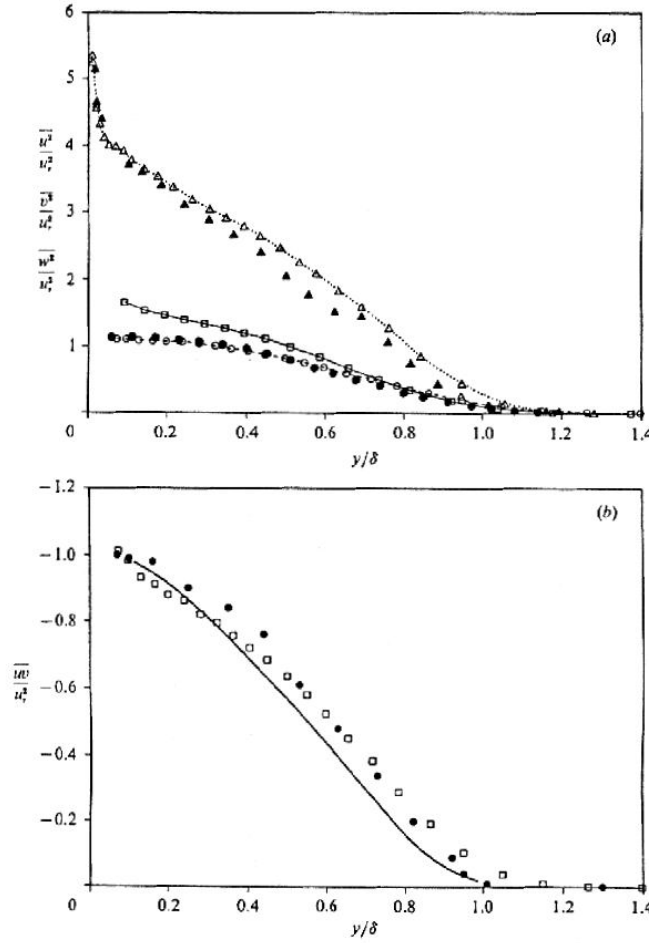
Figure 7.3: (a) Normal stresses in a zero pressure gradient boundary layer: △, $\overline{u'^2}/u_\tau^2$; □, $\overline{v'^2}/u_\tau^2$; ○, $\overline{w'^2}/u_\tau^2$ ($u_\tau = \sqrt{\tau_w/\rho}$). (b) Shear stress distribution. Results from Alving, 1988. Filled-in symbols from Erm, Smits & joubert, 1987. Solid line from Klebanoff, 1955.

coefficient R_{uv} is positive and quite high (in this case about 0.45 over most of the layer).

7.4   Turbulent Transport of Heat

For an incompressible flow, the energy equation is given by:

$$\rho C_p \frac{DT}{Dt} = \frac{Dp}{Dt} + k\nabla^2 T + 2\mu S_{ij}\frac{\partial U_j}{\partial x_i} \tag{7.12}$$

where k = thermal conductivity of fluid (W/mK), and

$$\bar{S}_{ij} \;=\; \frac{1}{2}\left(\frac{\partial \bar{U}_i}{\partial x_j} + \frac{\partial \bar{U}_j}{\partial x_i}\right),$$

$$\text{and} \quad 2\mu S_{ij}\frac{\partial U_j}{\partial x_i} \;=\; \Phi \;=\; \text{dissipation function.} \qquad (7.13)$$

Now, by an order of magnitude argument (not repeated here, but see for example White *Viscous Flow*, or Schlichting, or Panton pp. 254–258), we can show that for most purposes, as long as the Eckert number ($Ec = (\gamma - 1)Ma^2 T_0/\Delta T$) is small compared to one, the pressure term and the dissipation function are negligible compared to the other terms. Hence:

$$\rho C_p \frac{DT}{Dt} \;=\; k\nabla^2 T$$

$$\frac{\partial T}{\partial t} + U_j\frac{\partial T}{\partial x_j} \;=\; \alpha\nabla^2 T \qquad (7.14)$$

where α = thermal diffusivity (with dimensions L^2/T), and $Pr = \nu/\alpha$.

Substituting $T = T + \theta'$ etc., taking the mean, we get

$$U_j\frac{\partial \bar{T}}{\partial x_j} \;=\; \frac{\partial}{\partial x_j}\left(\alpha\frac{\partial \bar{T}}{\partial x_j} - \overline{\theta' u_j}\right) \qquad (7.15)$$

where the term in parenthesis is equal to $Q_j/\rho C_p$, where Q_j is the mean heat flux per unit area, that is, the rate of transport of mean heat, given by the sum of the contributions from molecular motion and turbulent motion. Note the similarity with equation 7.11 for the mean momentum: the transport of heat and momentum occurs in a similar way, even when the flow is turbulent.

7.5 The Reynolds Stress Equations

We can form equations for the evolution of the Reynolds stresses directly from the Navier-Stokes equation. For example, if we take equation 7.7, multiply by the fluctuating velocity u, time average and subtract the mean, we get:

$$\frac{\partial\left(\frac{1}{2}\overline{u^2}\right)}{\partial t} + U\frac{\partial\left(\frac{1}{2}\overline{u^2}\right)}{\partial x} + V\frac{\partial\left(\frac{1}{2}\overline{u^2}\right)}{\partial y} + W\frac{\partial\left(\frac{1}{2}\overline{u^2}\right)}{\partial z} \;=\; \frac{D\left(\frac{1}{2}\overline{u^2}\right)}{Dt}$$

$$=\; -\frac{1}{\rho}\overline{u\frac{\partial p'}{\partial x}} + \overline{\nu u\nabla^2 u} - \left(\overline{u^2}\frac{\partial U}{\partial x} + \overline{uv}\frac{\partial U}{\partial y} + \overline{uw}\frac{\partial U}{\partial z}\right)$$

$$-\left(\overline{u^2\frac{\partial u}{\partial x}} + \overline{uv\frac{\partial u}{\partial y}} + \overline{uw\frac{\partial u}{\partial z}}\right). \qquad (7.16)$$

By multiplying the continuity equation 7.6 by u^2 , and adding the result to equation 7.16, we can rewrite the last three terms as:

$$-\frac{1}{2}\left(\frac{\partial \overline{u^3}}{\partial x} + \frac{\partial \overline{u^2 v}}{\partial y} + \frac{\partial \overline{u^2 w}}{\partial z}\right)$$

These kinds of terms are called "transport" terms because their integral across the boundary layer or free shear layer is zero (the boundary conditions at the inner and outer edges dictate that the integral must be zero).

The first term on the right of equation 7.16 can be written as:

$$-\frac{1}{\rho}\frac{\partial \overline{p' u}}{\partial x} + \frac{1}{\rho}\overline{p'\frac{\partial u}{\partial x}}.$$

Here, $\overline{p' u}$ is the rate of work done by the fluid against fluctuations in pressure. The first term therefore represents the spatial transport of the Reynolds stress (alternatively, one component of the turbulent kinetic energy) by pressure gradients (sometimes called "pressure diffusion"). It can also be interpretedas the net loss of turbulent energy by work done in transporting fluid through regions of changing pressure. The second term on the right represents the transfer of turbulent energy from the u-component to v- and w-components. That this is a transfer of energy among components can be seen by noting that when we write an equation for q^2 these terms sum to zero because of continuity — there is no net change in q^2. This transfer of energy tends to isotropize the turbulence, and therefore it is called the "tendency-to-isotropy" term.

Similarly, equations for the other normal stresses can be derived. These can be written down by inspection from equation 7.16 by a cyclic interchange of x, y and z (and u, v and w).

By multiplying equation 7.7 by the fluctuating velocity v instead of u, and adding u times the y-component momentum equation we get an equation for the shear stress:

$$\frac{D\overline{uv}}{Dt} \;=\; -\frac{1}{\rho}\left(\frac{\partial \overline{p' u}}{\partial y} + \frac{\partial \overline{p' v}}{\partial x}\right) + \frac{1}{\rho}\overline{p'\left(\frac{\partial u}{\partial y} + \frac{\partial v}{\partial x}\right)} + \nu\left(\overline{u\nabla^2 v} + \overline{v\nabla^2 u}\right)$$

$$+ \text{ other terms involving second and third order correlations} \tag{7.17}$$

So, although we have written equations for the Reynolds stresses (that is, the additional unknowns introduced into the Navier-Stokes equations when they were averaged), these equations themselves contain third-order products, which again represent a new set of unknown quantities. Equations for the third-order products can also be derived from the Navier-Stokes equations but these will contain fourth-order moments, and so on. If these

Reynolds-stress equations are to be useful, then at some point the equations need to be <u>closed</u>, that is, the highest-order products need to be expressed in terms of lower-order products ($\overline{u^2}$, $-\overline{uv}$, $\bar{U}$, for example) so that the number of equations equals the number of unknowns. This is called turbulence modelling (see below), and most attention has been focussed on the turbulence kinetic energy, despite the fact that q^2 does not appear in any of the mean momentum equations.

7.6 The Turbulent Kinetic Energy Equation

In any case, by adding up the three equations for the normal stresses, we obtain:

$$
\begin{aligned}
\frac{D\left(\frac{1}{2}\overline{q^2}\right)}{Dt} &= -\frac{1}{\rho}\left(\frac{\partial \overline{p'u}}{\partial x} + \frac{\partial \overline{p'v}}{\partial y} + \frac{\partial \overline{p'w}}{\partial z}\right) + \frac{1}{\rho}\overline{p'\left(\frac{\partial u}{\partial x} + \frac{\partial v}{\partial y} + \frac{\partial w}{\partial z}\right)} \\
&\quad + \nu\left(\overline{u\nabla^2 u} + \overline{v\nabla^2 v} + \overline{w\nabla^2 w}\right) \\
&\quad - \left[\overline{u^2}\frac{\partial U}{\partial x} + \overline{uv}\frac{\partial U}{\partial y} + \overline{uw}\frac{\partial U}{\partial z} + \overline{uv}\frac{\partial V}{\partial x} + \overline{v^2}\frac{\partial V}{\partial y} + \overline{vw}\frac{\partial V}{\partial z}\right. \\
&\quad\left. + \overline{uw}\frac{\partial W}{\partial x} + \overline{vw}\frac{\partial W}{\partial y} + \overline{w^2}\frac{\partial W}{\partial z}\right] - \frac{1}{2}\left[\frac{\partial \overline{u^3}}{\partial x} + \frac{\partial \overline{u^2 v}}{\partial y} + \frac{\partial \overline{u^2 w}}{\partial z}\right. \\
&\quad\left. + \frac{\partial \overline{v^2 u}}{\partial x} + \frac{\partial \overline{v^3}}{\partial y} + \frac{\partial \overline{v^2 w}}{\partial z} + \frac{\partial \overline{w^2 u}}{\partial x} + \frac{\partial \overline{w^2 v}}{\partial y} + \frac{\partial \overline{w^3}}{\partial z}\right] \qquad (7.18)
\end{aligned}
$$

The second term on the right is zero by continuity. In tensor notation:

$$
\begin{aligned}
\frac{D\left(\frac{1}{2}\overline{q^2}\right)}{Dt} &= \frac{\partial\left(\frac{1}{2}\overline{q^2}\right)}{\partial t} + \overset{1a}{\overbrace{U_j\frac{\partial\left(\frac{1}{2}\overline{q^2}\right)}{\partial x_j}}} \\
&= -\frac{\partial}{\partial x_j}\left(\overset{2a}{\overbrace{\frac{\overline{p'u_j}}{\rho}}} + \overset{1b,2b}{\overbrace{\tfrac{1}{2}\overline{u_j q^2}}}\right) - \underbrace{\overline{u_i u_j}\frac{\partial U_i}{\partial x_j}}_{3} + \underbrace{\nu\,\overline{u_i\frac{\partial^2 u_i}{\partial x_j^2}}}_{4,5}. \qquad (7.19)
\end{aligned}
$$

It is useful to give the physical meaning associated with the various terms. In this we follow Bradshaw *An introduction to turbulence and its measurement* 1971 (Pergamon Press — out of print). See also figure 7.4.
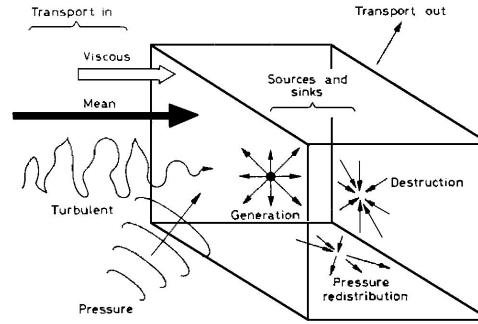
Figure 7.4: "The most general case of fluid motion, exhibiting all the complications allowed by the Navier-Stokes equations, is called turbulence," Peter Bradshaw, 1971.

(1) The instantaneous rate of transport of q^2 is q^2 times the instantaneous velocity, for example, the rate of transport in the x-direction is $q^2(U+u)$. [Note that the "rate of transport" is nothing more than the flux per unit area, where the flux of (something) is the amount of that (something) being transported across some surface per unit time. For example, the mass flux = $(\mathbf{n} \cdot \rho\mathbf{V})dA$, the momentum flux = $(\mathbf{n} \cdot \rho\mathbf{V})\mathbf{V}dA$, the energy flux = $(\mathbf{n} \cdot \rho\mathbf{V})\mathbf{V}^2 dA$, etc.] The <u>mean</u> rate of transport of q^2 in the x-direction is therefore $\overline{q^2}\bar{U} + \overline{q_2 u}$. The <u>net</u> rate at which $\overline{q^2}$ is leaving an elementary control volume in the x-direction is $\frac{\partial}{\partial x}(\overline{q^2}\bar{U} + \overline{q^2 u})dxdydz$. Summing up the contributions from the three directions gives terms (1a) + (1b), where (1a) is called the advection, or mean energy transport, and it is the rate of change of $\frac{1}{2}q^2$ along a mean streamline. [Note that any term that can be expressed as a spatial gradient of a mean quantity is a "transport" term (its integral over the flow volume must be zero). Terms not so expressible are called "source/sink" terms. Note that term (3) is the only one involving a mean velocity gradient, and it is the only term therefore that can act to take energy from the mean motion.]

(2) Terms like $\overline{p'u'}$ can be interpreted as the rate at which work is being done against the fluctuations in pressure (per unit area). Hence $\frac{\partial}{\partial x}(\overline{p'u})dxdydz$ represents the net loss of turbulent energy from an elemental volume by the work done in transporting the fluid through a region of changing pressure.

The sum of terms (2a) and (2b) (also called (1b)) is sometimes called the turbulent energy transport, or energy diffusion.

(3) Terms like $-\rho\overline{u^2}\frac{\partial U}{\partial x}dxdydz$ represent an extraction of energy from the mean flow by the turbulence: from the point of view of the turbulence

these are energy <u>production</u> terms, and from the point of view of the mean flow these are energy <u>loss</u> terms (we will see from the equation for the mean flow kinetic energy derived in section 7.7 that these same terms appear in that equation with the opposite sign). Note that $-\rho \overline{u^2} \frac{\partial U}{\partial x} dx dy dz$ is the rate at which work is done against the x-component of the Reynolds normal stress to stretch an element of fluid $dx dy dz$ in the x-direction at a rate $\frac{\partial U}{\partial x}$. Usually terms like $-\rho \overline{uv} \frac{\partial U}{\partial y} dx dy dz$ are more important, and these represent the work done against the shear stress $-\rho \overline{uv}$ to shear an element of fluid at the rate $\frac{\partial U}{\partial y}$.

(4) Now a term like $\left(\mu \frac{\partial U}{\partial y}\right) \frac{\partial U}{\partial y}$ represents the product of the instantaneous viscous stress and the instantaneous rate of strain, that is, a transfer of energy between the bulk motion and the molecular motion — a dissipation of bulk kinetic energy into thermal energy by viscosity. From the point of view of the temperature field it is a source of energy and is responsible for "aerodynamic" heating in high-speed flows.

The viscous term in the energy equation (the enthalpy equation) is:

$$\Phi = 2\mu S_{ij} \frac{\partial U_j}{\partial x_i} = \frac{\partial U_j}{\partial x_i}\left(\mu\left(\frac{\partial U_i}{\partial x_j} + \frac{\partial U_j}{\partial x_i}\right)\right) = \text{dissipation function}$$

(see section 7.7). If we substitute the Reynolds decomposition and take the time average, we obtain (see Schlichting, Chapter 18 Part e):

$$\bar{\Phi} = \frac{\partial \bar{U}_j}{\partial x_i}\left(\mu\left(\frac{\partial \bar{U}_i}{\partial x_j} + \frac{\partial \bar{U}_j}{\partial x_i}\right)\right) + \overline{\frac{\partial u_j}{\partial x_i}\left(\mu\left(\frac{\partial u_i}{\partial x_j} + \frac{\partial u_j}{\partial x_i}\right)\right)}. \tag{7.20}$$

The first term on the right represents the dissipation of mean flow kinetic energy into thermal internal energy (= Φ_m, the "direct" dissipation function), and the second term on the right represents the viscous dissipation of turbulent kinetic energy (= ε, the "turbulent" dissipation function). Since the instantaneous velocity gradients associated with the turbulence are much greater than the mean velocity gradients (except very close to a solid surface), $\varepsilon \gg \Phi_m$.

How does all this relate to the turbulent kinetic energy equation? Well, the viscous term in equation 7.19 may be written as:

$$\nu\left(\overline{u\nabla^2 u} + \overline{v\nabla^2 v} + \overline{w\nabla^2 w}\right)$$

$$= \nu\left(\tfrac{1}{2}\nabla^2\left(\overline{u^2} + \overline{v^2} + \overline{w^2}\right) - \overline{\left(\frac{\partial u}{\partial x}\right)^2} - \overline{\left(\frac{\partial u}{\partial y}\right)^2} - \overline{\left(\frac{\partial u}{\partial z}\right)^2} - \cdots\right)$$

We recognize the squares of velocity gradients as elements of ε. Not all the elements are there, because cross product terms like $\mu \frac{\partial^2 \overline{uv}}{\partial x \partial y}$ are

missing in the turbulent kinetic energy equation. However, these cross-product terms are usually interpreted as a diffusion term and these can be shown to be small, except near the wall (see Townsend Section 2.7). To explain this interpretation, we also bring in the other term $\mu \nabla^2 (\frac{1}{2}\overline{q^2})$. This is the viscous diffusion of $\overline{q^2}$), just as $\mu \nabla^2 U$ is the viscous diffusion of U. Similarly, $\mu \frac{\partial^2 \overline{uv}}{\partial x \partial y}$ is the viscous diffusion of $\overline{uv}$. Since all diffusion terms are small at all Reynolds numbers that are not too low we have:

$$\mu \overline{\left(\frac{\partial u_j}{\partial x_i}\right)^2} \approx \varepsilon \approx \mu \left(\overline{u'\nabla^2 u'} + \overline{v'\nabla^2 v'} + \overline{w'\nabla^2 w'}\right)$$

(5) Diffusion terms like $\mu \nabla^2 U$ are negligible (see Townsend Section 2.7).

Energy balances for the wake of a circular cylinder and a zero pressure gradient boundary layer are shown in figure 7.5, and for a fully developed pipe flow in figure 7.7. The wall bounded flows display large regions where the production term is approximately balanced by the dissipation term. The diffusion terms become important near the wall, as expected, and they are important near the outer edge of the layer, since all other terms become very small there. The wake flow is somewhat more complicated in that all terms appear to be important everywhere.

7.7   Mean Flow Kinetic Energy Equation

To derive the equation for the mean flow kinetic energy (this is not the same as the energy or enthalpy equation), we take the mean x-momentum equation 7.8 and multiply by U. Similarly, we take the y- and z-momentum equations and multiply by V and W respectively. Adding up the resulting equations gives:

$$\frac{D}{Dt}\left(\frac{\rho \overline{U_i^2}}{2}\right) = U_j \frac{\partial}{\partial x_j}\left(\frac{\rho \overline{U_i^2}}{2}\right) = -\bar{U}_i \frac{\partial p}{\partial x_i} + \bar{U}_i \frac{\partial}{\partial x_j}\left(2\mu S_{ij}\right) - \bar{U}_i \frac{\partial}{\partial x_j}\left(\rho \overline{u_i u_j}\right) \quad (7.21)$$

The term on the left in equation 7.21 is the rate of change of the kinetic energy of the mean motion. The first term on the right of equation 7.21 is the work done by the mean pressure forces to produce kinetic energy of the mean motion. The viscous term in equation 7.21 has both a spatial transfer part and a dissipation part:

$$\bar{U}_i \frac{\partial}{\partial x_j}\left(2\mu S_{ij}\right) = \frac{\partial}{\partial x_j}\left(2\mu \bar{U}_i S_{ij}\right) - 2\mu \bar{S}_{ij}\frac{\partial \bar{U}_i}{\partial x_j}$$
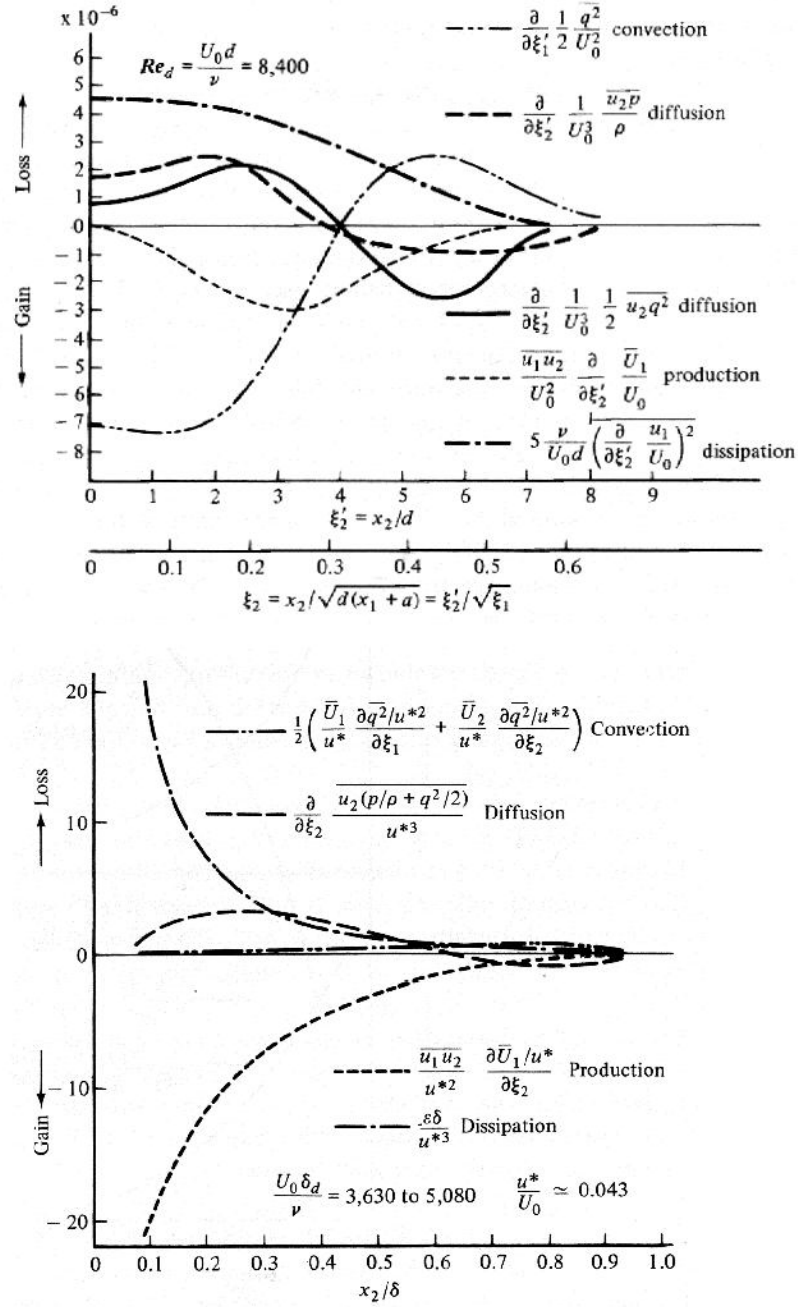
Figure 7.5: (a) Energy balance in the wake of a circular cylinder at $\xi = x/d = 160$. (b) Energy balance in a zero pressure gradient boundary layer (outer scaling). From Townsend (figures taken from Hinze).

where the first term on the right represents the spatial transport of mean kinetic energy by the stress gradients, and the second term represents the direct dissipation function Φ_m (the same Φ_m as in equation 7.20).
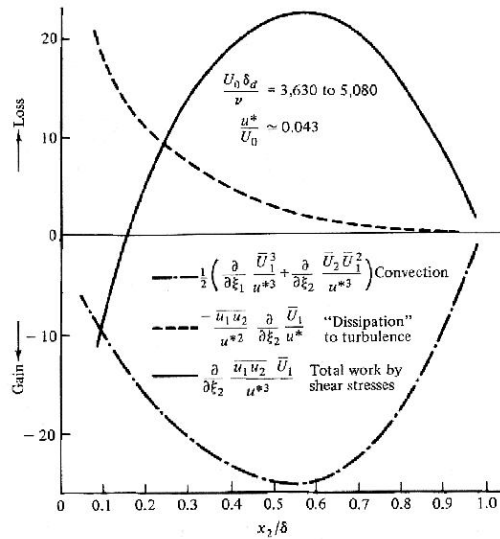
Figure 7.6: Mean flow energy balance in a zero pressure gradient boundary layer (outer scaling). From Townsend (figure taken from Hinze).

The last term on the right in equation 7.21 can be written as:

$$-\bar{U}_i \frac{\partial}{\partial x_j}\left(\rho\overline{u_i u_j}\right) = -\frac{\partial}{\partial x_j}\left(\bar{U}_i \rho\overline{u_i u_j}\right) + \rho\overline{u_i u_j}\frac{\partial \bar{U}_i}{\partial x_j}$$

where the first term on the right represents the spatial transport of mean kinetic energy by the turbulent fluctuations, and the second term represents the loss to turbulence: this is the extraction of turbulent energy from the mean flow.

Figure 7.6 shows the energy balance of the mean motion for a zero pressure gradient boundary layer. Obviously the term labelled "dissipation to turbulence" is identical in magnitude to the "production" term in figure 7.7b but with opposite sign.
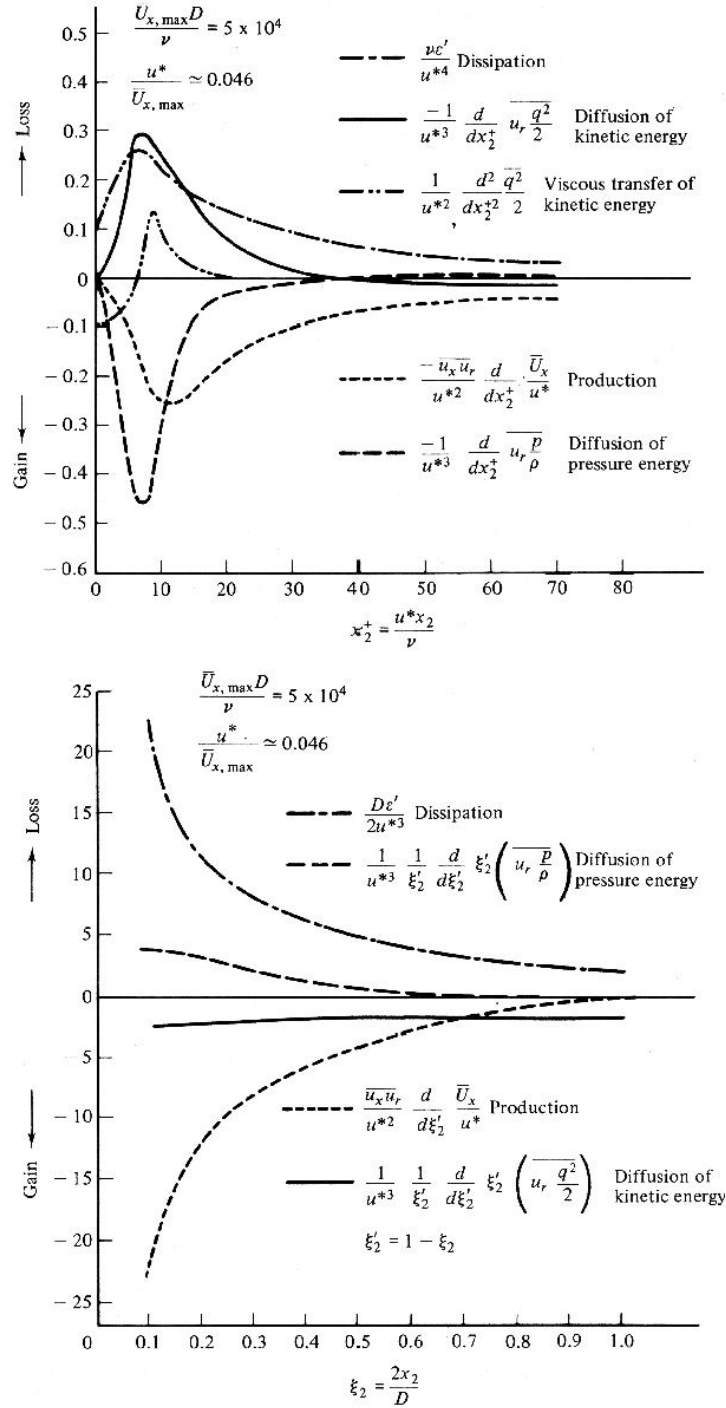
Figure 7.7: (a) Energy balance in the wall region of a pipe flow (inner scaling). (b) Energy balance in the core region of a pipe flow (outer scaling). From Laufer (figures taken from Hinze).

Chapter 8

Vorticity and Turbulence

8.1 Introduction

If you have ever looked over a river bridge and watched the surface patterns move downstream of the pylons then you will have seen swirling motions with both rotational and translational motion. Similar patterns have been observed in the wake of any bluff body (sharp plate, cylinder) as well as in boundary layers and free shear layers. They are generally disorganized in that their characteristic scales vary with time and space in an apparently random fashion. Their scales are also a function of Reynolds number in that the range of length scales that is observed increases with Reynolds number, as does the range of time scales, or frequencies.

We know that turbulent motions are characterized by intense three- dimensional fluctuations in velocity, even if the flow itself is nominally two-dimensional. How can we interpret these motions physically? Inherent in all thinking about turbulence is the concept of an eddy, which is regarded as a more or less coherent fluid motion and forms a subset of the larger velocity field (according to Townsend, p.6: "flow patterns with spatially limited distributions of vorticity and comparatively simple forms"). Any interpretation of eddy behavior is often based on analogies with simpler swirling motions such as that associated with vortices, for example, the Rankine or potential vortex, which leads to the concept of a line vortex, and the sink vortex. Turbulence is often seen in terms of vorticity distributed in a very intermittent fashion: the turbulent fluid is identified with fluid containing concentrated vorticity distributed as vortex tubes or sheets, and these tubes or sheets may be contained in a background field where the vorticity is at a relatively low level (almost zero). The eddying motions associated with this vorticity distribution interact with each other and they become distorted, they are transported and they change their intensity. There are two ways of interpreting eddies: as a perturbation imposed on the mean velocity field (a consequence of thinking in terms of the Reynolds-averaged equations of

motion) or as constituting the entire velocity field, both mean and fluctuating. The conceptual difference is clear: what is not usually so clear is how any particular researcher interprets the motions in terms of structure.

The concept of eddy structures arises from at least three sources:

1. Flow visualization;

2. Correlations and spectrum functions; and

3. The vorticity equation.

The concept of vorticity is crucial for a physical understanding of turbulence. Note that there is an important distinction between vorticity and vortices: for example, a laminar boundary layer has vorticity but no vortices. In turbulent flow, vortices are difficult to define unambiguously, but eddies are generally thought of as vortex tubes, at least qualitatively, and these are sometimes called the "muscles and sinews of turbulence." Here, we start with some basic definitions, then consider vortices in inviscid flow, and then vortices in a viscous flow. We will only consider barotropic, constant density flows.

8.2   Basic Concepts

8.2.1   Circulation

The circulation Γ is defined as

$$\Gamma = \oint \mathbf{V} \cdot d\ell \tag{8.1}$$

where counterclockwise is positive. That is, the circulation contained within a closed contour in a body of fluid is defined as the integral around the contour of the velocity vector which is locally tangential to the contour.

8.2.2   Vorticity

Vorticity is defined as the curl of the velocity:

$$\Omega = \nabla \times \mathbf{V}.$$

That is,

$$\Omega_i = \epsilon_{ijk} \frac{\partial u_j}{\partial x_k} = \left(\frac{\partial u_k}{\partial x_j} - \frac{\partial u_j}{\partial x_k} \right). \tag{8.2}$$

The vorticity is related to the instantaneous angular velocity of the fluid element, ω, by:

$$\Omega = 2\omega.$$
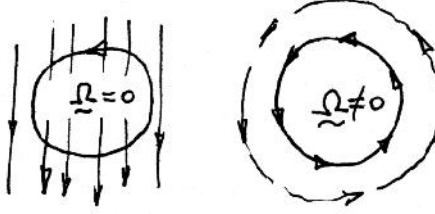
Figure 8.1: Rotational and irrotational motions.

By Stokes Theorem

$$\Gamma = \oint \mathbf{V} \cdot d\ell = \iint \nabla \times \mathbf{V} \cdot \mathbf{n} dA$$

Therefore:

$$\Gamma = \iint \mathbf{n} \cdot \mathbf{\Omega} dA \qquad (8.3)$$

Hence, if $\Omega = 0$ then $\Gamma = 0$, and the flow is called irrotational.

Consider a boundary layer developing on a flat plate in a zero pressure gradient (figure 8.2): If we evaluate the circulation from the line integral of the velocity (equation 8.1), we see that the circulation in the incoming flow is zero. This is true for an arbitrary contour, and therefore the vorticity in the incoming flow is zero everywhere. Now, if we take a contour enclosing the boundary layer at any station downstream of the leading edge, we see that the circulation per unit streamwise distance is constant (if we ignore the small contributions made to the circulation integral by the velocity component normal to the wall). This means that all the vorticity was created at the leading edge. However, the circulation only describes the average net vorticity present within the contour, but we do not know anything about the distribution of the vorticity within the contour. For a two-dimensional boundary layer, the mean vorticity at any point has only one component $\left(\frac{\partial v}{\partial x} - \frac{\partial u}{\partial y} \right) \mathbf{k}$, and it is clear that the distribution of the vorticity will change as
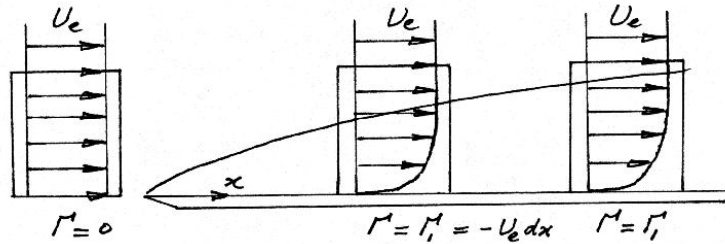
Figure 8.2: Overall circulation in a boundary layer.
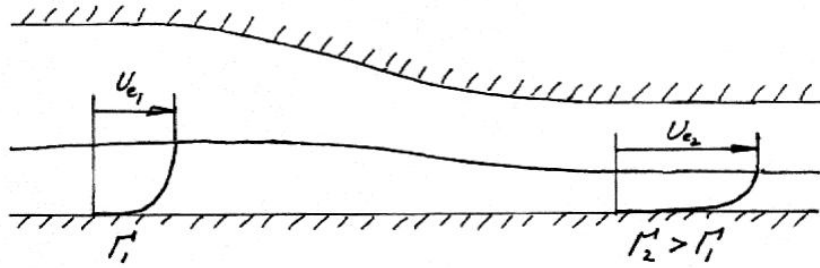
Figure 8.3: Circulation in a boundary layer in a favorable pressure gradient.

the layer grows. Note also that if the boundary layer is turbulent, the overall level of the fluctuating vorticity within the boundary layer a given volume must sum to zero, and we can expect that within any sub-volume it must on average be zero also, so that negative and positive vorticity must nearly cancel at any time.

If the boundary layer enters a region of streamwise pressure gradient, the freestream velocity will change, and therefore the circulation around a contour enclosing the layer must change accordingly. Therefore pressure gradients can change the circulation (favorable pressure gradients will increase the circulation, and vice versa). It is sometimes said that the pressure gradients at the wall act as a source or sink of vorticity[1].

8.2.3   Vortex tubes and filaments

Instantaneously, imagine a closed contour in the fluid. Each point on the contour will have a streamline passing through it. These streamlines define a volume called a *stream tube*. If the cross-sectional area is infinitesimal, we get a *stream filament*.

Similarly, we define a vortex line as a line whose tangents are parallel to the vorticity vector. For a closed contour, each point on the contour will have a vortex line passing through it. Hence, we can define a *vortex tube*, and a *vortex filament*.

For an incompressible flow, the velocity field is divergence-free, that is, $\nabla \cdot \mathbf{V} = 0$, and there are no sinks or sources of mass in the fluid. As a vector identity, the divergence of the curl of a vector is zero, that is, $\nabla \cdot \Omega = 0$ and there are no sinks or sources of vorticity inside the fluid. Therefore, vortex tubes must terminate on themselves, at a solid boundary, or at a free surface.

We can make a formal analogy between $\mathbf{V}$ in an incompressible flow and Ω.

---

[1]Note that all the vorticity in the layer is due to the no-slip condition: a pressure gradient by itself will not generate vorticity in a barotropic fluid — see section 8.4
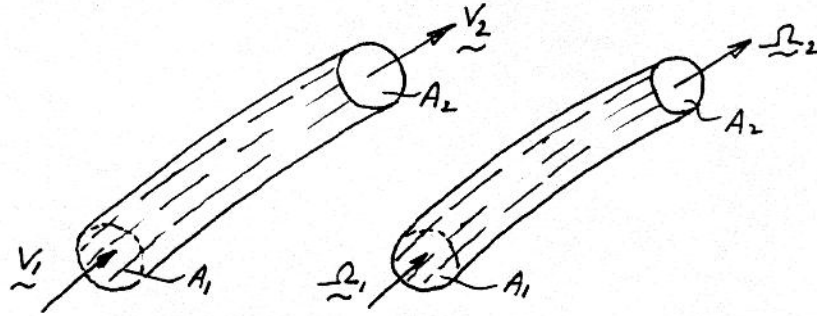
Figure 8.4: Comparison between a streamtube (left) and a vortex tube (right).

<table>
<tr><td>

Incompressible flow applied
to streamtube
$$\nabla \cdot \mathbf{V}$$
No sources or sinks of mass,
then
$$\int \int \int \nabla \cdot \mathbf{V}\, dv = 0$$
That is:
$$\int \int \mathbf{n} \cdot \mathbf{V}\, dA = 0$$
For stream tube, by definition
of streamlines, on walls
$$\nabla \cdot \mathbf{V} = 0$$
and
$$\int \int \mathbf{n} \cdot \mathbf{V_1}\, dA_1 + \int \int \mathbf{n} \cdot \mathbf{V_2}\, dA_2 = 0$$
Hence $\dot{q}_1 = \dot{q}_2 = $ constant
i.e. volume flow rate
for stream tube is constant,
and if area decreases, velocity
increases

</td><td>

Vorticity vector applied
to vortex tube
$$\nabla \cdot \mathbf{\Omega}$$
No sources or sinks of vorticity,
then
$$\int \int \int \nabla \cdot \mathbf{\Omega}\, dv = 0$$
That is:
$$\int \int \mathbf{n} \cdot \mathbf{\Omega}\, dA = 0$$
For vortex tube, by definition
of vortex lines, on walls
$$\nabla \cdot \mathbf{\Omega} = 0$$
and
$$\int \int \mathbf{n} \cdot \mathbf{\Omega_1}\, dA_1 + \int \int \mathbf{n} \cdot \mathbf{\Omega_2}\, dA_2 = 0$$
Hence $\Gamma_1 = \Gamma_2 = $ constant
i.e. circulation for vortex
tube is constant, and if area
decreases vorticity increases
(Helmholtz's Theorem)

</td></tr>
</table>

8.2.4 Vortex sheet

A vortex line or filament is a vortex tube of infinitesimal area. A vortex sheet can be though of as an infinite number of vortex filaments, placed side by side, each of which has an infinitesimal strength (circulation). The integral of the vorticity over an area centering a unit width of the sheet then has a finite value, which is called the strength of the sheet γ. That is,

$$\gamma = \lim_{\ell \to 0} \frac{1}{\ell} \oint \mathbf{V} \cdot d\ell$$

where ℓ is the width of the enclosed sheet (see figure 8.5).
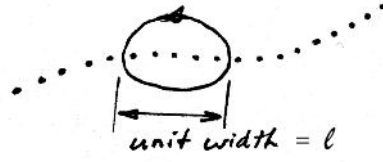
Figure 8.5: Circulation in a vortex sheet.

Vortex sheets represent velocity discontinuities in the flow, such as that which occurs between two uniform parallel flows of different velocity (see figure 8.6).
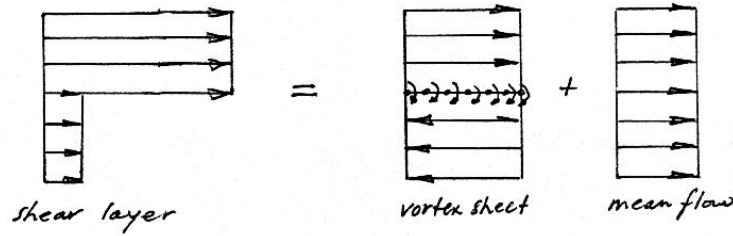

Figure 8.6: Decomposition of a two-stream shear layer.

8.3   Biot-Savart Law

This "law' gives the induced fluid velocity at any distance from an arbitrary infinite line with circulation Γ (line vortex). That is,

$$d\mathbf{V} = \frac{\Gamma}{4\pi r^3} d\ell \times \mathbf{r}. \tag{8.4}$$

That is:

$$|d\mathbf{V}| = \frac{\Gamma}{4\pi r^3} |d\ell| \, |\mathbf{r}| \sin \theta,$$

where the direction is given by the right hand screw rule.

Consider an infinite straight line vortex filament. The induced velocity at any point may be found as follows:

$$\mathbf{V} = \int_{-\infty}^{\infty} \frac{\Gamma}{4\pi r^3} d\ell \times \mathbf{r}.$$

That is:

$$|\mathbf{V}| = \int_{-\infty}^{\infty} \frac{\Gamma}{4\pi r^2} \sin \theta d\ell.$$
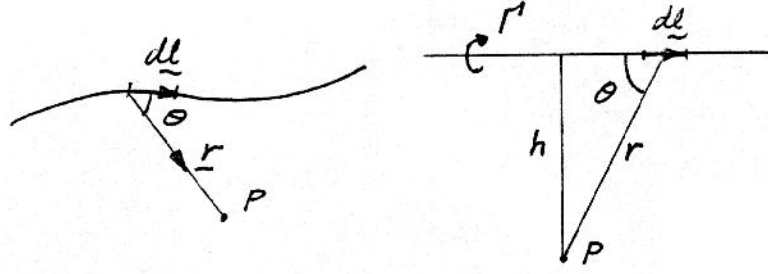
Figure 8.7: Velocity induced by a vortex filament.

With

$$r = \frac{h}{\sin\theta}, \quad \ell = \frac{h}{\tan\theta},$$

$$d\ell = \frac{-h(1 + \tan^2\theta)}{\tan^2\theta} d\theta = \frac{-h}{\sin^2\theta} d\theta.$$

Hence,

$$|\mathbf{V}| = \frac{\Gamma}{2\pi h}.$$

8.4 The Vorticity Transport Equation

By taking the curl of the Navier-Stokes equation we obtain the vorticity transport equation. For a constant density fluid this is given by:

$$\frac{D\mathbf{\Omega}}{Dt} = \mathbf{\Omega} \cdot \nabla\mathbf{V} + \nu\nabla^2\mathbf{\Omega}. \tag{8.5}$$

Note that when the density is contant

$$\frac{\nabla p}{\rho} = \nabla\left(\frac{p}{\rho}\right).$$

In other words, the forces due to pressure gradients are conservative and $\nabla\times\nabla(p/\rho) = 0$ That is, the pressure does not appear explicitly in the vorticity transport equation. We shall discuss the pressure field in more detail later.

Consider the terms in equation 8.5:

$\dfrac{D\mathbf{\Omega}}{Dt}$ = rate of change of vorticity following a fluid element;

$\nu\nabla^2\mathbf{\Omega}$ = rate of change of vorticity due to molecular diffusion of vorticity;

$\mathbf{\Omega}\cdot\nabla\mathbf{V}$ = part of this is the exchange of vorticity between components because of rotation of vortex lines due to presence of velocity
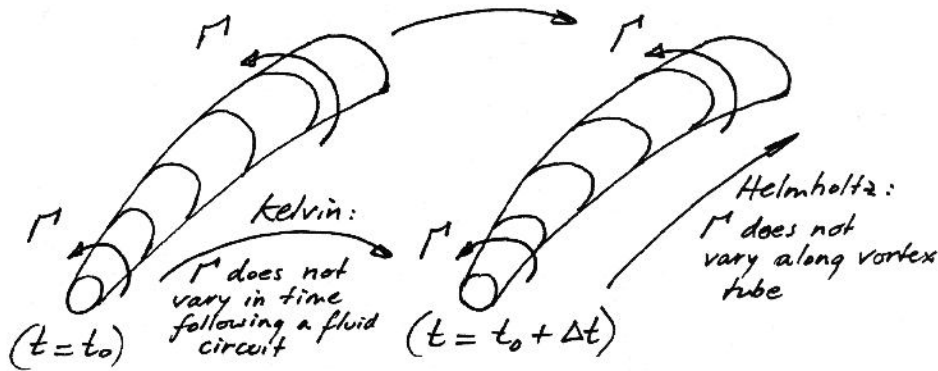
Figure 8.8: Illustrating the Kelvin and Helmholtz theorems.

gradients; another part gives the rate of change of vorticity due to stretching of vortex lines. This term is non-linear, since $\mathbf{\Omega}$ depends on $\mathbf{V}$.

For inviscid flows, we see that if the vorticity was initially zero then it will remain zero — so the vorticity of a fluid lump depends on its initial condition, and if it was zero initially it cannot gain vorticity ever. Also, for inviscid flows we have Kelvin's theorem, which says that the circulation around any closed material curve is invariant.

We can make the following observations from these two theorems:

1. Since the vorticity $\mathbf{\Omega} = \nabla \times \mathbf{V}$, this implies $\nabla \cdot \mathbf{\Omega} = 0$. Therefore, the vortex lines never end in a fluid. They either form closed loops or end at a boundary.

2. The circulation is the same for every contour enclosing the vortex line, that is, $D\Gamma/Dt = 0$.

3. If we have at some instant a flow without vorticity (such that the circulation around any contour is zero), then Kelvin's theorem states that at any future time the fluid must remain without vorticity. In particular, a fluid initially at rest has no vorticity, and must remain without vorticity.

4. Vortex tubes are in some sense permanent – a vortex tube specified at an initial instant by drawing the vortex-lines that intersect a given closed curve in the fluid has a continuing identity. We may say that in a barotropic, inviscid fluid a vortex-tube moves *with* the fluid and its strength remains constant (Batchelor p. 274).
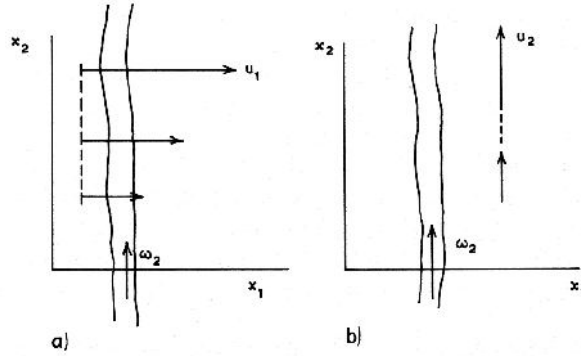
Figure 8.9: Effect of a velocity gradient on a vortex line. (a) Tilting: vorticity ω_2, velocity gradient $\partial u_1/\partial x_2$. (b) Stretching: vorticity ω_2, velocity gradient $\partial u_2/\partial x_2$. From Bradshaw, *Turbulence*, 1978.

8.4.1 Vortex tilting and stretching

(For the following see *Turbulence*, ed. P. Bradshaw, Springer-Verlag, 1978, p.9-10).

The vorticity/velocity-gradient interaction term $\mathbf{\Omega} \cdot \nabla \mathbf{V}$ can be written in tensor notation for the *i*th component as $\Omega_j \partial u_i / \partial x_j$.

1. A. When $i = j$, say $i = 1$; $j = 2$ (figure 8.9a). Here this term represents an exchange of vorticity between components because a velocity gradient $\partial u_1/\partial x_2$ tilts a vortex line which was originally in the x_2-direction so that it acquires a component in the x_1-direction.

2. B. When $i = j$, say $i = j = 2$ (figure 8.9b, the vortex line is stretched by the rate of tensile strain along the axis, without any change of direction of that axis. We have already seen that the circulation around a closed path enclosing a vortex filament is constant (incompressible flow) (equivalent to conserving angular momentum), and as the line is stretched its vorticity will increase.

8.5 Vortex Interactions

Vortex interactions play a very important role in many flow situations. For example, the generation of vortex trails behind aircraft, the formation of vortex sheets associated with lifting surfaces, the atmospheric phenomenon of tornadoes, vortex rings (for example, smoke rings) and the vortex shedding behind bluff bodies (for example, the von Kármán vortex street behind a cylinder) all involve vortex interaction. For example, the turbulent vortices behind an aircraft could disturb the flight of another aircraft moving into

the vortex system, and the stability and decay of the vortex system is particularly important. In the field of turbulence, the understanding of vortex interactions is crucial for the understanding of the kinematics and dynamics of turbulence.

Turbulent flows have many random or chaotic features. However, recent evidence has demonstrated the existence of organized motions in a wide variety of turbulent shear flows (mixing layers, boundary layers and wakes). These so called "coherent structures" are often modelled as interacting vortices. Turbulent flows have often been described as a complex collection of vortices entangled like spaghetti. The large dissipation of energy and the high rates of mass, momentum and energy diffusion in turbulent flows are due to the intense mixing and distortion of the interacting vortices. An example of such an interaction is seen in figures 5.19 and 5.27. It shows how two or three vortices in a mixing layer combine to form a larger scale structure. Notice that the vortices (while pairing) rotate about each other and amalgamate.

Therefore, it is easy to see why the study of vortex interaction is such an active field of research. Some of the more recent research in this area is illustrated in Van Dyke's Album of Fluid Motion. The study of vortex interactions is a very large field and we will restrict the discussion to the simplest flows, that is, inviscid, barotropic flows with conservative body forces. Under these conditions the vorticity field obeys Helmholtz's rules (see section 8.4).

The vorticity equation for an inviscid, incompressible fluid reduces to:

$$\frac{D\mathbf{\Omega}}{Dt} = \mathbf{\Omega} \cdot \nabla \mathbf{V},$$

where the term on the right-hand side is called the vorticity stretching vector. For two-dimensional flows, this equation reduces to:

$$\frac{D\mathbf{\Omega}}{Dt} = 0.$$

We will now consider a number of examples.

8.5.1   Velocity field induced by a vortex filament

By a vortex filament, we mean a vortex tube of concentrated vorticity such that, as its cross-sectional area A goes to zero, Ω goes to infinity to keep the product $\Omega A = \Gamma = $ constant. Therefore the integral of the velocity vector along a closed path containing the filament is Γ. The aim is to find the induced velocity field in the irrotational fluid surrounding the filament; we are interested in calculating u_r and u_θ. There are several methods of doing
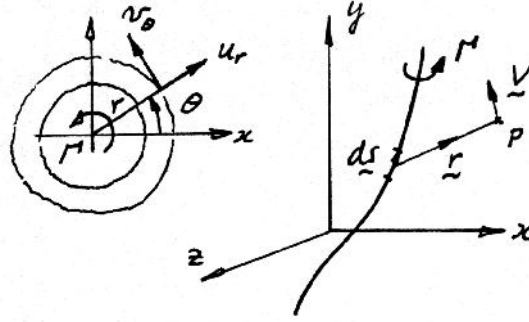
Figure 8.10: Notation for calculating the induced velocity field.

this. The most general method involves the use of the Biot-Savart law which can be expressed as (see section 8.3):

$$4\pi \mathbf{V} = \int \frac{\Gamma}{r^3} d\mathbf{s} \times \mathbf{r}.$$

 The integration is carried over the length of the vortex filament. The Biot-Savart law says that each element of the vortex filament contributes to the velocity induced at point P and the contribution is proportional to the inverse of (some) power of r. Therefore at any point P the induced velocity is largely determined by the elements nearest to P.

   For a filament aligned with the y-axis, the velocity at the point P in the x-z plane at a distance r from the origin is given by:

$$\mathbf{V} = u_\theta \mathbf{e}_\theta = \frac{\Gamma}{2\pi r} \mathbf{e}_\theta.$$

The induced velocity can also be found by using the complex potential function for a vortex filament. The complex potential in this case is

$$F(z) = \frac{-i\Gamma}{2\pi} \ln z$$
$$= \phi + i\psi$$

and

$$\mathbf{V} = \nabla \phi.$$

The velocity field is determined by differentiation of the velocity potential or stream function. Hence:

$$u_\theta = \frac{\Gamma}{2\pi r}$$

   So the velocity field for a vortex filament varies as l/r where r is the distance from the center of the vortex. Note that $u_\theta \to \infty$ at the center of
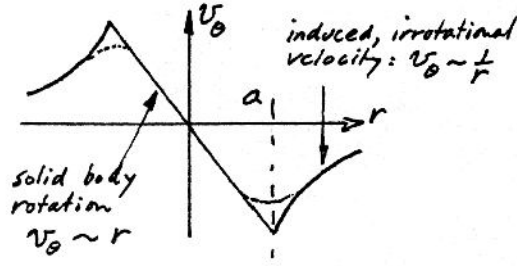
Figure 8.11: Rankine vortex velocity distribution.

the vortex: it is a singularity. In a real (viscous) fluid, viscosity damps out the velocity in the center of the vortex, leading to solid body rotation in the central region of the vortex. The pressure varies parabolically in this region and hyperbolically outside of this region.

8.5.2 The Rankine vortex

Consider the Rankine vortex — a solid body rotation in the core, surrounded by an irrotational field of the same circulation. In the core,

$$\frac{\partial p}{\partial r} = \frac{\rho u_\theta^2}{r}$$

so that

$$p - p_{min} = \frac{\rho u_\theta^2}{2}$$

and the kinetic energy per unit length

$$E = \pi \rho \int_0^a u_\theta^2 r \, dr$$

remains finite.

The vorticity is confined to the inner core, the energy is finite, and viscosity limits the energy in the irrotational flow from becoming infinite. Actual flows that approach this are the sink vortex, hurricane, cyclone, tornado.

This is our model for a line vortex. We can imagine any flow with vorticity to be made up of large numbers of infinitesimally slender vortices, or sometimes as vortex sheets which can be thought of as a layer of locally parallel vortex lines.

8.5.3 Filaments of opposite sign and equal strength

We can solve for the velocity field by considering a complex potential of the form:

$$F(z) = \frac{i\Gamma}{2\pi} \ln\left(\frac{z - c}{z + c}\right).$$
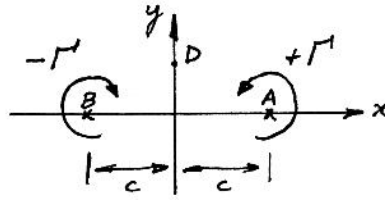
Figure 8.12: Two vortex filaments of opposite sign and equal strength.

But here we are more interested in vortex interactions. The vortex at A induces a velocity at point B in the y-direction and vice versa (figure 8.12). The magnitude of the velocity is

$$u_{induced} = \frac{\Gamma}{2\pi(2c)} = \frac{\Gamma}{4\pi c}.$$

Therefore both vortices move downwards at the speed $\Gamma/4\pi c$. The velocity of the fluid at the midpoint between the vortices equals the sum of induced velocities from each vortex:

$$u_{midpoint} = \frac{2\Gamma}{2\pi c} = \frac{\Gamma}{\pi c} = 4\left(\frac{\Gamma}{4\pi c}\right),$$

which is four times the velocity of the vortex pair, so there is a jet of fluid between the vortices.

Note the line of symmetry between the two vortices. Since this line is a streamline, the normal velocity in the x-direction at any point on the y-axis is zero. Therefore, $\mathbf{V} \cdot \mathbf{n} = 0$ on the y-axis, and this is the wall boundary condition for inviscid fluids. Thus the two vortex system above is equivalent to a single vortex next to a wall (figure 8.13). Therefore a vortex next to a wall will move parallel to the wall at the velocity. This fact is very useful because we can see now how to account for the effect of the wall in more complicated situations. This technique of replacing the wall with another vortex of the opposite sign is called the *Method of Images*.
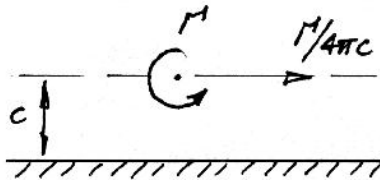
Figure 8.13: Single vortex moving along a wall, with image vortex in the wall.

If the strengths of the vortices are not equal in magnitude, then the motion is not in a straight line but in concentric circles. The center of rotation is
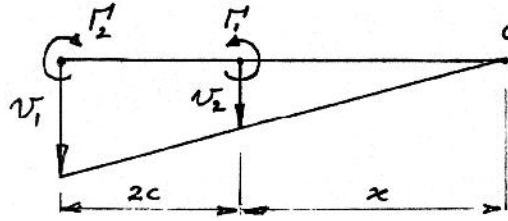
Figure 8.14: Two vortices of unequal strengths and opposite sign.

found as follows. In figure 8.14, u_1 and u_2 are the velocities induced by the vortices on each other and 0 is the center of rotation. Now,

$$u_1 = \frac{\Gamma_1}{4\pi c}, \quad u_2 = \frac{-\Gamma_2}{4\pi c} \quad (\Gamma_2 < 0).$$

Imposing the condition of irrotationality in the fluid surrounding the vortices (only solid body rotation is allowed), then by similar triangles:

$$\frac{u_2}{x} = \frac{u_1}{x + 2c}.$$

Substituting for u_1 and u_2 leads to:

$$\frac{-\Gamma_2}{x} = \frac{\Gamma_1}{x + 2c}.$$

That is,

$$x = \left(\frac{-\Gamma_2}{\Gamma_1 + \Gamma_2} \right) 2c.$$

When $\Gamma_1 + \Gamma_2 = 0$, $x = \infty$, and we get motion in a straight line.

8.5.4   Filaments of the same sign and strength

By using arguments similar to the previous case, we can show that the induced velocities are in opposite directions. Therefore it is obvious that the vortices will rotate about each other.

If the strengths of the vortices are not the same, then an analysis similar to that given earlier yields $x = [\Gamma_2/(\Gamma_1 + \Gamma_2)]2c$ and the motion is again in concentric circles (figure 8.15).

8.5.5   Filaments not parallel to each other

Until now, we have been considering filaments which were parallel to each other. We now consider two vortices, one along the x-axis and the other parallel to the z-axis at a distance y from the origin (figure 8.16). Let us
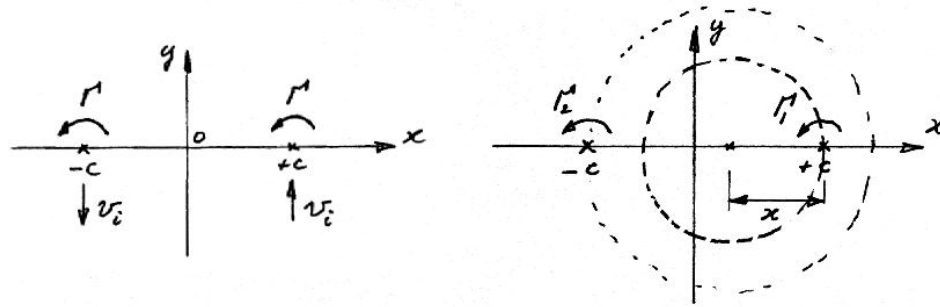
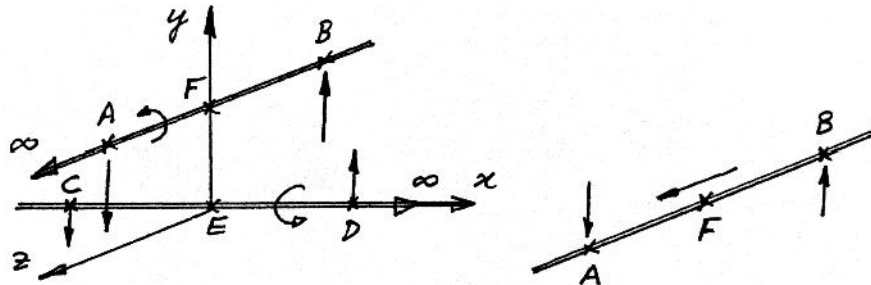Figure 8.15: Two vortices of the same sign and strength.

Figure 8.16: Two vortices not parallel to each other.

consider the induced velocities at some points on the two vortices. A vortex 1 induces a velocity in the downward direction $(-y)$. At B, it induces a velocity in the $+y$-direction. Similarly, the velocities induced by vortex 2 at points C and D are shown. At point E, there is a velocity in the $+x$-direction and at point F, the induced velocity is in the $+z$-direction. Therefore, on each filament there are points where the induced velocities are perpendicular to each other. This leads to the stretching of the filaments. As time goes on the distortions of the filaments (from straight lines) increase, leading to a mess which looks like spaghetti. In this process, it is clear from recent work (for example, by Orszag, Zabruski, and Hussain) that viscosity cannot be neglected: when the vortices come close enough the velocity gradients are high enough to make viscous forces become predominant. As a result, we have vortex "connection and reconnection" whereby, in the example given above, pieces of one vortex connect to a piece of the other vortex. This can only happen when viscous forces are important. See also the experiment by Lim & Nickels shown in figure 5.18.
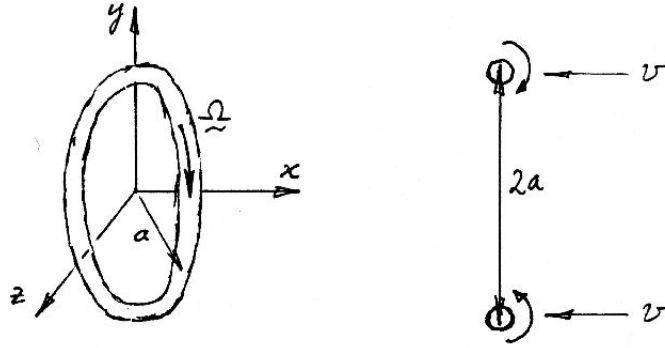
Figure 8.17: Vortex ring notation.

8.5.6   Vortex rings

Until now, we have considered only infinitely long straight filaments. Let us now consider a vortex ring where the vortex filament forms a loop.

(a) Self propulsion of the vortex ring

Consider a vortex ring of finite thickness 2c with radius a. (figure 8.17). The direction of r is shown also. It can be shown that the vortex ring propels itself forward ($-x$-direction in our case) with a velocity given by

$$u_{ring} = \frac{\Gamma}{4\pi a}\left[\ln\frac{8a}{c} - \frac{1}{4}\right].$$

Consider two points A and B diametrically opposite to each other. The vorticity at point A is directed into the page and this gives rise to an induced velocity at B as shown. Similarly, the velocity induced at A by the vorticity at B turns out to be in the same direction because $\mathbf{\Omega}$ at B is coming out of the page. Intuitively, this velocity should be proportional to $\Gamma/2\pi(2a)$ which is the multiplier in the above equation. The logarithmic term comes from integrating along the circle. Most importantly, the velocity is proportional to $1/a$.

(b) Interaction of two vortex rings

Consider two vortex rings of different sizes, moving on the same axis and having vorticity of the same sign (figure 8.18). The velocities induced at point A by the vorticity vector at C and vice versa are shown in the figure. The velocities induced on the bigger ring tend to enlarge its diameter, and therefore its velocity in the x-direction reduces. For the smaller vortex ring, its radius decreases and its velocity increases. It catches up with the bigger

ring and passes right through it. Now the roles are reversed and the "leap-frogging" repeats itself (see figure 8.19).

What if the two vortices are of opposite circulations? In this case, when the vortex rigns approach each other, each induces a radial outward velocity on the other, and they grow in size and slow down.

(c) Vortex ring near a wall

This system is equivalent to the one shown in figure 8.20. The velocities induced by the fictitious ring on the left tend to expand the ring. The vortex ring "sees" its image or reflection in the wall and behaves accordingly.

The mirror image principle also explains the "ground effect" — the extra lift an airplane experiences near the ground. An airfoil sees its mirror image and feels the induced velocity and pressure field from the reflection (figure 8.21). So the lift will be increased. The effect depends strongly on aspect ratio (see, for example, Ashley & Landahl p.218, Thwaites p.527). There are two basic mechanisms: (1) the image of the spanwise vortex induces an upwash on the front part of the physical wing, and a downwash over the rear — to counteract this, a vortex distribution is required, corresponding to a camber, which is such as to produce a force directed towards the ground; and (2) the images of the trailing vortices produce an upwash at the physical wing, thereby reducing the induced angle of incidence, which reduces the induced drag and increases the lift slightly.

8.6 Vorticity Diffusion

For two-dimensional, barotropic viscous flows the vorticity transport equation reduces to:

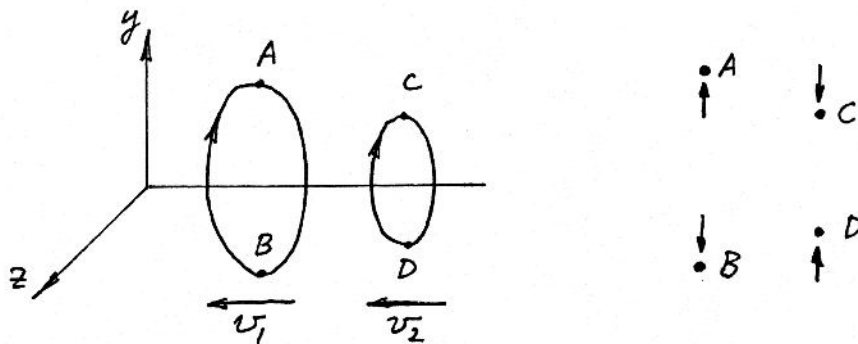$$\frac{D\mathbf{\Omega}}{Dt} = \nu \nabla^2 \mathbf{\Omega}. \tag{8.6}$$
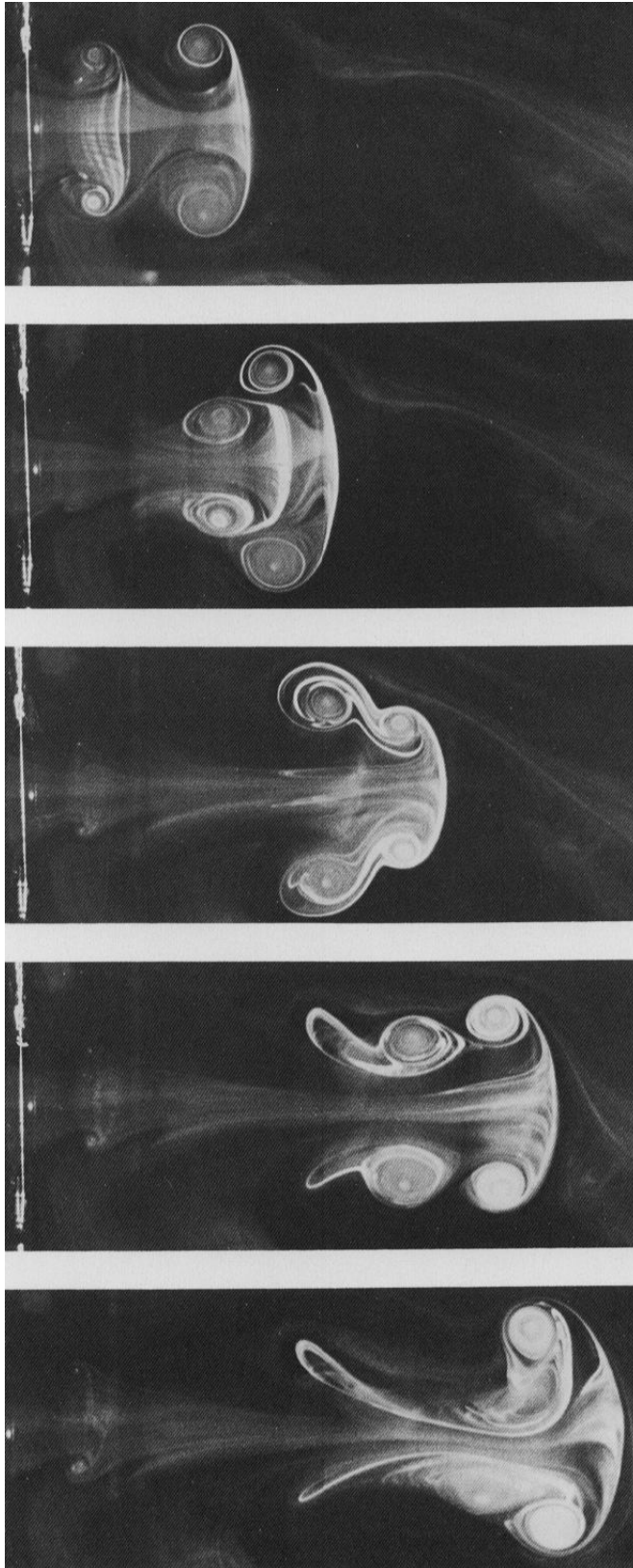

Figure 8.18: Vortex ring interaction.

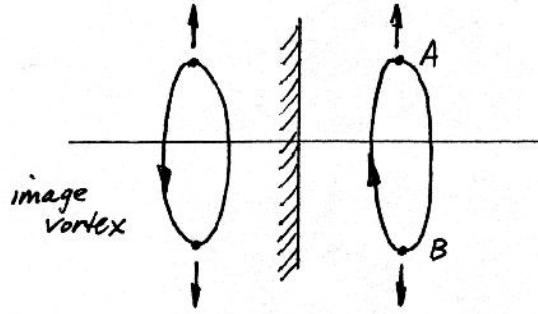Figure 8.19: Leapfrogging of two vortex rings. from Yamada & Matsui, 1978.

Figure 8.20: Vortex ring near a wall.

Now, the energy equation for constant property, low speed flow is given by:

$$\frac{DT}{Dt} = \alpha \nabla^2 T. \tag{8.7}$$

Note the similarity. In fact, both equations are diffusion equations and

$$\nu = \frac{\mu}{\rho} = \text{viscous diffusivity}$$

$$\alpha = \frac{k}{\rho C_p} = \text{thermal diffusivity}$$

In addition, if C represents the proportion of marked molecules in a fluid mixture (the concentration of one component of the mixture), then the concentration obeys a simple conservation law, where the concentration of a given fluid particle can only change by molecular transport across the surface, That is:

$$\frac{DC}{Dt} = \wp \nabla^2 C. \tag{8.8}$$

where $\wp$ is the mass diffusivity.

The ratio of these diffusivities give a measure of the relative diffusivity of vorticity, heat and mass:

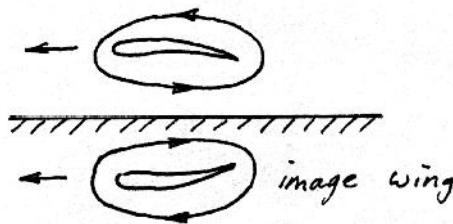$$\frac{\nu}{\alpha} = \frac{\mu C_p}{k} = Pr = \frac{\text{viscous diffusion rate}}{\text{thermal diffusion rate}}$$
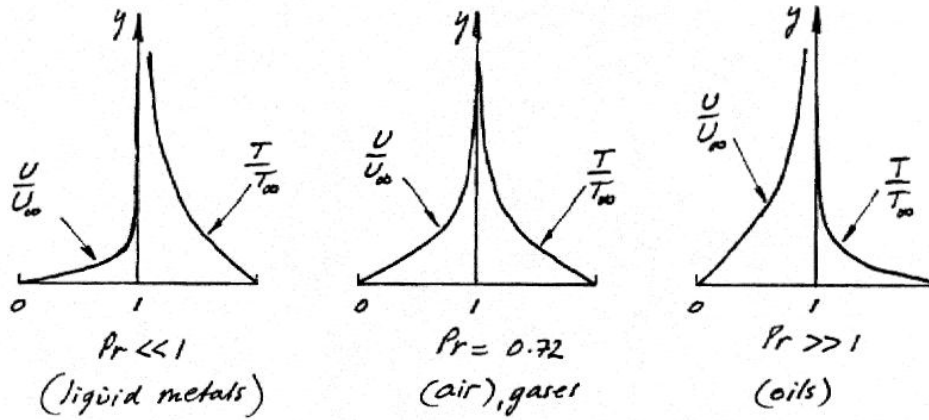

Figure 8.21: Ground effect due to image wing.

Figure 8.22: Relative diffusion of vorticity and temperature.

$$\frac{\nu}{\wp} \;=\; \frac{\mu}{\rho\wp} \;=\; Sc \;=\; \frac{\text{viscous diffusion rate}}{\text{mass diffusion rate}}$$

$$\frac{\wp}{\alpha} \;=\; \frac{\rho C_p \wp}{k} \;=\; Le \;=\; \frac{\text{mass diffusion rate}}{\text{thermal diffusion rate}}$$

Note: $Pr = ScLe$ and some typical value for the Prandtl number are 0.024 (mercury), 0.72 (air), 7.0 (water) and 3,500 (SAE 30 oil). Also, the Schmidt number is important for the interpretation of scalar fields: for most markers, such as smoke in air and dye in water, the Schmidt number is very large and the vorticity is diffused at a much higher rate than the marker is diffused (see recent work by Roshko, Rockwell, Dahm). In these cases, the extent of the marked fluid does not neccessarily coincide with the extent of the vorticity, even in turbulent flows where the dominant transport process of vorticity is by turbulent diffusion not viscous diffusion. Because of these considerations, there are considerable advantages to using temperature as a scalar marker in air flows.

For example, if we were to compare the temperature and velocity profiles in the Rayleigh problem, where a heated flat plate is suddenly accelerated from rest in a viscous fluid, we see that only for gases ($Pr \approx 1$) do the thermal and velocity profiles almost coincide (figure 8.22). .

8.6.1   Note on vorticity diffusion

Consider the Rayleigh problem, and evaluate the circulation around a fixed contour, of unit length in the x-direction (figure 8.23). . At $t = 0$, $\Gamma = -2U$/unit length. At $t > 0$, $\Gamma = -2U$/unit length. That is, the circulation has remained constant, despite the action of viscosity inside the contour. However, at $t \gg 0$, $\Gamma < -2U$/unit length because of viscous diffusion across

the contour, out of the control volume.

Of course, if the contour was large enough, then the circulation would always remain constant, although the vorticity distribution would be continually changing.

Another example is a bucket of radius R containing a viscous fluid, placed on a rotating turntable. If at $t < 0$, the fluid was moving with solid body rotation, then the circulation around any contour enclosing all the fluid would be $+2\pi R^2 \omega$. If at $t = 0$, the bucket was suddenly brought to rest, the no-slip condition at the wall would instantaneously cancel out this circulation. Within the bucket, the vorticity generated at the wall diffuses out with time until the vorticity everywhere is also zero.

Another example is the behavior of a line vortex being stretched in a viscous fluid.

8.7 The Pressure Field and Vorticity

So far we have not considered the pressure fluctuations in a turbulent field. We can obtain an equation for the instantaneous pressure (mean plus fluctuating) by taking the divergence of the Navier-Stokes equations. We obtain:

$$-\frac{1}{\rho}\nabla^2\left(\bar{p} + p'\right) = \frac{\partial^2 uv}{\partial x \partial y} + \frac{\partial^2 vw}{\partial y \partial z} + \frac{\partial^2 wu}{\partial z \partial x}$$

$$+ \frac{\partial^2 u^2}{\partial x^2}\frac{\partial^2 v^2}{\partial y^2} + \frac{\partial^2 w^2}{\partial z^2} \qquad (8.9)$$

where u, v and w are the instantaneous velocities. Note that the viscous stresses do not constribute to the pressure field — it is completely specified by the instantaneous velocity field. Equation 8.9 is in the form of a Poisson's equation $\nabla^2 p = f$, so that there exists a solution:

$$\bar{p} + p' = \frac{\rho}{4\pi}\int \frac{f(x')}{|\mathbf{x} - \mathbf{x}'|}\,dx'dy'dz',$$
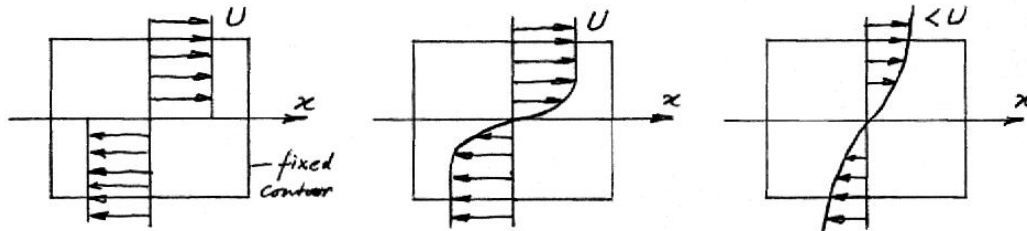

Figure 8.23: Vorticity diffusion as a function of time. (a) $t = 0$; (a) $t > 0$; (a) $t \gg 0$.

where

$$|\mathbf{x} - \mathbf{x}'|^2 = (x - x')^2 + (y - y')^2 + (z - z')^2$$

(x' is the position at which the pressure is to be found). That is

$$\bar{p} + p' = \frac{\rho}{4\pi} \int \frac{\partial^2 u_i u_j / \partial x_i \partial x_j}{|\mathbf{x} - \mathbf{x}'|} \, dx' dy' dz'. \qquad (8.10)$$

So the pressure is not local but it is given by the integral over the entire velocity field.

Note that it may be shown (exercise) that

$$p(\mathbf{x}') = \frac{\rho}{4\pi} \int \left[2 \frac{\partial \bar{u}_i}{\partial x_j} \frac{\partial u_j}{\partial x_i} + \frac{\partial^2}{\partial x_i \partial x_j} \left(u_i u_j - \overline{u_i u_j} \right) \right] \frac{dx' dy' dz'}{|\mathbf{x} - \mathbf{x}'|}.$$

Term I on the right hand side represents the contribution to p' due to the interaction between mean velocity gradients and turbulent velocity gradients; and Term II represents the contribution to p' due to fluctuations of the Reynolds stresses about their mean value (generally smaller than the contribution due to Term I).

8.8 Splat and Spin

We can rewrite equation 8.9 (for incompressible flow) as:

$$-\frac{1}{\rho} \frac{\partial^2 p}{\partial x_i^2} = \frac{\partial^2 u_i u_j}{\partial x_i \partial x_j} \qquad (8.11)$$

$$= \frac{\partial}{\partial x_j} \left(u_j \frac{\partial u_i}{\partial x_i} + u_i \frac{\partial u_j}{\partial x_i} \right)$$

$$= \frac{\partial u_i}{\partial x_j} \frac{\partial u_j}{\partial x_i} + u_i \frac{\partial}{\partial x_i} \left(\frac{\partial u_i}{\partial x_j} \right)$$

Hence

$$-\frac{1}{\rho} \frac{\partial^2 p}{\partial x_i^2} = \frac{\partial u_i}{\partial x_j} \frac{\partial u_j}{\partial x_i}. \qquad (8.12)$$

Now we have

$$S_{ij} == \frac{1}{2} \left(\frac{\partial u_i}{\partial x_j} + \frac{\partial u_j}{\partial x_i} \right),$$

and

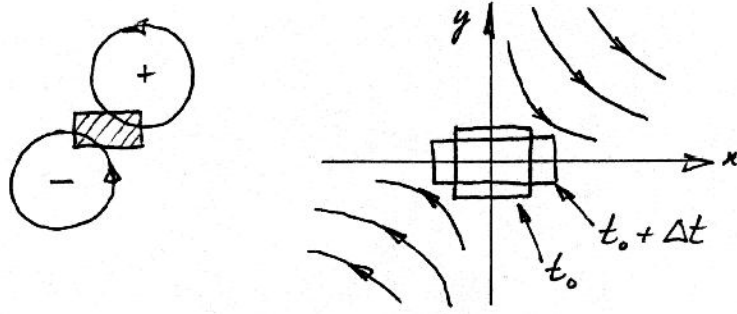$$\xi_{ij} == \frac{1}{2} \left(\frac{\partial u_i}{\partial x_j} - \frac{\partial u_j}{\partial x_i} \right),$$

Figure 8.24: A straining field formed by the collision of two vortices.

where S_{ij} and ξ_{ij} are the *rate-of-strain* tensor (symmetric) and the *rate-of-rotation* tensor (anti-symmetric), respectively, so that

$$\frac{\partial u_i}{\partial x_j} = S_{ij} + \xi_{ij}.$$

Hence,

$$-\frac{1}{\rho}\frac{\partial^2 p}{\partial x_i^2} = \left(S_{ij} + \xi_{ij}\right)\left(S_{ij} - \xi_{ij}\right)$$

$$= S_{ij}S_{ij} - \xi_{ij}\xi_{ij}$$

Now $S_{ij}S_{ij} = S^2 =$ sum of the squares of the principal strains, and $\xi_{ij}\xi_{ij} = \frac{1}{2}\Omega_i^2$, where Ω_i is the ith component of the vorticity vector.

[Note: $\xi_{ij} = \frac{1}{2}\epsilon_{ijk}\Omega_k$, where

$$\begin{aligned}
\epsilon_{ijk} &= 1 && \text{(cyclic } ijk) \\
\epsilon_{ijk} &= -1 && \text{(anti-cyclic } ijk) \\
\epsilon_{ijk} &= 0 && \text{(otherwise)}
\end{aligned}$$

and $\epsilon_{ijk}\epsilon_{ijm} = 2\delta_{km}$, so this result follows]

Hence

$$-\frac{1}{\rho}\frac{\partial^2 p}{\partial x_i^2} = S^2 - \frac{1}{2}\Omega_i^2 \tag{8.13}$$

where the first term on the right is called *splat*, and the second term is called *spin*.

But so what? Here we follow Bradshaw & Koh, Phys. Fluids **24**, 777, 1981. Consider a straining field caused by the collision of two vortices (figure 8.24). A small fluid element in the region of the collision will be compressed in the y-direction and elongated in the x-direction. The rotation will be small.
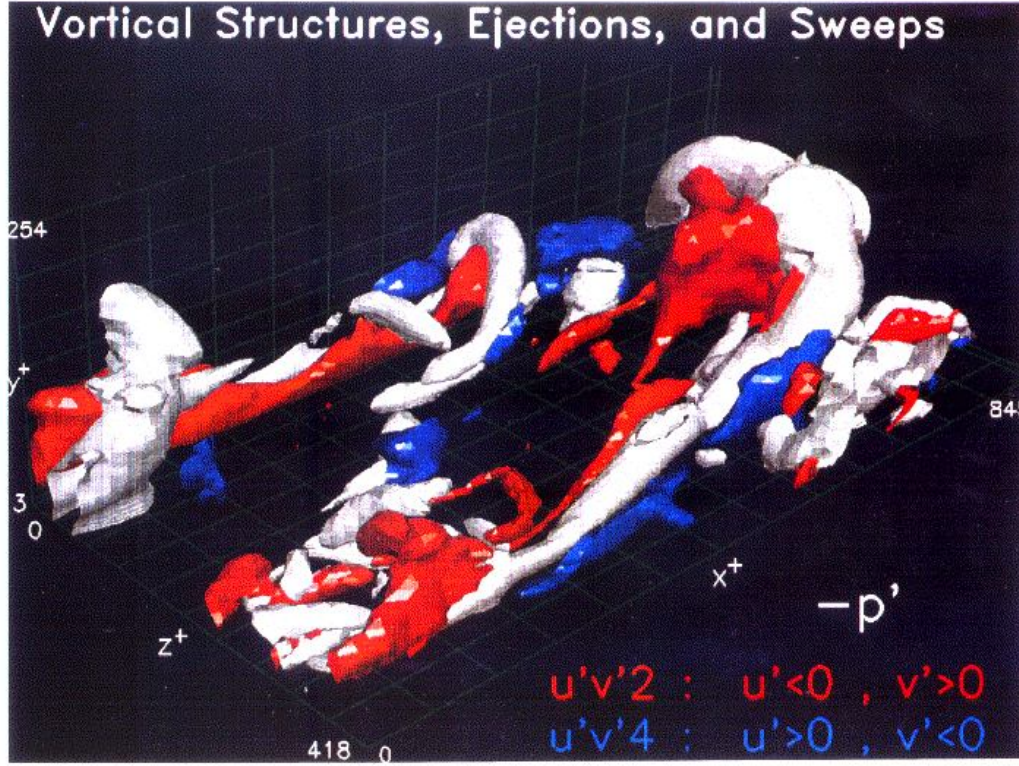
Figure 8.25: Visualization by Robinson of Spalart's simulations of a low Reynolds number turbulent wall layer ($Re_\theta \approx 640$). Here the pressure minima seem to mark the vortical motions well.

From Poisson's equation, $S^2 \approx 0$, which implies that $\partial^2 p / \partial x_i^2 < 0$. That is, the pressure is a maximum.

Next, consider a fluid element embedded in a vortex. In this case the vorticity term dominates

$$\left(\frac{\partial u_i}{\partial x_j} \approx -\frac{\partial u_i}{\partial x_i} \quad \text{and} \quad S_{ij} \approx 0, \quad \text{while} \quad \xi_{ij} \neq 0 \right)$$

and $\partial^2 p / \partial x_i^2 > 0$, implying that a pressure minimum will occur in the core of a vortex (which is fairly obvious from previous considerations). Bradshaw & Koh referred to these components as "splat" and "spin" (see equation 8.13). This provides a simple physical explanation of turbulent pressure fluctuations: high and low pressures are caused by the collision of eddies and the passage of eddies, respectively. This helps the interpretation of the pressure field, and it also helps the interpretation of DNS results (for example, see figure 8.25). .

Note that, despite this talk of vorticity, it is the pressure gradients that drive the flow. Pressure fluctuations can be viewed as the signatures of

fluid motion, but it is important to remember that the motions come about because of pressure gradients.

Chapter 9

Statistical Description of Turbulence

So far we have made extensive use of Reynolds averaging to describe turbulent flow behavior, especially in terms of the Reynolds-averaged equations of motion. Here we introduce other measures, including higher order moments, space-time correlations, spectra and wavelets. Parts of this presentation follows Tennekes & Lumley, Chapters 6 and 8.

In this chapter, we will denote the instantaneous values of the velocity components by capital letters (U, V, and W), time-averaged values by over-bars ($\bar{U}$, $\bar{V}$, and $\bar{W}$), and lower case letters for fluctuating velocities (u, v, and w). For the pressure p, the time-average value is $\bar{p}$, and the fluctuating value is p'. A capital P indicates a probability.

9.1 Probability Density

We will consider only statistically steady functions (stationary) — these have mean values which are not a function of time.

If we collect the contribution to $U(t)$ in the range from U_1 to $U_1 + \Delta U$ (see figure 9.1, over a long time T, then $P(U)$ is the probability density where

$$P(U)\,\Delta U = \lim_{T\to\infty} \frac{1}{T}\Sigma\,(\Delta t) = \Delta F(U)$$

where $F(U) = P(V < U)$, and Δt is the amount of time spent in the interval ΔU. The probability of finding $U(t)$ between U_1 and $U_1 + \Delta U$ is equal to the proportion of time spent there. Also:

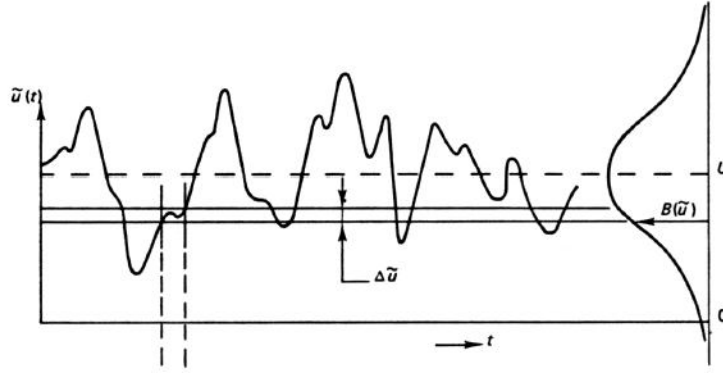$$P(U) \geq 0, \quad \text{and} \quad \int_{-\infty}^{\infty} P(U)\,dU = 1$$

Figure 9.1: A random signal and its probability density function. From Tennekes & Lumley, 1972.

Note that we can write:

$$\bar{f} = \lim_{T \to \infty} \frac{1}{T} \int_{t_0}^{t_0+T} f(U)\, dt$$

which is the definition of a mean. So:

$$\bar{f} = \int_{-\infty}^{\infty} f(U)\, P(U)\, dU,$$

and therefore

$$\overline{U} = \int_{-\infty}^{\infty} U\, P(U)\, dU.$$

If we now consider the fluctuations away from the mean, we obtain the variance (the mean square departure from the mean):

$$\overline{u^2} = \int_{-\infty}^{\infty} u^2\, P(U)\, dU = \int_{-\infty}^{\infty} u^2\, P(u)\, du$$

where $\sigma = \sqrt{\overline{u^2}}$ is the standard deviation (or intensity).

Now the value of $\overline{u^2}$ does not reflect the symmetry or anti-symmetry of the u distribution. However, the third moment $\overline{u^3}$ depends only on the lack of symmetry in $P(u)$:

$$\overline{u^3} = \int_{-\infty}^{\infty} u^3\, P(u)\, du.$$

For a symmetric distribution, $\overline{u^3} = 0$ (see figure 9.2).

The skewness S is defined by:

$$S = \frac{\overline{u^3}}{\sigma^3} = \frac{\overline{u^3}}{(\sqrt{\overline{u^2}})^3}.$$
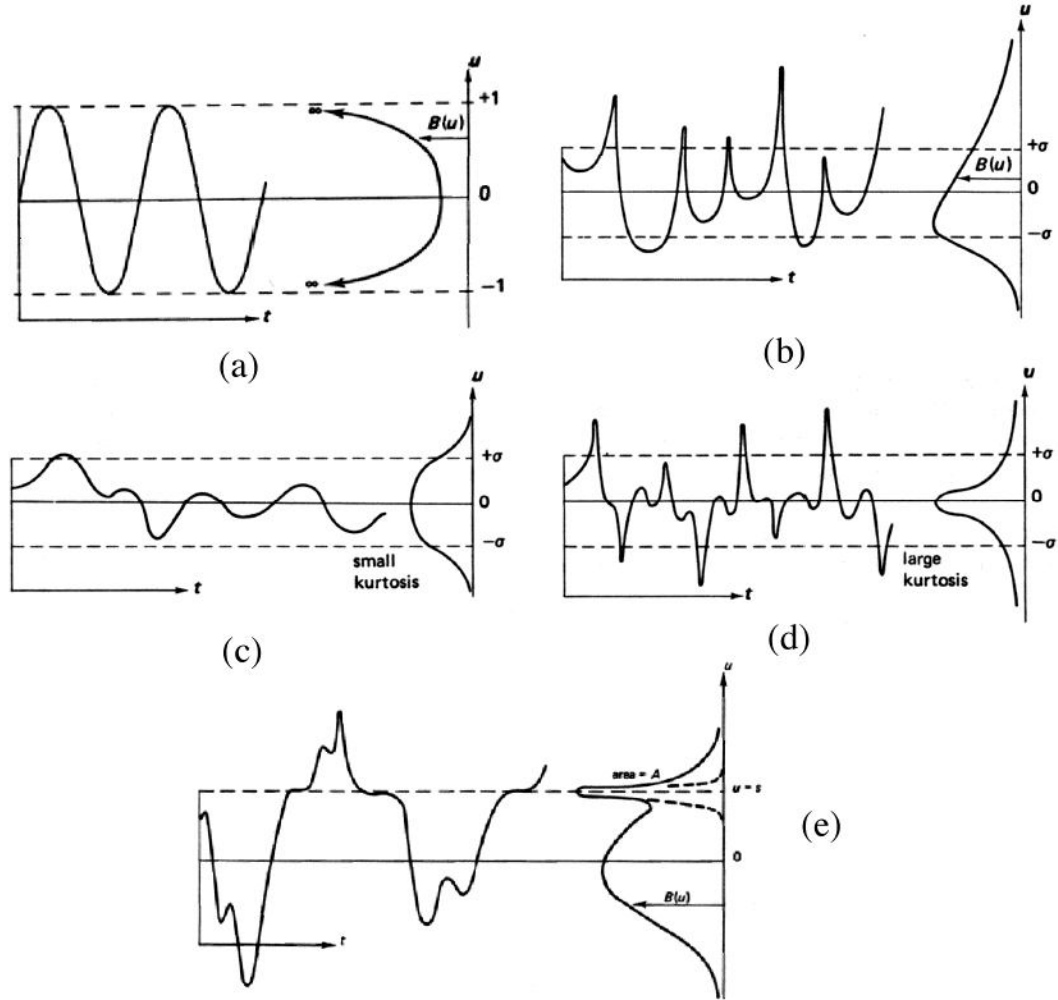
Figure 9.2: (a) Probability density distribution of a sine wave; (b) A function with positive skewness (3rd moment); (c) A function with small kurtosis (4th moment); (d) A function with large kurtosis; (e) bimodal probability density distribution indicating intermittent behavior. From Tennekes & Lumley, 1972.

The fourth-order moment is called the kurtosis K:

$$K = \frac{\overline{u^4}}{\sigma^4} = \frac{1}{\sigma^4} \int_{-\infty}^{\infty} u^4 P(u)\, du.$$

Some representative probability density distributions for boundary layers are shown in figures 9.3 and 9.4, and some representative distributions of skewness and kurtosis in a subsonic turbulent boundary layer are shown in figure 9.5. Bimodal distributions indicate that the signal is intermittent, that is, it is flipping between two preferred states. This is seen near the edge
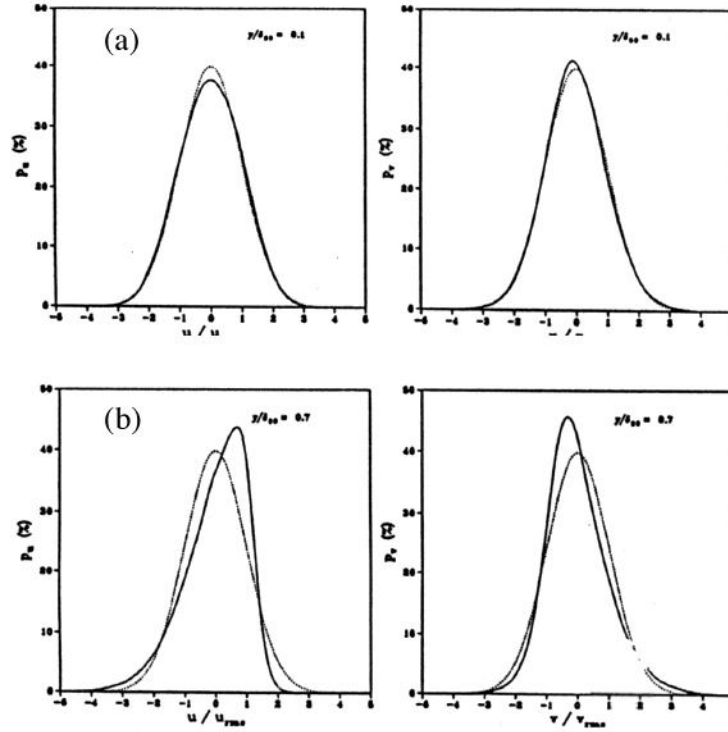
Figure 9.3: (a) Probability density distributions of u' and v' at $y/\delta = 0.1$ in an incompressible boundary layer (Alving, 1988); (b) As in (a) but at $y/\delta = 0.7$.

of a shear layer where the flow is intermittently turbulent. In the example given below, the relatively sharp peak would correspond to the free stream (the finite width of the peak is due to the irrotational fluctuations induced by the turbulent field), and the broad peak would correspond to the turbulence within the layer.

9.2   Joint Probability Density

Consider two variables, $u(t)$ and $v(t)$. Then $P(u,v)$, the joint probability density, is proportional to the fraction of time that the signals spend in a window defined by u and $u + \Delta u$, and v and $v + \Delta v$. As before:

$$P(u,v) \; \geq \; 0$$

$$\iint P(u,v)\,du dv \; = \; 1.$$
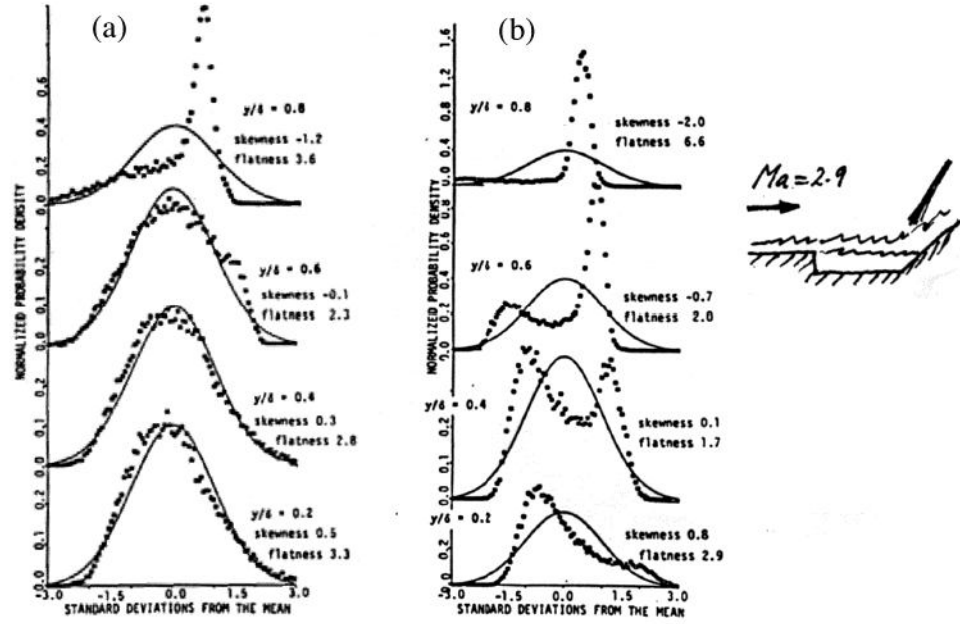
Note

$$\int P(u,v)\,dv \; = \; P(u)$$

Figure 9.4: (a) Probability density distributions of $(\rho u)'$ in a Mach 2.9 undisturbed boundary layer (Hayakawa & Smits, 1983); (b) As in (a) but downstream of reattachment.

$$\int P(u, v)\, du \;=\; P(v).$$

The most important moment is

$$\overline{uv} \;=\; \iint_{-\infty}^{\infty} uv\, P(u, v)\, du dv.$$

This is called the "covariance" or the correlation between u and v (see figure 9.6). It is a measure of the asymmetry of $P(u, v)$. If $P(-u, v) = P(u, v)$, then $-\overline{uv} = 0$ (see figure 9.7). In boundary layers $-\overline{uv} > 0$.

Some representative covariances for $-\overline{uv}$ are shown in figure 9.8.

9.3   Correlation Coefficients

To get an estimate of the length scales of the fluctuating motion we study the correlation between the same fluctuating quantity measured at two different points in space (and time). In general

$$R\,(\mathbf{x}, \mathbf{r}) = \frac{\overline{\mathbf{u}(\mathbf{x}, t)\mathbf{u}(\mathbf{x} + \mathbf{r}, t + \tau)}}{\sqrt{\mathbf{u}(\mathbf{x}, t)^2}\,\sqrt{\mathbf{u}(\mathbf{x} + \mathbf{r}, t + \tau)^2}}.$$
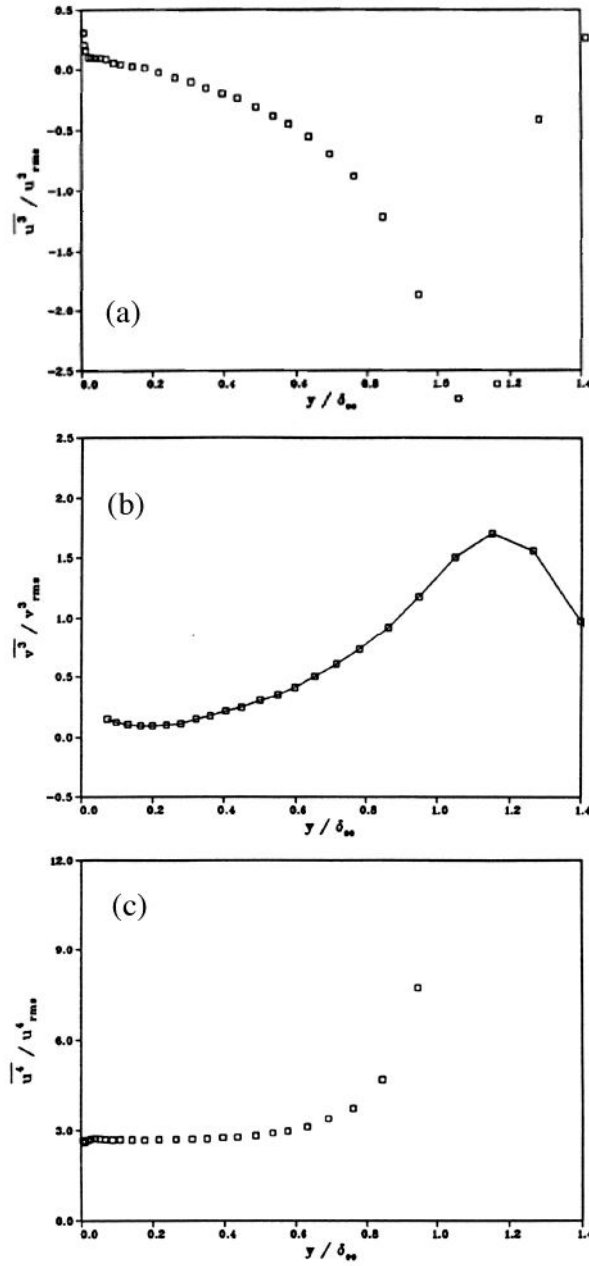
Figure 9.5: Skewness and kurtosis in a subsonic turbulent boundary layer. (a) Skewness of *u*; (b) Skewness of *v*; (c) Kurtosis of *u*. From Alving, 1988.

9.3.1   Space correlations: $\mathbf{r} \neq 0$, $\tau = 0$

Attention is usually given to correlations of the same component of velocity at points separated in a direction either parallel to or perpendicular to it (see figure 9.9). These are called the longitudinal *and* lateral correlations, respectively. Correlations will depend on the magnitude and direction of **r**.
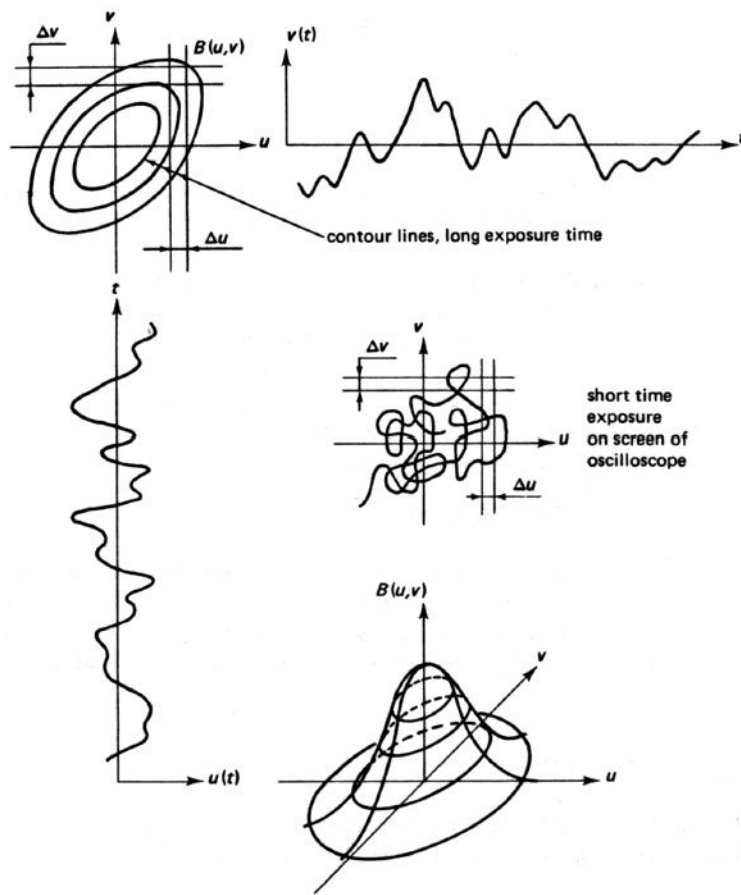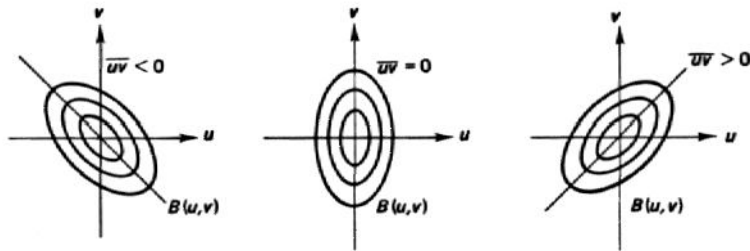
Figure 9.6: Covariance of u and v. From Tennekes & Lumley, 1972.

Figure 9.7: Functions with negative and positive covariances. From Tennekes & Lumley, 1972.

Different behaviors with different directions may provide information about the structure of turbulence. With $r = |\mathbf{r}| = 0$, and $\mathbf{u_1}$ parallel to $\mathbf{u_2}$, then $R = 1$. At large enough $\mathbf{r}$, $\mathbf{u_1}$ and $\mathbf{u_2}$ become independent so that $R \to 0$.

Townsend postulated some eddy forms (set up so that they satisfied
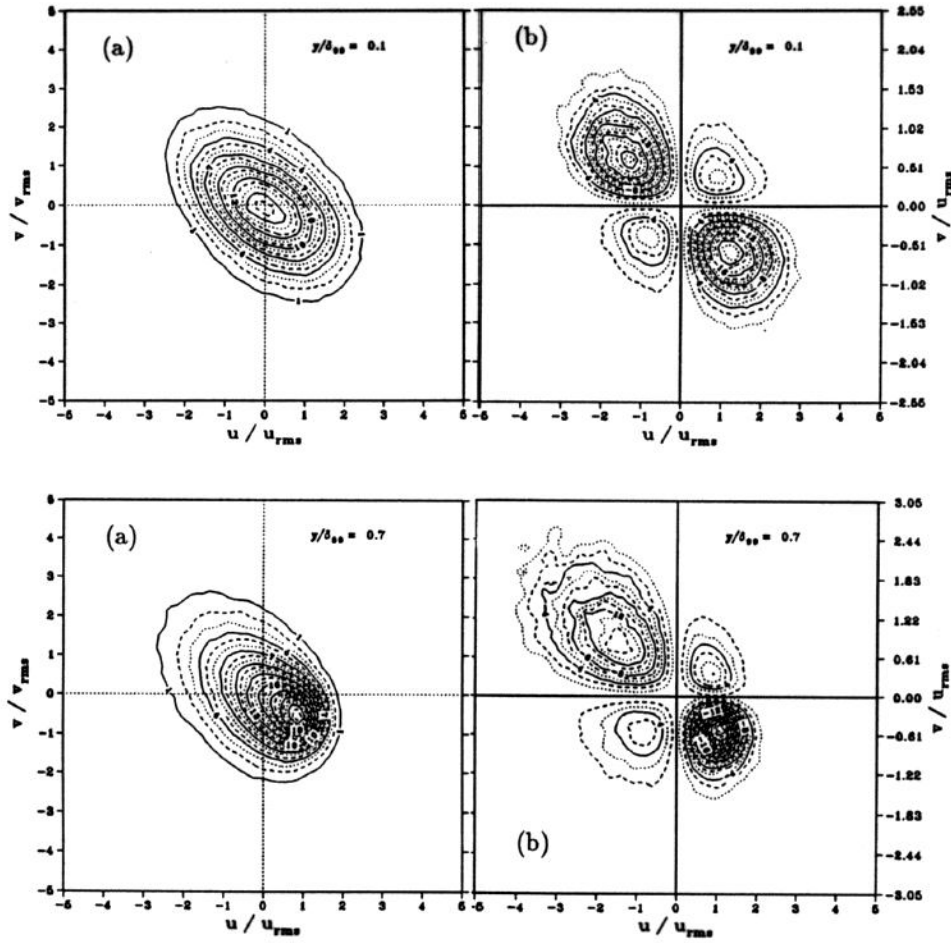
Figure 9.8: Contours in (u, v) space: (a) pdf; (b) contributions to $-\overline{uv}$. Top: $y/\delta =$ 0.1; Bottom : $y/\delta = 0.7$. From Alving *et al.*. 1989.
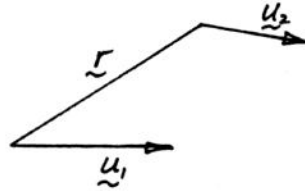

Figure 9.9: Velocities at two points separated by a distance **r**.

continuity) and examined how the correlation function might give some information regarding the shape of these eddies (shown in figure 9.10). The notation that is often used is best illustrated by an example. For instance, $R_{11}(r_2, 0, 0)$ is the space correlation in the y-direction of the u-component of velocity, and $R_{22}(r_1, 0, 0)$ is the space correlation in the x-direction of the
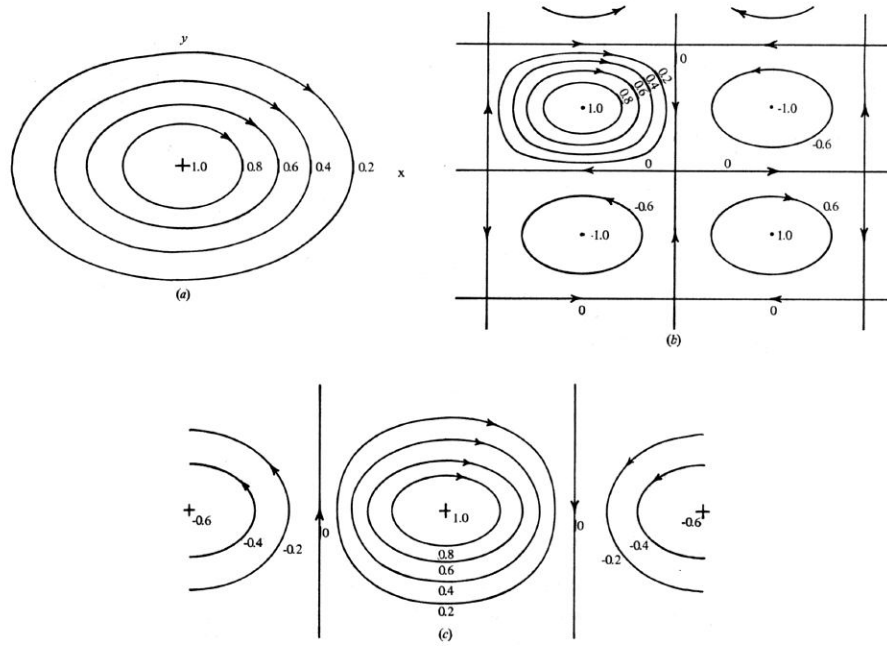
Figure 9.10: Simple eddy structures. (a) Isolated eddy; (b) Periodic array of eddies; (c) Finite row of simple eddies. From Townsend, 1976.

v-component of velocity. For Townsend's examples, consider R_{11}:

(a) For simple eddies, R_{11} decreases rapidly with r;

(b) For periodic eddies, R_{11} is also periodic; and

(c) For an array of eddies in line, R_{11} is periodic along the line but falls off rapidly in the normal direction.

However, if the wave number of these eddies varies around some mean then one loses correlation. That is, the periodicity of R_{11} becomes difficult to detect and it takes lower values — this is often described as "jitter" (see figure 9.11).

A negative region (curve B in figure 9.11b) implies u_1 and u_2 tend to be in opposite directions, which is commonly found in lateral correlations. Longitudinal correlations tend to be more like curve A.

The correlation curve indicates the distance over which the motion at one point affects the other. This suggests a (Eulerian) length scale based on the area of the curve called the integral scale L_E:

$$L_E = \int_0^\infty R(r)\, dr \qquad (9.1)$$

Another length scale that can be defined in terms of the space-correlation is
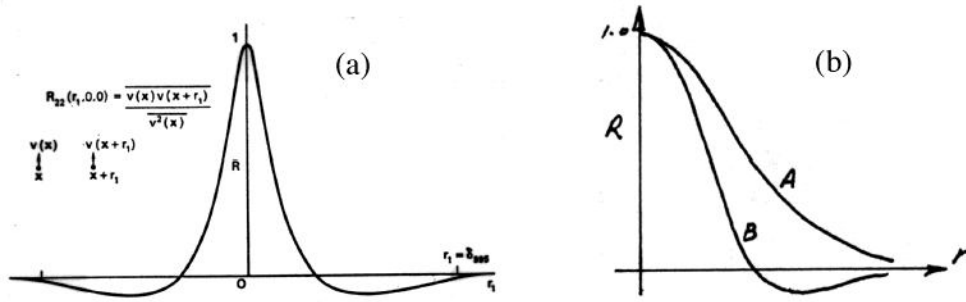
Figure 9.11: Examples of auto correlations: (a) Typical $R_{22}(r_1, 0, 0)$ correlation in a boundary layer at about $y/\delta = 0.5$ (Bradshaw, 1970); (b) Other possible forms.

the microscale λ_E, where:

$$\frac{1}{\lambda_E^2} = -\frac{1}{2} \frac{\partial^2 R}{\partial r^2}\bigg|_{r=0} \tag{9.2}$$

In figures 9.12 and 9.13 some examples are given of space correlations of the density fluctuations in a supersonic turbulent boundary layer (freestream Mach number of 2.9). Two side views are shown, as well as two plan views. The images were obtained by M.W. Smith using Rayleigh scattering to make the two-dimensional instantaneous density field visible.

9.3.2   Autocorrelations: r = 0, τ ≠ 0

An autocorrelation is the correlation of the same velocity component at a single point but at different instants in time. Such a correlation depends on τ in a similar way the space-correlation depends on **r**. Note that for a stationary flow

$$R(\tau) = \frac{\overline{u(t)u(t + \tau)}}{\overline{u^2}}.$$

We can define a typical time scale of the turbulence Λ_L:

$$\Lambda_L = \int_0^\infty R(\tau)\, d\tau \tag{9.3}$$

which is called the integral time scale (or Lagrangian integral scale).[1]

When a turbulent motion is being transported in a flow with a relatively large mean velocity it is possible that the turbulence is advected past the

[1] Lagrangian refers to moving points or following fluid elements; Eulerian refers to fixed points.
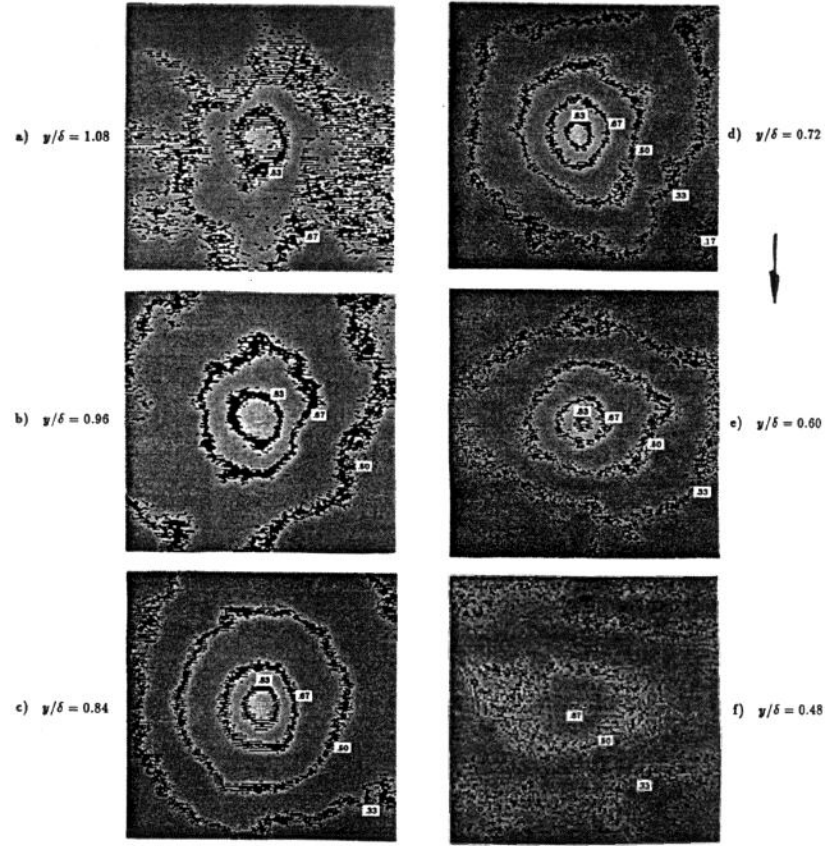
Figure 9.12: Space correlations of density fluctuations derived from Rayleigh scattering images taken in planes parallel to the wall at Mach 2.5. From Smith & Smits, 1996.

point of observation more rapidly than the pattern of fluctuation is changing (figure 9.14). An autocorrelation will then be related to the corresponding space correlation with a separation in the mean flow direction given by $r = \tau \bar{U}$, that is, $u(\tau)$ may be identified with $u(r/\bar{U})$. Effectively this assumes that the turbulence is "frozen:" this is valid only if $u/\bar{U} \ll 1$. This is known as Taylor's Hypothesis.

Another time scale defined in terms of the auto-correlation is the (Lagrangian) micro time-scale λ_L, where:

$$\frac{1}{\lambda_L^2} = -\frac{1}{2} \frac{\partial^2 R}{\partial \tau^2}\bigg|_{\tau=0}. \tag{9.4}$$

That is, λ_L is defined in terms of an osculating parabola fitted to the autocorrelation near zero time delay (figure 9.15). Since the autocorrelation is even,
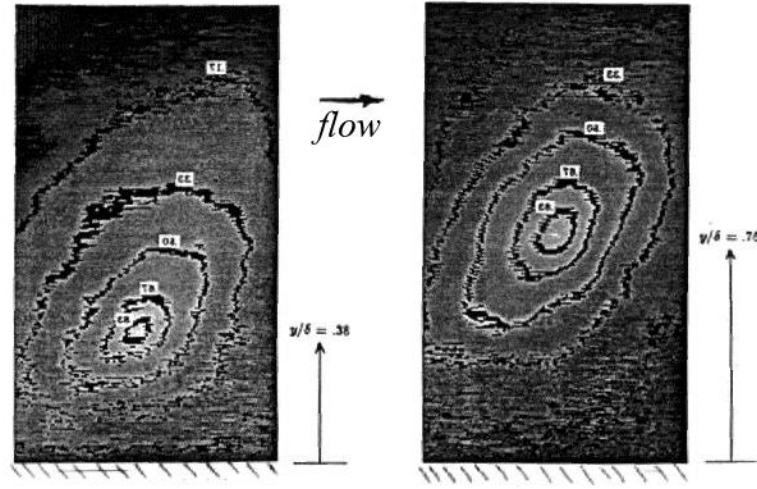
Figure 9.13: As in figure 9.12, but plane is in streamwise direction (flow is from right to left).
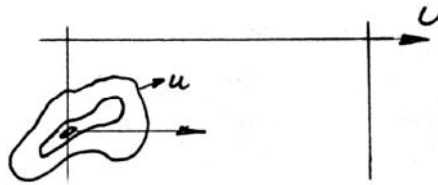
Figure 9.14: Turbulent motion (eddy) convected past the point of observation.

$\partial^2 R/\partial\tau^2\big|_{\tau=0} = 0$, and expanding the correlation in a Taylor series:

$$R = 1 - \frac{1}{2}\frac{\tau^2}{\lambda_L^2} + O(\tau^4) + \dots \quad \text{as} \quad \tau \to 0.$$

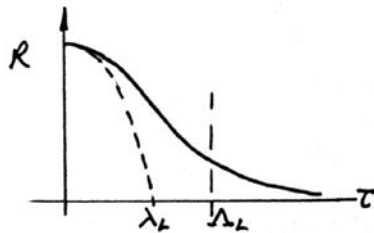In practice, the micro time-scale is not that different from the integral

Figure 9.15: The Lagrangian macro (Λ_L) and micro (λ_L) time scales.
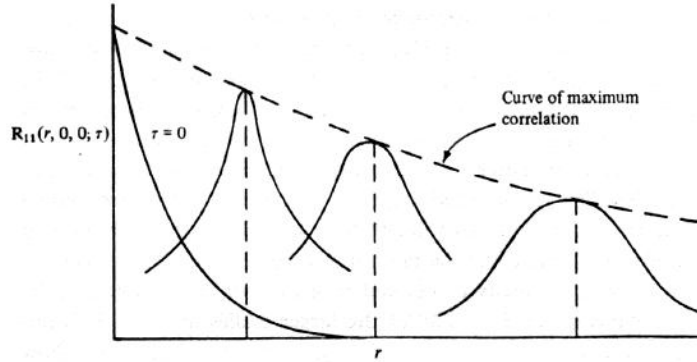
Figure 9.16: Variation of the longitudinal space-time correlation with increasing time delay τ. Measured with two probes separated in the streamwise direction. From Tennekes & Lumley.

time-scale (or Lagrangian integral scale) Λ_L. Also, λ_L is difficult to measure because its value depends critically on the accuracy of the measurements for short time delay.

Because $u(t)$ is stationary, we can write

$$0 = \frac{d^2 \overline{u^2}}{dt^2} = 2\,\overline{u\frac{d^2u}{dt^2}} + 2\overline{\left(\frac{du}{dt}\right)^2}$$

and so we have:

$$\overline{\left(\frac{du}{dt}\right)^2} = 2\frac{\overline{u^2}}{\lambda_L^2} \tag{9.5}$$

9.3.3 Space-time correlations

These correlations are taken at different positions and different instants, and they can be useful for indicating the evolution of certain features, such as the coherence length of an "average large-scale motion." Figure 9.16 illustrates how the space-time correlation changes with increasing time delay τ. Figure 9.18 shows the connection with an "equivalent" space correlation using Taylor's hypothesis.

Another example is given in figure 9.18. Here two hot wires were used to measure the space-time correlation curves for the streamwise component of the velocity and a separation in the streamwise direction (that is, R_{11}). The individual correlation curves are shown, as well as a curve drawn to connect the maxima. This curve gives some measure of the rate at which the large scale motions change their character. Note that the curve decays much more quickly in a subsonic boundary layer than it does in the supersonic case.
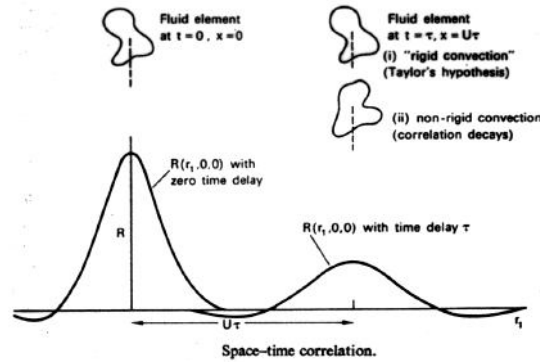
Figure 9.17: Correlation measurements showing the decay of maximum correlation level with increasing time delay τ.

Figure 9.19 shows some examples of space time correlations for the streamwise component of velocity in turbulent boundary layers (taken from Kovasznay *et al.* 1970). Here, the correlation was measured in a three perpendicular planes. The contour maps show the maximum value of the correlation at any point in these three planes, and they give some measure of the shape of an "average large- scale motion, although their interpretation is subject to the rate at which the structures evolve: if the structures develop rapidly, such contour maps can lead to erroneous conclusions.

In figure 9.20, some comparisons are made for a subsonic and a supersonic turbulent boundary layer. Here, two probes were used to measure the spanwise space correlation, and Taylor's hypothesis was used to convert the autocorrelation into a streamwise space correlation. The maximum values of the correlations were then used to produce the contour maps. Note that the spanwise dimension of the contour maps is nearly constant throughout the layer, and it is about the same in a subsonic and a supersonic flow. The streamwise extent is very much larger, and it depends strongly on the distance from the wall, and on the Mach number (Reynolds number also turns out to be important).

One particular space-time correlation of interest is the correlation for optimum time delay, R_0. Consider the experiment shown in figure 9.21. Here, two hot wires were used to measure the streamwise velocity fluctuations in a boundary layer as a function of time at two distances from the wall, that is, R_{12}, for a separation ζ. An example of the correlation as a function of time delay is shown. The time delay to the peak in the correlation τ_{max} may be used to define a "structure angle" θ, if the convection velocity of the large-scale motion is known. Some typical results for θ are shown in Figure 9.22 for subsonic and supersonic boundary layers. The result depends on wire spacing when that is small, but for large spacing the results appear to collapse onto a single curve. The angles are small near the wall, increase
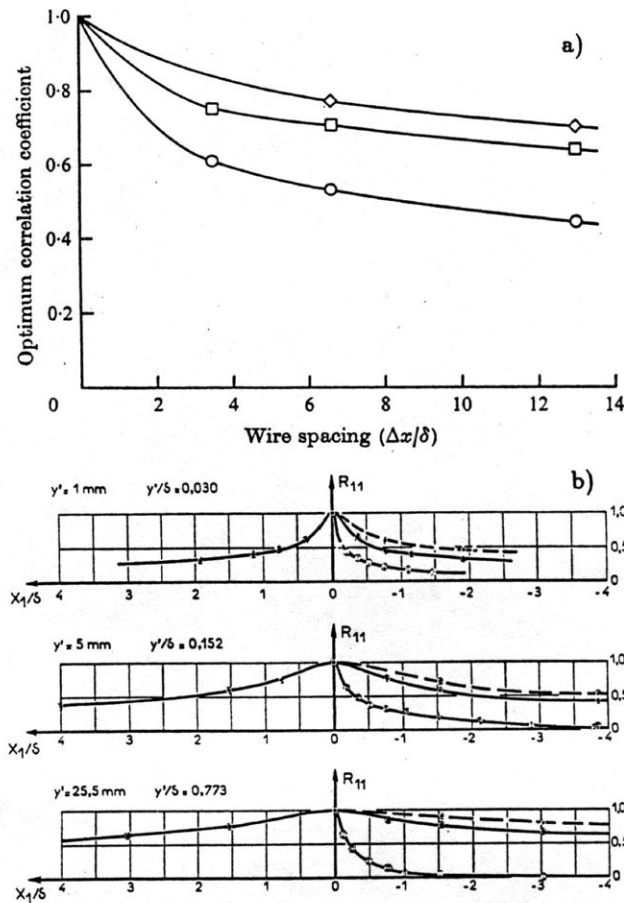
Figure 9.18: Correlation measurements showing the decay of maximum correlation level of R_{11} with increasing streamwise wire separation. (a) Owen & Horstman [1972], $Re_\theta = 7,300$, Ma = 7.2 (top curve: $y/\delta = 0.08$; middle curve: $y/\delta = 0.15$; bottom curve: $y/\delta = 0.30$); (b) Favre *et al.* [1958], $Re_\theta = 2,700$, Ma = 0.4 (top curve: band-pass 1–2,500 Hz; middle curve: band-pass 1–275 Hz; bottom curve: along a mean streamline with zero time delay).

to about 50° in the middle of the layer, and then increase further near the outer edge. The measurements are in broad qualitative agreement with the flow visualization results (see figures 6.14 to 6.19).

9.3.4 Recapitulation of correlations

The following summary has been reproduced from Hinze.
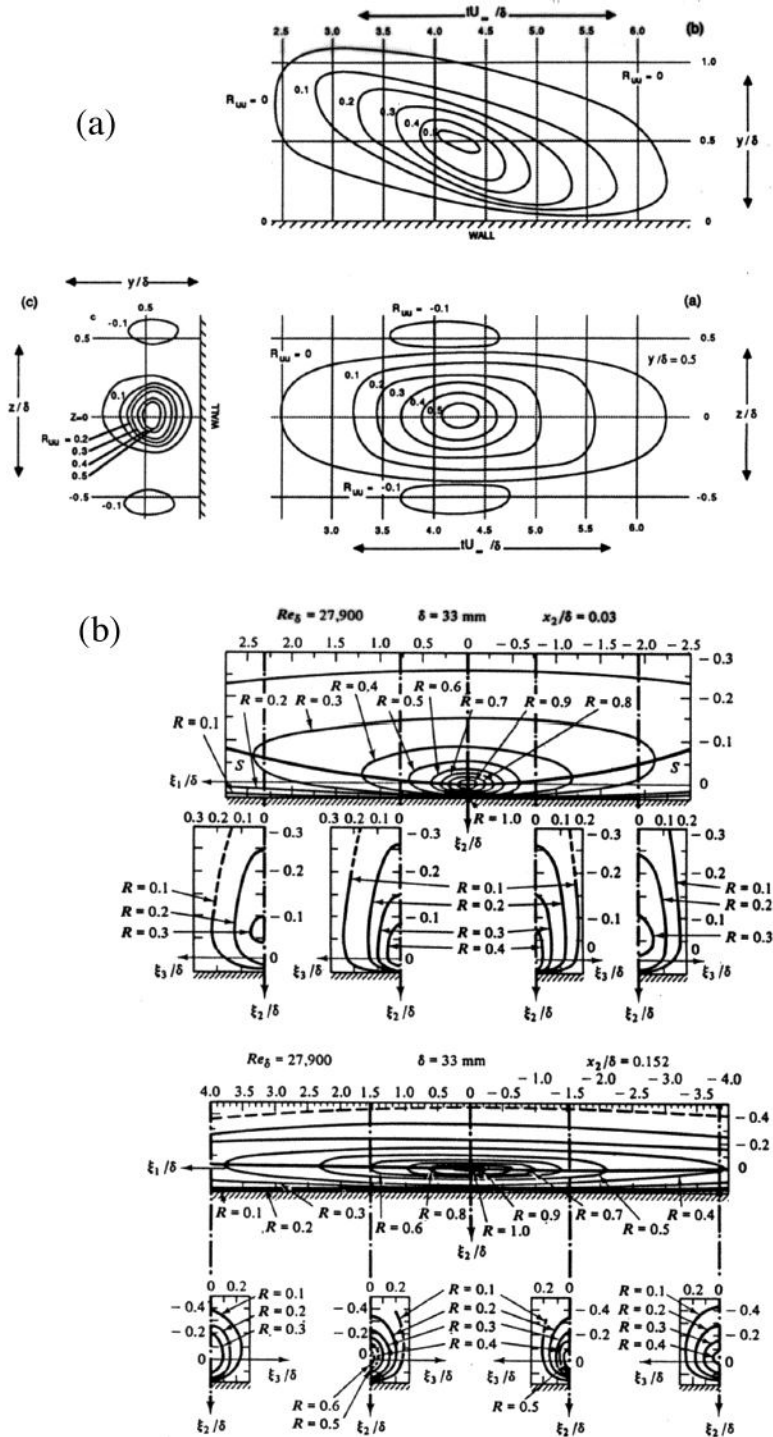
Figure 9.19: (a) Contours of constant space-time correlation of streamwise velocity fluctuations from Kovasznay *et al.*: spanwise/streamwise contours, vertical/streamwise contours, and spanwise/vertical contours are shown. Fixed point (wire) at $y/\delta = 0.5$. (b) Iso-space correlation contours of $R_{11}(\zeta_1, \zeta_2, \zeta_3, \tau_m)$ for optimum time delay τ_m. From Favre *et al.*. Fixed points at $y/\delta = 0.03$ and $y/\delta = 0.152$.
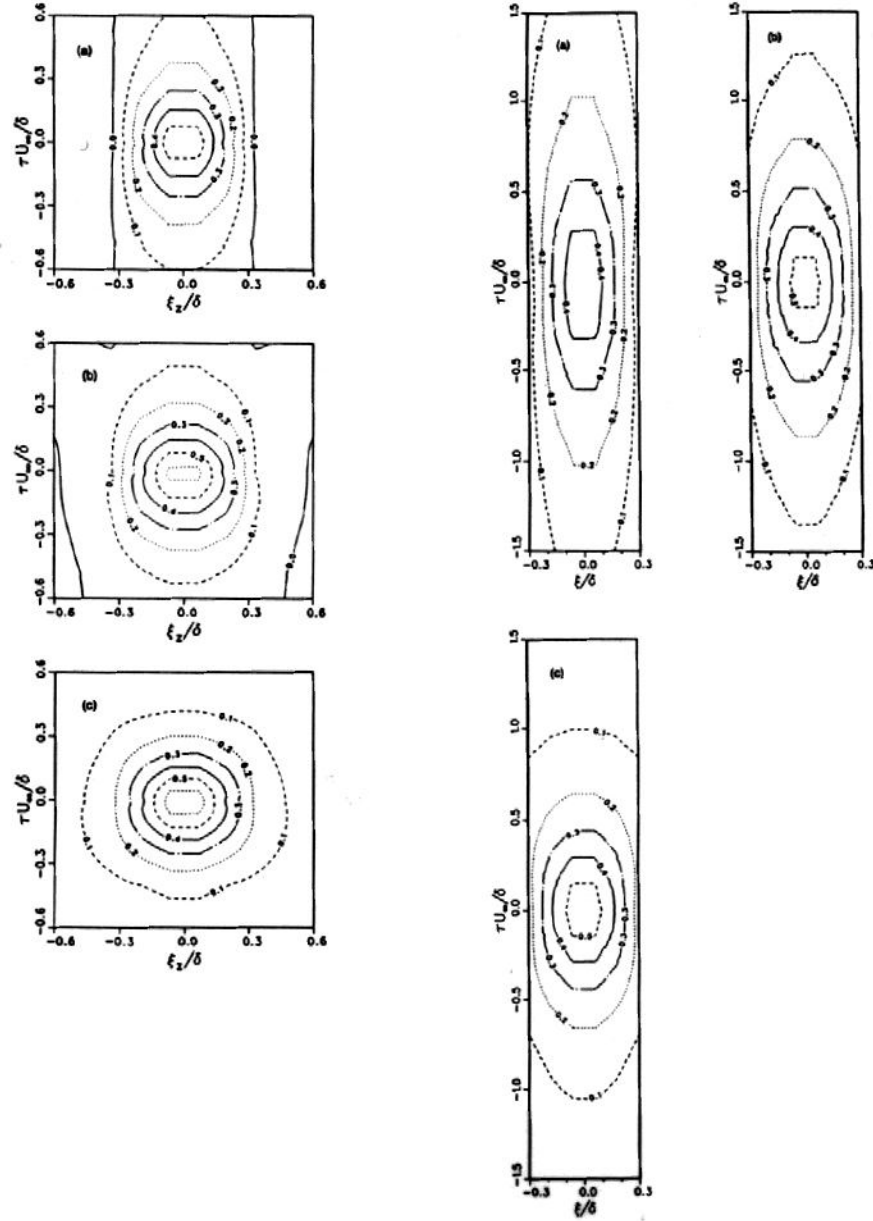
Figure 9.20: Left: Contours of constant space-time correlation of mass-flux fluctuations from spanwise separated probes in a supersonic boundary layer: from top to bottom $y/\delta = 0.20$, $y/\delta = 0.51$, $y/\delta = 0.82$. From Spina & Smits. Right: Contours of constant space-time correlation of streamwise velocity fluctuations from spanwise separated probes in a subsonic boundary layer: from top to bottom $y/\delta = 0.22$, $y/\delta = 0.52$, $y/\delta = 0.80$. From Alving *et al.*.

EULERIAN SPACE CORRELATIONS

Double Correlations between a Velocity Component and Pressure or Other Scalar Quantity. First-order tensor:

$$(\mathbf{K}_{i,p})_{A,B} = \overline{(u_i)_A p_B} \qquad (\mathbf{K}_{i,\gamma})_{A,B} = \overline{(u_i)_A \gamma_B}$$

Figure 9.21: Left: Experiment to measure structure angles. Right: Space-time correlation for a given probe spacing. From R. W. Smith Ph.D. Thesis.

Figure 9.22: Average structure angle profiles for several vertical wire spacings, subsonic and supersonic boundary layers. From Spina *et al.*.

Correlation coefficient:

$$(\mathbf{L}_{i,p})_{A,B} = \frac{(\mathbf{K}_{i,p})_{A,B}}{(u'_i)_A p'_B} \qquad \text{(no summation)}$$
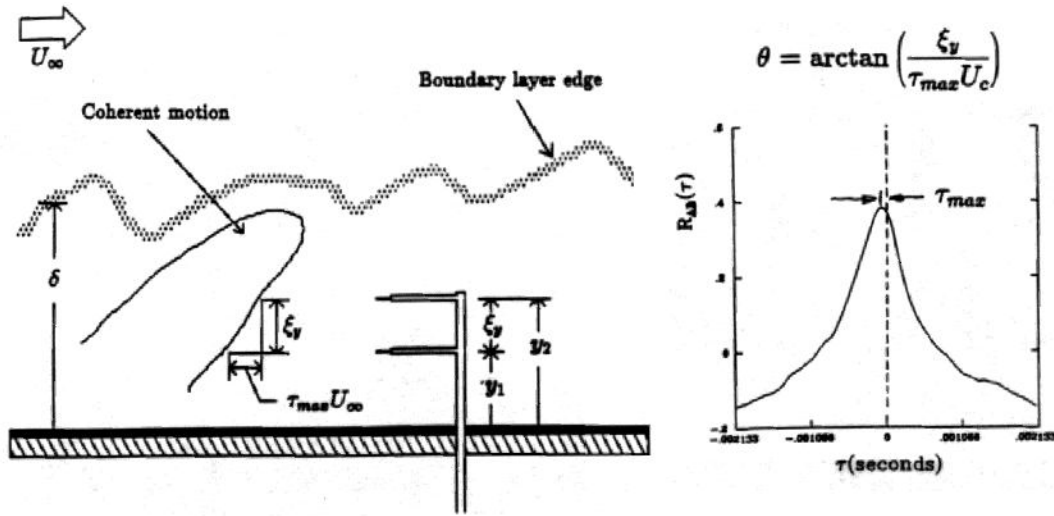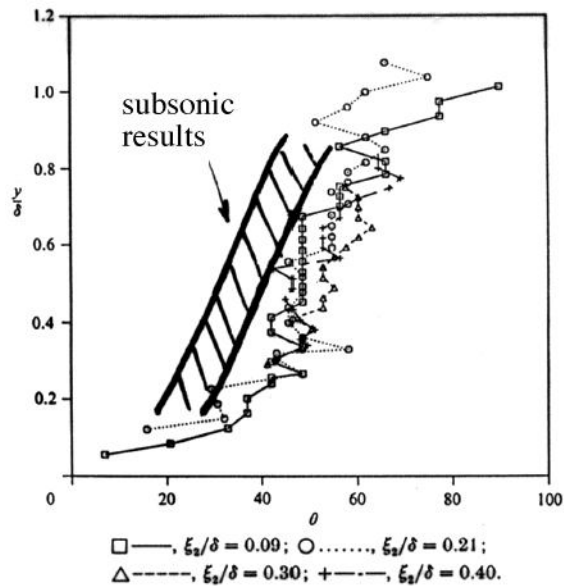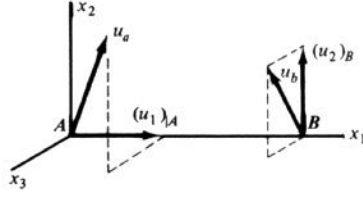
Figure 9.23: Double correlations between two velocity components. From Hinze.

Special case when $A \equiv B$:

$$\mathbf{K}_{i,\gamma}(0) = \overline{\gamma u_i} = -\varepsilon_\gamma \frac{\partial \Gamma}{\partial x_i} \qquad \text{(measure of "eddy" transport)}$$

Double Correlations between Two Velocity Components (see figure 9.23. Second-order tensor:

$$(\mathbf{Q}_{i,j})_{A,B} = \overline{(u_i)_A (u_j)_B}$$

Correlation coefficient:

$$(\mathbf{R}_{i,j})_{A,B} = \frac{\overline{(u_i)_A (u_j)_B}}{\overline{(u_i')_A (u_j')_B}}$$

Special case when $A \equiv B$:

$$\mathbf{Q}_{i,j}(0) = \overline{u_i u_j} = -(\varepsilon_m)_{ik} \left(\frac{\partial \bar{U}_k}{\partial x_j} + \frac{\partial \bar{U}_j}{\partial x_k} \right)$$

(measure of turbulence stresses, eddy "viscosity," or eddy-transport coefficient of momentum)

For the special case of homogeneous turbulence (see chapter 10):
Longitudinal correlation coefficient:

$$\mathbf{f}(r) = \frac{\overline{(u_r)_A (u_r)_B}}{u'^2}$$

Transverse correlation coefficient:

$$\mathbf{g}(r) = \frac{\overline{(u_n)_A (u_n)_B}}{u'^2}$$

Integral scale:

$$\Lambda_f = \int_0^\infty \mathbf{f}(r) \, dr \qquad = \Lambda_g = \int_0^\infty \mathbf{g}(r) \, dr$$

Dissipation scale:

$$\lambda_f \quad \text{from} \quad \frac{1}{\lambda_f^2} = -\frac{1}{2} \frac{\partial^2 \mathbf{f}}{\partial r^2}\bigg|_{r=0}$$
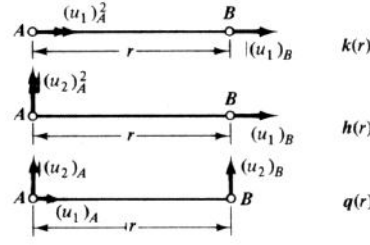
Figure 9.24: Triple correlations between velocity components in homogeneous turbulence. From Hinze.

$$\lambda_g \quad \text{from} \quad \frac{1}{\lambda_g^2} = -\frac{1}{2} \left. \frac{\partial^2 \mathbf{g}}{\partial r^2} \right|_{r=0}$$

Triple Correlations between Velocity Components. Third-order tensor:

$$(\mathbf{S}_{ik,j})_{A,B} = \overline{(u_i)_A (u_k)_A (u_j)_B}$$

Correlation coefficient:

$$(\mathbf{T}_{ik,j})_{A,B} = \frac{\overline{(u_i)_A (u_k)_A (u_j)_B}}{\overline{(u_i')_A (u_k')_A (u_j')_B}}$$

For the special case of homogeneous turbulence (see chapter 10 and figure 9.24):

$$\mathbf{k}(r) = \mathbf{T}_{rr,r} = \frac{\overline{(u_r)_A^2 (u_r)_B}}{u'^3}$$

$$\mathbf{h}(r) = \mathbf{T}_{nn,r} = \frac{\overline{(u_n)_A^2 (u_r)_B}}{u'^3}$$

$$\mathbf{q}(r) = \mathbf{T}_{nr,r} = \frac{\overline{(u_n)_A (u_r)_A (u_n)_B}}{u'^3}$$

EULERIAN TIME CORRELATION

For velocity u at a fixed point:

$$\mathbf{R}_E(t) = \frac{\overline{u(\tau)u(\tau - t)}}{u'^2}$$

For steady flowfield, averaging with respect to time:
Eulerian integral time scale:

$$T_E = \int_0^\infty \mathbf{R}_E \, dt$$

Eulerian dissipation time scale:

$$\tau_E \quad \text{from} \quad \frac{1}{\tau_E^2} = -\frac{1}{2} \left. \frac{\partial^2 \mathbf{R}_E}{\partial t^2} \right|_{t=0}$$

If the field has a uniform mean velocity $\bar{U}$, so that $\bar{U} \gg u$, there is a simple relationship between T_E and Λ_f: because of $x = \bar{U}t$,

$$\Lambda_f = \bar{U}T_E$$

and

$$\mathbf{f}(x) \equiv \mathbf{R}_E(t)$$

LAGRANGIAN TIME CORRELATION

$$\mathbf{R}_L(t) = \frac{\overline{v(\tau)v(\tau - t)}}{v'^2}$$

for the velocity components of a fluid particle. Homogeneous flowfield. Averaging over a large number of particles:
Lagrangian or diffusion integral time scale:

$$T_L = \int_0^\infty \mathbf{R}_L \, dt$$

Lagrangian dissipation time scale:

$$\tau_L \quad \text{from} \quad \frac{1}{\tau_L^2} = -\frac{1}{2} \left. \frac{\partial^2 \mathbf{R}_L}{\partial t^2} \right|_{t=0}$$

Lagrangian or diffusion integral length scale:

$$\Lambda_L = v'T_L$$

Coefficient of eddy diffusion for fluid particles:

$$\varepsilon = v'\Lambda_L = v'^2 \int_0^\infty \mathbf{R}_L \, dt$$

Similarly, for transport on Γ by fluid particles:

$$\varepsilon_\gamma(\alpha) = v'^2 \int_0^\infty f(\alpha, t)\mathbf{R}_L(t) \, dt$$

where $f(\alpha, t)$ accounts for the effect of exchange during the path of the particles.
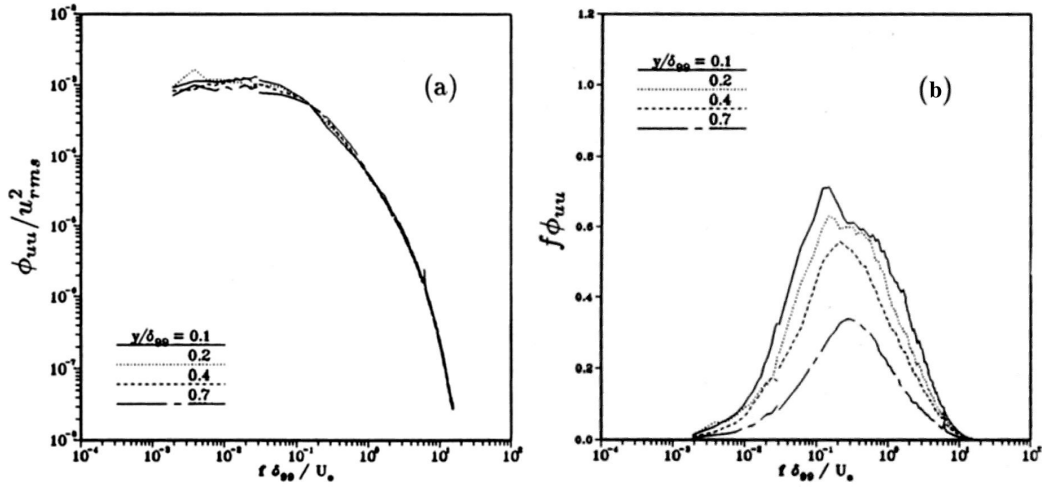
Figure 9.25: Some frequency spectra taken in a subsonic boundary layer: (a) log-log representation; (b) pre-multiplied representation. From Alving *et al.*.

9.4   Frequency Spectra

We define the *power spectral density* ϕ by saying that $\phi(\omega)d\omega$ is the contribution from frequencies $\omega - \frac{1}{2}d\omega$ and $\omega + \frac{1}{2}d\omega$ (where $d\omega$ is small but arbitrary) to the mean square of the signal. Note that:

$$\int_0^\infty \phi(\omega)\, d\omega = \overline{u^2} \quad \left(= \int_0^\infty \omega\phi(\omega)\, d(\log\omega) \right)$$

and ϕ is sometimes just called the spectrum. The first representation is usually plotted on log-log coordinates, and the second one (sometimes called the "pre-multiplied" form) is usually plotted on linear-log coordinates (see figure 9.25).

Now, the spectrum of $a \sin \omega_1 t$ is $\frac{1}{2}a^2\delta(\omega - \omega_1)$, where δ is the delta function, which is zero when $\omega \neq \omega_1$ and goes to infinity at $\omega = \omega_1$ such that $\delta(\omega - \omega_1)$ is unity. Thus the integral of the spectrum of $a \sin \omega_1 t$ over all ω is the mean square $\frac{1}{2}a^2$. The spectrum ϕ can be measured using a narrow band "notch" filter, that is, by measuring the mean square signal passing through a bandpass filter — the mean square of a convolution of $u(t)$ with a filter function. These are illustrated in figure 9.26. Some examples taken from a subsonic boundary layer are shown in figure 9.25.

Now there is a simple connection between the auto-correlation and its spectrum function:

$$\overline{u(t)u(t+\tau)} = \int_0^\infty \phi(\omega) \exp(i\omega\tau)\, d\omega$$
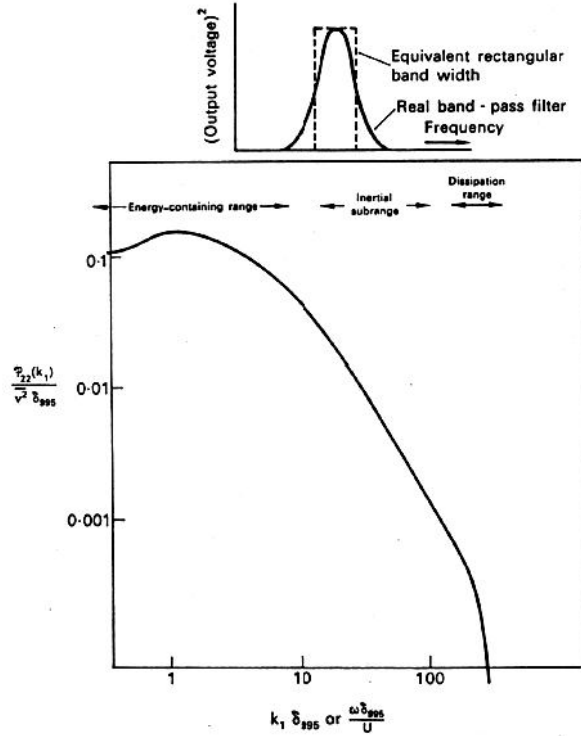
Figure 9.26: Typical $\phi_{22}(k_1)$ wave number (or frequency) spectrum in boundary layer at about $y/\delta = 0.5$. From Bradshaw.

Remember: $\exp(\pm i\omega\tau) = \cos\omega\tau \pm i\sin\omega\tau$, and complex numbers are used simply to identify different parts of the transform. Now $\phi(\omega)$ is an even function ($\phi(\omega) = \phi(-\omega)$), and since the time correlation is an even function of τ, we could write:

$$\overline{u(t)u(t + \tau)} = \int_0^\infty \phi(\omega)\cos\omega\tau\,d\omega$$

and so we have the inverse transform:

$$\phi(\omega) = \frac{1}{\pi}\int_{-\infty}^\infty \overline{u(t)u(t + \tau)}\cos\omega\tau\,d\tau$$

$$= \frac{2}{\pi}\int_0^\infty \overline{u(t)u(t + \tau)}\cos\omega\tau\,d\tau$$

Useful pairs of transforms are given in table 9.1 (source unknown).

Using Taylor's hypothesis, the autocorrelation with time delay $(-r_1/U)$ (r_1 is in the x-direction, that is, in the direction of the flow) should be nearly the same as the space correlation with a spacing r_1 in the x-direction. Then we can convert a frequency to a *wave number* using $k_1 = \omega/U$ (where the

$R_s(\tau) \! \int_0^\infty G_x(f) \cos 2\pi f \tau \, df$

$G_x(f) = 4 \int_0^\infty R_x(\tau) \cos 2\pi f \tau \, d\tau$

Table 3.2
Special Autocorrelation Functions

Type	Autocorrelation Function
Constant	$R_s(\tau) = c^2$
Sine wave	$R_s(\tau) = \frac{X^2}{2}\cos 2\pi f_o \tau$
White noise	$R_s(\tau) = a\,\delta(\tau)$
Low-pass, white noise	$R_s(\tau) = a B\left(\frac{\sin 2\pi B\tau}{2\pi B\tau}\right)$
Band-pass white noise	$R_s(\tau) = a B\left(\frac{\sin \pi B\tau}{\pi B\tau}\right)\cos 2\pi f_o \tau$
Exponential	$R_s(\tau) = e^{-a|\tau|}$
Exponential cosine	$R_s(\tau) = e^{-a|\tau|}\cos 2\pi f_o \tau$
Exponential cosine, exponential sine	$R_s(\tau) = e^{-a|\tau|}(b\cos 2\pi f_o \tau + c\sin 2\pi f_o |\tau|)$

Table 3.3
Special Power Spectral Density Functions

Type	(One-Sided) Power Spectral Density Function
Constant	$G_x(f) = c^2 \delta(f)$
Sine wave	$G_x(f) = \frac{X^2}{2}\delta(f - f_o)$
White noise	$G_x(f) = a, \; f \geq 0; \quad$ otherwise zero
Low-pass white noise	$G_x(f) = a, \; 0 \leq f \leq B; \quad$ otherwise zero
Band-pass white noise	$G_x(f) = a, \; 0 < f_o - (B/2) \leq f \leq f_o + (B/2)$ otherwise zero
Exponential	$G_x(f) = \frac{4a}{a^2 + 4\pi^2 f^2}$
Exponential cosine	$G_x(f) = 2a\left[\frac{1}{a^2 + 4\pi^2(f + f_o)^2} + \frac{1}{a^2 + 4\pi^2(f - f_o)^2}\right]$
Exponential cosine, exponential sine	$G_x(f) = \frac{2ab + 4\pi c(f + f_o)}{a^2 + 4\pi^2(f + f_o)^2} + \frac{2ab - 4\pi c(f - f_o)}{a^2 + 4\pi^2(f - f_o)^2}$

Table 9.1: Table of transforms.

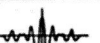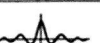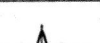frequency is in Hertz), assuming that the convection velocity of eddies with frequency ω is the local mean velocity, U, so that:

$$U^{-1}\phi(\omega) = \phi(k_1).$$

We usually write:

$$\phi'(\omega) \;=\; \frac{1}{2\pi} \int_{-\infty}^{\infty} e^{i\omega\tau} R_{uu} \, d\tau$$

$$\text{and} \quad R_{uu}(\tau) \;=\; \frac{1}{2\pi} \int_{-\infty}^{\infty} e^{-i\omega\tau} \phi'(\omega) \, d\omega.$$

Here we take into account positive and negative arguments in correlation *and* spectrum, and $\phi'(\omega)$ and $R_{uu}(\tau)$ are non-dimensionalized by u'^2 , or something similar.

We can also have co-spectra, such as the $u'v'$ co-spectrum, defined by:

$$\phi_{uv}(\omega) = \frac{1}{2\pi} \int_{-\infty}^{\infty} e^{i\omega\tau} R_{uv} \, d\tau$$

which is the sum of a real part (called the co-spectrum) and an imaginary part (called the quadrature spectrum).

What about the relation between Fourier transforms and the *space corre-lation*? For this we need wave number spectra.

9.5   Wave Number Spectra

Another method of determining time or length scales associated with tur-bulent motion is by Fourier analysis of the velocity fluctuations into three-dimensional wave-space.[2]

Specifically, we define:

$$\Phi_{ij}(\mathbf{x}, \mathbf{k}) = \frac{1}{(2\pi)^3} \int_{-\infty}^{\infty} R_{ij}(\mathbf{x}, \mathbf{r})e^{-i(\mathbf{k}\cdot\mathbf{r})} \, dV(\mathbf{r}) \tag{9.6}$$

where the integration is over all $\mathbf{r}$ space. The inverse relation

$$R_{ij}(\mathbf{x}, \mathbf{r}) = \int_{-\infty}^{\infty} \Phi_{ij}(\mathbf{x}, \mathbf{k})e^{i(\mathbf{k}\cdot\mathbf{r})} \, dV(\mathbf{k}) \tag{9.7}$$

is taken over all $\mathbf{k}$ space, where $\mathbf{k}$ is the wave number (= frequency in Hz divided by local velocity).

Now Φ_{ij} is known as the *energy spectrum function*, and it gives the con-tribution from $\mathbf{k}$ to the energy of the turbulence (also known as the "wave number spectrum"). That is, Φ_{ij} gives the contribution to $\overline{u_i u_j}$ from Fourier components of the velocity field with wave numbers in unit volume of $\mathbf{k}$ space.

Since R_{ij} and Φ_{ij} are Fourier transforms of each other, either is, in prin-ciple, calculable from the other. In practice, it is more accurate to measure directly the one required. Each quantity, however, makes a separate con-tribution to the understanding of turbulent flows: namely, correlation mea-surements tend to give information about the large scales, and spectra tend to give information about the small scales.

As an example, consider the one-dimensional (*x*-component) wave num-ber spectrum of the *v*-component of velocity. The space correlation was:

$$R_{22}(r_1, 0, 0) = \frac{\overline{v(\mathbf{x})v(\mathbf{x} + r_1)}}{\sqrt{\overline{v(\mathbf{x})^2}} \sqrt{\overline{v(\mathbf{x} + r_1)^2}}}$$

which according to Taylor's hypothesis is nearly the same as the *v*-component auto-correlation $\overline{v(t)v(t + \tau)}/\overline{v^2}$ with time delay $-r_1/U \, (= \tau)$.

Then

$$\Phi'_{22}(k_1) = \frac{1}{2\pi} \int_{-\infty}^{\infty} \overline{v(\mathbf{x})v(\mathbf{x} + r_1)}e^{-ik_1 r_1} \, dr_1$$

---

[2]In contrast, Fourier decomposition into component frequencies is one-dimensional.
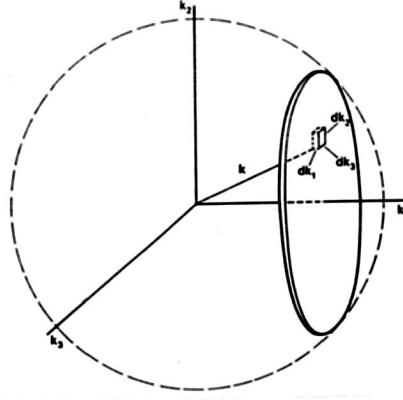
Figure 9.27: Energy distributed in three-dimensional wave number space.

and

$$\overline{v(\mathbf{x})v(\mathbf{x}+r_1)} = \int_{-\infty}^{\infty} \Phi'_{22}(k_1)e^{ik_1 r_1}\,dk_1.$$

Note

(1) Φ' is dimensional so that $\Phi = \Phi'/\sqrt{\overline{v(\mathbf{x})^2}}\sqrt{\overline{v(\mathbf{x}+r_1)^2}}$.

(2) k_1 is the x-component wave number, where $\lambda_1 = 2\pi/k_1$ (the y- and z-components are k_2 and k_3 respectively); and

(3) By putting $i = j = 2$ and $r_2 = r_3 = 0$ in Equation 9.7, we have

$$\overline{v(\mathbf{x})v(\mathbf{x}+r_1)} = \int\left[\iint \Phi'(k_1,k_2,k_3)\,dk_2 dk_3\right]e^{ik_1 r_1}\,dk_1.$$

so that

$$\Phi'(k_1) = \iint \Phi'(k_1,k_2,k_3)\,dk_2 dk_3 \neq \Phi'(k_1,0,0)$$

We can think of $\Phi(\mathbf{k})$ as being distributed in wave number space as a solid body, whose local density is equal to the local value of $\Phi(\mathbf{k})$. The energy content of an elemental volume is:

$$\Phi(\mathbf{k})\,dk_1 dk_2 dk_3.$$

The energy content of a slice of thickness dk_1 is:

$$\Phi(k_1)\,dk_1 = \left[\iint \Phi(\mathbf{k})\,dk_2 dk_3\right]dk_1$$

(This analogy is spelled out more clearly by Bradshaw in "Turbulence and Its Measurement).

Perhaps more useful than the energy spectrum function is the integrated spectrum function (or wave number magnitude spectrum):

$$E_{ij}(k) = \frac{1}{2} \oint_{|\mathbf{k}|=k} \Phi_{ij}(\mathbf{k}) \, dS(\mathbf{k}) \tag{9.8}$$

where the integration is over a spherical surface in $\mathbf{k}$ space of radius $|\mathbf{k}|$. This represents the contribution to $\overline{u_i u_j}$ from wave numbers with magnitude equal to $|\mathbf{k}|$. That is, $2E(k)dk$ is the weight of a spherical shell of radius $|\mathbf{k}| = k$, and thickness dk, cut from the imaginary solid. Of particular interest is the sum of the diagonal components of Φ_{ii}. Then:

$$R_{ii}(0) = \overline{u_i u_j} = \int_{-\infty}^{\infty} \Phi_{ii}(\mathbf{k}) \, dV(\mathbf{k}) \, d\mathbf{k}$$

and

$$E_{ii}(k) = \frac{1}{2} \sin \Phi_{ii}(\mathbf{k}) \, dk$$

So

$$\frac{1}{2}\overline{u_i u_j} = \int_{-\infty}^{\infty} E_{ii}(k) \, dk = \text{kinetic energy per unit mass}$$

The only practical way to measure true wave-number spectra is by taking the Fourier transform of the corresponding correlations, which can be very time consuming. Usually we measure $\phi(\omega)$ as an approximation to $\phi(k_1)$.

9.6 Wavelet Transforms

9.6.1 Introduction

Due to the well-known intermittent nature of turbulence, the traditional use of the Fourier decomposition for the analysis of turbulence data has some inherent disadvantages. These disadvantages arise from the fact that Fourier modes, while being discrete in the frequency domain, are infinite in the physical domain. Thus, Fourier decomposition is not well suited for highlighting the intermittency of the data or capturing individual localized "events ," especially when the events occur randomly in space and time. Relatively new analysis methods, using wavelet transforms, offer the possibility of overcoming some of the disadvantages associated with Fourier analysis techniques.

The wavelet transform is the result of convolving a function, termed an "analyzing wavelet," with a data signal. The wavelet transform is equivalent to a filter, and the characteristics of the filter depend on the characteristics of the analyzing wavelet function. The wavelet function is *localized* in space

(or time) and consequently is also localized, but not discrete, in frequency space. Therefore, wavelet analysis offers an advantage over Fourier analysis in that wavelet decomposition of turbulence data is better able to capture any events present in the data.

Furthermore, the shape of the analyzing wavelet is arbitrary, subject only to a few constraints (see section 9.6.3). The shape of the wavelet function may be chosen to correspond to the signature of some interesting event which is believed to be an important feature of the turbulent flow. In comparison, the wavelet function may also be chosen such that it exhibits a particular behavior in the frequency domain which also may have some physical significance. Thus, the wavelet transform may be viewed as a filter in both physical space and frequency space, and the two representations are intimately connected through the wavelet function (Brasseur & Wang, 1991).

Finally, the wavelet transform is is performed over a range of scale. The wavelet transform for a particular scale is obtained by convolving the data signal with a re-scaled, or dilated, version of the wavelet function (see section 9.6.2). Thus, wavelet analysis is capable of highlighting localized events which may occur at many different scales (spatial or temporal) and is a useful tool for investigating the scaling of turbulent flows.

9.6.2   One-Dimensional Continuous Wavelet Transforms

Much experimental fluid mechanics research is based on the analysis of one-dimensional time-series data of particular flow variables of interest, such as velocity, vorticity, or pressure. Therefore, the one-dimensional continuous wavelet transform is of great practical interest. This section briefly presents the definitions and relationships necessary to understand and compute continuous wavelet transforms in one dimension. See Grossman & Morlet (1984), Kronland-Martinet *et al.* (1987), Smith & Smits (1991a), and Wang *et al.* (1991) for more detailed discussions.

The wavelet transform, denoted by $T(b, a)$, is defined as the convolution of a wavelet function, $g(t)$, with a signal, $s(t)$. The wavelet function is re-scaled by a *scale factor*, a, where $a > 0$ and $a > 1$ corresponds to dilations, and pre-multiplied by a *weighting function*, $w(a)$, to yield $w(a)g(t/a)$. Thus,

$$T(b, a) = \frac{1}{\sqrt{a}} \int_{-\infty}^{\infty} \bar{g}\left(\frac{t - b}{a}\right) s(t) dt \qquad (9.9)$$

where the overbar denotes complex conjugation, b is the time-shift parameter, and the weighting function has been chosen to be equal to $1/\sqrt{a}$ to ensure that the product $w(a)g(t/a)$ has the same energy for all values of a. In general, $g(t)$ may be complex. and thus $T(b, a)$ may also be complex.

Equation 9.9 may be written in terms of Fourier transforms as

$$T(b,a) = \sqrt{a} \int_{-\infty}^{\infty} \bar{G}(a\omega)S(\omega)e^{j\omega b}\, d\omega \tag{9.10}$$

where $S(\omega)$ is the Fourier transform of $s(t)$ defined by

$$S(\omega) = \frac{1}{\sqrt{2\pi}} \int_{-\infty}^{\infty} s(t)e^{-j\omega t}\, dt \tag{9.11}$$

and $G(\omega)$ is the Fourier transform of $g(t)$.

The original signal may be reconstructed from its wavelet transform using the following:

$$s(t) = \frac{1}{C(g)} \int_{0}^{\infty} \int_{-\infty}^{\infty} \frac{1}{\sqrt{a}} g\left(\frac{t-b}{a}\right) T(b,a) \frac{db\,da}{a^2} \tag{9.12}$$

As in equation 9.9, the factor $1/\sqrt{a}$ arises from the weighting function. The factor $C(g)$ is a constant for a given wavelet function and will be discussed in section 9.6.3. Equation 9.12 may be used to show that the total energy of the signal can be computed from the wavelet transform using

$$\int_{-\infty}^{\infty} s(t)\bar{s}(t)\, dt = \frac{1}{C(g)} \int_{0}^{\infty} \int_{-\infty}^{\infty} T(b,a)\bar{T}(b,a)\, db \tag{9.13}$$

Let

$$E_a\left[s(t)\right] = \frac{1}{C(g)a^2} \int_{-\infty}^{\infty} T(b,a)\bar{T}(b,a)\, db \tag{9.14}$$

where $E_a\left[s(t)\right]$ is the energy of the function $s(t)$ at a scale a. Then, equation 9.13 becomes

$$\int_{-\infty}^{\infty} s(t)\bar{s}(t)\, dt = \int_{0}^{\infty} E_a\left[s(t)\right]\, da \tag{9.15}$$

Equation 9.14 may be used to compute an energy spectrum of the signal $s(t)$ in terms of wavelet scale a. Note that it has been implicitly assumed that both $g(t)$ and $s(t)$ are square-integrable functions.

9.6.3 The Admissibility Condition

The parameter $C(g)$ in equation 9.12 is defined as

$$C(g) = 2\pi \int_{-\infty}^{\infty} \frac{1}{|\omega|} G(\omega)\bar{G}(\omega)\, d\omega \tag{9.16}$$

The constraint that

$$C(g) < \infty \tag{9.17}$$

for both $\omega > 0$ and $\omega < 0$ is termed the "admissibility condition" and must be imposed to ensure that the reconstruction formula, equation 9.12, is well-behaved. This constraint requires that $G(0) = 0$, that is, the mean value of the function $g(t)$ must be zero. Thus the wavelet transform, regardless of the scale factor, will not contain any information about the mean value of the signal.

It is important to remember that $C(g)$ is a *constant* for a given wavelet function $g(t)$, and thus appears *outside* the integrals in equations 9.12, 9.13 and 9.14. Therefore, in principle, a function which does *not* satisfy the admissibility condition may still be used as a "wavelet." The consequence of using an inadmissable function as a wavelet is that the wavelet transform at all scales will carry information about the mean value of the signal. Therefore, when equation 9.12 is used to reconstruct the original signal from its wavelet transform, the result will be infinite.

Note that the formula for $C(g)$ given by equation 9.16 is not, in general, correct for all wavelet functions. For one-dimensional wavelet functions, $C(g)$ will be a function of the sign (positive or negative) of ω. For higher-dimensional wavelets, $C(g)$ will, in general, be a function of the wavenumber vector $\mathbf{k}$ (Wang *et al.* 1991). Any changes in the definition of $C(g)$ will also result in changes in the reconstruction formula given in equation 9.12.

9.6.4   Choice of Wavelet Function

Many different wavelet functions are available. A common choice is the *Mexican Hat* wavelet, which is given by

$$g_r(t) = \left(1 - t^2\right)e^{-t^2/2} \tag{9.18}$$

This function can be considered the real part of a complex function, $g(t)$, whose Fourier transform is given by

$$\begin{cases} 2\omega^2 e^{-\omega^2/2} & \text{for} \quad \omega > 0 \\ 0 & \text{for} \quad \omega \leq 0 \end{cases} \tag{9.19}$$

and thus satisfies the admissibility condition. The imaginary part of the function $g(t)$, denoted by $g_i(t)$, may be obtained by computing the inverse Fourier transform of equation 9.19. The real part, imaginary part, and modulus of $g(t)$ are shown in figure 9.28, as are its Fourier transforms as given by equation 9.19. These representations illustrate the localized nature of the wavelet function in both physical and frequency space.

Note that we can think of the wavelet transform as a microscope, where the "optics" are given by the specific wavelet function $g(t)$ that is chosen for the analysis, the "enlargement" is given by the parameter a, and the position is determined by the parameter b. This interpretation was first proposed by Lliandrat & Moret-Bailly (1990).
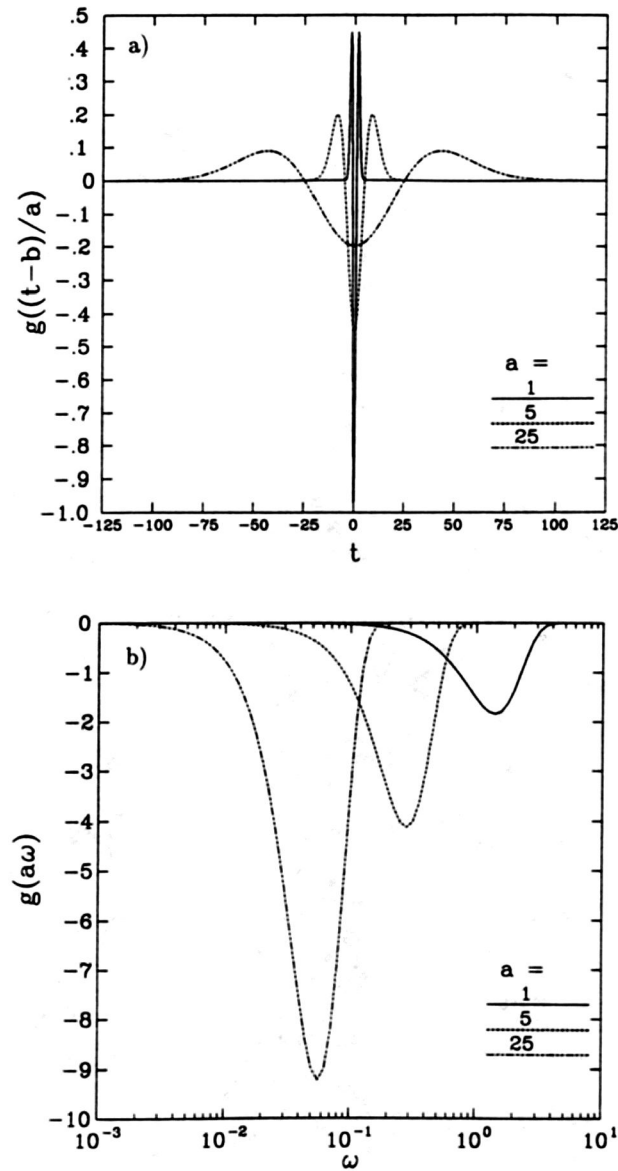
Figure 9.28: Top: The Mexican Hat wavelet function, $g(t)$, for three different scale factors, a; zero time shift ($b = 0$); and $w(a) = 1/\sqrt{a}$. Bottom: The Fourier transform, or frequency domain representation, of the Mexican Hat wavelet function. Note the long low-frequency tail. From Smith's Ph.D. Thesis.

9.6.5 Examples

Figure 9.29a shows the transform coefficients for the wavelet decomposition of a one-dimensional signal, in this case the streamwise velocity fluctuation in a turbulent boundary layer. Figure 9.29b shows the reconstruction of the signal using 13 scales; as can be seen the reconstruction is (qualitatively) very

Figure 9.29: (a) Fluctuating signal (the top trace) and associated wavelet transform. (b) Fluctuating signal (the top trace) and reconstructed signals from the wavelet transform.

good. These kind of diagrams are usually presented as shown in figure 9.30. There, the magnitude of the coefficients are represented by intensity, and the wavelet scales increase along the vertical scale. The particular example shows the streamwise velocity fluctuations obtained by two probes separated in the streamwise direction. The signals were both analyzed using the Mexican hat wavelet, and the change in the wavelet coefficients is a measure of the change in the correlation with streamwise evolution. It can be seen that the large scales retain good correlation but that the smaller scales do not (the largest wavelet scale corresponds to about a boundary layer thickness in size).

In figure 9.31 the results of a scale similarity study are given. Here, the similarity of the wavelet coefficients are studied, as a function of scale, by examining their probability density distributions and their spectra. Some similarity is seen in these crude measures, at least for the larger scales, but it is not compelling.

Two other uses for wavelet analysis of turbulence signals have been

Figure 9.30: Subsonic boundary layer results ($Re_\theta = 13,200$) using Mexican hat wavelet. Upstream signal is shown at top; downstream is shown below. The horizontal axis is time, and covers the equivalent of about 50δ.

proposed. The first is to use wavelet decomposition as a basis for conditional sampling, and the preliminary results obtained by Poggie, Poddar & Smits (1993) look promising. The second is to use it as a basis for identifying structure. Here, particular wavelet families are designed to match expected features in the flow. For example, Smith & Smits (1993) have suggested searching for vortex tubes by matching velocity signatures characteristic of these features. This was first suggested by Lumley (see section 9.6.6. See also Chapter 10.

9.6.6 A Simple Eddy

The following material is quoted verbatim from Tennekes & Lumley, 1972.

Let us recall that an autocorrelation and the corresponding spectrum

Figure 9.31: (a) Probability distribution function; (b) Scale decomposition of energy; (c) Power spectrum of fluctuating signal; (d) Power spectrum of reconstructed signal at different wavelet scales.

function are a Fourier-transform pair. If the correlation is a function of spatial separation, the spectrum is a function of wavenumber. A certain eddy size, say ℓ, is thus associated with a certain wavenumber, say κ. An "eddy"

of wavenumber κ may be thought of as some disturbance containing energy in the vicinity of κ. It would be tempting to think of an eddy as a disturbance contributing a narrow spike to the spectrum at κ. However, a narrow spike in the spectrum creates slowly damped oscillations (of wavelength $2\pi/\kappa$) in the correlation, as we discovered in section 6.2 (that is, section 6.2 in Tennekes & Lumley). Such a correlation is characteristic of wavelike disturbances, but not of eddies; we expect eddies to lose their identity because of interactions with others within one or two periods or wavelengths. Therefore, the contribution of an eddy to the spectrum should be a fairly broad spike, wide enough to avoid oscilatory behavior ("ringing") in the correlation.

It is convenient to define an eddy of wavenumber κ as a disturbance containing energy between, say 0.62κ and 1.62κ. This choice centers the energy around κ on a logarithmic scale, because $\ln(1.62) = \ln(1/0.62) \approx 0.5$; it also makes the width of the contribution to the spectrum equal to κ (figure 9.32). We recall from section 6.2 (in Tennekes & Lumley) that the transform of a narrow band around κ is a wave of wavelength $2\pi/\kappa$, with an envelop whose width is the inverse of the bandwidth. Now, because the bandwidth selected is κ, the width of the envelop is of order $1/\kappa$. This is sketched in figure 9.32; we see that an eddy defined this way is indeed the relatively compact disturbance we want it to be. The eddy size ℓ is roughly equal to $2\pi/\kappa$.

The schematic eddy presented in figure 9.32 suffices for the development of energy-cascade concepts (see section 10.5). This model, however, cannot deal with all of the problems associated with the distinction between waves and eddies. The Fourier transform of a velocity field is a decomposition into waves of different wavelengths; each wave is asociated with a single Fourier coefficient. An eddy, however, is associated with many Fourier coefficients and the phase relations among them. Fourier transforms are used because they are convenient (spectra can be measured easily); more sophisticated transforms are needed if one wants to decompose a velocity field into eddies instead of waves (Lumley, 1970).
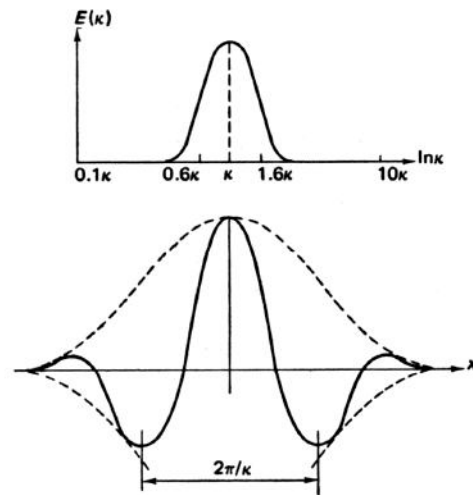
Figure 9.32: An eddy of wave number κ and wavelength $2\pi/\kappa$. From Tennekes & Lumley, 1972.

Chapter 10

Homogeneous Isotropic Turbulence

10.1 Introduction

The term *homogeneous* implies that the turbulence properties are independent of position. Here, averages such as the total energy of the fluctuations $\frac{1}{2}\overline{u_i(\mathbf{x})u_i(\mathbf{x})}$ are constants. More general correlations such as $\overline{u_i(\mathbf{x})u_j(\mathbf{x} + \mathbf{r})}$ are independent of x and depend only on r. The term *isotropy* implies that there is no preferred direction, such that, for example, $\overline{q^2} = 3\overline{u_1^2} = 3\overline{u_2^2} = 3\overline{u_3^2}$, and hence there can be no mean shearing.

In practice, most turbulent flows are not isotropic, nor are they homogeneous but the more important features of the energy transfer process are the same as in homogeneous flow, and it is easier to study the simpler case to obtain some physical insight.

A practical approximation to isotropic homogeneous turbulence is the turbulent flow found far downstream of a uniform grid of bars (see figure 6.10). The wakes of the individual bars become turbulent close behind the grid and interact in a complicated way so that at a large number of mesh lengths from the plane of the grid (> 20) the turbulence is more or less homogeneous (see figure 10.1) For a uniform grid the turbulence also approaches isotropy (see figure 10.2). In this case, the turbulent energy decays slowly as the distance from the grid increases because there is no source of turbulent energy other than the shear flow close to the grid.

For homogeneous turbulence, the turbulent kinetic energy equation becomes (show this as an exercise):

$$\frac{\partial}{\partial t}\left(\tfrac{1}{2}\overline{q^2}\right) = -\overline{u_i u_j}\frac{\partial U_i}{\partial x_j} - \nu\overline{\left(\frac{\partial u_i}{\partial x_j}\right)^2} \tag{10.1}$$

Note that, unless production equal dissipation, $\overline{q^2}$ varies with time and the
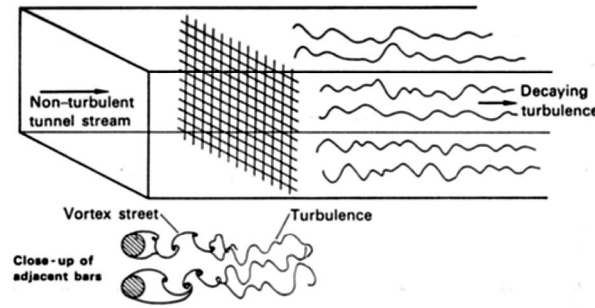
Figure 10.1: Generation of homogenous turbulence in a wind tunnel using a grid.

flow is not stationary.

Most theoretical work in homogeneous flows has concentrated on the behavior of the correlations and spectrum functions. We will only consider two principal observations from the study of isotropic homogeneous turbulence which have a larger implication for all turbulent flows: the decay of isotropic homogeneous turbulence, and the energy cascade.

Equation 10.1 shows that energy is produced by working of the Reynolds stresses against the mean flow, and it is dissipated as heat by working of the viscous stresses against the turbulent velocity gradients. Since the Reynolds stress tensor specifies the turbulent kinetic energy, the eddies containing most of the energy also contribute most to the Reynolds stresses and presumably receive most of the energy that is transferred from the mean flow. On the other hand, the rate of energy dissipation is determined by eddies which are much smaller than those containing most of the energy. So a simple consideration of the energy budget raises two questions: the nature of the energy transfer from the mean flow to the turbulent eddies, and the nature of the transfer from the large energy-containing eddies to the much smaller dissipating eddies (Townsend p.46).

From the turbulent kinetic energy equation for homogeneous turbulence (equation 10.1), we see that:

1. The action of viscosity is strongest where the instantaneous velocity gradients are largest – implies small scale motions. Dissipation is therefore controlled by small eddies.

2. The production term can be interpreted as the interaction of eddies with significant $-\overline{u'v'}$ working against the mean shear, that is, the extraction of energy from the mean flow by the motions which contain most of the Reynolds stress. These motions must be at least comparable to the scale of the mean flow for a reasonable interaction to occur. Also the smaller motions will contribute little to the shear stress — if the vortex stretching makes the smaller motions lose all sense of direction
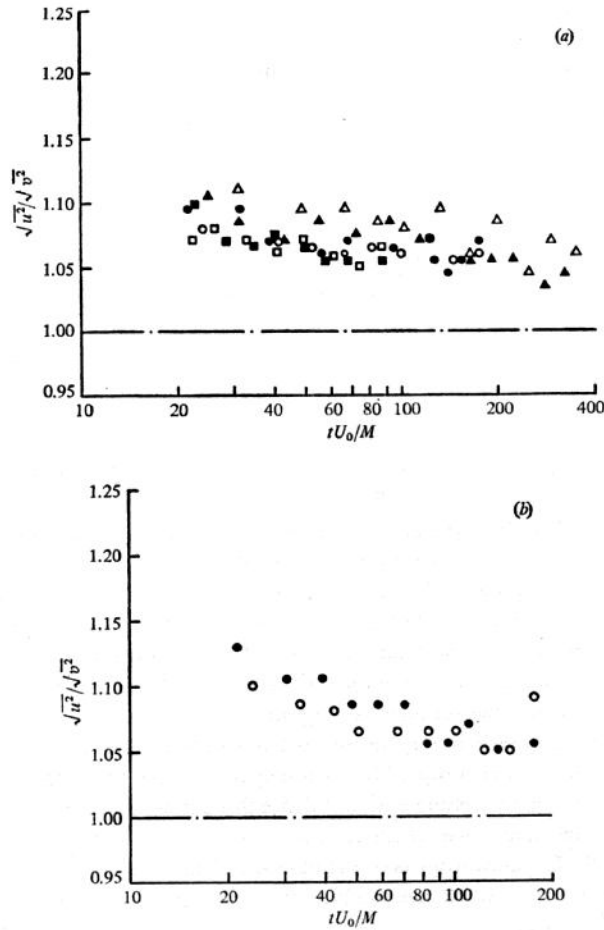
Figure 10.2: Approach to isotropy of decaying turbulence generated by different square biplane grids using square and round rods (from Comte-Bellot & Corrsin 1966).

then their contribution to $-\overline{u'v'}$ goes to zero. Hence the production term is said to be dominated by the large scale motions, and the energy is said to be transferred to the dissipating eddies by inviscid vortex stretching.

An important point to note is that the energy transfer occurs as an inviscid process so that the rate at which energy is transferred to the smaller eddies is constant and it is actually independent of viscosity — viscosity simply sets the size of the smallest eddies that finally dissipate the energy.

Now in grid turbulence (which is approximately isotropic if there is no mean shear), there is no source of turbulent energy far from the grid, and the turbulent energy decays slowly. This decay period is dominated by the decay of high Reynolds number turbulence and it is called the "initial period
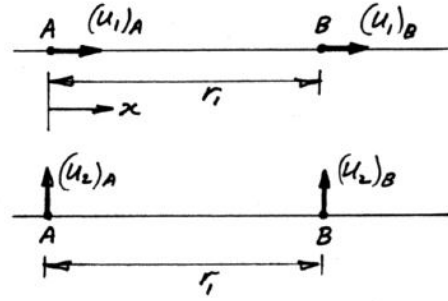
Figure 10.3: Two-point correlations.

of decay." As the turbulence decays, the energy transfer from the large eddies to the small eddies decreases so that the intensity of the small eddies decreases faster than that of the large eddies. Therefore, the dissipation rate decreases and the dissipating eddies become larger. Finally the intensity and the dissipation rate sink to such low levels that the dissipation in the largest eddies (which are of a size comparable to the mesh size) becomes relatively important: this deacy process is dominated by turbulence of very low Reynolds number based on $\sqrt{\overline{u'^2}}$ and λ. This is called the "final period of decay."

10.2   Lateral and Longitudinal Correlations

In isotropic turbulence $R_{ij}(\mathbf{x}, \mathbf{r})$ has a form independent of position and orientation of the reference axes. That is, R_{ij} is an isotropic tensor of second order. It is then possible to write

$$\overline{u_i u_j(r)}\, R_{ij} = Q_{ij} = r_i r_j A(r) + \delta_{ij} B(r) \tag{10.2}$$

where $A(r)$ and $B(r)$ are functions only of the scalar separation r (see Hinze, Chapter 3).

Suppose $\mathbf{r}$ lies on the x_1-axis (streamwise direction), then $r_1 = |\mathbf{r}|$ and $r_2 = r_3 = 0$. So:

$$Q_{11} \;=\; r^2 A(r) + B(r) = \overline{u_1^2} f(r) \;=\; \text{longitudinal correlation}$$

$$\text{and} \quad Q_{22} \;=\; 0 \cdot A(r) + B(r) \;=\; \overline{u_1^2} g(r) \;=\; \text{lateral correlation}$$

Note that

$$f(r) \;=\; \overline{(u_1)_A (u_1)_B}$$

$$g(r) \;=\; \overline{(u_2)_A (u_2)_B}$$

Hence

$$A(r) = \frac{1}{r^2}\overline{u_1^2}(f(r) - g(r))$$

$$B(r) = \overline{u_1^2}g(r)$$

And so equation 10.2 becomes (in this case):

$$Q_{ij} = \overline{u_1^2}\left[\frac{r_i r_j}{r^2}(f - g) + \delta_{ij}g\right] \tag{10.3}$$

We can find a relationship between f and g by considering the derivatives of R_{ij}. Now:

$$Q_{ij} = \overline{u_i(0)u_j(r)}$$

$$\frac{\partial Q_{ij}}{\partial x_j} = \left.\frac{\partial \overline{u_i(0)u_j(r)}}{\partial x_j}\right|_r$$

$$= \overline{u_i(0)\frac{\partial u_j(r)}{\partial x_j}}\bigg|_r + \overline{u_j(r)\frac{\partial u_i(0)}{\partial x_j}}\bigg|_r$$

The first term on the right is zero by continuity, and the second term is zero since $u_i(0)$ must be independent of the gradient at r. Hence

$$\frac{\partial Q_{ij}}{\partial x_j} = \frac{\partial Q_{ij}}{\partial r_j} = 0$$

and from equation 10.3 (see Hinze p. 185):

$$\frac{1}{\overline{u_1^2}}\frac{\partial Q_{ij}}{\partial r_j} = \frac{\partial}{\partial r_j}\left[\frac{r_i r_j}{r^2}(f - g) + \delta_{ij}g\right]$$

That is,

$$\frac{1}{\overline{u_1^2}}\frac{\partial Q_{ij}}{\partial r_j} = \frac{3(f - g)}{r^2}r_i + \frac{(f - g)}{r^2}\delta_{ij} - \frac{2(f - g)}{r^3}\frac{r_j r_j}{r^2}r_i$$

$$+ \frac{1}{r^3}\left(\frac{df}{dr} - \frac{dg}{dr}\right)r_j r_j r_i + \delta_{ij}\frac{r_j}{r}\frac{dg}{dr} = 0$$

Hence

$$f(r) + \frac{r}{2}\frac{df}{dr} = g(r) \tag{10.4}$$
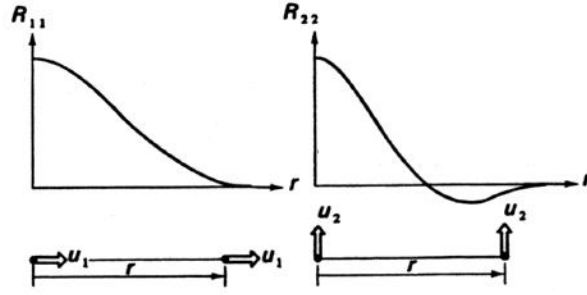
Figure 10.4: Longitudinal (R_{11}) and lateral (R_{22}) correlations.

and we have obtained a relationship between the lateral and longitudinal correlations, which results basically from the continuity equation for incompressible flow.

Now f and g are even functions of r. Expanding f and g in a series expansion for small separations we obtain:

$$f(r) = 1 + \frac{r^2}{2!} \left.\frac{\partial^2 f}{\partial r^2}\right|_{r=0} + \cdots$$

$$g(r) = 1 + \frac{r^2}{2!} \left.\frac{\partial^2 g}{\partial r^2}\right|_{r=0} + \cdots$$

Together with equation 7.2.3, we obtain (Hinze p.188):

$$\left.\frac{\partial^2 g}{\partial r^2}\right|_{r=0} = 2 \left.\frac{\partial^2 f}{\partial r^2}\right|_{r=0}$$

Therefore:

$$\lambda_f^2 = 2\lambda_g^2 \tag{10.5}$$

It is now possible to express Q_{ij} in terms of one scalar only:

$$\frac{Q_{ij}}{\overline{u_1^2}} = -\frac{r_i r_j}{2r}\frac{df}{dr} + \delta_{ij}\left(f + \frac{r}{2}\frac{df}{dr}\right) \tag{10.6}$$

Note that $Q_{ij}(r) = 0$ if $i = j$ and $R_{22} = R_{33}$ by symmetry, and f and g are even functions of r. So:

$$\frac{Q_{ij}(\mathbf{r})}{\overline{u_1^2}} = \begin{bmatrix} f(r) & 0 & 0 \\ 0 & g(r) & 0 \\ 0 & 0 & g(r) \end{bmatrix}$$

(see also figures 10.5, 10.6 and 10.7).
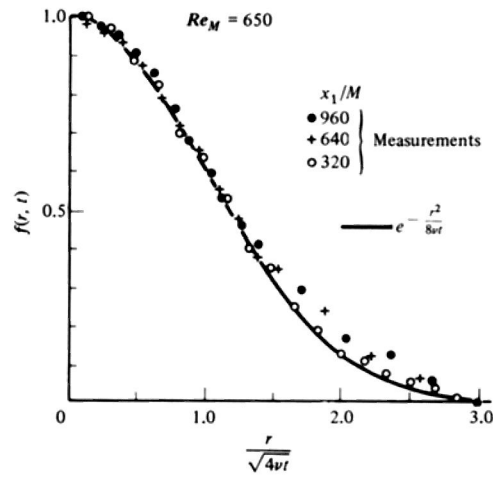
Figure 10.5: Longitudinal correlation coefficient in the final period ($UM/\nu = 650$). From Batchelor & Townsend, 1948.
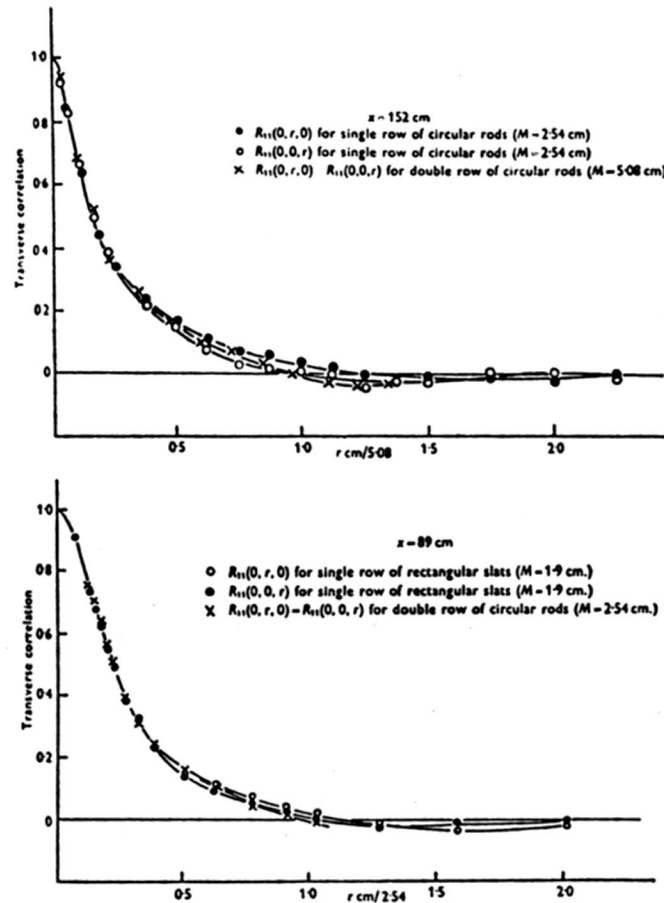
Figure 10.6: Transverse correlations for grids of different shapes. From Stewart & Townsend, 1951.
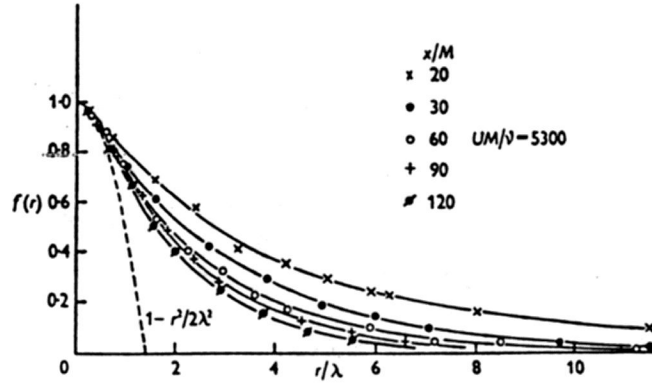
Figure 10.7: Correlation function at different stags of decay. From Stewart & Townsend, 1951.
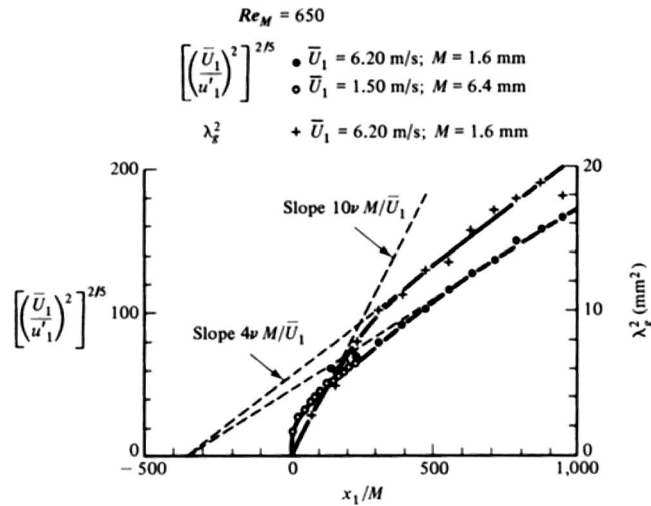
Figure 10.8: Decay of energy in the final period (UM/ν = 650). From Batchelor & Townsend, 1948.

10.3   Decay of Turbulence

The decay of turbulence has often been studied by forming an equation for the double correlations, called the Kármán-Howarth equation. To derive this equation, assume the mean velocity U_i is constant, put $U_i^A = U_{iA} + u_{iA}$ at point A and $U_j^B = U_{jB} + u_{jB}$ at point B. Now the Navier-Stokes equation for u_i at A and u_j at B are known. Multiply the $(u_i)_A$ equation by $(u_j)_B$ and vice versa, and add the two equations (see Hinze p.195 for details). In isotropic turbulence:

$$\overline{(u_i)_A(u_k)_B(u_j)_B} = -\overline{(u_k)_A(u_j)_A(u_i)_B}$$

Figure 10.9: Notation for $k(r,t)$.

and

$$\overline{p_A(u_j)_B} = -\overline{p_B(u_i)_A} = 0$$

(this is the only way they can be invariant under reflection). Finally we obtain an equation for the dynamic behavior of isotropic turbulence in terms of the double correlation (the Kármán-Howarth (1938) equation):

$$\frac{\partial}{\partial t}\left(\overline{u_1^2}f\right) - \frac{(\overline{u_1^2})^{3/2}}{r^4}\frac{\partial}{\partial r}\left(r^4 k\right) = 2\nu\frac{\overline{u_1^2}}{r^4}\frac{\partial}{\partial r}\left(r^4\frac{\partial f}{\partial r}\right) \tag{10.7}$$

where $k(r,t)$ is the correlation between two velocity components at one point, and one at another (all in the same direction; see figure 10.9), and

$$h(r,t) = -k(r,t)/2$$

Note that h and k are triple correlations, while f is a double correlation.

Equation 10.7 has more unknowns than equations (not unusual in turbulence theory). However, if we consider conditions where viscous effects dominate, so that the second term in the left of equation 10.7 (the convective term) can be neglected, then:

$$\frac{\partial}{\partial t}\left(\overline{u_1^2}f\right) = 2\nu\frac{\overline{u_1^2}}{r^4}\frac{\partial}{\partial r}\left(r^4\frac{\partial f}{\partial r}\right) \tag{10.8}$$

This is a diffusion equation, with the solution

$$f(r,t) = e^{-r^2/8\nu t} \tag{10.9}$$

This is the decay law for turbulence when viscous effects dominate – called the "final period of decay."

Consider a single point result for $r \to 0$. Now

$$f_{r \to 0} = 1 - \frac{r^2}{2\lambda^2} + \cdots$$

$$\text{where} \quad \lambda^2 = \frac{-1}{\frac{\partial^2 f(0,t)}{\partial r^2}} + \cdots$$

$$\text{Hence} \quad \frac{\partial \overline{u^2}}{\partial t} = -\frac{10\nu\overline{u^2}}{\lambda^2} \tag{10.10}$$

(this is true regardless of f for $r \to 0$; Batchelor, p. 100)

$$\text{Since} \quad f = e^{-r^2/8\nu t}$$

$$\text{and} \quad \frac{1}{\lambda^2} = \left.\frac{\partial^2 f(0,t)}{\partial r^2}\right|_{r=0} = \frac{1}{4\nu t}$$

$$\text{and so} \quad \frac{d\overline{u^2}}{dt} = -\frac{5}{2}\frac{\overline{u^2}}{t}$$

Using Taylors hypothesis we have $t = x/U$, and

$$\left(\frac{U^2}{\overline{u^2}}\right) = C\,(x - x_0) \tag{10.11}$$

where x_0 is the virtual origin. Experimental work supports this conclusion for $x \geq 500M$, where M is the mesh size (see figure 10.8).

Another useful result for isotropic turbulence is that a simple form can be found for the dissipation, where:

$$\varepsilon \equiv \nu \overline{\left(\frac{\partial u_i}{\partial x_j} + \frac{\partial u_j}{\partial x_i}\right)\frac{\partial u_j}{\partial x_i}}$$

We note that $\frac{\partial u_i}{\partial x_j}\frac{\partial u_j}{\partial x_i}$ is small, so that

$$\varepsilon = \nu \overline{\left(\frac{\partial u_i}{\partial x_j}\right)^2}$$

$$\frac{\varepsilon}{\nu} = \overline{\frac{\partial u_i}{\partial x_j}\frac{\partial u_i}{\partial x_j}}$$

$$= \left.\frac{\partial}{\partial x_j}\frac{\partial}{\partial x_j'}\left(\overline{u_i u_i'}\right)\right|_{x \to x'}$$

$$= \left.\frac{\partial}{\partial x_j}\frac{\partial}{\partial x_j'}\overline{u^2}\,R_{ii}\right|_{x \to x'} = \overline{u^2}\left.\frac{\partial}{\partial x_j}\frac{\partial R_{ii}}{\partial x_j}\right|_{r \to 0} = -\overline{u^2}\left.\frac{\partial^2 R_{ii}}{\partial r_j \partial r_j}\right|_{r \to 0}$$

$$\varepsilon = -\nu\overline{u^2}\left(\frac{8}{r}f' + 7f'' + rf'''\right)_{r \to 0}$$

$$= -\nu\overline{u^2}\left(f''(0) + 7f''(0)\right) = 15\nu\,\overline{u^2}f''(0)$$

So, for isotropic, homogeneous turbulence,

$$\varepsilon = 15\nu\,\frac{\overline{u^2}}{\lambda^2} \tag{10.12}$$

Note that this agrees with equation 10.11 in that:

$$\frac{\partial \frac{1}{2}\overline{q^2}}{\partial t} = -\varepsilon = -15\,\frac{\nu\overline{u^2}}{\lambda^2}$$

and since $\overline{q^2} = 3\overline{u^2}$, we obtain:

$$\frac{\partial \overline{u^2}}{\partial t} = -10\,\frac{\nu\overline{u^2}}{\lambda^2}$$

as before.

Note also that in the case of isotropic homogeneous turbulence:

$$\overline{\left(\frac{\partial u_i}{\partial x_j}\right)^2} = \overline{\left(\frac{\partial u_i}{\partial x_j} - \frac{\partial u_j}{\partial x_i}\right)\left(\frac{\partial u_i}{\partial x_j} - \frac{\partial u_j}{\partial x_i}\right)} = \overline{\omega_k \omega_k} \tag{10.13}$$

and therefore the viscous dissipation per unit mass is equal to the viscosity times the mean square of the rate of strain, and to the viscosity times the mean square vorticity (also called *enstrophy*).

10.4 Spectra and the Energy Cascade

An equation in terms of spectral functions instead of correlation functions may be found by taking Fourier transforms of the Kármán-Howarth equation. This gives:

$$\frac{\partial E(k,t)}{\partial t} = -\frac{\partial S(k,t)}{\partial t} - 2\nu k^2\, E(k,t) \tag{10.14}$$

where E is the integrated energy spectrum defined in section 9.5. Specifically, $E = E_{11}$, where

$$E_{ij}(k) = \frac{1}{2} \int_{|\mathbf{k}|=k} \Phi_{ij}(\mathbf{k})\, dS(\mathbf{k})$$

and S is a related Fourier transform of the triple correlations (that is, the spectrum function of $S_{i,i}$ given on p.196, Hinze).

> Term on left: represents the rate of change of energy associated with wave number k.

> First term on right: In considering the Kármán-Howarth equation, the term with the triple correlation may be interpreted as representing a "convective" action in the spread of the double correlation $f(r,t)$. This convective action may be caused by the interaction of eddies of different size. Hence this term represents the interaction of eddies of different wave numbers, thereby transferring energy between wave numbers. Specifically, $\frac{3}{2}S(k,t)$ is the flux of kinetic energy from components of wave number less than k to components of wave number larger than k.
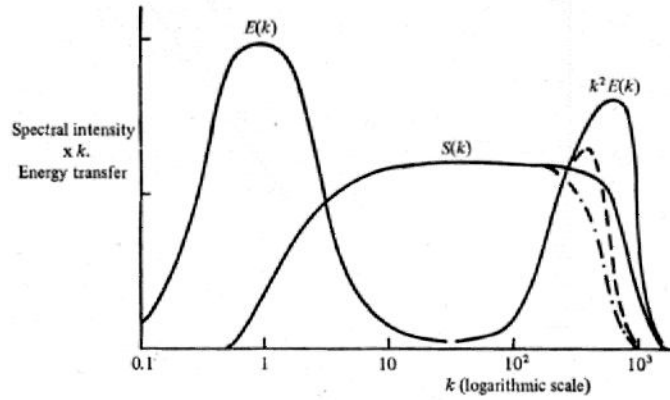
Figure 10.10: Spectral distributions of turbulent intensity, energy transfer and viscous dissipation (the broken curves indicate the effect of an increase of fluid viscosity). From Townsend, 1976.

> Second term on right: represents the viscous dissipation at each wave number k.

The distributions of the kinetic energy, viscous energy dissipation, and energy transfer are shown in figure 10.10 for two Reynolds numbers. The scale of the energy-containing eddies is $1/k_e$, and the scale of the dissipating eddies is $1/k_d$. The viscous dissipation is associated with high wave numbers, that is, small eddies. As Townsend points out, the Fourier components of the small wave number (large size) eddies that contribute most to the energy,

$$\tfrac{1}{2}\overline{q^2} = \tfrac{3}{2}\int_0^\infty E(k)\,dk = \tfrac{3}{2}\int_0^\infty kE(k)\,d(\log k)$$

contribute comparatively little to the viscous dissipation,

$$\varepsilon = 3v\int_0^\infty k^2 E(k)\,dk = 3v\int_0^\infty k^3 E(k)\,d(\log k)$$

(this result is derived in section 10.87). That is, the sizes of the energy-containing eddies are different by orders of magnitude from the sizes of the dissipating eddies. Since $S(k,t)$ transfers energy, we would expect a net transfer from the low wave number (large eddy) to the large wave number (small eddy) end of the spectrum. Energy fed to the turbulence is primarily fed to the large scales (of the order of the scale of the mean velocity gradients, or the mesh size in grid turbulence). From these large eddies, smaller eddies are generated by eddy interactions (see section 10.5), and then still smaller ones, until the eddies are small enough for viscosity to become important (that is, when the Reynolds numbers associated with the eddies is of order unity). We would expect that there is little direct
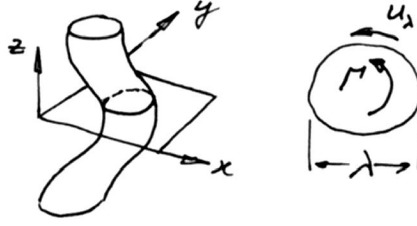
Figure 10.11: A vortex tube in an inviscid flow.
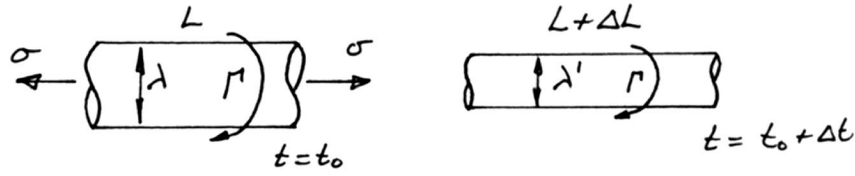
Figure 10.12: A vortex tube stretched by the surrounding strain field.

interaction between large energy-containing eddies and small dissipating ones. Increasing the Reynolds number (say by decreasing the viscosity), only extends this "energy cascade" at the small eddy end. That is, the viscosity just sets the scaleat which the dissipation occurs. The structure of all other scales is independent of Reynolds number — this observation is known as the Reynolds number similarity hypothesis (section 3.5 in Townsend).

10.5 Vortex Stretching and the Energy Cascade

The following notes were adapted from the lecture notes used by Professor T. Wei at Rutgers, who in turn adapted them from lecture notes used by Professor W. Wilmarth at Michigan.

Consider a vortex tube in an inviscid flow (figure 10.11). The vortex tube has circulation Γ, a characteristic diameter λ and velocity u_λ. Hence $\Gamma \propto u_\lambda \lambda$.

If this tube is being stretched by the surrounding strain field (figure 10.12), the length increases but Γ is conserved (note that in a viscous fluid, $\omega(r)$ will be different — see section 8.6). The strain rate

$$\sigma = \frac{1}{\Delta t} \frac{\Delta L}{L} = \frac{1}{L} \frac{dL}{dt}$$

Since the volume of the tube will be constant in an incompressible inviscid flow,

$$L \propto \frac{\text{volume}}{\lambda^2}$$
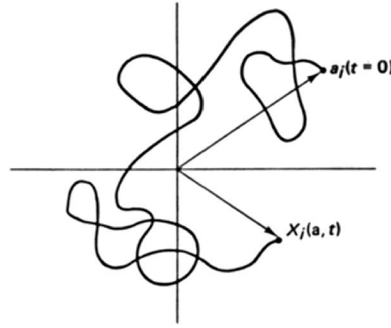
Figure 10.13: The motion of a wandering point.

and

$$\frac{dL}{dt} \propto -\frac{\text{volume}}{\lambda^3} \frac{d\lambda}{dt}$$

so that

$$\sigma = \frac{1}{L}\frac{dL}{dt} \propto -\frac{1}{\lambda}\frac{d\lambda}{dt}$$

So a positive strain rate will decrease the characteristic scale (and by implication increase the characteristic wave number). The concept of random walk implies that stretching will be statistically more likely than compression. The theory states that a particle subjected to random impulses will, on the average, increase its distance from its starting point. Hence, as Bradshaw observes, the distance between two particles will, on the average, increase. If those two particles are situated at the ends of a given element of vortex line, then, in a flow field approximating to random disturbances, the length of the element will on the average increase.

What happens to the kinetic energy? Now:

$$\text{KE} \propto (u_\lambda)^2 \propto \omega^2\lambda^2 \propto \frac{\Gamma^2}{\lambda^2}$$

and therefore, as the scale decreases, the kinetic energy goes up. In other words, vortex stretching is a means of transferring energy from the surrounding strain field (set up primarily by eddies with scales much larger than λ) to eddies which are smaller in scale than λ. That is, on the average vortex stretching transfers energy from low wavenumbers (large λ) to higher wavenumbers (small λ).

Consider the rate of kinetic energy transferred among wave numbers, that is, the kinetic energy flux ε_λ at a given wave number:

$$\varepsilon_\lambda \propto \frac{u_\lambda^2}{\tau} \propto \frac{u_\lambda^3}{\lambda}$$

Since energy is supplied from the large eddies (where the size of largest eddies depend on the mesh size, or shear layer thickness, or pipe diameter),

the rate of energy input depends on the characteristic velocity and length scales of the largest eddies (say U and δ). Hence,

$$\frac{u_\lambda^3}{\lambda} \propto \frac{U^3}{\delta}$$

That is,

$$u_\lambda \propto U \left(\frac{\lambda}{\delta}\right)^{1/3}$$

or

$$\mathrm{Re}_\lambda = \frac{u_\lambda \lambda}{\nu} \propto \frac{U\delta}{\nu} \left(\frac{\lambda}{\delta}\right)^{4/3} = \mathrm{Re}_\delta \left(\frac{\lambda}{\delta}\right)^{4/3}$$

The energy transfer process is inviscid as long as $\mathrm{Re}_\delta \gg 1$. For $\mathrm{Re}_\lambda O(1)$, viscous dissipation will become important. If the length scale for the dissipative scales is λ_v, then:

$$\lambda_v \propto \delta \, (\mathrm{Re}_\delta)^{-3/4}$$

(λ_v is the Kolmogorov scale, usually denoted by η).

10.5.1   The energy transfer process

If we consider the vorticity field to be made up of a mean vorticity and a fluctuating vorticity then we can see that two processes control the vortex stretching — random walk and the presence of a mean shear. The energy of the stretched vortex line increases and this must be extracted from the velocity field which does the stretching, in particular, the strain field that is present. Now it seems reasonable that an eddy of a given scale can only interact with an eddy of comparable scale and that the greater the difference between two eddy length scales the smaller their interaction will be: to a small eddy, the strain rate due to a neighboring much larger eddy will have little effect since the net change in velocity across the small scale eddy is comparatively small. So large eddies will feel the effect of the mean shear most directly and therefore will have forms which depend on the nature of the shear. The small eddies, formed by vortex stretching down to smaller and smaller sizes eventually lose all influence of the boundary conditions that affected their parents and are therefore held to be in some sense universal. That is, since the vortex-stretching process is essentially random (and three-dimensional) it does not tend to transmit directional preferences.

To summarize, if an element of fluid has rotation and it is subject to a strain rate in the z-direction $\partial W/\partial z$ then the element will be stretched in the z direction and its cross-section will get smaller in the x-y plane. If angular momentum is conserved then $\omega r^2 = $ constant, and when r decreases ω must increase. This means that the kinetic energy $\omega^2 r^2$ must increase. This energy must come from the flow field that does the stretching.
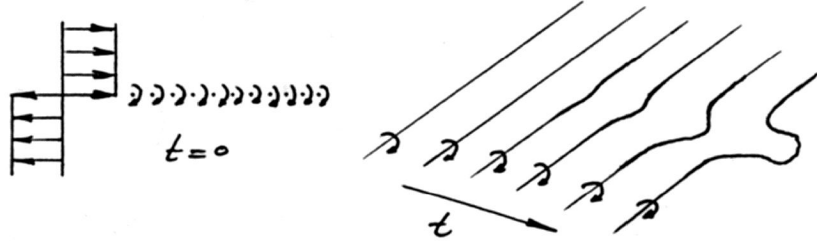
Figure 10.14: Three-dimensional perturbation in a vortex sheet.

Thus an extension in one direction decreases the length scales and increases the velocity components in the other two directions, which in turn stretch other elements of fluid with vorticity components in these directions, and so on. If the viscosity is negligible this distortion and spreading of length scales would go on indefinitely. The lower limit of the motions that survive will therefore depend on the Reynolds number, and the spread of scales increases with Reynolds number.

10.5.2   How does this get started?

Even if we started with a field where there was no stretching whatsoever going on then the smallest disturbance will produce a kink in a vortex line. If the Reynolds number is high enough so that viscous damping is not important then this disturbance will grow under its own induced velocity field (figure 10.14.

10.5.3   How does it continue?

A single disturbance will set up its own velocity field which interacts with other vortex lines and so on. General spatial and temporal unsteadiness, which needs to be only very small, depending on the Reynolds number, eventually produces a "continuous" distribution of length and frequency scales. Note that the strain field which maintains vortex stretching may be thought of as the resultant strain set up by the induced velocity fields of the surrounding motions.

So there is an energy cascade from δ down to λ_v. For $\delta > \lambda \gg \lambda_v$, the energy transfer is inviscid (inertial), and the rate is governed by

$$\varepsilon_\delta = \varepsilon_\lambda = \varepsilon_{\lambda_v} \ \rightarrow \ \text{heat}$$

and ε_{λ_v} is fixed by U and δ:

$$\frac{U^3}{\delta} = \frac{u_{\lambda_v}^3}{\lambda_v} = \text{dissipation rate.}$$
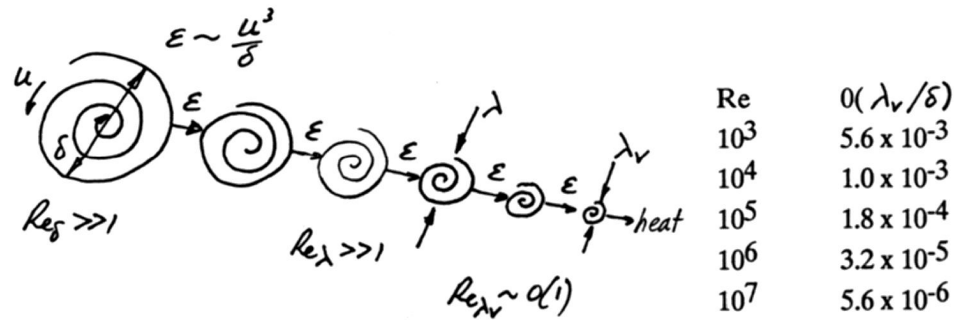
Figure 10.15: The energy cascade and the scale of the smallest motions.

As we stated before, the role of viscosity is to fix the scale λ_v at which the dissipation occurs (figure 10.15.

10.6   Isotropicity of the Small Scales

It is often argued that the small eddies, formed by vortex stretching down to smaller and smaller sizes, will eventually lose all influence of the boundary conditions that affected their parents and are therefore held to be in some sense universal. That is, since the vortex-stretching process is essentially random (and three-dimensional) it does not tend to transmit directional preferences. This argument is often used to justify the modelling of the small scales as an isotropic field, even when the energy containing eddies are neither homogeneous nor isotropic.

Now there are several objections to the notion that the small scale eddies are isotropic (see Bradshaw *Turbulence*):

1. Energy production varies across shear layer and therefore the intensity of the small eddies is likely to do likewise;

2. The instantaneous rate of energy transfer to the small eddies varies with time and space; and

3. Averaging the instantaneous intensity of the small scale motions over periods larger than typical time scales of smallest eddies but shorter than those of the large eddies will also vary with space and time.

10.7   The Initial Period of Decay

By physical arguments we can say that, for isotropic homogeneous turbulence, the initial period of decay ($x > 20M$) is dominated by the decay of

the energy containing eddies — there is a drain of energy from those eddies through inertial interactions towards the small eddies in the dissipation wave number range. Now a model for the dissipation may be given from our previous consideration (as long as $\lambda \gg \lambda_v$):

$$\varepsilon = \frac{u_\lambda^3}{\lambda} = \frac{q^3}{\Lambda}$$

where Λ is some macro-scale, and q is the velocity scale of the energy-containing eddies. The turbulent kinetic energy equation reduces to

$$\frac{d}{dt}\left(\tfrac{1}{2}\overline{q^2}\right) = -\frac{q^3}{\Lambda}$$

and by using Taylor's hypothesis:

$$U\frac{d}{dx}\left(\tfrac{1}{2}q^2\right) = -\frac{q^3}{\Lambda}$$

A similarity solution may be found for $q^2 = ax^n$, $\Lambda = bx^m$, and we find that $n = -1$, and $m = \tfrac{1}{2}$. Hence:

$$q^2 \; \propto \; \frac{1}{x} \tag{10.15}$$

$$\Lambda \; \propto \; \sqrt{x} \tag{10.16}$$

This is the initial period of decay law (see Batchelor *Homogeneous Turbulence* (1953) and Dickey & Mellor JFM Vol. 99, pp. 13-31 (1980)). Some experimental results are shown in figure 10.16. Note also that $q\Lambda/v = $ constant, that is, the turbulence decays so that the large-scale Reynolds number stays constant.

10.8   Kolmogorov Hypothesis

Inertial actions do not change the energy, they just move it from one place to another. But we expect on the basis of the previous discussion that strong interactions can occur only among wavenumbers with approximately similar wavenumbers (perhaps within an order of magnitude). This is so because the strain rates or velocity gradients associated with one eddy must have significant values over the size of the eddy it interacts with. We can divide the spectrum into three ranges: the production range (low wavenumber), the inertial range (intermediate wavenumber — here little production or dissipation takes place), and the dissipation range (high wavenumber).
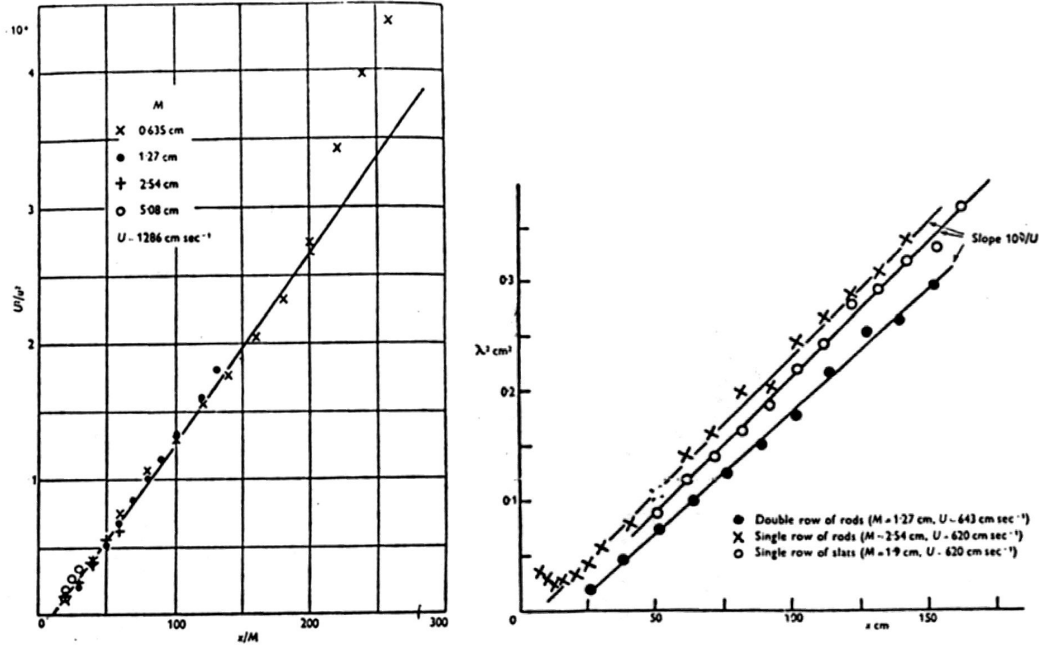
Figure 10.16: Left: Decay of energy during and beyond the initial period (after Batchelor & Townsend, 1948a). Right: Variation of λ^2 during the initial period (after Batchelor & Townsend, 1948a; and Stewart & Townsend, 1951).

If this hypothesis is correct, these wavenumber ranges are virtually independent. So the only effect of the production range on the higher wavenumber part of the spectrum is to determine the total rate of production of turbulent energy, and if the field is stationary than the rate of production = rate of dissipation ε. Therefore, the spectrum in the range where k is large enough to be independent of production can depend, at a given k, only on ε and ν. That is:

$$E = E(k, \nu, \varepsilon) \qquad (= \text{power per unit mass per wavenumber})$$

$$[E] = \frac{L^3}{T^2}, \qquad [\varepsilon] = \frac{L^2}{T^3}, \qquad [\nu] = \frac{L^2}{T}, \qquad [k] = \frac{1}{L}$$

But in the inertial subrange, the energy should be independent of ν. Hence, by dimensional analysis,

$$\frac{E(k)}{\varepsilon^{2/3} k^{-5/3}} = K_0 = \text{Kolmogorov constant} \approx 1.44$$

That is,

$$E(k) = K_0 \, \varepsilon^{2/3} \, k^{-5/3} \tag{10.17}$$

This famous result is known as the Kolmogorov (1941) -5/3 law. Experiment lends much support for this -5/3 behavior.

Further, in the dissipating range, we find

$$\frac{E(k)}{\varepsilon^{2/3}k^{-5/3}} = K\left(\nu^{3/4}\varepsilon^{-1/4}k\right) \tag{10.18}$$

We thus have the Kolmogorov microscales which describe the characteristics of the dissipating eddies:

$$\boxed{\eta \;(= \lambda_v) = \left(\tfrac{\nu^3}{\varepsilon}\right)^{1/4}, \qquad \tau_K = \left(\tfrac{\nu}{\varepsilon}\right)^{1/2}, \qquad \upsilon = (\nu\varepsilon)^{1/4}} \tag{10.19}$$

Note that the Reynolds number formed with these quantities is unity:

$$\frac{\eta\upsilon}{\nu} = 1$$

Now $E(k)$ (actually E_{ii}) is the three-dimensional integrated energy spectrum function. There is, however, no known way of measuring E_{ii} directly, but for isotropic flow it is related to the one-dimensional spectrum function $\Phi_{11}(k_1)$ by the relation:

$$E_{11}(k_1) = k_1^2\,\frac{\partial^2\Phi_{11}(k_1)}{\partial k_1^2} - k_1\,\frac{\partial\Phi_{11}(k_1)}{\partial k_1}$$

(Hinze 1959). If E_{ii} exhibits a power law relationship with wave number then the (measurable) one-dimensional spectrum function $\Phi(k_1)$ also follows the same power law relationship. Hence the "inertial subrange" defined by equation 10.17 for $E(k)$ would be evident from measurements of $\Phi(k_1)$. In fact, what is most often measured in the frequency spectrum $\Phi(\omega)$, and k_1 is found by $k_1 =$ frequency/mean velocity. Strictly, we should not use the mean velocity but the phase velocity associated with the particular wave number. This issue is discussed extensively by Perry & Abell (1977).

The dimensional reasoning that led to equations 10.17 and 10.18 has been criticized by many workers on the basis of the conceptual difficulties of a fluctuating energy dissipation rate ε being independent of the low wavenumber range (see for example Landau & Lifshitz 1959, Oboukhov 1962, Corrsin 1962, and Kraichnan 1974, and also section 10.10). However, the experimental evidence for the existence of an inertial subrange is extensive, and perhaps the best example is provided by Grant *et al.* (1962, JFM), obtained in a tidal channel (figure 10.17). See also the results obtained by Gurvich *et al.* (1967) in the atmospheric boundary layer (figure 10.18). (Note that in laboratory flows, the wavenumber span of the inertial subrange is often very small, due to the low turbulence Reynolds numbers encountered. See figure 10.19.)
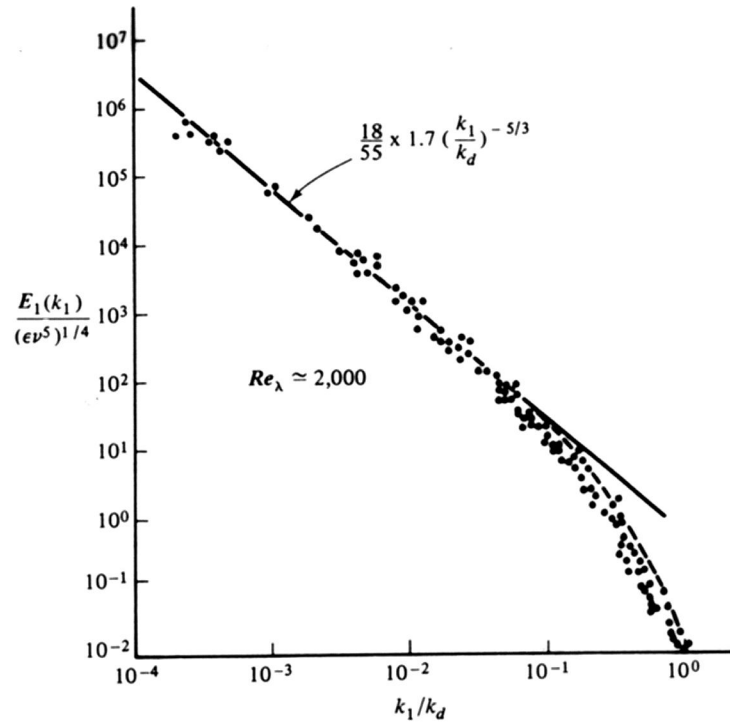
Figure 10.17: One-dimensional energy spectrum obtained in a tidal current. ——
computed according to Pao. From Grant & Stewart.
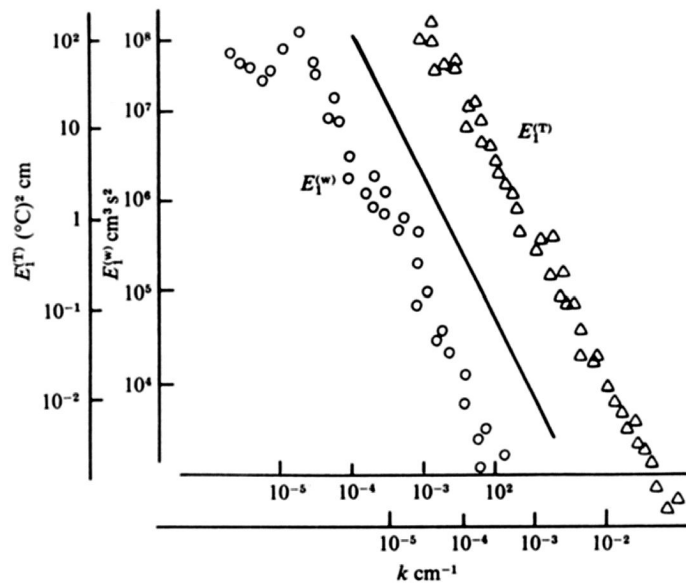
Figure 10.18: Spectra for temperature and vertical velocity fluctuations obtained
from measurements from aircraft and from a tower. From Gurvich *et al.* (1967).
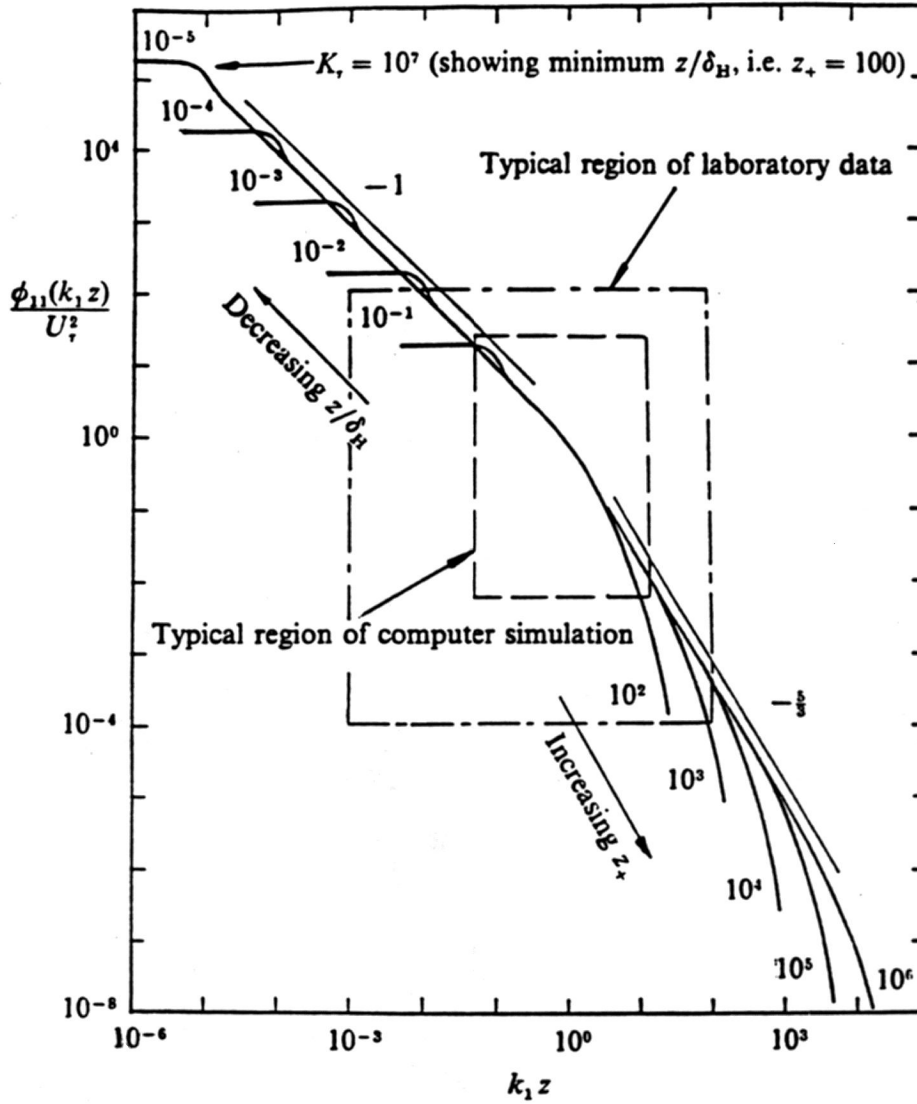
Figure 10.19: Power spectral density of the streamwise velocity fluctuations in the logarithmic law of the wall region of a turbulent boundary layer conjectured from recent similarity proposals. Here z = distance from the wall, k_1 is the streamwise wavenumber, and δ_H is the boundary layer thickness. From Perry.

10.9   Form of the Spectrum in the Dissipation Range

In the dissipation range we have

$$\frac{E(k)}{\varepsilon^{2/3}k^{-5/3}} = K\left(\nu^{3/4}\varepsilon^{-1/4}k\right) = K\left(k\eta\right)$$

(equation 10.18) but dimensional analysis does not say anything about the form of the function K. Suppose that for wavenumbers greater than the

energy containing range we have stationary turbulence. Then equation 10.14 becomes

$$\frac{dS(k)}{dk} = -2\nu k^2 E(k) \tag{10.20}$$

In the inertial range where viscous action is negligible, $S \approx$ constant and must equal $-\varepsilon$, since energy is transferred through the inertial range by inviscid interactions. Hence

$$\varepsilon = \int_0^\infty 2\nu k^2 E(k)\, dk \tag{10.21}$$

This is a useful way to measure the dissipation (if the probe has sufficient spatial resolution).

Now, to obtain a form for the function K, suppose that we could write that in the equilibrium range S is proportional to E (Pao, Physics of Fluids, 1965):

$$E = E(\varepsilon, k.\nu) = -\sigma\, S(\varepsilon, k, \nu)$$

where σ is the rate at which the energy is being transported through a cascade process across the wave number range. Now σ is unknown. However, in the inertial subrange

$$E = E(\varepsilon, k) = K_0\, \varepsilon^{2/3} k^{-5/3}$$

and $S \approx -\varepsilon$. So we obtain that (with $\sigma = E/\varepsilon$)

$$\sigma = \sigma(\varepsilon, k) = K_0 \varepsilon^{-1/3} k^{-5/3}$$

Pao postulated that σ was independent of ν over the entire wave number range, and would apply also in the dissipation range. Hence

$$\frac{dS}{dk} = -\nu K_0\, \varepsilon^{-1/3} k^{1/3} S$$

That is,

$$S = -\varepsilon\, \exp\left(-\frac{3}{2}K_0\left(\frac{\nu^3 k^4}{\varepsilon}\right)^{1/3}\right) = -\varepsilon\, \exp\left(-\frac{3}{2}K_0\,(k\eta)^{4/3}\right)$$

Finally

$$E = K_0\, \varepsilon^{2/3} k^{-5/3}\, \exp\left(-\frac{3}{2}K_0\,(k\eta)^{4/3}\right) \tag{10.22}$$

and

$$K = K_0\, \exp\left(-\frac{3}{2}K_0\,(k\eta)^{4/3}\right)$$

Equation 10.22 is called Pao's form of the dissipation spectrum. For some comparisons with experimental data see figures 10.17 and 10.20.
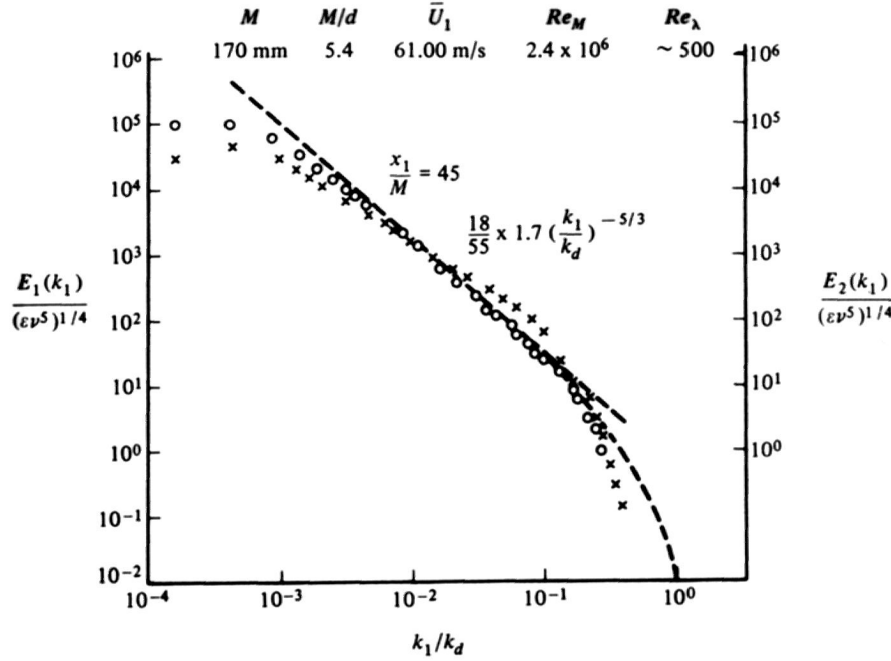
Figure 10.20: One-dimensional energy spectrum $E_1(k_{11}$ (○○○○), and $E_2(k_{11}$ (××××).
—— computed according to Pao. After Kistler & Vrebalovich.

10.10   The Decay of Isotropic Turbulence: Summary

As time goes on, we see that the energy containing motions (low wavenumbers) decay as their energy is drained by inertial interactions towards the high wavenumber dissipation range. In terms of the spectrum, there would be a range of wavenumbers in which the spectral amplitudes would remain invariant with time — the universal equilibrium range (see figure 10.21).

At later times, however, the energy transfer from the large eddies to the small eddies decreases (the energy-containing eddies have been depleted). Then, since the small eddies are no longer receiving energy to sustain them, they begin to disappear, and the small eddies will decay faster than the very weak large scales that remain. The dissipation rate decreases and the dissipating eddies get larger as the smallest scales continue to disappear:

$$\frac{1}{k_d} \propto \left(\frac{\nu^3}{\varepsilon}\right)^{1/4} , \text{ and since } \varepsilon \downarrow, \frac{1}{k} \uparrow, \text{ and } \lambda \downarrow$$

Finally, the intensity and the dissipation rate sink to such low levels that the energy in the largest eddies becomes relatively important: this is turbulence of very low Reynolds number and it is governed by viscous effects — this is the final period of decay.
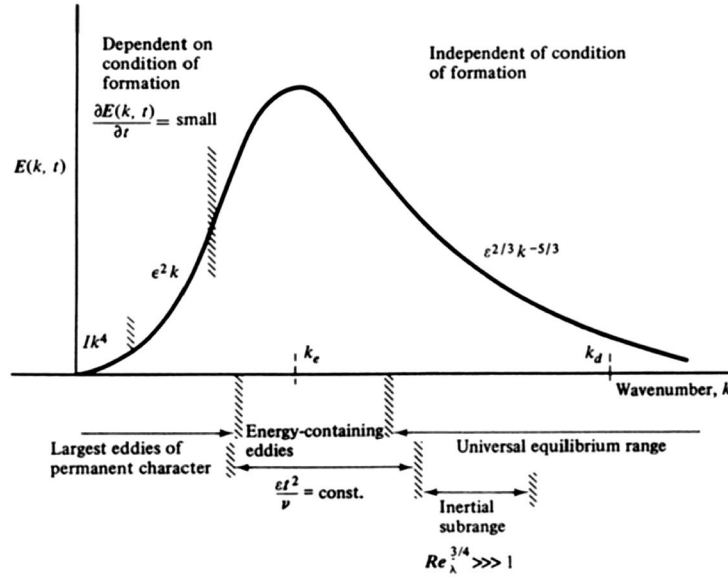
Figure 10.21: Form of the three-dimensional energy spectrum Ek, t in the various wavenumber ranges. Townsend, or Hinze.

So, curiously, we see that in the initial period of decay the energy containing motions increase their scale, and that in the final period of decay it is the large scales that are last to die because the small scales dissipate more rapidly (it looks a bit like an energy transfer from small scales to large but of course it is not).

10.11 Isotropicity in the Dissipation Range: The Concept of Local Isotropy

The vortex-stretching "cascade" process, being essentially random and three-dimensional, tends not to transmit directional preferences from large scales to small scales. Therefore motions at scales many times smaller than those of the main energy containing motions tend to be statistically isotropic. This notion is often applied even in inhomogeneous flows, and it is called the concept of "local isotropy."

Now there are several objections to the notion that the small scale eddies are isotropic (Bradshaw, *Turbulence*):

1. Energy production varies across shear layer hence intensity of small eddies likely to do likewise;

2. Instantaneous rate of energy transfer to the small eddies varies with time and space; and
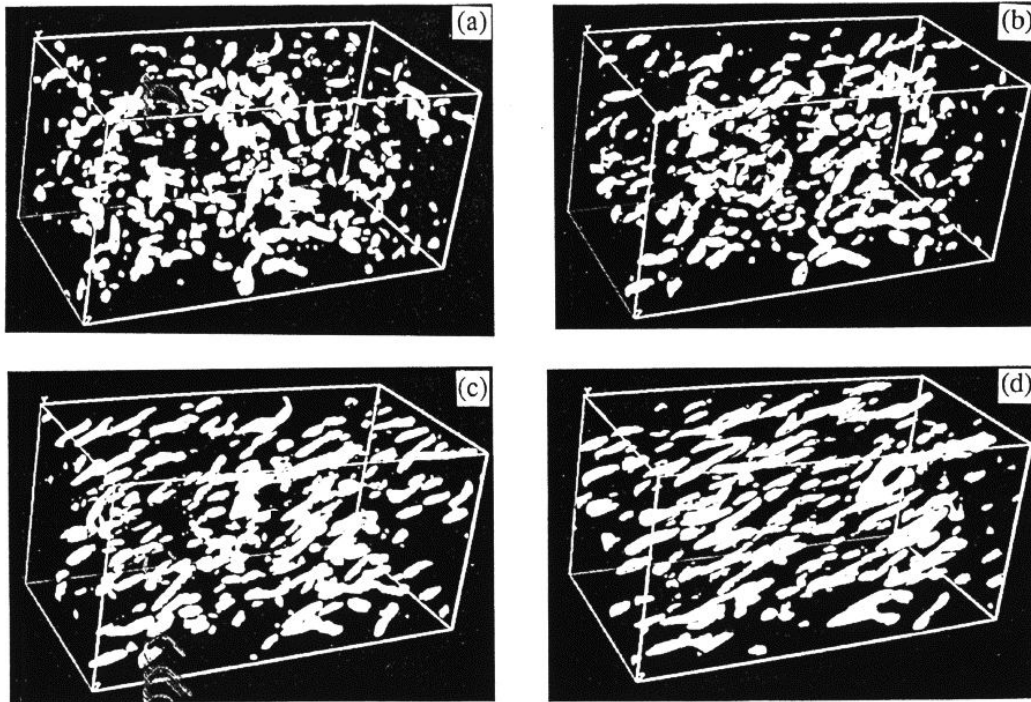
Figure 10.22: 3-D iso-contours for wavelet transformed enstrophy field. The peak in the wavelet filter is aligned with the peak in the dissipation rate spectrum, $k = 10$. The contour level is 2.5 times the r.m.s. value of the wavelet coefficients at that time step. (a) $St = 0.0$, (a) $St = 0.325$, (a) $St = 0.65$, (a) $St = 1.0$. Brasseur & Wang, Physics of Fluids, 1992.

3. Averaging the instantaneous intensity of the small scale motions over periods larger than typical time scales of smallest eddies but shorter than those of the large eddies will also vary with space and time.

In fact, simulations of homogeneous isotropic turbulence indicate that the regions of the flow where dissipation is high (where vorticity fluctuations are high) are dominated by rod-like structures of random orientation, where the diameter scales with η but the length can be many orders of magnitude larger (see figure 10.22). When this flow is subjected to a mean shear, then rods line-up in a preferred direction which depends on the mean strain rate (see figure 10.22 again), and therefore it can be argued that the dissipating structures will reflect the influence of the large scales, as well as the history of the strain field. For a full discussion see Brasseur (AIAA Paper 91-0230), Rogers *et al.* (Report TF25, Dept. Mech. Eng., Stanford 1986), and Rogallo (NASA TM 81315, 1981).

10.12 Summary

1. The two-point correlation tensor R_{ij} may be written in terms of a single correlation function $f(r)$

2. Using the Kármán-Howarth equation, we find that in the final period of decay, $f = \exp(-r^2/8\nu t)$.

3. $\varepsilon = 15\nu \overline{u^2} \frac{1}{\lambda^2}$

4. By taking the Fourier transform of the Kármán-Howarth equation, we see (at high enough reynolds number) the distinction between the energy-containing wavenumber range and the dissipation wavenumber range, and the presence of a wavnemuber range where energy is transferred inertially from lower to higher wavenumbers.

5. Kolmogorov (1941) proposed the "energy cascade," where

   (a) inertial transfer of energy from lower to higher wavenumbers (independent of ν)

   (b) The rate of energy transfer = rate of dissipation, and
   $$\varepsilon = \frac{q^3}{\Lambda}$$

   (c) Using the turbulent kinetic energy equation, we find a imilarity solution where
   $$q^2 \propto x^{-1} \quad \text{and} \quad \Lambda \propto \sqrt{x}$$

   (d) The transfer mechanism is vortex stretching

6. $\eta = \left(\frac{\nu^3}{\varepsilon}\right)^{1/4} \qquad \upsilon = (\nu\varepsilon)^{1/4}$

7. The wavenumber range that encompasses the inertial transfer region (the "inertial subrange") and the dissipation region is called the "universal equilibrium" range. It is often described as a region of "local isotropy."

8. By dimensional analysis in the "universal equilibrium" range
   $$\frac{E(k)}{\varepsilon^{2/3}k^{-5/3}} = K(k\eta)$$
   .

9. In the inertail subrange,
   $$E(k) = K_0 \varepsilon^{2/3} k^{-5/3}$$
   .

10. $\varepsilon' \gg \overline{\varepsilon}$

Chapter 11

Turbulent Shear Flows

In the logical progression of topics, we should now consider sheared homogeneous turbulence, then turbulent free shear flows (mixing layers, jets, wakes), and finally wall-bounded flows. However, it may actually be more instructive to move on to wall-bounded flows before considering other flows, particularly when some wall-bounded flows offer a certain degree of simplification. Such flows are "fully-developed" flows, such as pipe and channel flow sufficiently far downstream from the entrance, and turbulent Couette flow.

11.1   Channel Flow

Here we consider fully-developed, turbulent, two-dimensional channel flow. Fully developed flow means that the flow is statistically stationary (the pressure driving the flow is steady) and homogeneous in the downstream direction (x-direction in figure 11.1.   Hence $\partial \mathbf{V}/\partial x = 0$.   The boundary conditions are the no-slip conditions, so that on the top and bottom walls $U = V = W = 0$, and $u' = v' = w' = 0$.   From the the continuity equation (equation 7.5), we see that $V = 0$ everywhere.   Also, since the flow is two-dimensional, $W = 0$ everywhere, and $\overline{w'v'} = 0$.

From the mean flow Reynolds-averaged equations (equations 7.8 to 7.10):

$$\text{(x-momentum)} \quad 0 \;=\; -\frac{1}{\rho}\frac{\partial p}{\partial x} - \frac{\partial \overline{u'v'}}{\partial y} + \nu\frac{\partial^2 \bar{U}}{\partial y^2} \qquad (11.1)$$

$$\text{(y-momentum)} \quad 0 \;=\; -\frac{1}{\rho}\frac{\partial p}{\partial y} - \frac{\partial \overline{v'^2}}{\partial y} \qquad (11.2)$$

$$\text{(z-momentum)} \quad 0 \;=\; -\frac{1}{\rho}\frac{\partial p}{\partial z} \qquad (11.3)$$
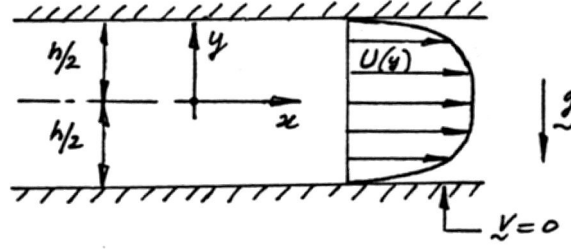
Figure 11.1: Notation for fully-developed turbulent, two-dimensional channel flow.

Integrate equation 11.2:

$$\frac{p}{\rho} = -\overline{v'^2} + \frac{p_w(x)}{\rho} \tag{11.4}$$

Substitute for the pressure in equation 11.1:

$$\frac{\partial}{\partial y}\left(-\overline{u'v'} + v\frac{\partial \bar{U}}{\partial y}\right) = \frac{1}{\rho}\frac{dp_w}{dx} + \frac{\partial\left(-\overline{v'^2}\right)}{\partial x}$$

Therefore

$$\tau_T \equiv -\overline{u'v'} + v\frac{\partial \bar{U}}{\partial y} = \frac{1}{\rho}\frac{dp_w}{dx}y + F(x)$$

because $\partial\left(-\overline{v'^2}\right)/\partial x = 0$ from streamwise homogeneity. Here, τ_T is the "total" stress, being the sum of the Reynolds shear stress and the viscous stress. From symmetry:

$$\left(\frac{\partial \bar{U}}{\partial y}\right)_{h/2} = -\left(\frac{\partial \bar{U}}{\partial y}\right)_{-h/2}$$

and so $F(x) = 0$, and:

$$-\overline{u'v'} + v\frac{\partial \bar{U}}{\partial y} = \frac{1}{\rho}\frac{dp_w}{dx}y = \text{constant} \times y \tag{11.5}$$

at a given x. Data indicate that $dp/dx < 0$. The stress distribution is illustrated in figure 11.2. Note that:

$$\frac{\tau_w}{\rho} = u_\tau^2 = \frac{\left(S_{xy}\right)_w}{\rho} = v\left(\frac{\partial \bar{U}}{\partial y}\right)_{-h/2}$$

If we consider the integral form of the momentum equation (x-component only, see Figure 37):
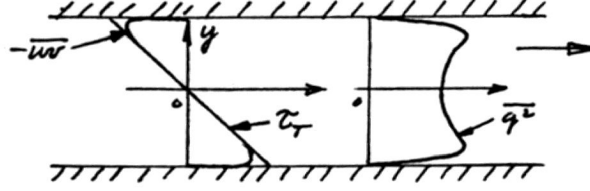
Figure 11.2: Stress and turbulent kinetic energy distributions in fully-developed turbulent, two-dimensional channel flow.
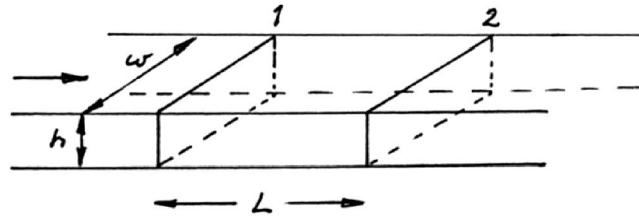
Figure 11.3: Fixed control volume for fully-developed turbulent, two-dimensional channel flow.

$$\int (\mathbf{n} \cdot \rho\mathbf{V})\,\mathbf{V}dA \; = \; \int \mathbf{n}pdA \quad + \quad \mathbf{F_v}$$

$$\underbrace{\phantom{\int (\mathbf{n} \cdot \rho\mathbf{V})\,\mathbf{V}dA}}_{\substack{\text{net outflux}\\ \text{of momentum}}} \quad \underbrace{\phantom{\int \mathbf{n}pdA}}_{\substack{\text{resultant force}\\ \text{due to pressure}\\ \text{differences}}} \quad \underbrace{\phantom{\mathbf{F_v}}}_{\substack{\text{net viscous}\\ \text{forces}}}$$

For a fully-developed flow this reduces to:

$$\int \mathbf{n}pdA \; = \; \mathbf{F_v}$$

Since the pressure difference is only a function of x (remember that $p_2 - p_1 = p_{w2} - p_{w2}$):

$$p_1 wh - p_2 wh = \tau_w L\,(2w + 2h)$$

For a two-dimensional flow, the channel width is much greater than the height and:

$$\tau_w = -\frac{h}{2}\frac{dp_w}{dx} \tag{11.6}$$

So that finally:

$$-\overline{uv} + v\frac{d\bar{U}}{dy} = -\frac{\tau_w}{\rho}\frac{2y}{h} \tag{11.7}$$

Now, very near the surface, we expect viscous forces to become dominant because the velocity gradients become very large and $-\overline{uv}$ approaches zero
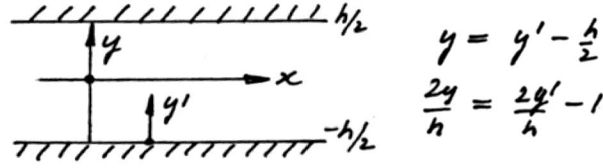
Figure 11.4: Notation for the region near the wall.

as the wall is approached. If y' is measured from the bottom surface, we are concerned with the region where $2y'/h \approx 0$ (see figure 11.4). So for a small region near the wall:

$$\nu \frac{d\bar{U}}{dy'} \approx \frac{\tau_w}{\rho}\left(\frac{2y'}{h} - 1\right) = \frac{\tau_w}{\rho} + \cdots$$

$$\text{Hence} \quad \frac{d\bar{U}}{dy'} = \frac{\tau_w}{\mu} + \ldots$$

$$\text{and} \quad \bar{U} = \frac{\tau_w y'}{\mu} + \ldots$$

which is usually written as

$$\frac{\bar{U}}{u_\tau} = \frac{y' u_\tau}{\nu}. \tag{11.8}$$

Here we have defined a velocity scale u_τ (sometimes called the friction velocity) based on the wall shear stress, so that $u_\tau = \sqrt{\tau_w/\rho}$.

Very near the wall, therefore, the velocity varies linearly with the distance from the wall. Note that the form given in equation 11.8 includes the density although it strictly does not belong in an expression describing a viscous-dominated region. This distinction is only important when considering flows with variable fluid properties, such as boundary layers in supersonic flow.

Experiments show that further out from the wall (where it is still true that $(2y/h - 1) \ll 1$):

$$\bar{U} = fn\left(\frac{\tau_w}{\rho}, \nu, y'\right)$$

so that:

$$\frac{\bar{U}}{u_\tau} = fn\left(\frac{y' u_\tau}{\nu}\right). \tag{11.9}$$

This is sometimes called "the law of the wall" (after Don Coles). With the notation

$$y^+ = \frac{y' u_\tau}{\nu}, \quad \text{and} \quad U^+ = \frac{\bar{U}}{u_\tau},$$
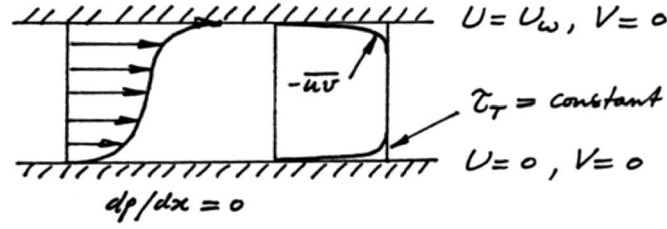
Figure 11.5: Mean flow and stress distributions in fully-developed turbulent, Couette flow.

equation 11.9 may be written as:

$$U^+ = fn\left(y^+\right). \tag{11.10}$$

11.2 Turbulent Couette Flow

Couette flow is the flow that occurs between two parallel, two-dimensional plates when these plates have differing velocities, as will occur when the bottom plate is stationary and the top plate is moving at a constant speed, as shown in figure 11.5. In this case the flow is not driven by a pressure gradient ($dp/dx = 0$) but by the viscous shear on the moving wall. When the flow is fully developed the equation of motion reduces to:

$$-\overline{uv} + v\frac{d\bar{U}}{dy} = -\frac{\tau_w}{\rho} = \text{constant.}$$

11.3 Turbulent Pipe Flow

Turbulent flow is characterized by unsteady eddying motions that are in constant motion with respect to each other. At any point in the flow, the eddies produce fluctuations in the flow velocity and pressure. If we were to measure the streamwise velocity in turbulent pipe flow, we would see a variation in time as shown in figure 11.6. We see that the velocity has a time-averaged value $\langle U \rangle$, defined by

$$\langle U \rangle = \lim_{T \to \infty} \frac{1}{T} \int_t^{t+T} U \, dt$$

and a fluctuating value u', so that $\langle U \rangle$ is not a function of time, but u' is.

The eddies interact with each other as they move around, and they can exchange momentum and energy. For example, an eddy that is near the
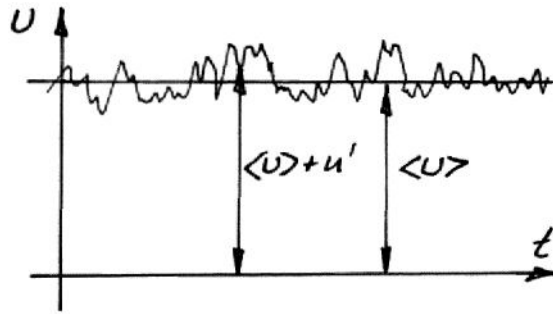
Figure 11.6: Velocity at a point in a turbulent flow as a function of time.

centerline of the pipe (and therefore has a relatively high velocity), may move towards the wall and interact with eddies near the wall (which typically have lower velocities). As they mix, momentum differences are smoothed out. This process is superficially similar to the action of viscosity which tends to smooth out momentum gradients by molecular interactions, and turbulent flows are sometimes said to have an equivalent "eddy" viscosity. Because turbulent mixing is such an effective transport process, the eddy viscosity is typically several orders of magnitude larger than the molecular viscosity.

The important point is that turbulent flows are very effective at mixing: the eddying motions can very quickly transport momentum, energy and heat from one place to another. As a result, velocity differences get smoothed out more effectively than in a laminar flow, and the time-averaged velocity profile in a turbulent pipe flow is much more uniform than in a laminar flow (see figure 11.7). The velocity profile is no longer parabolic, and it is sometimes approximated by a power law, such as

$$\frac{\langle U \rangle}{U_{CL}} = \left(\frac{2y}{D} \right)^{1/n} , \tag{11.11}$$

where U_{CL} is the velocity on the centerline, and the exponent n varies with Reynolds number (for a Reynolds number of about 100,000, $n = 7$). See section 11.8.

As a result of this mixing, the velocity gradient at the wall is higher than that seen in a laminar flow at the same Reynolds number, so that the shear stress at the wall is correspondingly larger. This observation is in agreement with the fact that the losses in a turbulent flow are much higher than in a laminar flow, and therefore the pressure drop per unit length will be greater, which is reflected in a larger frictional stress at the wall. Note that we cannot evaluate the wall stress from equation 11.11 since this approximation to the velocity profile actually gives an infinite velocity gradient (and therefore an
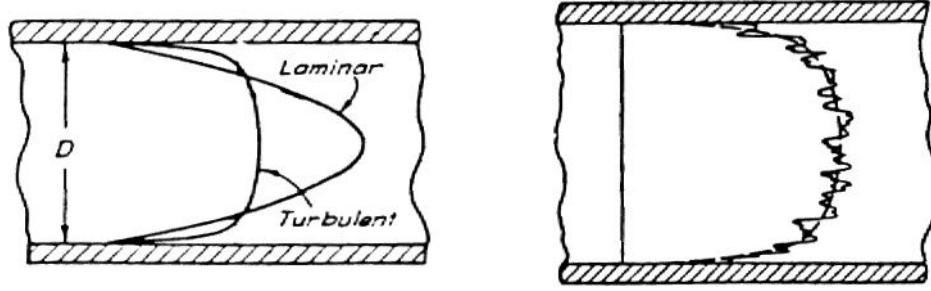
Figure 11.7: Velocity distributions in laminar and turbulent pipe flow.

infinite stress) at the wall. Instead, we often use the semi-empirical relation

$$\frac{1}{\sqrt{f}} = 2.0 \log\left(Re\ \sqrt{f}\right) - 0.8$$

which is known as Prandtl's universal law of friction for smooth pipes (this is the line corresponding to turbulent flow in a smooth pipe as given in the Moody diagram, figure 5.2). A more accurate form is given by

$$\frac{1}{\sqrt{f}} = 1.873 \log\left(Re\ \sqrt{f}\right) - 0.2631 - \frac{233}{\left(Re\ \sqrt{f}\right)^{0.90}} \qquad (11.12)$$

which describes the friction factor to within 1 % for Reynolds numbers from 10×10^3 to 35×10^6.[1]

11.4 Turbulent Boundary Layers

Turbulent pipe flows were discussed in section 11.3. Similar considerations apply to turbulent boundary layer flow. Transition to turbulence in boundary layers can occur for $Re_x > 10^5$, where Re_x is the Reynolds number based on the freestream velocity, U_e, and the distance from the leading edge, x. The major difference between pipe and boundary layer flows is that a boundary layer has an outer edge. Turbulence is unsteady, and therefore the edge between the inner turbulent and the outer non-turbulent fluid changes with time, and an instantaneous cross-section reveals a highly convoluted edge (figure 11.8). The boundary layer thickness δ can only be defined in a time-averaged sense. The velocity profile itself is fuller than a laminar boundary layer (see figure 11.9), and it is sometimes approximated by a power law similar to that used to describe turbulent pipe flow (see section 11.8). That is,

$$\frac{\langle U \rangle}{U_e} = \left(\frac{y}{\delta}\right)^{1/n}, \qquad (11.13)$$

---

[1]M.V. Zagarola & A.J. Smits, *Phys. Rev. Lett.,* January 1997.

where U_e is the time averaged velocity at the edge of the boundary layer, and the exponent n varies with Reynolds number (for a Reynolds number based on length of about 500,000, $n = 7$). The boundary layer grows approximately according to

$$\frac{\delta}{x} = \frac{0.37}{Re_x^{0.2}}$$

so that δ grows as $x^{0.8}$. That is, a turbulent boundary layer grows faster than a laminar boundary layer. Again, this is a reflection of the fact that turbulence diffuses momentum more efficiently than viscosity.

As in pipe flow, the velocity gradient at the wall is higher than that found in a laminar flow at the same Reynolds number, so that the shear stress at the wall is correspondingly larger. The wall stress is given approximately by the empirical relation

$$C_f = \frac{0.0576}{Re_x^{0.2}}$$

where the local skin friction coefficient was defined in equation 3.9.

Consider the case of a two-dimensional turbulent boundary layer developing on a flat wall. The external flow is steady, and since $\partial W/\partial z = 0$, $W = 0$ everywhere. The complete equations of motion are:

$$\text{continuity} \qquad \frac{\partial U}{\partial x} + \frac{\partial V}{\partial y} = 0 \qquad\qquad (11.14)$$

$$x\text{-momentum} \qquad U\frac{\partial U}{\partial x} + V\frac{\partial U}{\partial y} = -\frac{1}{\rho}\frac{\partial p}{\partial x} + \frac{\partial}{\partial x}\left(2\nu\frac{\partial U}{\partial x} - \overline{u^2}\right)$$

$$+ \frac{\partial}{\partial y}\left(\nu\left(\frac{\partial U}{\partial y} + \frac{\partial V}{\partial x}\right) - \overline{uv}\right) \qquad (11.15)$$

Figure 11.8: Streamwise section of a turbulent boundary layer. Rayleigh scattering image of a turbulent boundary layer at Mach 2.5, by M.W. Smith. Flow is from left to right. Reynolds number based on momentum thickness is about 25,000.
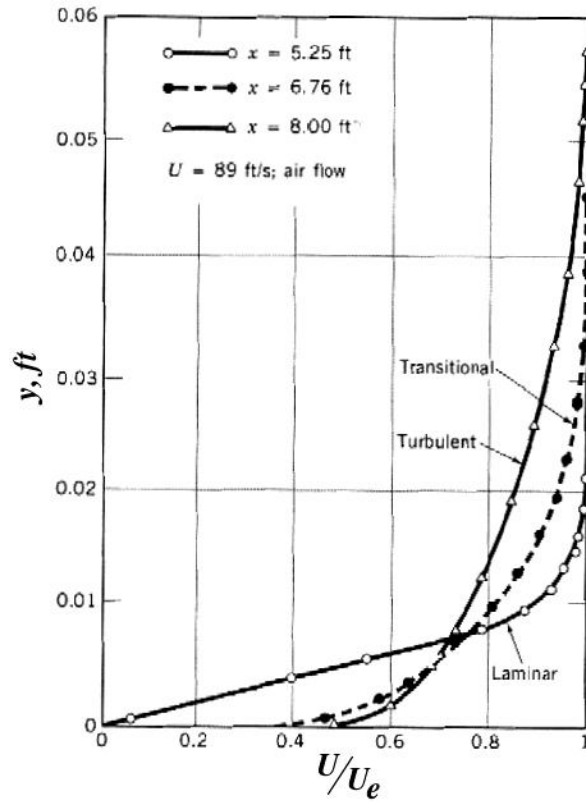
Figure 11.9: Mean velocity profiles in a boundary layer undergoing transition. From Munson, Young & Okiishi, *Fundamentals of Fluid Mechanics*.

$$y\text{-momentum} \quad U\frac{\partial V}{\partial x} + V\frac{\partial V}{\partial y} = -\frac{1}{\rho}\frac{\partial p}{\partial y} + \frac{\partial}{\partial x}\left(\nu\left(\frac{\partial U}{\partial y} + \frac{\partial V}{\partial x}\right) - \overline{uv}\right)$$

$$+\frac{\partial}{\partial y}\left(2\nu\frac{\partial V}{\partial y} - \overline{v^2}\right) \quad (11.16)$$

These equations could be simplified if we could show that some terms are more important than others. We need to make order-of-magnitude arguments, and therefore we need to choose suitable scales.

Some more-or-less typical velocity profiles are sketched in figure 11.10. In the outer part of the boundary layer we assume the local freestream velocity U_e will represent the order of magnitude of the mean velocity. Similarly, the streamwise length scale is the distance from the origin of the boundary layer L (this origin does not necessarily coincide with the leading edge of the plate since there will always be a region of laminar and transitional flow), and the length scale normal to the plate will be the boundary layer thickness δ. From this, velocity gradients in the direction normal to the plate will be of order U_e/δ, which probably over-estimates the actual velocity gradient magnitude.
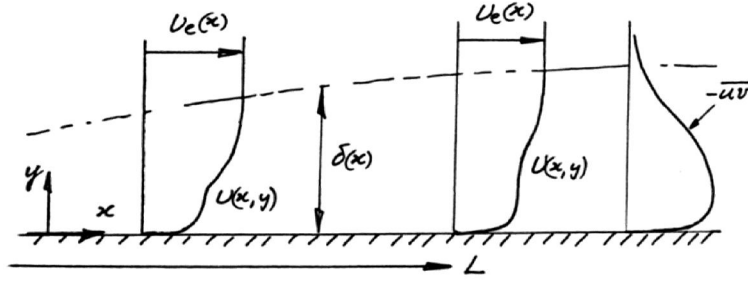
Figure 11.10: Typical mean velocity and Reynolds shear stress profiles in a boundary layer, with notation.

In the inner part of the boundary layer the mean velocity gradients are very much greater, and instead of the thickness of the boundary layer we should use the thickness of the viscous layer δ_v. The velocity scale for the mean flow in this region should still be U_e, or at least some fraction of U_e (see Townsend for a further discussion of this velocity scale, which he calls U_s since it seems to act as a slip velocity for the outer flow). For the turbulence, we assume that for the inner and outer flow all the stresses are of equal order and that

$$\overline{u^2} = O(u_\tau^2), \qquad \overline{v^2} = O(u_\tau^2), \qquad \overline{ww^2} = O(u_\tau^2),$$

although we should remember that all stresses must go to zero at the wall and in the freestream.

From the continuity equation we have that $V = O(U_e \delta / L)$ in the outer region, and $V = O(U_e \delta_v / L)$ in the inner region.

By considering the order of magnitude of the terms in the x-momentum equation, and eliminating obviously small terms, we obtain for the outer flow (assuming pressure differences are of the order of the dynamic pressure):

$$\underbrace{U\frac{\partial U}{\partial x} + V\frac{\partial U}{\partial y}}_{O\left(\frac{U_e^2}{L}\right)} = \underbrace{-\frac{1}{\rho}\frac{\partial p}{\partial x}}_{O\left(\frac{U_e^2}{L}\right)} + \underbrace{\frac{\partial}{\partial y}(-\overline{uv})}_{O\left(\frac{u_\tau^2}{\delta}\right)} + \underbrace{\frac{\partial}{\partial y}\left(v\frac{\partial U}{\partial y}\right)}_{O\left(\frac{vU_e}{\delta^2}\right)} \qquad (11.17)$$

Therefore:

$$\frac{\delta}{L} = O\left(\frac{u_\tau^2}{U_e^2}\right) = O\left(\frac{C_f}{2}\right)$$

$$\text{since} \qquad C_f \equiv \frac{\tau_w}{\frac{1}{2}\rho U_e^2} = \frac{2u_\tau^2}{U_e^2}$$

Consider the order of magnitude of the ratio of the last two terms on the right hand side in equation 11.17:

$$\text{Ratio} = O\left(\frac{u_\tau^2}{\delta} \cdot \frac{\delta^2}{\nu U_e}\right) = O\left(\frac{u_\tau \delta}{\nu} \div \frac{U_e}{u_\tau}\right)$$

We see that this ratio may be expressed as the product of two parts: a Reynolds number which represents the ratio of the largest to the smallest scale in the boundary layer (the viscous length scale ν/u_τ is taken to be representative of the smallest scale, and it is usually to be of the same order as the Kolmogorov scale); and a velocity ratio which is equal to $\sqrt{2/C_f}$. Both factors depend on Reynolds number, and the smallest value of their ratio will occur at the lowest Reynolds number. If we take a value of $u_\tau \delta/\nu = 180$ as probably the lowest value where a turbulent boundary layer has been observed, then $U_e/u_\tau = 18$ at the same Reynolds number. Therefore, the ratio is approximately 10, and since this is in some sense the worst case the last term in equation 11.17 will always be very small compared to the others in the outer flow.

For the inner flow:

$$\underbrace{U\frac{\partial U}{\partial x} + V\frac{\partial U}{\partial y}}_{O\left(\frac{u_e^2}{L}\right)} = \underbrace{-\frac{1}{\rho}\frac{\partial p}{\partial x}}_{O\left(\frac{u_e^2}{L}\right)} + \underbrace{\frac{\partial}{\partial y}(-\overline{uv})}_{O\left(\frac{u_\tau^2}{\delta_v}\right)} + \underbrace{\frac{\partial}{\partial y}\left(\nu\frac{\partial U}{\partial y}\right)}_{O\left(\frac{\nu U_e}{\delta_v^2}\right)} \tag{11.18}$$

Now consider the order of magnitude of the ratio of the last two terms on the right hand side of equation 11.18:

$$\text{Ratio} = O\left(\frac{u_\tau^2}{\delta_v} \cdot \frac{\delta_v^2}{\nu U_e}\right) = O\left(\frac{u_\tau \delta_v}{\nu} \div \frac{U_e}{u_\tau}\right)$$

This ratio will be of order unity when:

$$\frac{u_\tau \delta_v}{\nu} = \frac{U_e}{u_\tau}$$

That is:

$$\delta_v \approx 18\frac{\nu}{u_\tau}$$

As we shall see later, the actual extent of the viscous influence does not extend more than about $30\nu/u_\tau$ from the wall.

If we now consider the y-momentum equation (outer flow only):

$$\underbrace{U\frac{\partial V}{\partial x} + V\frac{\partial V}{\partial y}}_{O\left(\frac{u_e^2 \delta}{L^2}\right)} = \underbrace{-\frac{1}{\rho}\frac{\partial p}{\partial y}}_{O(??)} + \underbrace{\frac{\partial}{\partial y}(-\overline{v^2})}_{O\left(\frac{u_\tau^2}{\delta}\right)=O\left(\frac{u_e^2}{L}\right)} + \underbrace{2\nu\frac{\partial^2 V}{\partial y^2}}_{O\left(\frac{\nu U_e}{L\delta}\right)} \tag{11.19}$$

The viscous term is always negligible outside the sublayer. The terms on the left are an order of magnitude smaller than the stress gradients, and so the pressure gradient term must be of the same order as the stress gradients.

Now consider:

$$\frac{dp}{\rho} = \underbrace{\frac{1}{\rho}\frac{\partial p}{\partial x}dx}_{O\left(\frac{U_e^2}{L}L\right)} + \underbrace{\frac{1}{\rho}\frac{\partial p}{\partial y}dy}_{O\left(\frac{U_e^2}{L}\delta\right)}$$

Therefore

$$\frac{\partial p}{\partial x} \approx \frac{dp}{dx} = \frac{dp_w}{dx}$$

and since at the edge of the boundary layer $\partial/\partial y = 0$, we get from x-momentum equation in the freestream:

$$U_e\frac{dU_e}{dx} = \frac{dp_w}{dx}$$

and we speak of the pressure gradient as being "imposed" or "impressed" on the boundary layer.

Summary: Hence the two-dimensional turbulent boundary layer equation is given by:

$$U\frac{\partial U}{\partial x} + V\frac{\partial U}{\partial y} = -\frac{1}{\rho}\frac{dp_w}{dx} + \frac{\partial}{\partial y}\left(-\overline{uv} + v\frac{\partial U}{\partial y}\right) \qquad (11.20)$$

where the wall pressure pw is now a boundary condition given by Bernoulli's equation:

$$U_e\frac{dU_e}{dx} = \frac{dp_w}{dx} \qquad (11.21)$$

11.4.1   Turbulence characteristics

Figure 11.11 shows measurements of u', v', w' and $-\overline{u'v'}$ in a turbulent boundary layer on a flat plate at a Reynolds number $\mathrm{Re}_x = 10^7$. Note that: (i) the scaling is not based on similarity coordinates — as we shall see later; and (ii) the normal components are shown as intensities (r.m.s. values), although the shear stress is shown in the usual way.

The fluctuations are quite large, being up to about 11-12% of U_e near the wall, although different components differ in magnitude, for obvious physical reasons: u' is largest, being unimpeded by the wall, whereas v' is directly impeded by the wall and it is the smallest, and it also reaches its maximum value much further from the wall than u' or w'. The w'-component
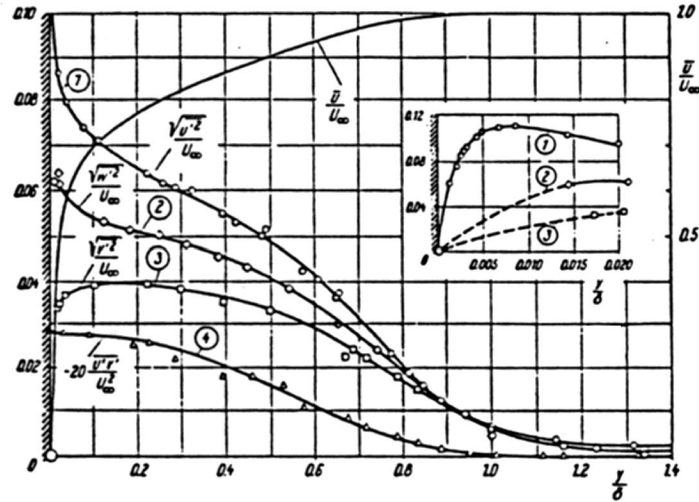
Figure 11.11: Variation of the fluctuating turbulent velocity components in the boundary layer on a flat plate at zero incidence, as measured by P. S. Klebanoff. From Schlichting.

lies between the other two in magnitude. It is important to note that a two-dimensional (in the mean sense) turbulent boundary layer will always have a non-zero lateral component w'. The quantity $\overline{u'v'}$, rescaled by a factor of 20 in figure 11.11, is small but of crucial importance in the understanding of the boundary layer. Near the wall, u', v' and w' all vanish due to the no-slip condition — this is most clearly seen in the inset of the figure showing the region $y/\delta < .015$. Turbulence resists damping and significant fluctuations exist as close to the wall as we are able to measure ($y/\delta < 0.01$ in this case).

Note also that the turbulence extends outside of the boundary layer, that is for $y > \delta$. Of course, δ is rather arbitrary and there is some freestream turbulence, but the main cause is "intermittency." Measurements of the turbulent velocity components show that there exists a fairly sharp boundary between the turbulent flow in the boundary layer and the nearly turbulent free external flow. The edge of a turbulent boundary layer consists of an interface, called the superlayer (Corrsin), separating the fully turbulent and external flows (see figure 11.12). The interface evolves as it travels downstream and irrotational fluid is "entrained" into the boundary layer, and to a stationary observer its position appears to fluctuate strongly with time.

An intermittency factor γ can be defined which is equal to 1 when the flow is fully turbulent at all times and equal to 0 when it is fully laminar. A typical distribution of γ is shown in figure 11.12. The boundary layer is observed to be intermittent from about $y/\delta = 0.4$ to $y/\delta = 1.2$. The mean position of the superlayer (where γ is 50%) is at about $y/\delta = 0.78$. It is usual to incorporate this intermittency factor in modelling the outer layer
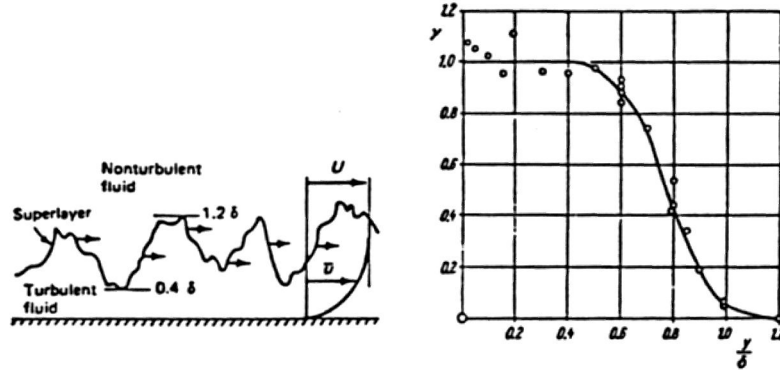
Figure 11.12: Left: Schematic showing the interface between turbulent and non-turbulent fluid in a boundary layer. Right: Variation of the intermittency factor in a turbulent boundary layer on a flat plate at zero incidence, as measured by P. S. Klebanoff. From Schlichting.

turbulence.

11.4.2   Stress Behavior Near the Wall

At the wall, U and V are zero, and therefore the acceleration terms are also zero. Thus, at the wall, the pressure gradient and stress gradient terms balance:

$$\frac{dp_w}{dx} = \frac{\partial}{\partial y}\left(\mu\frac{\partial U}{\partial y}\right)\Bigg|_{y=0} \qquad (11.22)$$

Hence we see that the order-of-magnitude argument used in the near-wall region, which suggested that the convective terms are of the same order as the pressure gradient term, fails in the limit at the wall. Thus, at some small distance from the wall, it is not true that the pressure gradient balances the gradient of total stress, as is sometimes stated: away from the wall the orders- of-magnitude of the pressure gradient and convective terms are equal, and it is not clear if a simple result can be obtained by neglecting one with respect to the others.

So for flows with arbitrary pressure gradients the order-of-magnitude argument indicates that:

$$\mu\frac{\partial U}{\partial y} - \rho\overline{u'v'} = \tau_w \qquad (11.23)$$

since at $y = 0$, $u' = v' = 0$ and $\mu\frac{\partial U}{\partial y} = \tau_w$.

Thus there exists a constant-stress region near the wall, where the sum of the viscous and turbulent shearing stresses is constant (see figure 11.13). If the pressure gradient is not zero, then the extent of this constant stress
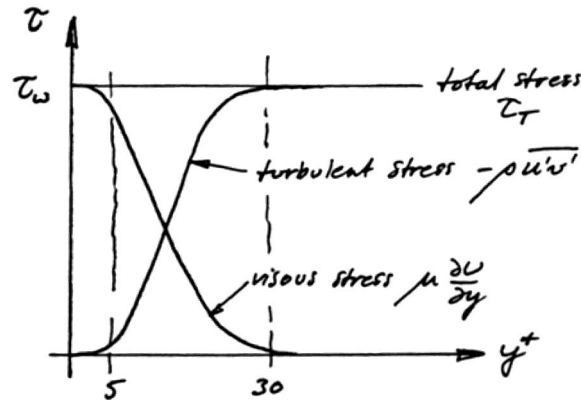
Figure 11.13: Viscous and turbulent shear stress distributions in the near-wall region of a zero pressure-gradient turbulent boundary layer (region highly magnified).

region may be reduced, or we may have to relax our standards on what we mean by "constant" since a small variation in the total stress across the near-wall layer will then exist.

At the wall, the flow is dominated by viscous effects. At some small distance from the wall, $-\overline{u'v'}$ becomes important, and experiments have shown that it rapidly dominates the momentum transport. This is what makes the prediction of turbulent boundary layers so difficult: for most of the flow, the momentum transport is dominated by $-\rho\overline{u'v'}$, and yet we know very little about its general behavior.

Before going on, we see that for adverse pressure gradients ($dp_w/dx > 0$), the gradient of the stress at the wall is positive, and for favorable pressure gradients it is negative (see figure 11.14). Hence, we expect to see a peak in the stress profile for the case of an adverse pressure gradient, and a reduced level of stress in the case of a favorable pressure gradient. This happens to be true, but it is difficult to make this quantitative: as noted above, the gradient of the total stress away from the wall will obviously be determined by the magnitude of the convective terms as well as the magnitude of the pressure gradient.

11.4.3 Scaling Laws for the Mean Velocity

We have already indicated that near the wall viscous effects are important, whereas away from the wall viscous effects are small and they can usually be neglected in the mean momentum equations. When viscous effects dominate, that is, very near the wall, the boundary layer equations for zero
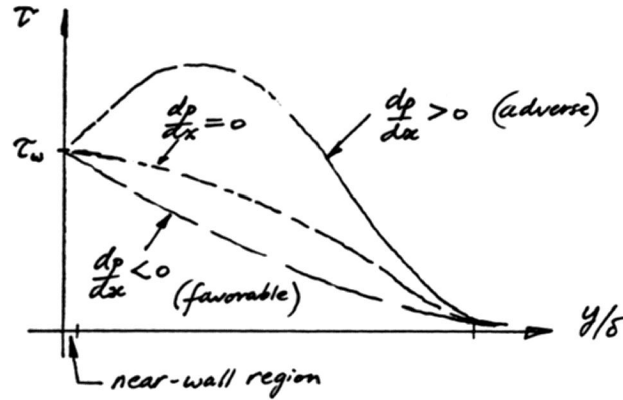
Figure 11.14: Total stress distributions in turbulent boundary layers with zero, favorable, and adverse pressure gradients.

pressure gradient flow give:

$$\frac{\partial}{\partial y}\left(\mu\frac{\partial U}{\partial y}\right)\Bigg|_0 = 0$$

That is,

$$\left(\mu\frac{\partial U}{\partial y}\right)\Bigg|_0 = \tau_w$$

and

$$U = \frac{\tau_w}{\mu}y + \cdots \tag{11.24}$$

Thus, for some small distance from the wall the velocity profile is linear, as it is in laminar flow. A similar result was found for channel flow in section 11.1. Note that the density does not enter this relation since the acceleration terms have been neglected. However, we often write this relationship by introducing the friction velocity $u_\tau = \sqrt{\tau_w/\rho}$:

$$\frac{U}{u_\tau} = \frac{yu_\tau}{\nu} \tag{11.25}$$

or

$$U^+ = y^+ \tag{11.26}$$

$$\text{where} \quad U^+ = \frac{U}{u_\tau}, \quad \text{and} y^+ = \frac{yu_\tau}{\nu}$$

This is the linear part of the sublayer. The density is only introduced for the sake of uniform notation rather than any physical reason (this distinction is important in variable density flows). Experimentally, this "linear" sublayer region is found to occupy a region where $y^+ \leq 5$ (a very thin region in terms of y/δ, as we shall see).

Viscous effects are still important for a larger region (up to $y^+ \approx 30$), [2] and it has been found experimentally that we can write for the general near-wall region the functional relationship:

$$U = f(y, u_\tau, v)$$

That is:

$$\frac{U}{u_\tau} = f\left(\frac{y u_\tau}{v}\right) \tag{11.27}$$

This is commonly known as the "law of the wall" (Coles).

In the outer region, viscosity is no longer important. The appropriate length scale is no longer v/u_τ, as it was in the inner layer but δ, the thickness of the layer. So it is proposed that the functional relationship is

$$U_e - U = g(y, u_\tau, \delta)$$

That is:

$$\frac{U_e - U}{u_\tau} = g\left(\frac{y}{\delta}\right) \tag{11.28}$$

This is commonly known as the "law of the wake" (Coles), or the velocity defect law.

Why should u_τ enter this relationship? We have assumed that the only influence of the wall on the outer flow is through the shear at the wall: this assumption, and all the others, have to be verified by experiment before we can believe the results. This has some interesting consequences, but for the time being we shall assume that the proper scale is u_τ, as given in equation 11.28.

Before we look at the experimental evidence, we can obtain an interesting result by dimensional analysis. It was Millikan (1938) who proposed that there must exist a small but discernible region of the flow where both the law-of-the- wall and the law-of-the-wake apply. This region will be found where $y^+ \gg 1$, and $\eta \ll 1$ ($\eta = y/\delta$), and therefore will only exist at a sufficiently high Reynolds number (see figure 11.15). In that region, the mean velocity distribution must be independent of v *and* δ. Since the velocity and the velocity gradient given by the two "laws" must be the same in this "overlap" region, we see that, from equations 11.27 and 11.28

$$y\frac{\partial U^+}{\partial y} = y^+\frac{df}{dy^+} \tag{11.29}$$

and

$$y\frac{\partial U^+}{\partial y} = -\eta\frac{dg}{d\eta} \tag{11.30}$$

---

[2]Recent evidence suggests that weak viscous effects may persist to $y^+ \approx 200$ or even more (Smits & Zagarola)
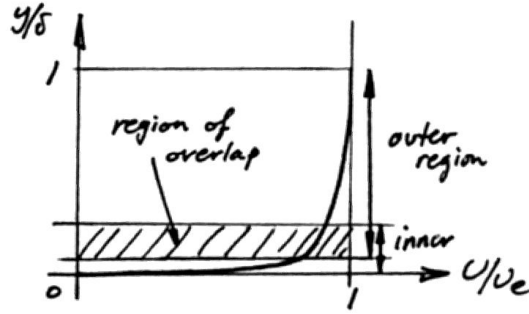
Figure 11.15: Inner and outer regions, showing region of overlap.

By matching the velocity gradients, and by noting that the right hand side of equation 11.29is only a function of y^+, and the right hand side of equation 11.30is only a function of η, then in the overlap region:

$$y^+\frac{df}{dy^+} = -\eta\frac{dg}{d\eta} = \frac{1}{\kappa}$$

where κ is a constant. That is,

$$\frac{df}{dy^+} = \frac{1}{\kappa y^+}$$

and

$$\frac{dg}{d\eta} = -\frac{1}{\kappa\eta}$$

By integrating, we obtain two forms of the log-law:

$$\frac{U}{u_\tau} = \frac{1}{\kappa}\ln\left(\frac{yu_\tau}{\nu}\right) + B \tag{11.31}$$

and

$$\frac{U_e - U}{u_\tau} = -\frac{1}{\kappa}\ln\left(\frac{y}{\delta}\right) + B' \tag{11.32}$$

Here κ is von Kármán's constant, and an often quoted value is 0.41.

The first form (equation 11.31) is the version most commonly seen. In this form, the additive constant B depends on the lower limit of integration and it may depend on Reynolds number (see for example Duncan, Thom & Young, and Zagarola & Smits). However, for all practical flows it seems that B is a constant and equal to about 5.2 (see Bradshaw & Brederode). Note that if we were to accept the suggestion by Bill George that the outer flow in a boundary layer should scale on U_e rather than u_τ, we would find that the velocity variation in the overlap region is then expressed as a power
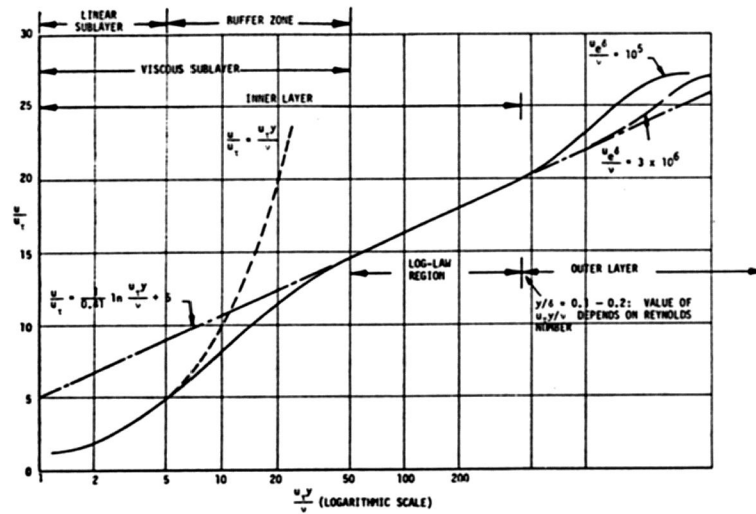
Figure 11.16: Regions of a turbulent boundary layer (inner layer coordinates). Outer-layer profile shown is for U_e = constant. From Cebeci & Bradshaw.
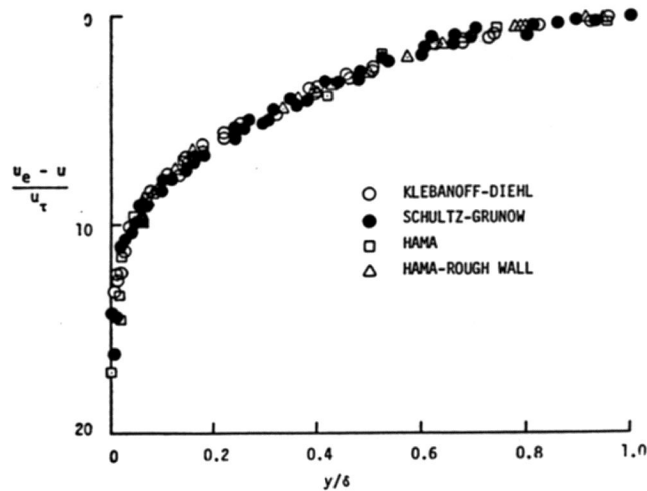
Figure 11.17: Universal plot of turbulent boundary layer profiles in zero pressure gradient (outer layer coordinates), after Clauser (1956). The symbols denote the experimental data. From Cebeci & Bradshaw.

law. In practice, the differences with a logarithmic variation are small, but philosophically it is an important distinction.

So we can plot the velocity profile in two ways: using inner-layer variables $(u_\tau, v/u_\tau)$ (see figure 11.16), or outer-layer variables, or "velocity defect coordinates" (u_τ, δ) (see figure 11.17).

Thus we can see an important difference between laminar and turbulent

boundary layers: laminar layers scale according to a single parameter η ($= y/\delta$), whereas turbulent layers scale according to two parameters y^+ and η (for zero pressure gradient flows). We cannot write down a similarity solution in the same way we could for the Blasius flow: the turbulent boundary layer profile is Reynolds number dependent. Before considering this aspect, we note the combined velocity profile representation suggested by Coles:

$$\frac{U}{u_\tau} = \frac{1}{\kappa} \ln\left(\frac{yu_\tau}{\nu}\right) + B + \frac{\Pi}{\kappa} W\left(\frac{y}{\delta}\right) \tag{11.33}$$

Here, Π is a function of Reynolds number but asymptotes to a constant approximately equal to 0.55 at high Reynolds number. Note that equation 11.33 does not include the viscous sublayer. The wake function W is well-fitted by a $\sin^2$ function:

$$W = 2\sin^2\left(\frac{\pi}{2}\frac{y}{\delta}\right) \tag{11.34}$$

where π is the usual Pythagorean constant = 3.14159 . . .

11.5   Reynolds-Number Dependence of Velocity Profile

First consider the ratio of the outer-layer and inner-layer length scales ($= \delta u_\tau / \nu$). As we shall see in section 11.8, in a zero pressure gradient turbulent boundary layer, we have, approximately:

$$\frac{\delta}{x} = \frac{0.37}{Re_x^{1/5}},$$

$$\frac{\theta}{x} = \frac{0.037}{Re_x^{1/5}},$$

and

$$C_f = \frac{0.0592}{Re_x^{1/5}} \equiv 2\frac{u_\tau^2}{U_e^2}$$

from which we get:

$$\frac{\delta u_\tau}{\nu} = 0.064 Re_x^{0.7} = 1.146 Re_\theta^{7/8} \tag{11.35}$$

So we can see that the viscous length scale becomes a decreasingly small fraction of the boundary layer thickness as the Reynolds number increases. For example, consider the fraction of the boundary layer thickness occupied by the viscous sublayer ($y^+ \leq 30$). This fraction varies from 20% at the lowest
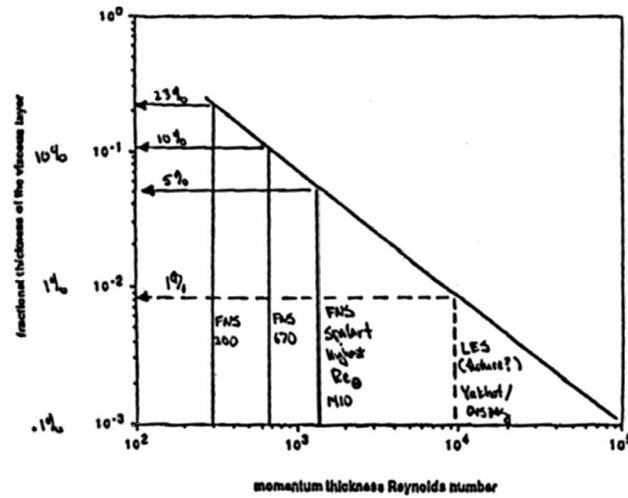
Figure 11.18: Fraction of the boundary layer thickness occupied by the viscous sublayer, as a function of momentum thickness Reynolds number Re_θ. from Jim Brasseur.

Reynolds number where a turbulent boundary layer is self-sustaining, to much less than 1% at very high Reynolds numbers (see figure 11.18.

What about the log-law? Experiments have shown that the lower limit of the log-law corresponds to about the upper limit of the viscous sublayer ($y+ \approx 30$), and the upper limit of the log-law corresponds to about $y/\delta \approx 0.2$.[3] According to these observations, a log-law can only exist when $\delta u_\tau/\nu > 150$, which corresponds to $Re_x > 65,000$ and $Re_\theta > 255$. In practice, turbulent boundary layers are not observed until $Re_\theta > 320$ (Preston 1956, Smits *et al.* 1982).

What about the wake region? Experiments have shown that the wake factor in Coles' "law of the wake" formulation (equation 11.33) is a function of Reynolds number for $Re_\theta < 5000$ (see figure 11.19).

Note also that the velocity profile is plotted as $U/U_e = f(y/\delta)$ (sometimes called "power-law" coordinates), the shape will continue to be a function of Reynolds number, even at high Reynolds numbers. When plotted in defect coordinates, however, the profiles collapse for $Re_\theta > 5000$ (see figures 11.17 and 11.20).

---

[3]Recent boundary layer and pipe flow data indicate a subtle but persistent influence of viscosity out to $y^+ = 200$ or even 500, so that the simple arguments adopted here concerning scaling may need to be modified.
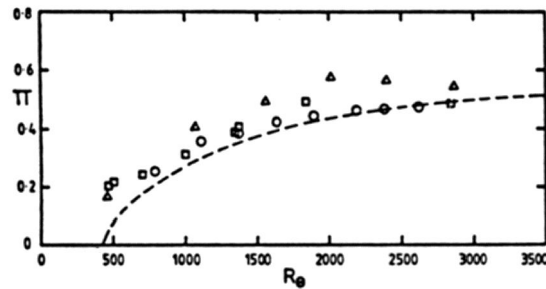
Figure 11.19: Wake factor Π as a function of Re_θ. The dotted line is the correlation derived by Coles (1962). See Smits *et al.* for the key to the symbols indicating experimental data.
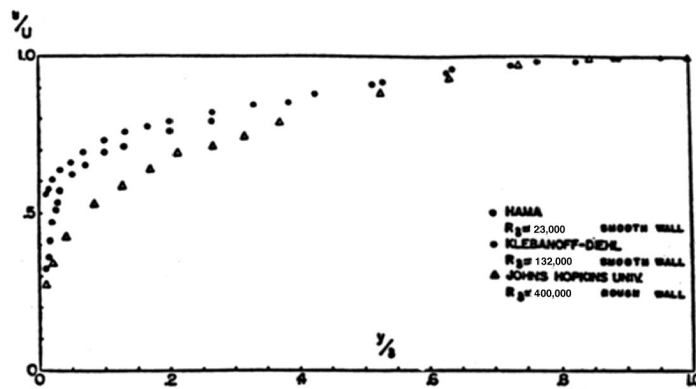
Figure 11.20: Turbulent boundary layer velocity profiles plotted in "power-law" coordinates, showing effect of increasing Reynolds number.

11.6   Friction Law for Pipe and Channel Flows

For a two-dimensional channel flow, we found a linear variation of total stress in the near-wall region. This linear variation also holds for pipe flow, where y is measured radially from the wall. Again, near the wall we can identify a region where viscous effects are important (the viscous sublayer, where $y^+ < 30$), and a region away from the wall where they are not (the core region). Here we also find a region of overlap where a logarithmic velocity variation occurs, and also a wake region but with a smaller value of the wake factor Π than seen in the boundary layer case. In fact, Π is so small that it is not a bad approximation to neglect it altogether (see Tennekes and Lumley, Section 5.2, for a fuller discussion).[4] If we assume that the log-law works

---

[4]As we shall see, if the wake component is independent of Reynolds number, it will integrate to a constant so that the result obtained by neglecting it is the same as the more complete result except for an additive constant.

all the way to the centerline, we can derive a skin- friction formulation very simply. From the log-law:

$$\frac{U}{u_\tau} = \frac{1}{\kappa} \ln \frac{y u_\tau}{\nu} + B$$

Evaluating the velocity at the centerline gives:

$$\frac{U_{max}}{u_\tau} = \frac{1}{\kappa} \ln \frac{h u_\tau}{2\nu} + B$$

To get the skin friction coefficient ($= \tau_w / \frac{1}{2}\rho U_{av}^2$), we need to evaluate the average velocity, U_{av}. If we further assume that the log-law holds all the way to the wall (since the thin viscous sublayer should not contribute significantly to the momentum defect, which means in effect that we are at a high Reynolds number), we get:

$$\frac{U_{max}}{u_\tau} = \frac{2}{h} \int_0^{h/2} \frac{U}{u_\tau} \, dy = \frac{1}{\kappa} \ln \frac{h u_\tau}{2\nu} + B - \frac{1}{\kappa}$$

Using Re$= U_{av} h / \nu$, we obtain:

$$\sqrt{\frac{2}{C_f}} = \frac{1}{\kappa} \ln \left(\frac{\text{Re}}{2} \sqrt{\frac{C_f}{2}} \right) + B - \frac{1}{\kappa}$$

or, with the friction factor $f = 4 C_f$,

$$\sqrt{\frac{8}{f}} = \frac{1}{\kappa} \ln \left(\frac{\text{Re}}{2} \sqrt{\frac{f}{8}} \right) + B - \frac{1}{\kappa}$$

With $\kappa = 0.41$ and $B = 5.2$, we get

$$\frac{1}{\sqrt{f}} = 0.862 \ln \left(\text{Re} \sqrt{f} \right) - 0.518 \tag{11.36}$$

If we repeat this analysis for pipe flow, we obtain

$$\frac{U_{av}}{u_\tau} = \frac{1}{\kappa} \ln \frac{D u_\tau}{2\nu} + B - \frac{3}{2\kappa}$$

and

$$\frac{1}{\sqrt{f}} = 0.862 \ln \left(\text{Re} \sqrt{f} \right) - 1.738 \tag{11.37}$$

There exists a concept of "hydraulic diameter" which is used to extend these simple cases to conduits of more complex cross-sectional shapes (Perry,

1962). Very simply, the pipe result is used for other conduit shapes by substituting for the diameter D with a hydraulic diameter D_H, where D_H is defined by

$$D_H = 4 \times \text{(cross-section area)/(wetted perimeter)}$$

It seems to work quite well, as we can see when we use the pipe result to obtain the channel result. For a channel,

$$D_H = \frac{4hw}{2(h + w)}$$

where h is the channel height, and w is its width. When we substitute in the pipe result the hydraulic diameter for the channel, and use the fact that $w \gg h$, we obtain:

$$\frac{1}{\sqrt{f}} = 0.862 \ln\left(\text{Re }\sqrt{f}\right) - 1.141$$

which is very similar to the earlier result (equation 11.37).

11.7   Momentum-Integral Methods for Turbulent Boundary Layers

The Reynolds shear-stress term $-\rho\overline{u'v'}$ in the turbulent boundary layer equations is obviously a source of difficulty in solving the equations: it represents a new unknown, so that the list of unknowns has been increased from two (U and V) as in the laminar case to three without increasing the number of equations. Trying to generate an expression for $-\rho\overline{u'v'}$ in terms of U and V is called the "closure" problem. We will discuss some of the more elementary methods for "closing" the set of equations later. Here we take a simpler approach, using the momentum integral equation and an expression for the profile to obtain information about the "integral" parameters δ, δ^*, θ and the skin friction coefficient C_f.

By integrating the boundary layer equations over the thickness of the layer, or by using the integral form of the momentum equation applied to a control volume enclosing the full extent of the layer (see, for example, Duncan, Thom & Young), we obtain the "momentum integral equation:"

$$\frac{d\theta}{dx} + \theta\,(H + 2)\,\frac{1}{U_e}\frac{dU_e}{dx} = \frac{C_f}{2} \tag{11.38}$$

for a two-dimensional, constant density, constant property, steady flow. This relationship holds for laminar *and* turbulent flows (to the boundary layer approximation).

For zero pressure gradient flow,

$$\frac{d\theta}{dx} = \frac{C_f}{2} \qquad (11.39)$$

For these relationships to be useful, we need a representation of the velocity profile.

11.8 Power Laws

Earlier, we mentioned the power-law velocity-profile similarity proposed by Bill George (1992). Simpler power-law relations have been used for many years as engineering approximations. They are based on the observation that the velocity profile in a zero pressure-gradient boundary layer can be approximated by a relationship such as:

$$\frac{\bar{U}}{U_e} = \left(\frac{y}{\delta}\right)^{\frac{1}{n}}, \qquad (11.40)$$

where the value of n depends weakly on the Reynolds number, varying from a value of 7 for $5 \times 10^5 < Re_x < 10^7$ to a value of 9 for $10^6 < Re_x < 10^8$. As a result, we obtain

$$\frac{\delta^*}{\delta} = \frac{1}{1+n} \qquad \text{and} \qquad \frac{\theta}{\delta} = \frac{n}{(1+n)(2+n)}. \qquad (11.41)$$

Therefore the shape factor H ($= \delta^*/\theta$) depends on n, and for $n = 7$, $\delta^*/\delta = 1/8$, $\theta/\delta = 7/72$, and $H = 9/7$ (compare these results with a laminar boundary layer).

Experiments show that the shape factor is not constant, especially at low Reynolds numbers, indicating to some extent the Reynolds-number-dependence of n.

Power-law approximations work reasonably well as a description for the outer-layer velocity distribution, but at the wall $\partial \bar{U}/\partial y \to \infty$, and they cannot be used to find the skin-friction. It is usually assumed instead that the Blasius relationship (derived as a curve-fit to pipe flow data) can be used, so that

$$\frac{U_e}{u_\tau} = C_b \left(\frac{u_\tau \delta}{\nu}\right)^{\frac{1}{n}}, \qquad (11.42)$$

where C_b is a constant. By using the momentum-integral equation, (Equation 11.39), we obtain, for $n = 7$,

$$C_f = \frac{0.0592}{Re_x^{1/5}}, \qquad \frac{\delta}{x} = \frac{0.37}{Re_x^{1/5}}, \qquad \text{and} \qquad \frac{\theta}{x} = \frac{0.037}{Re_x^{1/5}}, \qquad (11.43)$$

and for $n = 9$,

$$C_f = \frac{0.0375}{Re_x^{1/6}}, \qquad \frac{\delta}{x} = \frac{0.27}{Re_x^{1/6}}, \quad \text{and} \quad \frac{\theta}{x} = \frac{0.023}{Re_x^{1/6}}, \qquad (11.44)$$

where the constants have been adjusted to fit the experimental data (see Young, 1989).

Despite their questionable provenance, these relationships are useful for simple engineering estimates.

Note that equation 11.43 indicates that the growth of the turbulent boundary layer on a flat plate is proportional to $x^{0.8}$, which is a faster rate of growth than that of a laminar layer, which grows as $x^{0.5}$.

The *local* skin friction coefficient is C_f, defined as

$$C_f \equiv \frac{\tau_w}{\frac{1}{2}\rho U_e^2} \qquad (11.45)$$

The *total* skin friction coefficient C_F is defined as

$$C_F \equiv \frac{\text{Drag}}{\frac{1}{2}\rho U_e^2 b\ell}$$

and b and ℓ are the width and length of the plate respectively. Hence:

$$C_F = b \int_0^\ell \frac{\tau_w}{\frac{1}{2}\rho U_e^2 b\ell} \, dx = \frac{0.72}{\left(\frac{U_e\ell}{\nu}\right)^{0.2}} \qquad (11.46)$$

This equation agrees pretty well with experiment if the constant 0.072 is changed to 0.074. A comparison with experiment is shown in figure 11.21.

Because of the limitation on Blasius's pipe resistance formula, the validity of the equation is restricted to flows for which $U_e\delta/\nu < 10^5$. Using equation 11.43, this corresponds to $U_e\ell/\nu < 6 \times 10^6$. Since for $U_e\ell/\nu$ less than about 5×10^5 the boundary layer on a plate is fully laminar, equation 11.45 is valid in the range $5 \times 10^5 < U_e\ell/\nu < 10^7$.

Despite the fact that these power-laws do not represent the profile very well, the correlations derived for δ, δ^*, θ and C_f are quite reasonable (see, for example, Smits *et al.* 1983), and they are very useful for preliminary calculations.

11.9   Mixing Length and Eddy Viscosity Concepts

In turbulent shear flows, it is usually the Reynolds shear stresses that are most important. Consider a flow with $U(y)$, and $V = 0 = W$ (see figure 11.22a). If fluid element A moves to position y_0 by turbulent motion it
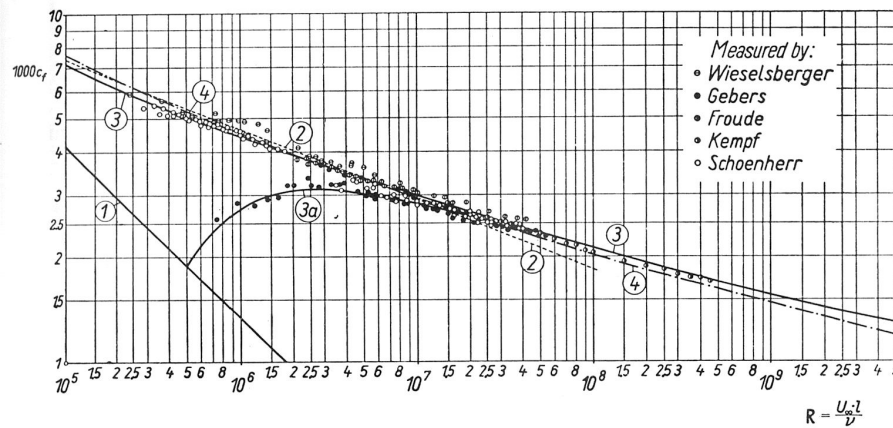
Figure 11.21: Local skin friction coefficient in a boundary layer as a function of Reynolds number based on freestream velocity and streamwise distance. From Schlichting, 7th edition.

gives rise to a $(-v')$ velocity fluctuation at that level. On average, the element A will have the mean streamwise momentum representative of level y_A. By moving from y_A to y_0, element A carries this momentum, or some fraction of it, and at y_0 this turbulent motion gives rise to a $(+u')$ velocity fluctuation. Hence the shear stress contribution $-\rho\overline{u'v'}$ is (on average) positive due to this movement. Similarly, if element B moves from y_B to y_0, we again find $-\rho\overline{u'v'} > 0$ due to this movement. So on average, we expect that $-\rho\overline{u'v'} > 0$ when the velocity profile has a positive gradient ($\partial U/\partial y > 0$). Hence, the presence of a mean shear gives rise to non- zero turbulent shear stresses. To see this more clearly, consider a flow where $U =$ constant ($V = W = 0$). See figure 11.22b. Here $\overline{v'2} \neq 0 \neq \overline{u'2}$, but $\overline{u'v'} = 0$ since there is no vertical gradient in streamwise momentum.

This turbulent transport of momentum, leading to a non-zero turbulent shear stress is reminiscent of simple kinetic models of the appearance of viscous stresses by molecular transport. In a gas, the molecules are generally far apart and there is little cohesion between them. They exchange properties (such as momentum) by collisions, and this also gives rise to a fluid friction. We can illustrate this as follows (which also demonstrates the smoothing effect of viscosity).

Consider two adjacent lumps of a gas, lump A and lump B (figure 11.23). Now A is moving faster than B, which means that, on the average, molecules in A move faster to the right than those in lump B. In addition to this bulk motion, the molecules have their own random motion. This results in a migration of molecules between A and B which, by collision, will tend to speed up the bulk velocity B and slow down the bulk velocity of A. Macroscopically, this exchange of momentum appears as a shear stress at
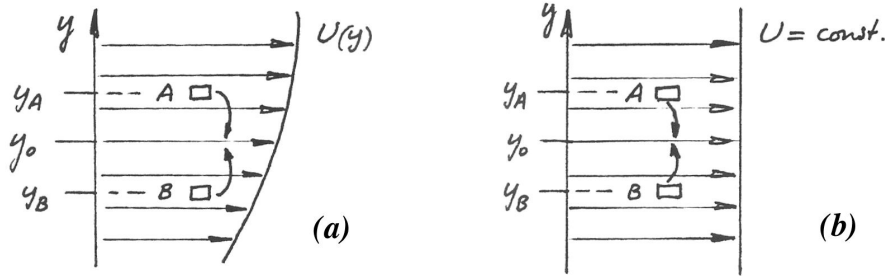
Figure 11.22: (a) Turbulent momentum transport with a positive velocity gradient; (b) Transport with a zero velocity gradient.
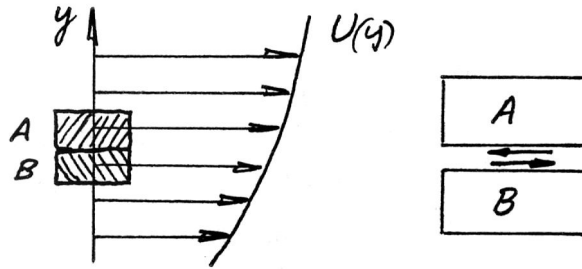
Figure 11.23: Momentum transport on a molecular scale with a positive velocity gradient.

the interface between the lumps (remember these are surface forces which act typically over a distance comparable to the mean free path).

Hence:

1. Viscosity tends to smooth out velocity differences between adjacent fluid lumps;

2. In a gas the viscosity must depend on the average molecular speed, the number density and the mean free path. The dimensions are

$$\left[\frac{\text{stress}}{\text{velocity gradient}}\right] = \frac{MLT^{-2}L^{-2}}{LT^{-1}L^{-1}} = \frac{M}{L^3} \times \frac{L}{T} \times L$$

$$= \text{density} \times \text{velocity} \times \text{length}$$

The proportionality constant between stress and velocity gradient is called the viscosity μ, and so we would expect, in a gas, $\mu \sim \rho \bar{v} \Lambda$, where $\bar{v}$ is the mean molecular speed, and Λ is the mean free path. In fact, using a hard sphere molecular model, we find:

$$\mu = \frac{5\pi}{32}\rho\bar{v}\Lambda \approx \tfrac{1}{2}\rho\bar{v}\Lambda \tag{11.47}$$

This relationship approximates observation, and the departures arise from the limitations of the hard sphere model;

3. In a gas, if we increase the temperature, the number of collisions will increase and we would expect the viscosity to increase, which it does;

4. In a liquid the mechanism is different. If the temperature increases the intermolecular forces decrease, and hence the viscosity will decrease.

11.9.1 Prandtl's eddy viscosity

These analogies with molecular motions lead to two simple closure schemes: the eddy viscosity and mixing length hypotheses. The eddy viscosity approach says that, since

$$S_{ij} = \mu \left(\frac{\partial U_i}{\partial x_j} + \frac{\partial U_j}{\partial x_i} \right)$$

why not

$$-\rho \overline{u'v'} = \mu_t \left(\frac{\partial U_i}{\partial x_j} + \frac{\partial U_j}{\partial x_i} \right)$$

Specifically, for two-dimensional thin shear layers, we write

$$-\rho \overline{u'v'} = \mu_t \frac{\partial U}{\partial y}$$

That is,

$$-\overline{u'v'} = \nu_t \frac{\partial U}{\partial y} \tag{11.48}$$

Here ν_t is known as the eddy viscosity. Its simplest form sets $\nu_t =$ constant, but variants such as $\nu_t = \nu_t(y)$ and $\nu_t = \nu_t(x, y)$ are widespread. A function for ν_t can always be formed that satisfies any set of experimental data, but it is not a universal function (see reasons given below, especially in the handout from Bradshaw's notes). A typical distribution for a zero pressure gradient boundary layer is shown in figure 11.25.

11.9.2 Taylor and von Kármán's mixing length method

Consider a mean flow where $U = U(y)$, with turbulence components u' and v'. If fluid elements at y_1 will, on average, come from levels $y_1 - \ell_m$ and $y_2 + \ell_m$, where ℓ_m is a length scale. If we assume that the fluid elements retain their initial velocities $U(y_1 - \ell_m)$ and $U(y_1 + \ell_m)$ before mixing at height y_1, then these velocities represent, on average, the overall spread of instantaneous
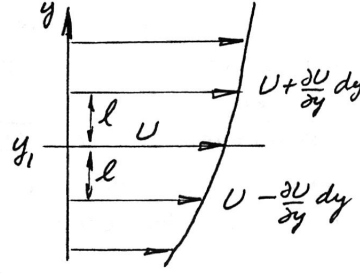
Figure 11.24: Vertical turbulent momentum transport over a characteristic distance ℓ_m.

velocities at that height: $U - u_{rms}$ and $U + u_{rms}$ (see figure 11.24). Now if ℓ_m is small,

$$\sqrt{\overline{u'^2}} = \ell_m \frac{\partial U}{\partial y}$$

If we assume that $\overline{u'v'}$ is proportional to $\overline{u'^2}$ then:

$$-\rho\overline{u'v'} = \rho\ell_m^2 \frac{\partial U}{\partial y}\left|\frac{\partial U}{\partial y}\right| \tag{11.49}$$

where the magnitude is used to ensure the correct sign of the shear stress.

All we need now is ℓ_m, the "mixing length." A typical distribution for a zero pressure gradient boundary layer is shown in figure 11.26. Again we find that there is no "universal" distribution, and the mixing length is flow dependent.

Now the kinetic arguments for the viscous stresses work because (1) $\partial U/\partial y$ is small compared with the gradient of the molecular velocities which are responsible for viscosity, and (2) memories of velocity gradients extend only over distances comparable to the mean free path and therefore the production of viscous stresses is purely a local phenomenon.

Neither of these statements is true for the large eddies responsible for the production of Reynolds stresses. While turbulent velocities are small compared with the mean velocity over most of the flow field, the largest eddies are as big as the whole of the turbulent field.

In short, in using these gradient diffusion models using forms of ν_t (the "Boussinesq" hypothesis[5] or mixing length models, we're trying to calculate turbulent flows without saying anything about the turbulence. So let's learn more about the turbulence.

---

[5]Boussinesq J. (1877) *Theorie de l'ecoulement tourbillant*, Men. Pres. Acad. Sci. XXIII, 46, Paris
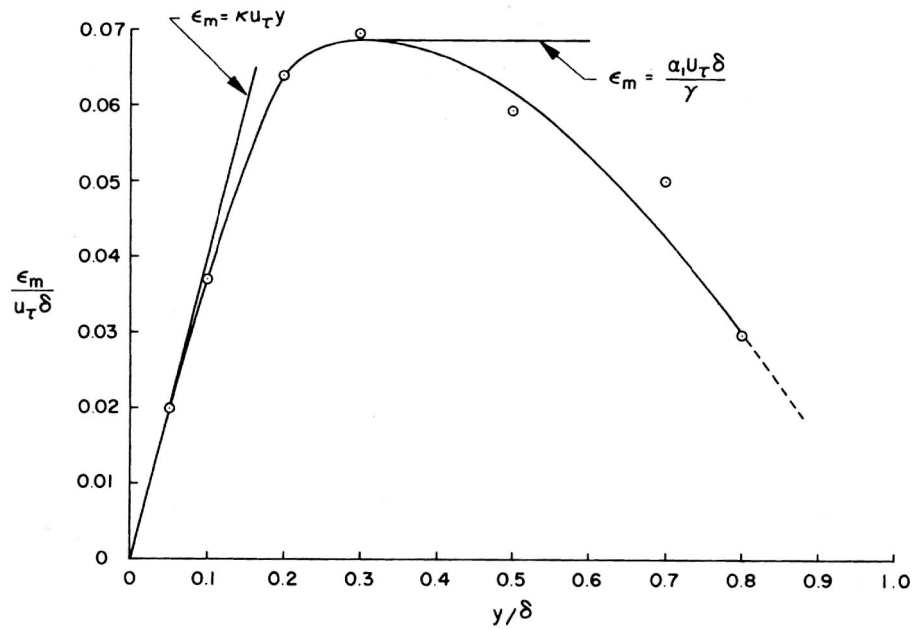
Figure 11.25: Dimensionless eddy viscosity distribution (ε_m in this plot) across a zero pressure gradient boundary layer, according to the data of Klebanoff (1954). From Cebeci & Smith, 1974.
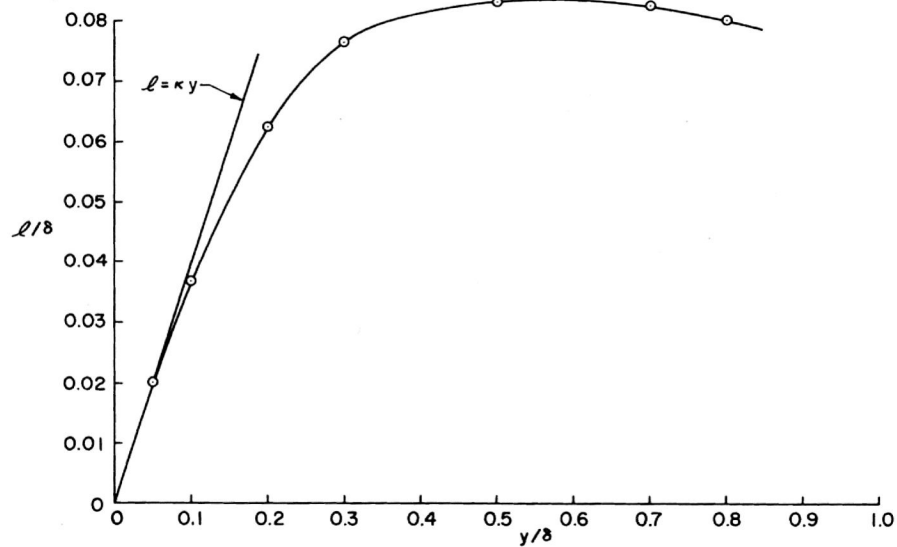
Figure 11.26: Dimensionless mixing length distribution across a zero pressure gradient boundary layer, according to the data of Klebanoff (1954). From Cebeci & Smith, 1974.

11.10   Mixing length and eddy viscosity

(from notes by Peter Bradshaw, September 1976)

We define a length ℓ by

$$\ell_m = \frac{(-\overline{uv})^{1/2}}{\partial U/\partial y}$$

and call it the "mixing length."

We also define a quantity ν_t, having the dimensions of kinematic viscosity, by

$$\nu_t = \frac{(-\overline{uv})}{\partial U/\partial y}$$

and call it the "(kinematic) eddy viscosity." These are purely the definitions of symbols: no assumption is involved, providing that we do not suppose that the mixing length necessarily corresponds directly to an eddy length scale or that the eddy viscosity is a property of the fluid like the molecular viscosity.

Since our object is to find some empirical equation for $-\overline{uv}$ there is no point in introducing ℓ_m or ν_t unless their behavior is simpler than that of $-\overline{uv}$ itself. What one would like to find is that ℓ_m is just some multiple of the shear layer thickness δ (or, more reasonably, that $\ell_m/\delta = f(y/\delta)$) or that ν_t is similarly related to $U_e\delta$). There are several methods of calculating thin shear layers, especially boundary layers, that rely on relations like these, with empirical constants chosen to give the best agreement between calculation and experiment. What is the justification for this? The justification used by the proprietors of these calculation methods is usually "It works, doesn't it?" — the defense used by witch-doctors from time immemorial. A more scientific assessment is possible and, particularly in the case of the mixing length, gives some ideas of the errors likely to be incurred by using simple empirical relations between ℓ_m or ν_t and the mean properties of the shear layer. For simplicity we consider only *thin shear layers* so that Reynolds stresses other than $-\overline{uv}$ do not affect the mean flow.

11.10.1   Early ideas about turbulence

Soon after it was recognized that turbulent flow carried a much larger shear stress than a laminar flow with the same value of $\partial U/\partial y$, Boussinesq (1877) suggested that turbulence might have a simply-behaved eddy viscosity. Any idea of a direct connection between turbulence and molecular diffusion, making ν_t a universal multiple of ν, was soon contradicted by experiment, but the concept of a simply-behaved ν_t underlay several attempts to treat turbulent flow (for instance the Ekman layer model (1905) of cyclonic motion

in the lower atmosphere was first formulated using an eddy viscosity and only later rewritten in the laminar-flow form usually quoted in textbooks).

In 1925 Prandtl, who had invented the boundary layer concept in 1904, postulated a more definite analogy between turbulence and molecular motion. Specifically he supposed that turbulent eddies conserved their momentum between collisions with other eddies, and the "mixing length" as defined above came out as the mean free path of this imaginary process. Now the idea that eddies are separate entities that collide every so often can be disproved simply by watching a plume of smoke; the eye of faith can distinguish eddies but their interaction is continuous, and not discrete as in the case of molecules. Unfortunately when the mixing length idea was tried out in the inner layer of a turbulent wall flow, using the plausible assumption that ℓ_m was proportional to y, it successfully predicted the logarithmic profile observed in practice if the constant of proportionality was taken as 0.4. The witch doctors took over and the mixing length was in. It was 1950 before the paradox was resolved.

11.10.2 Special cases where ℓ_m and ν_t are simple functions

In the inner layer of a wall flow, it is plausible to assume that the flow depends only on u , y and ; the physical justification is that the eddies near the wall are small so that they are unconscious of the comparatively slow fluctuations of the larger eddies further out or of the even slower changes (with x) of the free stream. Dimensional analysis gives the familiar

$$\frac{U}{u_\tau} = f_1\left(\frac{u_\tau y}{\nu}\right)$$

or

$$\frac{\partial U}{\partial y} = \frac{u_\tau}{y} f_2\left(\frac{u_\tau y}{\nu}\right)$$

If we further argue that viscosity should not affect the shear-stress-carrying eddies outside the viscous sublayer then (outside the sublayer) $\partial U/\partial y$ simplifies to

$$\frac{\partial U}{\partial y} = \frac{u_\tau}{\kappa y} \qquad \text{for} \quad \frac{u_\tau y}{\nu} < 30, \quad \text{say}$$

which is the mixing length formula with $(-\overline{uv})^{1/2} = u_\tau$ and $\ell_m = \kappa y$.

In the outer layer of a boundary layer in zero pressure gradient, plausible arguments and dimensional analysis lead to

$$\frac{U_e - U}{u_\tau} = f_3\left(\frac{y}{\delta}\right), \qquad \frac{(-\overline{uv})^{1/2}}{u_\tau} = f_4\left(\frac{y}{\delta}\right)$$

and

$$\frac{\partial U}{\partial y} = \frac{u_\tau}{\delta} f_5\left(\frac{y}{\delta}\right) \qquad \text{or} \qquad \frac{\partial U}{\partial y} = \frac{(-\overline{uv})^{1/2}}{\delta} f_6\left(\frac{y}{\delta}\right)$$

There is no reason to suppose that f_6 is a constant (implying $\ell = $ constant $\times\delta$) but obviously f_6 must tend to $1/(\kappa y/\delta)$ in the log law region where the inner-layer and outer-layer analyses are simultaneously valid.

Now what we have done, *for these special cases only*, is to obtain the mixing length formula, with $\ell_m = \kappa y$ or $\ell/\delta = f_6(y/\delta)$, by dimensional analysis, based on the ideas that the inner-layer eddies are not directly affected by the outer layer eddies ("local equilibrium") and that the outer layer flow changes only in scales but not in behavior as the boundary layer flows downstream ("self-preservation"). The eddy viscosity formula, with $\nu_t = \kappa u_\tau y$ in the inner layer and $\nu_t = u_\tau\delta f_7(y/\delta)$ in the outer layer, can be obtained from the same analysis. In neither case do we need any concepts borrowed from the kinetic theory of gases. The outer layer "self-preserving" results also apply, with different functions of y/δ, to other self-preserving flows like jets in still air or wakes in zero pressure gradient (and in these two cases quite good agreement with experiment is obtained by taking ν_t or ℓ_m constant across the width of the shear layer). Again no physical meaning need be attached to ν_t or ℓ_m. By coincidence, the function f_7 in the eddy viscosity in the outer layer of a boundary layer is nearly the same for a wide range of (constant) values of the presure-gradient parameter $(\delta^*/\tau_w)dp/dx$.

If we look more closely, the essential lack of physical meaning in ν_t and ℓ_m becomes more obvious. Near the center line of a symmetrical jet or wake, $U = u_\tau + O(y^2)$ so that $\partial U/\partial y$ is proportional to y. Again by symmetry, $-\overline{uv}$ is proportional to y. Therefore $\ell_m \propto y^{-1/2}$ and $\ell_m \to \infty$ as $y \to 0$! In this case ν_t is well behaved near the center line, but in an asymmetrical jet (for instance a wall jet from a nozzle blowing tangential to a wall) $\partial U/\partial y$ and $-\overline{uv}$ change sign at different points, between which ν_t is negative and ℓ_m is *imaginary*.

If we extend the idea of eddy viscosity to the normal stresses in a turbulent flow and write

$$-\overline{u^2} = \nu_t\frac{\partial U}{\partial x}$$

$$-\overline{v^2} = \nu_t\frac{\partial V}{\partial y}$$

$$-\overline{w^2} = \nu_t\frac{\partial W}{\partial z}$$

then adding these three equations and using the continuity equation

$$\frac{\partial U}{\partial x} + \frac{\partial V}{\partial y} + \frac{\partial W}{\partial z} = 0$$

gives

$$\overline{u^2} + \overline{v^2} + \overline{w^2} = 0$$

so the turbulence vanishes altogether, a result to gladden the heart of any witch doctor. (There are ways round this).

In three-dimensional flow it is found that the eddy viscosity for $-\overline{vw}$, namely $-\overline{vw}/(\partial W/\partial y)$, is in general not equal to the eddy viscosity for $-\overline{uv}$, namely $-\overline{uv}/(\partial U/\partial y)$.

11.10.3 Relation between ℓ_m and eddy length scales

If the turbulence is in local equilibrium, then, by definition, the mean and turbulent transport terms in the turbulent energy equation (or the other exact equations for the rates of change of Reynolds stress along a mean streamline) are negligible. Thus, in the turbulent energy equation, we get

"production" = "dissipation"

or

$$-\overline{uv}\frac{\partial U}{\partial y} = \varepsilon$$

where ε stands for complicated viscous terms. Now we know that ε is really the rate of transfer of energy to the smaller eddies from the energy-containing, shear-stress-carrying eddies, and should therefore depend on typical scales of the latter. A dimensionally-correct form is

$$\varepsilon = \frac{(-\overline{uv})^{3/2}}{L}$$

where L, defined by this expression, is called the "dissipation length parameter." Then

$$-\overline{uv}\frac{\partial U}{\partial y} = \frac{(-\overline{uv})^{3/2}}{L}$$

so that $\ell_m == L$ ($= \kappa y$ in the inner layer of a boundary layer). This derivation adds little to the purely dimensional arguments above. The point is that L is defined by a relation between two turbulence qualities involved in the fundamental process of energy transfer from large eddies to small and is therefore a real eddy length scale, which should be much less dependent on the mean flow than ℓ_m, which is a relation between one turbulence quantity and one mean flow quantity. Therefore, in cases where the flow is changing significantly with distance downstream, so that the transport terms in the turbulent energy equation become significant and ℓ_m is no longer equal to L, it is L and not ℓ_m that is more likely to obey simple rules. In fact a calculation method that I (peter Bradshaw) devised, assuming $L/\delta = F(y/\delta)$, gives distinctly better results than $\ell_m/\delta = f(y/\delta)$ in rapidly-changing flows, and enables one to assess the errors in the latter assumption.

11.10.4   Conclusions

(i) ℓ_m and ν_t have no physical significance; they are just quantities defined by the equations at the beginning of this section.

(ii) ℓ_m and ν_t obey simple rules only in local-equilibrium layers and self-preserving flows, and only in a local-equilibrium layer, where all length scales are proportional, can ℓ_m be identified with a true turbulence length scale.

(iii) By coincidence ℓ_m/δ is nearly the same function of y/δ in self-preserving boundary layers over a wide range of $(\delta^*/\tau_w)dp/dx$ (as well as being independent of x in any one such boundary layer). This is explicable from the analysis of section 11.10.3 if we note that mean transport and turbulent transport of turbulent energy are by coincidence nearly equal and opposite *throughout* a self-preserving boundary layer, leaving production dissipation.

(iv) From (ii) and (iii) it follows that simple rules for ℓ_m or ν_t can give good results in boundary layers — or other thin shear layers — that are not too far from being self-preserving.

(v) In more demanding cases ℓ_m and ν_t do not obey simple formulae and may exhibit ludicrously unphysical behavior.

(vi) It is frequently useful to phrase qualitative arguments in terms of mixing length or eddy viscosity, or even to make qualitative hypotheses about ℓ_m or ν_t rather than $-\overline{uv}$ directly. This is acceptable if pathological cases (such as asymmetrical jets) are avoided but the student must beware being conned into forgetting conclusion (i).

Chapter 12

Engineering Calculation Methods for Turbulent Flows

12.1   Introduction

Here we discuss methods for calculating turbulent flows at Reynolds numbers of engineering interest. As we have noted previously , at very low Reynolds numbers we can use Direct Numerical Simulations (DNS) where the smallest resolved scale is the smallest eddy of interest, that is, the grid scale Δ is $0(\eta)$, where η is of order the Kolmogorov scale. At higher Reynolds numbers, we can use LES (where the smallest scales are modelled in some way but the time-dependent anisotropic large (energy-containing) scales are computed directly. However, turbulent flows found in engineering applications have Reynolds numbers which are typically much larger than the regimes suitable for DNS or LES approaches, and calculations are usually based on the Reynolds-Averaged Navier-Stokes equations (RANS), together with some turbulence model to close the equations. In any case, routine engineering calculations will almost certainly continue to use turbulence models since LES and DNS are unlikely to transcend the status of research-type calculations and become design tools (they are immensely labor and computer intensive, and they require highly skilled users). A good survey of engineering calculation methods is given by Wilcox, including computer programs and homework problems.

The early efforts in calculating turbulent boundary layers used methods based on the momentum integral equations. These "integral" methods were discussed briefly in section 11.7, and a more detailed survey is given by Cebeci in *Turbulence*. Here we will consider one representative example. Current calculation methods are all based directly on the partial differential equations derived from the N-S equation by using Reynolds decomposition. According to Reynolds (in *Turbulence*), different levels of turbulent flow pde models can be identified. We can modify this hierarchy somewhat to suggest

355

the following ordering:

1. Integral methods — these are based on the momentum integral equation which is an ode for the integral properties of the boundary layer.

2. Zero-equation models — models using only the pde's for the mean velocity field, and no turbulence models (for example eddy viscosity or mixing length models). Also called "algebraic stress models."

3. One-equation models — models involving one pde relating to a turbulence velocity scale, in addition to the mean pde's.

4. Two-equation models — models using an additional pde related to a turbulence length scale (for example k–ε, or k–ω)).

5. Stress-equation models (Reynolds-Averaged Navier Stokes, or RANS) — models involving pde's for all components of the Reynolds stress tensor, and in general for a length scale as well.

6. Very Large-Eddy Simulations (VLES) – c-omputations of the three-dimensional time- dependent large eddy structure and a high-level model for smaller-scale turbulence (for example a Smagorinski eddy-viscosity model).

7. Large-Eddy Simulations (LES) — computations of the three-dimensional time- dependent large eddy structure and a low-level model for the small-scale turbulence (for example, k–ε).

8. Direct Numerical Simulations (DNS) — computations of the full three-dimensional time-dependent flow field with no modelling assumptions.

12.2   Integral Methods

By integrating the mean momentum equation from the wall out to the boundary layer edge for a two-dimensional incompressible flow, we obtain the momentum-integral equation (equations 3.29 and 3.30). If the shape factor H and the wall stress τ_w, can be expressed as functions of the momentum thickness θ, this equation can be solved for θ. The simplest empirical input is to assume H = constant, and $\tau_w = f(Re_\theta)$. A more realistic version is that by Head who used the concept of an entrainment velocity V_e, which is a velocity scale defined in terms of the growth of the velocity deficit in the boundary layer. That is:

$$\frac{V_e}{U_e} = \frac{1}{U_e}\frac{d}{dx}\left(U_e\left(\delta - \delta^*\right)\right) = F\left(H_1\right) \tag{12.1}$$

Head assumed that $V_e = F(H_1)$, where H_1 is a new shape parameter defined by $H_1 = (\delta - \delta^*)/\theta$, and also that $H_1 = G(H)$. The functions F and G can be obtained from experimental data. By additionally using some skin friction correlation, such as that proposed by Ludwieg & Tillman:

$$C_f = 0.24610^{-0.678H} Re_\theta^{-0.268}, \tag{12.2}$$

a closed set of equations is obtained which can be solved for the skin friction and other integral properties. This method was widely used and it was extended in a number of ways by Green (who allowed F to be a function of the streamwise distance) and Myring (who extended the method to three dimensions). The integral approach avoided the complexity of solving the partial differential equations describing the shear layer development, but it quickly lost popularity when computers became available that made possible the rapid solution of multiple pde's.

12.3 Zero-Equation Models

Most of these methods are based on the eddy viscosity concept in some form (see also sections 11.9) and 11.10. For a boundary layer method, for a flow with constant properties,

$$U\frac{\partial U}{\partial x} + V\frac{\partial U}{\partial y} = U_e\frac{dU_e}{dx} + \frac{\partial}{\partial y}\left(-\overline{u'v'} + v\frac{\partial U}{\partial y}\right) \tag{12.3}$$

The two most popular models for the Reynolds shear stress are

$$-\overline{u'v'} = v_t\frac{\partial U}{\partial y} \qquad \text{eddy viscosity}$$

and

$$-\rho\overline{u'v'} = \rho\ell_m^2\frac{\partial U}{\partial y}\left|\frac{\partial U}{\partial y}\right| \qquad \text{mixing length}$$

Here v_t or ℓ_m are prescribed as functions of y (see figures 11.25 and 11.26) for particular flows. The methods lack generality but are still widely used. Note that implicitly we assume that v_t or ℓ_m are better behaved quantities than τ and $\partial U/\partial y$ themselves – that in some sense they are more "universal."

The notes in the next few sections are based on material in Launder $\$$ Spalding's *Mathematical Models of Turbulence*, Academic Press, 1972.

12.3.1 Nature of the hypothesis

- The originator was Prandtl (1925), who used as a starting point the kinetic theory of gases, which gives:

$$\mu \approx \tfrac{1}{3}\rho\bar{v}\Lambda$$

where Λ is the mean free path, and $\bar{v}$ is the molecular velocity.

- First part of the hypothesis:

$$\frac{\tau}{\partial U/\partial y} \equiv \mu_t = \rho \ell_m V_t$$

where ℓ_m is the mixing length, and V_t is the turbulent velocity.

- Second part of the hypothesis:

$$V_t \equiv \ell_m \left|\frac{\partial U}{\partial y}\right|$$

As a consequence,

$$\tau \equiv \mu_t \frac{\partial U}{\partial y} = \rho \ell_m \left|\frac{\partial U}{\partial y}\right| \frac{\partial U}{\partial y}$$

so that

$$\mu_t = \rho \sqrt{\frac{\tau}{\rho}} \, \ell_m$$

The question is: "What determines ℓ_m?"

Values of mixing length for some free turbulent flows:

For a plane mixing layer:

$$\ell_m/\delta = 0.07, \qquad \text{where} \quad \delta \equiv \text{layer width}$$

For a plane jet in stagnant surroundings:

$$\ell_m/\delta = 0.09, \qquad \text{where} \quad \delta \equiv \text{width of half jet}$$

For a "fan" jet in stagnant surroundings:

$$\ell_m/\delta = 0.125, \qquad \text{where} \quad \delta \equiv \text{width of half jet}$$

For a round jet in stagnant surroundings:

$$\ell_m/\delta = 0.075, \qquad \text{where} \quad \delta \equiv \text{width of half jet}$$

Mixing length distribution in boundary layers near a single wall:

The Escudier formula gives:

$$\frac{y}{\delta} \le \frac{\lambda}{\kappa}, \qquad \frac{\ell_m}{\delta} = \kappa \frac{y}{\delta}$$

$$\frac{y}{\delta} > \frac{\lambda}{\kappa}, \qquad \frac{\ell_m}{\delta} = \lambda$$

where $\kappa = 0.41$ and $\lambda = 0.09$ (see figure 12.1). Note that this formula needs modification very near the wall.

Figure 12.1: Mixing length distribution in boundary layers near a single wall.

Figure 12.2: Mixing length very near a wall; van Driest's (1956) hypothesis.

Mixing length very near a wall; van Driest's (1956) hypothesis:

The effective viscosity, μ_{eff}, is given by:

$$\mu_{eff} = \mu + \rho \ell_m^2 \left| \frac{\partial u}{\partial y} \right|$$

The mixing length is given by:

$$\ell_m = \kappa y \left[+1 - \exp\left(-\frac{y \sqrt{\tau_s \rho}}{A\mu} \right) \right]$$

where $A = 26.0$. The resulting distribution is shown in figure 12.2.

12.3.2 Mixing-Length Hypothesis

Advantages

In favor of the Mixing Length Hypothesis (MLH) are three important attributes:

- It is simple, requiring no additional differential equations to be solved;

- Provided that good choices are made for the mixing-length distributions, the MLH allows realistic predictions to be made of the velocity and shear-stress distributions, and the general behavior, of boundary-layer flows;

Figure 12.3: The MLH implies that the effective viscosity vanishes where the velocity gradient is zero.

- Much experience of using the MLH has been accumulated and made available through publications.

Disadvantages

Against the MLH, it must however be said:

- That there is almost no successful experience of predicting recirculating flows with its aid, for the relations between the stresses and the velocity gradients are too complicated;

- It implies that the effective viscosity vanishes where the velocity gradient is zero (see figure 12.3). For a finite effective Prandtl number, the effective thermal conductivity also goes to zero under these conditions.;

- The MLH takes no account of processes of convection or diffusion of turbulence.

It is true that care and ingenuity can make good some of the deficiencies of the MLH; and for many practical purposes it is still the best model to employ.

12.4   One-Equation Models

In typical one-equation turbulence models, the Turbulent Kinetic Energy equation (TKE equation — equation 7.19) forms the basis for a model equation for the turbulence velocity scale $q = \sqrt{\overline{q^2}} = \sqrt{\overline{u_i^2}}$, following Prandtl

(1945). The velocity scale k is determined from the solution of a convective transport equation. The TKE equation is given by:

$$\frac{D\left(\frac{1}{2}\overline{q^2}\right)}{Dt} = -\underbrace{\frac{\partial}{\partial x_j}\left(\frac{\overline{p'u_j}}{\rho} + \frac{1}{2}\overline{u_j q^2}\right)}_{1,2} - \underbrace{\overline{u_i u_j}\frac{\partial U_i}{\partial x_j}}_{3} + \underbrace{\nu\, \overline{u_i\frac{\partial^2 u_i}{\partial x_j^2}}}_{4}. \tag{12.4}$$

The term on the left is the *advection* of TKE. The first term on the right represents the net loss of TKE by the work done in transporting the fluid through a region of changing pressure; the second term represents the transport of TKE by the turbulence itself; the third term represents the production of TKE (the extraction of energy from the mean flow by the turbulence), and the fourth term is the *dissipation*, ε.

In general, the scalar eddy viscosity is defined by:

$$\overline{u_i u_j} = \frac{1}{3}\overline{q^2}\delta_{ij} - 2\nu_t S_{ij} \tag{12.5}$$

In one-equation models, ν_t is modelled by

$$\nu_t = C_2 q \ell_m \tag{12.6}$$

which still requires the length scale distribution $\ell_m(y/\delta)$ to be specified.

We also need to do some work with the TKE equation. In particular, we need to model the diffusion term (1 and 2) and the dissipation (4). To start with the dissipation, we found from considerations of isotropic homogeneous turbulence that in the initial period of decay the dissipation may be modelled by:

$$\varepsilon = C_3 \frac{q^3}{\ell_m} \tag{12.7}$$

For high Reynolds number turbulence in inhomogeneous flows, we make the same assumption on the grounds that the dissipation will still be determined by the properties of the energy containing eddies.

For the diffusion term we write:

$$\frac{\overline{p'u_j}}{\rho} + \frac{1}{2}\overline{u_j q^2} = -C_4 \nu_t \frac{\partial \overline{q^2}}{\partial x_j} \tag{12.8}$$

Whenever we model a higher-order moment as being proportional to the gradient of a related lower-order moment, it is called a *gradient diffusion hypothesis*.

Consider the forms appropriate to thin shear layers (the boundary layer approximation). The TKE equation becomes

$$\frac{D\left(\frac{1}{2}\overline{q^2}\right)}{Dt} = -\frac{\partial}{\partial x_j}\left(\frac{\overline{p'v'}}{\rho} + \frac{1}{2}\overline{q^2 v'}\right) - \overline{u'v'}\frac{\partial U}{\partial y} - \varepsilon \tag{12.9}$$

In the usual notation, we start with the exact boundary-layer form of the *k*-equation:

$$\rho \frac{Dk}{Dt} = -\frac{\partial}{\partial y}\left(\rho \overline{v'k'} + \overline{v'p'}\right) - \rho \overline{u'v'} \frac{\partial u}{\partial y} - \mu \sum \left(\overline{\frac{\partial u'_i}{\partial x_j}}\right)^2$$

where $k = \frac{1}{2}\overline{q^2}$. On the left we have *convective flow*, and on the right we have *diffusion*, *production*, and *dissipation*. The various terms are modelled according to:

-
$$\rho \overline{v'k'} + \overline{v'p'} = \text{constant} \times \rho \sqrt{k}\, \ell \frac{\partial k}{\partial y} = \frac{\mu_t}{\sigma_k} \cdot \frac{\partial k}{\partial y}$$

-
$$\rho \overline{u'v'} = \nu_t \frac{\partial u}{\partial y}$$

-
$$-\mu \sum \left(\overline{\frac{\partial u'_i}{\partial x_j}}\right)^2 \rightarrow \text{local isotropy} \rightarrow c_D \frac{\rho k^{3/2}}{\ell}$$

and so:

$$\rho \frac{Dk}{Dt} = -\frac{\partial}{\partial y}\left(\frac{\mu_t}{\sigma_k}\frac{\partial k}{\partial y}\right) + \mu_t \left(\frac{\partial u}{\partial y}\right)^2 - c_D \frac{\rho k^{3/2}}{\ell}$$

This is one way of developing a one equation model. A different approach was given by Bradshaw, Ferris & Atwell in 1967.

The Bradshaw-Ferris-Atwell Method

Consider one very popular version of a one equation model in more detail – this is the model by Bradshaw, Ferris & Atwell (1967) sometimes called the BFA method.. This method was the "winner" at the 1968 Stanford Olympics, that is, the 1968 AFOSR-IFP-Stanford Conference on Computation of Turbulent Boundary Layers (the runner-up was Cebeci & Smith's algebraic eddy viscosity model — a zero-equation model).

Bradshaw's modelling of the energy equation

-
$$\text{Dissipation: } \propto \frac{\rho k^{3/2}}{\ell}, \quad \text{as before}$$

-
$$\text{Diffusion: } -\overline{v'k'} = Bk\sqrt{\frac{\tau_{max}}{\rho}}, \quad B \equiv \frac{\tau_{max}}{\rho u_G^2} g\left(\frac{y}{\delta}\right)$$

where $\tau = a \cdot \rho k$, and $a = 0.3$.

Figure 12.4: Values of a_1 measured by Alving (1988) in a boundary layer recovering from a sudden application of convex curvature.

- $$\frac{\ell}{\delta} = f\left(\frac{y}{\delta}\right)$$

  The functions f and g are shown in figure 12.5 (where $f = L$, $g = G$).

- The diffusion assumption renders the equation hyperbolic.

BFA actually start with the equation for the turbulent kinetic energy but transform it into an equation for the shear stress by the assumption that

$$\frac{-\overline{uv}}{\overline{q^2}} \equiv a_1 = \text{constant} \ (= 0.15 \text{ for boundary layers})$$

(the constant $a_1 = a$, where the subscript was introduced by Townsend). This assumption is in reasonable agreement with experiment in many boundary layers, and it avoids the use of the turbulent viscosity concept. See figure 12.4.

The treatment of the diffusion is also quite different. Instead of the "gradient diffusion" assumption, Bradshaw supposed that the diffusive flux of energy is proportional to the energy itself times a diffusion velocity of the large eddies of turbulence: this is taken as $\sqrt{\tau_{max}/\rho}$. That is:

$$-\overline{q^2 v'} = q^2 \sqrt{\frac{\tau_{max}}{\rho}} = \frac{\tau}{\rho a_1} \sqrt{\frac{\tau_{max}}{\rho}}$$

Figure 12.5: Distributions of a_1, L, and G according to the BFA method.

So that

$$-\overline{q^2v'} = \frac{1}{a_1}G\frac{\tau}{\rho}\sqrt{\frac{\tau_{max}}{\rho}}$$

and G is a function of y/δ.

Note that the $\overline{p'v'}$ term has been neglected on the basis that it is probably small. Or you could argue that it has been included but modelled in the same way as $\overline{q^2v'}$. Since $\overline{p'v'}$ cannot be measured directly, the jury is out.

The model equation for the shear stress becomes:

$$\frac{D}{Dt}\left(\frac{\tau}{2a_1\rho}\right) = \frac{\tau}{\rho}\frac{\partial U}{\partial y} - \left(\frac{\tau_{max}}{2a_1\rho}\right)^{1/2}\frac{\partial}{\partial y}\left(\frac{G\tau}{\rho}\right) - \frac{(\tau/\rho)^{3/2}}{L} \qquad (12.10)$$

where

$$
\begin{aligned}
a_1 &= \text{constant} = \text{Townsend's structure parameter} \\
L/\delta &= L(y/\delta) = \text{dissipation length} - \text{prescribed} \\
G/\sqrt{\tau_{max}/\rho U_e^2} &= f(y/\delta) = \text{diffusion function} - \text{prescribed}
\end{aligned}
$$

(see figure 12.5).

Now the BFA method could have started directly with the shear stress equation (after all, it is $\overline{u'v'}$ that we need to know). To the boundary layer approximation the shear stress equation is given by:

$$\frac{D\overline{u'v'}}{Dt} = \underbrace{-\overline{v'^2}\frac{\partial u}{\partial y}}_{\text{production}} \underbrace{-\frac{\partial}{\partial y}\left(\overline{u'v'^2} + \frac{\overline{p'u'}}{\rho}\right)}_{\text{diffusion}}$$

$$+ \overline{\frac{p'}{\rho} \left(\frac{\partial u'}{\partial y} + \frac{\partial v'}{\partial x} \right)} \underbrace{}_{\text{redistribution}} - 2\nu \sum_{l} \overline{\left(\frac{\partial u'}{\partial x_l} \frac{\partial v'}{\partial x_l} \right)} \underbrace{}_{\text{dissipation}}$$

However, the terms in the TKE equation have been measured and studied experimentally much more extensively than the terms in the shear stress equation. So the advantage of the BFA approach is that a_1, L, and G have all been measured. (A minor advantage is that with this model the set of pde's comprising equations 12.3, 12.5 and the continuity equation is hyperbolic, and therefore ode's can be written along the characteristic directions. These ode's do not contain V, so that, to the boundary layer approximation, the effect of the V-component velocity is merely to displace the flow in the y-direction, leaving the development of U and τ along a given streamline unaltered.

Implicitly it is assumed that a_1, L, and G change much more slowly than τ and U in the x-direction, so that they can be regarded as well-behaved coefficients rather than variables. This is probably satisfied as long as the flow remains hyperbolic in its response to disturbances.

Note that near the surface, production will equal dissipation. That is,

$$-\overline{uv} \frac{\partial U}{\partial y} = \varepsilon$$

or according to BFA:

$$\tau \frac{\partial U}{\partial y} = \frac{\tau^{3/2}}{L}$$

That is,

$$\frac{\partial U}{\partial y} = \frac{\sqrt{\tau}}{L}$$

and therefore in this region, L reduces to the mixing length which is known to be equal to κy in this region (the logarithmic region). L is not equal to the mixing length in regions where the advection or diffusion is appreciable. Since L is a quantity relating one turbulence parameter to another it is likely to be more universal than the mixing length which is a quantity relating a turbulence parameter to the mean velocity gradient.

Also, near the outer edge of the boundary layer, the TKE equation reduces to diffusion equals advection, so that:

$$\left(U \frac{\partial}{\partial x} + V \frac{\partial}{\partial y} \right) \frac{\tau}{2a_1} = -\frac{\partial}{\partial y} (G\tau)$$

If we assume self-preservation, such that $\partial/\partial x = -\eta \partial/\partial y$, and we integrate over a region in η where $\tau \to 0$ (the outer edge), then we find

$$\frac{dQ}{dx} = \frac{d}{dx}\left(U_e(\delta - \delta^*)\right) = \text{entrainment rate} = 2a_1 G(y = \delta)$$

This helps to define the empirical function G.

Assessment of Bradshaw's model

Advantage:

- The local shear stress is not tied to the local mean velocity gradient.

Disadvantages:

- Transport of length scale is not accounted for.

- The shear stress/kinetic energy relation is of limited validity; in practice, it is applicable only to external boundary layers without velocity maxima.

What about the performance of Bradshaw's model? It does have one advantage over the energy model of Prandtl and others: the shear stress is freed from the local mean velocity gradient. However, the advantage turns out to be conceptual rather than actual. Recent surveys by Ng & Spalding (1970) and Sivasegaram & Whitelaw (1970) have concluded there is little to choose, in the way of accuracy, between predictions obtained with Bradshaw's model and with the MLH. Like the MLH and Prandtl's energy model, it fails to allow for the transport of length scale.

Moreover, the assumed proportionality of τ and ρk has only limited validity. Along the axis of a pipe, for example, the stress is zero but the turbulence energy is finite. In practice therefore only external boundary-layer flows can be predicted. Even then the model in its original form may not be applied to wall-jets or natural-convection boundary layers; for in these flows the shear stress changes sign but the turbulence energy, of course, cannot.

12.5   Two-Equation Models

The principal feature of two-equation models

- Two-equation models determine k, the kinetic energy of turbulence, and ℓ, the length scale, from transport equations.

- Then, $\mu_t = \rho \sqrt{k}\ell$

Figure 12.6: Length scale variations.

Figure 12.7: (a) Recirculating flow downstream of a backward-facing step. (b) Duct with complex cross-section.

Why we need two-equation models: boundary-layer flows

- Experiments show that viscous influences alter length-scale profiles. In figure 12.6, we can guess ℓ at x_1; but what distribution should be chosen at x_2 and x_3?

Why we need two-equation models: elliptic flows

- In recirculating flows (figure 12.7a), convective transport of ℓ may be large.

- In fully developed duct flows (figure 12.7b), complex cross-sections give rise to large difusive effects on ℓ that cannot be accounted for by algebraic formulae.

A means of constructing the length-scale-determining equation

- Define a variable $z \equiv k^m \ell^n$, with m and n constants.

- Derive an exact equation for z from the Navier-Stokes equations.

- Express unknown correlations in terms of knowable quantities, for example,

$$-\overline{z'v'} \propto \sqrt{k}\ell\frac{\partial z}{\partial y}$$

Kolmogorov (1942)	$k^{1/2}/\ell$	f
Chou (1945), Davidov (1961) Harlow-Nakayama (1968) Jones-Launder (1942)	$k^{3/2}/\ell$	ε
Rotta (1951), Spalding (1967)	ℓ	ℓ
Rotta (1968, 1971) Rodi-Spalding (1970) Ng-Spalding (1972)	$k\ell$	$k\ell$
Spalding (1969)	$k\ell^2$	W

Table 12.1: Some proposals for the dependent variable of the second equation.

- Deduce ℓ from k and z, each being determined by its differential equation. See table 12.1.

A general form of the z-equation

-
$$\frac{Dz}{Dt} = \frac{\partial}{\partial y}\left(\frac{\mu_t}{\sigma_z}\frac{\partial z}{\partial y}\right) + z\left[c_1\frac{\mu_t}{k}\left(\frac{\partial u}{\partial y}\right)^2 - c_2\frac{\rho^2 k}{\mu_t}\right] + s_z$$

  where s_z represents secondary source terms, and c_z, c_1 and c_2 are constants in many flows.

- Note: the k-equation may be written (for a thin shear layer):
$$\frac{Dk}{Dt} = \frac{\partial}{\partial y}\left(\frac{\mu_t}{\sigma_k}\frac{\partial k}{\partial y}\right) + k\left[\frac{\mu_t}{k}\left(\frac{\partial u}{\partial y}\right)^2 - c_D\frac{\rho^2 k}{\mu_t}\right]$$

Estimate of c_2 from decay of turbulence behind a grid

- Decay of turbulence behind a grid:
$$\rho_G u_G\frac{dk}{dx} = -c_D\frac{\rho^2 k^2}{\mu_t} \quad \propto x^{-2} \quad \text{(from experiment)}$$

  and
$$\rho_G u_G\frac{dz}{dx} = -c_2\frac{\rho^2 kz}{\mu_t}$$

Hence,

$$c_2 = c_D (m - n/2)$$

Thus, if $z \equiv k/\ell^2$ ($m = 1$, $n = -2$), $c_D = 0.09$, and $c_2 = 0.18$ (recommended value = 0.17).

Estimate of c_1 from near-wall turbulence

- With $\tau/\rho k = \sqrt{c_D}$, and $\partial u/\partial y = \sqrt{\tau/\rho}/\kappa y$:

$$c_1 = \frac{c_2}{c_D} - \frac{\kappa^2 n^2}{\sigma_z \sqrt{c_D}}$$

So, if $z \equiv k^{3/2}/\ell$ ($m = 3/2$, $n = -1$), $\kappa = 0.4$, $\sigma_z = 1.0$, $c_1 = 1.5$ (recommended value = 1.45).

- Final tuning of all c's and σ's by computer optimization.

Boundary conditions

-

Free stream: $$\rho_G u_G \frac{dk_G}{dx} = c_D \frac{\rho_G^2 k_G^2}{\mu_{t_G}}$$

$$\rho_G u_G \frac{dz_G}{dx} = c_2 \frac{\rho_G^2 k_G z_G}{\mu_{t_G}}$$

-

Near a wall: $$u^+ = \frac{1}{\kappa} \ln E y^+$$

$$k^+ = c_D^{1/2}$$

$$z^+ = c_D^{(n/2-m)/2} (\kappa y^+)^n$$

-

Plane, or axis of symmetry: $$\frac{\partial k}{\partial y} = 0; \quad \frac{\partial z}{\partial y} = 0$$

.

As it turns out, the most successful approach is probably that based on $z = k^{3/2}/\ell = \varepsilon$, which is widely known as the $k-\varepsilon$ model (Jones & Launder, 1972). It is without doubt the model that has received the most attention. Now, the terms in the ε-equation (formed by differentiating the x-component of the N-S equations with respect to x_j, multiplying by $\partial u_i/\partial x_j$ and averaging) have
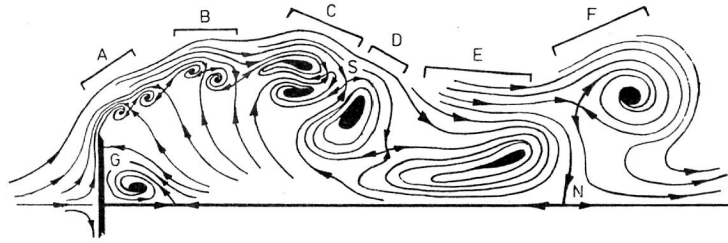
Figure 12.8: Instantaneous streamlines for bluff plate with splitter plate, according to Smits (1979).

never been measured, so the reason for this success is not clear. Nevertheless, the $k - \varepsilon$ model has been widely applied, with conspicuous success, for a long time. It has become clear, however, that all is not well. The 1980-81 Stanford meetings basically concluded that while we can calculate a much wider range of flows, there are no *a priori* means of judging which model will work best. This has led some people to pursue "zonal modelling" where the search for a universal turbulence model has been abandoned and the constants (or models) used in the calculation are optimized for different regions in the flow. For example, a backward-facing step problem (see figure 12.8) may use different constants for the upstream boundary layer, the free-shear layer, and the redeveloping boundary layer downstream. Alternatively, some people feel that more equations will allow more physics to be modelled — this naturally leads to calculation methods which use separate equations for all the Reynolds stresses, plus a length-scale (or other additional) equation. These are called "stress-equation" models.

12.6   Stress-Equation Models

Motives for developing more elaborate models

-

Hydrodynamic models: the question of "closure"

-

Some practical considerations

-

In turbulent shear flows, the energy is usually first produced in one component and then transferred to the others by turbulent processes. One

of the key terms in the equations of motion is the pressure strain term. The set of differential equations governing the transport of the (kinematic) Reynolds stresses $\overline{u_i u_j}$ may be written in the form:

$$
\frac{D\overline{u_i u_j}}{Dt} = -\underbrace{\left[\overline{u_j u_k}\frac{\partial U_i}{\partial x_k} + \overline{u_i u_k}\frac{\partial U_j}{\partial x_k}\right]}_{\text{generation}} - \underbrace{2\nu\overline{\frac{\partial u_i}{\partial x_k}\frac{\partial u_j}{\partial x_k}}}_{\text{dissipation}} + \underbrace{\overline{\frac{p}{\rho}\left(\frac{\partial u_i}{\partial x_j} + \frac{\partial u_j}{\partial x_i}\right)}}_{\text{pressure strain}}
$$

$$
-\underbrace{\frac{\partial}{\partial x_k}\left[\overline{u_i u_j u_k} - \nu\frac{\partial \overline{u_i u_j}}{\partial x_k} + \overline{\frac{p}{\rho}\left(\delta_{jk}u_i + \delta_{ik}u_j\right)}\right]}_{\text{diffusion}} \qquad (12.11)
$$

- The dissipation is handled in the usual way, that is,

$$
2\nu\overline{\frac{\partial u_i}{\partial x_k}\frac{\partial u_j}{\partial x_k}} = \tfrac{2}{3}\delta_{ij}\varepsilon \qquad (12.12)
$$

where ε comes from the dissipation (or length scale) equation. For example, Launder, Reece & Rodi (JFM, 1975) use:

$$
\frac{D\varepsilon}{Dt} = C_\varepsilon\frac{\partial}{\partial x_k}\left(\frac{k}{\varepsilon}\overline{u_k u_l}\frac{\partial \varepsilon}{\partial x_l}\right) - C_{\varepsilon_1}\varepsilon\frac{\overline{u_i u_k}}{k}\frac{\partial U_i}{\partial x_k} - C_{\varepsilon_2}\frac{\varepsilon^2}{k} \qquad (12.13)
$$

- The diffusion term is usually modelled using a gradient diffusion hypothesis. For example, Daly & Harbour (1970) use:

$$
\overline{u_i u_j u_k} = C'_s\frac{k}{\varepsilon}\frac{\partial \overline{u_k u_l}}{\partial x_l} \qquad (12.14)
$$

This is an example of an isotropic effective diffusion formulation — more complicated forms are obviously possible.

- The generation term can be calculated directly.

- The pressure-strain term, or the pressure-strain redistribution tensor is a crucial element, and needs to be considered in detail.

The pressure-strain term

As in Chapter 11, we can write the pressure-strain term as:

$$
-\frac{1}{\rho}\overline{u'\frac{\partial p'}{\partial x}} = -\frac{1}{\rho}\frac{\overline{\partial p' u'}}{\partial x} + \frac{1}{\rho}\overline{p'\frac{\partial u'}{\partial x}} \qquad (12.15)
$$

The first term on the right is the spatial transport of turbulent energy by pressure gradients (sometimes called the *pressure diffusion*). The second term on the right represents the transfer of turbulent energy from u' to v' and w' by pressure fluctuations. This process tends to isotropize turbulence, and it is part of the *tendency-to-isotropy* term. There is no net change of energy — when we write the equation for the rate of change of $\overline{q^2}$ these kinds of terms sum to zero because of continuity. However, in stress-equation modelling, this redistribution term needs to be dealt with explicitly.

Following Chou (1945), the explicit appearance of the pressure in the correlation is eliminated by taking the divergence of the equation for the fluctuating velocity u_i, thus obtaining a Poisson equation for p. The pressure-strain correlation may then be re-expressed in the following form for a position x in the flow:

$$
\frac{\overline{p}}{\rho}\frac{\partial u_i}{\partial x_j} = \frac{1}{4\pi}\int_{\text{vol}}\left\{\underbrace{\overline{\left(\frac{\partial^2 u_l u_m}{\partial x_l \partial x_m}\right)'\frac{\partial u_i}{\partial x_j}}}_{\phi_{ij,1}}\right.
$$

$$
\left.+ 2\underbrace{\left(\frac{\partial U_l}{\partial x_m}\right)'\overline{\left(\frac{\partial u_m}{\partial x_l}\right)'\left(\frac{\partial u_i}{\partial x_j}\right)}}_{\phi_{ij,2}}\right\}\frac{d\,\text{vol}}{|\mathbf{x}-\mathbf{y}|} + S_{ij}
$$

$$\tag{12.16}$$

where capital letters indicate mean values and lower case letters indicate fluctuating quantities, and where terms with and without a prime relate to values at y and x respectively (the integration being carried out over y-space), and S_{ij} is a surface integral which will be negligible away from the vicinity of a solid boundary. Equation 12.16 suggests that there are two distinct kinds of interaction giving rise to the correlation $\overline{p\partial u_i/\partial x_j}$; one involving just fluctuating quantities ($\phi_{ij,1}$) and another arising from the presence of the mean rate of strain ($\phi_{ij,2}$).

Nearly every worker who has made closure approximations for equation 12.11 has adopted Rotta's (1951) proposal for $\phi_{ij,1}$, which may be written as:

$$\phi_{ij,1} + \phi_{ji,1} = -c_1\left(\frac{\varepsilon}{k}\right)\left(\overline{u_i u_j} - \tfrac{2}{3}\delta_{ij}k\right) = \phi_{ij,1}, \quad \text{for brevity} \tag{12.17}$$

where c_1 is supposed to be a constant (at any rate, at high Reynolds numbers) and k and ε are the time-averaged turbulence kinetic energy and energy dissipation rate respectively: the quotient k/ε thus represents a characteristic decay time of the turbulence. According to equation 12.17, the sign of $\phi_{ij,1}$ is always such as to promote a change towards isotropy, its magnitude being proportional to the local level of anisotropy. Rotta (1951) originally proposed

that c_1 should be about 1.4, though later he showed (Rotta, 1962) that a value about twice as large provided a better fit to Uberoi's (1957) data on the decay of highly anisotropic turbulence.

$\phi_{ij,1}$ is called the *return-to-isotropy* part of the pressure strain tensor, since in flows without any mean strain this term is responsible for the return to isotropy, and $\phi_{ij,2}$ is called the *rapid part* of the pressure strain tensor, since under conditions of rapid distortion the effects of far outweigh the effects of $\phi_{ij,1}$ (Townsend 1971). There is considerable disagreement on what the correct form for $\phi_{ij,2}$ is, and it is an area of current work (see, for example, Shih & Lumley 1990, JFM).

12.7 Large Eddy Simulation

The following material was taken from the Ph.D thesis by Ugo Piomelli (Stanford, 1987.)

12.7.1 General considerations

Numerical solution of the Navier-Stokes equations is made very difficult by the large number of grid points required to adequately resolve all the scales of motion. It is easy to show (Tennekes & Lumley, 1972) that the ratio of the largest and smallest scales of motion varies with the 3/4 power of the flow Reynolds number. This implies that the number of grid points required for three-dimensional Direct Numerical Simulation (DNS) of a turbulent flow increases with the 9/4 power of the Reynolds number of the flow.

Thus only very low Reynolds number, geometrically simple flows have been treated by means of DNS. Only recently has simulation of wall bounded flows been successfully attempted. Moser & Moin (1984, 1987) studied the turbulent flow in a mildly curved channel, Spalart & Leonard (1985) and Spalart (1986a,b) simulated a boundary layer and Kim, Moin & Moser (1987) studied the flow in a plane channel.

These efforts are limited to very low Reynolds numbers: 3200 for the channel (based on channel half-width and centerline velocity) and 1400 for the boundary layer (based on edge velocity and momentum thickness). Even then, they require very large amounts of computer CPU time, tens of hours on supercomputers. These limits restrict the usefulness of DNS to basic research.

The simulation of turbulent flows for engineering application is usually based on the Reynolds-Averaged Navier-Stokes equations (RANS), in which the effect of all the turbulent structures is modelled. This approach is limited by the fact that it is difficult, if not impossible, to model the large structures which differ greatly from one flow to the other. Even the most complex

models have not been successfully applied to widely different classes of flows.

Large Eddy Simulation (LES) is an approach to the simulation of turbulent flows in which the large scales of motion are computed explicitly, while the effect of the small scales (subgrid scales or SGS) is modelled. The rationale for this method is based on two experimental observations: first, the small scales, which are created by interactions among larger scales, are more isotropic and universal in nature than the large scales, which are determined by the boundary conditions; one should therefore be able to model them in a more general way. Secondly, since the small scales carry only a smal1 fraction of the total turbulent energy, it may be possible to model them in a fairly crude way without overly affecting the structure of the large scales.

In LES one solves the equations of motion for the large scale structures, which can be formally obtained by multiplying the Navier-Stokes equations by a filtering function and integrating them over the computational domain. The smallest scale admitted by the filter, A, determines the cutoff between subgrid and resolved scales.

LES was first applied to engineering flows by Deardorff (1970), who carried out a simulation of turbulent flow in a channel at very high Reynolds number using only 6720 grid points. The effect of the subgrid scales was modelled by the eddy viscosity model introduced by Smagorinsky t1963). The agreement of the mean velocity profile with the experimental data was fair, and good agreement was obtained for the Reynolds stress profiles.

Schumann (1973, 1975) extended Deardorff's results by using more points (up to 65536), as well as a subgrid scale model which divided the subgrid scale (SOS) stress into a locally isotropic and an inhomogeneous part. His calculations were carried out at Reynolds number 150,000 and constitute a marked improvement over Deardorff's.

Both Deardorff and Schumann used approximate boundary conditions designed to ensure that the logarithmic law-of-the-wall is obeyed; they did not attempt to compute the dynamics of the wall layer, in which most of the turbulence is produced.

During the period 1970–1978 LES was applied by the Stanford group to homogeneous unbounded flows (Kwak, Reynolds & Ferziger, 1975; Shaanan, Ferziger & Reynolds, 1975; Clark, Ferziger & Reynolds, 1977, 1979 and others).

Moin, Reynolds & Ferziger (1978) were the first to attempt the simulation of a wall-bounded flow in which the wall layer was computed. In their simulation they used 16 points in the streamwise and spanwise directions and 63 unequally spaced points in the direction normal to the walls. They also used the Smagorinsky model to account for the effect of the subgrid scales. Although the grid resolution, especially in the streamwise and spanwise directions, was insufficient to resolve the streaky structures near the wall, the

results of the simulation were encouraging: mean velocity, Reynolds stress
and turbulent intensity profiles were in good agreement with experiments,
except very near the wall.

Moin & Kim (1982) (hereafter called MK) improved on the results by
Moin *et al..* (1978) by using a much finer grid ($64 \times 63 \times 128$ points re-
spectively in the streamwise, normal and spanwise directions). Following
Schumann, they divided the SGS stress into a locally isotropic part and an
inhomogeneous part meant to account for the poor spanwise resolution. The
simulation was very successful; not only were the mean velocity, Reynolds
stress and turbulent intensities predicted accurately, but the higher order
statistics agreed well with experimental results. The streaks were captured,
although their spacing was too large. The poor resolution of the wall layer
was held responsible for the errors in the streak spacing and in the location of
the peak in the streamwise turbulent intensity, as well as for discrepancies
between experimental and computed values of the higher order statistics
near the wall.

Horiuti (1987) analyzed the numerical method used by Moin *et al.* (1978)
and MK, and showed that their use of the rotational form of the Navier-
Stokes equations coupled with finite differences in the normal direction
produces very large truncation errors near the wall. He suggested use of a
modification of Arakawa's (1966) scheme which is conservative and more
accurate than MK's approximation near the wall. Horiuti's 1987 simulation,
which used ($64 \times 63 \times 64$ grid points (and was therefore capable of resolving
the wall layer) and the Smagorinsky model, showed extremely good agree-
ment with experimental results, and with the DNS of Moser & Moin (1984,
1987). The computed streak spacing was slightly larger than the value pre-
dicted by MK, but the grid resolution was only half as fine in the spanwise
direction; the position of the peak in the streamwise turbulent intensity was
closer to the experimental value than in MK. The turbulent energy budgets
were in good qualitative agreement with those computed by Moser & Moin
(1984, 1987) for a curved channel.

12.7.2 Governing equations

The equations governing the motion of an incompressible fluid in a channel
are the Navier-Stokes equations and the continuity equation:

$$\frac{\partial u_i}{\partial t} + \frac{\partial u_i u_j}{\partial x_j} = -\frac{1}{\rho}\frac{\partial p}{\partial x_i} + \delta_{i1} + \frac{1}{\text{Re}_\tau}\frac{\partial^2 u_i}{\partial x_j \partial x_j} \tag{12.18}$$

$$\frac{\partial u_i}{\partial x_i} = 0 \tag{12.19}$$

where the variables are made dimensionless using the channel half-width
δ and the friction velocity $u_\tau = (\tau_w/\rho)^{1/2}$. The summation rule applies to

repeated indices. In the present work we shall use the convention that x_1 or x is the streamwise direction, x_2 or y the direction normal to the walls and x_3 or z the spanwise or transverse direction. The velocity components in those directions will be denoted by u_1, u_2 and u_3 or u, v and w.

In large eddy simulation we decompose the velocity u_i in a large scale component $\bar{u}_i$ and a subgrid component u'_i.

$$u_i = \bar{u}_i + u'_i \tag{12.20}$$

The large scale field is defined by filtering:

$$\bar{u}_j(x_1, x_2, x_3) = \int_D \prod_{i=1}^{3} G_i(x_i, x'_i) u_j(x'_1, x'_2, x'_3) dx'_1 dx'_2 dx'_3 \tag{12.21}$$

where the integral is extended to the entire flow field and G_i is the filter function in the i-th direction. In the present simulations we have used two different filters in the planes parallel to the wall: the Gaussian filter

$$G_i(x_i, x'_i) = \left(\frac{6}{\pi \Delta_i}\right) \exp\left[-6(x_i - x'_i)^2 / \Delta_i^2\right] \qquad (i = 1, 3) \tag{12.22}$$

and the sharp cutoff filter which is defined, in real space, by (Leonard, 1974):

$$G_i(x_i, x'_i) = \frac{2 \sin\left[\pi(x_i - x'_i)/\Delta_i\right]}{\pi(x_i - x'_i)} \qquad (i = 1, 3) \tag{12.23}$$

With this filter the subgrid scales represent the effect of all the structures with wavenumbers $|k_i| > \pi/k_i$. The sharp cutoff filter is implicitly applied whenever an infinite series is approximated by a finite number of modes.

In the direction normal to the wall it is desirable to use a filter with variable width to account for the variation of the turbulence length scales with distance from the wall. This was accomplished by employing a box filter of variable width:

$$G_2(y, y') = \begin{cases} \left[\Delta^+ y_j + \Delta^- y_j\right]^{-1} & \text{for } y - \Delta^- y_j < y' < y + \Delta^+ y_j, \\ 0 & \text{for } y' < y - \Delta^- y_j, \ y' > y + \Delta^+ y_j; \end{cases} \tag{12.24}$$

with
$$\left.\begin{array}{l} \Delta^+ y_j = \frac{1}{2}(y_{j+1} - y_j) \\ \Delta^- y_j = \frac{1}{2}(y_j - y_{j-1}) \end{array}\right\} \quad \text{for} \quad \frac{1}{2}(y_j + y_{j-1}) < y < \frac{1}{2}(y_{j+1} + y_j)$$

where y_j is the vertical coordinate of the j-th computational point. Application of the filtering function G_2 defined by equation 12.24 to u_i can be interpreted as averaging u_i over the grid spacing.

When any of the filters described here is used, partial differentiation and filtering commute (see Moin *et al.*, 1978 and also Moin & Kim, 1982). For the Gaussian and sharp cutoff filter, the linear dimension of the filter in the *i*-th direction, Δ_i is usually twice the grid spacing h_i (see Kwak *et al.*, 1975).

Applying the filtering operation to the non-linear term in the Navier-Stokes equations we obtain

$$\frac{\partial}{\partial x_j} = \frac{\partial}{\partial x_j}\left[\bar{u}_i\bar{u}_j + L_{ij} + C_{ij} + R_{ij}\right] \tag{12.25}$$

where

$$\begin{cases} L_{ij} &=& \overline{\bar{u}_i\bar{u}_j} - \bar{u}_i\bar{u}_j \\ C_{ij} &=& \overline{\bar{u}_i u'_j} + \overline{\bar{u}_j u'_i} \\ L_{ij} &=& \overline{u'_i u'_j} \end{cases} \tag{12.26}$$

The terms in equation 12.26 are referred to as, respectively, Leonard stresses, cross (or outscatter) terms and subgrid scale Reynolds stresses (or backscatter). While the cross terms and SGS Reynolds stresses are invariably modelled, the Leonard stresses can be either modelled or computed. When second-order accurate difference schemes are used, the Leonard stresses L_{ij} are of the same order as the truncation error (Shaanan *et al.*, 1975). When higher order difference schemes or spectral methods are employed, it is desirable to compute L_{ij} exactly. If the Leonard stresses are computed (as in MK) the filtered Navier-Stokes equations assume the form

$$\frac{\partial \bar{u}_i}{\partial t} + \frac{\partial \overline{\bar{u}_i\bar{u}_j}}{\partial x_j} = -\frac{\partial P}{\partial x_i} + \delta_{i1} - \frac{\partial \tau_{ij}}{\partial x_j} + \frac{1}{\text{Re}_\tau}\frac{\partial^2 \bar{u}_i}{\partial x_j\partial x_j} \tag{12.27}$$

where

$$\begin{cases} \tau_{ij} &=& Q_{ij} - \frac{1}{3}Q_{kk}\delta_{ij} \\ P &=& \bar{p}/\rho + \frac{1}{3}Q_{kk} \\ Q_{ij} &=& R_{ij} + C_{ij} \end{cases} \tag{12.28}$$

The term τ_{ij} in equation 12.28 is also frequently referred to as *subgrid scale Reynolds stress*.

The filtered continuity equation is

$$\frac{\partial \bar{u}_i}{\partial x_i} = 0 \tag{12.29}$$

12.7.3 The residual stress model

The assumptions on which LES is based, such as the universality and homogeneity of the small eddies and the hypothesis that the small eddies do not contribute much to the total turbulent kinetic energy, imply use of fairly

crude models to simulate the effect of the small eddies on the large ones that are simulated.

The model that has been used most frequently in LES of turbulent flows is an eddy viscosity model due to Smagorinsky (1963):

$$\tau_{ij} = -2\nu_T S_{ij} \tag{12.30}$$

where

$$S_{ij} = \frac{1}{2}\left(\frac{\partial \bar{u}_i}{\partial x_j} + \frac{\partial \bar{u}_j}{\partial x_i}\right) \tag{12.31}$$

is the strain-rate tensor, and ν_T is an eddy viscosity. To determine the eddy viscosity we assume that, in the balance of subgrid scale turbulent kinetic energy $\overline{q^2} = \overline{u_i' u_i'}$, the two dominant effects are production and dissipation.

The production $\wp$ is given by

$$\wp = -\overline{u_i' u_j'} S_{ij} = 2\nu_T S_{ij} S_{ij} \tag{12.32}$$

while dimensional analysis suggests that the dissipation ε is given by

$$\wp = c_1 \frac{\left(\overline{u_i' u_i'}\right)^{3/2}}{\ell} \tag{12.33}$$

in which ℓ is the characteristic length scale of the subgrid eddies.

Equating equation 12.32 to 12.33 and assuming that the eddy viscosity is proportional to the characteristic length and velocity scales of the small eddies:

$$\nu_T = c_2 \ell \left(\overline{u_i' u_i'}\right)^{1/2} \tag{12.34}$$

we obtain Smagorinsky's (1963) model:

$$\nu_T = \ell^2 \sqrt{2 S_{ij} S_{ij}} \tag{12.35}$$

in which all the constants have been absorbed by the length scale ℓ.

Since ℓ is the size of a representative subgrid scale eddy, it must be related to the filter size Δ, which is in turn related to the grid size h. If the cutoff is within the inertial sub-range of homogeneous isotropic turbulence, Lilly (1966, 1967) found that ℓ can be expressed as

$$\ell = C_S \Delta \tag{12.36}$$

with $C_S = 0.23$.

For anisotropic filters no uniquely superior expression for ℓ has yet been found. Near the wall the growth of turbulence structures is inhibited, and the reduction of the length scales must be taken into account. Non-uniformity

of the computational grid in the normal direction is not usually sufficient to account for the variation of the length scales, and empirical corrections are used near the wall.

MK modified the formulation used by Deardorff (1970) to include the reduction of the length scales near the wall by Van Driest (1956) damping; the latter is often used in one-point closure models. This leads to

$$\ell_{MK} = C_S \left[1 - \exp\left(-y^+/A^+\right)\right] (\Delta_1 \Delta_2 \Delta_3)^{1/3} \tag{12.37}$$

where $A^+ = 25$. The exponential damping can be added to the length scale proposed by Bardina, Ferziger & Reynolds (1980) to yield

$$\ell_{BFR} = C_S \left[1 - \exp\left(-y^+/A^+\right)\right] \sqrt{\Delta_1^2 + \Delta_2^2 + \Delta_3^2} \tag{12.38}$$

An alternative formulation proposed by Mwn and Callen (1986) is

$$\frac{1}{\ell_{MC}} = \frac{1}{C_S (\Delta_1 \Delta_2 \Delta_3)^{1/3}} + \frac{1}{\kappa \left(1 - |y|\right)} \tag{12.39}$$

in which κ is the von Kármán constant. Equation 12.39 matches Deardorff's length scale to Prandll mixing length on the assumption that, near the walls, at $y = \pm l$, the size of the subgrid eddies scales with the distance from the wall.

Another expression for ℓ was proposed by Leslie (1985):

$$\ell_L = C_S \left[1 - \exp\left(-y^+/A^+\right)\right] \left(\Delta_1^{-3/4} + \Delta_2^{-3/4} + \Delta_3^{-3/4}\right)^{-4/3} \tag{12.40}$$

We suggest an expression of the form

$$\ell_{PFM} = C_S \left[1 - \exp\left(-y^{+3}/A^{+3}\right)\right]^{1/2} (\Delta_1 \Delta_2 \Delta_3)^{1/3} \tag{12.41}$$

which ensures the proper behavior for the SGS Reynolds stress τ_{12} near the wall ($\tau_{12} \sim y^{+3}$).

The two-part model, introduced by Schumann (1975) and employed by MK, is usually written:

$$\tau_{ij} = -2\nu_T \left(S_{ij} - \langle S_{ij} \rangle\right) - 2\nu_T^* \langle S_{ij} \rangle \tag{12.42}$$

where $\langle \rangle$ represents averaging over a plane parallel to the wall. The first term in equation 12.42 is a modified Smagorinsky model with

$$\nu_T = \ell^2 \sqrt{2 \left(S_{ij} - \langle S_{ij} \rangle\right)\left(S_{ij} - \langle S_{ij} \rangle\right)} \tag{12.43}$$

The second term, in which

$$v_T^* = \ell^{*2} \sqrt{2\langle S_{ij}\rangle\langle S_{ij}\rangle} \tag{12.44}$$

is supposed to account for the production of subgrid turbulent kinetic energy in the viscous sublayer, where the grid resolution is inadequate. While the length scale ℓ represents an average of length scales in all directions, ℓ^* only represents the spanwise structures that the grid cannot resolve. The form of ℓ^* originally proposed by Schumann (1975) is

$$\ell_S^* = \min\left[c\,\sqrt{\Delta_1\Delta_3},\, \kappa y_w\right] \tag{12.45}$$

in which y_w is the distance from the nearest wall and $c = 0.065$.

Moin & Kim (1982) used

$$\ell_{MK}^* = c\Delta_3^2\left[1 - \exp\left(-y^{+3}/A^{+3}\right)\right]^2 \tag{12.46}$$

Another model that has been very successful for the simulation of homogeneous turbulence, as well as for shear flows, is the mixed model. This model, developed by Bardina *et al.* (1980) is based on the assumption that the main interaction between resolved and subgrid scale eddies takes place between the smallest resolved eddies and the largest subgrid scale eddies. Since filtering a velocity field removes the smallest scales of the flow, a velocity field that is filtered twice will contain only the very largest scales of motion. The difference between a filtered velocity field and one that has been filtered twice, $\bar{u}_i - \bar{\bar{u}}_i$, will therefore contain predominantly intermediate scales of motion, that is, the smallest resolved scales. On the basis of these considerations Bardina *et al.* (1980) introduced the scale similarity model, which is of the form

$$\tau_{ij} = C_B\left(\bar{u}_i\bar{u}_j - \bar{\bar{u}}_i\bar{\bar{u}}_j\right) \tag{12.47}$$

Bardina *et al.* (1980) found that the scale similarity model correlates well with the subgrid scale Reynolds stresses, but does not dissipate energy. They then proposed the mixed model, which is a linear combination of the scale similarity model (equation 12.47) and the Smagorinsky model (equation 12.30):

$$\tau_{ij} = C_B\left(\bar{u}_i\bar{u}_j - \bar{\bar{u}}_i\bar{\bar{u}}_j\right) - 2v_T S_{ij} \tag{12.48}$$

The constant C_B was set to 1.1 by fitting numerical results to experimental data.

Speziale (1985) showed that, if the Leonard stresses are computed, Galilean invariance of the equations of motion is not preserved if either the Smagorinsky or the two-part model is employed, but is preserved only if the mixed

model is used with $C_B = 1$. If the Leonard stresses are modelled, however, then either the Smagorinsky or the two-part model guarantees Galilean invariance, and the mixed model cannot be used in the form given by (equation 12.48).

It should also be noticed that when one uses either the Smagorinsky or the two-part model, the trace of the subgrid scale stress tensor has to be added to the pressure, since the strain tensor is trace-free. With the mixed model, however, such is not the case, and one can replace (equation 12.28) with

$$\begin{cases} \tau_{ij} & = & R_{ij} + C_{ij} \\ P & = & \bar{p}/\rho \end{cases} \tag{12.49}$$

Chapter 13

Structure of Turbulence in Wall-Bounded Shear Flows

13.1   Physical Models for Turbulent Boundary Layers

There have been many studies of organized motions in turbulent boundary layers. The following extract from the MSE thesis of J. Goldstein (Princeton, 1991) provides a convenient summary of this work.

Hussain (1983) defines a coherent structure as "a connected large-scale turbulent fluid mass with phase correlated vorticity over its spanwise extent." He states that organized structures are responsible for significant transport of mass, momentum, and energy without actually being energetic themselves, and that they must be spatially mutually exclusive. He theorizes that it is this exclusivity that makes the interaction of coherent structures, such as pairing and tearing, a highly non-linear process. Hussain writes that "the presence of coherent structures everywhere in a turbulent shear flow suggests a sequence of formation, evolution, and decay." The formation of these structures seems to be due to some instability mechanism, even though this mechanism and the processes by which these structures evolve are not yet fully understood. Decay of coherent structures seems to be a result of inter-structure interaction and viscous diffusion.

Yule (1980) proposed that coherent structures are "repetitive, have survival distances much larger than the structure size, and contribute significantly to the kinetic energy." Hussain, however, states that the last two conditions do not occur in general, but are dependent on where the coherent structure exists in the boundary layer. Brown & Thomas (1978) state that an organized structure is "a recognizable large-scale motion which has its own internal dynamics which of itself and through its interactions with other similar structures dominates the mechanism of the flow."
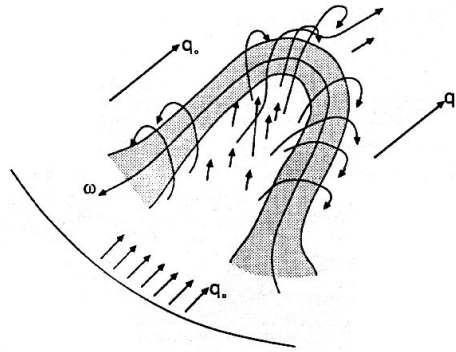
Figure 13.1: Schematic of a horseshoe vortex, the dominant coherent structure in a turbulent boundary layer according to Theodorson (1952).

It was Theodorsen (1952) who first suggested the existence of organized structures in turbulent boundary layers. He went so far as to propose that the dominant coherent structure in a turbulent boundary layer is a horseshoe-shaped vortex loop inclined downstream at 45° to the wall (see figure 13.1). Theodorsen theorized that vortex stretching is the only available mechanism by which the concentration of vorticity can be increased to lead to turbulence. Based on his analysis of the enstrophy equation, Theodorsen concluded that the.vortex stretching term in the equation will be a maximum on a plane inclined 45o to the wall. His physical reasoning seems to be quite sound, but it is still not known why the breakdown of laminar shear flows to turbulence should be accompanied by the formation of horseshoe vortices inclined at 45°, although the existence of horseshoe vortices in turbulent shear flows and their corresponding average angle of inclination has been verified by large numbers of direct observations, beginning with Theodorsen himself (working with Prof. John Weske in the early 1950's). See figure 13.2. This structure in particular has received particular attention over the years, since the horseshoe vortex seems to serve as the dominant dynamical link between the different regions of a turbulent boundary layer. This point will be discussed further in later sections.

It is common practice to catalog organized structures depending on where they occur in the boundary layer. Inner-layer structures, according to taxonomy by Robinson (1991), consist primarily of low- and high-speed streaks, vortical structures such as *legs* and *arches* and the burst-sweep cycle. Outer layer structures basically consist of large-scale long-lived structures such as *bulges* and *backs*. Other coherent structures include *pockets*, high pressure *potatoes*, near-wall shear layers, vortical structures, and wall pressure fluctuations. Horseshoe vortices of various scales are found in both the inner and outer layers. Structures relevant to the present work will be discussed further in later sections.
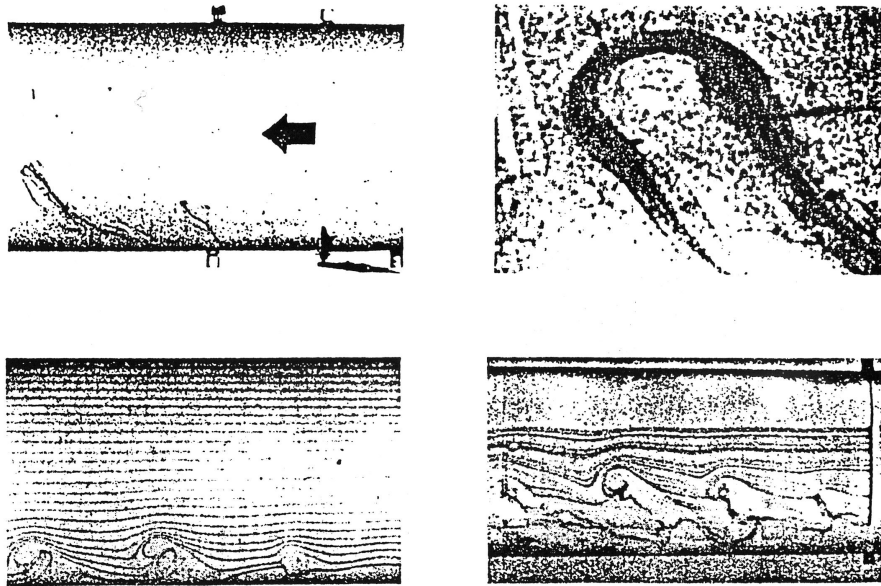
Figure 13.2: Early flow visualization studies of horseshoe vortices by Theodorson and Weske.

13.2 Inner Layer Structures

Kline et al. (1967), using hydrogen bubbles in water to visualize a turbulent boundary layer, found that the bubbles, when introduced very close to the floor, collect into streamwise streaks with an average spanwise separation of about 100 wall units (see figure 13.3). These streak patterns migrate slowly downstream, with a velocity less than the local mean, and are therefore called *low-speed streaks*. Additional probe measurements showed that regions where velocity is greater than the local mean exist between the low-speed streaks. These regions are known as *high-speed streaks*. Robinson *et al.* (1989) studied the low-speed and high-speed streaks in the interpretation of the Spalart (1986) turbulent boundary layer DNS data. They found that the length of the low-speed streaks often exceeds 1500 wall units, and were between 20 and 80 wall units wide. These low-speed streaks are certainly coherent structures, but are not particularly energetic. In contrast, the length of high-speed streaks rarely exceeds 800 wall units, and their widths range between 40 and 100 wall units (see figure 13.4).

Kline it et al. also noted that the low-speed streaks rise very slowly from the floor. When the streak reaches a y^+ of about 10, it begins to oscillate. The oscillation increases in magnitude and the lift-up continues until a y^+ of about 15 (on average), when the streak breaks up. This can occur at a y^+ as high as 30. The remnants of the streak continue moving away from the wall. This streak lift-up, oscillation, and break-up is termed an *ejection*. One
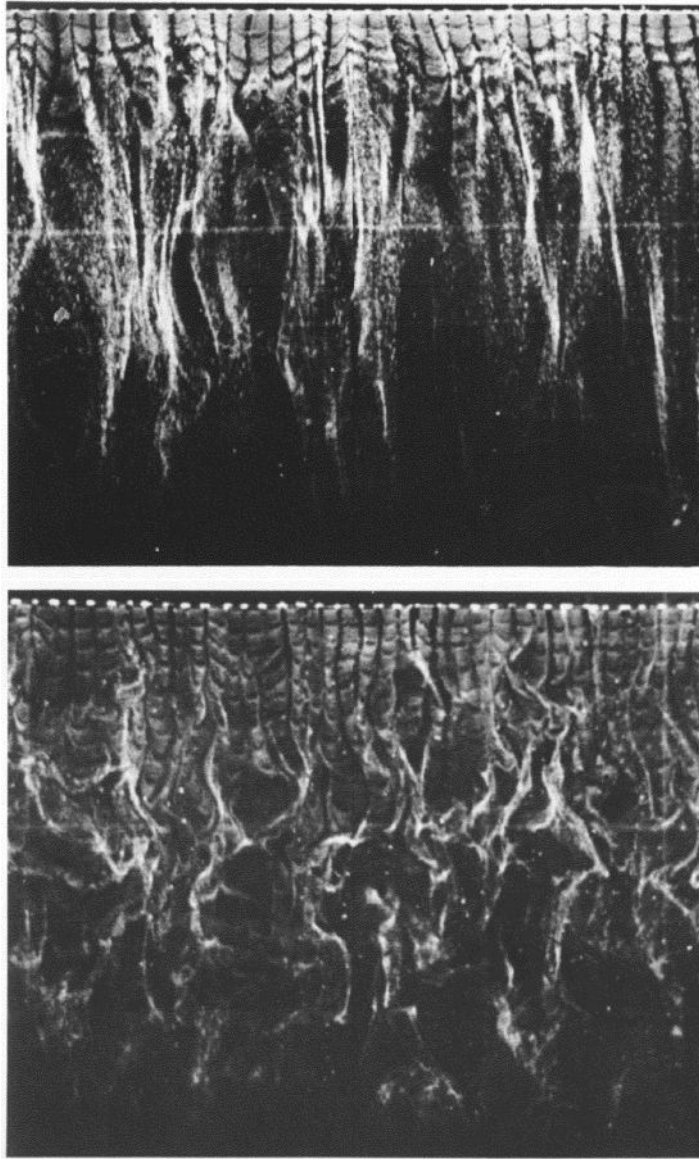
Figure 13.3: Hydrogen bubbles marking low-speed streaks in the sublayer, from Kline *et al.* (1967). Wire located at (a) $y^+ = 3$; and (b) $y^+ = 38$. The flow direction is from top to bottom.

or more ejections from the same low-speed streak is termed a *burst*, which is usually followed by an inrush of high momentum fluid from above, called a sweep. Blackwelder (1978) suggests that the upward motion of streaks cease upon the arrival of the sweep imposed by the outer flow field. The sweep motion results in an inflectional velocity profile, which according to Chen & Blackwelder (1978) cause instabilities that trigger ejections. This sequence of events is called the burst-sweep cycle, and seems to be responsible for most of the turbulent energy and instantaneous Reynolds stress ($-\rho u'v'$)
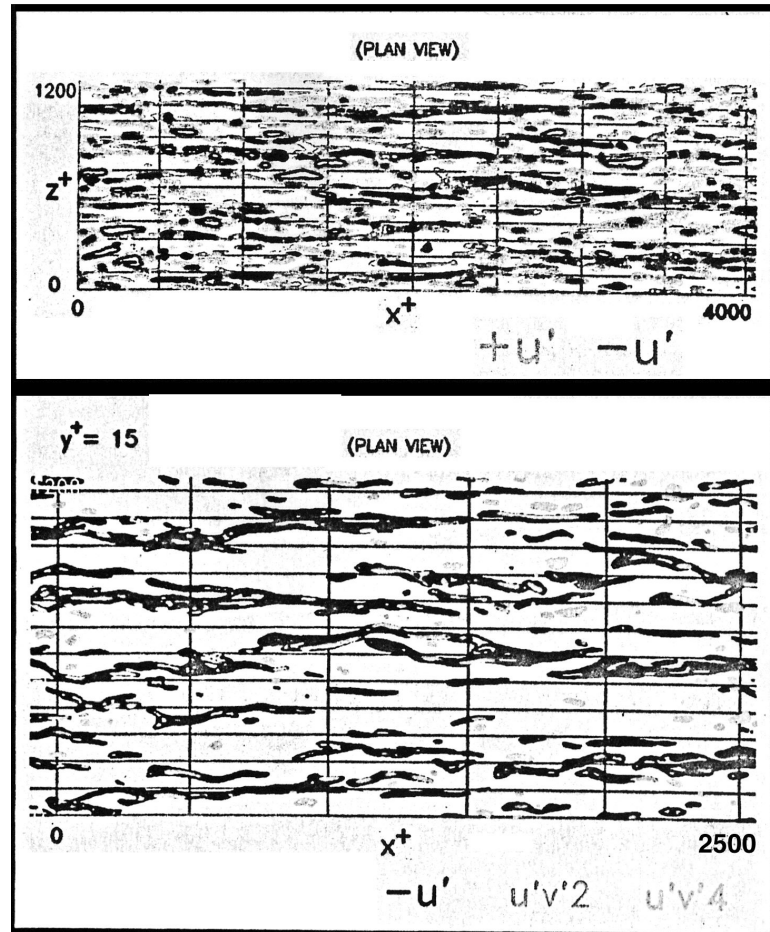
Figure 13.4: (a) Low- and high-speed streaks; and (b) Low-speed streaks with ejections ($u'v'$ second quadrant) and sweeps ($u'v'$ fourth quadrant). From the analysis of Spalart's DNS of a turbulent boundary layer by Robinson *et al.* (1989). Flow is from left to right, $Re_\theta = 640$, $y^+ = 15$.

production in the boundary layer, hence its importance.

Hot-wire anemometry has been used extensively to study the structure of coherent motions. However, identifying ejections and sweeps in hot wire data is a complicated task. Various conditional sampling techniques have been developed to cope with this problem. Wallace *et al.* (1972) and Wilmarth & Lu (1972) introduced the quadrant technique, a method for classifying $u'v'$ events. They labelled a burst a quadrant two (Q2) event ($u' < 0$, $v' > 0$), and a sweep a quadrant four (Q4) event ($u' > 0$, $v' < 0$). Events in the other two quadrants (Q1 and Q3) were labelled interactions. There are other methods used to detect ejections and sweeps, such as $u'v'$-threshold, $u'v'$ slope threshold, u' threshold (U-level), u' slope threshold, and variable-interval time-averaging (VITA). The effectiveness of each detection criterion were compared in Bogard & Tiederman (1986). They concluded that the

quadrant technique, with an appropriate threshold, can most readily iden-
tify ejections. The VITA and U-level techniques also had low probabilities
for error, but were more sensitive to the threshold chosen. Identifying bursts
and sweeps in visualization data is an even more complicated task, to be
discussed later.

There is considerable controversy as to what part of the burst-sweep cy-
cle contributes most to turbulent energy production. Grass (1971) showed
that the production of turbulent energy is an intermittent process, and that
it occurs through contributions by both sweeps and bursts. He also con-
cluded that the contribution of sweeps to turbulent energy production is
limited to the wall region, while the contribution of ejections extended well
into the outer region. Kim *et al.* (1971) concluded that nearly all of the tur-
bulent energy production occurs during ejections in the inner layer. Corino
& Brodkey (1969) concluded that bursting occurs 18% of the time and is
responsible for 50 to 70% of the total turbulence production. Kline & Corino
separately estimated that 70% of the Reynolds stress production occurs dur-
ing ejections. In contrast, Willmarth & Lu (1972) concluded that 60% of
the Reynolds stress production occurs during the sweep cycle. Lu & Will-
marth (1973) concluded that bursts account for 77% of $u'v'$ production, while
sweeps account for 55%. The excess over 100% is accounted for by inter-
actions with negative contributions. Wallace *et al.* (1972) measured equal
contributions (70%) from ejections and sweeps. These values are the result
of analysis of hot wire data.

A number of investigators have attributed the existence of the high-
and low-speed streaks and the bursting cycle in the viscous sublayer to the
presence of counter-rotating streamwise vortex pairs. Bakewell & Lumley
(1967) found, through an eigenfunction decomposition of the fluctuating
streamwise velocity, that the dominant coherent structure in the inner layer
was a streamwise counter-rotating vortex pair elongated in the streamwise
direction, with an average spanwise separation of 90–100 wall units (see
figure 13.5). The planes of circulation of these vortices were found to be
inclined slightly upstream from wall normal. The effect of these streamwise
vortices on the surrounding fluid is to sweep near-wall low-momentum
fluid between them and induce an upward motion. Bakewell & Lumley
suggested the ejections result from the plane of circulation of the stream-
wise vortices becoming normal to the wall, coupled with an increase in
circulation. Townsend (1970) proposed that a pair of counter-rotating vor-
tices inclined 30° to the floor was the dominant-coherent structure in the
near-wall region. Head & Bandyopadhyay (1981) found visual evidence for
these vortices (see figure 13.6). How are these vortices formed?

Tu (1966) hypothesized that the vortices are formed when transverse
vorticity undergoes local distension near the wall. The distended vortex
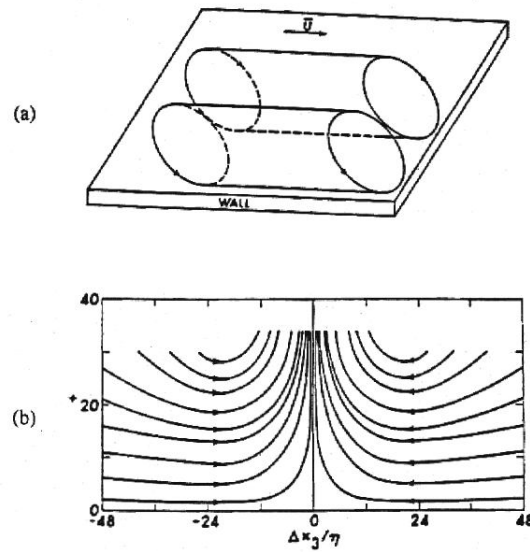loop is stretched and distorted into counter-rotating vortex pairs. Brown &

Figure 13.5: A streamwise counter-rotating vortex pair, proposed by Bakewell & Lumley (1967) to be the dominant vortical structure in the inner layer: (a) proposed structure; (b) corresponding streamlines on centerline.
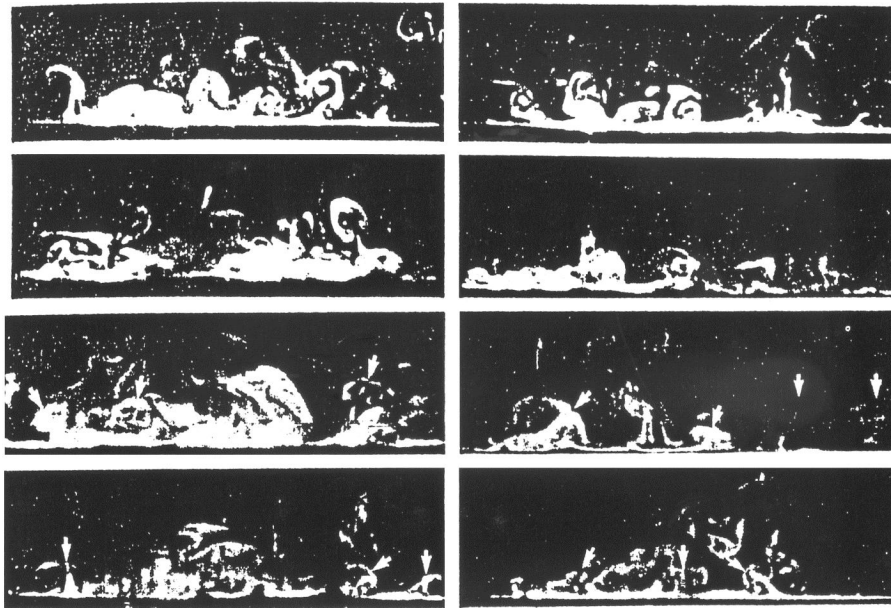

Figure 13.6: Streamwise vortex pairs from the visualization by Head & Bandyopadhyay (1981).

Thomas (1978) found that the large-scale structure streamlines are concave near the wall (see figure 13.7). Here, the mean vorticity and the circulation are of opposite signs, which according to Rayleigh is the criterion for an
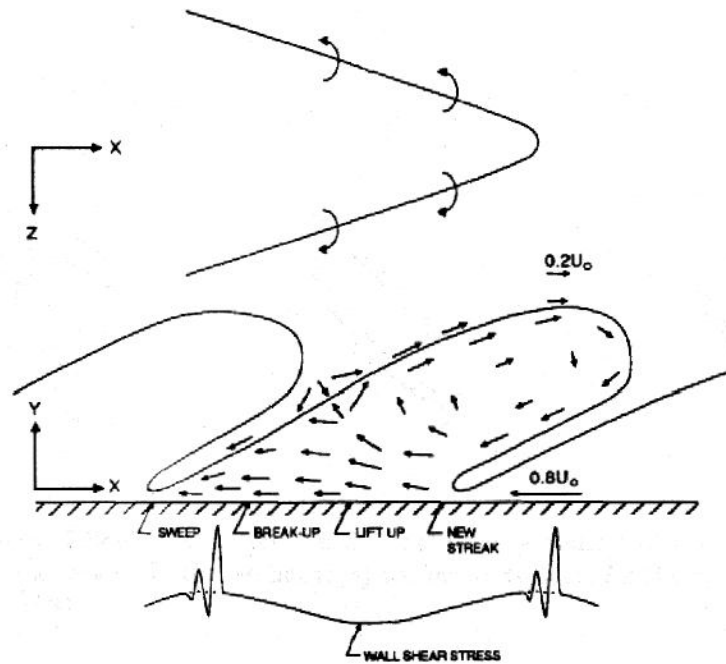
Figure 13.7: Curvature of the inner layer streamlines which may give rise to Taylor-Görtler instabilities. From Brown & Thomas (1978).

inviscid instability. In a viscous flow, if the streamline curvature is large enough, the condition may give rise to Taylor-Görtler vortices. This, Brown & Thomas concluded, is the mechanism for the formation of the streamwise vortices. Alternatively, it has been suggested that the streamwise vortices are actually the legs of the horseshoe vortices. However, Robinson *et al.* showed that not all these quasi-streamwise vortices, as they called them, are the legs of horseshoe vortices, and that whole horseshoe vortices with two trailing legs are very rare. In addition, the length of these legs (vortices having a predominantly streamwise orientation, according to Robinson *et al.*) is much less than the expected length of the streamwise counter-rotating vortex pairs according to Bakewell & Lumley.

In addition to legs, Robinson *et al.* classified vortices as necks, extending upward from the floor at an angle of about 45° to the floor, and heads, having a predominantly transverse orientation (see figure 13.8). The vortices were extracted from the numerical data by assuming that the vortices have a low-pressure core, and setting an appropriate pressure threshold. Changing the pressure threshold alters the connectivity of the vortices, but the basic shape of the vortices is maintained. Robinson *et al.* found that strong ejections, in general, occur in two locations: on the inboard sides of legs, and behind heads. This is to be expected, since the vortices there, through Biot-Savart interactions, induce an upward velocity in the surrounding fluid. Likewise,
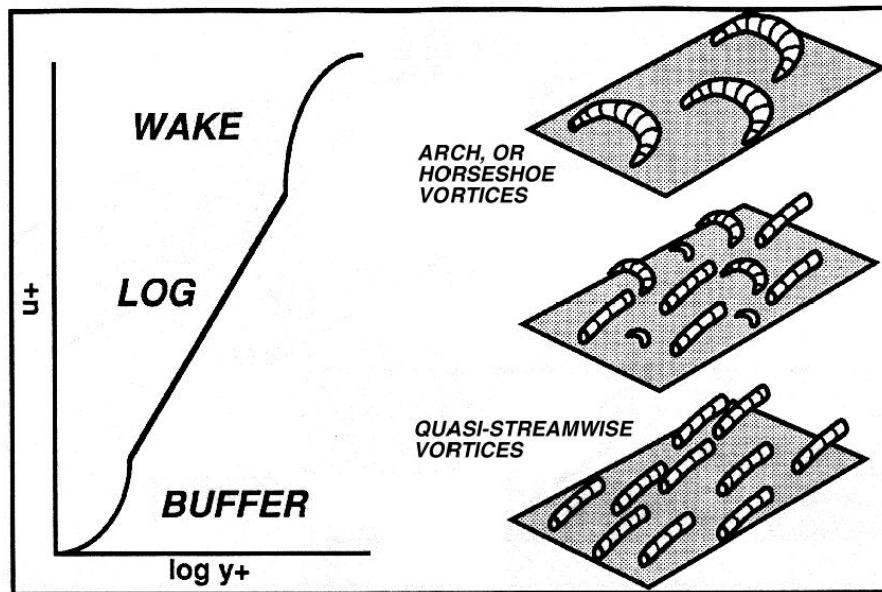
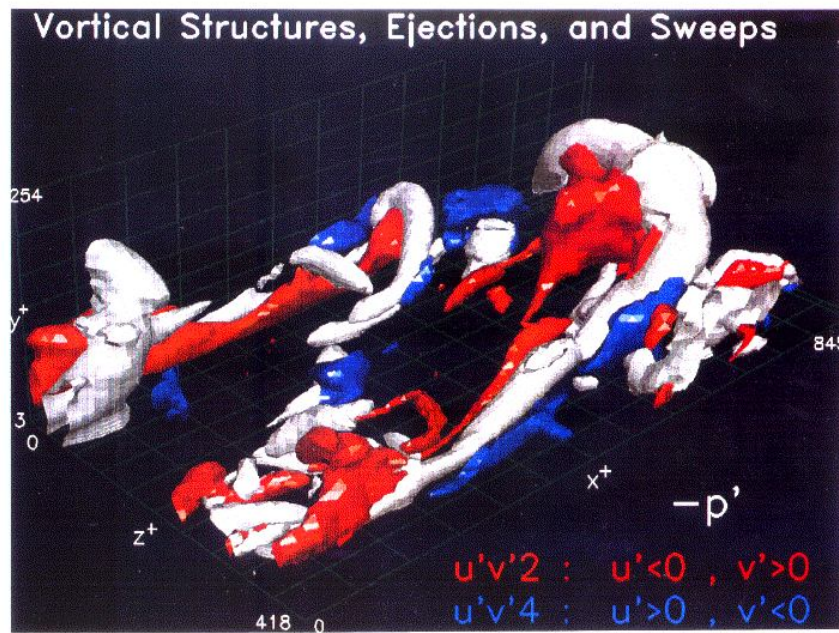Figure 13.8: Vortex taxonomy by Robinson *et al.* (1989).

Figure 13.9: Location of ejection ($u'v'$ second quadrant) and sweep ($u'v'$ fourth quadrant) events with respect to vortical structures. From Robinson *et al.* (1989).

strong sweeps are generally found on the outboard sides of legs and necks (see figure 13.9).

13.3   Outer Layer Structures

Since it was an accepted fact that most of the turbulent energy production occurs in the inner layer, and it appeared that the outer layer was rather passive, most of the early coherent structure studies focused on the inner layer. There has been, however, renewed interest in the outer layer in recent years. Large-scale structures appear to play an important role in the dynamics of the turbulent boundary layer. They are responsible for large-scale mixing in the outer layer, and play a dominant role in the entrainment of high-momentum freestream fluid into the boundary layer. Large-scale structures may also provide the trigger for inner layer instabilities to develop.

Chen & Blackwelder (1978) used temperature tagging to study the large-scale structures in a turbulent boundary layer. They heated the wall slightly so that low momentum, near-wall fluid would be "hot," and high momentum, outer layer fluid would be "cold" Using two vertically displaced hot-wire probes, they found the average time delay between when the hot-cold interface marking a large-scale structure reached the lower and higher probes. They were thus able to determine the average large-scale structure angle to be approximately $45°$ between $y/\delta = 0.15$ and 0.67.

The outer layer appears to be dominated by large scale vortical structures, called bulges, and large scale incursions of irrotational fluid that may reach almost all the way to the floor. These bulges have spanwise and streamwise dimensions of the order of δ, and have long survival distances. The convection velocity of bulges was found to be between 0.8 and $0.9U_\infty$. Kovasznay *et al.* (1970) found that if the flow were viewed from a coordinate system moving at this convection velocity, a stagnation point appears on the back of the large-scale structure at about $y/\delta = 0.8$. This phenomenon was also observed by Brown & Thomas (1978) and Falco (1977) (see figure 13.10). Kovasznay *et al.* concluded that the upstream-facing side of the structure is the most active. This phenomenon of increased turbulence activity on the upstream-facing region of a turbulent/non-turbulent interface is found in a number of flows.

Head & Banyopadhyay (1981) performed an extensive survey of outer layer coherent structures at various Reynolds numbers. The visualization study consisted of seeding the turbulent boundary layer with smoke and illuminating it with a laser sheet at various orientations. These included transverse light planes inclined downstream at $45°$, the average characteristic angle of the horseshoe vortices, and upstream at $45°$, perpendicular to the plane of the horseshoes (see figure 13.11). The visualization with the laser sheet oriented at $45°$ downstream showed a number of inverted U-shaped structures which were interpreted as being horseshoe vortices. It was noted that the aspect ratio of these U-shaped structures increased with Reynolds number. With the laser sheet oriented at $45°$ upstream, the visual-
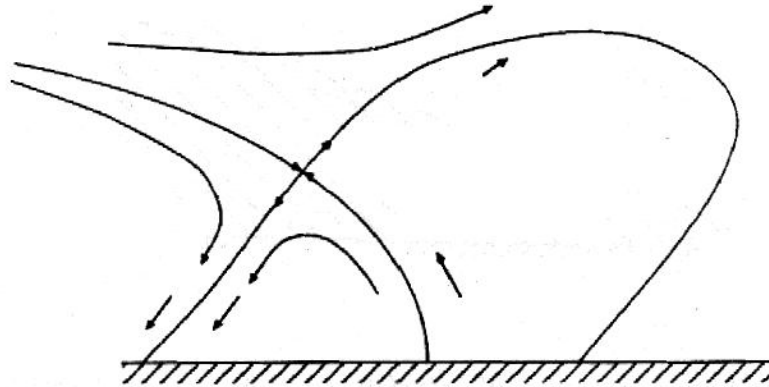
Figure 13.10: Streamlines in a large-scale bulge with the observer moving at $0.8U_\infty$, showing the saddle point on the back of the structure. From Falco (1977).
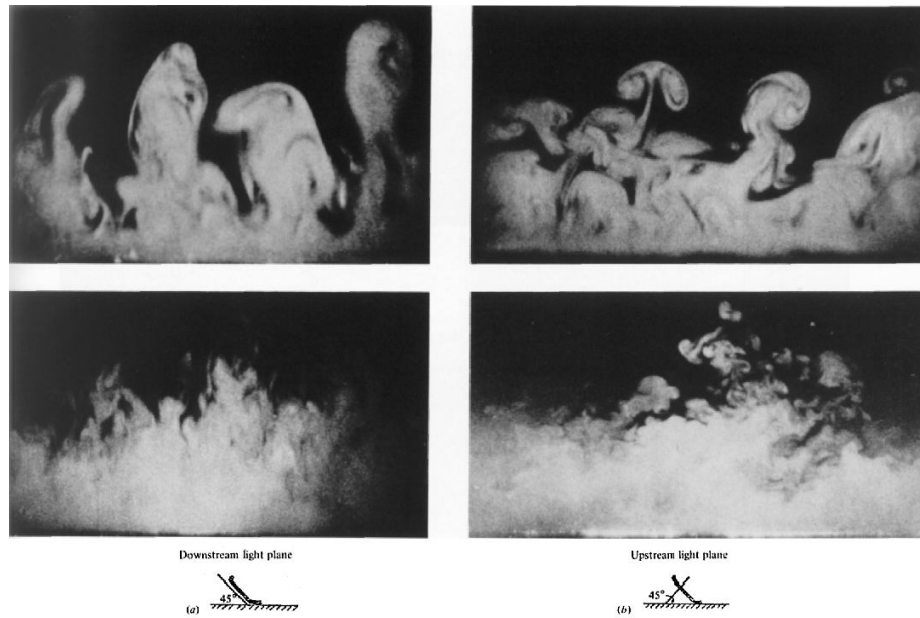

Figure 13.11: Cuts along and perpendicular to the plane of the horseshoe vortices, showing (a) inverted U-shaped loops; and (b) mushrooms. Top: low Reynolds number; Bottom: high Reynolds number. From Head & Bandyopadhyay (1981).

ization revealed counter-rotating vortex pairs resembling mushrooms. This seemed to confirm that horseshoe vortices were, in fact, the dominant coherent structure in the turbulent boundary layer. However, the upstream- and downstream-facing plane cuts were never of the same structure at the same instant in time. Tnerefore, that these structures were horseshoe vortices could not be proven conclusively.

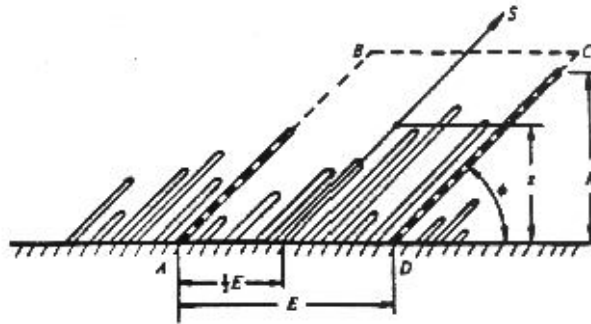When the flow was visualized using a streamwise-oriented laser sheet,

Figure 13.12: Random distribution of horseshoe vortices. From Perry & Chong's (1982) model of a turbulent boundary layer.

it was observed that, at least occasionally, the horseshoe vortices would rise from the floor in an ordered fashion, their heads making a 20° angle to the floor. This, in addition to being another level of coherence, could suggest that the formation of a horseshoe vortex and its rise from the wall creates conditions which are beneficial to the formation of a smaller horseshoe behind it.

Perry & Chong (1982) proposed a model for the turbulent boundary layer consisting of different distributions of Λ-shaped vortices, inclined at a characteristic angle to the floor, embedded in an irrotational flow (see figure 13.12). The model assumes that all the circulation in the flow resides in these vortices. The vortices, through Biot-Savart interactions, move and stretch each other. This stretching results in an increase in the vortex's aspect ratio, causing the vortex legs to come closer together. This results in vorticity cancellation and eventually, death by viscous dissipation. Perry & Chong used random, discrete, and continuous distributions of vortex heights in their model. They set both the discrete and continuous distributions to satisfy the law of the wall, and their model in turn predicts other known turbulent boundary layer parameters such as spectra. Their work helped validate the findings of many previous studies which suggested that horseshoe vortices are the dominant structure in turbulent boundary layers.

The combined visualization and hot wire study by Palco (1977) introduced the notion of the "typical" eddy as the coherent structure responsible for a large part of the Reynolds stress production in the outer layer. Typical eddies are highly coherent three-dimensional vortical structures, and are found in turbulent boundary layers, wakes, jets, and mixing layers. In turbulent boundary layers, they are found embedded in large-scale bulges, and resemble distorted laminar vortex rings (see figure 13.13). Falco determined the average height and length of the typical eddies, but since his visualization study was conducted along a streamwise plane, no information about
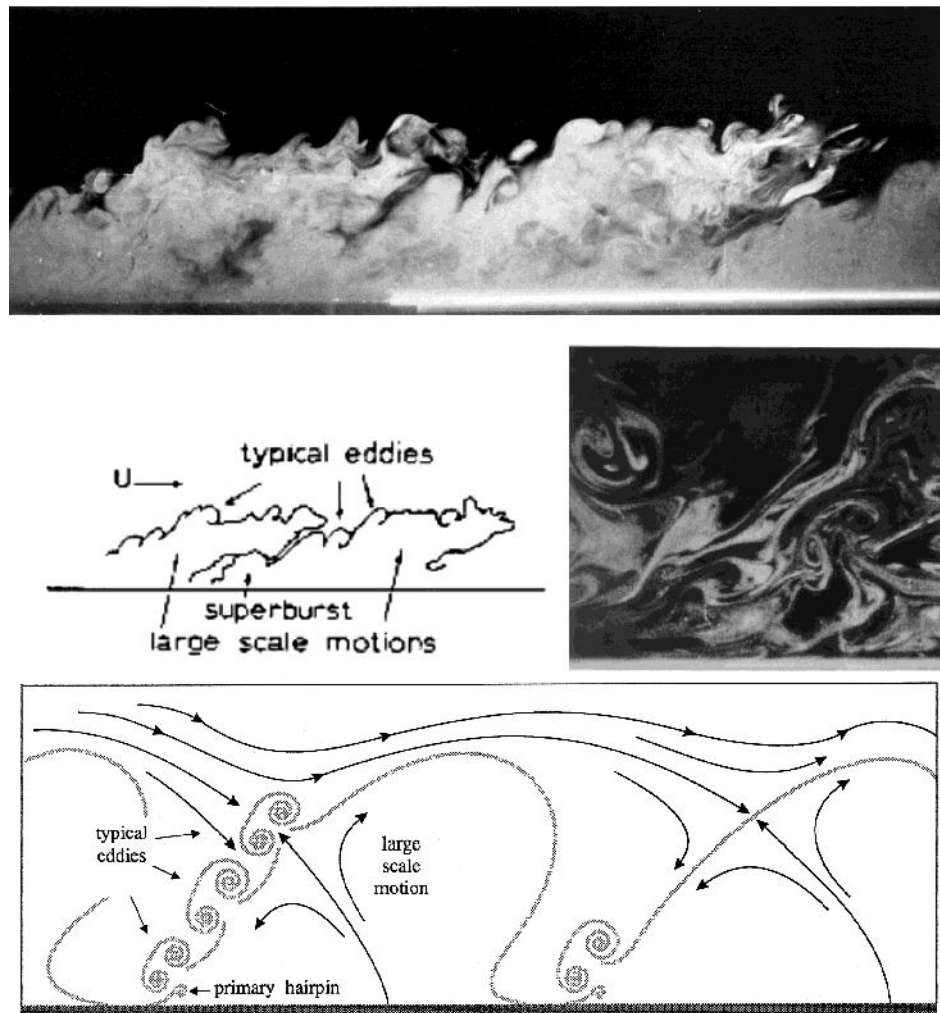
Figure 13.13: (a) "Typical" eddies in a turbulent boundary layer; (b) Idealized spanwise; and (c) cross-sections of a typical eddy. From Falco (1977). The flow is from left to right.

the spanwise scale of these eddies could be obtained. The average typical eddy streamwise size was found to be constant at around 200 wall units. It is interesting that the streamwise scale of these eddies is fixed when the length is scaled on inner layer parameters. This point will be discussed further in later sections. Typical eddies in the log region were found to have a convection velocity less than the convection velocity of the bulges they appear in, and usually became part of bulges upstream that overtook them. In contrast, typical eddies in the outer layer convect downstream faster than the large scale structure they appear in and will move to the front of the bulge.

13.4   Interactions

When the bursting cycle was first studied, it was assumed to be a purely inner layer phenomenon which scaled on inner layer parameters. Kline *et al.* (1967) proposed that the bursting period scaled on v and u_τ. However, in 1971, Rao *et al.* showed that, over a large range of Reynolds numbers, the mean bursting period scales on U_∞ and δ. They proposed a strongly interactive relationship between the inner and outer layers, one where large scale structures scour the inner layer, causing intense shear which triggers local instabilities, resulting in ejections. Laufer & Badri Narayanan (1971) noted that the mean bursting frequency is approximately equal to the frequency of the passage of large scale structures in the outer layer. Blackwelder & Kaplan (1976) also concluded that the bursting frequency scales on outer variables. In contrast, Blackwelder & Haritonidis (1983) and Luchik & Tiederman (1987) concluded that the bursting frequency scales on inner variables. This ongoing controversy suggests a complex relationship between the inner end outer layers.

There is further evidence which points to strong interactions between the inner and outer layers. Blackwelder & Kaplan (1976) examined the velocity signals from an array of ten hotwires arranged vertically or in the spanwise direction (see figure 13.14). They found a high degree of correlation in the large scales in the vertical direction throughout the boundary layer, but almost none in the spanwise direction (at a y^+ of 15). This is due to the small scale of the structures at this height in the sublayer. Palco found that the Reynolds number dependence of the typical eddy scale was removed by non-dimensionalizing the eddy lengths with inner variables, a strange notion since typical eddies are a turbulent phenomena, not a viscous phenomena. Over this range, the average eddy streamwise scale is approximately constant at 200 wall units, and the average vertical scale increases slowly from an initial value of about 100 wall units. He reports that the Lu & Willmarth (1972) measurements of the duration of intense turbulent production in the outer layer, when non-dimensionalized with inner variables, fit on the specified range. Head & Bandyopadhyay (1981) concluded that Falco's typical eddies were actually longitudinal sections of horseshoe vortex tips. This seems to explain the scaling of the typical eddies on inner layer variables, and lends credence to Antonia's (1972) conclusion that "there seems to bc little doubt that large-scale bursts (of high shear stress) observed near the outer region of the boundary layer originate from or at least extend through to the inner layer region of the flow."

Praturi & Brodkey (1978) performed a stereoscopic study of a turbulent boundary layer ($\text{Re}_\theta = 900$) by photographing the motion of tracer particles, using a camera moving with the flow at 70% of the freestream velocity. They concluded that "wall-region vortex motions are a result of in-
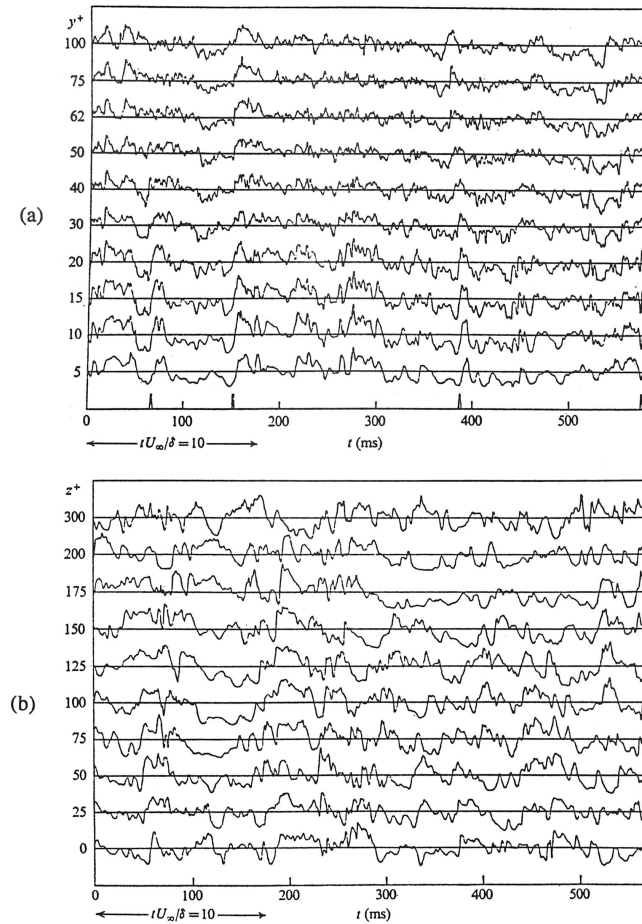
Figure 13.14: Velocity traces from an array of ten hot wires placed in a turbulent boundary layer, arranged (a) vertically; and (b) spanwise. From Blackwelder & Kaplan (1976).

teraction between the incoming higher-speed fluid from the outer region of the boundary-layer and the outflowing low-speed wall-region fluid." This observation is in direct contradiction to all models which suggest that the outflow of low-speed fluid in the near wall region is caused by counter-rotating vortex pairs. In addition, even though large numbers of frames were studied, complete horseshoe vortices were not detected, although the vortex elements which make up horseshoes were observed. This conclusion agrees with that of Robinson *et al.* (1989).

Brown & Thomas (1978) correlated wall shear stress data with velocity data at various heights in the boundary layer. They found a line of maximum correlation tilted 18° from the horizontal, which they hypothesized was due to a large-scale organized structure moving at a characteristic convection velocity and angle producing a wall shear stress response. Offen &
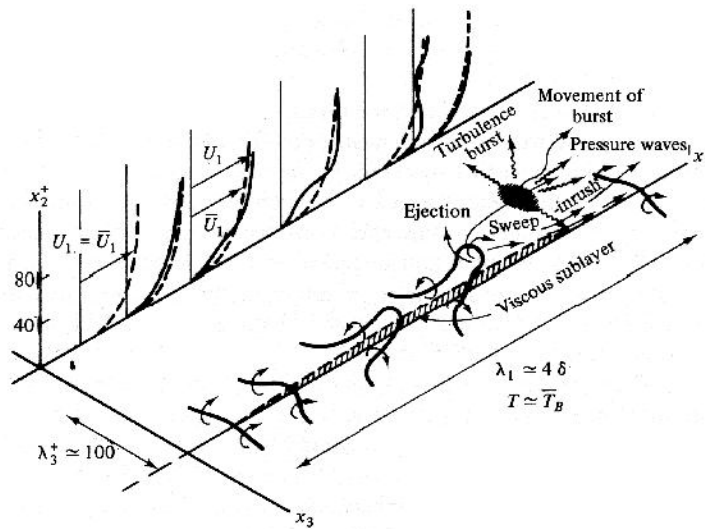
Figure 13.15: Model of the interaction between a horseshoe vortex and a low-speed streak. From Hinze (1975).

Kline (1975) suggested that structures in the logarithmic region are responsible for sweeps, which in turn, establish conditions which cause ejections further downstream. They also hypothesized that large scale outer layer structures are formed as a result of vortex pairing by a number of remnants of the vortices associated with the bursting cycle. Smith (1978) studied the relationship between inner and outer layer coherent structures using flow visualization from a moving frame of reference. He proposed that bursting is directly related to the passage of a large-scale motion, usually a transverse vortex. Logarithmic-layer typical eddies could very well be the large-scale structure in question.

Researchers have long believed that a strong dynamical link exists between horseshoe vortices and the bursting cycle. Hinze (1975) proposed the following model: due to some outer-layer disturbance, he states, a horseshoe vortex forms close to the wall (see figure 13.15). The vortex tip rises from the wall due to self-induction, and the velocity gradient stretches the vortex. The stretching causes the vorticity to become more concentrated, inducing an outward flow between its legs. As the horseshoe rises from the floor, an intense shear layer with an inflection point forms, giving rise to local instabilities which produces breakdown of the vortex tip. The pressure wave of this chaotic break-up, or burst, propagate through the boundary layer. An inrush of high-momentum fluid follows. Interactions between this sweep and slower fluid may give rise to another horseshoe vortex, and the cycle repeats itself.

Acarlar & Smith (1984) studied the formation and evolution of horse-

shoe vortices using hydrogen bubbles. The viscous sublayer was tripped with a hemispherical disturbance embedded in the tunnel floor, causing vortex-sheet roll-up and the formation of a horseshoe vortex. Based on their observations, they proposed a model for the burst/sweep cycle (see figure 13.16): in a turbulent boundary layer, a disturbance, possibly from the outer layer, imposes an adverse pressure gradient on the near-wall fluid, causing a local deceleration. When the decelerated fluid interacts with faster-moving fluid in the near-wall region, a highly unstable inflectional velocity profile results, giving rise to a roll-up of the vortex sheet into horse-shoe vortices. Due to self-induction, the horseshoe moves away from the wall, and is stretched by the action of the shear flow. This creates a lateral pressure gradient which maintains the low-speed streaks. They attribute ejections to the strong streamwise pressure gradient created by the horse-shoe vortex tip. The ejection of low-speed fluid outward stops when the vortex tip rises too far from the wall. Smith also noted, as did Head & Bandyopadhyay, that as the horseshoe vortices rise from the wall, their tips align themselves at an angle between 15° and 30° to the wall. Moin & Kim (1985) concluded from their large-eddy-simulation of a turbulent channel flow that horseshoe vortices are formed from agglomerated vortex lines which coalesce into U-shaped vortex loops after having been perturbed (see figure 13.17).

Another interesting finding of the Head & Bandyopadhyay study was that the average spanwise extent of the horseshoe vortices was approximately 100 wall units regardless of Reynolds number (in the Re_θ range 600 to 9400), which coincides with the average spacing of the low-speed streaks in the viscous sublayer (see figure 13.18). This would seem to suggest that the spanwise scale of the horseshoe vortices is set in the inner layer, and as they rise from the floor (Head & Bandyopadhyay showed that the horseshoe vortices originate very close to the wall in a low Reynolds number turbulent boundary layer), their spanwise scale is maintained. However, by what mechanism does a horseshoe vortex originating at the wall with an average scale of 100 wall units get to be a δ-sized outer-layer structure? This question is more perplexing at high Reynolds numbers, where the separation of scales between the inner and outer layers is extreme. It could be that at intermediate to high Reynolds numbers, large-scale horseshoe vortices form in the logarithmic region due to inviscid instabilities, not at the wall due to viscous instabilities. If this is the case, Head & Bandyopadhyay's observation that the spanwise scale of the horseshoe vortices is maintained at 100 wall units throughout the boundary layer is particularly perplexing.

Moin & Kim (1986) analyzed both DNS and LES turbulent channel flow data to find the connection between the bursting cycle and horse-shoe vortices. Using the VISA (Variable-Interval Space-Averaging) detection technique proposed by Kim (1983), they were able to obtain the three-
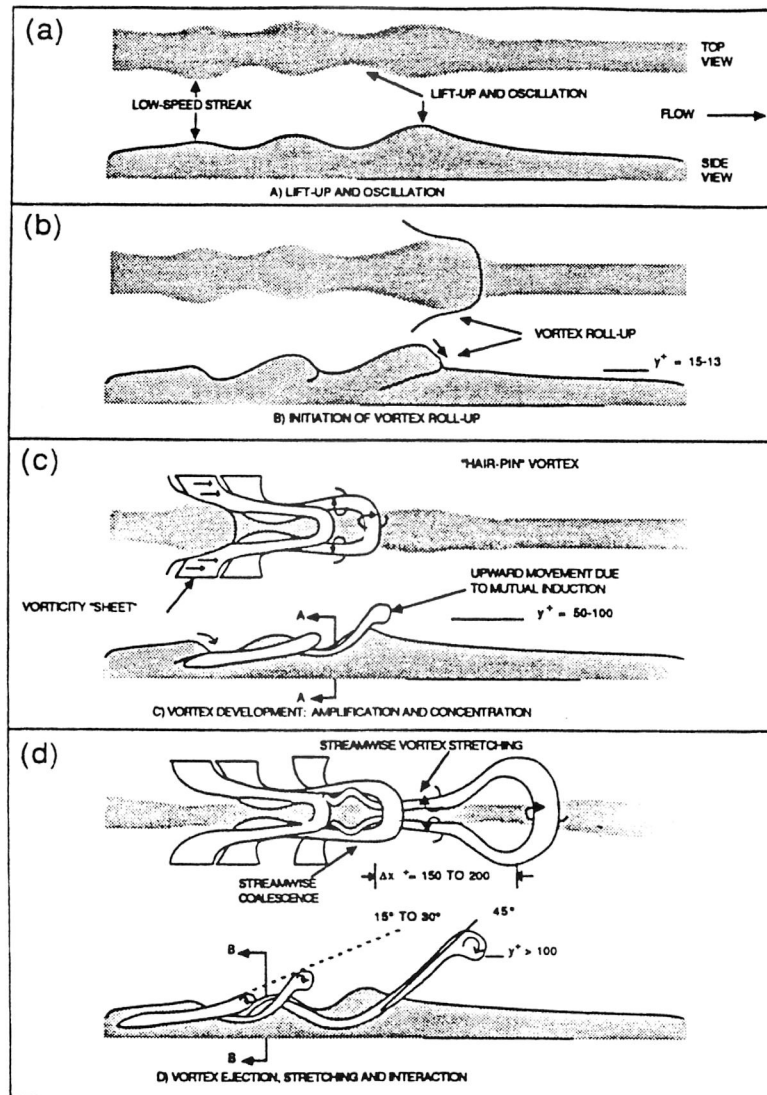
Figure 13.16: Model of the birth and evolution of a horseshoe vortex, and its interaction with a low-speed streak. From Acarlar & Smith (1984).

dimensional vorticity vector field coinciding with any single ejection or a sweep (see figure 13.19). Looking at the ensemble-averaged vortex lines resulting from the detection of Q2 (ejection) events, they found a pronounced horseshoe-shaped structure inclined at roughly 45° to the wall very near the detection point. They also found that the ensemble-averaged vortex lines of a Q4 (sweep) event revealed an inverted horseshoe vortex, pointing downward and upstream, slightly downstream of the detection point. This shows that, at least, horseshoe vortices are present during ejections and sweeps, and could be responsible for these events.
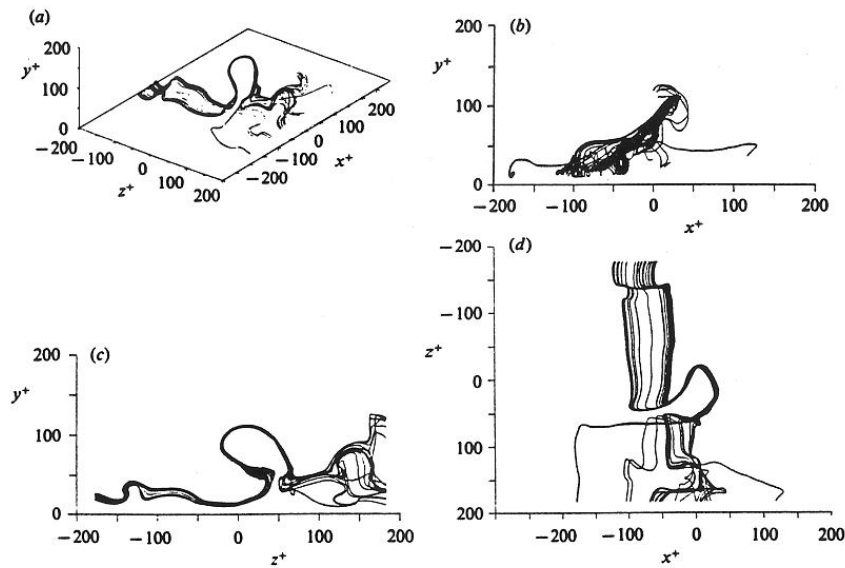
Figure 13.17: Instantaneous distribution of vortex filaments in a simulated channel flow, showing a horseshoe-like structure. From DNS of turbulent channel flow by Moin & Kim (1986).

13.5 A Study of Near Wall Scaling Laws

The following section was taken from Li Jun-de "The Turbulence Structure of Wall Shear Flows," Ph.D. Thesis, 1989, University of Melbourne, and Perry, Lim & Henbest (1985). Note that in their analysis (reproduced here), x is the streamwise direction (u'), y is the lateral direction (v'), and z is the wall-normal direction (w'). This conforms with the notation used in the geophysical fluid dynamics community, but it is different from the notation used elsewhere in these notes.

A characteristic of the turbulent boundary layer is that there exist many different length scales. These include the boundary layer thickness δ_H, the distance from the wall z, the Kolmogorov scale η and the viscous scale ν/u_τ, etc. Perry & Abell (1977), by using a dimensional analysis in conjunction with physical arguments, were able to show that in the turbulent wall region, the turbulence spectrum in different wavenumber regions scales with different length scales for the streamwise component. Their approach was based partly on the Townsend attached eddy hypothesis and was extended to the spanwise and normal to the wall components by Perry, Henbest & Chong (1986).

Figure 13.20 shows a schematic of three attached eddies of different scale with the instantaneous streamline pattern they each generate relative to the fluid at infinity. Imagine that these eddies are surrounded by fine scale
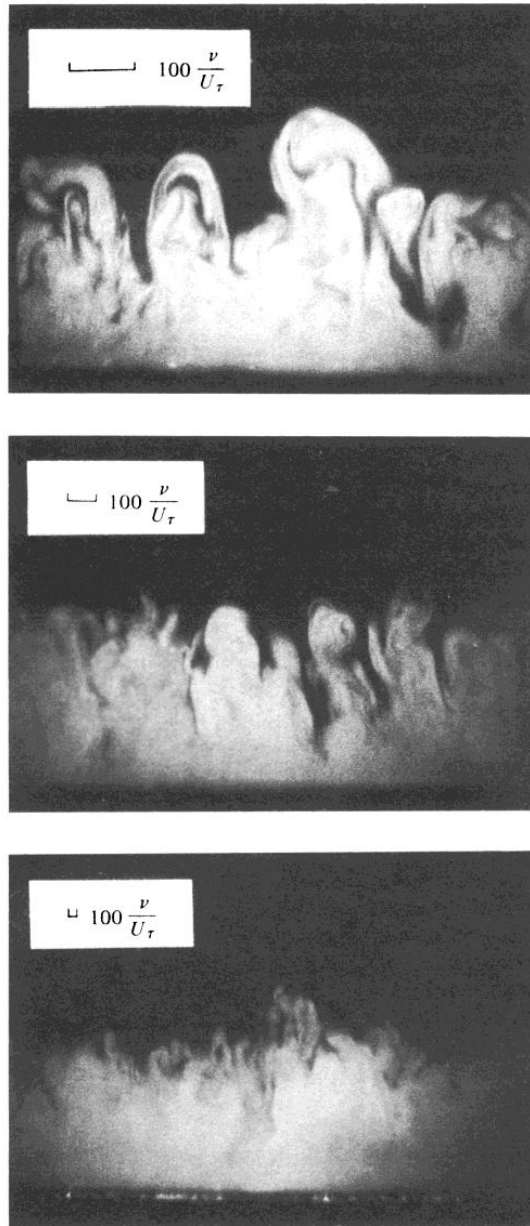
Figure 13.18: Visualizations showing preservation of the spanwise scale of horse-shoe vortices at 100 wall units for an order of magnitude change in Reynolds number. From Head & Bandypadhyay (1981).

"detached" motions, probably made up of the debris of older eddies that have been broken up and convected throughout the turbulent region. These detached motions are assumed to be locally isotropic and are thought to be responsible for a large part of the turbulent energy dissipation, but do not contribute to the mean vorticity and the Reynolds shear stress.
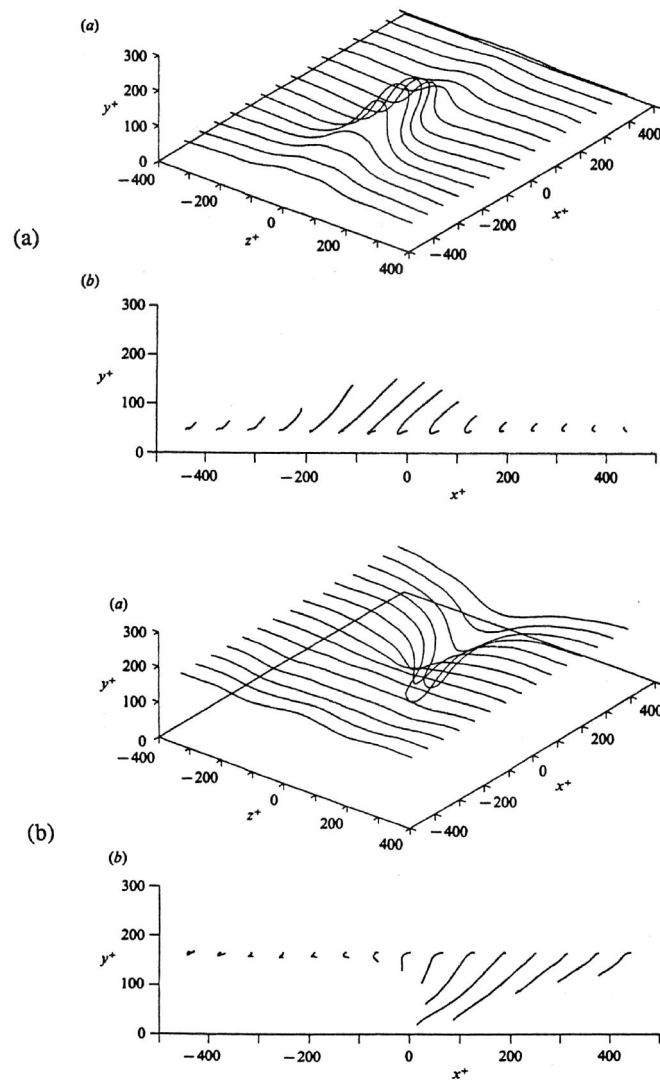
Figure 13.19: Ensemble average of vortex lines in the vicinity of an (a) ejection; and (b) a sweep, showing a horseshoe vortex and an inverted horseshoe, respectively. From DNS of turbulent channel flow by Moin & Kim (1986).

From figure 13.20 it can be seen that a hot-wire probe at a distance z from the wall will see contributions to u' (longitudinal velocity fluctuations) and to v' (lateral velocity fluctuations) from eddies of scale z and larger, whereas contributions to w' (normal velocity fluctuations) will only be made from eddies of height of order z.

The following analysis is applicable for $z \ll \delta_H$ and for $z \gg v/u_\tau$ (the turbulent wall region) on a smooth wall. Here, δ_H is the boundary layer thickness using the Hama (1954) velocity defect formulation for constant
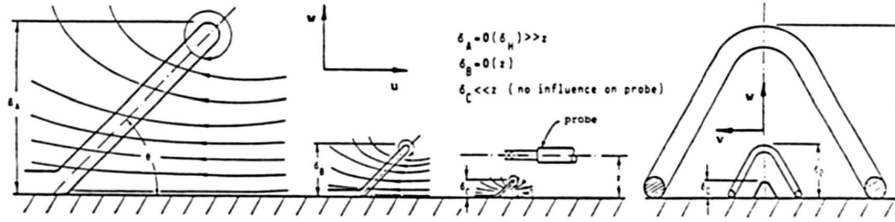
Figure 13.20: A sketch of three attached eddies of varying scales together with the instantaneous streamline pattern they each generate.
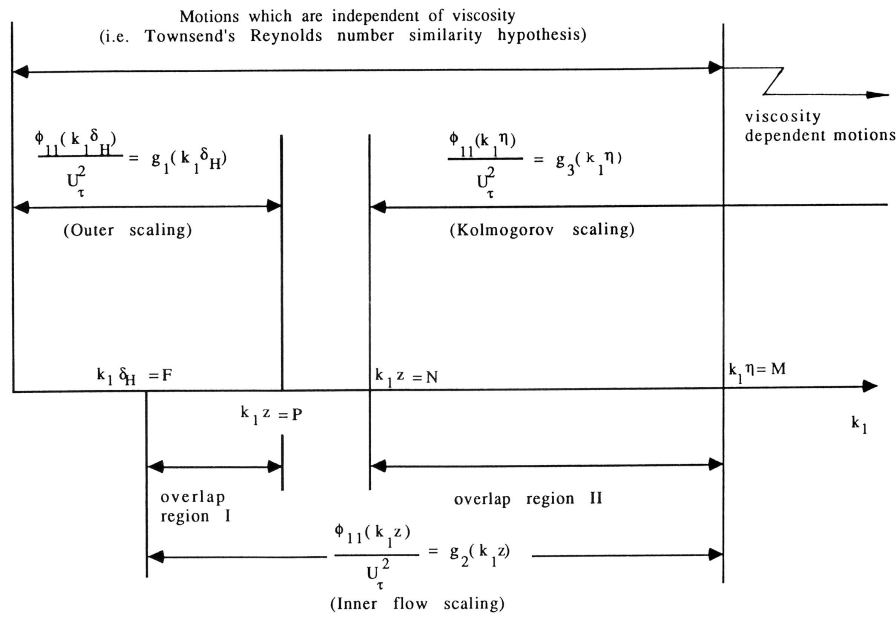

Figure 13.21: Wavenumber regions for the longitudinal spectrum showing regions of overlap.

pressure layers.

The behavior of the velocity fluctuation spectra in the wall region can be separated into three different wavenumber regions. Let $\phi_{11}(k_1)$, $\phi_{22}(k_1)$ and $\phi_{33}(k_1)$ be the one-dimensional spectra for u, v and w respectively. According to Perry & Abell (1977) and Perry *et al.* (1986), $\phi_{11}(k_1)$ scales with the boundary layer thickness δ_H in the low wavenumber region, with the Kolmogorov length scale in the higher wavenumber region and with the local distance z from the wall in the wavenumbers in between. Figure 13.21 shows the summary of the various regions.

In the first region, we have "outer flow" scaling:

$$\frac{\phi_{11}(k_1\delta_H)}{u_\tau^2} = g_1(k_1\delta_H) = \frac{\phi_{11}(k_1)}{\delta_H u_\tau^2} \tag{13.1}$$

In the Kolmogorov region:

$$\frac{\phi_{11}(k_1\eta)}{\upsilon^2} = g_3(k_1\eta) = \frac{\phi_{11}(k_1)}{\eta\upsilon^2} \tag{13.2}$$

where υ is the Kolmogorov velocity scale. In between, we have "inner flow" scaling:

$$\frac{\phi_{11}(k_1z)}{u_\tau^2} = g_2(k_1z) = \frac{\phi_{11}(k_1)}{zu_\tau^2} \tag{13.3}$$

In the turbulent wall region, they adopted Townsend's assumption that the local energy production $\wp$ equals the local energy dissipation rate ε.

$$\wp = -\overline{u_1u_3}\frac{\partial U}{\partial z} = \varepsilon \tag{13.4}$$

By using the law of the wall in the wall region, they obtained

$$\upsilon = \left(\frac{\nu u_\tau^3}{\kappa z}\right)^{1/4}$$

and

$$\eta = \left(\frac{\nu^3 \kappa z}{u_\tau^3}\right)^{1/4} \tag{13.5}$$

When the Reynolds number is high enough, Perry *et al.* (1986) anticipated that there will be two overlap regions existing in the streamwise spectra.

Figure 13.21 shows these overlap regions,where F is a characteristic constant and P, N and M are universal constants.

In the overlap region from $k_l\delta_H = F$ to $k_lz = \wp$,

$$\frac{\phi_{11}(k_1z)}{u_\tau^2} = \frac{A_1}{k_1z} = g_2(k_1z) \tag{13.6}$$

and

$$\frac{\phi_{11}(k_1\delta_H)}{u_\tau^2} = \frac{A_1}{k_1\delta_H} = g_1(k_1\delta_H) \tag{13.7}$$

These relations are compatible only if there exists the -1 law as shown and A_1 is a universal constant. In the second overlap region, that is, from $k_1z = N$ to $k_1\eta = M$, by requiring that the spectrum is independent of viscosity ν,they obtained:

$$\frac{\phi_{11}(k_1\eta)}{\upsilon^2} = \frac{K_0}{(k_1\eta)^{5/3}} = g_3(k_1\eta) \tag{13.8}$$

$$\frac{\phi_{11}(k_1z)}{u_\tau^2} = \frac{K_0}{\kappa^{2/3}}\frac{1}{(k_1z)^{5/3}} = g_3(k_1z) \tag{13.9}$$
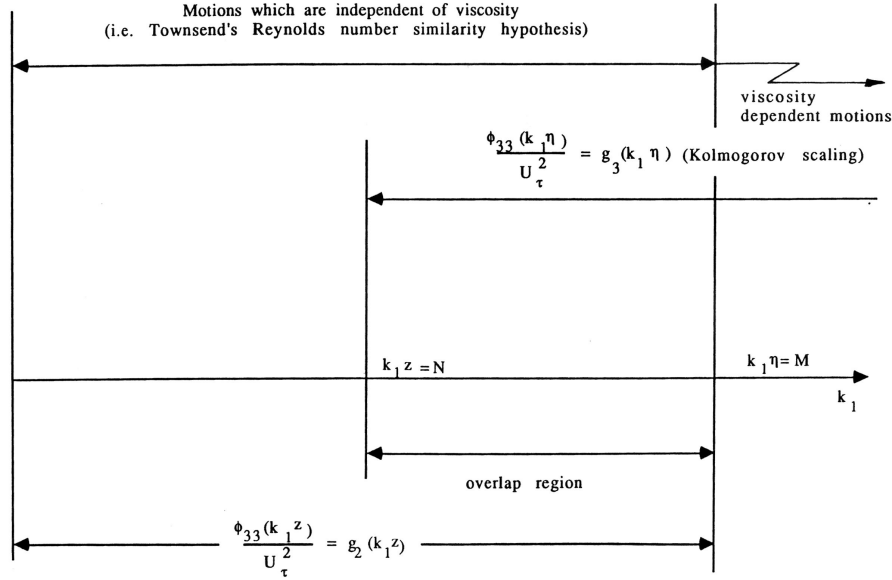
Figure 13.22: Wavenumber regions for the normal to the wall spectrum showing regions of overlap.

where K_0 is the Kolmogorov universal constant. Townsend (1976) proposed that $K_0 \approx 0.5$.

By using the attached eddy hypothesis, it can be seen that the spanwise spectrum $\phi_{22}(k_1)$ is of the same functional form as $\phi_{11}(k_1)$. In the first overlap region the universal constant becomes A_2 and in the second overlap region there is a 4/3 factor which results from the isotropic condition.

For $\phi_{33}(k_1)$, they argued that the only eddies that contribute to the normal to the wall component are the eddies that scale with the distance from the wall. Thus there is no outer flow scaling and only two regions exist for $\phi_{33}(k_1)$. This has been shown in figure 13.21. Again, when the Reynolds number is high enough, there is one overlap region. For this region they derived:

$$\frac{\phi_{33}(k_1\eta)}{v^2} = \frac{4}{3}\frac{K_0}{(k_1\eta)^{5/3}} \tag{13.10}$$

and

$$\frac{\phi_{33}(k_1z)}{u_\tau^2} = \frac{4}{3}\frac{K_0}{\kappa^{2/3}}\frac{1}{(k_1z)^{5/3}} \tag{13.11}$$

The inconvenience of the above scaling laws for spectra is that they are not given by a single formula which is valid over the entire wavenumber range. Perry, Li, Henbest & Marušić (1988b) derived such a formula from a curve fitting procedure for each component. Although there is no physical basis for these more general formulae, they are designed to give a fairly ac-

curate indication of the shape of the spectra while preserving the asymptotic laws such as the -1 law and the -5/3 law with all the correct scaling.

The streamwise velocity component spectrum which incorporates these scaling laws is:

$$\frac{\phi_{11}(k_1\delta_H)}{u_\tau^2} = \frac{A'}{G_1 G_2} \frac{1}{(k_1 z)^{5/3}} \tag{13.12}$$

where

$$G_1 = \left(1 + \left[\tfrac{1}{2}\left\{1 + \tanh\left(\theta(k_1\delta_H - q)\right)\right\}\alpha k_1\delta_H\right]^2\right)^{1/2}$$

and

$$G_2 = \left(1 + \left[\beta\frac{u_\tau^2}{v^2}A'\frac{1}{(k_1\eta)K_{11}(k_1\eta)}\right]^m\right)^{1/m}$$

with $A' = 2.06$, $\alpha = 2.0$, $\beta = 0.500$, $\theta = 1.8$, $q = 0.9$ and $m = 0.4$.

The normal to the wall velocity component spectrum is:

$$\frac{\phi_{33}(k_1 z)}{u_\tau^2} = B'\left(1 + \left[\beta\frac{u_\tau^2}{v^2}\frac{z}{\eta}\frac{1}{(K_{33}(k_1\eta))}\right]^m\right)^{-1/m} \tag{13.13}$$

where $B' = 0.9$, $m = 0.8$ and $\beta = 0.903$.

The various constants in equations 13.12 and 13.13 are chosen according to the data from Lim (1985) and Perry *et al.* (1987) and according to Perry *et al.* (1988b) "they are subject to alteration without notice."

The terms $K_{11}(k_1\eta)$ and $K_{33}(k_1\eta)$ in equations 13.12 and 13.13 are the one-dimensional spectra derived by using the Kovasznay's spectral expression in the Kolmogorov equilibrium region (Kovasznay, 1948). They are:

$$K_{11}(k_1\eta) = 0.500(k_1\eta)^{-5/3} - 6.04(k_1\eta)^{-1/3} - 1.8(k_1\eta) + 0.306(k_1\eta)^2 + 7.03 \tag{13.14}$$

and

$$K_{33}(k_1\eta) = 0.669(k_1\eta)^{-5/3} - 4.02(k_1\eta)^{-1/3} - 0.153(k_1\eta)^2 + 3.51 \tag{13.15}$$

Figures 13.23 and 13.25 show the results calculated from equations 13.12 and 13.13 respectively and figures 13.24 and 13.26 show the pre-multiplied forms of these spectra. The figures show that the -1 law and the -5/3 law are very pronounced only when K_τ approaches 10^6 ($K_\tau = \delta_h u_\tau / v$). This K_τ value is reached only in meteorological data.

The broadband turbulence intensities can be obtained by integrating the streamwise spectrum over different regions, for example:

$$\begin{aligned}\frac{\overline{u^2}}{u_\tau^2} = & \int_0^F g_1(k_1\delta_H)d(k_1\delta_H) + \int_{Fz/\delta_H}^P g_2(k_1 z)d(k_1 z) + \int_P^N g_2(k_1 z)d(k_1 z) \\ & + \int_N^{Mk^{-1/4}z^{+3/4}} g_2(k_1 z)d(k_1 z) + \frac{u_\tau^2}{v^2}\int_M^\infty g_3(k_1\eta)d(k_1\eta)\end{aligned} \tag{13.16}$$
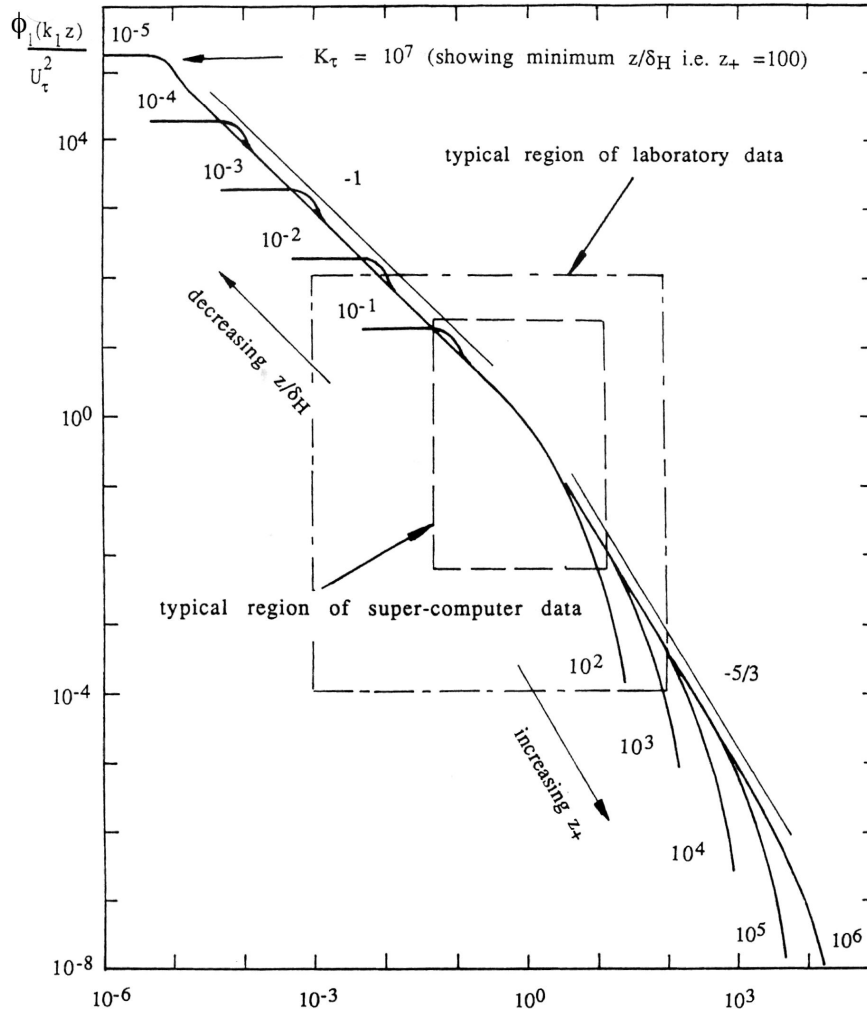
Figure 13.23: u' spectra in the turbulent wall region generated using equation 13.12.

By neglecting the last term in equation 13.16, Perry *et al.* (1986) derived:

$$\frac{\overline{u^2}}{u_\tau^2} = B_1 - A_1 \ln\left(\frac{z}{\delta_H}\right) - C\,(z^+)^{-1/2} \tag{13.17}$$

For the other two components, they give:

$$\frac{\overline{v^2}}{u_\tau^2} = B_2 - A_2 \ln\left(\frac{z}{\delta_H}\right) - \frac{4}{3}C\,(z^+)^{-1/2} \tag{13.18}$$

and

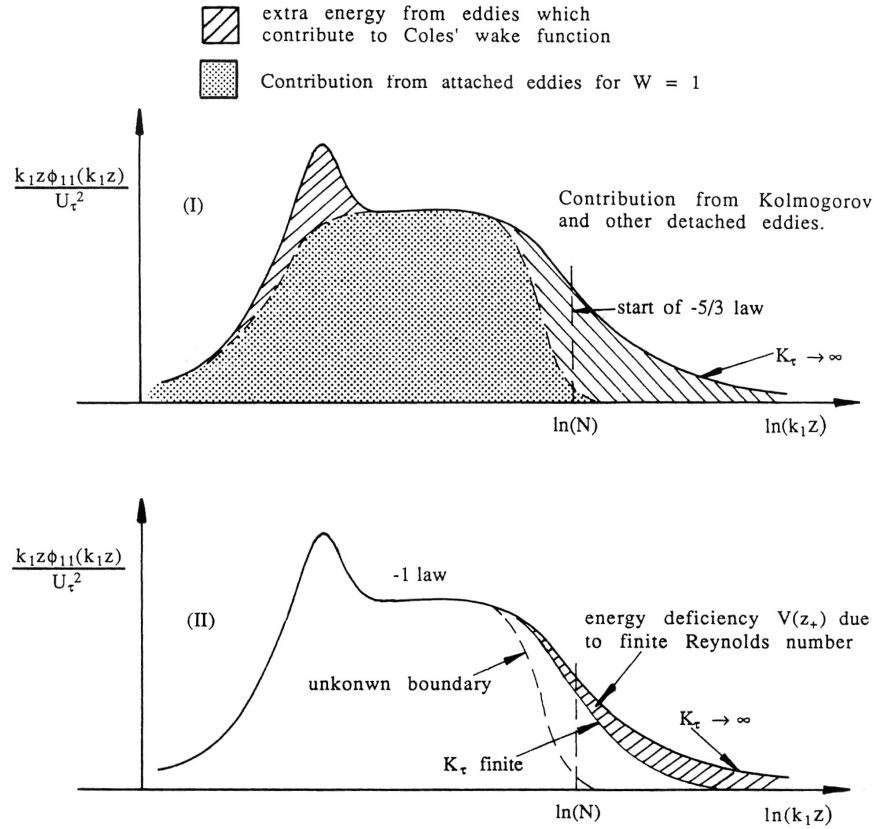$$\frac{\overline{w^2}}{u_\tau^2} = A_3 - \frac{4}{3}C\,(z^+)^{-1/2} \tag{13.19}$$

Figure 13.24: Premultiplied u' spectra. (I) Energy contribution from $K_\tau \to \infty$; (II) finite Reynolds number case.

where B_1 and B_2 are characteristic constants and A_1, A_2, A_3 and C are universal constants. All the formulaes in this section apply only to the turbulent wall region, that is, $100\nu/u_\tau < z < 0.156\delta_H$.

Perry, Lim & Henbest (1987) have attempted to verify experimentally these scaling laws and the broadband turbulence intensity profiles in the turbulent boundary layer. They showed that, in the turbulent wall region, the -1 laws exist in the u and v spectra and the -5/3 law exists in the spectra of the three components. These agree with the above scaling predictions.

Lim (1985) and Perry,Lim & Henbest (1987) have also attempted to verify the broadband turbulence intensity formulae (equations 13.17, 13.18 and 13.19) for turbulent boundary layers over smooth and rough walls. They found that the broadband turbulence intensities for the streamwise and the spanwise components agree well with the equations 13.17 and 13.18. For the normal to the wall component, the results were inconclusive. They attributed this to errors in the hot-wire anemometry techniques used and found that the data from other workers also gave inconclusive results.
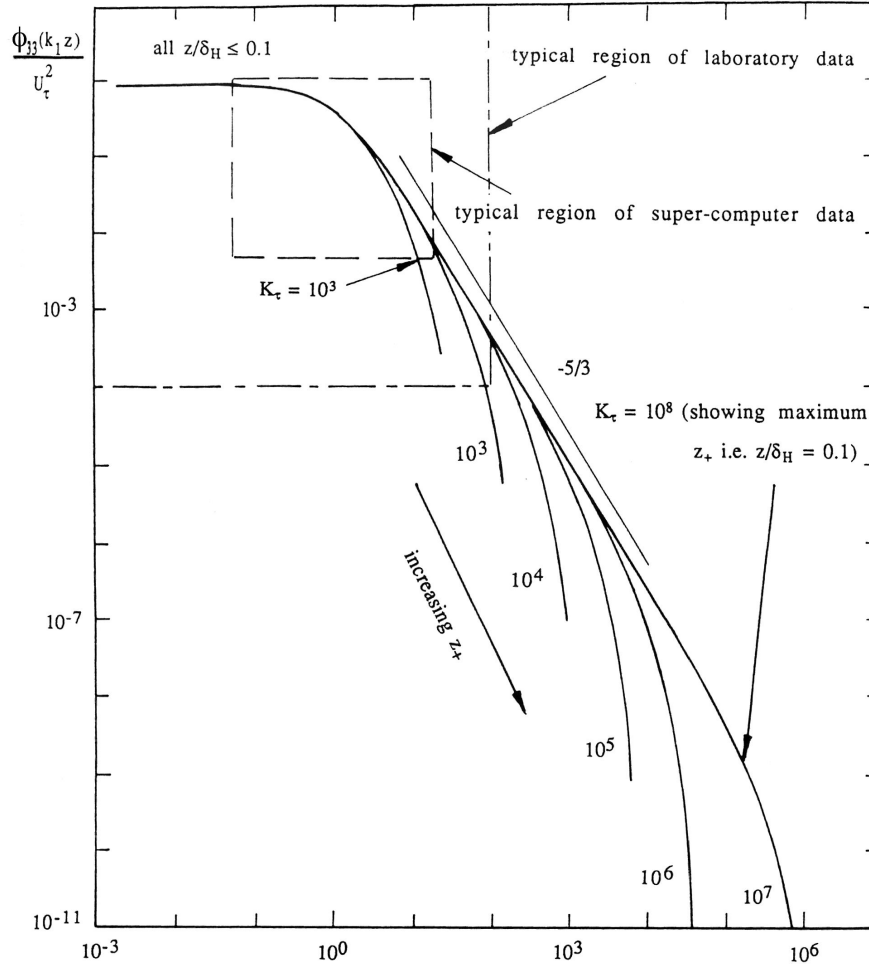
Figure 13.25: Wall-normal w' spectra in the turbulent wall region generated using equation 13.13.

Spalart (1988) has pointed out that the factor 4/3 in equations 13.18 and 13.19 should not be present and the viscous correction term in the equations should be isotropic because it has been assumed that the flow is isotropic in the Kolmogorov equilibrium region.

In equation 13.16, neglecting the last term on the right hand side introduces two problems. Firstly, as mentioned earlier, the amount of energy neglected is not fractionally the same for the three different components because near the wall $\overline{u^2} > \overline{v^2} > \overline{w^2}$. For the $\overline{w^2}$ quantity the contribution made by the last term in equation 13.16 is by no means negligible while for $\overline{u^2}$, the contribution is negligible. Secondly, for isotropic flow, the following
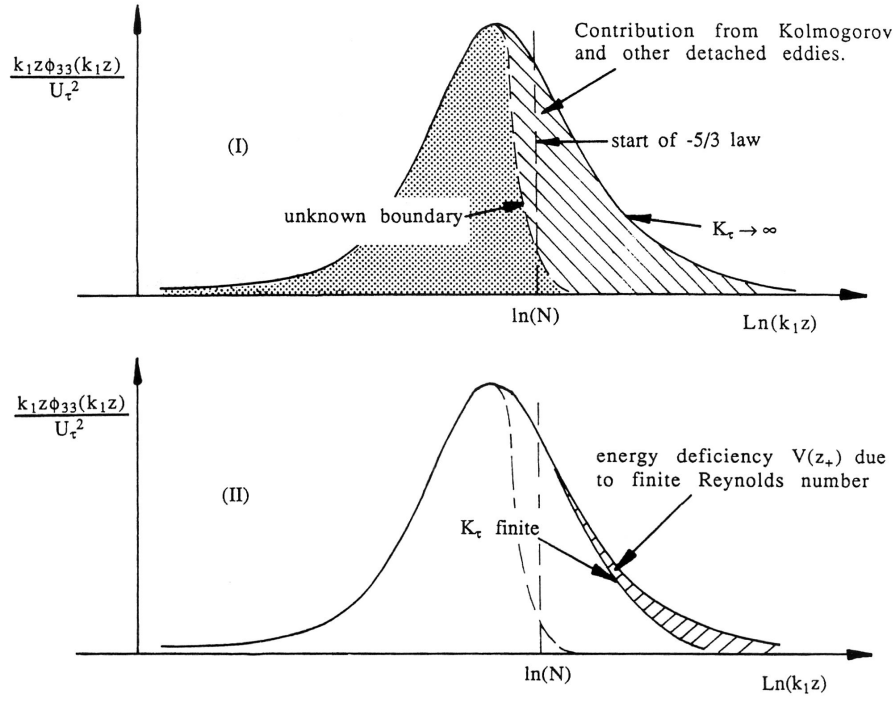
Figure 13.26: Premultiplied wall-normal w' spectra. (I) Energy contribution from $K_\tau \to \infty$; (II) finite Reynolds number case.

relation exists (Batchelor, 1953, or Hinze, 1975) for one-dimensional spectra:

$$\phi_{33}(k_1) = \phi_{22}(k_1) = \frac{1}{2}\left(\phi_{11}(k_1) - k_1 \frac{d\phi_{11}(k_1)}{dk_1}\right) \tag{13.20}$$

Equation 13.20 shows that the sudden arbitrary cut off of the $\phi_{11}(k_1)$ at $k_1\eta = M$ introduces a delta function for $\phi_{22}(k_1)$ and $\phi_{33}(k_1)$. This delta function was erroneously excluded in Perry *et al.*'s (1986) analysis and with its inclusion the factor 4/3 mentioned earlier becomes unity.

To resolve these issues Perry & Li (1990) first incorporated a more general viscous term such that

$$\frac{\overline{u^2}}{u_\tau^2} = B_1 - A_1 \ln\left(\frac{z}{\delta_H}\right) - V(z^+) \tag{13.21}$$

$$\frac{\overline{v^2}}{u_\tau^2} = B_2 - A_2 \ln\left(\frac{z}{\delta_H}\right) - V(z^+) \tag{13.22}$$

$$\frac{\overline{w^2}}{u_\tau^2} = A_3 - V(z^+) \tag{13.23}$$

where $B_1 = 2.39$ and $B_2 = 1.20$ are characteristic constants and $A_1 = 1.03$, $A_2 = 0.475$, $A_3 = 1.78$. $V(z^+)$ is the viscous correction and it is isotropic. Many forms have been suggested for $V(z^+)$ and they have been obtained from various sources ranging from DNS to fitting the spectrum given by the Kovasznay (1948) formula. The most recent algebraic form, obtained from the model spectra of Perry & Li (1990) at high wavenumbers, which is used by Marusic & Perry (1995) and Marusic, Uddin & Perry (1997) is

$$V(z^+) = 5.58 \left(1 - z^{+-0.9}\right) z^{+-0.5} \qquad (13.24)$$

Equations 13.21 – 13.23 have the same functional forms obtained by Townsend (1976) using the attached eddy hypothesis at large Reynolds number (as $z^+ \to \infty$, $V(z^+)$ becomes negligible over most of the boundary layer).

Appendix A

Equations of Motion

A.1   Continuity equation

Integral forms of the continuity equation for a fixed control volume:

$$\frac{\partial}{\partial t} \int \rho \, dv + \int \mathbf{n} \cdot \rho \mathbf{V} \, dA \; = \; 0$$

$$\int \mathbf{n} \cdot \rho \mathbf{V} \, dA \; = \; 0 \qquad \text{Fixed mass}$$

$$\int \mathbf{n} \cdot \rho \mathbf{V} \, dA \; = \; 0 \qquad \text{Steady flow}$$

$$\int \mathbf{n} \cdot \mathbf{V} dA \; = \; 0 \qquad \text{Incompressible flow}$$

Differential forms of the continuity equation:

$$\frac{\partial \rho}{\partial t} + \nabla \cdot \rho \mathbf{V} \; = \; 0$$

$$\nabla \cdot \mathbf{V} \; = \; -\frac{1}{\rho}\frac{D\rho}{Dt}$$

In tensor notation:

$$\frac{\partial \rho}{\partial t} + \frac{\partial \rho u_i}{\partial x_i} = 0$$

A.2   Linear momentum equation

Integral form of the momentum equation for a fixed control volume, where gravity is the only body force:

$$\mathbf{F}_{\text{ext}} + \int \vec{\Sigma}\,dA + \int \rho\mathbf{g}dv \;=\; \frac{\partial}{\partial t}\int \rho\mathbf{V}dv + \int (\mathbf{n}\cdot\rho\mathbf{V})\,\mathbf{V}dA$$

For an inviscid fluid:

$$\int \vec{\Sigma}\,dA = \int p\,dA$$

Differential form of the momentum equation (the Navier-Stokes equation):

$$\rho\frac{Du_i}{Dt} = \rho\frac{\partial u_i}{\partial t} + \rho u_j\frac{\partial u_i}{\partial x_j} = \rho g_i + \frac{\partial \sigma_{ij}}{\partial x_j}$$

or

$$\frac{\partial(\rho u_i)}{\partial t} + \frac{\partial(\rho u_i u_j)}{\partial x_j} = \rho g_i + \frac{\partial \sigma_{ij}}{\partial x_j}$$

where

$$\sigma_{ij} = -p\delta_{ij} + d_{ij}$$

and d_{ij} depends on the motion of the fluid only and it is called the shear stress tensor, or the deviatoric stress tensor (= σ'_{ij} in my notes, or τ_{ij} in Currie). For isotropic, Newtonian fluids,

$$d_{ij} = \lambda S_{kk}\delta_{ij} + 2\mu S_{ij}$$

where λ is called the "second viscosity coefficient" (μ'' in Batchelor),

$$\frac{\partial u_i}{\partial x_j} = S_{ij} + R_{ij}$$

$S_{ij} = e_{ij}$ and $R_{ij} = \xi_{ij}$ in my notes, and

$$S_{ij} = \tfrac{1}{2}\left(\frac{\partial u_i}{\partial x_j} + \frac{\partial u_j}{\partial x_i}\right) \;\text{ and }\; R_{ij} = \tfrac{1}{2}\left(\frac{\partial u_i}{\partial x_j} - \frac{\partial u_j}{\partial x_i}\right).$$

With the definition of the bulk viscosity μ'' (K in Currie, and κ in Batchelor):

$$\mu'' = \lambda + \tfrac{2}{3}\mu$$

we have

$$d_{ij} = \mu'' S_{kk}\delta_{ij} + 2\mu\left(S_{ij} - \tfrac{1}{3}S_{kk}\delta_{ij}\right)$$

and

$$\sigma_{ij} = -p\delta_{ij} + \mu'' S_{kk}\delta_{ij} + 2\mu\left(S_{ij} - \tfrac{1}{3}S_{kk}\delta_{ij}\right).$$

Differential form of the momentum equation where only the dynamic viscosity is retained:

$$\rho\frac{\partial u_i}{\partial t} + \rho u_j\frac{\partial u_i}{\partial x_j} = -\frac{\partial p}{\partial x_i} + \frac{\partial}{\partial x_j}\left(\mu\left(\frac{\partial u_i}{\partial x_j} + \frac{\partial u_j}{\partial x_i} - \tfrac{2}{3}\frac{\partial u_k}{\partial x_k}\delta_{ij}\right)\right)$$

For a constant-property fluid:

$$\rho\frac{D\mathbf{V}}{Dt} = -\nabla p + \rho\mathbf{g} + \mu\nabla^2\mathbf{V}$$

or, with $\psi = $ altitude:

$$\rho\frac{D\mathbf{V}}{Dt} = -\nabla p - \rho g\nabla\psi + \mu\nabla^2\mathbf{V}.$$

For an inviscid fluid we obtain Euler's equation:

$$\rho\frac{D\mathbf{V}}{Dt} = -\nabla p + \rho\mathbf{g}$$

A.3   Energy equation

Integral form of the energy equation for a fixed control volume:

$$\frac{\partial}{\partial t}\int \rho\left(e + \tfrac{1}{2}\rho V^2\right) dv + \int (\mathbf{n}\cdot\rho\mathbf{V})\left(e + \tfrac{1}{2}\rho V^2\right) dA = \int \mathbf{n}\cdot k\nabla T\, dA$$
$$+ \int \sigma_{ij}n_i u_j\, dA + \int \rho\mathbf{g}\cdot\mathbf{V}\, dA.$$

Differential form ($h = e + p/\rho$):

$$\frac{D}{Dt}\left(h + \tfrac{1}{2}V^2 + g\psi\right) = \frac{1}{\rho}\frac{\partial p}{\partial t} + \frac{\partial}{\partial t}(g\psi) + \frac{1}{\rho}\left[\frac{\partial}{\partial x_i}\left(\sigma_{ij}u_j\right) + \nabla\cdot k\nabla T\right]$$

Therefore, for a steady flow of an inviscid fluid where heat conduction effects are negligible, along along a streamline (streamlines are pathlines in steady flow):

$$h + \tfrac{1}{2}V^2 + g\psi = \text{constant}$$

When the fluid is incompressible as well, the specific internal energy e is constant, and

$$\frac{p}{\rho} + \tfrac{1}{2}V^2 + g\psi = \text{constant}$$

which is Bernoulli's equation.

Enthalpy equation

By using the momentum equation, we can write the energy equation as an enthalpy equation:

$$\rho\frac{Dh}{Dt} = \frac{Dp}{Dt} + \nabla \cdot k\nabla T + d_{ij}\frac{\partial u_j}{\partial x_i}$$

where

$$d_{ij}\frac{\partial u_j}{\partial x_i} = \Phi \quad \text{(the dissipation function)}$$

Entropy equation

From the enthalpy equation

$$\rho\frac{Dh}{Dt} - \frac{Dp}{Dt} = \nabla \cdot k\nabla T + \Phi.$$

Using $dh - dp/\rho = Tds$, we get

$$\rho T\frac{Ds}{Dt} = \nabla \cdot k\nabla T + \Phi$$

Note: when $\mathbf{q} = 0$ (adiabatic flow), and there is no dissipation, then the flow is *isentropic* (the rate of change of entropy following a fluid particle is zero). If this is true for all fluid particles, the flow is *homentropic*, that is, s is constant everywhere.

A.4   Summary

The equations of motion for a compressible, viscous, heat conducting fluid are:

$$\frac{\partial \rho}{\partial t} + \frac{\partial \rho u_i}{\partial x_i} = 0, \tag{A.1}$$

$$\rho\frac{\partial u_i}{\partial t} + \rho u_j\frac{\partial u_i}{\partial x_j} = -\frac{\partial p}{\partial x_i} + \frac{\partial d_{ij}}{\partial x_j}, \tag{A.2}$$

$$\rho\frac{\partial h}{\partial t} + \rho u_j\frac{\partial h}{\partial x_j} = \frac{Dp}{Dt} - \frac{\partial}{\partial x_i}\left(k\frac{\partial T}{\partial x_i}\right) + d_{ij}\frac{\partial u_i}{\partial x_j}, \tag{A.3}$$

which are, respectively, the continuity, momentum and energy equations. The deviatoric stress tensor d_{ij} is given by

$$d_{ij} = \mu \left(\frac{\partial u_i}{\partial x_j} + \frac{\partial u_j}{\partial x_i} - \frac{2}{3} \frac{\partial u_k}{\partial x_k} \delta_{ij} \right). \tag{A.4}$$

With the addition of an equation of state and the known variation of viscosity and thermal conductivity with temperature and pressure, this is a complete set of equations describing compressible fluid flow, provided that: the continuum hypothesis holds, the fluid particles are in local thermodynamic equilibrium, body forces can be neglected, the fluid is Newtonian, heat conduction follows Fourier's law and radiative heat transfer can be neglected.

Appendix B

References

S.B. Pope, "Turbulent Flows," Cambridge University Press, 2000

P.S. Bernard and J.M. Wallace, "Turbulent Flow: Analysis, Measurement, and Prediction," John Wiley & Sons, 2002

J. Mathieu and J. Scott, "An Introduction to Turbulent Flow," Cambridge University Press, 2000

H. Tennekes and J.L. Lumley, "A First Course in Turbulence," MIT Press, 1972

Hinze, J.O., "Turbulence," McGraw-Hill, New York, 2nd edition, 1975

P. Bradshaw, "An Introduction to Turbulence and Its Measurement," Pergamon Press, 1971

P. A. Libby, "Introduction to Turbulence," Taylor & Francis,1996

J. T. Davies, "Turbulence Phenomena," Academic Press, 1972

M. Lesieur, "Turbulence in Fluids," Kluwer, 3rd edition, 1993

H. Schlichting and K. Gersten, "Boundary-Layer Theory," McGraw-Hill, 8th edition, 2000

D. C. Wilcox, "Turbulence Modeling for CFD," DCW Industries, 1993

B. E. Launder and D. B. Spalding, "Mathematical Models of Turbulence," Academic Press, 1972

U. Frisch, "Turbulence," CUP paperback, 1995

Cebeci, T. and Smith, A. M. O., "Analysis of Turbulent Boundary Layers," Academic Press, 1974

Bradshaw, P., Cebeci, T. and Whitelaw, J. H., "Engineering Calculation Methods for Turbulent Flow," Academic Press, 1981

Cebeci, T. and Bradshaw, P., "Momentum Transfer in Boundary Layers," Hemisphere, 1977

Cebeci, T. and Bradshaw, P., "Physical and Computational Aspects of Convective Heat Transfer," Springer-Verlag, 1984

Smits, A.J. and Dussauge, J.P., "Turbulent Shear Layers in Supersonic Flow," Springer Verlag, AIP Imprint, 1996